IMMUNE REGULATION IN KIDNEY DISEASES: IMPORTANCE, MECHANISM AND TRANSLATION

EDITED BY: Cheng Yang and Songjie Cai

PUBLISHED IN: Frontiers in Medicine and Frontiers in Cell and Developmental Biology

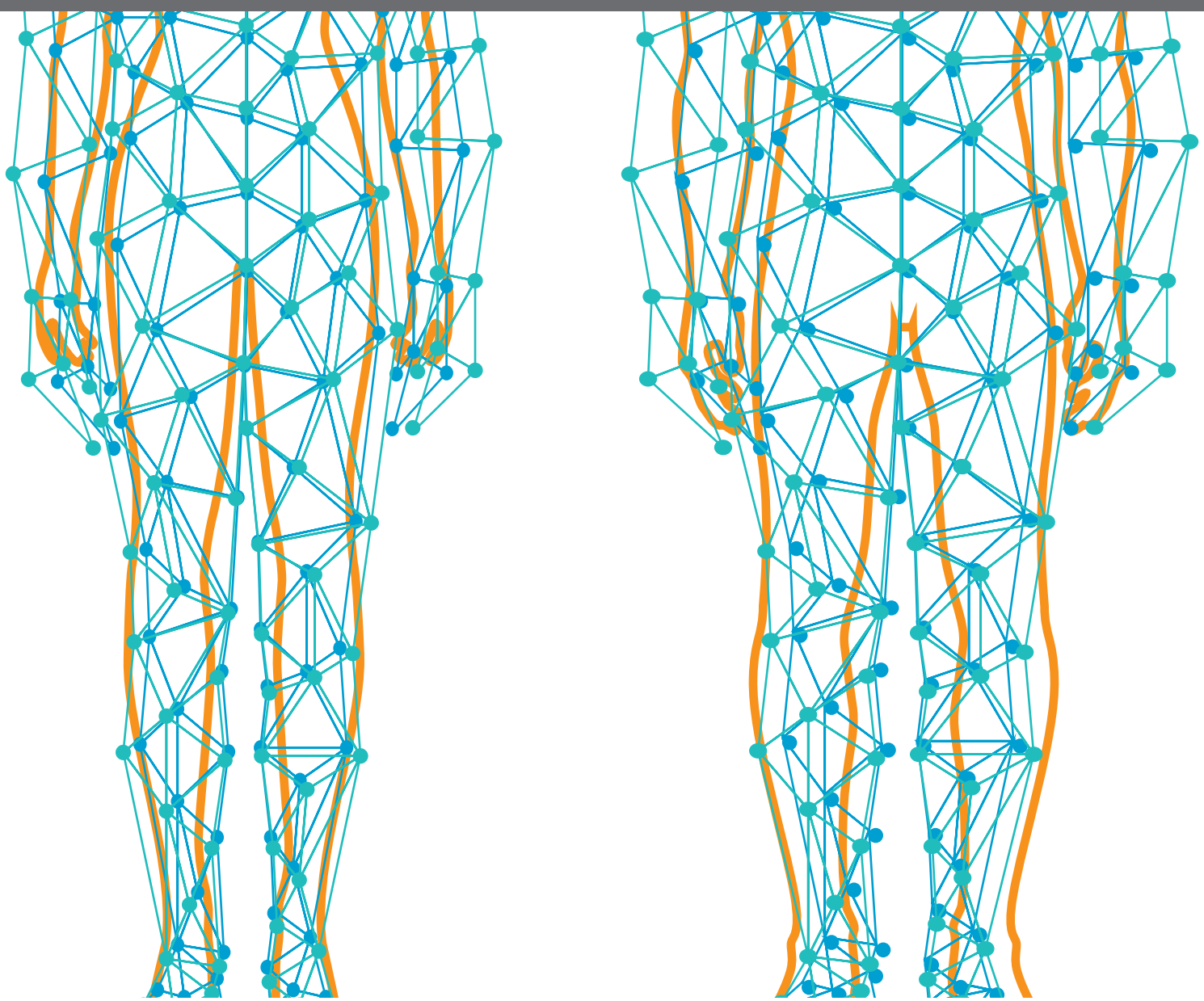

frontiers Research Topics

ISSN 1664-8714
ISBN 978-2-88966-604-1
DOI 10.3389/978-2-88966-604-1

About Frontiers

Frontiers is more than just an open-access publisher of scholarly articles: it is a pioneering approach to the world of academia, radically improving the way scholarly research is managed. The grand vision of Frontiers is a world where all people have an equal opportunity to seek, share and generate knowledge. Frontiers provides immediate and permanent online open access to all its publications, but this alone is not enough to realize our grand goals.

Frontiers Journal Series

The Frontiers Journal Series is a multi-tier and interdisciplinary set of open-access, online journals, promising a paradigm shift from the current review, selection and dissemination processes in academic publishing. All Frontiers journals are driven by researchers for researchers; therefore, they constitute a service to the scholarly community. At the same time, the Frontiers Journal Series operates on a revolutionary invention, the tiered publishing system, initially addressing specific communities of scholars, and gradually climbing up to broader public understanding, thus serving the interests of the lay society, too.

Dedication to Quality

Each Frontiers article is a landmark of the highest quality, thanks to genuinely collaborative interactions between authors and review editors, who include some of the world's best academicians. Research must be certified by peers before entering a stream of knowledge that may eventually reach the public - and shape society; therefore, Frontiers only applies the most rigorous and unbiased reviews.
Frontiers revolutionizes research publishing by freely delivering the most outstanding research, evaluated with no bias from both the academic and social point of view. By applying the most advanced information technologies, Frontiers is catapulting scholarly publishing into a new generation.

What are Frontiers Research Topics?

Frontiers Research Topics are very popular trademarks of the Frontiers Journals Series: they are collections of at least ten articles, all centered on a particular subject. With their unique mix of varied contributions from Original Research to Review Articles, Frontiers Research Topics unify the most influential researchers, the latest key findings and historical advances in a hot research area! Find out more on how to host your own Frontiers Research Topic or contribute to one as an author by contacting the Frontiers Editorial Office: frontiersin.org/about/contact

IMMUNE REGULATION IN KIDNEY DISEASES: IMPORTANCE, MECHANISM AND TRANSLATION

Topic Editors:
Cheng Yang, Fudan University, China
Songjie Cai, Brigham and Women's Hospital, Harvard Medical School, United States

Citation: Yang, C., Cai, S., eds. (2021). Immune Regulation in Kidney Diseases: Importance, Mechanism and Translation. Lausanne: Frontiers Media SA. doi: 10.3389/978-2-88966-604-1

Table of Contents

05 ***Editorial: Immune Regulation in Kidney Diseases: Importance, Mechanism and Translation***
Cheng Yang and Songjie Cai

08 ***Exosomes Derived From Mesenchymal Stem Cells Ameliorate Renal Ischemic-Reperfusion Injury Through Inhibiting Inflammation and Cell Apoptosis***
Long Li, Rulin Wang, Yichen Jia, Ruiming Rong, Ming Xu and Tongyu Zhu

16 ***The First Case of Ischemia-Free Kidney Transplantation in Humans***
Xiaoshun He, Guodong Chen, Zebin Zhu, Zhiheng Zhang, Xiaopeng Yuan, Ming Han, Qiang Zhao, Yitao Zheng, Yunhua Tang, Shanzhou Huang, Linhe Wang, Otto B. van Leeuwen, Xiaoping Wang, Chuanbao Chen, Liqiu Mo, Xingyuan Jiao, Xianchang Li, Changxi Wang, Jiefu Huang, Jun Cui and Zhiyong Guo

22 ***Erythropoietin Derived Peptide Improved Endoplasmic Reticulum Stress and Ischemia-Reperfusion Related Cellular and Renal Injury***
Yufang Zhang, Qian Wang, Aifen Liu, Yuanyuan Wu, Feng Liu, Hui Wang, Tongyu Zhu, Yaping Fan and Bin Yang

36 ***Oral Administration of Si-Based Agent Attenuates Oxidative Stress and Ischemia-Reperfusion Injury in a Rat Model: A Novel Hydrogen Administration Method***
Masataka Kawamura, Ryoichi Imamura, Yuki Kobayashi, Ayumu Taniguchi, Shigeaki Nakazawa, Taigo Kato, Tomoko Namba-Hamano, Toyofumi Abe, Motohide Uemura, Hikaru Kobayashi and Norio Nonomura

46 ***The Role of Immune Modulation in Pathogenesis of IgA Nephropathy***
Sheng Chang and Xiao-Kang Li

61 ***Inhibition of Inflammatory Cytokine Expression Prevents High-Fat Diet-Induced Kidney Injury: Role of Lingonberry Supplementation***
Susara Madduma Hewage, Suvira Prashar, Samir C. Debnath, Karmin O and Yaw L. Siow

74 ***A 14-Year Follow-Up of a Combined Liver-Pancreas-Kidney Transplantation: Case Report and Literature Review***
Geng Zhang, Weijun Qin, Jianlin Yuan, Changsheng Ming, Shuqiang Yue, Zhengcai Liu, Lei Yu, Ming Yu, Xiaokang Gao, Yu Zhou, Longxin Wang, Xiaojian Yang, Kefeng Dou and He Wang

80 ***MicroRNA-381-3p Functions as a Dual Suppressor of Apoptosis and Necroptosis and Promotes Proliferation of Renal Cancer Cells***
Cong Zhao, Yifei Zhou, Qiao Ran, Ying Yao, Haoran Zhang, Jie Ju, Tao Yang, Wei Zhang, Xiaoliang Yu and Sudan He

91 ***Transcriptome Profiling Reveals Indoxyl Sulfate Should Be Culpable of Impaired T Cell Function in Chronic Kidney Disease***
Fangfang Xiang, Xuesen Cao, Bo Shen, Xiaohong Chen, Man Guo, Xiaoqiang Ding and Jianzhou Zou

101 ***Serum N-terminal Pro-B-type Natriuretic Peptide Predicts Mortality in Cardiac Surgery Patients Receiving Renal Replacement Therapy***

Ying Su, Jun-yi Hou, Yi-jie Zhang, Guo-guang Ma, Guang-wei Hao, Jing-chao Luo, Zhe Luo and Guo-wei Tu

110 ***Kidney Ischemia-Reperfusion Elicits Acute Liver Injury and Inflammatory Response***

Yue Shang, Susara Madduma Hewage, Charith U. B. Wijerathne, Yaw L. Siow, Cara K. Isaak and Karmin O

119 ***Cathepsin S and Protease-Activated Receptor-2 Drive Alloimmunity and Immune Regulation in Kidney Allograft Rejection***

Yutian Lei, Benjamin Ehle, Santhosh V. Kumar, Susanne Müller, Solange Moll, Andrew F. Malone, Benjamin D. Humphreys, Joachim Andrassy and Hans-Joachim Anders

131 ***Histone Methylation Inhibitor DZNep Ameliorated the Renal Ischemia-Reperfusion Injury* via *Inhibiting TIM-1 Mediated T Cell Activation***

Jiawei Li, Yue Qiu, Long Li, Jiyan Wang, Yin Celeste Cheuk, Ruirui Sang, Yichen Jia, Jina Wang, Yi Zhang and Ruiming Rong

142 ***The Double-Edged Sword of Immunosuppressive Therapy in Kidney Transplantation: A Rare Case Report of Pulmonary Mucormycosis Post-Transplant and Literature Review***

Hengcheng Zhang, Ke Wang, Hao Chen, Li Sun, Zijie Wang, Shuang Fei, Ruoyun Tan and Min Gu

148 ***Plasma Soluble CD146 as a Potential Diagnostic Marker of Acute Rejection in Kidney Transplantation***

Jun Liao, Qian Fu, Wenfang Chen, Jun Li, Wenhui Zhang, Huanxi Zhang, Yifang Gao, Shicong Yang, Bowen Xu, Huiting Huang, Jiali Wang, Xirui Li, Longshan Liu and Changxi Wang

frontiers in Medicine

EDITORIAL
published: 11 February 2021
doi: 10.3389/fmed.2021.616880

Editorial: Immune Regulation in Kidney Diseases: Importance, Mechanism and Translation

Cheng Yang[1,2,3]* *and Songjie Cai*[4]*

[1] Department of Urology, Zhongshan Hospital, Fudan University, Shanghai, China, [2] Shanghai Key Laboratory of Organ Transplantation, Shanghai, China, [3] Zhangjiang Institute of Fudan University, Shanghai, China, [4] Transplantation Research Center, Renal Division, Brigham and Women's Hospital and Harvard Medical School, Boston, MA, United States

Keywords: kidney, immune regulation, acute kidney injury, ischemia reperfusion injury, transplantation—kidney, chronic kidney disease, erythropoietin

Editorial on the Research Topic

Immune Regulation in Kidney Diseases: Importance, Mechanism and Translation

Immune system is the vital system in humans. Our defense to infection relies on the system, which is regulated precisely. In our immune system, it exists a balance between offensive and defensive powers. The attack by immune cells cannot be amplified infinitely. Uncontrollable immune response will elicit autoimmune disease. On the other hand, weak immune response cannot kill tumor cells. Therefore, immune regulation by many regulatory immune cells and cytokines is of importance in physiological and pathological condition. The kidneys, both native and transplant, are closely related with the immune system. In this Research Topic, we bring you some excellent original studies, reviews, and case reports.

In this issue, these are three case reports related on kidney transplantation. In kidney transplantation, ischemia reperfusion (IR) injury is an evitable process, which is associated with delayed graft function, rejection, and long-term allograft survival. The immune system participates in the IR injury in terms of innate immunity activation, inflammation and stress. In previous study, He et al. established a novel procedure called ischemia-free liver transplantation during which the donor livers can be procured, preserved, and implanted without cessation of oxygenated blood supply to the grafts. In this issue, their team reported the first case of ischemia-free kidney transplantation (IFKT) in human. In brief, the left kidney was procured after ligating the left renal artery and vein and immediately cold flushed through the left kidney artery. This graft was preserved in ice-cold University of Wisconsin solution. The right kidney was subjected to IFKT. This method provides a unique solution to reduce IR injury or delayed graft function morbidity (He et al.). The second case by Zhang G. et al. reported a patient with combined liver-pancreas-kidney transplantation who had been followed up by 14 years. This patient suffered from end-stage liver disease, post-chronic hepatitis B, cirrhosis, chronic renal failure, and insulin-dependent diabetes mellitus caused by chronic pancreatitis. In 14 years of follow-up, no severe rejection or other complications were observed. Simultaneous piggyback orthotopic liver and heterotopic pancreas-duodenum and renal transplantation is a good therapeutic option for patients with exocrine pancreatic insufficiency and insulin-dependent diabetes combined with hepatic and renal failure (Zhang G. et al.). In kidney transplant patients, immunosuppression therapy is inevitable. The immune system is generally suppressed because all immunosuppression drugs are not specific to the allografts. Therefore, infection after transplantation is a very common but complicated problem. Opportunistic infections such as fungal is not rare in kidney transplant patients. In this case, Fumet et al. reported a patient with *pulmonary mucormycosis* 38 days after kidney

Edited and reviewed by:
Shrikant R. Mulay, Central Drug Research Institute (CSIR), India

***Correspondence:**
Cheng Yang
esuperyc@163.com
Songjie Cai
scai2@bwh.harvard.edu

Specialty section:
This article was submitted to Nephrology, a section of the journal Frontiers in Medicine

Received: *13 October 2020*
Accepted: *21 January 2021*
Published: *11 February 2021*

Citation:
Yang C and Cai S (2021) Editorial: Immune Regulation in Kidney Diseases: Importance, Mechanism and Translation. Front. Med. 8:616880. doi: 10.3389/fmed.2021.616880

transplantation (1). This case is a reminder that early diagnosis of fungal infection is imperative.

Acute kidney injury (AKI) brings heavy burden to the healthcare system with high morbidity and mortality. AKI occurs in about 13.3 million people per year, 85% of whom live in the developing world, and, although no direct link between AKI and death has yet been shown, AKI is thought to contribute to about 1.7 million deaths every year (2). Therefore, it is urgent to discover novel useful biomarkers and drugs of AKI. N-terminal pro-B-type natriuretic peptide (NT-proBNP) is a useful cardiac biomarker that is associated with acute kidney injury (AKI) and mortality after cardiac surgery. However, its prognostic value in cardiac surgical patients receiving renal replacement therapy (RRT) remains unclear. In this study, Su et al. established a prediction model based on NT-proBNP in cardiac surgical patients receiving RRT. The area under the receiver operating characteristic curve of NT-proBNP before surgery, at RRT initiation, and on the first day after RRT for predicting 28-day mortality was 0.64, 0.71, and 0.68, respectively (Su et al.). This study demonstrated that serum NT-proBNP was an independent predictor of 28-day mortality in cardiac surgical patients with AKI requiring RRT.

As mentioned above, no specific and effective therapy is available for AKI. In this issue, researchers investigated several novel molecule and peptide drugs, as well as cell therapy. Previous study found that 3-Deazaneplanocin A (DZNep), an inhibitor of Ezh2, had an inhibitory effect on graft-vs.-host disease (GVHD) in a kidney or bone marrow transplantation model, and it can only induce apoptosis of activated T cells but has no effect on naïve T cells. In this study, Li J. et al. further investigated the role of DZNep in kidney IR injury. They demonstrated that DZNep alleviated renal IR injury in mice by inhibiting T cell activation through direct and indirect pathways. The indirect pathway may involve the impairment of interactions between T cells and macrophages by the TIM-1–TIM-4 axis, suggesting that DZNep can be a novel strategy for preventing renal IRI following kidney transplantation (Li J. et al.). Erythropoietin (EPO), an evolutionarily conserved hormone mainly produced in the kidney, has been well-documented for its indispensable role in erythropoiesis. In recent years, numerous studies have shown that EPO acts far beyond erythropoiesis (3). EPO modulates immune cells function and protects tissue against injury. Our group synthesized a series of cyclic analogs and found that the head-to-tail thioether-cyclized HBSP, namely, cyclic helix B peptide (CHBP), remained stable in human plasma and had a 2.5-folds longer half-life than its counterpart in human hepatocytes (4). Zhang Y. et al. demonstrated that CHBP reduced endoplasmic reticulum stress through CHOP/PERK/JNK pathway. CHBP also inhibited the increase of CHOP protein, not only in tubular epithelia cells, but also in the IR injury kidneys at 2 weeks. Moreover, CHBP reduced the expression of PERK mRNA and protein, JNK and HMGB-1 protein, as well as early and later apoptosis. This study revealed a novel mechanism of CHBP in AKI, and CHOP might be a potential biomarker of IR-induced AKI (Zhang Y. et al.).

Mesenchymal stem cells (MSCs) have been found to exert several biological functions, such as repairing tissue damage, suppressing inflammatory responses, and modulating the immune system. Exosomes originated from mesenchymal stem cell were reported to activate signaling pathways by binding to receptors. In this issue, Li L. et al. found that exosomes from MSCs ameliorated kidney tubular epithelia cell apoptosis and interstitial inflammation through NK-κB pathway. Although the efficacy of molecular hydrogen (H_2) in IR injury has been reported, oral intake of H_2-rich water and inhalation of H_2 gas are still not widely used in clinical settings because of the lack of efficiency and difficulty in handling. Kawamura et al. successfully generated large quantities of H_2 molecules by crushing silicon (Si) to nano-sized Si particles (nano-Si) which were allowed to react with water. They investigated whether oral administration of H_2 could ameliorate kidney IR injury. In a rat kidney IR model, oral nano-Si intake downregulated immune response, cytokine production, and extrinsic apoptosis. This study might provide a novel gas therapy for renal IR injury (Kawamura et al.). As we know, hepatorenal syndrome is a complicated disease in clinic. The liver function is often compromised in patients with AKI and in animal models. However, the underlying mechanisms are not fully understood. Here, Shang et al. found that renal IR injury elicited acute liver injury and inflammation response. They demonstrated that renal IR can directly activate NF-kB and induce acute production of proinflammatory cytokines in the liver. Renal IR-induced hepatic inflammatory response may contribute to impaired liver function and systemic inflammation (Shang et al.).

Besides AKI, there are two researchers about chronic kidney disease (CKD). Chronic low-grade inflammation is a major stimulus for progression of CKD in individuals consuming high-fat diet. Lingonberry is rich in anthocyanins with demonstrated anti-inflammatory effect. Madduma Hewage et al. investigated the potential renal protective effect of lingonberry and its anthocyanin (cyanidin-3-glucoside) in high-fat diet fed obese mice and in human proximal tubular cells. They found that lingonberry supplementation can reduce inflammatory response, suggesting lingonberry might be a complementary fruit for chronic kidney disease (CKD) therapy (Madduma Hewage et al.). Since chronic inflammation and immune system dysfunction play a key role in the pathogenesis of CKD, Xiang et al. explored the genome-wide expression profile in human peripheral blood T cells under stimulation by indoxyl sulfate (IS) which was one of the protein-bound renal toxins. A total of 5,129 DEGs were identified, and IS may influence multiple biological functions of T cells including inflammatory response and cell cycle regulation. This study provided an immune regulation network in T cells stimulated by IS (Xiang et al.). IgA nephropathy is a common factor of end stage renal disease in China. A variety of immune cells (e.g., dendritic cells, NK cells, macrophages, T-lymphocyte subsets, and B-lymphocytes, etc.) and molecules (e.g., IgA receptors, Toll-like receptors, complements, etc.) in innate and adaptive immunity are involved in the pathogenesis of IgA nephropathy. Chang and Li reviewed the role of immune regulation in IgA nephropathy. This review focus on both innate and adaptive immunity, as well as mucosal immunity (Chang and Li).

In the field of kidney transplantation, there are two original researches. Liao et al. retrospectively enrolled fifty-six patients with biopsy-proved rejection or non-rejection and 11 stable allograft function patients. Both soluble CD146 in plasma and local CD146 expression in kidney allografts were detected. They found plasma soluble CD146 could be a biomarker of acute rejection after kidney transplantation, whose area under the receiver operating characteristic curve was 0.895 (Liao et al.).

In conclusion, all published articles covered immune regulation in acute, chronic kidney injury and kidney transplantation. We believe this Research Topic can provide new findings of immune regulation in kidney diseases. Thanks to all contribution authors, reviewers and editors.

AUTHOR CONTRIBUTIONS

CY and SC wrote the editorial. Both authors contributed to the article and approved the submitted version.

REFERENCES

1. Fumet JD, Limagne E, Thibaudin M, Ghiringhelli F. Immunogenic cell death and elimination of immunosuppressive cells: a double-edged sword of chemotherapy. *Cancers*. (2020) 12:2637. doi: 10.3390/cancers12092637
2. Mehta RL, Cerda J, Burdmann EA, Tonelli M, Garcia-Garcia G, Jha V, et al. International Society of Nephrology's 0by25 initiative for acute kidney injury (zero preventable deaths by 2025): a human rights case for nephrology. *Lancet*. (2015) 385:2616–43. doi: 10.1016/S0140-6736(15)60126-X
3. Peng B, Kong G, Yang C, Ming Y. Erythropoietin and its derivatives: from tissue protection to immune regulation. *Cell Death Dis*. (2020) 11:79. doi: 10.1038/s41419-020-2276-8
4. Yang C, Xu Z, Zhao Z, Li L, Zhao T, Peng D, et al. A novel proteolysis-resistant cyclic helix B peptide ameliorates kidney ischemia reperfusion injury. *Biochimica et Biophysica Acta*. (2014) 1842:2306–17. doi: 10.1016/j.bbadis.2014.09.001

Conflict of Interest: The authors declare that the research was conducted in the absence of any commercial or financial relationships that could be construed as a potential conflict of interest.

frontiers in Medicine

ORIGINAL RESEARCH
published: 19 November 2019
doi: 10.3389/fmed.2019.00269

Exosomes Derived From Mesenchymal Stem Cells Ameliorate Renal Ischemic-Reperfusion Injury Through Inhibiting Inflammation and Cell Apoptosis

Long Li[1,2†], *Rulin Wang*[3†], *Yichen Jia*[1,2†], *Ruiming Rong*[1,2], *Ming Xu*[1,2*] *and Tongyu Zhu*[1,2*]

[1] Department of Urology, Zhongshan Hospital, Fudan University, Shanghai, China, [2] Shanghai Key Laboratory of Organ Transplantation, Shanghai, China, [3] Department of Urology, The First Affiliated Hospital of Zhengzhou University, Zhengzhou, China

OPEN ACCESS

Edited by:
Songjie Cai,
Department of Medicine, Brigham and Women's Hospital, United States

Reviewed by:
Rajeev Rohatgi,
Northport VA Medical Center, United States
Bassam G. Abu Jawdeh,
University of Cincinnati, United States

***Correspondence:**
Ming Xu
xu.ming@zs-hospital.sh.cn
Tongyu Zhu
zs_tyzhu@163.com

[†]These authors have contributed equally to this work

Specialty section:
This article was submitted to Nephrology, a section of the journal Frontiers in Medicine

Received: 18 August 2019
Accepted: 01 November 2019
Published: 19 November 2019

Citation:
Li L, Wang R, Jia Y, Rong R, Xu M and Zhu T (2019) Exosomes Derived From Mesenchymal Stem Cells Ameliorate Renal Ischemic-Reperfusion Injury Through Inhibiting Inflammation and Cell Apoptosis. Front. Med. 6:269. doi: 10.3389/fmed.2019.00269

This study aimed to investigate the underlying mechanism of mesenchymal stem cells (MSCs) on protection of renal ischemia reperfusion injury (IRI). Exosomes originated from MSCs (MSC-ex) were extracted according to the instructions of Total Exosome Isolation Reagent. Rats were divided into five groups: sham-operated, IRI, MSC, MSC-ex, and MSC-ex + RNAase group. MSCs or MSC-ex were injected via carotid artery. The renal function test and pathological detection were applied to determine the renoprotection of MSC-ex on IRI. Western blotting and quantitative reverse transcription polymerase chain reaction (RT-qPCR) were conducted to examine the levels of apoptosis-related proteins and inflammatory cytokines. Our results revealed that MSC-derived exosomes attenuated renal dysfunction, histologic damage, and decreased apoptosis. The expression levels of inflammatory cytokines, such as interleukin 6 (IL-6), tumor necrosis factor-α (TNF-α), nuclear factor kappa B (NF-κB), and interferon gamma (IFN-γ), were decreased by the MSC-ex treatment. The expression levels of caspase-9, cleaved caspase-3, Bax, and Bcl-2 caused by IR were also inhibited by MSC-ex. MSC-ex + RNAase group shared the similar pattern of changes with IRI group, likely due to the ability of RNA hydrolase to eliminate the function of exosomes. Our results demonstrated that exosomes originating from MSCs have protective effects on IRI via inhibiting cell apoptosis and inflammatory responses. Out findings may provide a new insight into therapeutic mechanism of MSCs on renal IRI.

Keywords: mesenchymal stem cells, exosomes, ischemic-reperfusion injury, inflammation, apoptosis

INTRODUCTION

Ischemia reperfusion injury (IRI), one of the major causes of post-operative renal allograft complications, is inevitable during transplantation (1, 2). It has been reported that IRI may cause acute renal failure and delayed graft function, thereby impairing long-term survival of the graft and recovery in post-transplantation (3–5). Therefore, understanding the pathogenesis may assist scholars to present new strategies to prevent IRI after renal transplantation.

Mesenchymal stem cells (MSCs) have been found to exert several biological functions, such as repairing tissue damage, suppressing inflammatory responses, and modulating the immune system (6, 7). They may protect acute kidney injury (AKI) induced by cisplatin, glycerol, and IRI in rats, however, the underlying mechanism has still remained elusive. Accumulating evidence supported that MSCs act in a paracrine manner (8). Therefore, the biological factors in conditioned medium, including exosomes and soluble factors, derived from MSCs have been extensively studied in recent years. Exosomes were reported to activate signaling pathways by binding to receptors (9–11). Compared with MSCs, exosomes are more stable and reservable, have no risk of aneuploidy, with lower possibility of immune rejection following allogeneic administration, and may provide alternative therapies for a variety of diseases (12). A previous study demonstrated that exosomes from MSC can reduce remnant kidney fibrosis in a 5/6 subtotal nephrectomy mice model (13). Furthermore, it has been revealed that infusing exosomes from MSC reduce the expression levels of 8- hydroxy-2′ -deoxyguanosine (8-OHdG), malonaldehyde (MDA), Bax, and caspase-3 in a cis-platinum-induced AKI mouse model (14). However, to date, the underlying mechanism of MSC-derived exosomes on renoprotection of IRI has remained obscure. Thus, the present study aimed to identify the protective effects and mechanism of MSC-ex on renal IRI.

Nuclear factor kappa B (NF-κB) is a family of dimeric transcription factors that participate in inflammatory responses, innate and adaptive immunity during kidney transplantation (15–17). It has been reported that MSCs can protect tissues against injury by regulating the activation of NF-κB. In the present research, we demonstrated that: (1) MSC-ex mitigated IRI-induced renal structural injury and improved renal function in rats; (2) the renoprotection of MSC-ex is due to downregulation of inflammatory factors and suppressing NF-κB signaling pathway.

MATERIALS AND METHODS

Animals

Male Sprague-Dawley (SD) rats (weight, 200–250 g) were purchased from Shanghai SLAC Laboratory Animal Co., Ltd. (Shanghai, China), and housed in temperature-controlled, SPF condition with free access to food and water. Animals were fasted for 1 day prior to surgery. All animal procedures were performed in accordance with the guidelines of the bioethics, and the study was approved by the Ethics Committee of Zhongshan Hospital Affiliated to Fudan University (Shanghai, China).

Separation, Cultivation, and Authentication of MSCs

The SD-MSC line RASMX-01001 was purchased from Cyagen Biosciences (Guangzhou, China). Cells were cultured at 37°C with 5% CO_2 under humidity conditions.

Extraction and Authentication of Exosomes

MSCs were cultivated overnight without serum according to the instructions of Total Exosome Isolation Reagent (Thermo Fisher Scientific, Waltham, MA, USA). Then, culture fluid was collected, and centrifuged at 2,000 g for 30 min at 4°C. The Total Exosome Isolation Reagent was added and mixed thoroughly, and the liquid was stored at 4°C overnight. The liquid was then centrifuged at 1,000 g for 60 min at 4°C, and supernatant was removed, and the exosomes were left at the bottom of the centrifuge tubes. Phosphate-buffered saline (PBS) was used to re-suspend exosomes, which was diluted to 100 μg/ml, and stored at −80°C until further analysis. The isolated exosomes were identified by transmission electron microscopy (TEM) (**Supplementary Image 1**) and detected by flow cytometry (**Supplementary Image 2**).

An *in vivo* Model of Renal IRI

SD rats were anesthetized by intraperitoneal injection of pentobarbital at 0.1 g/kg. All rats were divided into five groups: sham-operated group, IR group, IR + MSC group (IR + MSC, 2 *10^6 MSC/1 ml PBS), IR + MSC-ex group (exosome 100 μg/ml in PBS), and IR + MSC-ex + RNAase (exosome 100 μg/ml in PBS). Renal IRI was induced by clamping the left renal artery via a median abdominal incision for 45 min, plus a right nephrectomy. Following clamp removal, adequate restoration of blood flow was made before abdominal closure and the right kidney was removed. The left carotid artery was separated by para-tracheal incision using a 24G arteriovenous puncture needle to make the carotid puncture. Sham-operated animals underwent the same surgical procedure without clamping. The MSCs (1.5×10^5 cells in PBS), exosomes (30 μg in PBS) or RNAase were given via carotid artery 1 h after I/R.

Assessment of Renal Function

Whole blood was centrifuged at 1,600 g for 25 min at 4°C to obtain serum. An auto biochemistry instrument was used to measure the levels of serum creatinine (SCr) and blood urea nitrogen (BUN).

Histological Assessment

Hematoxylin and eosin (H&E) staining was performed to assess histological injury. The tissue sections were blind-labeled and reviewed by two pathologists. Renal damage was graded based on the percentage of damaged tubules in the sample: 0 = normal kidney (no damage); 1 = minimal damage (<25% damage); 2 = mild damage (25%−50% damage); 3 = moderate damage (50%−75% damage); 4 = severe damage (75%-100% damage); and 5 = extremely damaged (100% damage), as previously described. Injury included inflammatory cell infiltration, dilation

TABLE 1 | Sequences of gene-specific primers used in RT-qPCR.

IL-6	Forward	5′-CGAGCCCACCAGGAACGAAAGTC-3′
	Reverse	5′-CTGGCTGGAAGTCTCTTGCGGAG-3′
TNF-α	Forward	5′ -CCTTATCTACTCCCAGGTTCTC-3′
	Reverse	5′-AGGGGCCATCCACAGTCTTC-3′
NF-κB	Forward	5′-TGTCCATGCAGCTTCGGCGG-3′
	Reverse	5′-GGCCGGGGTTCAGTTGGTCC-3′
IFN-γ	Forward	5′-AAAGACAACCAGGCCATCAG-3′
	Reverse	5′-CTTTTCCGCTTCCTTAGGCT-3′

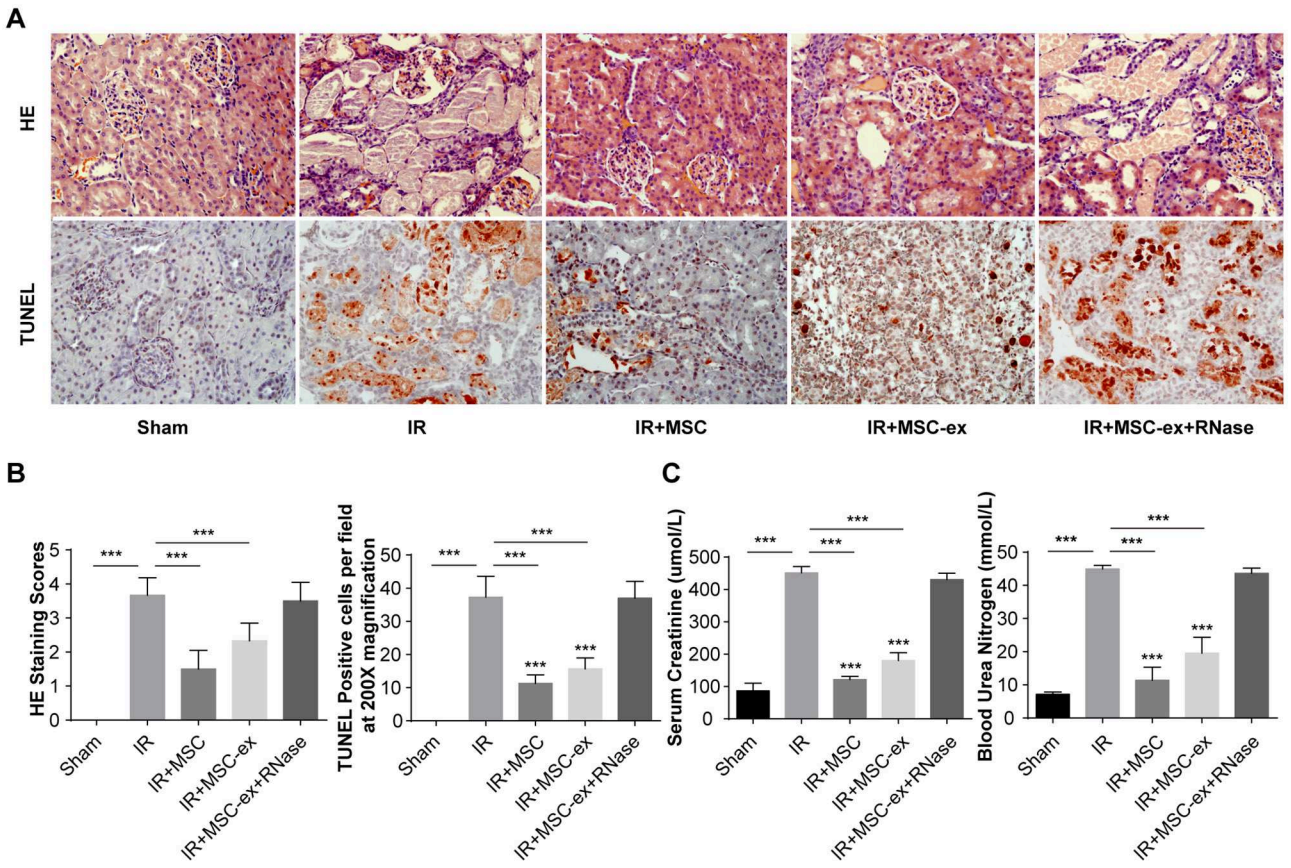

FIGURE 1 | MSCs and exosomes ameliorated renal IRI. **(A)** Representative images of HE and TUNEL staining methods in rat kidneys with administration of MSC, MSC-ex, and MSC-ex+RNAase after IR. Images were captured at x 200× magnification, scale bar = 10 μm. The levels of SCr and BUN were measured using the peripheral blood automatic biochemical analyzer. **(B)** Shows scores of HE staining and the number of TUNEL positive cells. Histopathological grading of tissue injury was assessed using the 0- to 4-point scoring system. **(C)** The levels of SCr and BUN were measured using the peripheral blood automatic biochemical analyzer. $^{***}P < 0.001$, $n = 6$.

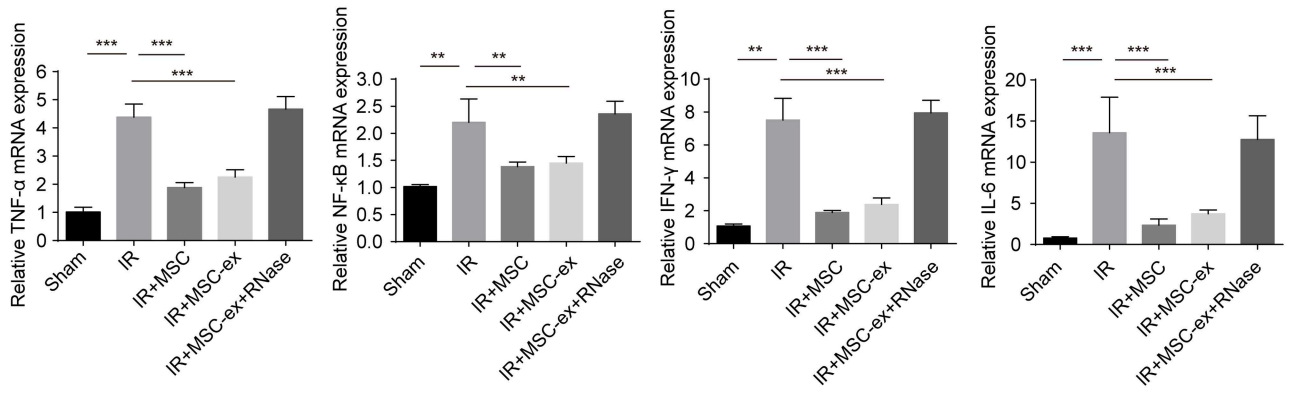

FIGURE 2 | MSCs and exosomes from MSCs decreased proinflammatory Total RNA was extracted from renal tissue 48 h after IR, and then reversely transcribed into cDNA. Treatment with MSCs or MSC-ex reduced the mRNA levels of TNF-α, NF-κB, IFN-γ, and IL-6, while MSC-ex + RNAase had no influence, $^{**}P < 0.01$, $^{***}P < 0.001$, $n = 6$.

of renal tubules, and interstitial edema. Scores of 1 or 2 represent mild injury, and scores of 3 or 4 and 5 represent moderate and severe injuries, respectively. The scores are the average of two reads.

Detection of Apoptosis

The terminal deoxynucleotidyl transferase-mediated dUTP-biotin nick end labeling (TUNEL) assay was used to detect apoptotic cells according to the manufacturer's instructions.

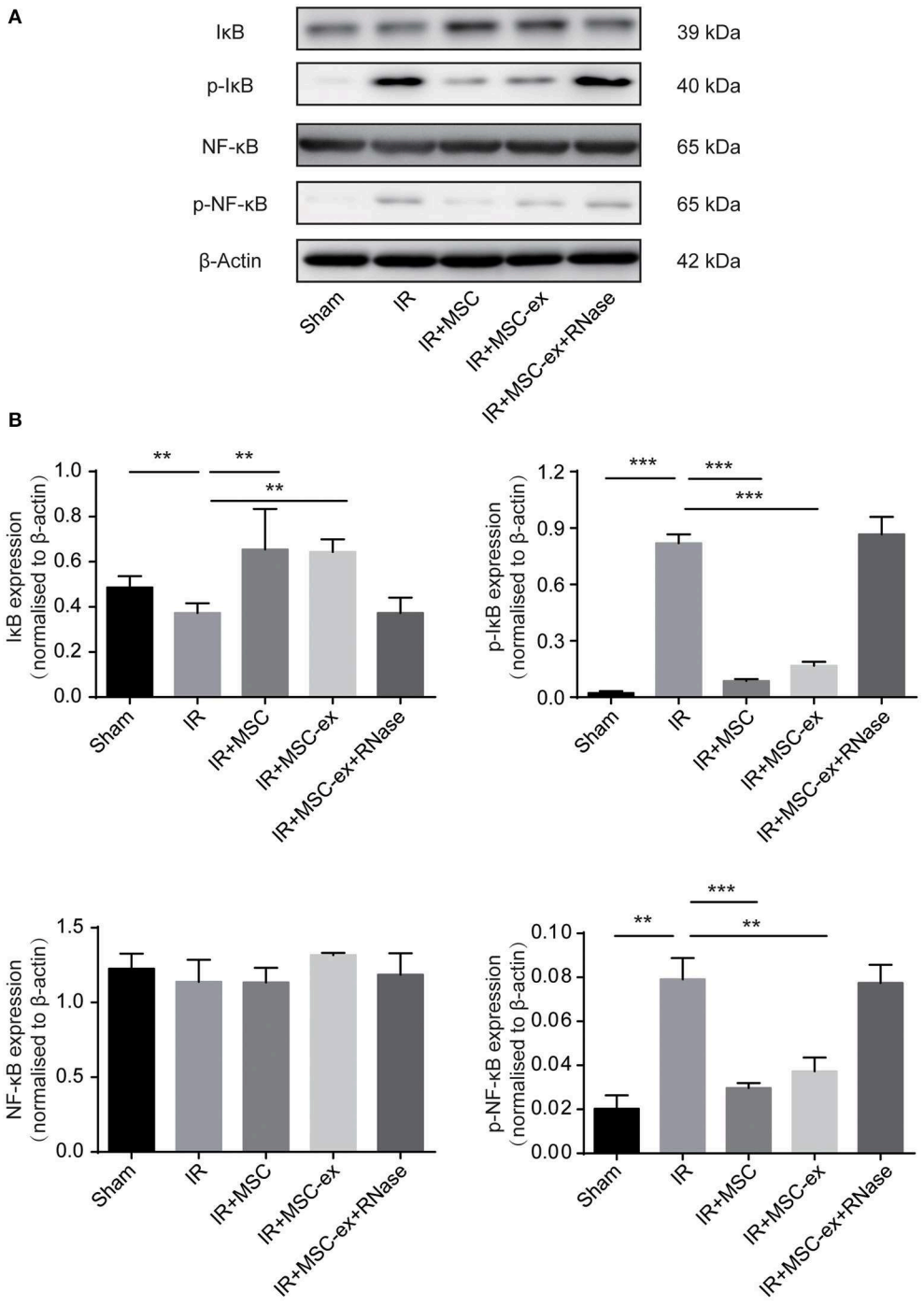

FIGURE 3 | MSC and exosomes from MSC inhibited the NF-κB signaling pathway by decreasing expression levels of p-NF-κB and p-IκB, and increasing expression level of IκB. **(A)** Representative images show the protein levels of IκB, p-IκB, NF-κB, and p-NF-κB. **(B)** The expression levels of IκB, p-IκB, NF-κB, and p-NF-κB were normalized to β-actin levels within the same sample. $^{**}P < 0.01$, $^{***}P < 0.001$, $n = 6$.

Apoptotic cells were examined at 400× magnification over 20 fields of tubular areas.

Quantitative Reverse Transcription Polymerase Chain Reaction (RT-qPCR)

Total RNA was extracted from rat kidneys by TRIzol reagent (Invitrogen, Carlsbad, CA, USA) according to the manufacturer's instructions. Total RNA (3–5 μg) was transcribed into cDNA by Superscript II reverse transcriptase and random primer oligonucleotides. Our gene-specific primers, such as interleukin 6 (IL-6), tumor necrosis factor-α (TNF-α), NF-κB, and interferon gamma (IFN-γ), are presented in **Table 1**.

Western Blot Analysis

Renal tissue homogenates were prepared, and the supernatant was maintained at 4°C. Besides, 30 μg protein from each sample was separated by sodium dodecyl sulfate-polyacrylamide gel electrophoresis (SDS-PAGE), and then transferred onto polyvinylidene fluoride (PVDF) membranes. The primary antibodies, including anti-cleaved caspase-3 (Cell Signaling Technology, Inc., Danvers, MA, USA), anti-NF-κB (Cell Signaling Technology, Inc., Danvers, MA, USA), anti-p-NF-κB (Cell Signaling Technology, Inc., Danvers, MA, USA), anti-IκB (Cell Signaling Technology, Inc., Danvers, MA, USA), and anti-p-IκB (Cell Signaling Technology, Inc., Danvers, MA, USA) were added and incubated at 4°C overnight, followed by incubation with horseradish peroxidase (HRP)-conjugated secondary antibodies at room temperature. Immunoreactive bands were visualized using ECL Western Blotting Substrate (Thermo Fisher Scientific, Waltham, MA, USA). For the loading control, the same membranes were simultaneously probed with anti-GAPDH (Abcam, Cambridge, UK). The signals were quantified by scanning densitometry using a Bio-Image Analysis System. Relative protein expression was subsequently quantitated by normalizing to GAPDH levels using the Image-Pro plus 6.0 software.

Statistical Analysis

Data were expressed as mean ± standard deviation (SD), and statistical analysis was performed by Student's *t*-test or one-way analysis of variance (ANOVA) with *post-hoc* Student-Newman-Keuls test. $P < 0.05$ was considered statistically significant.

RESULTS

Exosomes Attenuated Renal Dysfunction, Histologic Damage, and Decreased Apoptosis

To evaluate the renoprotective effects of exosomes from MSCs, we analyzed two indicators of renal function, including BUN and SCr. Rats underwent renal IRI showed significant increase in the levels of SCr (482 ± 37 vs. 86 ± 24 μmol/L) and BUN (45.42 ± 2.73 vs. 7.13 ± 0.74 mmol/L) compared with the sham-operated group. Additionally, MSC treatment and MSC-ex treatment decreased the levels of SCr (148 ± 16 μmol/L; 231 ± 30 μmol/L) and BUN (20.49 ± 5.70 mmol/L; 31.36 ± 5.53 mmol/L), while this protective effect was not observed in the MSC-ex + RNAase group (**Figure 1C**).

Moreover, H&E and TUNEL staining methods were performed to assess the degree of renal injury and tissue apoptosis in each treatment group. The 0- to 4-point scoring system was used to evaluate tissue injury. The results demonstrated that rats that underwent renal IRI had tissue injury, increased inflammatory cell infiltration, and larger areas of tubular necrosis, vacuolization and cast formation. Rats treated with MSC and MSC-ex experienced significant attenuation of pathological damage in kidney, while no significant therapeutic effect was found on rats in MSC-ex + RNAase group (**Figures 1A,B**).

TUNEL staining demonstrated that cell apoptosis was increased after IRI. In addition, treatment with MSC and MSC-ex remarkably decreased cell apoptosis, while no significant decrease was observed in the MSC-ex + RNAase group (**Figures 1A,B**).

Exosomes Alleviated Inflammatory Responses by Reducing the Levels of TNF-α, NF-κB, IFN-γ, and IL-6

To detect the anti-inflammatory function of exosomes, we further assessed the mRNA level of inflammatory cytokines and transcription factors. Results showed that mRNA levels of TNF-α, NF-κB, IFN-γ, and IL-6 were significantly increased in IRI, while those levels were reduced after undergoing MSC and MSC-ex. The MSC-ex+RNAase had no significant effect. The result suggested that MSC-ex may have a protective role in IRI through suppressing inflammation (**Figure 2**).

Exosomes Inhibited NF-κB Signaling Pathway and Inflammatory Response

It has been reported that activation and translocation of NF-κB can be involved in pro-inflammatory responses. Therefore, we detected the levels of phosphorylated NF-κB and IκB in renal tissue of rats in each group. The results revealed that protein levels of p-NF-κB and p-IκB were increased after renal IR. On the contrary, the level of IκB, which is an inhibitor of NF-κB, was decreased after IR, and the expression of NF-κB did not remarkably change. Both MSC and MSC-ex inhibited IR-induced increase of p-NF-κB, p-IκB and decrease of IκB. The expression levels of NF-κB, IκB, p-IκB, and p-NF-κB in IR + MSC-ex + RNAase group were similar to those of IRI (**Figure 3**).

Exosomes Inhibited Activation of Caspase-3 and Cell Apoptosis Caused by IRI

As demonstrated earlier, cell apoptosis increased after IRI. Additionally, treatment with MSC and MSC-ex significantly decreased the number of apoptotic cells (**Figures 1A,B**). In the subsequent experiment, we examined the expression levels of apoptosis-related proteins, such as caspase-9, Bax, and cleaved caspase-3 to further verify the anti-apoptotic effects of MSC and exosomes from MSC. Results showed that both of them notably inhibited the expression levels of caspase-9

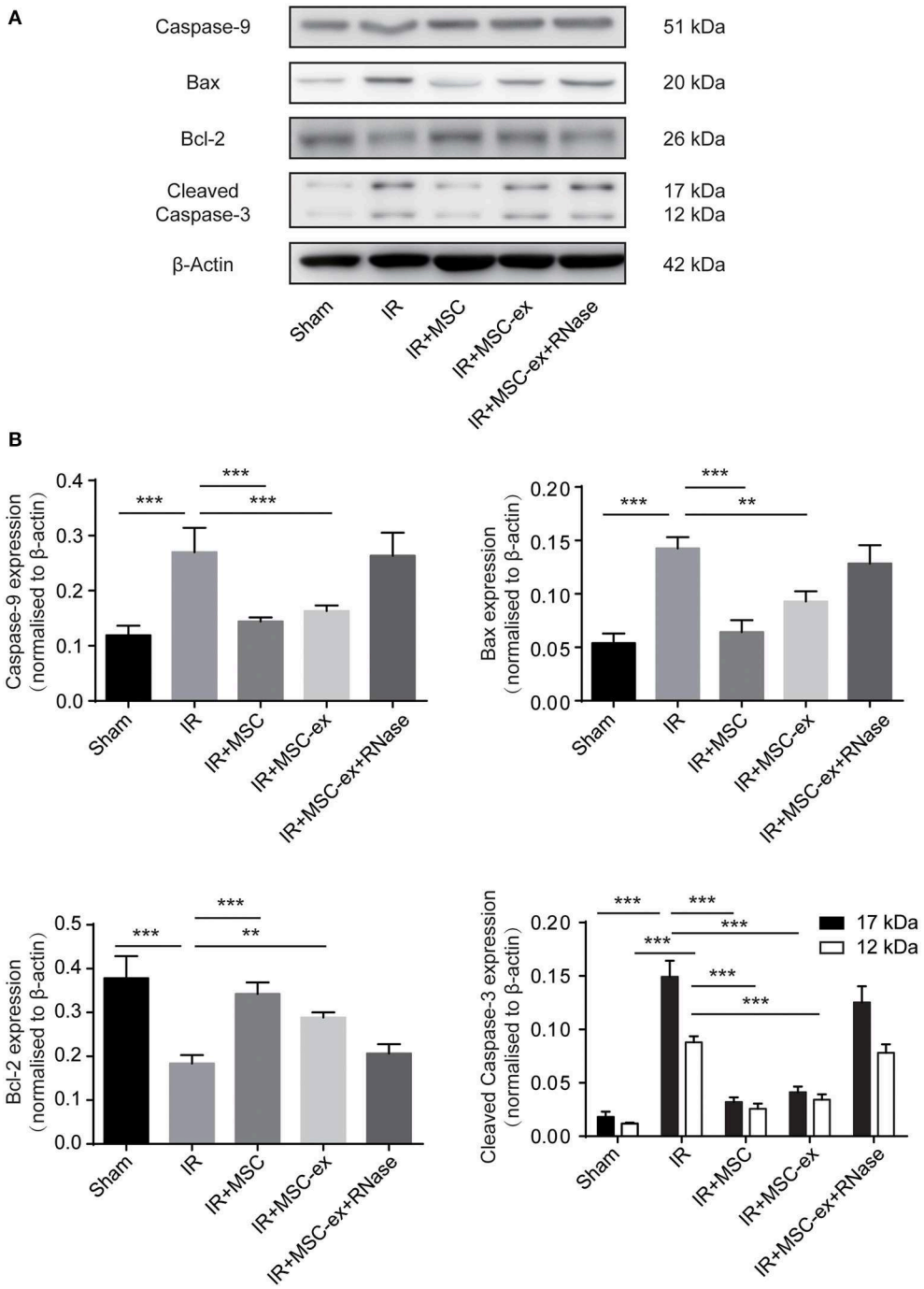

FIGURE 4 | MSC and exosomes from MSC reduced apoptosis by inhibiting expression levels of caspase-9, cleaved caspase-3, and Bax, and increasing expression level of Bcl-2. **(A)** Representative images show the protein levels of caspase-9, Bax, Bcl-2, and cleaved caspase-3. **(B)** The expression levels of caspase-9, Bax, Bcl-2, and cleaved caspase-3 were normalized to β-actin levels within the same sample. $^{**}P < 0.01$, $^{***}P < 0.001$, $n = 6$.

in kidneys after IRI, as well as cleaved caspase-3, compared with the IRI group. However, MSC and exosomes from MSC downregulated the expression levels of the pro-apoptotic proteins (caspase-9, cleaved caspase-3, and Bax), while upregulated the expression level of the anti-apoptotic protein, Bcl-2, indicating that both of them inhibited IR-induced apoptosis. Furthermore, the expression levels of caspase-9, Bax, and cleaved caspase-3 were slightly higher, whereas the expression level of Bcl-2 was lower in the MSC-ex group compared with the MSC group. The expression levels of these proteins were similar in the IR + MSC-ex + RNAase group and IRI group (**Figure 4**).

DISCUSSION

A previous study demonstrated that MSCs can repair IR-induced AKI (18, 19). MSCs have shown promising effects in experimental models of AKI and CKD, and have been used in clinical practice for more than one decade. The regenerative effects of MSCs do not rely on their ability to differentiate and replace damaged tissue, while those effects are primarily mediated by the release of paracrine factors (20). Therefore, we hypothesized that MSCs affect AKI rats via paracrine network.

In the immune system, exosomes have been demonstrated to play a pivotal role in mediating both adaptive and innate immune responses, thereby participating in antigen presentation associated with MHC-II and MHC-I molecules (9, 21). It has been suggested that aggregation of MSCs, which could differentiate into renal tubular epithelial cells, is directly involved in the repair and reconstruction of renal tubules mediated by chemotaxis, with homing ability in injured kidneys (22, 23). In the present studys, we detected protective effect of MSCs and MSC-ex on renal IRI, respectively. The results confirmed that MSCs and MSC-ex could alleviate tissue injuries and apoptosis after IRI. We found that treatment with MSC and MSC-ex significantly attenuated pathological damage to the kidney. To investigate the specific mechanism, we examined the expression levels of associated pro-inflammatory and transcription factors. The mRNA levels of TNF-α, NF-κB, IFN-γ, and IL-6 were noticeably after undergoing MSC and MSC-ex, suggesting that MSCs and exosomes could inhibit the inflammatory response in renal IRI (**Figure 2**). TNF-α has been deemed to play a substantial factor in the inflammatory cascade and systemic inflammatory response (24), resulting in aggravation of renal IRI.

NF-κB can be activated in kidney cells during IRI, and is highly involved in immune responses (17, 25–27). It is activated through phosphorylation of IκB, followed by proteasome-mediated degradation. Accordingly, we tested the expression levels of NF-κB, IκB, p-NF-κB, and p-IκB (15, 17, 25, 26). In the current research, it was unveiled that the expression levels of p-NF-κB and p-IκB were decreased after undergoing MSC and MSC-ex, while the expression level of IκB was increased. However, in the MSC-ex + RNAase group, the expression levels of NF -κB, IκB, p- NF-κb, and p- IκB were similar to those in the IR group. These results suggest that both MSC and MSC-ex can inhibit NF-κB activation after IRI, and RNA hydrolase can eliminate the effects of MSC-ex.

Apoptosis is a marker of severe tissue injury in IRI. We, in the present study, observed significant reduction of apoptotic cells in the IR + MSC-ex group compared with the IR group, providing further evidence for protective effects of MSC-ex on renal IRI. Cleaved caspase-3 plays a significant role in the downstream signaling pathway. During the renal IRI, Bax/Bcl-2 ratio could be upregulated to activate mitochondria-mediated apoptosis and release intracellular cytochrome C (28–30). In the present study, we found that MSCs and exosomes inhibited the expression levels of cleaved caspase-3, caspase-9 and Bax, and upregulated expression level of Bcl-2, confirming the effects of MSCs and exosomes on mitochondria-mediated apoptosis (**Figure 4**). However, we also observed that exosomes alone were not as effective as MSCs, suggesting that exosomes may be the main effector of MSCs on anti-inflammatory function. MSCs may be able to exert protective effect through other mechanisms, such as releasing cytokines.

Taken together, the results of this study demonstrate that exosomes originating from MSCs have protective effects on IRI via inhibition of apoptosis and inflammatory response, in which NF-κB signaling pathway may play a key role.

DATA AVAILABILITY STATEMENT

The datasets analyzed in this manuscript are not publicly available. Requests to access the datasets should be directed to ljlmjw@163.com.

ETHICS STATEMENT

All animal procedures were performed in accordance with the guidelines of the bioethics, and was approved by the Bioethics Committee of Zhongshan Hospital, Fudan University, Shanghai.

AUTHOR CONTRIBUTIONS

LL, RW, and YJ carried out the molecular biology studies and the immunoassays, analyzed the data, and drafted the manuscript. RR performed the cell experiments. TZ and MX designed and supervised the study, revised the manuscript, and gave final approval for publication.

ACKNOWLEDGMENTS

This study was financially supported by Shanghai Sailing Program (Grant No. 19YF1427600), the National Natural Science Foundation of China (Grant No. 81570674), and the Scientific and Technological Project of Henan Province (Grant No. 162102310134).

SUPPLEMENTARY MATERIAL

The Supplementary Material for this article can be found online at: https://www.frontiersin.org/articles/10.3389/fmed.2019.00269/full#supplementary-material

Supplementary Image 1 | The identification of isolated exosomes by TEM.

Supplementary Image 2 | The exosomal protein CD63 was verified by flow.

REFERENCES

1. Eltzschig HK, Eckle T. Ischemia and reperfusion–from mechanism to translation. *Nat Med.* (2011) 17:1391–401. doi: 10.1038/nm.2507
2. Kim SP, Thompson RH. Kidney function after partial nephrectomy: current thinking. *Curr Opin Urol.* (2013) 23:105–11. doi: 10.1097/MOU.0b013e32835d8ec1
3. Wood KJ, Goto R. Mechanisms of rejection: current perspectives. *Transplantation.* (2012) 93:1–10. doi: 10.1097/TP.0b013e31823cab44

4. van den Akker EK, Manintveld OC, Hesselink DA, de Bruin RW, Ijzermans JN, Dor FJ. Protection against renal ischemia-reperfusion injury by ischemic postconditioning. *Transplantation.* (2013) 95:1299–305. doi: 10.1097/TP.0b013e318281b934
5. Saat TC, van den Akker EK, IJzermans JN, Dor FJ, de Bruin RW. Improving the outcome of kidney transplantation by ameliorating renal ischemia reperfusion injury: lost in translation? *J Transl Med.* (2016) 14:20. doi: 10.1186/s12967-016-0767-2
6. Uccelli A, Moretta L, Pistoia V. Mesenchymal stem cells in health and disease. *Nat Rev Immunol.* (2008) 8:726–36. doi: 10.1038/nri2395
7. Furuichi K, Shintani H, Sakai Y, Ochiya T, Matsushima K, Kaneko S, et al. Effects of adipose-derived mesenchymal cells on ischemia-reperfusion injury in kidney. *Clin Exp Nephrol.* (2012) 16:679–89. doi: 10.1007/s10157-012-0614-6
8. Katsha AM, Ohkouchi S, Xin H, Kanehira M, Sun R, Nukiwa T, et al. Paracrine factors of multipotent stromal cells ameliorate lung injury in an elastase-induced emphysema model. *Mol Ther.* (2011) 19:196–203. doi: 10.1038/mt.2010.192
9. Lange C, Togel F, Ittrich H, Clayton F, Nolte-Ernsting C, Zander AR, et al. Administered mesenchymal stem cells enhance recovery from ischemia/reperfusion-induced acute renal failure in rats. *Kidney Int.* (2005) 68:1613–7. doi: 10.1111/j.1523-1755.2005.00573.x
10. Deregibus MC, Cantaluppi V, Calogero R, Lo Iacono M, Tetta C, Biancone L, et al. Endothelial progenitor cell derived microvesicles activate an angiogenic program in endothelial cells by a horizontal transfer of mRNA. *Blood.* (2007) 110:2440–8. doi: 10.1182/blood-2007-03-078709
11. Li T, Yan Y, Wang B, Qian H, Zhang X, Shen L, et al. Exosomes derived from human umbilical cord mesenchymal stem cells alleviate liver fibrosis. *Stem Cells Dev.* (2013) 22:845–54. doi: 10.1089/scd.2012.0395
12. Liao Z, Luo R, Li G, Song Y, Zhan S, Zhao K, et al. Exosomes from mesenchymal stem cells modulate endoplasmic reticulum stress to protect against nucleus pulposus cell death and ameliorate intervertebral disc degeneration *in vivo*. *Theranostics.* (2019) 9:4084–100. doi: 10.7150/thno.33638
13. He J, Wang Y, Sun S, Yu M, Wang C, Pei X, et al. Bone marrow stem cells-derived microvesicles protect against renal injury in the mouse remnant kidney model. *Nephrology.* (2012) 17:493–500. doi: 10.1111/j.1440-1797.2012.01589.x
14. Zhou Y, Xu H, Xu W, Wang B, Wu H, Tao Y, et al. Exosomes released by human umbilical cord mesenchymal stem cells protect against cisplatin-induced renal oxidative stress and apoptosis *in vivo* and *in vitro*. *Stem Cell Res Ther.* (2013) 4:34. doi: 10.1186/scrt194
15. Brines M, Cerami A. The receptor that tames the innate immune response. *Mol Med.* (2012) 18:486–96. doi: 10.2119/molmed.2011.00414
16. Lin M, Li L, Li L, Pokhrel G, Qi G, Rong R, et al. The protective effect of baicalin against renal ischemia-reperfusion injury through inhibition of inflammation and apoptosis. *BMC Complement Altern Med.* (2014) 14:19. doi: 10.1186/1472-6882-14-19
17. Mitchell S, Vargas J, Hoffmann A. Signaling via the NFkappaB system. *Wiley Interdiscip Rev Syst Biol Med.* (2016) 8:227–41. doi: 10.1002/wsbm.1331
18. Cao H, Qian H, Xu W, Zhu W, Zhang X, Chen Y, et al. Mesenchymal stem cells derived from human umbilical cord ameliorate ischemia/reperfusion-induced acute renal failure in rats. *Biotechnol Lett.* (2010) 32:725–32. doi: 10.1007/s10529-010-0207-y
19. Alzahrani FA. Melatonin improves therapeutic potential of mesenchymal stem cells-derived exosomes against renal ischemia-reperfusion injury in rats. *Am J Transl Res.* (2019) 11:2887–907.
20. Chen YT, Sun CK, Lin YC, Chang LT, Chen YL, Tsai TH, et al. Adipose-derived mesenchymal stem cell protects kidneys against ischemia-reperfusion injury through suppressing oxidative stress and inflammatory reaction. *J Transl Med.* (2011) 9:51. doi: 10.1186/1479-5876-9-51
21. van Kooten C, Rabelink TJ, de Fijter JW, Reinders MEJ. Mesenchymal stromal cells in clinical kidney transplantation. *Curr Opin Organ Transplant.* (2016) 21:550–8. doi: 10.1097/MOT.0000000000000364
22. Kale S, Karihaloo A, Clark PR, Kashgarian M, Krause DS, Cantley LG. Bone marrow stem cells contribute to repair of the ischemically injured renal tubule. *J Clin Invest.* (2003) 112:42–9. doi: 10.1172/JCI17856
23. Li N, Li XR, Yuan JQ. Effects of bone-marrow mesenchymal stem cells transplanted into vitreous cavity of rat injured by ischemia/reperfusion. *Graefes Arch Clin Exp Ophthalmol.* (2009) 247:503–14. doi: 10.1007/s00417-008-1009-y
24. Furuichi K, Kokubo S, Hara A, Imamura R, Wang Q, Kitajima S, et al. Fas ligand has a greater impact than TNF-alpha on apoptosis and inflammation in ischemic acute kidney injury. *Nephron Extra.* (2012) 2:27–38. doi: 10.1159/000335533
25. Sanz AB, Sanchez-Nino MD, Ramos AM, Moreno JA, Santamaria B, Ruiz-Ortega M, et al. NF-kappaB in renal inflammation. *J Am Soc Nephrol.* (2010) 21:1254–62. doi: 10.1681/ASN.2010020218
26. Diamant G, Dikstein R. Transcriptional control by NF-κB: elongation in focus. *Biochim Biophys Acta.* (2013) 1829:937–45. doi: 10.1016/j.bbagrm.2013.04.007
27. Prakoura N, Kavvadas P, Kormann R, Dussaule JC, Chadjichristos CE, Chatziantoniou C. NFkappaB-induced periostin activates integrin-beta3 signaling to promote renal injury in GN. *J Am Soc Nephrol.* (2016) 28:1475–90. doi: 10.1681/ASN.2016070709
28. Yang B, Jain S, Ashra SY, Furness PN, Nicholson ML. Apoptosis and caspase-3 in long-term renal ischemia/reperfusion injury in rats and divergent effects of immunosuppressants. *Transplantation.* (2006) 81:1442–50. doi: 10.1097/01.tp.0000209412.77312.69
29. Brooks C, Wei Q, Cho SG, Dong Z. Regulation of mitochondrial dynamics in acute kidney injury in cell culture and rodent models. *J Clin Invest.* (2009) 119:1275–85. doi: 10.1172/JCI37829
30. Wei Q, Dong G, Chen JK, Ramesh G, Dong Z. Bax and Bak have critical roles in ischemic acute kidney injury in global and proximal tubule-specific knockout mouse models. *Kidney Int.* (2013) 84:138–48. doi: 10.1038/ki.2013.68

Conflict of Interest: The authors declare that the research was conducted in the absence of any commercial or financial relationships that could be construed as a potential conflict of interest.

frontiers in Medicine

CASE REPORT
published: 11 December 2019
doi: 10.3389/fmed.2019.00276

The First Case of Ischemia-Free Kidney Transplantation in Humans

Xiaoshun He[1,2,3†], Guodong Chen[1,2,3†], Zebin Zhu[1,2,3†], Zhiheng Zhang[1,2,3], Xiaopeng Yuan[1,2,3], Ming Han[1,2,3], Qiang Zhao[1,2,3], Yitao Zheng[1,2,3], Yunhua Tang[1,2,3], Shanzhou Huang[1,2,3], Linhe Wang[1,2,3], Otto B. van Leeuwen[4], Xiaoping Wang[1,2,3], Chuanbao Chen[1,2,3], Liqiu Mo[5], Xingyuan Jiao[1,2,3], Xianchang Li[1,2,3,6], Changxi Wang[1,2,3], Jiefu Huang[1,7], Jun Cui[8] and Zhiyong Guo[1,2,3*]*

[1] Organ Transplant Center, The First Affiliated Hospital, Sun Yat-sen University, Guangzhou, China, [2] Guangdong Provincial Key Laboratory of Organ Donation and Transplant Immunology, Guangzhou, China, [3] Guangdong Provincial International Cooperation Base of Science and Technology (Organ Transplantation), Guangzhou, China, [4] Department of Surgery, University Medical Center Groningen, University of Groningen, Groningen, Netherlands, [5] Department of Anesthesiology, The First Affiliated Hospital, Sun Yat-sen University, Guangzhou, China, [6] Immunobiology and Transplant Science Center, Houston Methodist Research Institute, Houston, TX, United States, [7] Peking Union Medical College Hospital, Beijing, China, [8] MOE Key Laboratory of Gene Function and Regulation, State Key Laboratory of Biocontrol, School of Life Sciences, Sun Yat-sen University, Guangzhou, China

OPEN ACCESS

Edited by:
Songjie Cai,
Brigham and Women's Hospital,
United States

Reviewed by:
Biruh Workeneh,
University of Texas, United States
Ajay Kumar Baranwal,
Armed Forces Medical College,
Pune, India

***Correspondence:**
Xiaoshun He
gdtrc@163.com
Zhiyong Guo
rockyucsf1981@126.com

†These authors have contributed equally to this work and share first authorship

Specialty section:
This article was submitted to Nephrology, a section of the journal Frontiers in Medicine

Received: 04 August 2019
Accepted: 12 November 2019
Published: 11 December 2019

Citation:
He X, Chen G, Zhu Z, Zhang Z, Yuan X, Han M, Zhao Q, Zheng Y, Tang Y, Huang S, Wang L, van Leeuwen OB, Wang X, Chen C, Mo L, Jiao X, Li X, Wang C, Huang J, Cui J and Guo Z (2019) The First Case of Ischemia-Free Kidney Transplantation in Humans. Front. Med. 6:276. doi: 10.3389/fmed.2019.00276

Background: Ischemia-reperfusion injury (IRI) has been considered an inevitable event in organ transplantation since the first successful kidney transplant was performed in 1954. To avoid IRI, we have established a novel procedure called ischemia-free organ transplantation. Here, we describe the first case of ischemia-free kidney transplantation (IFKT).

Materials and Methods: The kidney graft was donated by a 19-year-old brain-dead donor. The recipient was a 47-year-old man with end-stage diabetic nephropathy. The graft was procured, preserved, and implanted without cessation of blood supply using normothermic machine perfusion.

Results: The graft appearance, perfusion flow, and urine production suggested that the kidney was functioning well-during the whole procedure. The creatinine dropped rapidly to normal range within 3 days post-transplantation. The levels of serum renal injury markers were low post-transplantation. No rejection or vascular or infectious complications occurred. The patient had an uneventful recovery.

Conclusion: This paper marks the first case of IFKT in humans. This innovation may offer a unique solution to optimizing transplant outcomes in kidney transplantation.

Keywords: kidney transplantation, ischemia-reperfusion injury, normothermic machine perfusion, ischemia-free kidney transplantation, ischemia-free organ transplantation

INTRODUCTION

Since the first successful case of kidney transplantation was performed in 1954 (1), all transplant procedures have caused cessation of blood supply to donor organs during procurement, preservation, and implantation. The subsequent restoration of blood supply after ischemia exacerbates the initial cellular damage; this is known as ischemia-reperfusion injury (IRI) (2). Not only can IRI lead to primary non-function (PNF) or delayed graft function (DGF) in the early stage, but it can also cause chronic fibrosis and allograft rejection in the long run (3).

For decades, great efforts have been made to treat IRI (4). However, limited success has been achieved because none of the research methods is able to prevent the donor organs from experiencing initial ischemic injury. It has been shown that hypothermic machine perfusion (HMP) is superior to static cold storage (SCS) in preserving donor kidneys (5). Recently, the Leicester group has translated the use of normothermic machine perfusion (NMP) from animal studies to clinical use and performed the first kidney transplantation in a male patient after 60 min of *ex vivo* NMP in 2011 (6). Since then, the same group has used NMP for assessment and resuscitation of marginal donor kidneys (7, 8). However, since they used NMP following many hours of SCS, ischemic injury of grafts and subsequent IRI was still inevitable.

We have established a novel procedure called ischemia-free liver transplantation (IFLT) during which the donor livers can be procured, preserved, and implanted without cessation of oxygenated blood supply to the grafts (9). During IFLT, IRI can be largely avoided. In this study, we report the first case of ischemia-free kidney transplantation (IFKT).

CASE PRESENTATION

The kidney donor was a 19-year-old male patient who died of a craniocerebral trauma. The terminal serum creatinine was 54 μmol/L. The donor and recipient were co-located in the First Affiliated Hospital of Sun Yat-sen University. The left kidney was procured after ligating the left renal artery and vein and immediately cold flushed through the left kidney artery. This graft was preserved in ice-cold University of Wisconsin solution. The right kidney was subjected to IFKT. The study protocol was approved by the Ethical Committee of our hospital. Written informed consent for the publication of the case report was obtained from the patient undergoing this ischemia-free kidney transplantation.

IFKT PROCEDURE

Figure 1A shows the technical details of the procedure. Firstly, the abdominal aorta (AA) and right renal artery, inferior vena cava (IVC), and right renal vein were well-dissected. The ureter was cut off, and a tube was placed in the ureter for urine drainage. A 34Fr caval cannula was placed in the infrarenal IVC for blood outflow to the organ reservoir of the Liver Assist device (Organ Assist, Groningen, the Netherlands, **Figure 1B**). A straight 20Fr cannula was inserted into the infrarenal AA of the donor. Subsequently, the arterial cannula was connected to the artery perfusion line of Liver Assist, and the suprarenal AA was blocked. The venous drainage of suprarenal IVC was also blocked. After the circuit of *in vivo* NMP was established, the right kidney was harvested and moved to the organ reservoir for *ex vivo* NMP (**Figure 1C**). Simultaneously, the donor liver was procured after cold flush via a cannula in the superior mesenteric vein. We sutured part of the suprarenal IVC with 6-0 Prolene and reduced its diameter to 1.5 cm on the organ reservoir of NMP *ex vivo*.

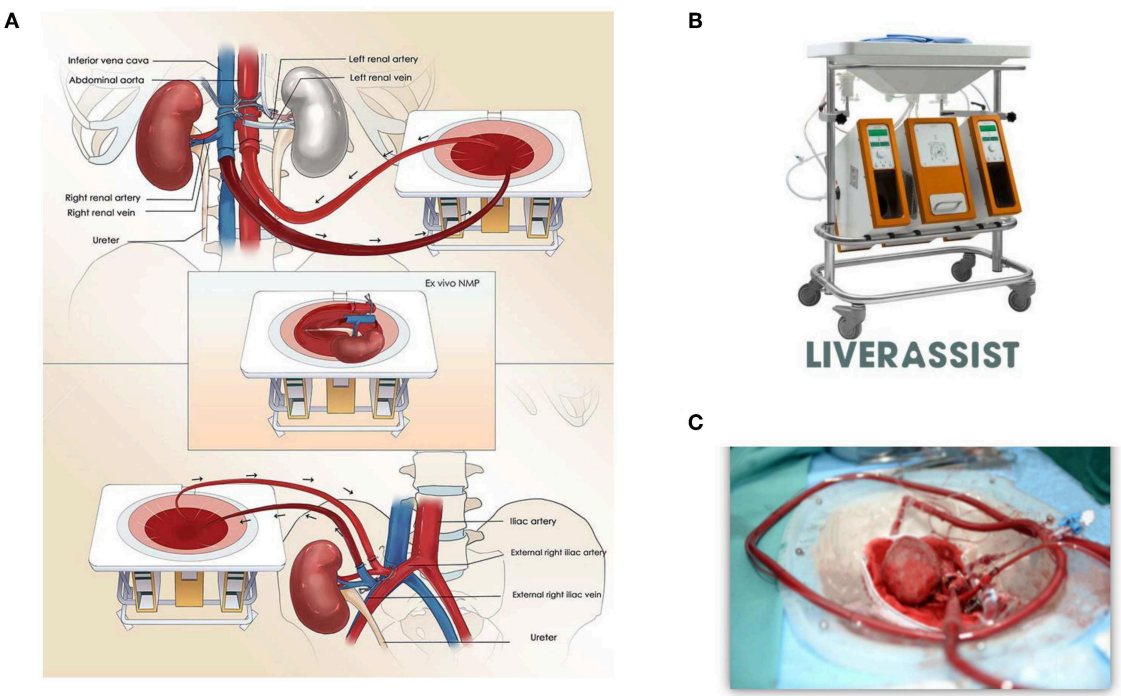

FIGURE 1 | (A) Ischemia-free kidney transplant procedure. The diagram shows procurement, preservation, and implantation of the donor kidney without cessation of blood supply using normothermic machine perfusion. **(B)** Normothermic machine perfusion device, Liver Assist (Organ Assist, Groningen, the Netherlands). **(C)** Donor kidney circuit on the organ reservoir of the NMP device.

TABLE 1 | Components of the perfusate solution.

Components	
Crossed-matched leucocyte-depleted washed red cells	1,000 mL
Sodium, potassium, magnesium, calcium, and glucose injection	600 mL
Succinylated gelatinor	400 mL
5% sodium bicarbonate	50 mL
Heparin	25,000 units
Metronidazole	0.5 g
Miropeen for injection	1 g
10% calcium gluconate	8 mL
Compound amino acid injection	40 mL
Dexamethason	15 mg
Insulin	100 units
20% mannitol	20 mL

The kidney graft underwent continuous NMP for 110 min. The perfusate components are shown in **Table 1**. The perfusate was warmed up to 37°C, and the oxygenator was supplied with air. The viability of the graft was assessed based on the appearance of graft and perfusion flow, as well as urine production. No creatinine was added to the perfusate for the graft function test. The perfusion pressure (52–70 mmHg) and flow (130–184 mL/min) were stable during the whole procedure (**Figure 2A**). The creatinine and urea levels in the perfusate were stable and low (**Figure 2B**). The kidney graft continued to produce urine during the whole procedure (**Figure 2C**). The pH values and specific gravity of the urine produced before procurement were comparable to those produced during NMP and after reperfusion (**Figure 2D**).

The donor kidney was then moved from the reservoir and placed in the right iliac fossa of the recipient so that an *in vivo* NMP circuit was re-established. The donor suprarenal AA and suprarenal IVC were anastomosed to the recipient right external iliac artery and vein in an end-to-side fashion using 6-0 Prolene. During the vascular anastomoses, caution was taken to prevent twisted perfusion lines. After that, the clamp on the donor suprarenal AA was released so that recipient blood supply for the donor kidney was established. In the meantime, NMP was stopped. Around 50 mL perfusate was flushed out of the kidney, followed by release of the clamp on the donor suprarenal IVC. The cannulas in the IVC and AA were removed, and the infrarenal IVC and AA were sutured closed. Finally, after withdrawal of the draining tube, the donor ureter was anastomosed to the bladder of the recipient. The recipient operation time was 135 min.

OUTCOMES

The recipient was a 47-year-old man with diabetic nephropathy who had been on hemodialysis for more than 2 years. The recipient had immediate graft function, and the serum creatinine levels fell from 1100 μmol/L pre-transplantation to 95 μmol/L on post-operative day (POD) 3 (**Figure 3A**). The mean urine output over the first 5 days post-transplantation was 4,987 mL/day compared with a pre-transplant daily output of <100 mL.

The post-transplant estimated glomerular filtration rate (eGFR) increased from 3.99 mL/min/1.73m^2 pre-transplantation to 103.28 mL/min/1.73m^2 on POD 7 (**Figure 3B**). The post-transplant level of cystatin C (Cys C) was quite low (1.76 mg/L on POD 1 and 1.26 mg/L on POD 7) (**Figure 3C**). The levels of other serum kidney injury biomarkers (10–13), including neutrophil gelatinase-associated lipocalin (NGAL), liver fatty acid-binding protein (L-FABP), kidney injury molecule-1 (KIM-1), and glutathione s-transferase alpha 1 (GSTA1), all sharply decreased after IFKT (**Figures 3D–G**). No acute rejection, renal artery or renal vein thrombosis, or infectious complications occurred. The patient was discharged with a serum creatinine of 80 μmol/L on POD 15.

DISCUSSION

Kidney transplantation is inevitably associated with IRI, which can cause acute cellular injury and renal dysfunction (14–18). Several methods to ameliorate IRI have been proposed, including ischemic pre-conditioning, pharmacological interventions, protective gases, and gene and stem cell therapies (4). However, few of these methods have been translated into clinical practice. In contrast to the intention to "treat" IRI in earlier studies (4), our group focused on "preventing" IRI. We have shown that the concept of ischemia-free organ transplantation (IFOT) is feasible, safe, and effective in liver transplantation (9). Histological analysis, inflammatory cytokine production, and pathway analysis suggested that IRI is largely avoidable.

In this case report, we showed for the first time that IFOT can be expanded to kidney transplantation. The kidney was continuously functioning, with urine production during procurement, preservation, and implantation during IFKT. The serum creatinine dropped rapidly to normal range within 3 days, and eGFR increased rapidly post-transplantation. A recent study indicated that CysC can maintain its predictive power for adverse outcomes in patients with no meaningful GFR (19). The serum CysC level and the other renal injury markers were quite low post-transplantation. Since the kidney experienced ongoing NMP, for the safety of the recipient, no biopsy was obtained to confirm the absence of IRI. The recipient had an uneventful recovery without infectious or surgical complications.

Successful IFKT is established based on efficient NMP. To our knowledge, all studies concerning kidney NMP in humans are from the Leicester group (6, 7, 20, 21). They have reported that NMP can resuscitate human kidneys deemed untransplantable and can help assess kidney quality (20, 21). Moreover, the use of NMP is associated with significant decrease in DGF (6). However, the 1-h NMP is preceded by a period of cold storage after procurement and followed by a cold flush before implantation. Therefore, ischemic injury and subsequent graft IRI are still unavoidable. In contrast, IFKT maintains continuous oxygenated blood supply to the kidney, and thus IRI is probably avoided, and this may further reduce the DGF rate and improve long-term outcome after kidney transplantation, although the donor and

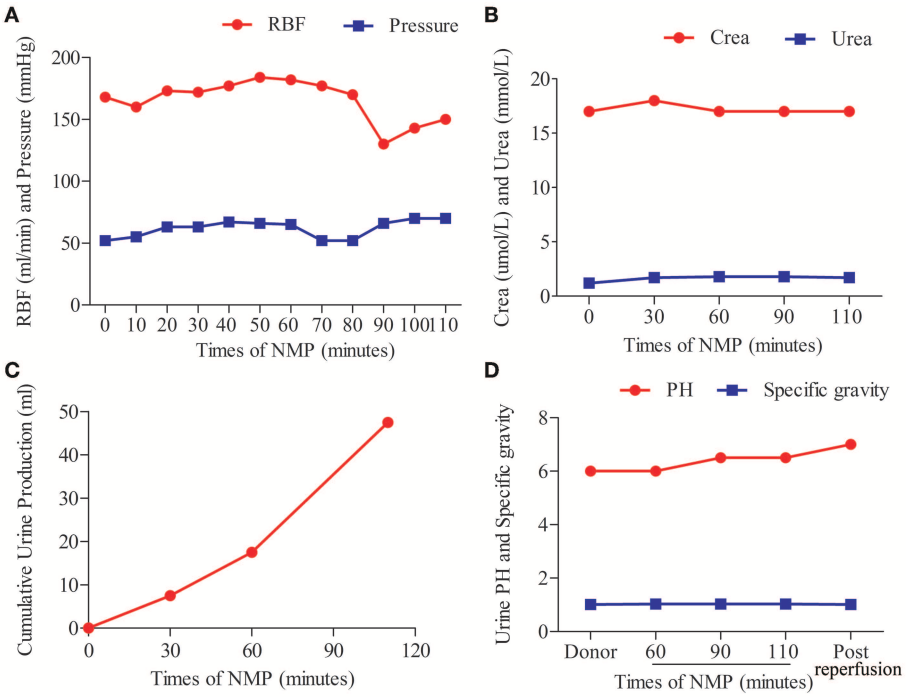

FIGURE 2 | Normothermic machine perfusion and allograft viability. **(A)** Arterial flow rates and pressure. **(B)** Creatinine (Crea) and urea concentration in the perfusate. **(C)** Volume of urine production during machine perfusion. **(D)** pH values and specific gravity levels of the urine produced before procurement, during machine perfusion, and post-reperfusion.

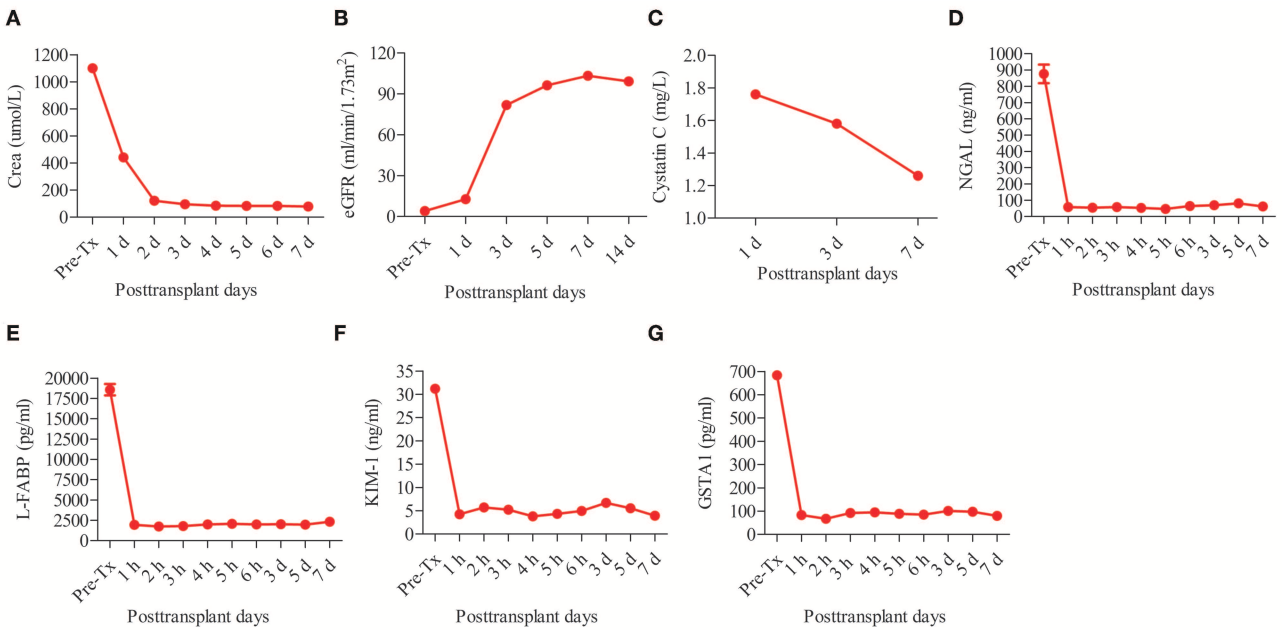

FIGURE 3 | Post-transplant renal function and serum biomarker levels of kidney injury of the recipient. The renal function tests including **(A)** creatinine (Crea) and **(B)** estimated glomerular filtration rate (eGFR). The serum biomarker levels of kidney injury including **(C)** cystatin C, **(D)** neutrophil gelatinase-associated lipocalin (NGAL), **(E)** liver fatty acid-binding protein (L-FABP), **(F)** kidney injury molecule-1 (KIM-1), and **(G)** glutathione s-transferase alpha 1 (GSTA1).

recipient need to be at the same hospital because of the limited NMP time. This method may be more useful in expanded criteria donor (ECD) kidneys, since ECD kidneys are more susceptible to IRI. It would be highly interesting to compare the transplant outcomes of IFKT, kidney transplantation using NMP as a preservation method, and conventional kidney transplantation in the future.

Undoubtedly, there are several limitations to this study. Firstly, the donor and recipient are usually not co-located. Therefore, a portable kidney NMP device is required for this procedure. However, to our knowledge, this kind of device is not commercially available. Secondly, it is difficult to conduct IFKT of both donor kidneys for two recipients. In addition, although serum kidney injury marker levels have been tested to assess IRI severity, a biopsy of the graft should be done to confirm the absence of IRI. Finally, the kidney in this case was from a young standard brain-death donor. No significant difference in transplant outcomes and renal graft function was documented between the two recipients of the left and right renal grafts. The potential benefits should be tested in a prospective, randomized controlled study in a predefined subgroup of ECD kidneys.

In summary, we report here that IFKT is technically feasible. This innovation might be able to optimize transplant outcomes and maximize graft utilization.

DATA AVAILABILITY STATEMENT

The raw data supporting the conclusions of this manuscript will be made available by the authors, without undue reservation, to any qualified researcher.

ETHICS STATEMENT

The studies involving human participants were reviewed and approved by The Ethical Committee of First Affliated Hospital of Sun Yat-sen University. The patients/participants provided their written informed consent to participate in this study.

AUTHOR CONTRIBUTIONS

XH and ZG conceived of the IFKT, they designed the procedure, performed the operation, enrolled the patient into the study, and wrote the report. GC and ZZhu designed the procedure and study protocol, followed up with the patient, analyzed the data, and critically revised the report. ZZha, XY, MH, and QZ assisted with the design of the procedure, preclinical preparation, the operation, analyzed the data, and revised the report. YZ, YT, SH, LW, OL, XW, and CC assisted with the design of the procedure, preclinical preparation, and the operation. LM, XJ, and CW assisted with the design of the procedure, the operation, preclinical preparation, and collected clinical data. XL and JH assisted with the design of the procedure, study protocol, and critically revised the manuscript. JC assisted analysis of the data and revision of the article.

FUNDING

This study was supported by the National Natural Science Foundation of China (81373156, 81471583, 81570587, and 81871257), the Special Fund for Science Research by Ministry of Health (201302009), the Key Clinical Specialty Construction Project of National Health and Family Planning Commission of the People's Republic of China, the Guangdong Provincial Key Laboratory Construction Projection on Organ Donation and Transplant Immunology (2013A061401007), Guangdong Provincial International Cooperation Base of Science and Technology (Organ Transplantation) (2015B050501002), Guangdong Provincial Natural Science Funds for Major Basic Science Culture Project (2015A030308010 and 2018A030313612), Guangdong Provincial Natural Science Funds for Distinguished Young Scholars (2015A030306025), the Special Support Program for Training High-Level Talents in Guangdong Province (2015TQ01R168), the Pearl River Nova Program of Guangzhou (201506010014), and the Science and Technology Program of Guangzhou (201704020150).

ACKNOWLEDGMENTS

We thank all members of the organ procurement organization, surgical intensive care unit, transplant anesthesia team, and cardiopulmonary bypass team, as well as all the donors and patients.

REFERENCES

1. Merrill JP, Murray JE, Harrison JH, Guild WR. Successful homotransplantation of the human kidney between identical twins. *J Am Med Assoc*. (1956) 160:277–82. doi: 10.1001/jama.1956.02960390027008
2. Snoeijs MG, van Heurn LW, Buurman WA. Biological modulation of renal ischemia-reperfusion injury. *Curr Opin Organ Transplant*. (2010) 15:190–9. doi: 10.1097/MOT.0b013e32833593eb
3. Menke J, Sollinger D, Schamberger B, Heemann U, Lutz J. The effect of ischemia/reperfusion on the kidney graft. *Curr Opin Organ Transplant*. (2014) 19:395–400. doi: 10.1097/MOT.0000000000000090
4. Eltzschig HK, Eckle T. Ischemia and reperfusion–from mechanism to translation. *Nat Med*. (2011) 17:1391–401 doi: 10.1038/nm.2507
5. Moers C, Smits JM, Maathuis MH, Treckmann J, van Gelder F, Napieralski BP, et al. Machine perfusion or cold storage in deceased-donor kidney transplantation. *N Engl J Med*. (2009) 360:7–19. doi: 10.1056/NEJMoa0802289
6. Nicholson ML, Hosgood SA. Renal transplantation after *ex vivo* normothermic perfusion: the first clinical study. *Am J Transplant*. (2013) 13:1246–52. doi: 10.1111/ajt.12179
7. Hosgood SA, Barlow AD, Hunter JP, Nicholson ML. *Ex vivo* normothermic perfusion for quality assessment of marginal donor kidney transplants. *Br J Surg*. (2015) 102:1433–40. doi: 10.1002/bjs.9894
8. Hosgood SA, Barlow AD, Dormer J, Nicholson ML. The use of *ex-vivo* normothermic perfusion for the resuscitation and assessment of human kidneys discarded because of inadequate *in situ* perfusion. *J Transl Med*. (2015) 13:329. doi: 10.1186/s12967-015-0691-x

9. He X, Guo Z, Zhao Q, Ju W, Wang D, Wu L, et al. The first case of ischemia-free organ transplantation in humans: a proof of concept. *Am J Transplant*. (2018) 18:737–44 doi: 10.1111/ajt.14583
10. Obeidat MA, Luyckx VA, Grebe SO, Jhangri GS, Maguire C, Zavodni A, et al. Post-transplant nuclear renal scans correlate with renal injury biomarkers and early allograft outcomes. *Nephrol Dial Transplant*. (2011) 26:3038–45. doi: 10.1093/ndt/gfq814
11. Sabbisetti VS, Waikar SS, Antoine DJ, Smiles A, Wang C, Ravisankar A, et al. Blood kidney injury molecule-1 is a biomarker of acute and chronic kidney injury and predicts progression to ESRD in type I diabetes. *J Am Soc Nephrol*. (2014) 25:2177–86. doi: 10.1681/ASN.2013070758
12. Kawai A, Kusaka M, Kitagawa F, Ishii J, Fukami N, Maruyama T, et al. Serum liver-type fatty acid-binding protein predicts recovery of graft function after kidney transplantation from donors after cardiac death. *Clin Transplant*. (2014) 28:749–54. doi: 10.1111/ctr.12375
13. Mir MC, Pavan N, Parekh DJ. Current paradigm for ischemia in kidney surgery. *J Urol*. (2016) 195:1655–63. doi: 10.1016/j.juro.2015.09.099
14. Thadhani R, Pascual M, Bonventre JV. Acute renal failure. *N Engl J Med*. (1996) 334:1448–60. doi: 10.1056/NEJM199605303342207
15. Perico N, Cattaneo D, Sayegh MH, Remuzzi G. Delayed graft function in kidney transplantation. *Lancet*. (2004) 364:1814–27. doi: 10.1016/S0140-6736(04)17406-0
16. Yarlagadda SG, Coca SG, Formica RJ, Poggio ED, Parikh CR. Association between delayed graft function and allograft and patient survival: a systematic review and meta-analysis. *Nephrol Dial Transplant*. (2009) 24:1039–47. doi: 10.1093/ndt/gfn667
17. Chen GD, Shiu-Chung KD, Wang CX, Qiu J, Han M, He XS, et al. Kidney transplantation from donors after cardiac death: an initial report of 71 cases from China. *Am J Transplant*. (2013) 13:1323–1326. doi: 10.1111/ajt.12190
18. Kosmoliaptsis V, Salji M, Bardsley V, Chen Y, Thiru S, Griffiths MH, et al. Baseline donor chronic renal injury confers the same transplant survival disadvantage for DCD and DBD kidneys. *Am J Transplant*. (2015) 15:754–63. doi: 10.1111/ajt.13009
19. Ho LC, Sung JM, Tsai YS, Wang HH, Li YC, Chen YT, et al. Cystatin C as a predictor for outcomes in patients with negligible renal function. *Blood Purif*. (2014) 38:81–8. doi: 10.1159/000365837
20. Hosgood SA, Saeb-Parsy K, Hamed MO, Nicholson ML. Successful transplantation of human kidneys deemed untransplantable but resuscitated by *ex vivo* normothermic machine perfusion. *Am J Transplant*. (2016) 16:3282–5. doi: 10.1111/ajt.13906
21. Hosgood SA, Nicholson ML. An assessment of urinary biomarkers in a series of declined human kidneys measured during *ex vivo* normothermic kidney perfusion. *Transplantation*. (2017) 101:2120–5. doi: 10.1097/TP.0000000000001504

Conflict of Interest: The authors declare that the research was conducted in the absence of any commercial or financial relationships that could be construed as a potential conflict of interest.

frontiers in Medicine

ORIGINAL RESEARCH
published: 24 January 2020
doi: 10.3389/fmed.2020.00005

Erythropoietin Derived Peptide Improved Endoplasmic Reticulum Stress and Ischemia-Reperfusion Related Cellular and Renal Injury

Yufang Zhang[1†], Qian Wang[2†], Aifen Liu[1], Yuanyuan Wu[3], Feng Liu[2], Hui Wang[2], Tongyu Zhu[4,5], Yaping Fan[2] and Bin Yang[2,3]*

[1] Renal Group, Basic Medical Research Centre, Medical College of Nantong University, Nantong, China, [2] Department of Nephrology, Nantong-Leicester Joint Institute of Kidney Science, Affiliated Hospital of Nantong University, Nantong, China, [3] Department of Cardiovascular Sciences, University of Leicester, University Hospitals of Leicester, Leicester, United Kingdom, [4] Department of Urology, Zhongshan Hospital, Fudan University, Shanghai, China, [5] Shanghai Key Laboratory of Organ Transplantation, Shanghai, China

OPEN ACCESS

Edited by:
Songjie Cai,
Brigham and Women's Hospital,
United States

Reviewed by:
Matsuda Yoshiko,
University of California, San Francisco,
United States
Ryoichi Imamura,
Osaka University, Japan

***Correspondence:**
Bin Yang
by5@le.ac.uk;
dryangbin@hotmail.com

[†]These authors have contributed equally to this work

Specialty section:
This article was submitted to Nephrology, a section of the journal Frontiers in Medicine

Received: 01 November 2019
Accepted: 08 January 2020
Published: 24 January 2020

Citation:
Zhang Y, Wang Q, Liu A, Wu Y, Liu F, Wang H, Zhu T, Fan Y and Yang B (2020) Erythropoietin Derived Peptide Improved Endoplasmic Reticulum Stress and Ischemia-Reperfusion Related Cellular and Renal Injury. Front. Med. 7:5. doi: 10.3389/fmed.2020.00005

Ischemia-reperfusion (IR) injury often affects transplant and native kidneys alike. IR injury is one of the main causes of acute kidney injury (AKI) and further associated with the progression of chronic kidney disease. Our previous study revealed the renoprotection of erythropoietin derived cyclic helix-B surface peptide (CHBP) against IR injury. However, the precise role and underlying mechanism of endoplasmic reticulum stress (ERS) in the injury and the renoprotection induced by IR or CHBP, respectively, have not been fully defined. This study using mouse kidney epithelial cells (TCMK-1) revealed that the level of CHOP (a key marker of ERS), PERK, and JNK (regulators of CHOP) was gradually increased by the prolonged time of hydrogen peroxide (H_2O_2) stimulation. In addition, CHOP mRNA and protein were significantly reduced by small interfering RNA (siRNA) target CHOP, as were apoptotic and inflammatory mediator caspase-3 and HMGB-1, and early apoptosis. Furthermore, *CHOP* mRNA was correlated positively with PERK protein, active caspase-3, HMGB-1 and apoptosis, but negatively with cell viability *in vitro,* while CHOP protein was also correlated positively with the level of tubulointerstitial damage and active caspase-3 protein *in vivo*. Finally, CHBP improved the viability of TCMK-1 cells subjected to H_2O_2 stimulation time-dependently, with reduced level of *CHOP* mRNA. CHBP also inhibited the increase of CHOP protein, not only in TCMK-1 cells, but also in the IR injury kidneys at 2 weeks. Moreover, CHBP reduced the expression of *PERK* mRNA and protein, JNK and HMGB-1 protein, as well as early and later apoptosis. In addition, raised CHOP at 12 h post IR injury might be an early time window for intervention. In conclusion, the differential role of ERS and CHBP in IR-related injury was proved in mouse TCMK-1 cells and kidneys, in which the mechanistic signaling pathway was associated with CHOP/PERK/JNK, HMGB-1/caspase-3, and apoptosis. CHOP might be a potential biomarker and CHBP might be therapeutic drug for IR-induced AKI.

Keywords: apoptosis, CHOP, cyclic helix-B surface peptide (CHBP), endoplasmic reticulum stress (ERS), inflammation, ischemia-reperfusion injury

INTRODUCTION

Renal ischemia-reperfusion (IR) injury is inevitable in kidney transplantation, which greatly affects the survival of allograft (1–3). IR injury also often occurs in native kidneys subjected to a variety of causes such as cardiovascular surgery, dehydration, and sepsis. IR injury is a major inducement of acute kidney injury (AKI) and further associated with its progression to chronic kidney disease (CKD). It is imperative to disclose the mechanism of IR injury in order to achieve time diagnosis and specific treatment for IR-induced AKI and prevent CKD. Renal tubular epithelial cells (TECs) are most vulnerable to renal IR insult, underwent to autophagy, apoptosis or necrosis, which contributes to the loss of renal function, and subsequent repair/recovery or fibrosis (4–6). The underlying mechanisms of IR injury and repair are complicated including endoplasmic reticulum stress (ERS), mitochondria dysfunction, cell death, and inflammation (7–10). Improving ERS and TEC apoptosis have been considered to be effective methods to alleviate renal IR injury (3, 11).

Newly synthesized proteins fold in the lumen of ER prior to exit into various compartments of the cell and extracellular space. In response to adverse conditions, these proteins could folded incorrectly and unable to exit, but accumulate inside ER resulting in ERS (9, 12). A series of adaptions were subsequently activated, called the unfolded protein response (UPR) (9, 13, 14). The UPR is attributed to the activation of one ER transmembrane protein, named protein kinase RNA-like ER kinase (PERK) (15–17). Growing evidence has shown that ERS associated with apoptosis and inflammation plays important roles in IR injury (18, 19). UPR could gradually develop into apoptosis and further induces inflammation, if ERS is too severe to overcome. CCAAT/enhancer-binding protein homologous protein (CHOP) is an ERS-induced transcriptional regulator and key to ERS-mediated apoptotic pathway (20, 21). The over expression of CHOP plays an important role in the activation of C-Jun N-terminal kinase (JNK) that contributes to apoptotic cell death (22, 23). CHOP-mediated apoptosis and inflammation exacerbate myocardial IR injury, whereas $CHOP^{-/-}$ mice have been shown to be resistant to apoptosis in various disease models (24).

Erythropoietin (EPO), on the other hand, could protect various organs including kidney against IR injury (25). The renoprotection of EPO is through a heterodimer EPO receptor and β-common receptor (EPOR/βcR). EPOR/βcR is pharmacologically distinct from the homodimer $(EPOR)_2$ that mediates erythropoiesis (26–28). The renoprotection of EPO against IR injury has been shown by our previous studies, in terms of reducing tubular cell apoptosis, but promoting inflammatory apoptotic cell clearance (29, 30). However, the large dosage of EPO was required to achieve tissue protection, which often causes hypertension and thrombosis *in vivo* (31). Therefore, a helix B surface peptide (HBSP) derived from EPO was developed, which is composed by 11 amino acids (QEQLERALNSS) and interacts with EPOR/βcR only, but with very short serum half-life (32). A metabolic stable cyclic HBSP (CHBP) was further generated, having prolonged half-life and potent tissue protection. The renoprotection of HBSP and CHBP against IR injury has also been confirmed in our previous research projects (33, 34). The pretreatment of CHBP reduced the active level of oxidative damage and ERS induced hydrogen peroxide (H_2O_2) in human proximal tubular cell line, HK-2 cells (35), but its underlying mechanisms have still not been well-defined, especially the impact of CHBP on ERS regulators in TECs, as well as in kidneys post IR injury with extended time to 2 and 8 weeks.

We hypothesized that ERS and CHBP plays differential role in renal IR-related injury, which is associated CHOP and its regulators, apoptotic and inflammatory mediators, as well as subsequent apoptosis. To verify this hypothesis, TCMK-1 cells, mouse kidney epithelial cell line, stimulated by H_2O_2 and mouse kidneys subjected to IR injury were used to evaluate the change of CHOP, the key marker of ERS, and its regulators PERK and JNK, and their relations to apoptotic and inflammatory mediators caspase-3 and HMGB-1, and apoptosis. The impacts of intervention using siRNA target CHOP and CHBP treatment, on above biological events were further studied. It has been proved in this study that ERS plays key roles in IR-related injury and CHBP induced renoprotection in mouse TCMK-1 cells at the early stage and in kidneys with prolonged IR time, and the underlying mechanistic pathway is associated with CHOP/PERK/JNK, HMGB-1/ caspase-3, and apoptosis. CHOP might be a potential biomarker and CHBP might be therapeutic drug for IR-induced AKI.

METHODS AND MATERIALS

TCMK-1 Cell Culture and H_2O_2 Stimulation

TCMK-1 cells (a mouse kidney epithelial cell line, CCL-139™, American Type Culture Collection, Manassas, USA) were cultured in DMEM/F12 medium, supplemented with 10% (v/v) of fetal bovine serum (FBS, Gibco Technologies, Logan, USA), 100 unit/ml penicillin G (Gibco), and 100 μg/ml streptomycin (Gibco), defined as completed medium, at 37°C in 5% CO_2 atmosphere. TCMK-1 cells grown about 80% confluent in monolayer in 6-well plates were treated with or without 500 μmol/L H_2O_2 (Merck KGaA, Darmstadt, Germany) diluted in basic culture medium. At 4, 8, 12 h after the exposure of H_2O_2, the cells were washed three times with PBS (Ji Nuo, Hangzhou, China) and harvested for further analysis. Twenty ng/ml of CHBP (synthesized by Shanghai Institute of Materia Medica, Chinese Academy of Sciences) was added at the same time upon H_2O_2 stimulation and cultured for 12 h (35).

According to the instruction of manufacturer, the small interfering RNA (siRNA) was diluted to 5 nM transfected into TCMK-1 cells using Lipofectamine® RNAiMAX (Invitrogen, Carlsbad, USA). A double-stranded CHOP siRNA (Thermo Fisher Scientific, Waltham, USA) targeting mouse *CHOP* mRNA was designed and constructed. The sequences of CHOP siRNA are: sense: GGAAGAACUAGGAAACGGATT, antisense: UCCGUUUCCUAGUUCUUCCTT. The negative control siRNA (# 4390843, Thermo Fisher Scientific) does not target any known mammalian genes. The transfected cells were cultured at 37°C for 8 h before 12-h H_2O_2 stimulation.

Renal IR Injury Model

Male BALB/c mice weighing 20–25 g were obtained from the Experimental Animal Center of Nantong University, China. They were housed in constant temperature (25°C) and humidity (55%) on a 12-h light/dark cycle, fed *ad libitum* on standard laboratory mouse chow and tap water. All animal procedures were performed according to the guidelines of the Animal Care and Use Committee of Nantong University and the Jiangsu Province Animal Care Ethics Committee (36).

The mice were anesthetized using 80 mg/kg sodium pentobarbital by intraperitoneal injections. The bilateral renal pedicles were exposed by flank incision and clamped for 30 min. For reperfusion, the clamping was released and confirmed blood reflow by monitoring the color change of the kidney before suturing the incision. The mice were randomly divided into 7 groups with different reperfusion time: control, 6, 12, 24, 72 h, and 1 w or 3 groups ($n = 6$): (1) Control group: the abdominal cavity and renal pedicles were exposed without clamping-induced IR injury, (2) IR group: mice were subjected to ischemia 30 min followed by reperfusion for 2 and 8 weeks, (3) IR + CHBP group: IR injury with 24 nmol/kg CHBP dissolved in 0.9% saline intraperitoneally injected after reperfusion every 3 days (37).

Cell Viability Analysis

TCMK-1 cells (1×10^5) were seeded in 96-well plates and cultured in the completed medium 24 h before adding 500 μmol/L of H_2O_2 apart from the control group. In the treatment groups, 20 ng/ml of CHBP was added at the same time upon H_2O_2 stimulation. Ten microliter of CCK-8 (Beyotime, Nantong, China) was then added after 1, 4, and 12 h and further incubated for 1–4 h. The cell viability was measured by absorbance using a microplate reader (MDC, Hayward, USA).

Quantitative Real-Time Polymerase Chain Reaction

Total RNA was extracted from cultured cells with Trizol reagent (Invitrogen) according to the manufacturer's instructions. Complementary DNA (cDNA) was synthesized using 1 μg of total RNA, oligo d(T) 18 Primer and Reverse Transcription Kit (Bio-Rad, Hercules, USA). Quantitative RT-PCR analysis was performed in the real time PCR system (CFX96, Bio-Rad) with AceQ® qPCR SYBR® Green system (Vazyme biotech, Nanjing, China). The oligonucleotide primers for target genes were used as follows: CHOP: forward 5′- ATGTGCGTGTGACCTCTGTT-3′ and reverse 5′-TATCTCATCCCCAGGAAACG, PERK: forward 5′-TAGATGAAACCAAGGAACCAGA-3′, and reverse 5′-ATCAGCACTTTAGATGGACGAA-3′). We amplified 2 μl cDNA for each sample in a 20 μl reaction system containing SYBR Green Master Mix and primers with the following cycling conditions: 2 min at 95°C, 40 cycles of 95°C for 10 s, then 60°C for 10 s. Expression levels were normalized with GAPDH in the same samples using the $2^{-\Delta\Delta Ct}$ method.

Western Blot Analysis

RIPA lysis buffer (Beyotime) containing phenylmethylsulfonyl fluoride, protease inhibitor, and phosphatase inhibitor was used to crack renal tissues or cells. Total protein was isolated according to the standard methods (34). The protein was measured by Pierce BCA Protein Quantitation Kit (Pierce, Rockland, USA). Twenty five micrograms of protein from TCMK-1 cells or kidney cortex was separated on a 12–15% (w/v) polyacrylamide denaturing gel and electronically blotted onto 0.45 μm polyvinylidene difluoride (PVDF) membranes (Roche Diagnostics GmbH, Mannheim, Germany) on 14 volts for 16 h at 4°C or 100 volts for 1 h at room temperature. After 2-h blocking with 5% milk, caspase-3 or CHOP antibody (both at 1:200, Santa Cruz Biochemicals, Santa Cruz, USA), or PERK, JNK, HMGB-1, β-actin or α-Tubulin antibody (all at 1:1,000, Cell Signaling Technology, Beverly, USA) was incubated overnight at 4°C. The horseradish peroxidase-conjugated secondary antibody (Jackson ImmunoResearch Laboratories, West Grove, USA) was then incubated for 2 h at room temperature. Antibody binding was detected by enhanced chemiluminescent (ECL, Pierce) and a Molecular Imager, Chemi Doc, XRS+ System (Bio-Rad, Berkeley, USA) (36). Developed images were semi quantitatively analyzed by scanning volume density using Alpha View Software 3.3 (Cell Biosciences Inc., Santa Clara, USA). The expression of target protein was normalized against to the expression of β-actin or α-Tubulin, and presented as an ratio.

Determination of Apoptosis by Flow Cytometry

Adherent TCMK-1 cells were harvested by tripsinizing and centrifuged at 1,000 rpm/min for 5 min, then washed twice with PBS. The pellet was resuspended in 100 μl of 1× binding buffer and incubated with 5 μl of FITC-conjugated annexin-V and 5 μl of propidium iodide (PI) for 15 min at room temperature in the dark. Another three tubes: annexin-V only, PI only and none dye was prepared as controls. Four hundred μl of 1× binding buffer was added to each sample tube, and the samples were analyzed by BD FACS Calibur flow cytometer (Becton Dickinson, San Jose, USA) using Cell Quest Research Software (BD Biosciences, Franklin Lakes, USA), a minimum of 10,000 cells were counted.

The results were shown as quadrant dot plots with survival cells (Annexin V-/PI-), early apoptotic cells (Annexin V+/PI-), later apoptotic cells or necrotic cells (Annexin V+/PI+). The number of each type of cells was expressed as the percentage of each type of cells against the total number of gated cells.

Correlation Analysis

The correlation analysis was used to measure the correlation between two parameters. The range of R value between 0 and 1 or −1 and $P < 0.05$ implies positive or negative correlation (38). This method was used to analyze the correlation between CHOP and PERK, JNK, apoptosis, or cell viability in the *in vitro* model.

Statistical Analysis

All data are representative of at least three independent experiments, while the data are presented as the mean ± standard error of the mean (SEM). The results among three or more groups were compared by one-way analysis of variance (ANOVA), while those in any two groups were compared

using a two-tailed independent Student's *t*-test. All statistical analysis were performed using GraphPad Prism 6.0 (GraphPad Software Inc., San Diego, USA), with $P < 0.05$ considered statistically significant.

RESULTS

ERS Induced by H_2O_2 in TCMK-1 Cells

To study the dynamic change of CHOP and its regulator PERK, the expression of CHOP mRNA and protein, and *PERK* mRNA was measured by qPCR and western blot in TCMK-1 cells treated with 500 μmol/L H_2O_2 for 4, 8, 12 h. The mRNA expression of CHOP and PERK was gradually increased with the time, and reached significance at 8 h compared with the control, and peaked at 12 h compared with the control or 4 h (all $P < 0.01$, **Figures 1A,B**). The expression of CHOP protein was also increased at 12 h (1.06 ± 0.13) compared with the control or 4 h, respectively (0.79 ± 0.04 or 0.67 ± 0.10, both $P < 0.05$, **Figures 1C,D**).

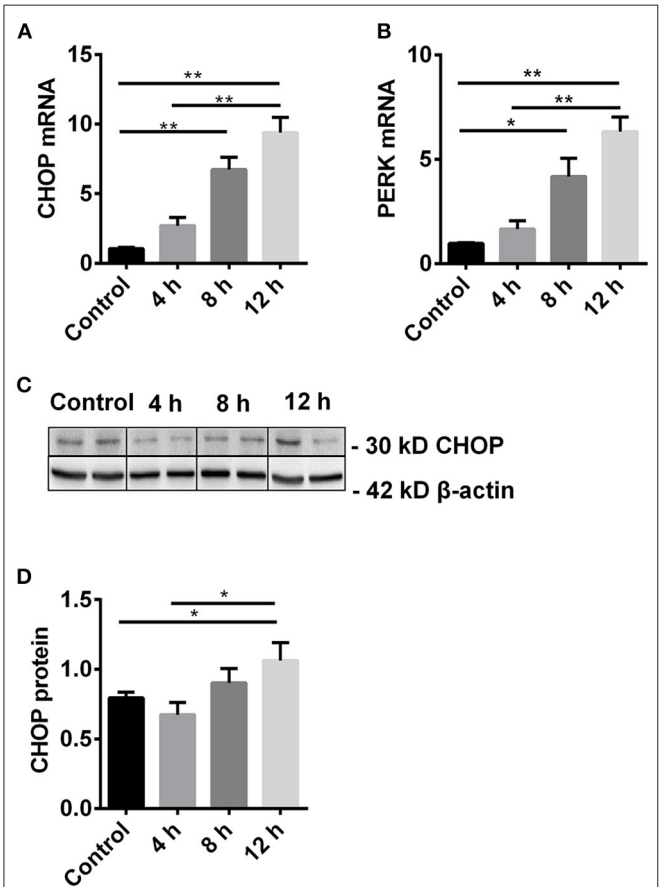

FIGURE 1 | The dynamic change of CHOP and its regulator PERK. **(A,B)** The mRNA level of CHOP and PERK was gradually increased and reached the significance at 8 h and peaked at 12 h. **(C,D)** The expression of CHOP protein was significantly increased at 12 h. Data are expressed as mean ± SEM ($n = 3$). The volume density of western blots was corrected by against 42 kD β-actin as a loading control. *$P < 0.05$, **$P < 0.01$. h, hours.

CHOP siRNA Downregulated Its mRNA and Protein *in vitro*

In the TCMK-1 cells transfected with CHOP siRNA, the expression of *CHOP* mRNA was reduced by 53% and 56% compared to the cells treated by H_2O_2 or the negative control (NC) siRNA, respectively (both $P < 0.01$, **Figure 2A**). In addition, CHOP siRNA also reduced the expression of CHOP protein (0.69 ± 0.08 vs. 1.17 ± 0.17 or 1.42 ± 0.10, $P < 0.05$ or 0.01, **Figures 2B,C**) in the same comparisons.

CHOP siRNA Decreased Caspase-3 and HMGB-1 Expression in TCMK-1 Cells

The effect of CHOP siRNA on caspase-3 expression was further investigated. The level of *caspase-3* mRNA (**Figure 2D**) and 17 kD protein (**Figures 2E,G**), contrary to 32 kD protein (**Figures 2E,F**), was increased in the H_2O_2 or NC siRNA group. However, they all were significantly decreased by CHOP siRNA (mRNA: 1.88 ± 0.21 vs. 3.33 ± 0.19 or 3.04 ± 0.17, 17 kD: 1.21 ± 0.08 vs. 1.57 ± 0.01 or 1.55 ± 0.07, 32 kD: 0.34 ± 0.04 vs. 0.62 ± 0.03 or 0.60 ± 0.07, $P < 0.05$ or 0.01).

The level of HMGB-1 protein was significantly up-regulated in the H_2O_2 group ($P < 0.05$, **Figures 3A,B**), but was down-regulated by CHOP siRNA compared to the H_2O_2 and NC siRNA group (0.81 ± 0.11 vs. 1.27 ± 0.34 and 1.18 ± 0.11, $P < 0.05$).

CHOP siRNA Decreased Apoptosis in TCMK-1 Cells

The cells stimulated by H_2O_2, NC siRNA or CHOP siRNA post H_2O_2 stimulation were presented (**Figure 3C**). The percentage of survival cells was decreased by H_2O_2 and NC siRNA compared with the control group, but reversed by CHOP siRNA (81.55 ± 1.74 vs. 75.66 ± 1.54, $P < 0.05$, **Figure 3D**). The early apoptotic cells and later apoptotic cells were increased, respectively, by H_2O_2 and NC siRNA treatment compared with the control group (**Figures 3E,F**). Only the early apoptotic cells were reduced by CHOP siRNA compared to the H_2O_2 and NC siRNA group (7.07 ± 1.28 vs. 14.58 ± 1.71 and 16.84 ± 2.74, $P < 0.01$, and 0.05).

CHOP Correlated With PERK, Caspase-3, HMGB-1, and Apoptosis Positively, but Cell Viability Negatively

To further investigate the role of CHOP in IR-related injuries, the correlation between *CHOP* mRNA and PERK, 17 kD active caspase-3, HMGB-1, apoptosis, and cell viability was analyzed, respectively. *CHOP* mRNA was correlated positively with PERK protein, active caspase-3, HMGB-1 and apoptosis ($R = 0.7219$, 0.9343, 0.7129, and 0.8823, all $P < 0.01$, **Figure 4**), but negatively with cell viability ($R = -0.5248$, $P < 0.05$) in the *in vitro* model.

CHBP Increased TCMK-1 Cell Viability Post H_2O_2 Stimulation

In order to observe the effect of CHBP, renoprotective peptide derived from erythropoietin, on cell viability, the CCK-8 assay was used to detect the value of optical density (OD) at 1, 4, 12 h after H_2O_2 stimulation (**Figure 5A**). The cell viability gradually decreased with the time of H_2O_2 stimulation with or without

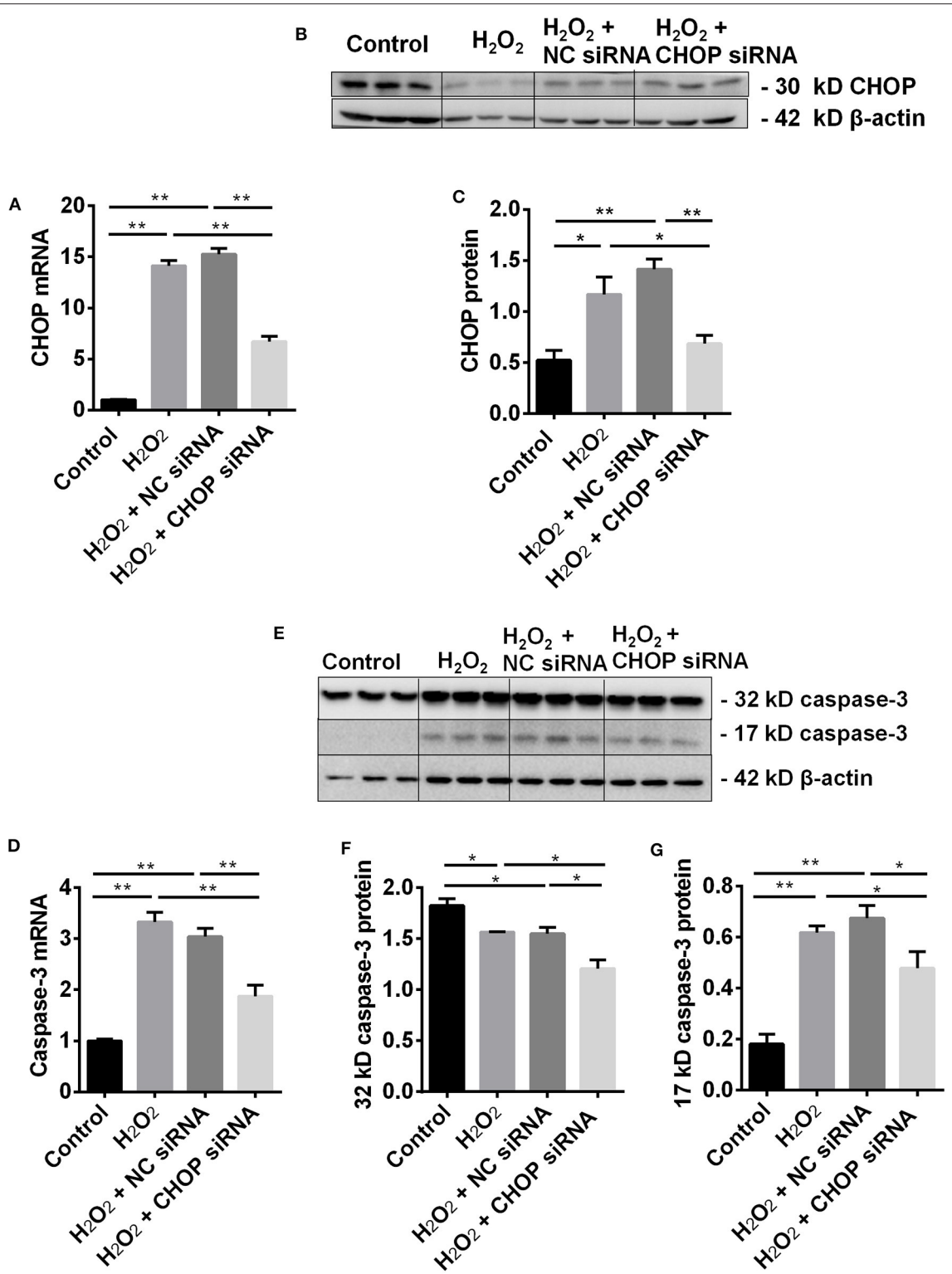

FIGURE 2 | CHOP siRNA downregulated its mRNA, protein and caspase-3 in TCMK-1 cells. **(A)** The expression of *CHOP* mRNA in the TCMK-1 cells transfected with CHOP siRNA was reduced by 53% and 56% compared to the cells treated by the H_2O_2 and the NC siRNA. **(B,C,E,G)** The expression of CHOP protein as well as *caspase-3* mRNA **(D)** and 17 kD caspase-3 protein was increased at the H_2O_2 and the NC siRNA group but reversed by CHOP siRNA. **(E,F)** The expression of 32 kD caspase 3 protein was decreased by H_2O_2 or NC siRNA and further decreased by CHOP siRNA. Data are expressed as mean ± SEM ($n = 3$). The volume density of western blots was corrected by against 42 kD β-actin as a loading control. $^*P < 0.05$, $^{**}P < 0.01$.

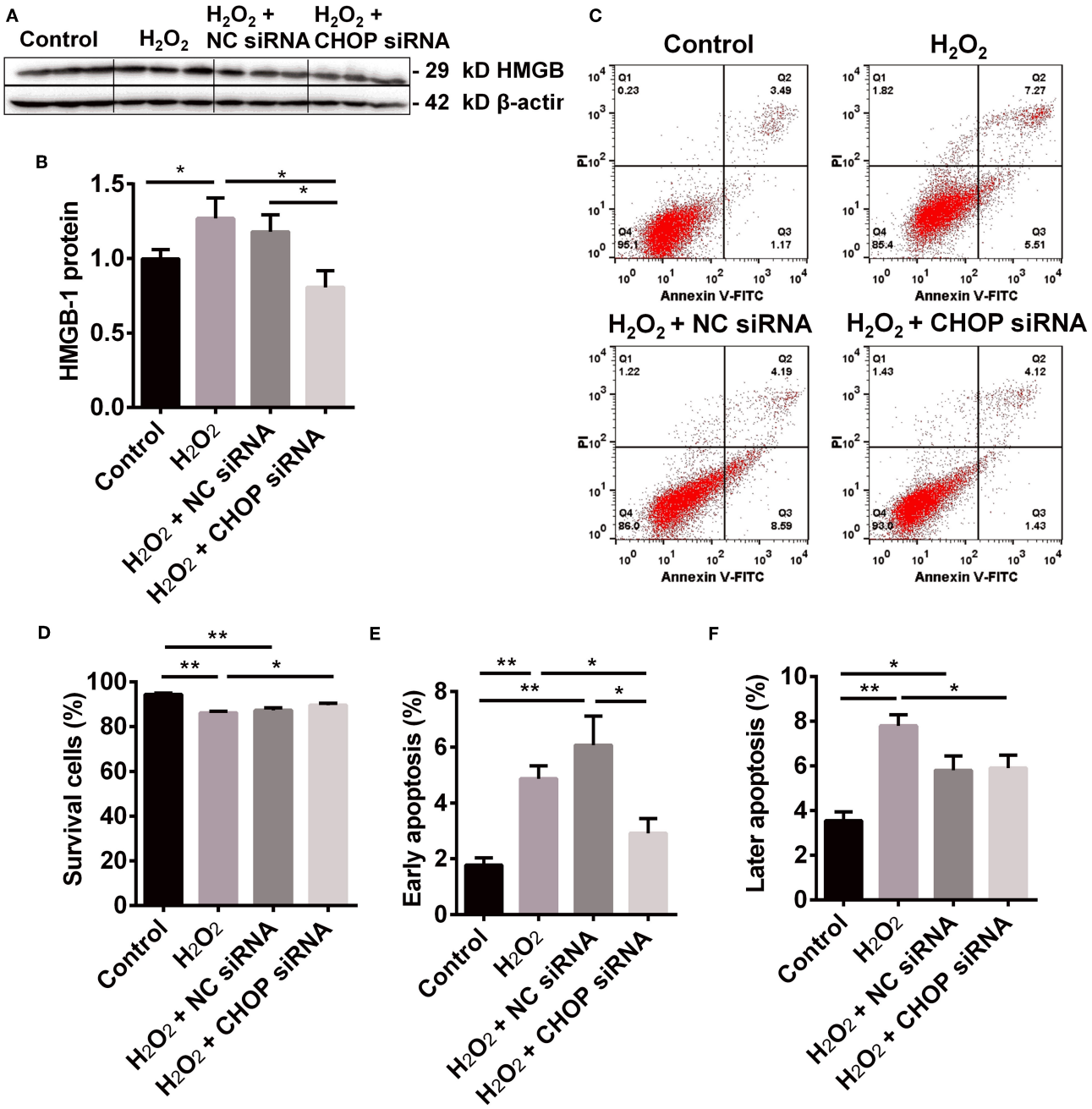

FIGURE 3 | The renoprotection of CHBP associated with ERS improvement, apoptosis and inflammation. **(A,B)** HMGB-1 protein was significantly up-regulated by H_2O_2, but was down-regulated by CHOP siRNA compared to the H_2O_2 and NC siRNA groups. **(C,D)** The percentage of living cells was decreased by H_2O_2 and H_2O_2 + NC siRNA but reversed by H_2O_2 + CHOP siRNA. **(E,F)** The both early and later apoptotic cells were increased by H_2O_2 and H_2O_2 + NC siRNA, but only the early apoptotic cells were reduced by H_2O_2 + CHOP siRNA. Data are expressed as mean ± SEM ($n = 3$). The volume density of western blots was corrected by against 42 kD β-actin as a loading control. *$P < 0.05$, **$P < 0.01$.

CHBP and reached the significance from 1 to 12 h compared with the control ($P < 0.01$ or 0.05).

More importantly, the cell viability was significantly increased in the H_2O_2 + CHBP group at 4 and 12 h (0.74 ± 0.08 and 0.46 ± 0.06) compared with the H_2O_2 group (0.49 ± 0.06 and 0.24 ± 0.04, $P < 0.05$ and 0.01).

CHBP Reduced ERS Induced by H_2O_2 and IR Injury

To further dissect the mechanism of CHBP renoprotection in association with ERS, the mRNA and protein of CHOP were measured in the TCMK-1 cells stimulated by H_2O_2 for 12 h (**Figures 5B–D**). It has been revealed that the mRNA and protein

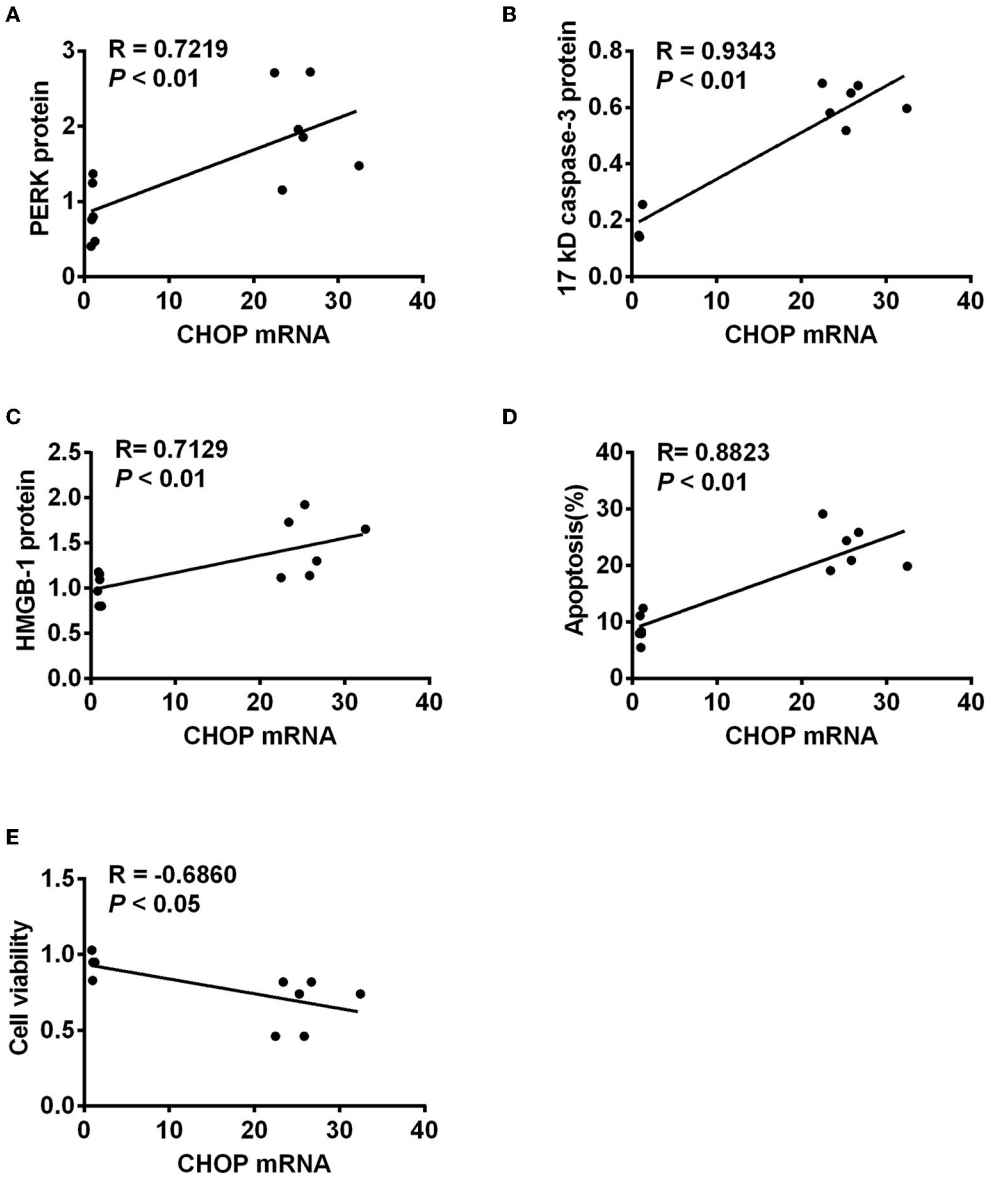

FIGURE 4 | The correlation between *CHOP* mRNA and other detected parameters. *CHOP* mRNA was positively correlated with PERK protein **(A)**, active caspase-3 **(B)**, HMGB-1 **(C),** and apoptosis **(D)** ($R = 0.7219$, 0.9343, 0.7129, and 0.8823, all $P < 0.01$) but negatively with cell viability (**E**, $R = -0.5248$, $P < 0.05$) in the *in vitro* model.

of CHOP were increased ($P < 0.01$ or 0.05), whereas the increased CHOP mRNA and protein were reversed by CHBP treatment (mRNA: 8.82 ± 0.79 vs. 13.06 ± 0.44, protein: 0.85 ± 0.06 vs. 1.26 ± 0.04, $P < 0.01$).

In addition, the expression of CHOP protein was significantly increased in the IR kidneys at 2 and 8 weeks (both $P < 0.05$), which was decreased by CHBP only at 2 weeks (1.30 ± 0.28 vs. 3.10 ± 0.66, $P < 0.05$, **Figures 5E,F**). The CHOP protein was also correlated positively with the level of tubulointerstitial damage (TID) and active caspase-3 protein at 2 weeks ($R = 0.7764$ and 0.9464, $P < 0.05$ or 0.01, **Figures 5G,H**). Besides that, a trend of positive correlation between CHOP protein and apoptosis or interstitial fibrosis was showed at 2 weeks, respectively, even though there was no statistical significance ($R = 0.5612$, $P = 0.1478$; $R = 0.4467$, $P = 0.2671$). However, the original data of TID, active caspase-3 protein, apoptosis and interstitial fibrosis have not been shown here.

Moreover, the level of *PERK* mRNA and protein (**Figures 6A–C**), JNK protein (**Figures 6D,E**) and HMGB-1 protein (**Figures 6F,G**) was significantly up-regulated by H_2O_2 ($P < 0.05$ or 0.01), which was down-regulated by CHBP (*PERK* mRNA: 2.24 ± 0.22 vs. 3.20 ± 0.26, PERK protein: 1.15 ± 0.15 vs. 1.98 ± 0.17, JNK protein: 1.10 ± 0.08 vs. 1.48 ± 0.11, HMGB-1 protein: 0.89 ± 0.04 vs. 1.21 ± 0.11, all $P < 0.05$).

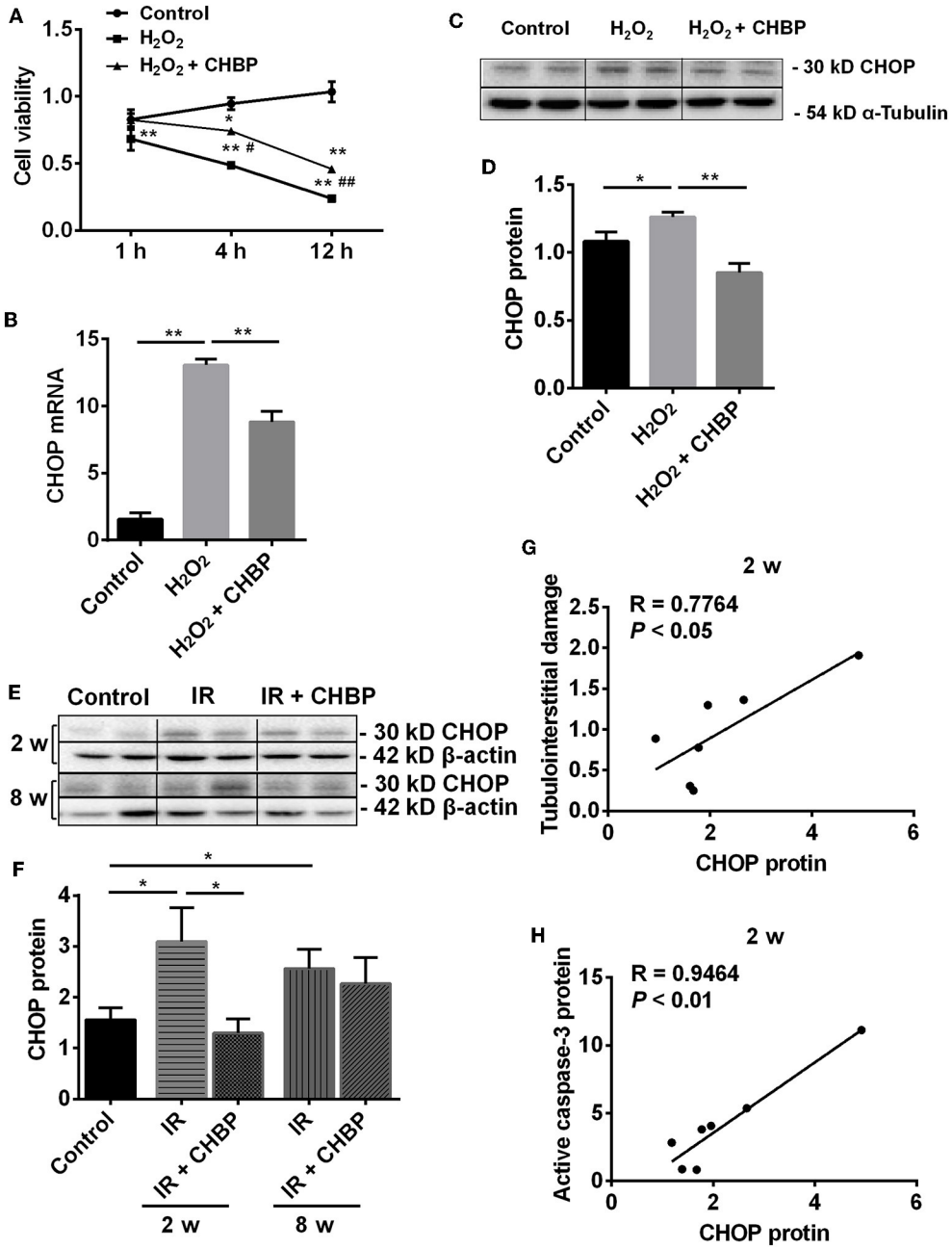

FIGURE 5 | The dynamic change of cell viability and the expression of CHOP mRNA and protein in TCMK-1 cells and kidneys. **(A)** The cell viability was gradually decreased with the time of H_2O_2 treatment, reached the significance from 1 to 12 h, but was significantly improved in the H_2O_2 + CHBP group after 4 h. **(B–D)** The mRNA and protein of CHOP were significantly increased in the TCMK-1 cells stimulated by H_2O_2, but reversed by CHBP. **(E,F)** CHOP protein was also significantly increased in the IR group at 2 and 8 weeks, but was decreased by CHBP only at 2 weeks. Data are expressed as mean ± SEM ($n = 3$–6). The volume density of western blots was corrected by against 42 kD β-actin or 54 kD α-Tubulin as a loading control. **(G,H)** CHOP protein was positively correlated with the level of TID and active caspase-3 protein at 2 weeks. *, #$P < 0.05$, **, ##$P < 0.01$ vs. Control, 4 h or H_2O_2 + CHBP.

CHBP Inhibited Cell Apoptosis *in vitro*

Apoptotic cells were detected by flow cytometry using Annexin V/PI staining. The population of cells in the control, H_2O_2, CHBP, or CHBP post H_2O_2 stimulation group was presented (**Figure 7A**). The percentage of survival cells (Annexin V-/PI-) was decreased by H_2O_2 treatment compared with the control groups with or without CHBP treatment, but effectively reversed by CHBP (88.15 ± 0.57 vs. 43.23 ± 2.88, $P < 0.01$, **Figure 7B**). Both the early apoptotic cells (Annexin V+/PI-) and later apoptotic cells (Annexin V+/PI+) were increased, respectively,

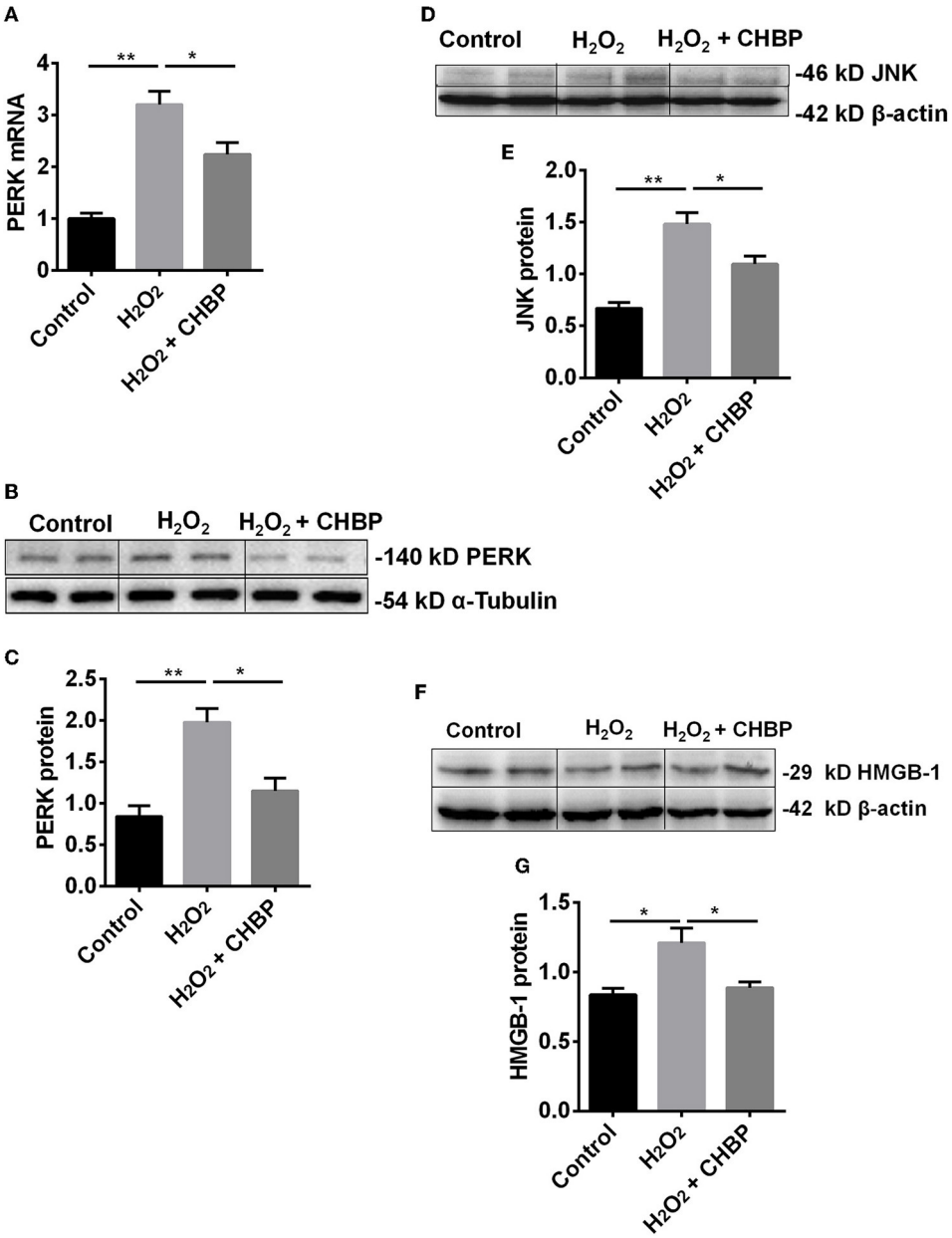

FIGURE 6 | The expression of PERK, JNK and HMGB-1 protein and/or mRNA. The mRNA **(A)** and protein **(B,C)** of PERK, as well as JNK protein **(D,E)** and HMGB-1 protein **(F,G)**, were significantly increased by H_2O_2 in the TCMK-1 cells. However, these effects were reversed by CHBP. Data are expressed as mean ± SEM ($n = 3$). The volume density of western blots was corrected by against 42 kD β-actin or 54 kD α-Tubulin as a loading control. *$P < 0.05$, **$P < 0.01$.

by H_2O_2 treatment compared with the control group and the CHBP group (**Figures 7C,D**), but reduced by CHBP almost to the baseline level (1.85 ± 0.22 vs. 6.67 ± 0.13, 7.88 ± 0.61 vs. 45.55, both $P < 0.01$).

Dynamic Change of CHOP at Different Time Post IR Injury

The expression of CHOP mRNA was significantly increased from 12 h after IR injury, peaked at 24 h, and then significantly decreased at 48 h compared with both 12 and 24 h, and also at 1 week compared with 24 h. CHOP protein was also significantly raised at 12, 24, 48, and 72 h compared with the control with a peak at 12 h, and decreased at 1 week compared with 12 h ($P <$ 0.05 or 0.01, **Figures 7E–G**).

DISCUSSION

The role and its underlying mechanism of ERS in IR-related injury and CHBP-induced renoprotection have been well-investigated in this study using *in vitro* and *in vivo* models. The

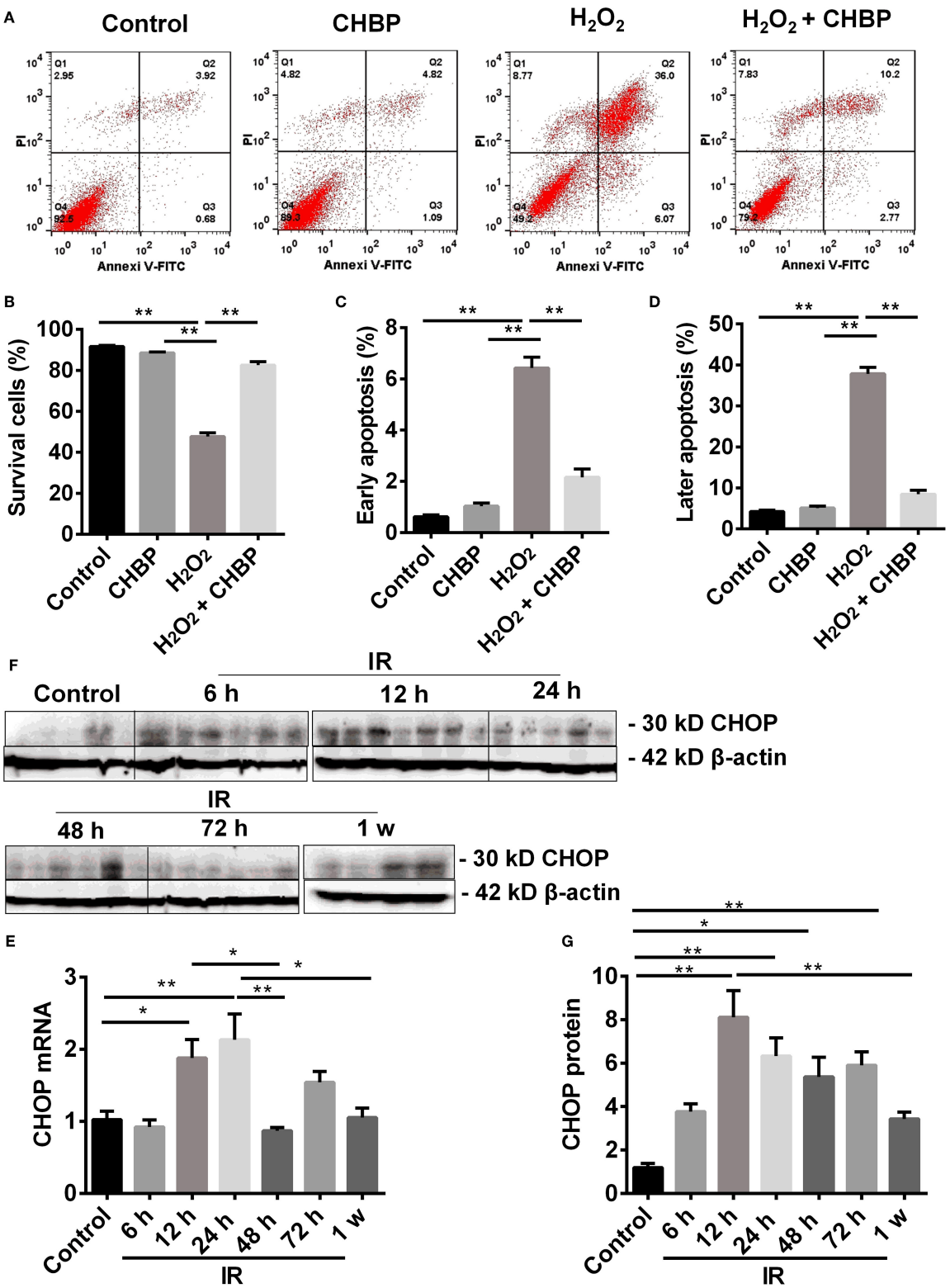

FIGURE 7 | Cell apoptosis analyzed by flow cytometry and CHOP protein detected by western blot. (**A,B**: Annexin V-FITC-/PI-) The percentage of living cells was decreased by H_2O_2, but reversed by CHBP. (**A,C**: Annexin V +/PI-; **A,D**: Annexin V +/PI+) The early apoptotic cells, as well as later apoptotic cells were increased, respectively, by H_2O_2, but reduced by CHBP. **(E–G)** The dynamic expression of CHOP at mRNA and protein level. **(E,F)** CHOP protein was significantly raised and picked at 12 h. **(G)** CHOP mRNA was also significantly increased at 12 h and peaked at 24 h after IR injury. Both CHOP protein and mRNA were decreased at 1 week. Data are expressed as mean ± SEM ($n = 3$). The volume density of western blots was corrected by against 42 kD β-actin as a loading control. $^*P < 0.05$, $^{**}P < 0.01$.

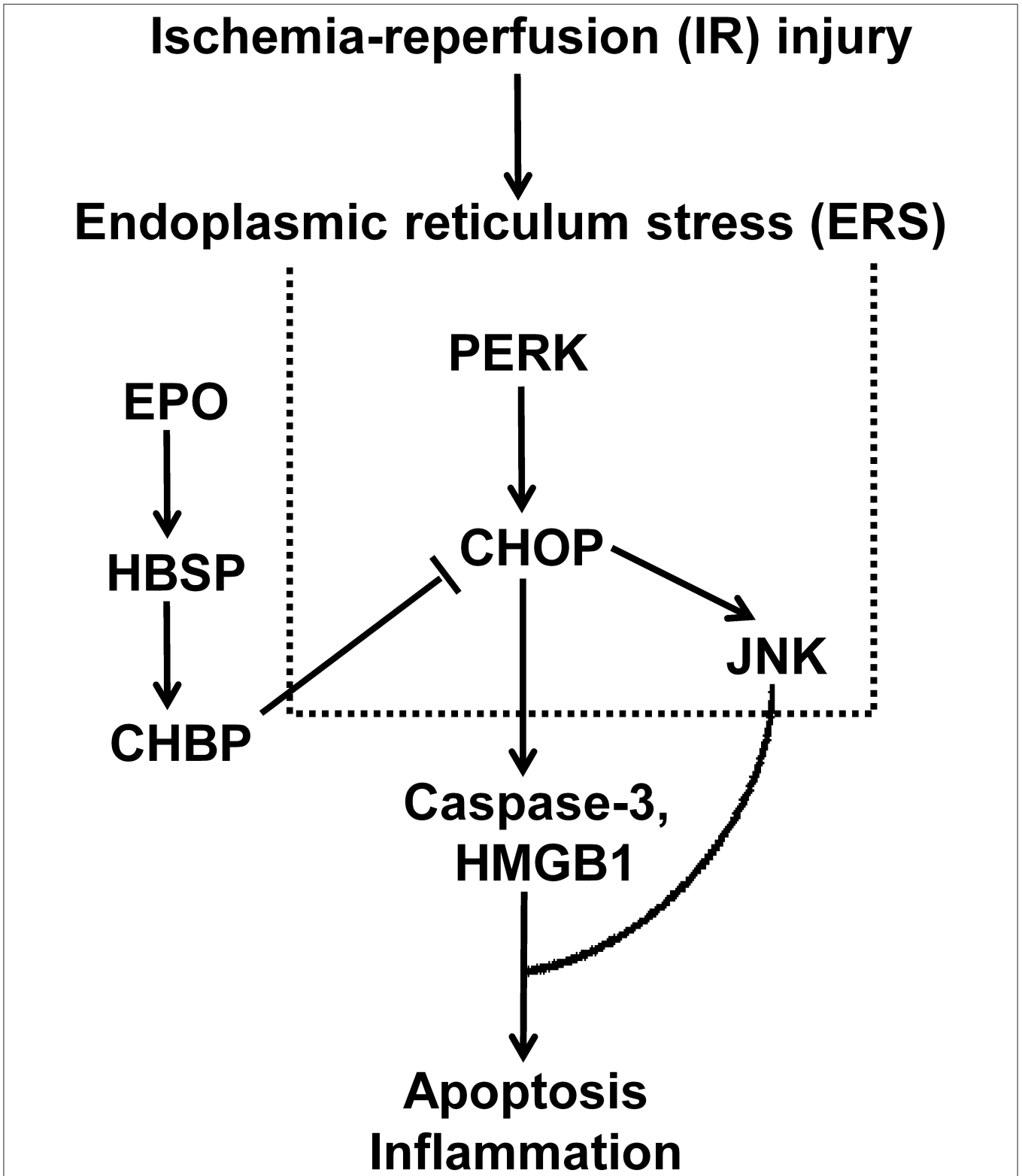

FIGURE 8 | The schematic illustration shows that the key role of ERS in IR-related injury, and CHBP-incuced renoprotection was associated with CHOP/PERK/JNK, HMGB-1/caspase-3, and apoptosis.

expression of CHOP, a key marker of ERS, was increased in IR-related and IR injury. In addition, the intervening CHOP using siRNA reduced CHOP expression at both mRNA and protein level, subsequent decreased caspase-3 and HMGB-1 protein, and early apoptosis. Furthermore, CHBP treatment significantly improved ERS, in terms of decreased CHOP expression in TCMK-1 cells and kidneys subjected to IR-related and IR injury, as well as its regulators PERK and JNK, apoptotic and inflammatory mediator HMGB-1, and early and later apoptosis *in vitro*. Therefore, the key role of ERS in IR-related injury and CHBP induced renoprotection was proved in both mouse TCMK-1 cells and kidneys, in which its mechanistic signaling pathway was associated with CHOP/PERK/JNK, HMGB-1/caspase-3, and apoptosis (**Figure 8**).

The dynamic change of *CHOP* and *PERK* mRNA was evaluated in TCMK-1 at different time points after H_2O_2 stimulation. The consequential increase of these key parameters was observed, which reflected the gradual occurrence of ERS. The expression of CHOP protein was also increased significantly with time from 8 to 12 h compared with the control and 4 h. The change of CHOP at mRNA level represents transcriptional change, while that of CHOP at protein level represents translational change. The divergence of both at 4 h reflected differential regulations between transcription and translation. In addition, the temporary decline of CHOP protein at 4 h may be due to consumption involved in apoptosis, a self-protective regulation of cells, which subsequently stimulated the increase of CHOP at mRNA. It has been confirmed that 500 μmol/L H_2O_2 for stimulation over a period of 12 h were the most suitable experimental condition for the following investigation.

CHOP is a key player in ERS-mediated apoptotic pathway (20, 39). In response to severe ERS, CHOP activates the expression of Bim, leading to caspase-3 cleavage and apoptosis (40). Caspase-3 associated with apoptosis and inflammation involved in renal IR-related and IR injury. The precursor of caspase-3 could be cleaved into 17 and 12 kD subunits, both of which contribute to caspase-3 activity (34, 37, 41, 42). The changes of CHOP activate the ER-associated caspase cascades, including caspase-12 and caspases-3 (37). Therefore, we further investigate the effect of CHOP intervention by its siRNA on apoptotic and inflammatory mediator caspase-3 and HMGB-1, and apoptosis in renal IR-related injury. CHOP siRNA decreased the expression of CHOP mRNA and protein, as well as *caspase-3* mRNA, 32 and 17 kD caspase-3, and HMGB-1 protein. Moreover, the number of early apoptotic cells was also reduced by CHOP siRNA compared to the H_2O_2 and NC siRNA groups, and the cell survival was improved. These data were consistent to the $CHOP^{-/-}$ knockout model *in vivo* (21, 43, 44). Furthermore, the correlation analysis revealed that *CHOP* mRNA was positively correlated with PERK, 17 kD active caspase-3 and HMGB-1, and apoptosis, but negatively related to cell viability. These results were in accordance with some other studies (40, 45, 46). Therefore, our data convincingly proved that CHOP was involved in the process of apoptosis, especially in its early stage, in renal IR-related injury.

The decreased cell viability upon H_2O_2 stimulation, in addition, was significantly reversed by CHBP treatment time-dependently, which confirmed the cellular protection of CHBP. More interestingly, CHBP also reduced CHOP mRNA and protein expression in TCMK-1 cells, while increased CHOP protein expression in the IR kidneys at prolonged time points was also decreased by CHBP treatment at 2 weeks, even though not at 8 weeks. Therefore, our data demonstrated that CHOP involved in renal IR-related and IR injuries, and CHBP-induced renoprotection might be through regulating CHOP or improving ERS. However, when UPR response cannot restore the homeostasis of endoplasmic reticulum upon IR injury, PERK pathway could trigger off downstream apoptosis via the activation of CHOP, caspase-12 and Bcl-2 family (44, 47, 48). Additional correlation analysis revealed that CHOP protein was positively correlated with the level of TID and active caspase-3 protein at 2 weeks. A trend of positive correlation between CHOP protein and interstitial fibrosis, apoptosis was also revealed at 2 weeks. But because the sample size is insufficient, it was not reached statistical significance. Therefore, CHBP might be renoprotective against IR-induced apoptosis and tubular damage mediated by CHOP, which could be more effective at 2 weeks than 8 weeks, as the level of CHOP could be alleviated with the time post IR injury naturally. These results also indicate that the efficacy of CHBP renoprotection might depend on the level of CHOP in certain degree, the higher of ERS, the better of CHBP renoprotection. In order to study the underlying relationship between CHBP and ERS, the changes in two main up and down-stream regulators of CHOP, PERK, and JNK, were further explored. PERK mRNA and protein, and JNK protein, were all increased significantly in the TCMK-1 cells stimulated by H_2O_2, but was reversed by CHBP treatment. These results imply that the renoprotection of CHBP was attributed to the improvement of CHOP associated ERS, especially at the early stage of renal IR injury. Furthermore, both early and later apoptotic cells increased by H_2O_2 stimulation all reversed by CHBP treatment that was more potent than CHOP siRNA. However, there was no impact of CHPB on apoptosis at baseline level. The change of HMGB-1 protein (49), a mediator of apoptosis and inflammation, has a similar trend with that of CHOP, PERK, and JNK *in vitro*. These results revealed that the protective effects of CHBP were related to not only ERS improvement, but also apoptotic and inflammatory mediator, and apoptosis. To confirm whether ERS plays key roles at the early stage of IR injury, we established a time course model with reperfusion at 6, 12, 24, 48, 72 h, and 1 week. The dynamic change of CHOP showed that the expression of CHOP mRNA and protein was significantly increased as early as 12 h post IR injury peaked at 24 and 12 h respectively, and then both decreased at 1 week. Therefore, the intervention at early time points is worth to be further investigated.

In conclusion, ERS and CHBP play differential roles in IR-related injury in TCMK-1 cells and kidneys. The mechanistic signaling pathway is associated with CHOP/PERK/JNK, HMGB-1/caspase-3, and apoptosis. This study, therefore, indicates that CHOP might be a potential biomarker for diagnosis and treatment of IR-induced acute kidney injury, and CHBP might also have therapeutic application clinically.

DATA AVAILABILITY STATEMENT

The datasets generated for this study are available on request to the corresponding author.

ETHICS STATEMENT

The animal study was reviewed and approved by Ethics committee of affiliated hospital of Nantong University.

AUTHOR CONTRIBUTIONS

BY, YF, and TZ conceived and designed the study. YZ, QW, AL, YW, FL, and HW acquired, analyzed, and interpreted the data. YZ and BY wrote the paper. BY final approval of submitted version. All authors participated in the design, interpretation of the studies and analysis of the data and review of the manuscript.

FUNDING

This research was funded by the National Natural Science Foundation of China (81170689, 81570677, and 81873622 to BY), and the Science and Technology Projects of Nantong (MS12015117 to YZ).

ACKNOWLEDGMENTS

We would like to acknowledge the Basic Medical Research Center of Nantong University for providing all facilities to accommodate this study. In addition, we thank Professor Yaqiu Long (Key Laboratory of Receptor Research, Shanghai Institute of Materia Medica, Chinese Academy of Sciences) for providing CHBP for this study.

REFERENCES

1. Lobb I, Davison M, Carter D, Liu W, Haig A, Gunaratnam L, et al. Hydrogen sulfide treatment mitigates renal allograft ischemia-reperfusion injury during cold storage and improves early transplant kidney function and survival following allogeneic renal transplantation. *J Urol.* (2015) 194:1806–15. doi: 10.1016/j.juro.2015.07.096
2. Chatauret N, Badet L, Barrou B, Hauet T. Ischemia-reperfusion: from cell biology to acute kidney injury. *Prog Urol.* (2014) 24 (Suppl. 1):S4–12. doi: 10.1016/S1166-7087(14)70057-0
3. Chiang WC, Huang YC, Fu TI, Chen PM, Chang FC, Lai CF, et al. Angiopoietin 1 influences ischemic reperfusion renal injury via modulating endothelium survival and regeneration. *Mol Med.* (2019) 25:5. doi: 10.1186/s10020-019-0072-7
4. Dong G, Liu Y, Zhang L, Huang S, Ding HF, Dong Z. mTOR contributes to ER stress and associated apoptosis in renal tubular cells. *Am J Physiol Renal Physiol.* (2015) 308:F267–74. doi: 10.1152/ajprenal.00629.2014
5. Li L, Wang ZV, Hill JA, Lin F. New autophagy reporter mice reveal dynamics of proximal tubular autophagy. *J Am Soc Nephrol.* (2014) 25:305–15. doi: 10.1681/ASN.2013040374
6. Rong S, Hueper K, Kirsch T, Greite R, Klemann C, Mengel M, et al. Renal PKC-epsilon deficiency attenuates acute kidney injury and ischemic allograft injury via TNF-alpha-dependent inhibition of apoptosis and inflammation. *Am J Physiol Renal Physiol.* (2014) 307:F718–26. doi: 10.1152/ajprenal.00372.2013
7. Wadosky KM, Shourideh M, Goodrich DW, Koochekpour S. Riluzole induces AR degradation via endoplasmic reticulum stress pathway in androgen-dependent and castration-resistant prostate cancer cells. *Prostate.* (2019) 79:140–50. doi: 10.1002/pros.23719
8. Wang J, Wen Y, Lv LL, Liu H, Tang RN, Ma KL, et al. Involvement of endoplasmic reticulum stress in angiotensin II-induced NLRP3 inflammasome activation in human renal proximal tubular cells *in vitro*. *Acta Pharmacol Sin.* (2015) 36:821–30. doi: 10.1038/aps.2015.21
9. Senft D, Ronai ZA. UPR, autophagy, and mitochondria crosstalk underlies the ER stress response. *Trends Biochem Sci.* (2015) 40:141–8. doi: 10.1016/j.tibs.2015.01.002
10. Ozkok A, Ravichandran K, Wang Q, Ljubanovic D, Edelstein CL. NF-kappaB transcriptional inhibition ameliorates cisplatin-induced acute kidney injury (AKI). *Toxicol Lett.* (2016) 240:105–13. doi: 10.1016/j.toxlet.2015.10.028
11. Pressly JD, Hama T, Brien SO, Regner KR, Park F. TRIP13-deficient tubular epithelial cells are susceptible to apoptosis following acute kidney injury. *Sci Rep.* (2017) 7:43196. doi: 10.1038/srep43196
12. Simon N, Hertig A. Alteration of fatty acid oxidation in tubular epithelial cells: from acute kidney injury to renal fibrogenesis. *Front Med.* (2015) 2:52. doi: 10.3389/fmed.2015.00052
13. Cao SS. Endoplasmic reticulum stress and unfolded protein response in inflammatory bowel disease. *Inflamm Bowel Dis.* (2015) 21:636–44. doi: 10.1097/MIB.0000000000000238
14. Hetz C. The unfolded protein response: controlling cell fate decisions under ER stress and beyond. *Nat Rev Mol Cell Biol.* (2012) 13:89–102. doi: 10.1038/nrm3270
15. O'Hayre M, Vazquez-Prado J, Kufareva I, Stawiski EW, Handel TM, Seshagiri S, et al. The emerging mutational landscape of G proteins and G-protein-coupled receptors in cancer. *Nat Rev Cancer.* (2013) 13:412–24. doi: 10.1038/nrc3521
16. Hottenrott C. Next-generation, genome- and mutational landscape heterogeneity-based novel biomarkers for personalized neoadjuvant treatment and laparoscopic rectal cancer resection. *Surg Endosc.* (2013) 27:1441–3. doi: 10.1007/s00464-012-2570-3
17. Sommerweiss D, Gorski T, Richter S, Garten A, Kiess W. Oleate rescues INS-1E β-cells from palmitate-induced apoptosis by preventing activation of the unfolded protein response. *Biochem Biophys Res Commun.* (2013) 441:770–6. doi: 10.1016/j.bbrc.2013.10.130
18. Lv Z, Liu C, Zhai M, Zhang Q, Li J, Zheng F, et al. LPS pretreatment attenuates cerebral ischaemia/reperfusion injury by inhibiting inflammation and apoptosis. *Cell Physiol Biochem.* (2018) 45:2246–56. doi: 10.1159/000488170
19. Yang JR, Yao FH, Zhang JG, Ji ZY, Li KL, Zhan J, et al. Ischemia-reperfusion induces renal tubule pyroptosis via the CHOP-caspase-11 pathway. *Am J Physiol Renal Physiol.* (2014) 306:F75–84. doi: 10.1152/ajprenal.00117.2013
20. Mei S, Livingston M, Hao J, Li L, Mei C, Dong Z. Autophagy is activated to protect against endotoxic acute kidney injury. *Sci Rep.* (2016) 6:22171. doi: 10.1038/srep22171
21. Tian H, Li Y, Kang P, Wang Z, Yue F, Jiao P, et al. Endoplasmic reticulum stress-dependent autophagy inhibits glycated high-density lipoprotein-induced macrophage apoptosis by inhibiting CHOP pathway. *J Cell Mol Med.* (2019) 23:2954–69. doi: 10.1111/jcmm.14203
22. Guo G, Meng Y, Tan W, Xia Y, Cheng C, Chen X, et al. Induction of apoptosis coupled to endoplasmic reticulum stress through regulation of CHOP and JNK in bone marrow mesenchymal stem cells from patients with systemic lupus erythematosus. *J Immunol Res.* (2015) 2015:183738. doi: 10.1155/2015/183738
23. Wolberg AS, Cushman M. Illustrated review article: a new format for disseminating scientific progress. *Res Pract Thromb Haemost.* (2018) 2:405–06. doi: 10.1002/rth2.12124
24. Miyazaki Y, Kaikita K, Endo M, Horio E, Miura M, Tsujita K, et al. C/EBP homologous protein deficiency attenuates myocardial reperfusion injury by inhibiting myocardial apoptosis and inflammation. *Arterioscler Thromb Vasc Biol.* (2011) 31:1124–32. doi: 10.1161/ATVBAHA.111.224519
25. Aronson JP, Katnani HA, Pomerantseva I, Shapir N, Tse H, Miari R, et al. Sustained intrathecal therapeutic protein delivery using genetically

transduced tissue implants in a freely moving rat model. *Int J Pharm.* (2017) 534:42–9. doi: 10.1016/j.ijpharm.2017.10.002
26. van Rijt WG, van Goor H, Ploeg RJ, Leuvenink HG. Erythropoietin-mediated protection in kidney transplantation: nonerythropoietic EPO derivatives improve function without increasing risk of cardiovascular events. *Transpl Int.* (2014) 27:241–8. doi: 10.1111/tri.12174
27. Uversky VN, Redwan EM. Erythropoietin and co.: intrinsic structure and functional disorder. *Mol Biosyst.* (2016) 13:56–72. doi: 10.1039/C6MB00657D
28. Zhang Y, Chen W, Wu Y, Yang B. Renoprotection and mechanisms of erythropoietin and its derivatives helix b surface peptide in kidney injuries. *Curr Protein Pept Sci.* (2017) 18:1183–90. doi: 10.2174/1389203717666160909144436
29. Yang B, Hosgood SA, Bagul A, Waller HL, Nicholson ML. Erythropoietin regulates apoptosis, inflammation and tissue remodelling via caspase-3 and IL-1beta in isolated hemoperfused kidneys. *Eur J Pharmacol.* (2011) 660:420–30. doi: 10.1016/j.ejphar.2011.03.044
30. Hu L, Yang C, Zhao T, Xu M, Tang Q, Yang B, et al. Erythropoietin ameliorates renal ischemia and reperfusion injury via inhibiting tubulointerstitial inflammation. *J Surg Res.* (2012) 176:260–6. doi: 10.1016/j.jss.2011.06.035
31. Forbes JA, Reig AS, Tomycz LD, Tulipan N. Intracranial hypertension caused by a depressed skull fracture resulting in superior sagittal sinus thrombosis in a pediatric patient: treatment with ventriculoperitoneal shunt insertion. *J Neurosurg Pediatr.* (2010) 6:23–8. doi: 10.3171/2010.3.PEDS09441
32. Brines M, Patel NS, Villa P, Brines C, Mennini T, De Paola M, et al. Nonerythropoietic, tissue-protective peptides derived from the tertiary structure of erythropoietin. *Proc Natl Acad Sci USA.* (2008) 105:10925–30. doi: 10.1073/pnas.0805594105
33. Yang C, Hosgood SA, Meeta P, Long Y, Zhu T, Nicholson ML, et al. Cyclic helix B peptide in preservation solution and autologous blood perfusate ameliorates ischemia-reperfusion injury in isolated porcine kidneys. *Transplant Direct.* (2015) 1:e6. doi: 10.1097/TXD.0000000000000515
34. Wu Y, Zhang J, Liu F, Yang C, Zhang Y, Liu A, et al. Protective effects of HBSP on ischemia reperfusion and cyclosporine a induced renal injury. *Clin Dev Immunol.* (2013) 2013:758159. doi: 10.1155/2013/758159
35. Li L, Lin M, Zhang L, Huang S, Hu C, Zheng L, et al. Cyclic helix B peptide protects HK2 cells from oxidative stress by inhibiting ER stress and activating Nrf2 signalling and autophagy. *Mol Med Rep.* (2017) 16:8055–61. doi: 10.3892/mmr.2017.7588
36. Liu A, Wu J, Yang C, Wu Y, Zhang Y, Zhao F, et al. TRPM7 in CHBP-induced renoprotection upon ischemia reperfusion-related injury. *Sci Rep.* (2018) 8:5510. doi: 10.1038/s41598-018-22852-2
37. Yang C, Zhang Y, Wang J, Li L, Wang L, Hu M, et al. A novel cyclic helix B peptide inhibits dendritic cell maturation during amelioration of acute kidney graft rejection through Jak-2/STAT3/SOCS1. *Cell Death Dis.* (2015) 6:e1993. doi: 10.1038/cddis.2015.338
38. Wang L, Mo Q, Wang J. MIrExpress: a database for gene coexpression correlation in immune cells based on mutual information and pearson correlation. *J Immunol Res.* (2015) 2015:140819. doi: 10.1155/2015/140819
39. Shu S, Zhu J, Liu Z, Tang C, Cai J, Dong Z. Endoplasmic reticulum stress is activated in post-ischemic kidneys to promote chronic kidney disease. *EBioMedicine.* (2018) 37:269–80. doi: 10.1016/j.ebiom.2018.10.006
40. Decuypere JP, Ceulemans LJ, Agostinis P, Monbaliu D, Naesens M, Pirenne J, et al. Autophagy and the kidney: implications for ischemia-reperfusion injury and therapy. *Am J Kidney Dis.* (2015) 66:699–709. doi: 10.1053/j.ajkd.2015.05.021
41. Yang C, Xu Z, Zhao Z, Li L, Zhao T, Peng D, et al. A novel proteolysis-resistant cyclic helix B peptide ameliorates kidney ischemia reperfusion injury. *Biochim Biophys Acta.* (2014) 1842:2306–17. doi: 10.1016/j.bbadis.2014.09.001
42. Yang C, Zhao T, Lin M, Zhao Z, Hu L, Jia Y, et al. Helix B surface peptide administered after insult of ischemia reperfusion improved renal function, structure and apoptosis through beta common receptor/erythropoietin receptor and PI3K/Akt pathway in a murine model. *Exp Biol Med.* (2013) 238:111–9. doi: 10.1258/ebm.2012.012185
43. Shang L, Dong P, Du L, Yang X, Wang H, Li S. SERP1 prevents hypoxia-reoxygenation-induced H9c2 apoptosis through activating JAK2/STAT3 pathway-dependent attenuation of endoplasmic reticulum stress. *Biochem Biophys Res Commun.* (2019) 508:256–62. doi: 10.1016/j.bbrc.2018.11.119
44. Choi AY, Choi JH, Hwang KY, Jeong YJ, Choe W, Yoon KS, et al. Correction to: licochalcone A induces apoptosis through endoplasmic reticulum stress via a phospholipase Cgamma1-, Ca(2+)-, and reactive oxygen species-dependent pathway in HepG2 human hepatocellular carcinoma cells. *Apoptosis.* (2019) 24:200–03. doi: 10.1007/s10495-018-1493-4
45. Bhavsar D, Subramanian K, Sethuraman S, Krishnan UM. Translational siRNA therapeutics using liposomal carriers: prospects & challenges. *Curr Gene Ther.* (2012) 12:315–32. doi: 10.2174/156652312802083611
46. Coselli JS, Amarasekara HS, Green SY, Price MD, Preventza O, de la Cruz KI, et al. Open repair of thoracoabdominal aortic aneurysm in patients 50 years old and younger. *Ann Thorac Surg.* (2017) 103:1849–57. doi: 10.1016/j.athoracsur.2016.09.058
47. Melk A, Baisantry A, Schmitt R. The yin and yang of autophagy in acute kidney injury. *Autophagy.* (2016) 12:596–7. doi: 10.1080/15548627.2015.1135284
48. Yang TY, Wu YJ, Chang CI, Chiu CC, Wu ML. The effect of bornyl cis-4-hydroxycinnamate on melanoma cell apoptosis is associated with mitochondrial dysfunction and endoplasmic reticulum stress. *Int J Mol Sci.* (2018) 19:1370. doi: 10.3390/ijms19051370
49. Mousavi Jarahi A, Keihani P, Vaziri E, Feizabadi M. Indicators of evaluating research at article level: recommendation for effective evaluation of APJCP' scientific performances. *Asian Pac J Cancer Prev.* (2018) 19:1151–54. doi: 10.22034/APJCP.2018.19.5.1151

Conflict of Interest: The authors declare that the research was conducted in the absence of any commercial or financial relationships that could be construed as a potential conflict of interest.

frontiers in Medicine

ORIGINAL RESEARCH
published: 20 March 2020
doi: 10.3389/fmed.2020.00095

Oral Administration of Si-Based Agent Attenuates Oxidative Stress and Ischemia-Reperfusion Injury in a Rat Model: A Novel Hydrogen Administration Method

Masataka Kawamura[1], Ryoichi Imamura[1], Yuki Kobayashi[2], Ayumu Taniguchi[1], Shigeaki Nakazawa[1], Taigo Kato[1], Tomoko Namba-Hamano[3], Toyofumi Abe[1], Motohide Uemura[1], Hikaru Kobayashi[2] and Norio Nonomura[1]*

[1] Department of Urology, Osaka University Graduate School of Medicine, Suita, Japan, [2] The Institute of Scientific and Industrial Research, Osaka University, Ibaraki, Japan, [3] Department of Nephrology, Osaka University Graduate School of Medicine, Suita, Japan

OPEN ACCESS

Edited by:
Songjie Cai,
Brigham and Women's Hospital,
United States

Reviewed by:
Bin Yang,
University of Leicester,
United Kingdom
Thierry Hauet,
University of Poitiers, France

***Correspondence:**
Ryoichi Imamura
imamura@uro.med.osaka-u.ac.jp

Specialty section:
This article was submitted to Nephrology, a section of the journal Frontiers in Medicine

Received: 04 January 2020
Accepted: 04 March 2020
Published: 20 March 2020

Citation:
Kawamura M, Imamura R, Kobayashi Y, Taniguchi A, Nakazawa S, Kato T, Namba-Hamano T, Abe T, Uemura M, Kobayashi H and Nonomura N (2020) Oral Administration of Si-Based Agent Attenuates Oxidative Stress and Ischemia-Reperfusion Injury in a Rat Model: A Novel Hydrogen Administration Method. Front. Med. 7:95. doi: 10.3389/fmed.2020.00095

Organ ischemia-reperfusion injury (IRI), which is unavoidable in kidney transplantation, induces the formation of reactive oxygen species and causes organ damage. Although the efficacy of molecular hydrogen (H_2) in IRI has been reported, oral intake of H_2-rich water and inhalation of H_2 gas are still not widely used in clinical settings because of the lack of efficiency and difficulty in handling. We successfully generated large quantities of H_2 molecules by crushing silicon (Si) to nano-sized Si particles (nano-Si) which were allowed to react with water. The nano-Si or relatively large-sized Si particles (large-Si) were orally administered to rats with renal IRI. Animals were divided into four groups: sham, IRI, IRI + nano-Si, and IRI + large-Si. The levels of serum creatinine and urine protein were significantly decreased 72 h following IRI in rats that were administered nano-Si. The levels of oxidative stress marker, urinary 8-hydroxydeoxyguanosine were also significantly decreased with the nano-Si treatment. Transcriptome and gene ontology enrichment analyses showed that the oral nano-Si intake downregulated the biological processes related to oxidative stress, such as immune response, cytokine production, and extrinsic apoptotic signaling pathway. Alterations in the regulation of a subset of genes in the altered pathways were validated by quantitative polymerase chain reaction. Furthermore, immunohistochemical analysis demonstrated that the nano-Si treatment alleviated interstitial macrophage infiltration and tubular apoptosis, implicating the anti-inflammatory and anti-apoptotic effects of nano-Si. In conclusion, renal IRI was attenuated by the oral administration of nano-Si, which should be considered as a novel H_2 administration method.

Keywords: silicon, ischemia reperfusion injury, hydrogen, oxidative stress, kidney, rat

INTRODUCTION

Ischemia-reperfusion injury (IRI), which is unavoidable in organ transplantation, is severely detrimental to renal graft function and survival. Prolonged time of cold ischemia during renal transplantation is associated with delayed graft function and decreased long-term graft survival (1, 2). One of the major events in ischemia reperfusion is the generation of cytotoxic oxygen radicals (3), increases in which lead to cellular injury by inducing DNA damage, protein oxidation, lipid peroxidation, and apoptosis (4).

Since the discovery of the selective antioxidant properties of molecular hydrogen (H_2) in 2007, multiple studies have shown its beneficial effects in diverse animal oxidative stress models *in vivo* (5–7). H_2 treatment has been shown to abrogate ischemia-reperfusion following warm and cold ischemia and has been identified as a potential therapy in improving kidney transplantation outcomes (8). Studies have explored several delivery systems for H_2 administration, including inhalation, oral intake of H_2-rich water, injection of H_2-rich saline, and direct incorporation (9). Nevertheless, to our knowledge, these methods are not widely used in clinical settings because of the lack of efficacy and difficulty in handling.

We have recently reported that nano-sized silicon (Si) particles (nano-Si) react with water in the pH range between 7.0 and 8.6, generating a large amount of H_2 (10). We have found that the H_2 generation rate strongly depended on the crystallite size of particles and pH of the water reacting with Si. In water with a pH of 8.0, nano-Si with a median diameter of 9.6 nm could generate up to 55 mL/g H_2 within 1 h, which corresponds to that contained in ∼3 L saturated H_2-rich water. Si and its oxide are non-poisonous materials and are therefore considered as appropriate for medical applications (11).

We hypothesized that oral administration of a diet containing nano-Si would react with water in the intestinal tract where alkaline pancreatic juices are secreted, thereby leading to the generation of H_2 and suppression of reactive oxygen species. Therefore, in the current study we investigated the potential of nano-Si in mitigating IRI *in vivo* and reducing oxidative stress and related biological processes. To that end, we administered a diet containing nano-Si or larger-sized Si particles (large-Si) with a minimum diameter of 1 μm in rats with renal IRI.

MATERIALS AND METHODS

Animals

All experiments were performed in male Sprague-Dawley rats weighing 170–190 g that were purchased from SLC Japan (Shizuoka, Japan) and maintained at the Institute of Experimental Animal Sciences of Osaka University Medical School. All animal studies were approved by the Osaka University Animal Research Committee and according to relevant regulatory standards.

Si Particles Containing Feed

As normal diet, we used AIN93M (Oriental Yeast Co., Ltd., Tokyo, Japan). In addition, we made special Si-based agent containing 1.0 wt.% nano-Si or large-Si particles in AIN93M, respectively. Before animal experiments, we examined the hydrogen production from the agent containing 1.0 wt.% nano-Si particles and water using a sensor gas chromatograph, SGHA-P2-A (FIS Inc., Hyogo, Japan).

Experimental Protocol

Experimental groups ($n = 6$ per group) were as follows: (i) sham operation (sham group), (ii) normal diet with IRI (IRI group), (iii) nano-Si-based agent diet with IRI (IRI + nano-Si group), and (iv) large-Si-based agent diet with IRI (IRI + large-Si group). The animals in the sham and IRI groups were fed a normal diet. The animals in the IRI + nano-Si and IRI + large-Si groups were fed a Si-based agent containing 1.0% nano-Si and large-Si in a diet, respectively. The Si-based agent was initiated at 6 weeks of age. Renal IRI or sham surgery was performed at 7 weeks of age, as previously described (12). Briefly, rats were anesthetized with isoflurane and placed on a heating pad to maintain body temperature during surgery. A midline abdominal incision was made, and left renal pedicles were isolated and clamped for 60 min. Complete reperfusion was visually confirmed after the clamp removal. After reperfusion of the left kidney, right nephrectomy was performed and the surgical wound was sutured. Sham surgery was performed in an identical fashion with the exception of renal pedicle clamping. The rats were euthanized 72 h after reperfusion, and blood, urine, and kidney samples were obtained.

Measurement of H_2 Concentration Diffused From Whole Blood Samples

After 1-week administration of the normal diet or the diet containing 1.0% nano-Si or large-Si, 200 μL whole blood samples were immediately collected into 20-mL glass tubes. The glass tubes were filled with fresh air before putting the samples, and the tops were covered using screw tops with attached silicon caps. Next, the tubes with the samples were placed for 30 min at room temperature, and 2 mL gas (vapor) were aspirated from the tube and injected into a sensor gas chromatography device, SGHA-P2-A. The H_2 concentrations in blood samples were adjusted to the H_2 concentrations in air which fluctuated daily.

Histological Analysis

For histological evaluation, the frozen renal sections extracted from rats were embedded in 4% paraformaldehyde. Histological sections were stained with hematoxylin and eosin and assessed by a transplant pathologist blinded to the conditions. Tubular damage was graded based on the following scale ranging from 0 to 5 by estimating the percentage of tubules in the corticomedullary junction showing epithelial necrosis, loss of nuclei, or cast formation: 0, none; 1, <10%; 2, 10–25%; 3, 26–50%; 4, 51–75%; and 5, >75%.

Measurement of Oxidative Damage

8-hydroxy-2′-deoxyguanosine (8-OHdG), a product of oxidative DNA damage, is widely used as a marker of oxidative stress. We measured urinary 8-OHdG levels using an enzyme-linked immunosorbent assay kit (Japan Institute for the Control of

Aging, Shizuoka, Japan). A monoclonal antibody against 8-OHdG and urine samples or standards were added to microtiter plates precoated with 8-OHdG. An enzyme-labeled secondary antibody was then added to the plates and allowed to bind to the monoclonal 8-OHdG antibody on the coated plates. The unbound enzyme-labeled secondary antibody fraction was removed by washing, and a chromatic substrate was added for color development. The color reaction was terminated, and the absorbance at 450 nm was measured by a microplate reader. Malondialdehyde (MDA) is used as an indicator of free radical-mediated lipid peroxidation. We measured serum malondialdehyde levels using the OxiSelect TBARS assay kit (Cell Biolabs, San Diego, CA, USA). Briefly, 100 mL of serum samples or a solution with a known MDA concentration were mixed with 100 mL SDS lysis solution and 250 mL thiobarbituric acid solution and heated at 95°C in a water bath for 1 h. After cooling, the samples were centrifuged to collect the supernatants, which were mixed with n-butanol followed by centrifugation. The butanol fractions were transferred to 96-well microplates and the change in color was determined at 532 nm using a spectrophotometric plate reader (ELx808, Bio Tek Instruments).

RNA Microarray

Total RNA from postoperative frozen kidneys was isolated by homogenization followed by the RNeasy Plus universal kit (Qiagen, Hilden, Germany). RNA was treated with DNAse and reverse transcribed to cDNA by the PrimeScript RT reagent kit (Takara Bio, Shiga, Japan). RNA quality was assessed using a 2100 Bioanalyzer (Agilent Technologies, Santa Clara, CA, USA) and the RNA 6000 Nano kit (Caliper Life Sciences, CA, USA). The RNA samples isolated from the IRI and IRI + nano-Si groups ($n = 2$ per group) were hybridized to Rat GeneChip Clariom^{TM} S array (Applied Biosystems, CA, USA). The hybridization and microarray scanning procedures were performed according to the Whole Transcript (WT) expression array user guide. After the probe set signal integration and background correction, the files were transferred to the Applied Biosystems Transcriptome Analysis Console software to analyze gene expression patterns. The threshold for upregulated and downregulated genes was set as a fold change of $\geq$1.5 with a $p < 0.05$.

Gene Ontology and Pathway Enrichment Analyses

Functional enrichment analysis was performed by Metascape (http://metascape.org) according to the genes assigned to each biological function. The resulting gene ontology terms with a $p < 0.05$ were considered significantly enriched among the differentially expressed genes.

Quantitative Real-Time Reverse-Transcriptase Polymerase Chain Reaction

Quantitative real-time reverse-transcriptase polymerase chain reaction was performed using TB Green Premix Ex Taq II and a Thermal Cycler Dice Real Time System TP800 (Takara). The primer sequences were as follows: C-C motif chemokine ligand 2 (*Ccl2*): forward: CTATGCAGGTCTCTGTCACGCTTC, reverse: CAGCCGACTCATTGGGATCA; interleukin 6 (*Il6*): forward: ATTGTATGAACAGCGATGATGCAC, reverse: CCAGGTAGAAACGGAACTCCAGA; intercellular adhesion molecule 1 (*Icam1*): forward: TGTATGAACTGAGCAATGTGCAAGA, reverse: CACCTGGCAGCGTAGGGTAA; inducible nitric oxide synthase (*iNos*): forward: CTCACTGTGGCTGTGGTCACCTA, reverse: GGGTCTTCGGGCTTCAGGTTA; tissue inhibitor of metalloproteinase-1 (*Timp1*): forward: CGAGACCACCTTATACCAGCGTTA, reverse: TGATGTGCAAATTTCCGTTCC; phorbol-12-myristate-13-acetate-induced protein 1 (*Pmaip1*): forward: GGAGTGCACCGGACATAACTG, reverse: TGCCGTAAATTCACTTTGTCTCCA; catalase (*Cat*): forward: GAACATTGCCAACCACCTGAAAG, reverse: GTAGTCAGGGTGGACGTCAGTGAA; peroxisome proliferator-activated receptor alpha (*PPARa*): forward: GGCAATGCACTGAACATCGAG, reverse: GCCGAATAGTTCGCCGAAAG; and beta-actin (*Actb*): forward: GGAGATTACTGCCCTGGCTCCTA, reverse: GACTCATCGTACTCCTGCTTGCTG. We used the $^{\Delta\Delta}$ cycle threshold technique to calculate the cDNA content of each sample. Target gene signals were normalized to *Actb*. Melting curve analysis showed a single dissociation peak for all polymerase chain reaction gene products, confirming the specificity of the reactions.

Immunohistochemical Analysis

The terminal deoxynucleotidyl transferase dUTP nick end labeling assay was used to assess apoptosis in frozen renal sections, according to the manufacturer's instructions (Japan Institute for the Control of Aging). In addition, frozen sections were incubated with an antibody against the macrophage surface molecule CD68. Anti-CD68 antibody was bound to a biotinylated secondary antibody which reacted with several peroxidase-conjugated streptavidin molecules using the LSAB + System-HRP kit (Dako, Copenhagen, Denmark). The sections were then visualized with the DAB chromogen. The images were captured using a BZ-X700 (Keyence, Osaka, Japan) microscope and the areas or cells with positive immunohistochemical signals were assessed using the software of the BZ-x700 microscope. In TUNEL staining, the ratio of the number of positive cells to total cells in the entire area including interstitium was calculated, and in the staining for CD68, the ratio of the area of the positive cells to the entire area was calculated.

Statistical Analysis

GraphPad Prism version 5.0 (GraphPad, San Diego, CA, USA) was used for all statistical analyses. Multiple groups were compared using one-way analysis of variance with Tukey's *post-hoc* multiple comparison test. Results were expressed as means ± standard error of the mean. Differences with a $p < 0.05$ were considered to indicate statistical significance.

RESULTS

Oral Nano-Si Administration Preserves Renal Function and Reduces Tubular Damage Due to IRI

We first confirmed that oral administration of nano-Si could generate H_2 in rats in the absence of IRI by gas chromatography (**Figure 1**). Compared with those maintained on a normal

diet, the H_2 concentrations diffused from the whole blood samples were significantly increased in those administered a diet comprising nano-Si but not large-Si. Next, we evaluated renal function by measuring serum creatinine and urine protein levels at 72 h after surgery. As shown in **Figures 2A,B**, the serum creatinine and urine protein levels were significantly decreased in the IRI + nano-Si group compared with the IRI group whereas there was no significant decrease in either parameter in the IRI + large-Si group compared with the IRI group. Additionally, the structural injury in the renal corticomedullary junction such as epithelial necrosis, loss of nuclei, and cast formation occurred as a result of IRI. Consistent with the detected changes in renal function, the kidneys in the IRI + nano-Si group had significantly less tubular damage than those in the IRI and IRI + large-Si groups, as evidenced by the tubular injury score (**Figures 2C,D**).

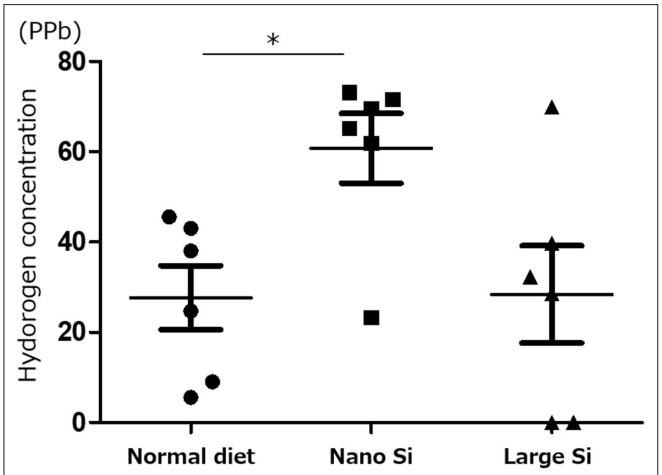

FIGURE 1 | Measurement of hydrogen (H_2) concentration diffused from whole blood samples using gas chromatography. All H_2 concentrations were adjusted to the H_2 concentration in air. Bars represent means ± standard error of the mean. $^*p < 0.05$, $n = 6$.

Effect of Nano-Si Treatment on Oxidative Stress

8-OHdG and malondialdehyde are major forms of DNA and lipid damage induced by reactive oxygen species, respectively. Therefore, we next measured the urinary 8-OHdG and serum malondialdehyde levels to assess oxidative stress. There was a significant reduction in oxidative DNA damage assessed by urinary 8-OHdG 72 h after surgery in the IRI + nano-Si group (**Figure 3A**). Additionally, the serum malondialdehyde levels were significantly decreased in the IRI + nano-Si group compared with the IRI + large-Si group (**Figure 3B**). Albeit not significant, there was a difference in lipid peroxidation between the IRI and IRI + nano-Si groups.

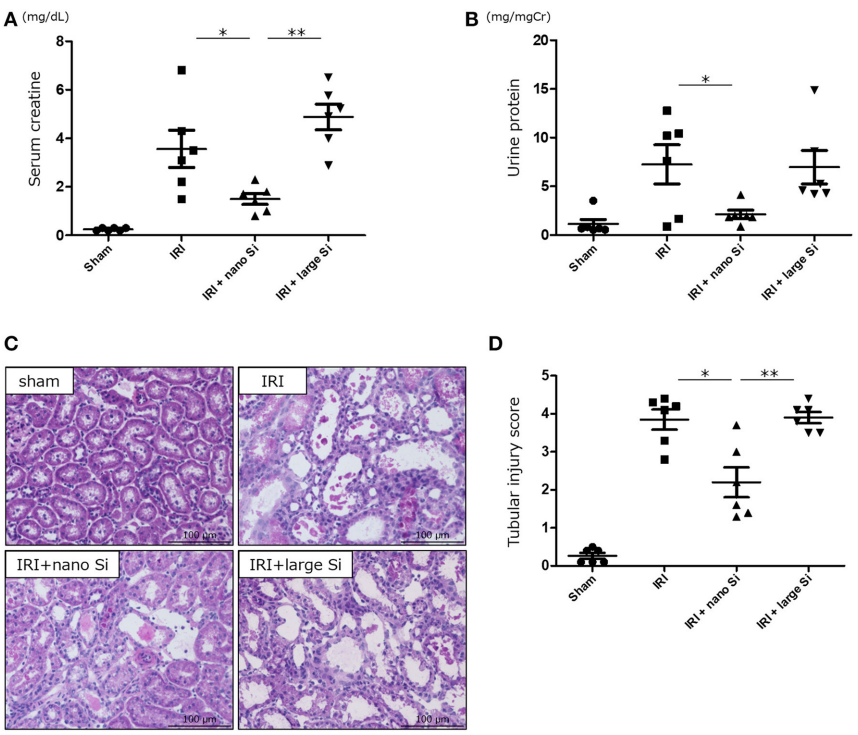

FIGURE 2 | Oral administration of nano-sized silicon (Si) particles (nano-Si) improves renal function and tubular damage following ischemia-reperfusion injury (IRI). Serum creatinine **(A)** and urine protein levels **(B)** at 72 h after surgery for ischemia-reperfusion in animals receiving normal diet (IRI group) or a diet comprising nano-Si (IRI + nano-Si group) or large-sized Si (IRI + large-Si group) as well as those undergoing sham surgery (sham group). **(C)** Representative images of renal sections stained with hematoxylin and eosin at 72 h after surgery in the sham, IRI, IRI + nano-Si, and IRI + large-Si groups. **(D)** Semiquantitative analysis of the images using tubular injury score. Bars represent means ± standard error of the mean. $^*p < 0.05$, $^{**}p < 0.01$, $n = 6$.

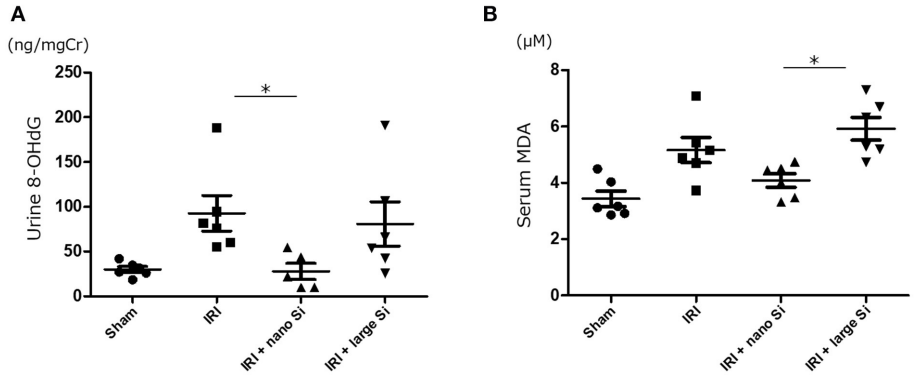

FIGURE 3 | Effect of nano-Si treatment on markers of oxidative stress. **(A)** Urine 8-hydroxy-2'-deoxyguanosine (8-OHdG) and **(B)** serum malondialdehyde (MDA) levels at 72 h after surgery in the sham, IRI, IRI + nano-Si, and IRI + large-Si groups. Bars represent means ± standard error of the mean. *$p < 0.05$, $n = 6$.

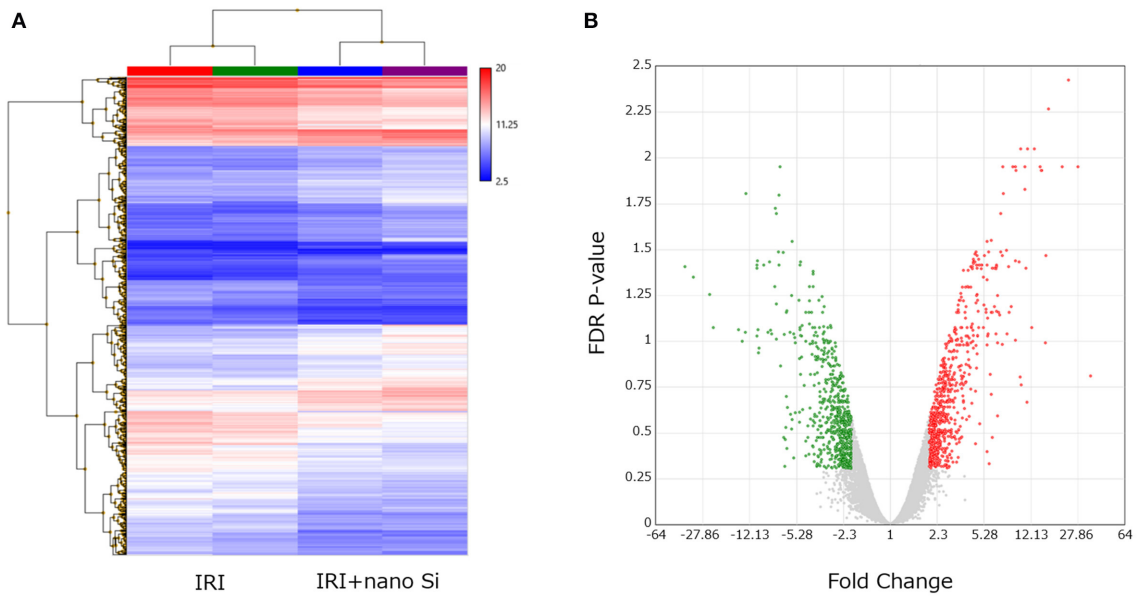

FIGURE 4 | Changes in the renal transcriptome at 72 h after IRI. **(A)** Hierarchical clustering of each sample dataset by renal tissue microarray. **(B)** Volcano plot showing the upregulated and downregulated genes in the kidneys of rats with IRI treated with nano-Si compared to those maintained with a normal diet (fold change, >2.0 or <2.0; $p < 0.05$). $n = 2$.

Effect of Nano-Si Treatment on Renal Transcriptome and Biological Functions

Renal RNA microarray analysis was performed to compare the IRI and the IRI + nano-Si groups for changes in renal transcriptomes of rats with IRI treated with nano-Si (**Figure 4A**). As shown in **Figure 4B**, we identified 666 downregulated genes and 703 upregulated genes (**Figure 4B**). We first performed gene ontology and pathway enrichment analysis of the 666 downregulated genes. **Figure 5A** lists the top 20 downregulated biological processes with *p* values, including pathways associated with immune response such as cytokine production and phagocytosis as well as the extrinsic apoptotic pathway. The gene ontology and pathway enrichment analysis of the 703 upregulated genes revealed that the top 20 upregulated pathways included primarily the processes related to some kind of amino acid metabolism such as fatty acids (**Figure 5B**). The biological processes involved in peroxisome were also ranked in the top 20 upregulated pathways.

Validation of Changes in Gene Expression Levels by Quantitative Polymerase Chain Reaction

Real-time reverse-transcription polymerase chain reaction was performed to validate the changes in expression of genes related to the biological processes modulated by nano-Si administration which we identified in the gene enrichment analysis (**Figure 6**). We assessed the expression levels of pro-inflammatory genes including *Cccl2*, *Il6*, and *Icam1*; those involved in extrinsic

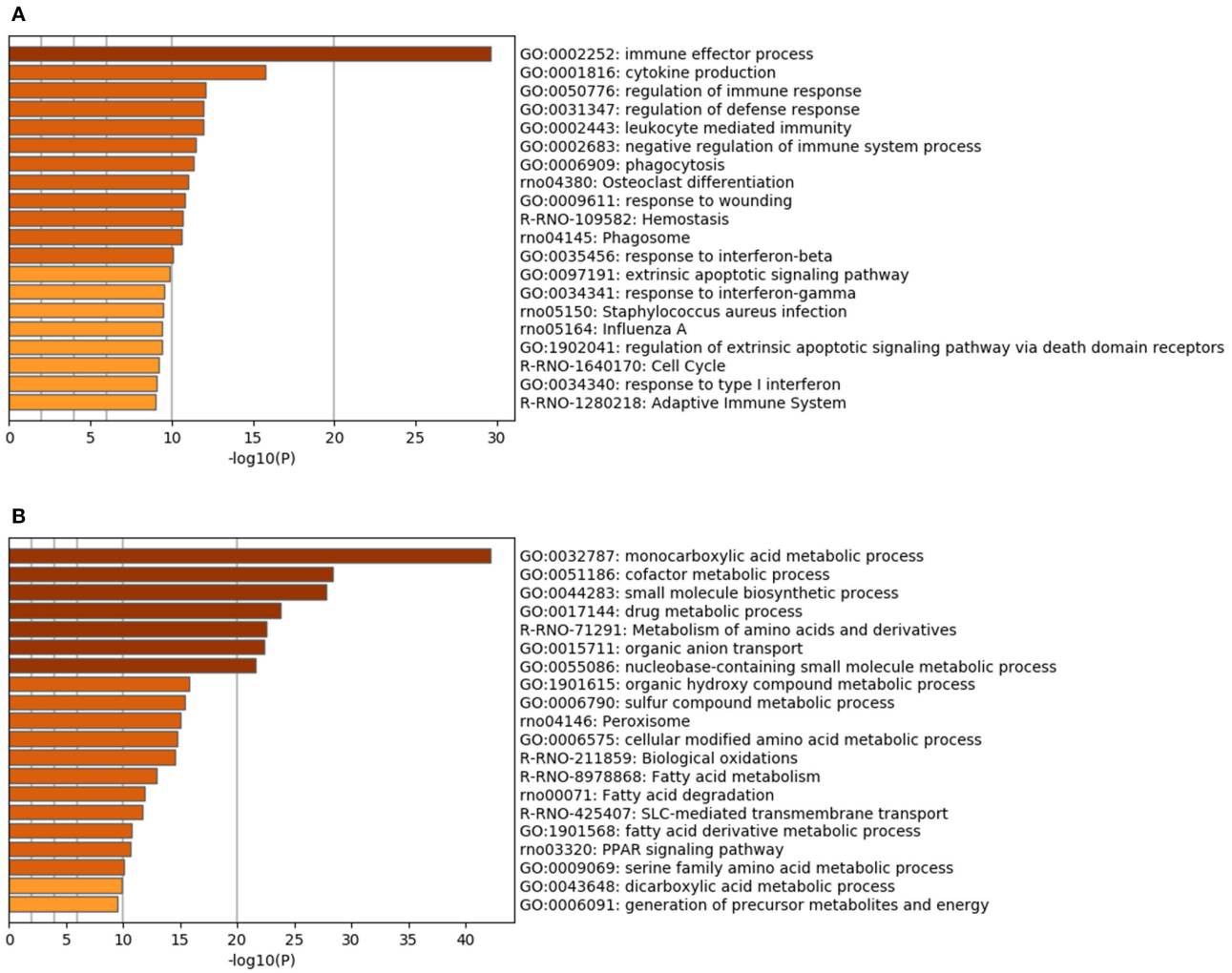

FIGURE 5 | Functional enrichment analysis of the genes modulated with the nano-Si treatment. Top 20 biological processes with upregulated **(A)** and downregulated **(B)** genes, with *p*-values, in the renal tissue samples at 72 h following IRI.

apoptotic signaling pathway including *Timp1* and *Pmaip1*; *iNOS* which is induced by oxidative stress; and those induced by the peroxisome including *Cat* and *PPARa*. **Figure 6** shows the fold changes in mRNA levels of the indicated genes in the IRI + nano-Si group compared with the sham group, normalized to *Actb*. Overall, the oral nano-Si treatment of rats with IRI led to significant reductions in the mRNA levels of *Cccl2*, *Il6*, *Timp1*, and *iNos* compared with the IRI group. Conversely, the expression levels of *Cat* and *PPARa* were significantly decreased in the kidneys of the IRI group compared with the sham group and increased in the IRI + nano-Si group compared with the IRI group.

Nano-Si Treatment Alleviates Interstitial Macrophage Infiltration and Tubular Apoptosis

Finally, we evaluated interstitial infiltration of macrophages and tubular apoptosis in the kidneys of rats with IRI that were treated with nano-Si (**Figures 7A,B**). Immunohistochemical analysis demonstrated that the nano-Si treatment led to a significant reduction in the CD68-positive macrophage infiltration at both the corticomedullary junction and the cortex of kidneys following IRI compared with the sham and the IRI + large-Si groups (**Figure 7C**). Moreover, the tubular apoptosis observed in the IRI and IRI + large-Si groups was significantly inhibited by the oral nano-Si administration (**Figure 7D**).

DISCUSSION

H_2 is a noble gas that eliminates reactive oxygen species that cause IRI. Studies on the role of H_2 in biology and medicine have been rapidly expanding since the first report of Ohsawa et al. (5) demonstrating that H_2 gas displays antioxidant properties that can protect the brain against IRI by selectively neutralizing hydroxyl radicals. Several delivery systems for H_2 administration that have been explored include inhalation using a ventilator

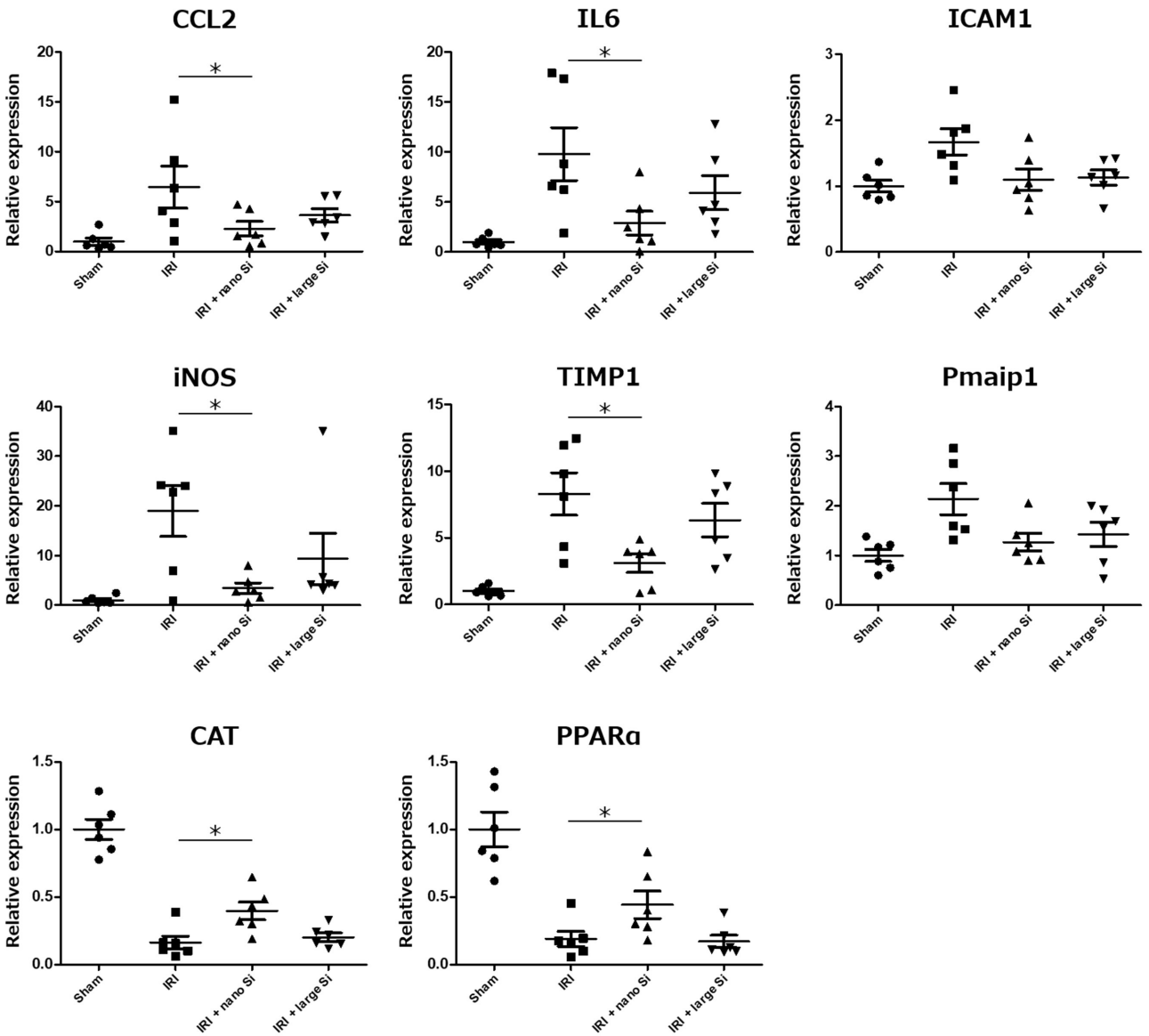

FIGURE 6 | Relative mRNA expression levels of eight genes associated with inflammation, apoptosis, and oxidative stress determined using real-time reverse-transcription polymerase chain reaction in the renal tissue samples at 72 h following surgery in the sham, IRI, IRI + nano-Si, and IRI + large-Si groups. *$p <$ 0.05, $n = 6$.

circuit, facemask, or nasal cannula, which has been reported to reduce IRI in the brain (13), heart (14), lungs (15), liver (16), skin (17), and intestines (6). Although inhaled H_2 gas may act rapidly, this method might be impractical in daily clinical use or unsuitable for continuous consumption for preventive use, because of the difficulty in handling high-pressure H_2 gas.

In contrast, oral intake of solubilized H_2 in H_2-rich water is easy to use as a portable and safe method of delivering molecular H_2 (18). However, H_2 in water evaporates over time, and H_2 might be lost before reaching the stomach or the intestines (9). Administration of H_2 via injectable H_2-rich saline can potentially deliver more precise H_2 concentrations and has been demonstrated to attenuate IRI in brain in neonates (19), heart (20), lungs (21), liver (22), intestines (23, 24), and kidneys (25) in animal models of oxidative stress. Nevertheless, the amount of H_2 dissolved in solutions is limited: up to 0.8 mM (1.6 mg/L) H_2 can be dissolved in water under atmospheric pressure at room temperature (26).

We have developed a new strategy to successfully generate large amounts of H_2 molecules by crushing Si to nano-sized particles and allowing these nanoparticles to react with alkaline water. Si is not an essential nutrient for mammals, and the underlying biological function remains unclear; however, oral Si supplementation for mammals is reportedly harmless (11).

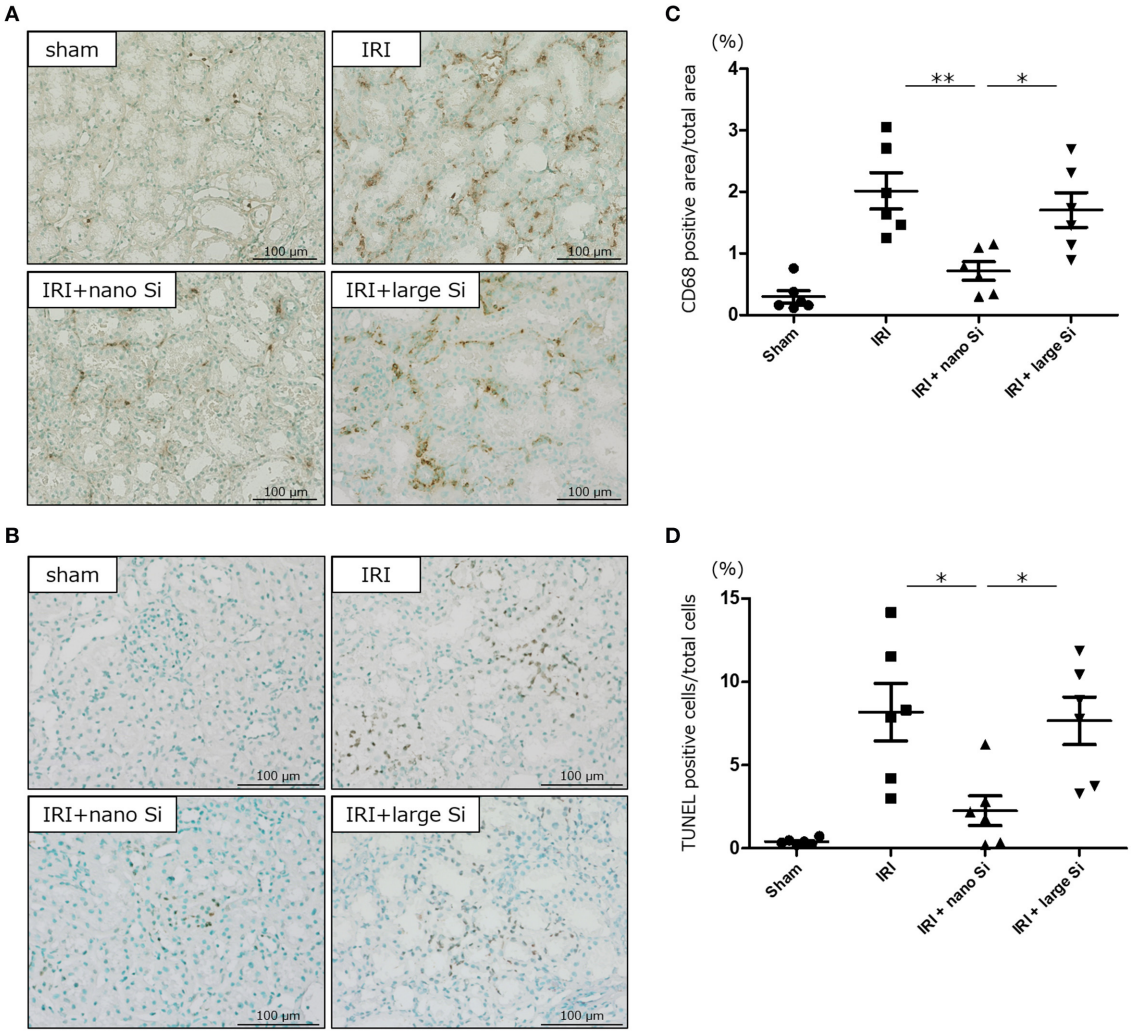

FIGURE 7 | Oral administration of nano-Si particles alleviates interstitial macrophage infiltration and tubular apoptosis. Representative images of **(A)** CD68 staining and **(B)** terminal deoxynucleotidyl transferase dUTP nick end labeling (TUNEL) of the renal tissues at 72 h after surgery in the sham, IRI, IRI + nano-Si, and IRI + large-Si groups. **(C)** Quantitative analysis of the images showing changes in the ratio of CD68-positive areas to the total area of the section. **(D)** Quantitative analysis of the images showing changes in the ratio of TUNEL-positive cells to the total number of cells. Bars represent means ± standard error of the mean. $^{*}p < 0.05$, $^{**}p < 0.01$, $n = 6$.

We therefore evaluated the efficacy of nano-Si administration in an *in vivo* model of acute renal IRI. Our serological, urinary, and histological analyses showed the deterioration of renal function and damage to tubular epithelial cells following ischemia-reperfusion surgery. In contrast, the administration of nano-Si-containing diet significantly reduced these changes. This benefit of nano-Si is considered to be due to the generation of H_2 reacting with alkaline water such as that found in intestinal fluids *in vivo*. In support of this hypothesis, the diet containing relatively larger Si particles with poor H_2 generation efficiency, which was administered following ischemia-reperfusion surgery using the same dosing schedule, did not lead to a similar effect.

Given that H_2 molecules can mitigate IRI by selectively removing reactive oxygen species that lead to oxidative damage to DNA, lipids, and proteins, we evaluated oxidative stress by monitoring urinary 8-OHdG and serum malondialdehyde levels. 8-OHdG and malondialdehyde, which are peroxidation products of DNA and lipids, respectively, are widely used as oxidative stress markers (27–29). The treatment with nano-Si led to a reduction in the increased urinary 8-OHdG levels due to IRI. Conversely, albeit not reaching statistical significance, we also found that there was a difference in the serum malondialdehyde levels between the IRI and IRI + nano-Si groups.

H_2 has been shown to exert anti-inflammatory and anti-apoptotic effects by suppressing oxidative stress (30). In fact, specific pathways and modulators underlying these effects have not been fully elucidated. In the present study, we demonstrated that the nano-Si treatment inhibited the

infiltration of macrophages into the tubulointerstitium and the upregulated expression of inflammation-related genes such as *Il6* and *Ccl2* in renal tissue. Macrophages are critical early initiators of innate immunity with important roles in inflammation following ischemia-reperfusion (31, 32). Additionally, activated endothelial cells and tubular epithelial cells produce cytokines and chemokines that induce inflammatory cell infiltration. We also demonstrated that the administration of the nano-Si reduced apoptosis in tubular epithelial cells after the induction of ischemia by hypoxia using terminal deoxynucleotidyl transferase dUTP nick end labeling assay to detect early apoptosis based on the presence of DNA fragmentation (33). Overall, these results suggest that the reduction in oxidative stress leads to anti-inflammatory and anti-apoptotic effects by regulating the expression levels of various genes. The proteins encoded by these genes, which may not be primary responders to H_2, might indirectly act to enable the various beneficial effects of nano-Si.

In conclusion, we demonstrated that the nano-Si treatment protected IRI rat kidneys, at least partially, via the reduction in oxidative stress through oral intake of nano-Si. To our knowledge, these findings are the first evidence for the protective effect with nano-Si in renal IRI. Given our results, the clinical use of nano-Si in kidney allograft donors prior to kidney transplantation should be considered as a means to improve kidney allograft outcomes. Thus, further investigation is needed to establish the feasibility and efficacy of using nano-Si in this way in the clinical setting.

DATA AVAILABILITY STATEMENT

The datasets generated for this study can be found on ArrayExpress, accession number E-MTAB-8687.

ETHICS STATEMENT

The animal study was reviewed and approved by Osaka University Animal Research Committee.

AUTHOR CONTRIBUTIONS

MK and RI designed, performed, and interpreted all the experiments. YK and HK developed and offered the experimental materials. Histological and immunohistochemical sections were assessed by TN-H. AT, SN, and TK participated in the interpretation of data and editing of the manuscript. TA, MU, and NN interpreted the data, edited, and finalized the manuscript.

FUNDING

This research was supported by Grants-in-aid for Scientific Research (18K16697) and Center of Innovation Program (JPMJCE1310).

ACKNOWLEDGMENTS

The authors deeply appreciate M. Tsuchiya and A. Yasumoto for technical assistance with the experiments.

REFERENCES

1. Ojo AO, Wolfe RA, Held PJ, Port FK, Schmouder RL. Delayed graft function: risk factors and implications for renal allograft survival. *Transplantation*. (1997) 63:968–74. doi: 10.1097/00007890-199704150-00011
2. Shoskes DA, Halloran PF. Delayed graft function in renal transplantation: etiology, management and long-term significance. *J Urol*. (1996) 155:1831–40. doi: 10.1016/s0022-5347(01)66023-3
3. Noiri E, Nakao A, Uchida K, Tsukahara H, Ohno M, Fujita T, et al. Oxidative and nitrosative stress in acute renal ischemia. *Am J Physiol Renal Physiol*. (2001) 281:F948–57. doi: 10.1152/ajprenal.2001.281.5.F948
4. Rodrigo R, Bosco C. Oxidative stress and protective effects of polyphenols: comparative studies in human and rodent kidney. A review. *Comp Biochem Physiol C Toxicol Pharmacol*. (2006) 142:317–27. doi: 10.1016/j.cbpc.2005.11.002
5. Ohsawa I, Ishikawa M, Takahashi K, Watanabe M, Nishimaki K, Yamagata K, et al. Hydrogen acts as a therapeutic antioxidant by selectively reducing cytotoxic oxygen radicals. *Nat Med*. (2007) 13:688–94. doi: 10.1038/nm1577
6. Buchholz BM, Kaczorowski DJ, Sugimoto R, Yang R, Wang Y, Billiar TR, et al. Hydrogen inhalation ameliorates oxidative stress in transplantation induced intestinal graft injury. *Am J Transplant*. (2008) 8:2015–24. doi: 10.1111/j.1600-6143.2008.02359.x
7. Wang F, Yu G, Liu SY, Li JB, Wang JF, Bo LL, et al. Hydrogen-rich saline protects against renal ischemia/reperfusion injury in rats. *J Surg Res*. (2011) 167:e339–44. doi: 10.1016/j.jss.2010.11.005
8. Abe T, Li XK, Yazawa K, Hatayama N, Xie L, Sato B, et al. Hydrogen-rich University of Wisconsin solution attenuates renal cold ischemia-reperfusion injury. *Transplantation*. (2012) 94:14–21. doi: 10.1097/TP.0b013e318255f8be
9. Ge L, Yang M, Yang NN, Yin XX, Song WG. Molecular hydrogen: a preventive and therapeutic medical gas for various diseases. *Oncotarget*. (2017) 8:102653–73. doi: 10.18632/oncotarget.21130
10. Kobayashi Y, Matsuda S, Imamura K, Kobayashi H. Hydrogen generation by reaction of Si nanopowder with neutral water. *J Nanopart Res*. (2017) 19:176. doi: 10.1007/s11051-017-3873-z
11. Domingo JL, Gomez M, Colomina MT. Oral silicon supplementation: an effective therapy for preventing oral aluminum absorption and retention in mammals. *Nutr Rev*. (2011) 69:41–51. doi: 10.1111/j.1753-4887.2010.00360.x
12. Tsutahara K, Okumi M, Kakuta Y, Abe T, Yazawa K, Miyagawa S, et al. The blocking of CXCR3 and CCR5 suppresses the infiltration of T lymphocytes in rat renal ischemia reperfusion. *Nephrol Dial Transplant*. (2012) 27:3799–806. doi: 10.1093/ndt/gfs360
13. Cui J, Chen X, Zhai X, Shi D, Zhang R, Zhi X, et al. Inhalation of water electrolysis-derived hydrogen ameliorates cerebral ischemia-reperfusion injury in rats—a possible new hydrogen resource for clinical use. *Neuroscience*. (2016) 335:232–41. doi: 10.1016/j.neuroscience.2016.08.021
14. Gao Y, Yang H, Chi J, Xu Q, Zhao L, Yang W, et al. Hydrogen gas attenuates myocardial ischemia reperfusion injury independent of postconditioning in rats by attenuating endoplasmic reticulum stress-induced autophagy. *Cell Physiol Biochem*. (2017) 43:1503–14. doi: 10.1159/000481974
15. Zhang J, Zhou H, Liu J, Meng C, Deng L, Li W. Protective effects of hydrogen inhalation during the warm ischemia phase against lung ischemia-reperfusion injury in rat donors after cardiac death. *Microvasc Res*. (2019) 125:103885. doi: 10.1016/j.mvr.2019.103885
16. Li H, Chen O, Ye Z, Zhang R, Hu H, Zhang N, et al. Inhalation of high concentrations of hydrogen ameliorates liver ischemia/reperfusion injury through A2A receptor mediated PI3K-Akt pathway. *Biochem Pharmacol*. (2017) 130:83–92. doi: 10.1016/j.bcp.2017.02.003

17. Fang W, Wang G, Tang L, Su H, Chen H, Liao W, et al. Hydrogen gas inhalation protects against cutaneous ischaemia/reperfusion injury in a mouse model of pressure ulcer. *J Cell Mol Med*. (2018) 22:4243–52. doi: 10.1111/jcmm.13704
18. Nagata K, Nakashima-Kamimura N, Mikami T, Ohsawa I, Ohta S. Consumption of molecular hydrogen prevents the stress-induced impairments in hippocampus-dependent learning tasks during chronic physical restraint in mice. *Neuropsychopharmacology*. (2009) 34:501–8. doi: 10.1038/npp.2008.95
19. Cai J, Kang Z, Liu K, Liu W, Li R, Zhang JH, et al. Neuroprotective effects of hydrogen saline in neonatal hypoxia-ischemia rat model. *Brain Res*. (2009) 1256:129–37. doi: 10.1016/j.brainres.2008.11.048
20. Sun Q, Kang Z, Cai J, Liu W, Liu Y, Zhang JH, et al. Hydrogen-rich saline protects myocardium against ischemia/reperfusion injury in rats. *Exp Biol Med*. (2009) 234:1212–9. doi: 10.3181/0812-rm-349
21. Mao YF, Zheng XF, Cai JM, You XM, Deng XM, Zhang JH, et al. Hydrogen-rich saline reduces lung injury induced by intestinal ischemia/reperfusion in rats. *Biochem Biophys Res Commun*. (2009) 381:602–5. doi: 10.1016/j.bbrc.2009.02.105
22. Lu Z, Lin Y, Peng B, Bao Z, Niu K, Gong J. Hydrogen-rich saline ameliorates hepatic ischemia-reperfusion injury through regulation of endoplasmic reticulum stress and apoptosis. *Dig Dis Sci*. (2017) 62:3479–86. doi: 10.1007/s10620-017-4811-8
23. Wu MJ, Chen M, Sang S, Hou LL, Tian ML, Li K, et al. Protective effects of hydrogen rich water on the intestinal ischemia/reperfusion injury due to intestinal intussusception in a rat model. *Med Gas Res*. (2017) 7:101–6. doi: 10.4103/2045-9912.208515
24. Shigeta T, Sakamoto S, Li XK, Cai S, Liu C, Kurokawa R, et al. Luminal injection of hydrogen-rich solution attenuates intestinal ischemia-reperfusion injury in rats. *Transplantation*. (2015) 99:500–7. doi: 10.1097/tp.0000000000000510
25. Shingu C, Koga H, Hagiwara S, Matsumoto S, Goto K, Yokoi I, et al. Hydrogen-rich saline solution attenuates renal ischemia-reperfusion injury. *J Anesth*. (2010) 24:569–74. doi: 10.1007/s00540-010-0942-1
26. Ohta S. Molecular hydrogen as a novel antioxidant: overview of the advantages of hydrogen for medical applications. *Methods Enzymol*. (2015) 555:289–317. doi: 10.1016/bs.mie.2014.11.038
27. Kato S, Yoshimura K, Kimata T, Mine K, Uchiyama T, Kaneko K. Urinary 8-hydroxy-2'-deoxyguanosine: a biomarker for radiation-induced oxidative DNA damage in pediatric cardiac catheterization. *J Pediatr*. (2015) 167:1369–74.e1. doi: 10.1016/j.jpeds.2015.07.042
28. Wu LL, Chiou CC, Chang PY, Wu JT. Urinary 8-OHdG: a marker of oxidative stress to DNA and a risk factor for cancer, atherosclerosis and diabetics. *Clin Chim Acta*. (2004) 339:1–9. doi: 10.1016/j.cccn.2003.09.010
29. Tsikas D. Assessment of lipid peroxidation by measuring malondialdehyde (MDA) and relatives in biological samples: analytical and biological challenges. *Anal Biochem*. (2017) 524:13–30. doi: 10.1016/j.ab.2016.10.021
30. Ichihara M, Sobue S, Ito M, Ito M, Hirayama M, Ohno K. Beneficial biological effects and the underlying mechanisms of molecular hydrogen—comprehensive review of 321 original articles. *Med Gas Res*. (2015) 5:12. doi: 10.1186/s13618-015-0035-1
31. Day YJ, Huang L, Ye H, Linden J, Okusa MD. Renal ischemia-reperfusion injury and adenosine 2A receptor-mediated tissue protection: role of macrophages. *Am J Physiol Renal Physiol*. (2005) 288:F722–31. doi: 10.1152/ajprenal.00378.2004
32. Lee HT, Kim M, Kim M, Kim N, Billings FT, D'Agati VD, et al. Isoflurane protects against renal ischemia and reperfusion injury and modulates leukocyte infiltration in mice. *Am J Physiol Renal Physiol*. (2007) 293:F713–22. doi: 10.1152/ajprenal.00161.2007
33. Daemen MA, van 't Veer C, Denecker G, Heemskerk VH, Wolfs TG, Clauss M, et al. Inhibition of apoptosis induced by ischemia-reperfusion prevents inflammation. *J Clin Invest*. (1999) 104:541–9. doi: 10.1172/jci6974

Conflict of Interest: The authors declare that the research was conducted in the absence of any commercial or financial relationships that could be construed as a potential conflict of interest.

frontiers in Medicine

REVIEW
published: 24 March 2020
doi: 10.3389/fmed.2020.00092

The Role of Immune Modulation in Pathogenesis of IgA Nephropathy

Sheng Chang[1,2] *and Xiao-Kang Li*[2,3]*

[1] Institute of Organ Transplantation, Tongji Hospital, Tongji Medical College, Huazhong University of Science and Technology, Key Laboratory of Organ Transplantation, Ministry of Education NHC Key Laboratory of Organ Transplantation Key Laboratory of Organ Transplantation, Chinese Academy of Medical Sciences, Wuhan, China, [2] Division of Transplantation Immunology, National Research Institute for Child Health and Development, Tokyo, Japan, [3] Department of Hepatobiliary and Pancreatic Surgery, The First Affiliated Hospital of Zhengzhou University, Zhengzhou, China

IgA nephropathy (IgAN) is the most prevalent primary glomerulonephritis worldwide, with diverse clinical manifestations characterized by recurrent gross hematuria or microscopic hematuria, and pathological changes featuring poorly O-galactosylated IgA1 deposition in the glomerular mesangium. Pathogenesis has always been the focus of IgAN studies. After 50 years of research, most scholars agree that IgAN is a group of clinicopathological syndromes with certain common immunopathological characteristics, and multiple mechanisms are involved in its pathogenesis, including immunology, genetics, and environmental or nutritional factors. However, the precise pathogenetic mechanisms have not been fully determined. One hypothesis about the pathogenesis of IgAN suggests that immunological factors are engaged in all aspects of IgAN development and play a critical role. A variety of immune cells (e.g., dendritic cells, NK cells, macrophages, T-lymphocyte subsets, and B-lymphocytes, etc.) and molecules (e.g., IgA receptors, Toll-like receptors, complements, etc.) in innate and adaptive immunity are involved in the pathogenesis of IgAN. Moreover, the abnormality of mucosal immune regulation is the core of IgAN immunopathogenesis. The roles of tonsil immunity or intestinal mucosal immunity, which have received more attention in recent years, are supported by mounting evidence. In this review, we will explore the latest research insights on the role of immune modulation in the pathogenesis of IgAN. With a better understanding of immunopathogenesis of IgAN, emerging therapies will soon become realized.

Keywords: glomerular mesangium, IgA nephropathy, immunopathogenesis, mucosal immune, innate immunity, adaptive immunity

OPEN ACCESS

Edited by:
Songjie Cai,
Brigham and Women's Hospital, United States

Reviewed by:
Laureline Berthelot,
Institut National de la Santé et de la Recherche Médicale (INSERM), France
Hitoshi Suzuki,
Juntendo University, Japan

***Correspondence:**
Xiao-Kang Li
ri-k@ncchd.go.jp

Specialty section:
This article was submitted to Nephrology, a section of the journal Frontiers in Medicine

Received: *13 January 2020*
Accepted: *03 March 2020*
Published: *24 March 2020*

Citation:
Chang S and Li X-K (2020) The Role of Immune Modulation in Pathogenesis of IgA Nephropathy. Front. Med. 7:92. doi: 10.3389/fmed.2020.00092

INTRODUCTION

IgA nephropathy (IgAN) is a clinicopathological syndrome, with diverse clinical manifestations characterized by repeated episodes of gross or microscopic hematuria, and pathological changes featuring IgA1 deposition in the glomerular mesangium, mesangial cell proliferation, and matrix expansion (1). IgAN is the most common primary glomerulonephritis worldwide, and it causes 25–50% of patients to develop end-stage renal disease (ESRD) within 20 years of diagnosis and shortens life expectancy by 10 years, although the course usually evolves gradually (2). The incidence of IgAN is influenced by region, ethnicity, and race; the highest incidence is in Asia, where it accounts for up to 60% of glomerular disease, which is significantly more than the incidence in Europe (30%) and America (10%) (3). Available data confirm that the prevalence of IgAN varies among different races and that IgAN has a high tendency for family aggregation. Genetic factors are

thought to be related to the occurrence and development of IgAN, although differences in the strategies and techniques for renal biopsy in different countries or regions should be considered. More specifically, the histopathological manifestations of IgAN based on characteristic IgA1, which is immunoprecipitated in the glomerulus alone or concomitant with immunoglobulin, may help to elucidate the autoimmune disease properties of IgAN. Immunological events play a decisive role in the pathogenesis of IgAN.

The most widely accepted hypothesis about the pathogenesis of IgAN has been known as a "four-hit" hypothesis (**Figure 1**) (4). That is, the development of IgAN requires at least four processes (called "hits"): (1) increased synthesis of poorly O-galactosylated IgA1 (also called Galactose-deficient IgA1, Gd-IgA1) in circulation; (2) production of autoantibodies against Gd-IgA1; (3) formation of immune complexes containing pathogenic O-galactosylated IgA1; and (4) mesangial deposition of these immune complexes activating mesangial cells and subsequently impairing glomeruli. In fact, multiple immune cells and many immune molecules in the immune system participate in the pathogenesis of IgAN through diverse mechanisms. This review focuses on the immune modulation of IgAN and summarizes the mechanisms associated with its pathogenesis.

ROLE OF POORLY O-GALACTOSYLATED IGA1 AND IGA RECEPTORS IN IGAN

Abundant clinical and laboratory evidence show that both innate and adaptive immunity play important roles in various aspects of the immunological pathogenesis of IgAN. It is generally agreed that IgAN does not originate from a single "hit" of pathogenic disease, but from the result of multiple consecutive but distinct "hits" of different pathogenic diseases. As mentioned in the Introduction, the first hit is that individuals with a genetic predisposition develop aberrant immune responses to common and environmental causes, which leads to an increase of poorly O-galactosylated IgA1 in the serum. As previously reported (5), IgA accounts for about 15% of total serum immunoglobulins in humans and it is mainly present in

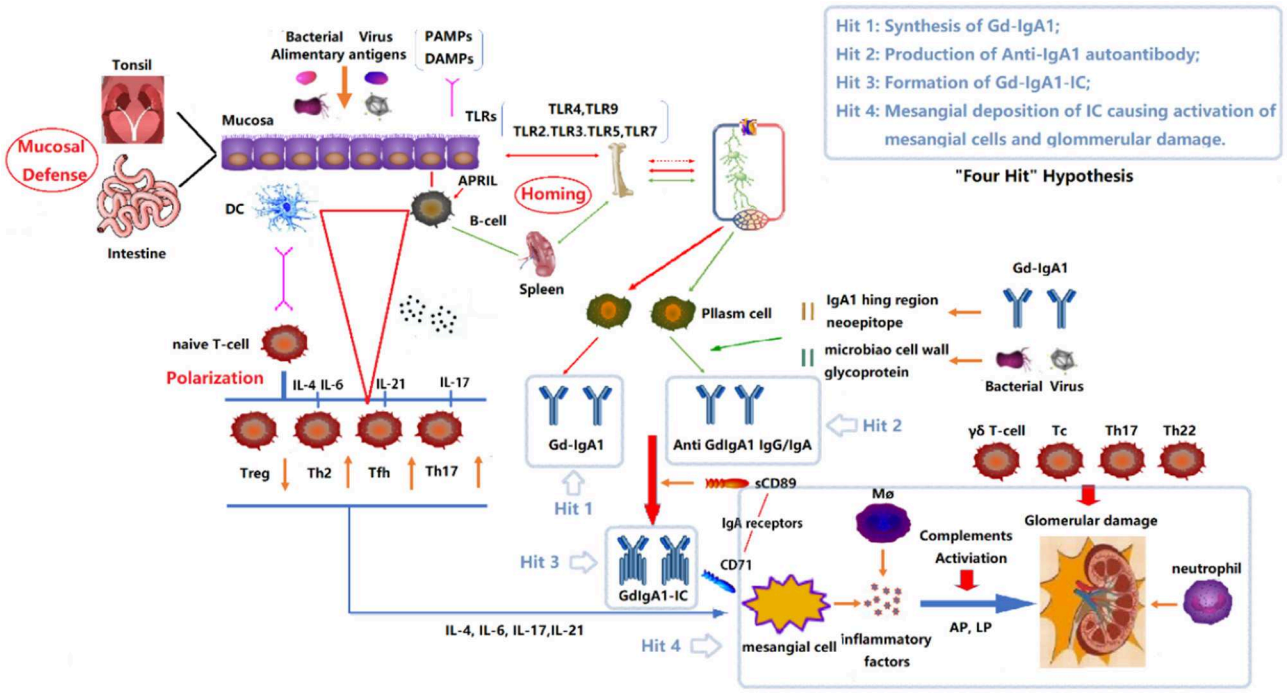

FIGURE 1 | "Four Hits" Hypothesis of IgA Nephropathy. In individuals with a genetic predisposition to IgA nephropathy, infection, or other events destroy the mucosal barrier defense function. Chronic stimulation such as pathogenic microbial or alimentary antigens are taken up by antigen-presenting cells, thereby activating B cells, and differentiating into plasma cell secreted IgA in T-cell-dependent or non-dependent manners. Due to the abnormal regulation of mucosal-bone marrow axis, the mis-expression of homing receptors on the surface of B/plasm cells leads to increased synthesis of poorly glycosylated IgA1 (Gd-IgA1) and self-aggregation to form aggregated Gd-IgA1 (Hit 1). The aberrant exposure of GalNAc of Gd-IgA1 as antigen stimulates B cells to differentiate into plasma cells and synthesizes anti-Gd-IgA1 autoantibodies (Hit 2). The Gd-IgA1 immune complex (Gd-IgA1-IC) is formed by anti-Gd-IgA1 autoantibodies binding to Gd-IgA1 along with soluble sCD89 (Hit 3). Macromolecular Gd-IgA1-IC binds to the IgA receptor (CD71) expressed on mesangial cells and deposits on the glomerular mesangium. Subsequently, the mesangial cells release various inflammatory factors (cytokines, chemokines, growth factors, etc.) under the stimulation of ICs, attracting and recruiting multiple subsets of T cells, macrophages, neutrophils infiltration, and activating the lectin pathway and alternative pathway of the complement system. Synergistic effects lead to glomerular injuries such as mesangial hyperplasia, matrix expansion, and interstitial fibrosis (Hit 4). DC, Dendritic cell; TLRs, Toll like receptors; APRIL, a proliferation-inducing ligand; DAMPs, damage-associated molecular patterns; PAMPs, pathogen-associated molecular patterns; Gd-IgA1, poorly glycosylated IgA1/Galactose-deficient IgA1; AP, The alternative pathway; LP, The lectin pathway.

the mucosal area (i.e., alimentary, respiratory, and urogenital tracts), but is also found in the blood. Structurally, IgA exists in two isotypes, IgA1 and IgA2, each of which can be divided into monomeric (mIgA) and polymeric (pIgA, mainly dimeric) forms. Based on location, it can also be categorized as serum IgA or secretory IgA (SIgA). Monomeric IgA is found predominantly in the serum, most of which is produced in the bone marrow. SIgA is mainly present in the mucosal areas and secretions, whereas PIgA is present at low levels in serum. The pIgA1 components are diverse, including dimeric IgA, SIgA, and IgA immune complexes (6). The primary function of SIgA on the mucosa and secretions is to neutralize toxins and prevent the infiltration and invasion of microbes (commensals and pathogens) through the mucosal epithelial barrier, thereby preventing systemic infection and maintaining a physiologically essential symbiotic relationship with commensals (7). The difference between human IgA1 and IgA2 lies only in the absence of 13 amino acids in the hinge region of IgA2. The hinge region of IgA1, however, consists of unusual repeated sequences rich in proline, serine, and threonine, with serine-containing O-linked oligosaccharide chains (8). The O-glycosylation consists of a core N-acetylgalactosamine (GalNAc), which is extended with β-1,3-linked Gal or further with sialic acid in α-2,3 and/or α-2,6 linkage. However, in the peripheral blood and renal tissues of patients with IgAN, the glycosylation of IgA1 molecules often lacks galactose molecules (Gal), resulting in the formation of monosaccharide side chains (i.e., aberrant glycosylation) containing only a single GalNAc, which may be related to the impaired function of β-1,3-galactosyltransferase. Altered glycosylation favors self-aggregation of IgA1 (9); in addition, aberrant glycosylation results in GalNAc exposure and is recognized by normal IgG and IgA1 antibodies in the body to form immune complexes (10). IgA immune complexes, which are composed of aberrantly glycosylated IgA1, may escape clearance from the liver and preferentially deposit in the kidney due to enhanced lectin reactivity with fibronectin, laminin, and collagen in the glomerular mesangial matrix.

Although aberrant IgA1 levels have been observed in peripheral blood and kidney biopsies from patients with IgAN, the source of this poorly O-galactosylated IgA1 has been of concern and several clinical observations have generated interest. Time-zero renal transplant biopsies were performed in 510 renal transplant donors in a controlled study from Japan (11). They found that mesangial IgA deposition was present in 16.1% of donor kidneys with no statistically significant difference between living donors and cadaveric donors or between related donors and non-related donors. IgA mesangial deposition often occurs in untreated celiac disease, and although IgA appears to be deposited, it rarely induces clinically significant glomerulonephritis. Another considerable phenomenon associated with kidney transplantation is IgA deposition. This frequently recurs in the allograft, with published recurrence rates of 10–53%, and recurrence tends to occur in the late phase of the post-transplant period. Additionally, after the kidney of a subclinical IgAN donor is implanted into a non-IgAN recipient, IgA deposits were removed from the kidney within a few weeks. The above data suggest that IgA1 immune complexes in glomerular mesangium of patients with IgAN are a result of deposition as opposed to *in situ* synthesis (12). Moreover, IgA deposition alone is not necessarily the main cause of kidney damage, and sometimes these subclinical IgA deposits are cleared and alleviated spontaneously (13).

To identify the molecular basis for aberrant IgA1 levels, an *in vitro* model analyzed the pathway of IgA1-producing cells from peripheral blood cells of patients with IgAN. The results showed that β-1,3-galactosyltransferase activity decreased, and N-acetylgalactosamine-specific α-2,6-sialyltransferase activity increased in IgA1-producing cells of patients with IgAN. Consequently, the data suggest that premature sialylation may contribute to abnormal IgA1 glycosylation in IgAN (14).

It has been demonstrated that aberrant glycosylation of IgA1, irrespective of O-glycans or N-glycans (15), significantly contributes to the pathogenesis of IgAN. An *in vitro* study using a model of human mesangial cells found that the aggregated IgA1 with underglycosylation from patients with IgAN bound glomerular mesangial cells with more high affinity and could induce profibrotic cytokine production and proliferation in mesangial cells, and the effects were more significant compared to aggregated IgA1 from a healthy control group (16). In addition, aberrantly glycosylated IgA1 acts as an autoantigen and forms IgG autoantibodies against Gal-deficient IgA1 molecules; these bind to the aberrantly glycosylated IgA1 molecules to form circulating immune complexes that are deposited in the glomerular mesangium, thereby causing kidney damage (17).

In recent years, the role of receptor-ligand binding between IgA1 circulating immune complexes and IgA receptors of mesangial cells in the pathogenesis of IgAN has attracted much attention. The deposition of circulating immune complexes in the renal mesangium mainly depends on its high affinity to IgAl receptors on mesangial cells. After binding, mesangial cells are induced to secrete inflammatory factors and activate complements, leading to pathological changes and clinical symptoms of IgAN. It is generally believed that the IgA receptor family comprises polymeric Ig receptors, involved in epithelial transport of IgA/IgM, myeloid-specific IgA Fc receptors (FcαRI or CD89), Fcα/μR, and some other IgA receptors. These are asialoglycoprotein receptors, transferrin receptors (TfR1 or CD71), FCRL4, and DC-SIGN/SIGNR1, which are involved in IgA catabolism and tissue IgA deposition (18). Recently, another new IgA receptor has been identified, namely β-1,4-galactosyltransferase 1 (β-1,4-GalT1). It is expressed constitutively by the human mesangial cells and its levels are increased in patients with IgAN. This receptor plays an important role in the deposition and clearance of mesangial IgA (19).

However, CD89 and CD71 are currently considered more important than other receptors and have accordingly attracted more attention. In a transgenic murine model co-expressing human IgA1 and CD89, the mice exhibited IgA1-sCD89 complexes in circulation, mesangial deposits, and subsequent glomerular inflammation in a similar manner as IgAN patients, whereas mice expressing only IgA1 did not experience mesangial impairment or renal dysfunction. However, following sCD89 injection, sCD89 and IgA1 deposits were detected in the mesangium of IgA1-expressing mice (20). It is proposed

that the pathogenic complexes containing polymeric Gd-IgA1 could facilitate IgA binding to CD89 on blood monocytes (21). The cleavage of FcRc-less CD89 would produce soluble CD89/Gd-IgA1 complexes, that would be deposited in the mesangium via IgA1-sCD89 complexes binding to CD71. The interaction of sCD89 with CD71 could induce expression of transglutaminase 2 (TGase2) at the mesangial surface, which upregulates CD71 and triggers an inflammatory feedback loop through enhanced expression and mesangial cell proliferation as well as inflammatory factors. These data indicate that interactions among IgA1, sCD89, CD71, and TGase2 in mesangial cells are required for IgAN progression.

A previous study demonstrated that the aberrantly glycosylated IgA from IgAN patients contained higher molecular weight pIgA than the normal IgA1 from healthy individuals. And more importantly, the serum IgA immune complexes from patients with IgAN bound more strongly to CD71, but soluble CD71 could significantly block this binding (22). It has been suggested that deposited pIgA1 or IgA1 immune complexes could initiate a process of auto-amplification involving the hyperexpression of CD71, allowing increased IgA1 mesangial deposition of pIgA1 or IgA1 immune complexes may trigger the self-amplification, which correlates to upregulation of CD71, thereby prompting IgA1 deposits in glomerular mesangium (23). Nevertheless, the novel findings in a recent study should be considered seriously (24), as the authors found that human IgA1 can cause glomerular damage in people without significant glycosylation defects, as long as serum levels are high enough or affinity is immature. Similarly, they observed that human IgA1 induced glomerular lesions independent of the IgA receptor CD89 molecule. These findings still need to be verified by more research.

The deposition of O-galactosylated IgA1 immune complexes on the mesangium activates mesangial cells to release inflammatory factors and complements. The activation of the inflammatory cascade responds to podocyte and tubule interstitial damage as well as renal fibrosis through crosstalk among glomerulus-podocyte-tubular epithelial cells (25). Podocytes are considered an important hub between the glomerulus and tubulointerstitial cells (25). Previous studies have confirmed that the mesangial cells incubated with supernatant of co-cultured IgA1 from sera of patients with IgAN can promote the expression of TNF-α and its receptor, and increase the secretion of IL-6 in podocytes (26). PIgA1 triggers mesangial cells to secrete cytokines (such as TNF-α and TGF-β), thereby activating podocytes and causing high permeability of the glomeruli and proteinuria. Simultaneously, the cytokines secreted by mesangial cells also stimulate the tubulointerstitial cells to produce other inflammatory factors or chemokines, leading to renal tubular damage, interstitial inflammatory cell infiltration and fibrosis (25). The TNF-α released by mesangial cells can not only stimulate podocytes to secrete TNF-α in an autocrine manner but also upregulate podocyte secretion of TNF-αR1 and TNF-αR2. Additionally, when TNF-α combines with TNF-αR1, it will increase IL-6 secretion and induce podocyte apoptosis and renal tubular atrophy (26, 27). It has been reported that IgA1 from blood of IgAN patients stimulates mesangial cells to produce some substances, promoting synthesis of TGF-β via activation of the renin-angiotensin system in podocytes, which then causes renal interstitial fibrosis (28). In addition, mesangial cells also release aldosterone, inducing apoptosis of renal tubular epithelial cells, which leads to tubular atrophy (29).

DIFFERENT PERSPECTIVES ON THE INVOLVEMENT OF MUCOSAL IMMUNE RESPONSE IN THE PATHOGENESIS OF IGAN

The mucosal immune response has been shown to be important in the pathogenesis of IgAN (30–33). It has long been found that during mucosal infection, hematuria and proteinuria are increased in patients with IgAN (34–36), and some cases have an episode of upper respiratory infection at onset (37, 38). Thus, this abnormal mucosal immune response is thought to be related to the occurrence and development of IgAN.

Since the concept of mucosal immunity was proposed in the 1960s, the mucosal immune system (MIS), as a relatively independent immune system in the body has been a concern. More than 95% of infections occur in or from the mucosa. Mucosa-associated lymphoid tissue (MALT) is present in the induction area that forms lymphoepithelial tissue. In these areas, mucosal IgA production is induced in a T-cell-independent and T-cell-dependent manner (39, 40). Primed B cells move to mucosal lamina propria, where they synthesize polymeric mucosal sIgA1 with poor O-galactosylation and low affinity; they are secreted to the mucosal surface but rarely enter the circulatory system. In contrast, most circulating IgA1 produced by bone marrow intrinsic plasma cells is monomeric and heavily O-galactosylated (41, 42).

The current hypothesis is that persistent exogenous antigen stimulation and mucosal-bone marrow axis dysfunction cause the production of pathogenic IgA1 and deposition in glomerular mesangial area, leading to the onset of IgAN (43, 44). The increased level of serum IgA1 with poor O-galactosylation in IgAN may be due to "wrong transfer" to the bone marrow due to the misexpression of homing receptors on the surface of B/plasma cells secreting IgAl in the mucosa, rather than homing to the mucosal surface, resulting in the direct release of "mucosal IgA" into the systemic circulation (45–47).

Role of the Tonsils in IgAN Pathogenesis

The first study on the relationship between tonsils and IgAN was carried out by Tomino in 1983 (48). It has been demonstrated that the antibodies eluted from the renal tissues of patients with IgAN specifically bound to tonsillar cells, and this effect was entirely suppressed by the addition of anti-human IgA antisera. It has also been reported that the serum IgA levels were increased in about half of patients with IgAN, but levels decreased after receiving a tonsillectomy, suggesting a relationship between tonsils and IgAN (49). Increased levels of circulating immune complexes have been observed after tonsil provocation tests in patients with IgAN complicated by chronic

tonsillitis (50). However, following a series of studies, the Japan Society of Stomato-Pharyngology (51) officially analyzed the relevant literature on the clinical benefits of tonsillar provocation test to patients with IgAN and suggested that it lacked value in determining indication for tonsillectomy in patients with IgAN. Nevertheless, the worse urinary findings after tonsillar irritation may be distinct, indicating that tonsil and kidney diseases are related (52). *Haemophilus parainfluenzae* is one of the common bacteria in tonsils. It has been reported that the antigen and antibodies of this bacterium are present in the glomerular mesangium and sera of IgAN patients, suggesting that *H. parainfluenzae* infection may contribute to the pathogenesis of IgAN (53). Another study also found that tonsil mononuclear cells in patients with IgAN can release high levels of IgAl after stimulation with lipopolysaccharide (LPS) and *Streptococcus hemolyticus*, and this effect may be due to its activation-induced cytidine deaminase and increased Iα-Cα expression (54). A single-center controlled study confirmed that the amount of interfollicular monocyte-derived dendritic cells (DCs) in the palatine tonsils is associated with the formation of crescents in IgAN, indicating that DCs in the interfollicular region of tonsils are involved in the course of glomerular vasculitis (55). Analysis in a group of patients with IgAN with gross hematuria found that the expression of chemokine receptor CX3CR1 in the circulating leukocytes was up-regulated, which was consistent with the results from whole-genome sequencing of these patients (56). This finding was supported by another study, which presented that CD8+ lymphocytes from patients with IgAN expressed significantly increased levels of CX3CR1, but this expression declined after tonsillectomy, accompanied by the remission of hematuria. Therefore, the excessive immune response to microbial DNA raises the expression of CX3CR1 of CD8+ lymphocytes in the tonsils of patients with IgAN, subsequently these lymphocytes transfer to renal glomeruli, giving rise to renal damage and hematuria (57). All these findings suggest that local mucosal infection of the tonsil is related to the pathogenesis of IgAN. In light of the above findings, in Asia (especially in Japan), tonsillectomy is generally considered to be beneficial for effective control of IgAN (58). Many studies have claimed that tonsillectomy had a favorable effect on long-term kidney function in patients with IgAN (59–63). A Chinese single-center cohort study found increased frequencies of memory B cells in the blood and tonsils in IgAN (64), but following tonsillectomy, these frequencies were significantly decreased. The author speculated that this may be related to the aberrant mucosa-bone marrow axis in IgAN patients, and IgAN has a Th2-related immunopathogenesis because memory B lymphocytes are mainly involved in the humoral immune response. A meta-analysis of non-randomized studies including 858 Asian IgAN patients that underwent tonsillectomy or not, suggested that the overall clinical remission rate was higher in the patients that received a tonsillectomy. Meanwhile, more patients who did not undergo surgery developed ESRD. The best clinical remission rates occurred in patients who received tonsillectomy combined with steroid pulse therapy. However, it is worth noting that the clinical remission rate of tonsillectomy alone is not superior to that of conventional treatment (65). A recent study from a Japanese group suggested that the timing of tonsillectomy and steroid pulse therapy is very important for the effect on IgAN. It is recommended that tonsillectomy be performed in a short window before and after steroid pulse therapy, which may be helpful for improving IgAN. The potential mechanism is that a steroid pulse can temporarily destroy the tonsil germinal center, causing tonsil atrophy. Before reconstructing the germinal center and restoring proliferation of local immune cells, tonsillectomy may be more conducive to enhancing the effect of therapy (66).

Numerous studies have sought to find a pathogenic correlation between tonsils and IgAN, however, the results are often contradictory. The ability of tonsillectomy to alleviate disease has rarely been observed in European cohorts. In a study involving a large European cohort of patients with IgAN, there was no improvement in IgAN progression after tonsillectomy (67). Furthermore, tonsillectomy did not influence the activation of innate immunity, even though the aberrant galactosylation of IgA1 was obvious in patients with IgAN. The research hardly encourages the involvement of tonsillectomy in the modification of mucosal immune response in patients with IgAN, but implies that activation of the gut mucosal immune network may potentially contribute to glomerulonephritis (68). This may indicate that the role of tonsils in IgAN pathogenesis is not significant enough, at least not in the numerous patients outside Asia. The reasons may involve the influence of genetics, environmental factors, attitude and timing of kidney biopsy, and other factors (39, 69–72). In Japan and China, early screening including renal biopsy is being used more aggressively, and even routinely in some centers.

Role of Intestinal Mucosal Immune in IgAN Pathogenesis

In recent years, the role of commensal microorganisms (microbiota) colonized on the surface of human intestinal mucosa, in both healthy and diseased conditions, has attracted attention. The microbes on the mucosal surface are in close contact with the intestinal epithelium and exert a significant effect on the modulation of intestinal mucosal immune by influencing the intestinal barrier against pathogens and the host immune system (73). Under normal circumstances, when the intestinal mucosa is stimulated, intestinal B cells switch from secreted IgM to secreted IgA1. SIgA1 and other secretory components (such as antimicrobial peptides and mucus secreted by Paneth cells and goblet cells, respectively) synergetically play a host defense role against the invasion of pathogens on the mucosa (74). Altered intestinal barriers might facilitate an abnormal response to microbiota, triggering MALT activation and subclinical intestinal inflammation (75). This can induce an abnormal response to alimentary antigens or commensal microbes, along with the synthesis of poorly glycosylated pIgA1, which eventually deposits in the mesangium through circulation.

In patients with IgAN, several clinical observations have shown activation of the innate immune system on the intestinal mucosa (76–78). A link between IgAN and genes concerned with the immunity of intestinal pathogens has been reported in a genome-wide association study (GWAS). The results of the

GWAS support the hypothesis that genetic risk, geospatial risk, and environmental variables may collectively induce alteration of the gut mucosal immunomodulation, which facilitates the course of IgAN (30). A clinical investigation from China (79) found that chronic enteritis was the second most common mucosal symptom of IgAN patients after chronic pharyngitis, with 35.2% of patients with IgAN presenting with chronic enteritis simultaneously. The incidence of chronic enteritis in patients with hematuria was markedly higher than that in patients without hematuria, indicating that gastrointestinal mucosal immunity is also closely related to IgAN.

It has been demonstrated that increased bacterial LPS exposure is related to poorly galactosylated IgA. B cells stimulated by LPS can promote the methylation of the chaperone Cosmc, thereby downregulating the expression of the Cosmc gene, which is the basis of abnormal O-glycosylation in the IgA1 hinge region of patients with IgAN, and thus promotes the formation of poorly galactosylated IgA (80). Other experimental models suggest the involvement of alimentary antigens (e.g., gluten) (81, 82). Increased IgA levels in response to alimentary antigens has been observed in the peripheral blood, which is correlated to increased intestinal permeability (83, 84). Coppo et al. (82) successfully established a murine model of gluten-induced experimental IgA glomerulopathy. Following this report, Papista et al. studied the relationship between gluten and IgA deposition in a spontaneous IgAN murine model expressing human IgA1 and CD89 (85). The mice were fed a gluten-free diet for three generations, and they observed an improvement of mesangial IgA1 deposits, alleviation of glomerular inflammation, and reduction of IgA1-sCD89 immune complex levels in the blood and renal eluates. On the contrary, a high-gluten diet could induce glomerular inflammation and IgA1-sCD89 complex deposition. In combination with the finding that high levels of anti-gliadin IgA are closely associated with the degree of proteinuria in patients with IgAN, a gluten-free diet may be useful in ameliorating the development of IgAN. All the above findings suggest that the gut mucosal immune system of patients with IgAN is hyper-reactive to mucosal antigens, such as alimentary antigens or microbial components.

INNATE IMMUNITY AND IGAN

Role of Toll-Like Receptors in IgAN Pathogenesis

It is well-known that the mucosal surface is the main site of innate immunity. As mentioned above, the innate immune system works through the recognition of pathogen- and damage-associated molecular patterns (PAMPs and DAMPs, respectively) induced by macrophages, DCs, leukocytes, and other cells. The system increases opsonification and phagocytosis, which facilitate the swift elimination of pathogens. Toll-like receptors (TLRs) are the key components of the mammalian innate immune system and mediate immune and inflammatory responses through binding PAMPs and/or DAMPs (86). Myeloid differentiation factor 88 (MyD88) is the adaptor for TLR-mediated signal transduction (87).

Antigen components from air, food, microorganisms, or necrotic cells are recognized as a DAMP or PAMP by TLRs on the surface of the mucosa, thereby initiating the innate immune response (88). Upon activation, TLRs initiate an intracellular signaling cascade, the release of cytokines, and the enhanced expression of cell surface costimulatory molecules (89). TLR activation induces DC maturation, chemokine release, and recruitment of inflammatory cells in the infected site. Subsequently, the mature DCs move to the lymph nodes, where they interact with T cell receptors (TCRs) of T cells and activate specific T cells and antibody synthesis (90). Consequently, infection can exacerbate kidney inflammation in diverse pathways by activating TLRs. Additionally, inflammatory products can also activate TLRs expressed on intrinsic renal cells, which can further trigger inflammation and tissue impairment. TLRs are expressed not only on circulating immune cells and in infiltrating macrophages/DCs, but also on resident renal cells (91), and they have been considered as mediators of renal diseases, playing a role in DC maturation and in autoimmunity (92). There has been a series of evidence supporting the involvement of TLRs in the pathogenesis of IgAN.

TLR4 recognizes LPS in gram-negative bacteria. It has been observed that the expression of TLR4 mRNA and protein in renal tissue is significantly increased in IgAN rats treated with oral and intravenous immunization of bovine serum albumin (BSA) for 12 weeks (93). The elevated TLR4 expression on monocytes of peripheral blood in patients with IgAN was significantly associated with proteinuria or clinical activity (94). Previous studies have mentioned that activation of TLR4 triggered by bacterial LPS promotes Cosmc methylation, thereby reducing the degree of glycosylation of the IgA1 molecule, which is also the basis of the pathogenesis of IgA nephropathy (80). In an *in vitro* co-culture system of IgA and mesangial cells, TLR4 mediates MAPK activation and MCP-1 secretion, indicating that TLR4 is engaged in glomerular mesangium damage by inducing inflammatory cytokines in IgAN (95). It has been confirmed that TLR4 is involved in the activation of NF-κB. The nuclear translocation of NF-κB triggers the transcription of mRNA encoding many inflammatory mediators, such as cytokines, chemokines, fibrinogen, etc., which contribute significantly to the effects of the innate and adaptive immune responses (96). For example, the nuclear translocation of NF-κB is conducive to B cell proliferation, thus increasing the synthesis of IgA (97). Animal experiments showed that TLRs are involved in the conversion of B cells from IgM to IgA (97). In addition, TLR4 is constitutively expressed in podocytes. Podocytes responding to immune complex-mediated glomerular filtration barrier damage will upregulate the expression of TLR4, thereby resulting in the local release of chemokines, which may allow the recruitment of inflammatory leukocytes and exacerbate glomerular damage (98). Recently, renal TLR4-mediated and profibrotic signaling have been demonstrated in chronic kidney disease. TLR4 expression was significantly associated with the expression of TGF-β1 and altered susceptibility of renal cells to TGF signaling (99, 100).

TLR9 has been characterized as the receptor of viral and bacterial cytosine-phosphate-guanosine (CpG)-DNA. A previous study reported that the IgAN-susceptible ddY

mice fed normally showed enhanced transcriptional levels of TLR9 and MyD88 in the splenocytes. These mice treated with nasal CpG-oligodeoxynucleotides can induce Th1 polarization, IgA expansion in circulation and mesangium, and exhibit exacerbated renal lesions. In the same study, TLR9 polymorphism was found to be involved in the development, but not occurrence, of human IgAN, revealing that an analogous mechanism relevant to TLR9/MyD88 may play a role in murine and human IgAN (101). The latest study found that CpG-ODN activates TLR9/MyD88 signaling and induces the production of glycosylated IgA1 and IgG-IgA ICs through the IL-6 and/or a proliferation-inducing ligand (APRIL) pathway, and further aggravates kidney damage. B cells and DCs are directly or indirectly involved in the process of inducing the excessive production of abnormally glycosylated IgA1, respectively (102). A non-randomized controlled study in Japan investigated expression of tonsillar TLR9 in a group of patients with IgAN patients who received tonsillectomy in combination with steroid pulse therapy (103). The results indicated that elevated tonsillar TLR9 levels existed in 22.4% of patients, and TLR9-positive patients showed better response to treatment, reflected in more effective alleviation in urine findings. This indirectly reflects the involvement of TLR9 in IgAN development. Additionally, up-regulation of TLR 4, TLR 7, TLR 8, and TLR 9 has also been observed in the renal tissues of patients with IgAN (104). A real-time RT-PCR analysis suggested the mRNA expression of TLR2, TLR3, TLR4, TLR5, TLR7, and TLR9 were markedly increased in the peripheral blood mononuclear cells of patients with IgAN. Among them, more obvious proteinuria was present in the patients with high mRNA levels of TLR2, TLR3, TLR5, or TLR9, while increased serum IgA was observed in patients with high mRNA levels of TLR4 (105). The above data suggest that PAMPs and/or DAMPs can aggravate glomerular inflammation in various ways by activating TLRs. In addition, inflammatory mediators can also activate TLRs present on the renal intrinsic cells, which can further trigger inflammation and tissue damage (90).

Role of Complements in IgAN Pathogenesis

Based on laboratory evidence and results of renal biopsy in patients with IgAN, it is known that complements play important roles in IgAN; however, the specific role of complement activation in the mechanisms of disease is still not fully clear. The complement system consists of the activation cascade of ∼50 proteins located in the plasma, tissues, and cells, including complement component proteins (C3, C5, etc.), complement regulatory proteins (factors H, I, etc.) and complement receptor proteins (CRl, CR2, etc.). There are three commonly accepted complement activation pathways, including the classical pathway (CP), the alternative pathway (AP), and the lectin pathway (LP). Each pathway has a respective triggering mechanism initiated by the interaction of complement proteins with distinct structures.

In IgAN, one of the characteristic manifestations is that IgA is generally co-deposited in mesangium with complement proteins. Immunohistochemical evidence shows deposits of C3, complement factor P (CFP), C4d, mannose-binding lectin (MBL), and membrane attack complex (MAC) in the mesangium of IgAN, along with the lack of C1q usually. Although some studies showed that glomerular mesangial C1q deposition in patients with IgAN was associated with poor renal prognosis and serious pathological features, this finding has not been generally accepted (106, 107). C1q is rare in the renal tissue of patients with IgAN (108), and its presence and clinical significance in IgAN are still inconclusive. AP is considered the most important effect pathway in the pathogenesis of IgAN. It has been proposed that pIgA, aggregated IgA, and abnormally glycosylated IgA have a powerful ability to activate AP (109, 110). *In vitro* assays using IgA coated directly on plastic surfaces, or serum pIgA showed that IgA1 is capable of triggering the cascade and cleaving C3 through AP (111, 112). Evidence for AP-dependent complement activation and essential effector molecular regulation of IgAN suggests that a gd-IgA1-immunocomplex can be used as a complement activation surface.

The co-deposition of C3 with IgA1in the mesangium is correlated with the severity and progression of IgAN. Previous studies have shown that poorly glycosylated pIgA1 in the peripheral blood can bind with IgA-binding M protein from *Streptococcus pyogenes* serotype M4 and co-deposit in the mesangium, which enhances the synthesis and secretion of IL-6 and C3 as well as the proliferation of mesangial cells, thereby promoting the inflammatory progression of IgAN (113). Besides C3 deposition in the kidney, lower C3 with higher C3 cleavage (iC3b and C3d) is detected in the peripheral blood of some patients with IgAN, suggesting systemic complement activation (114). A Korean observational cohort study involving a total of 343 patients with biopsy-proven IgAN showed that serum C3 and glomerular mesangial C3 deposits are independently associated with poor prognosis of IgAN (115). Similarly, a Chinese single-center cohort study analyzed the correlations of serum/urinary C3a and C5a with clinical manifestation and histopathology in patients with IgAN. They found that C3a and C5a depositions in IgAN were obviously enhanced, and they increased with the exacerbation of pathological impairment (116). In addition, another study found that the IgA/C3 ratio in the peripheral blood shows a significant positive correlation with quantities of protein in the urine of patients with IgAN (117).

Several previous reports indicated that AP complement components (factors B and P, CFB, and CFP) and complement regulatory protein (complement factor H, CFH) are widely present in the kidney tissues of patients with IgAN, and that there are also significantly increased CFB and CFP levels in the circulation of patients with IgAN (118, 119). CFH is the most important regulatory protein in AP, whose main function is to make the complement system clear pathogens or other dangerous substances, but not impair their own tissues. In addition to CFH, there is also a group of proteins that shows high sequence homology with CFH, namely complement FH-related proteins (CFHRs, including CFHR-1, CFHR-2, CFHR-3, CFHR-4, and CFHR-5). Functionally, CFHRs deregulate CFH by competing with CFH to bind C3b and promote activation of AP (120).

A GWAS of IgAN in Chinese and European cohorts found that a CFH gene variant on chromosome 1q32 (*rs6677604*) is

associated with IgAN (121). The same team also found that the *rs6677604-A* allele is involved in increased CFH and decreased C3a levels in serum (122). Moreover, serum C3 levels negatively correlated with mesangial C3 levels, whereas CFH levels were positively correlated with serum C3 levels. Decreased or absent CFHR1/CFHR3 levels further weakened the deregulation effect of CFH. This synergistic effect increased the negative regulation of complement activation caused by aberrant glycosylation of IgAl in IgAN, which may influence the formation of circulating immune complexes, thereby reducing risk of IgAN occurrence. It has been reported that in patients with IgAN, CFH levels were normal, but CFHR-1 levels were enhanced (123), and increased CFHR-1/CFH ratios were consistent with impaired renal function. In IgAN pathogenesis, CFHR-1 antagonizes CFH, thereby inhibiting the activation of C3. A study from another group also came to a similar conclusion (124).

In addition to CFH, CFHRl, and CFHR3, the role of CFHR5, another complement FH-related protein, has attracted extensive attention regarding its role in the pathogenesis of IgAN. A prospective clinical study showed that glomerular FHR5 deposition existed in all patients with IgAN, just in the same manner that C3 and sc5b-9 did (125). Recently, a study of a large Chinese cohort suggested that *CFHR5* is an IgAN predisposition gene (126), and another study also indicated that serum CFHR-5 level was independently correlated with IgAN progression (127). It has been proposed that FHR1 and FHR5 homodimers can disturb the physiological effects of FH. In addition, aberrant FHR levels may trigger and promote AP activation, resulting in complement cascade-associated inflammation and renal lesions (128).

In IgAN, different research teams found that about 25% of patients with IgAN exhibited positive renal local MBL staining, suggesting the presence of complement activation of LP (129). MBL, L-ficolin, M-ficolin, and H-ficolin are all complement-activating soluble pattern recognition molecules, which interact with PAMPs and/or DAMPs and initiate complement activation through MBL-associated serine protease (MASP)-1, MASP-2, and MASP-3, activating C4 and C2 and leading to C4b2a formation and C3 cleavage. LP activation on the surface of pathogens plays a first-line role in host defense (130). Clinical analysis showed that M-ficolin, L-ficolin, and MASP-1 were elevated, whereas MASP-3 levels were reduced in the blood of patients with IgAN, indicating that MASP-3 levels may be related to IgAN severity (131). The abnormal glycosylation of IgA1 is characterized by high levels of GalNac exposure, which may interact with ficolins to activate LP (132). In the absence of CP activity, MBL-MASP causes C3 and C4 to deposit on immobilized IgA, suggesting that a dose-dependent binding of MBL can bind pIgA, but not monomeric IgA, and activate complement LP (133). It has been reported in IgAN that positive renal local MBL staining and urinary MBL levels are associated with poor prognosis, suggesting that complement activation of LP is involved in IgAN pathogenesis (134, 135). In addition, the MBL level of patients with IgAN was closely related to the MBL2 genotype. In patients with IgAN, the incidence of prodromic infection and gross hematuria is significantly higher in individuals with MBL deficiency, and the long-term prognosis is poor. The possible underlying mechanism is that the risk of infection is increased in patients with MBL deficiency, and infection may induce impaired mucosal immune regulation, which promotes the progression of IgAN (136). The findings of many studies have suggested that the activated fragments of C4 deposited in the glomerular mesangium of patients with IgAN are more likely to be produced by the MBL pathway (137, 138). Mesangial deposition of C4d has been identified as a significant risk factor for worsening renal function (139–141). A retrospective study on renal biopsies of 15 cases of IgAN showed that segmental and global deposition of C4d was particularly associated with endocapillary proliferation; moreover, interstitial fibrosis and tubular atrophy were more severe in C4d-positive patients with IgAN (142).

In addition to AP and LP, it is worth noting that the complement terminal pathway also is involved in IgAN pathogenesis. Treatments targeting this pathway are starting to be used clinically. As early as the 1980s, studies on histopathological analysis of IgAN biopsies began to demonstrate glomerular C5b9 deposition (143). Using immunofluorescence, researchers quantified MAC, properdin, CFH, and complement receptor type 1 (CR1, an inhibitor of the complement system) in urine samples of patients with IgAN (144). There was glomerular deposition of C5, CFH, and properdin; urinary MAC, CFH, and properdin levels were obviously elevated, but CR1 levels were apparently reduced. A proteomics study of IgAN kidney biopsy specimens from Norway showed an increased abundance of proteins of the terminal complement pathway, suggesting complement-mediated impairment in progressive IgAN. Meanwhile, one study reported a lower abundance of CR1 in progressive IgAN, which may reflect an underlying mechanism involved in reducing complement inhibitory control in IgAN (145).

ADAPTIVE IMMUNITY AND IGAN

Adaptive immunity is certainly correlated with IgAN pathogenesis. Under physiological circumstances, as previously mentioned, T cells activated by DCs presenting mucosal antigens (bacterial or viral products, alimentary antigens, etc.) trigger naive B cells to undergo IgM-to-IgA class switch in a T-cell-dependent manner in Peyer's patches and tonsils. Activated B cells migrate to regional lymph nodes and home to MALT, where they eventually differentiate into IgA-secreting plasma cells. In addition, IgA can be produced in a T-cell-independent manner in the MALT. The IgA dimers move through the mucosal epithelium to become SIgAs, which act in defense against pathogens. In the pathogenesis of IgAN, the continued exogenous antigen stimulation, abnormal mucosal immune response, and the incorrect expression of homing receptors on the surface of IgAl-secreting B/plasma cells can result in elevated aberrantly glycosylated IgA1, which tends to self-aggregate into pIgA1. Meanwhile, glycosylation deficiency brings about GalNAc exposure and is recognized by natural IgG and IgA1 antibodies as an antigen, thereby resulting in the formation of immune complexes. Furthermore, soluble CD89/Gd-IgA1-IgG

complexes are deposited in the mesangium by binding to their receptors and continuous release of cytokines and growth factors in the local mesangium, leading to inflammatory damage, matrix accumulation, and glomerulosclerosis. Finally, further recruitment of T lymphocytes leads to renal tubular interstitial damage and fibrosis (146).

Role of T Cells in IgAN Pathogenesis

Multiple T-cell subsets, especially Tc, Th2, Th17, Th22, T follicular helper (Tfh), and regulatory T-cells (Tregs), are major contributors to the pathogenesis and pathophysiology of IgAN. Th1 lymphocytes are primarily involved in cell-mediated immunity, secreting IFN-γ, IL-2, TNF-β, and facilitating the elimination of intracellular pathogens, whereas Th2 lymphocytes regulate humoral immunity and mediate the clearance of parasites by producing IL-4, IL-5, IL-9, and IL-13. It is generally believed that patients with IgAN have Th1/Th2 imbalances that tend to favor Th2 shift (147–149). Previous study had shown that the ratio of Th1/Th2 in tonsil lymphocytes in IgAN patients with tonsillitis was lower than that in patients with common chronic tonsillitis, and Th1/Th2 ratio was consistent with proteinuria and histopathology features in IgAN group (147). It has been observed that Th2 differentiation promoted poor galactosylation of IgA in a murine model of IgAN (148). Subsequent studies demonstrated that IL-4 treatment resulted in decreased expression of C1GALT1C1 mRNA of B cells from patients with IgAN, by methylation modification, which is beneficial to the secretion of aberrantly glycosylated IgA1 (149). Moreover, the response of glomerular cells to Gd-IgA immunocomplexes could be enhanced by Th2 lymphocytes, thereby reducing the glomerular filtration rate (GFR) (148). In addition, as a Th1-type cytokine, IFN-γ may be beneficial for preventing the progression of IgAN (150). Some studies also reported that IFN-γ serum levels were rarely significantly increased in patients with IgAN compared with the obvious elevation of Th2-type cytokines (151, 152). Moreover, as another major cytokine secreted by Th1 cells, the level of IL-2 has no correlation with serum IgA levels, the severity of renal histological changes, or other clinical parameters in patients with IgAN (153). Additionally, it should be emphasized that IL-2 is not unique to the Th1 subgroup. Other Th subgroups, activated Tc cells, NK T cells, and dendritic cells also can secrete a large amount of IL-2 (154). It has been shown that Th1 cells may be predominant during the late stage of IgAN with crescent formation and tissue damage (155). Another Italian study of whole-genome DNA methylation screening in CD4+ T cells in patient with IgAN proposed that there are specific methylation abnormalities in CD4+ T cells in patients with IgAN, which may cause reduced TCR function and decreased T cell activation, thereby leading to a Th1/Th2 imbalance with an enhanced IL2/IL5 ratio. These abnormalities may be related to the subsequent immunoglobulin class-switch to IgG production (156).

Tfh cells were first discovered in human tonsils and described as a subset of CD4+ T cells expressing the chemokine receptor CXCR5. They are localized in the B-cell region of lymphoid tissues and play a pivotal function in the formation of memory B cells and long-lived plasma cells (157). It was reported that there is a higher frequency of CD4+CXCR5+ Tfh cells in patients with IgAN, and there is a negative correlation between this subpopulation and estimated GFR. In addition, there are positive correlations among CD4+CXCR5+PD-1+ Tfh cells and serum IL-21, Gd-IgA1, and proteinuria. This indicates that high Tfh frequency may be involved in the development of IgAN (158). Another study indicated that Tfh might be involved in IL-21-mediated production of IgA and Gd-IgA1 (159). The study also found that IL-21 promoted the level of activation-induced cytidine deaminase in B cells, thereby promoting somatic hypermutation. According to a previous study, anti-Gd-IgA1 autoantibodies originate from somatic hypermutation of heavy-chain gene segments in anti-Gd-IgA1-producing cells (160).

Th17 and Treg cells are frequently found on the mucosal surface, where they implement their defenses against microbial invasion and prevent excessive immune responses, respectively. It has been identified that Th17 cells, driven by IL-23, are involved in autoimmune inflammation (161), whereas Tregs suppress the immune responses and inflammation, and maintain peripheral tolerance. Studies have shown that these two T-cell subsets can be transformed into each other under certain conditions. RORγt and Foxp3 are the main modulators of Th17 cells and Tregs, respectively, and the balance of their expression levels determines the direction in which T-cell subsets differentiate (162). The balance of Th17 and Treg cells *in vivo* maintains immune homeostasis (163).

It has already been demonstrated that patients with IgAN present a reduced frequency of CD45RA(-) FoxP3 (high) activated Treg subset, elevated frequency of Th17, as well as correspondingly elevated serum levels of Th17-associated cytokines, such as IL-17A, IL-21, IL-23, IL-1β, and IL-6, and decreased serum levels of Treg-associated cytokine, IL-10. The patients with high IL-17A expression had lower renal function, greater proteinuria, and more severe tubulointerstitial damage (164). Upon IL-17 stimulation, B lymphocytes proliferate and lead to increased production of underglycosylated IgA1 *in vitro* (165). Moreover, mesangial cells stimulated by Gd-IgA1 are capable of producing CCL20, and therefore, inflammatory Th17 cells recruited to the kidney induce further glomerular lesions in IgAN (166). Previous studies suggested that the frequencies of Tregs in the peripheral blood and tonsils of patients with IgAN were significantly lower than those in the healthy controls. The reduction is primarily ascribed to the decreased levels of induced Tregs, but no significant alteration in levels of natural Tregs is observed (167, 168). In addition, another study revealed not only a deficient quantity but also poor immunosuppressive function of Tregs in IgAN. Perhaps because of the dual defect in both quantity and function, Tregs of patients with IgAN hardly prevent formation of Gd-IgA1 mesangial deposits, and subsequent infiltration of inflammatory cells as well as proliferation of the mesangial matrix (169). T cell development is regulated by microRNAs (miRNAs) post-transcription. As one of the post-transcriptional regulator of miRNAs, miR-155 can regulate mammalian immunity in various ways. It has been demonstrated that peripheral blood lymphocytes of patients with IgAN express extremely low

levels of mir-155. This causes a T-cell subset shift that makes individuals prone to the development of autoimmune diseases (i.e., elevated frequencies of Th2 and Th17 along with reduced frequencies of Th1 and Treg), which is beneficial for inhibiting the expression of Cosmc gene and aggravating poor IgA1 glycosylation (151).

Concerning the role of Tc cells in the pathogenesis of IgAN, it has been previously mentioned that the high expression of CX3CR1 is presented in the peripheral blood CD8+ Tc of patients with IgAN, which boosts lymphocytes moving across the glomerular endothelium and causes glomerular capillary wall destruction and hematuria (56, 57).

Role of B Cells in IgAN Pathogenesis

B cells are essential in the early stage of IgAN pathogenesis. The existing data indicate that besides TLRs, the mucosal response of B cells also involves APRIL and B-cell activation factor (BAFF), which makes an important contribution in IgAN progression (170, 171). APRIL and BAFF are two important factors for B cell homeostasis; they share two receptors–transmembrane activator and calcium modulator cyclophilin ligand interactor (TACI) and B cell maturation antigen (BCMA), and BAFF also has a unique receptor: BAFF receptor (BAFF-R) (172). APRIL synthesis is enhanced when pathogens on the mucosal surface induce TLR9 expression, which further contributes to T-cell-independent IgA class switching on B cells. One study showed that TLR9 stimulation can induce abnormal expression of APRIL in B cells of the tonsil germinal center of patients with IgAN (173). APRIL promotes increased production of IgA, mainly Gd-IgA1. The findings from a controlled study showed that the expression of APRIL and its receptors is elevated in B cells from patients with IgAN, which promotes the hypersecretion of Gd-IgA1 (174). A recent study identified that over-production of IgA from tonsillar mononuclear cells of patients with IgAN is induced by the APRIL pathway and that high expression of TACI on patients' B-cells induced by oligodeoxynucleotides with CpG will promote APRIL-associated IgA production (175). In a group of patients with IgAN recurrence after renal transplantation, the serum levels of APRIL remained relatively high for nearly 3 years after surgery (176). Moreover, it has been demonstrated that IL-6-mediated overproduction of Gd-IgA1 can be entirely inhibited by treatment with APRIL-specific siRNA in ddY mice (102).

BAFF is involved in B cell survival, maturation, proliferation, and differentiation. During mucosal infection, myeloid cells secrete IL-12, IL-8, and IFN-α, and these cytokines boost the secretion of IFN-γ by NK cells, which further up-regulates the expression of BAFF. Excessive BAFF levels hinder B cell proliferation and differentiation into antibody-secreting cells, promoting the production of aberrantly glycosylated IgA1. Several groups have previously measured BAFF expression in IgAN. Treating tonsillar mononuclear cells from IgAN patients *in vitro* by physical or chemical stimulation may activate BAFF, and induce secretion of aberrant O-glycosylated IgA1 by suppressing the expression of C1GALT1 and Cosmc (177, 178). It has been identified that elevated levels of TLR9 and BAFF are conducive to the overexpression of serum IgA1 and associated with renal function and disease activity of IgAN (179). Interestingly, the findings from a clinical cohort study proposed that *Streptococcus pyogenes* infection was closely associated with BAFF production in patients with IgAN, but the levels of BAFF were decreased (172). In addition, a study of comprehensive transgenic animal models and clinical data indicated that although BAFF-overexpressing Tg mice can induce IgAN, peripheral blood in patients with IgAN revealed a unique elevation of APRIL levels and no significant change in BAFF levels (180). Martín-Penagos et al. hypothesized that this phenomenon may have occurred because TACI expressed in B cells in the human small intestine upregulates APRIL-induced IgA synthesis and downregulates BAFF-mediated responses *in vitro*. Upon binding to TACI, APRIL is more strongly correlated to IgA class switching than BAFF (176).

Evidence from animal models suggests that CD19+ B cells are essential for the pathogenesis of IgAN. Furthermore, the reconstitution of IgAN by transfusion of murine spleen cells without CD90+ pan T cells and transfusion of CD19+ cells in SCID mice indicates that the responsible B cells are involved in nephritogenic IgA synthesis in a T-cell-independent manner (181). A Chinese clinical cohort study demonstrated that the levels of tonsillar CD19+CD5+B cells of patients with IgAN were positively associated with the severity of renal histopathology (182). Another study investigated the features of CD19+CD5+ B cells in the circulation, ascites, and biopsy tissues of patients with IgAN. The results revealed that the frequency of CD19+CD5+ B cells can be observed in above samples of all patients with IgAN. Furthermore, higher levels of IgA and IFN-γ are secreted by CD19+CD5+ B cells in patients with untreated IgAN (183).

SUMMARY

The most widely accepted "four-hit" hypothesis about the pathogenesis of IgAN implies that immunological factors are engaged in all aspects of IgAN development and play a critical role. Chronic stimulation of harmless antigens, such as bacteria or virus products, alimentary antigens or airborne antigens contributes to abnormal mucosal immunoregulation. In pathological conditions, abnormal expression of effector molecules and disordered activation and differentiation of immune cells in the innate and adaptive immune system synergistically cause poorly glycosylated IgA1 self-aggregation, immune complex formation, and deposition on the mesangium, which further stimulates local inflammation and immune response, causing tissue damage and pathological repair.

Aiming at all aspects of immune mechanism involvement, it is helpful to develop novel and promising clinical early-diagnosis and prognostic indicators, as well as ideal specific targeted therapeutic drugs in translational medicine. In fact, there are already some promising detection indicators and therapeutic approaches in preclinical stages of development. Certainly, we must also be aware that the current research progress on the immunological mechanism of IgAN is incomplete, and sometimes even contradictory. It is still very difficult for us to systematically link all evidence into fully clear pathogenesis. The

following work will require continued efforts to systematically understand IgAN.

AUTHOR CONTRIBUTIONS

SC is responsible for writing the review. X-KL is responsible for determining the topic and supervising the content of the article.

FUNDING

This work was supported by National Natural Science Foundation of China (No. 81873511) and the Non-Profit Central Research Institute Fund of Chinese Academy of Medical Sciences (2018PT32018).

REFERENCES

1. Berger J, Hinglais N. Intercapillary deposits of IgA-IgG. *J Urol Nephrol*. (1968) 74:694–5.
2. D'Amico G, Imbasciati E, Barbiano Di Belgioioso G, Bertoli S, Fogazzi G, Ferrario F, et al. Idiopathic IgA mesangial nephropathy. Clinical and histological study of 374 patients. *Medicine*. (1985) 64:49–60. doi: 10.1159/000183538
3. Zhu L, Zhang H. The genetics of IgA nephropathy: an overview from China. *Kidney Dis*. (2015) 1:27–32. doi: 10.1159/000381740
4. Suzuki H, Kiryluk K, Novak J, Moldoveanu Z, Herr AB, Renfrow MB, et al. The pathophysiology of IgA nephropathy. *J Am Soc Nephrol*. (2011) 22:1795–803. doi: 10.1681/ASN.2011050464
5. de Sousa-Pereira P, Woof JM. IgA: structure, function, and developability. *Antibodies*. (2019) 8:E57. doi: 10.3390/antib8040057
6. Oortwijn BD, van der Boog PJ, Roos A, van der Geest RN, de Fijter JW, Daha MR, et al. A pathogenic role for secretory IgA in IgA nephropathy. *Kidney Int*. (2006) 69:1131–8. doi: 10.1038/sj.ki.5000074
7. Perse M, Veceric-Haler Z. The role of IgA in the pathogenesis of IgA nephropathy. *Int J Mol Sci*. (2019) 20:6199. doi: 10.3390/ijms20246199
8. Kerr MA. The structure and function of human IgA. *Biochem J*. (1990) 271:285–96. doi: 10.1042/bj2710285
9. Kokubo T, Hiki Y, Iwase H, Horii A, Tanaka A, Nishikido J, et al. Evidence for involvement of IgA1 hinge glycopeptide in the IgA1-IgA1 interaction in IgA nephropathy. *J Am Soc Nephrol*. (1997) 8:915–9.
10. Tomana M, Novak J, Julian BA, Matousovic K, Konecny K, Mestecky J. Circulating immune complexes in IgA nephropathy consist of IgA1 with galactose-deficient hinge region and antiglycan antibodies. *J Clin Invest*. (1999) 104:73–81. doi: 10.1172/JCI5535
11. Suzuki K, Honda K, Tanabe K, Toma H, Nihei H, Yamaguchi Y. Incidence of latent mesangial IgA deposition in renal allograft donors in Japan. *Kidney Int*. (2003) 63:2286–94. doi: 10.1046/j.1523-1755.63.6s.2.x
12. Novak J, Vu HL, Novak L, Julian BA, Mestecky J, Tomana M. Interactions of human mesangial cells with IgA and IgA-containing immune complexes. *Kidney Int*. (2002) 62:465–75. doi: 10.1046/j.1523-1755.2002.00477.x
13. Ibels LS, Gyory AZ, Caterson RJ, Pollock CA, Mahony JF, Waugh DA, et al. Recognition and management of IgA nephropathy. *Drugs*. (1998) 55:73–83. doi: 10.2165/00003495-199855010-00006
14. Suzuki H, Moldoveanu Z, Hall S, Brown R, Vu HL, Novak L, et al. IgA1-secreting cell lines from patients with IgA nephropathy produce aberrantly glycosylated IgA1. *J Clin Invest*. (2008) 118:629–39. doi: 10.1172/JCI33189
15. Kobayashi I, Nogaki F, Kusano H, Ono T, Miyawaki S, Yoshida H, et al. Interleukin-12 alters the physicochemical characteristics of serum and glomerular IgA and modifies glycosylation in a ddY mouse strain having high IgA levels. *Nephrol Dial Transplant*. (2002) 17:2108–16. doi: 10.1093/ndt/17.12.2108
16. Wang Y, Zhao MH, Zhang YK, Li XM, Wang HY. Binding capacity and pathophysiological effects of IgA1 from patients with IgA nephropathy on human glomerular mesangial cells. *Clin Exp Immunol*. (2004) 136:168–75. doi: 10.1111/j.1365-2249.2004.02408.x
17. Tumlin JA, Madaio MP, Hennigar R. Idiopathic IgA nephropathy: pathogenesis, histopathology, and therapeutic options. *Clin J Am Soc Nephrol*. (2007) 2:1054–61. doi: 10.2215/CJN.04351206
18. Monteiro RC, Van De Winkel JG. IgA Fc receptors. *Ann Rev Immunol*. (2003) 21:177–204. doi: 10.1146/annurev.immunol.21.120601.141011
19. Molyneux K, Wimbury D, Pawluczyk I, Muto M, Bhachu J, Mertens PR, et al. beta1,4-galactosyltransferase 1 is a novel receptor for IgA in human mesangial cells. *Kidney Int*. (2017) 92:1458–68. doi: 10.1016/j.kint.2017.05.002
20. Berthelot L, Papista C, Maciel TT, Biarnes-Pelicot M, Tissandie E, Wang PH, et al. Transglutaminase is essential for IgA nephropathy development acting through IgA receptors. *J Exp Med*. (2012) 209:793–806. doi: 10.1084/jem.20112005
21. Lechner SM, Papista C, Chemouny JM, Berthelot L, Monteiro RC. Role of IgA receptors in the pathogenesis of IgA nephropathy. *J Nephrol*. (2016) 29:5–11. doi: 10.1007/s40620-015-0246-5
22. Moura IC, Arcos-Fajardo M, Sadaka C, Leroy V, Benhamou M, Novak J, et al. Glycosylation and size of IgA1 are essential for interaction with mesangial transferrin receptor in IgA nephropathy. *J Am Soc Nephrol*. (2004) 15:622–34. doi: 10.1097/01.ASN.0000115401.07980.0C
23. Moura IC, Arcos-Fajardo M, Gdoura A, Leroy V, Sadaka C, Mahlaoui N, et al. Engagement of transferrin receptor by polymeric IgA1: evidence for a positive feedback loop involving increased receptor expression and mesangial cell proliferation in IgA nephropathy. *J Am Soc Nephrol*. (2005) 16:2667–76. doi: 10.1681/ASN.2004111006
24. Wehbi B, Oblet C, Boyer F, Huard A, Druilhe A, Paraf F, et al. Mesangial deposition can strongly involve innate-like IgA molecules lacking affinity maturation. *J Am Soc Nephrol*. (2019) 30:1238–49. doi: 10.1681/ASN.2018111089
25. Lai KN, Leung JC, Chan LY, Saleem MA, Mathieson PW, Tam KY, et al. Podocyte injury induced by mesangial-derived cytokines in IgA nephropathy. *Nephrol Dial Transplant*. (2009) 24:62–72. doi: 10.1093/ndt/gfn441
26. Lai KN, Leung JC, Chan LY, Saleem MA, Mathieson PW, Lai FM, et al. Activation of podocytes by mesangial-derived TNF-alpha: glomerulo-podocytic communication in IgA nephropathy. *Am J Physiol Renal Physiol*. (2008) 294:F945–55. doi: 10.1152/ajprenal.00423.2007
27. Chan LY, Leung JC, Tsang AW, Tang SC, Lai KN. Activation of tubular epithelial cells by mesangial-derived TNF-alpha: glomerulotubular communication in IgA nephropathy. *Kidney Int*. (2005) 67:602–12. doi: 10.1111/j.1523-1755.2005.67116.x
28. Wang C, Liu X, Peng H, Tang Y, Tang H, Chen Z, et al. Mesangial cells stimulated by immunoglobin A1 from IgA nephropathy upregulates transforming growth factor-beta1 synthesis in podocytes via renin-angiotensin system activation. *Arch Med Res*. (2010) 41:255–60. doi: 10.1016/j.arcmed.2010.05.003
29. Chan LY, Leung JC, Tang SC, Choy CB, Lai KN. Tubular expression of angiotensin II receptors and their regulation in IgA nephropathy. *J Am Soc Nephrol*. (2005) 16:2306–17. doi: 10.1681/ASN.2004121117
30. Kiryluk K, Li Y, Scolari F, Sanna-Cherchi S, Choi M, Verbitsky M, et al. Discovery of new risk loci for IgA nephropathy implicates genes involved in immunity against intestinal pathogens. *Nat Genet*. (2014) 46:1187–96. doi: 10.1038/ng.3118
31. Harabuchi Y, Takahara M. Recent advances in the immunological understanding of association between tonsil and immunoglobulin a nephropathy as a tonsil-induced autoimmune/inflammatory syndrome. *Immun Inflamm Dis*. (2019) 7:86–93. doi: 10.1002/iid3.248
32. Meng H, Ohtake H, Ishida A, Ohta N, Kakehata S, Yamakawa M. IgA production and tonsillar focal infection in IgA nephropathy. *J Clin Exp Hematopathol JCEH*. (2012) 52:161–70. doi: 10.3960/jslrt.52.161
33. Novak J, Moldoveanu Z, Julian BA, Raska M, Wyatt RJ, Suzuki Y, et al. Aberrant glycosylation of IgA1 and anti-glycan antibodies in IgA nephropathy: role of mucosal immune system. *Adv Otorhinolaryngol*. (2011) 72:60–3. doi: 10.1159/000324607

34. Bene MC, Hurault De Ligny B, Kessler M, Faure GC. Confirmation of tonsillar anomalies in IgA nephropathy: a multicenter study. *Nephron*. (1991) 58:425–8. doi: 10.1159/000186474
35. Sugiyama N, Shimizu J, Nakamura M, Kiriu T, Matsuoka K, Masuda Y. Clinicopathological study of the effectiveness of tonsillectomy in IgA nephropathy accompanied by chronic tonsillitis. *Acta Otolaryngol Suppl*. (1993) 508:43–8. doi: 10.3109/00016489309130265
36. Harper SJ, Allen AC, Bene MC, Pringle JH, Faure G, Lauder I, et al. Increased dimeric IgA-producing B cells in tonsils in IgA nephropathy determined by *in situ* hybridization for J chain mRNA. *Clin Exp Immunol*. (1995) 101:442–8. doi: 10.1111/j.1365-2249.1995.tb03132.x
37. Feehally J, Beattie TJ, Brenchley PE, Coupes BM, Mallick NP, Postlethwaite RJ. Sequential study of the IgA system in relapsing IgA nephropathy. *Kidney Int*. (1986) 30:924–31. doi: 10.1038/ki.1986.274
38. Floege J. The pathogenesis of IgA nephropathy: what is new and how does it change therapeutic approaches? *Am J Kidney Dis*. (2011) 58:992–1004. doi: 10.1053/j.ajkd.2011.05.033
39. Kiryluk K, Novak J. The genetics and immunobiology of IgA nephropathy. *J Clin Invest*. (2014) 124:2325–32. doi: 10.1172/JCI74475
40. Macpherson AJ, Gatto D, Sainsbury E, Harriman GR, Hengartner H, Zinkernagel RM. A primitive T cell-independent mechanism of intestinal mucosal IgA responses to commensal bacteria. *Science*. (2000) 288:2222–6. doi: 10.1126/science.288.5474.2222
41. Khera AK, Afkhami S, Lai R, Jeyanathan M, Zganiacz A, Mandur T, et al. Role of B cells in mucosal vaccine-induced protective CD8+ T cell immunity against pulmonary tuberculosis. *J Immunol*. (2015) 195:2900–7. doi: 10.4049/jimmunol.1500981
42. Fernandes JR, Snider DP. Polymeric IgA-secreting and mucosal homing pre-plasma cells in normal human peripheral blood. *Int Immunol*. (2010) 22:527–40. doi: 10.1093/intimm/dxq037
43. Floege J, Feehally J. The mucosa-kidney axis in IgA nephropathy. *Nat Rev Nephrol*. (2016) 12:147–56. doi: 10.1038/nrneph.2015.208
44. Harper SJ, Allen AC, Pringle JH, Feehally J. Increased dimeric IgA producing B cells in the bone marrow in IgA nephropathy determined by *in situ* hybridisation for J chain mRNA. *J Clin Pathol*. (1996) 49:38–42. doi: 10.1136/jcp.49.1.38
45. Batra A, Smith AC, Feehally J, Barratt J. T-cell homing receptor expression in IgA nephropathy. *Nephrol Dial Transplant*. (2007) 22:2540–8. doi: 10.1093/ndt/gfm228
46. Kennel-de March A, Bene MC, Renoult E, Kessler M, Faure GC, Kolopp-Sarda MN. Enhanced expression of L-selectin on peripheral blood lymphocytes from patients with IgA nephropathy. *Clin Exp Immunol*. (1999) 115:542–6. doi: 10.1046/j.1365-2249.1999.00823.x
47. Buren M, Yamashita M, Suzuki Y, Tomino Y, Emancipator SN. Altered expression of lymphocyte homing chemokines in the pathogenesis of IgA nephropathy. *Contrib Nephrol*. (2007) 157:50–5. doi: 10.1159/000102304
48. Tomino Y, Sakai H, Endoh M, Suga T, Miura M, Kaneshige H, et al. Cross-reactivity of IgA antibodies between renal mesangial areas and nuclei of tonsillar cells in patients with IgA nephropathy. *Clin Exp Immunol*. (1983) 51:605–10.
49. Tomino Y, Sakai H. Clinical guidelines for immunoglobulin a (IgA) nephropathy in Japan, second version. *Clin Exp Nephrol*. (2003) 7:93–7. doi: 10.1007/s10157-003-0232-4
50. Masuda Y, Terazawa K, Kawakami S, Ogura Y, Sugiyama N. Clinical and immunological study of IgA nephropathy before and after tonsillectomy. *Acta Otolaryngol Suppl*. (1988) 454:248–55. doi: 10.3109/00016488809125036
51. Akagi H, Nishizaki K, Hattori K, Kosaka M, Fukushima K, Doi A, et al. Prognosis of tonsillectomy in patients with IgA nephropathy. *Acta Otolaryngol Suppl*. (1999) 540:64–6. doi: 10.1080/00016489950181224
52. Xie Y, Chen X, Nishi S, Narita I, Gejyo F. Relationship between tonsils and IgA nephropathy as well as indications of tonsillectomy. *Kidney Int*. (2004) 65:1135–44. doi: 10.1111/j.1523-1755.2004.00486.x
53. Suzuki S, Nakatomi Y, Sato H, Tsukada H, Arakawa M. Haemophilus parainfluenzae antigen and antibody in renal biopsy samples and serum of patients with IgA nephropathy. *Lancet*. (1994) 343:12–6. doi: 10.1016/S0140-6736(94)90875-3
54. Liu H, Peng Y, Liu F, Xiao W, Zhang Y, Li W. Expression of IgA class switching gene in tonsillar mononuclear cells in patients with IgA nephropathy. *Inflamm Res*. (2011) 60:869–78. doi: 10.1007/s00011-011-0347-0
55. Takechi H, Oda T, Hotta O, Yamamoto K, Oshima N, Matsunobu T, et al. Clinical and immunological implications of increase in CD208+ dendritic cells in tonsils of patients with immunoglobulin a nephropathy. *Nephrol Dial Transplant*. (2013) 28:3004–13. doi: 10.1093/ndt/gft399
56. Cox SN, Sallustio F, Serino G, Loverre A, Pesce F, Gigante M, et al. Activated innate immunity and the involvement of CX3CR1-fractalkine in promoting hematuria in patients with IgA nephropathy. *Kidney Int*. (2012) 82:548–60. doi: 10.1038/ki.2012.147
57. Otaka R, Takahara M, Ueda S, Nagato T, Kishibe K, Nomura K, et al. Up-regulation of CX3CR1 on tonsillar CD8-positive cells in patients with IgA nephropathy. *Hum Immunol*. (2017) 78:375–83. doi: 10.1016/j.humimm.2017.02.004
58. Nagayama Y, Nishiwaki H, Hasegawa T, Komukai D, Kawashima E, Takayasu M, et al. Impact of the new risk stratification in the 2011 Japanese society of nephrology clinical guidelines for IgA nephropathy on incidence of early clinical remission with tonsillectomy plus steroid pulse therapy. *Clin Exp Nephrol*. (2015) 19:646–52. doi: 10.1007/s10157-014-1052-4
59. Ponticelli C. Tonsillectomy and IgA nephritis. *Nephrol Dial Transplant*. (2012) 27:2610–3. doi: 10.1093/ndt/gfs093
60. Ohya M, Otani H, Minami Y, Yamanaka S, Mima T, Negi S, et al. Tonsillectomy with steroid pulse therapy has more effect on the relapse rate than steroid pulse monotherapy in IgA nephropathy patients. *Clin Nephrol*. (2013) 80:47–52. doi: 10.5414/CN107861
61. Ochi A, Moriyama T, Takei T, Uchida K, Nitta K. Comparison between steroid pulse therapy alone and in combination with tonsillectomy for IgA nephropathy. *Inter Urol Nephrol*. (2013) 45:469–76. doi: 10.1007/s11255-012-0251-8
62. Maeda I, Hayashi T, Sato KK, Shibata MO, Hamada M, Kishida M, et al. Tonsillectomy has beneficial effects on remission and progression of IgA nephropathy independent of steroid therapy. *Nephrol Dial Transplant*. (2012) 27:2806–13. doi: 10.1093/ndt/gfs053
63. Kawaguchi T, Ieiri N, Yamazaki S, Hayashino Y, Gillespie B, Miyazaki M, et al. Clinical effectiveness of steroid pulse therapy combined with tonsillectomy in patients with immunoglobulin A nephropathy presenting glomerular haematuria and minimal proteinuria. *Nephrology*. (2010) 15:116–23. doi: 10.1111/j.1440-1797.2009.01147.x
64. Wu G, Peng YM, Liu FY, Xu D, Liu C. The role of memory B cell in tonsil and peripheral blood in the clinical progression of IgA nephropathy. *Hum Immunol*. (2013) 74:708–12. doi: 10.1016/j.humimm.2012.10.028
65. Wang Y, Chen J, Wang Y, Chen Y, Wang L, Lv Y. A meta-analysis of the clinical remission rate and long-term efficacy of tonsillectomy in patients with IgA nephropathy. *Nephrol Dial Transplant*. (2011) 26:1923–31. doi: 10.1093/ndt/gfq674
66. Adachi M, Sato M, Miyazaki M, Hotta O, Hozawa K, Sato T, et al. Steroid pulse therapy transiently destroys the discriminative histological structure of tonsils in IgA nephropathy: tonsillectomy should be performed before or just after steroid pulse therapy. *Auris Nasus Larynx*. (2018) 45:1206–13. doi: 10.1016/j.anl.2018.04.009
67. Feehally J, Coppo R, Troyanov S, Bellur SS, Cattran D, Cook T, et al. Tonsillectomy in a European cohort of 1,147 patients with IgA nephropathy. *Nephron*. (2016) 132:15–24. doi: 10.1159/000441852
68. Vergano L, Loiacono E, Albera R, Coppo R, Camilla R, Peruzzi L, et al. Can tonsillectomy modify the innate and adaptive immunity pathways involved in IgA nephropathy? *J Nephrol*. (2015) 28:51–8. doi: 10.1007/s40620-014-0086-8
69. Sissons JG, Woodrow DF, Curtis JR, Evans DJ, Gower PE, Sloper JC, et al. Isolated glomerulonephritis with mesangial IgA deposits. *Br Med J*. (1975) 3:611–4. doi: 10.1136/bmj.3.5984.611
70. Power DA, Muirhead N, Simpson JG, Nicholls AJ, Horne CH, Catto GR, et al. IgA nephropathy is not a rare disease in the United Kingdom. *Nephron*. (1985) 40:180–4. doi: 10.1159/000183457
71. Liu H, Peng Y, Liu H, Liu Y, Yuan S, Liu F, et al. Renal biopsy findings of patients presenting with isolated hematuria: disease associations. *Am J Nephrol*. (2012) 36:377–85. doi: 10.1159/000342233

72. Kiryluk K, Novak J, Gharavi AG. Pathogenesis of immunoglobulin a nephropathy: recent insight from genetic studies. *Annu Rev Med*. (2013) 64:339–56. doi: 10.1146/annurev-med-041811-142014
73. Shreiner AB, Kao JY, Young VB. The gut microbiome in health and in disease. *Curr Opin Gastroenterol*. (2015) 31:69–75. doi: 10.1097/MOG.0000000000000139
74. Chairatana P, Nolan EM. Defensins, lectins, mucins, and secretory immunoglobulin a: microbe-binding biomolecules that contribute to mucosal immunity in the human gut. *Crit Rev Biochem Mol Biol*. (2017) 52:45–56. doi: 10.1080/10409238.2016.1243654
75. Coppo R. The intestine-renal connection in IgA nephropathy. *Nephrol Dial Transplant*. (2015) 30:360–6. doi: 10.1093/ndt/gfu343
76. Russell MW, Mestecky J, Julian BA, Galla JH. IgA-associated renal diseases: antibodies to environmental antigens in sera and deposition of immunoglobulins and antigens in glomeruli. *J Clin Immunol*. (1986) 6:74–86. doi: 10.1007/BF00915367
77. Wang J, Anders RA, Wu Q, Peng D, Cho JH, Sun Y, et al. Dysregulated LIGHT expression on T cells mediates intestinal inflammation and contributes to IgA nephropathy. *J Clin Invest*. (2004) 113:826–35. doi: 10.1172/JCI20096
78. Smerud HK, Fellstrom B, Hallgren R, Osagie S, Venge P, Kristjansson G. Gluten sensitivity in patients with IgA nephropathy. *Nephrol Dial Transplant*. (2009) 24:2476–81. doi: 10.1093/ndt/gfp133
79. Jiang J, Wang XX, Shen PC, Sun C, He LQ. Clinical investigation of mucosal immune system in IgA nephropathy patients. *J Dalian Med Univ*. (2016) 38:558–61.
80. Qin W, Zhong X, Fan JM, Zhang YJ, Liu XR, Ma XY. External suppression causes the low expression of the cosmc gene in IgA nephropathy. *Nephrol Dial Transplant*. (2008) 23:1608–14. doi: 10.1093/ndt/gfm781
81. Emancipator SN, Gallo GR, Lamm ME. Experimental IgA nephropathy induced by oral immunization. *J Exp Med*. (1983) 157:572–82. doi: 10.1084/jem.157.2.572
82. Coppo R, Mazzucco G, Martina G, Roccatello D, Amore A, Novara R, et al. Gluten-induced experimental IgA glomerulopathy. *Lab Invest*. (1989) 60:499–506.
83. Kloster Smerud H, Fellstrom B, Hallgren R, Osagie S, Venge P, Kristjansson G. Gastrointestinal sensitivity to soy and milk proteins in patients with IgA nephropathy. *Clin Nephrol*. (2010) 74:364–71. doi: 10.5414/CNP74364
84. Coppo R, Amore A, Roccatello D, Gianoglio B, Molino A, Piccoli G, et al. IgA antibodies to dietary antigens and lectin-binding IgA in sera from Italian, Australian, and Japanese IgA nephropathy patients. *Am J Kidney Dis*. (1991) 17:480–7. doi: 10.1016/S0272-6386(12)80644-5
85. Papista C, Lechner S, Ben Mkaddem S, LeStang MB, Abbad L, Bex-Coudrat J, et al. Gluten exacerbates IgA nephropathy in humanized mice through gliadin-CD89 interaction. *Kidney Int*. (2015) 88:276–85. doi: 10.1038/ki.2015.94
86. Chen JQ, Szodoray P, Zeher M. Toll-like receptor pathways in autoimmune diseases. *Clin Rev Allergy Immunol*. (2016) 50:1–17. doi: 10.1007/s12016-015-8473-z
87. O'Neill LA, Bowie AG. The family of five: TIR-domain-containing adaptors in toll-like receptor signalling. *Nat Rev Immunol*. (2007) 7:353–64. doi: 10.1038/nri2079
88. Zhu L, Zhang Q, Shi S, Liu L, Lv J, Zhang H. Synergistic effect of mesangial cell-induced CXCL1 and TGF-beta1 in promoting podocyte loss in IgA nephropathy. *PLoS ONE*. (2013) 8:e73425. doi: 10.1371/journal.pone.0073425
89. Gay NJ, Gangloff M. Structure and function of Toll receptors and their ligands. *Ann Rev Biochem*. (2007) 76:141–65. doi: 10.1146/annurev.biochem.76.060305.151318
90. Takeda K, Kaisho T, Akira S. Toll-like receptors. *Ann Rev Immunol*. (2003) 21:335–76. doi: 10.1146/annurev.immunol.21.120601.141126
91. Anders HJ, Schlondorff D. Toll-like receptors: emerging concepts in kidney disease. *Curr Opin Nephrol Hypertens*. (2007) 16:177–83. doi: 10.1097/MNH.0b013e32803fb767
92. Patole PS, Zecher D, Pawar RD, Grone HJ, Schlondorff D, Anders HJ. G-rich DNA suppresses systemic lupus. *J Am Soc Nephrol*. (2005) 16:3273–80. doi: 10.1681/ASN.2005060658
93. He L, Peng X, Liu G, Tang C, Liu H, Liu F, et al. Anti-inflammatory effects of triptolide on IgA nephropathy in rats. *Immunopharmacol Immunotoxicol*. (2015) 37:421–7. doi: 10.3109/08923973.2015.1080265
94. Coppo R, Camilla R, Amore A, Peruzzi L, Dapra V, Loiacono E, et al. Toll-like receptor 4 expression is increased in circulating mononuclear cells of patients with immunoglobulin a nephropathy. *Clin Exp Immunol*. (2010) 159:73–81. doi: 10.1111/j.1365-2249.2009.04045.x
95. Lim BJ, Lee D, Hong SW, Jeong HJ. Toll-like receptor 4 signaling is involved in IgA-stimulated mesangial cell activation. *Yonsei Med J*. (2011) 52:610–5. doi: 10.3349/ymj.2011.52.4.610
96. Chen X, Peng S, Zeng H, Fu A, Zhu Q. Toll-like receptor 4 is involved in a protective effect of rhein on immunoglobulin a nephropathy. *Indian J Pharmacol*. (2015) 47:27–33. doi: 10.4103/0253-7613.150319
97. McCarthy DD, Chiu S, Gao Y, Summers-deLuca LE, Gommerman JL. BAFF induces a hyper-IgA syndrome in the intestinal lamina propria concomitant with IgA deposition in the kidney independent of LIGHT. *Cell Immunol*. (2006) 241:85–94. doi: 10.1016/j.cellimm.2006.08.002
98. Banas MC, Banas B, Hudkins KL, Wietecha TA, Iyoda M, Bock E, et al. TLR4 links podocytes with the innate immune system to mediate glomerular injury. *J Am Soc Nephrol*. (2008) 19:704–13. doi: 10.1681/ASN.2007040395
99. Campbell MT, Hile KL, Zhang H, Asanuma H, Vanderbrink BA, Rink RR, et al. Toll-like receptor 4: a novel signaling pathway during renal fibrogenesis. *J Surg Res*. (2011) 168:e61–9. doi: 10.1016/j.jss.2009.09.053
100. Skuginna V, Lech M, Allam R, Ryu M, Clauss S, Susanti HE, et al. Toll-like receptor signaling and SIGIRR in renal fibrosis upon unilateral ureteral obstruction. *PLoS ONE*. (2011) 6:e19204. doi: 10.1371/journal.pone.0019204
101. Suzuki H, Suzuki Y, Narita I, Aizawa M, Kihara M, Yamanaka T, et al. Toll-like receptor 9 affects severity of IgA nephropathy. *J Am Soc Nephrol*. (2008) 19:2384–95. doi: 10.1681/ASN.2007121311
102. Makita Y, Suzuki H, Kano T, Takahata A, Julian BA, Novak J, et al. TLR9 activation induces aberrant IgA glycosylation via APRIL- and IL-6-mediated pathways in IgA nephropathy. *Kidney Int*. (2020) 97:340–9. doi: 10.1016/j.kint.2019.08.022
103. Sato D, Suzuki Y, Kano T, Suzuki H, Matsuoka J, Yokoi H, et al. Tonsillar TLR9 expression and efficacy of tonsillectomy with steroid pulse therapy in IgA nephropathy patients. *Nephrol Dial Transplant*. (2012) 27:1090–7. doi: 10.1093/ndt/gfr403
104. Ciferska H, Honsova E, Lodererova A, Hruskova Z, Neprasova M, Vachek J, et al. Does the renal expression of Toll-like receptors play a role in patients with IgA nephropathy? *J Nephrol*. (2019). doi: 10.1007/s40620-019-00640-z. [Epub ahead of print].
105. Saito A, Komatsuda A, Kaga H, Sato R, Togashi M, Okuyama S, et al. Different expression patterns of toll-like receptor mRNAs in blood mononuclear cells of IgA nephropathy and IgA vasculitis with nephritis. *Tohoku J Exp Med*. (2016) 240:199–208. doi: 10.1620/tjem.240.199
106. Lee HJ, Choi SY, Jeong KH, Sung JY, Moon SK, Moon JY, et al. Association of C1q deposition with renal outcomes in IgA nephropathy. *Clin Nephrol*. (2013) 80:98–104. doi: 10.5414/CN107854
107. Nasri H. Letter to the article: association of C1q deposition with renal outcomes in IgA nephropathy. *Clin Nephrol*. 2013; 80:98–104. *Clin Nephrol*. (2014) 81:228–9. doi: 10.5414/CN108075
108. Katafuchi R, Nagae H, Masutani K, Tsuruya K, Mitsuiki K. Comprehensive evaluation of the significance of immunofluorescent findings on clinicopathological features in IgA nephropathy. *Clin Exp Nephrol*. (2019) 23:169–81. doi: 10.1007/s10157-018-1619-6
109. Oortwijn BD, Roos A, Royle L, van Gijlswijk-Janssen DJ, Faber-Krol MC, Eijgenraam JW, et al. Differential glycosylation of polymeric and monomeric IgA: a possible role in glomerular inflammation in IgA nephropathy. *J Am Soc Nephrol*. (2006) 17:3529–39. doi: 10.1681/ASN.2006040388
110. Shinohara H, Nagi-Miura N, Ishibashi K, Adachi Y, Ishida-Okawara A, Oharaseki T, et al. Beta-mannosyl linkages negatively regulate anaphylaxis and vasculitis in mice, induced by CAWS, fungal PAMPS composed of mannoprotein-beta-glucan complex secreted by *Candida albicans*. *Biol Pharm Bull*. (2006) 29:1854–61. doi: 10.1248/bpb.29.1854
111. Russell MW, Mansa B. Complement-fixing properties of human IgA antibodies. Alternative pathway complement activation by plastic-bound, but not specific antigen-bound, IgA. *Scand J Immunol*. (1989) 30:175–83. doi: 10.1111/j.1365-3083.1989.tb01199.x

112. Hiemstra PS, Gorter A, Stuurman ME, Van Es LA, Daha MR. Activation of the alternative pathway of complement by human serum IgA. *Eur J Immunol*. (1987) 17:321–6. doi: 10.1002/eji.1830170304
113. Schmitt R, Stahl AL, Olin AI, Kristoffersson AC, Rebetz J, Novak J, et al. The combined role of galactose-deficient IgA1 and streptococcal IgA-binding M Protein in inducing IL-6 and C3 secretion from human mesangial cells: implications for IgA nephropathy. *J Immunol*. (2014) 193:317–26. doi: 10.4049/jimmunol.1302249
114. Zwirner J, Burg M, Schulze M, Brunkhorst R, Gotze O, Koch KM, et al. Activated complement C3: a potentially novel predictor of progressive IgA nephropathy. *Kidney Int*. (1997) 51:1257–64. doi: 10.1038/ki.1997.171
115. Kim SJ, Koo HM, Lim BJ, Oh HJ, Yoo DE, Shin DH, et al. Decreased circulating C3 levels and mesangial C3 deposition predict renal outcome in patients with IgA nephropathy. *PLoS ONE*. (2012) 7:e40495. doi: 10.1371/journal.pone.0040495
116. Liu L, Zhang Y, Duan X, Peng Q, Liu Q, Zhou Y, et al. C3a, C5a renal expression and their receptors are correlated to severity of IgA nephropathy. *J Clin Immunol*. (2014) 34:224–32. doi: 10.1007/s10875-013-9970-6
117. Mizerska-Wasiak M, Maldyk J, Rybi-Szuminska A, Wasilewska A, Miklaszewska M, Pietrzyk J, et al. Relationship between serum IgA/C3 ratio and severity of histological lesions using the Oxford classification in children with IgA nephropathy. *Pediatr Nephrol*. (2015) 30:1113–20. doi: 10.1007/s00467-014-3024-z
118. Moresco RN, Speeckaert MM, Delanghe JR. Diagnosis and monitoring of IgA nephropathy: the role of biomarkers as an alternative to renal biopsy. *Autoimmun Rev*. (2015) 14:847–53. doi: 10.1016/j.autrev.2015.05.009
119. Zhang JJ, Jiang L, Liu G, Wang SX, Zou WZ, Zhang H, et al. Levels of urinary complement factor H in patients with IgA nephropathy are closely associated with disease activity. *Scand J Immunol*. (2009) 69:457–64. doi: 10.1111/j.1365-3083.2009.02234.x
120. Ricklin D, Reis ES, Lambris JD. Complement in disease: a defence system turning offensive. *Nat Rev Nephrol*. (2016) 12:383–401. doi: 10.1038/nrneph.2016.70
121. Gharavi AG, Kiryluk K, Choi M, Li Y, Hou P, Xie J, et al. Genome-wide association study identifies susceptibility loci for IgA nephropathy. *Nat Genet*. (2011) 43:321–7. doi: 10.1038/ng.787
122. Zhu L, Zhai YL, Wang FM, Hou P, Lv JC, Xu DM, et al. Variants in complement factor h and complement factor H-related protein genes, CFHR3 and CFHR1, affect complement activation in IgA nephropathy. *J Am Soc Nephrol*. (2015) 26:1195–204. doi: 10.1681/ASN.2014010096
123. Tortajada A, Gutierrez E, Goicoechea de Jorge E, Anter J, Segarra A, Espinosa M, et al. Elevated factor H-related protein 1 and factor H pathogenic variants decrease complement regulation in IgA nephropathy. *Kidney Int*. (2017) 92:953–63. doi: 10.1016/j.kint.2017.03.041
124. Medjeral-Thomas NR, Lomax-Browne HJ, Beckwith H, Willicombe M, McLean AG, Brookes P, et al. Circulating complement factor H-related proteins 1 and 5 correlate with disease activity in IgA nephropathy. *Kidney Int*. (2017) 92:942–52. doi: 10.1016/j.kint.2017.03.043
125. Murphy B, Georgiou T, Machet D, Hill P, McRae J. Factor H-related protein-5: a novel component of human glomerular immune deposits. *Am J Kidney Dis*. (2002) 39:24–7. doi: 10.1053/ajkd.2002.29873
126. Zhai YL, Meng SJ, Zhu L, Shi SF, Wang SX, Liu LJ, et al. Rare variants in the complement factor H-related protein 5 gene contribute to genetic susceptibility to IgA nephropathy. *J Am Soc Nephrol*. (2016) 27:2894–905. doi: 10.1681/ASN.2015010012
127. Zhu L, Guo WY, Shi SF, Liu LJ, Lv JC, Medjeral-Thomas NR, et al. Circulating complement factor H-related protein 5 levels contribute to development and progression of IgA nephropathy. *Kidney Int*. (2018) 94:150–8. doi: 10.1016/j.kint.2018.02.023
128. Tortajada A, Gutierrez E, Pickering MC, Praga Terente M, Medjeral-Thomas N. The role of complement in IgA nephropathy. *Mol Immunol*. (2019) 114:123–32. doi: 10.1016/j.molimm.2019.07.017
129. Roos A, Rastaldi MP, Calvaresi N, Oortwijn BD, Schlagwein N, van Gijlswijk-Janssen DJ, et al. Glomerular activation of the lectin pathway of complement in IgA nephropathy is associated with more severe renal disease. *J Am Soc Nephrol*. (2006) 17:1724–34. doi: 10.1681/ASN.2005090923
130. Coppo R, Amore A, Peruzzi L, Vergano L, Camilla R. Innate immunity and IgA nephropathy. *J Nephrol*. (2010) 23:626–32.
131. Medjeral-Thomas NR, Troldborg A, Constantinou N, Lomax-Browne HJ, Hansen AG, Willicombe M, et al. Progressive IgA nephropathy is associated with low circulating mannan-binding lectin-associated serine protease-3 (MASP-3) and increased glomerular factor h-related protein-5 (FHR5) deposition. *Kidney Inter Rep*. (2018) 3:426–38. doi: 10.1016/j.ekir.2017.11.015
132. Thiel S. Complement activating soluble pattern recognition molecules with collagen-like regions, mannan-binding lectin, ficolins and associated proteins. *Mol Immunol*. (2007) 44:3875–88. doi: 10.1016/j.molimm.2007.06.005
133. Roos A, Bouwman LH, van Gijlswijk-Janssen DJ, Faber-Krol MC, Stahl GL, Daha MR. Human IgA activates the complement system via the mannan-binding lectin pathway. *J Immunol*. (2001) 167:2861–8. doi: 10.4049/jimmunol.167.5.2861
134. Liu LL, Jiang Y, Wang LN, Liu N. Urinary mannose-binding lectin is a biomarker for predicting the progression of immunoglobulin (Ig)A nephropathy. *Clin Exp Immunol*. (2012) 169:148–55. doi: 10.1111/j.1365-2249.2012.04604.x
135. Shi B, Wang L, Mou S, Zhang M, Wang Q, Qi C, et al. Identification of mannose-binding lectin as a mechanism in progressive immunoglobulin a nephropathy. *Inter J Clin Exp Pathol*. (2015) 8:1889–99.
136. Guo WY, Zhu L, Meng SJ, Shi SF, Liu LJ, Lv JC, et al. Mannose-binding lectin levels could predict prognosis in iga nephropathy. *J Am Soc Nephrol*. (2017) 28:3175–81. doi: 10.1681/ASN.2017010076
137. Fabiano RC, Pinheiro SV, de Almeida Araujo S, Simoes ESAC. Immunoglobulin a nephropathy: pathological markers of renal survival in paediatric patients. *Nephrology*. (2016) 21:995–1002. doi: 10.1111/nep.12850
138. Sato Y, Sasaki S, Okamoto T, Takahashi T, Hayashi A, Ogawa Y, et al. Mesangial C4d deposition at diagnosis in childhood immunoglobulin a nephropathy. *Pediatr Int*. (2019) 61:1133–9. doi: 10.1111/ped.13921
139. Maeng YI, Kim MK, Park JB, Cho CH, Oh HK, Sung WJ, et al. Glomerular and tubular C4d depositions in IgA nephropathy: relations with histopathology and with albuminuria. *Int J Clin Exp Pathol*. (2013) 6:904–10.
140. Nasri H, Ahmadi A, Rafieian-Kopaei M, Bashardoust B, Nasri P, Mubarak M. Association of glomerular C4d deposition with various demographic data in IgA nephropathy patients; a preliminary study. *J Nephropathol*. (2015) 4:19–23. doi: 10.12860/jnp.2015.04
141. Sahin OZ, Yavas H, Tasli F, Gibyeli DG, Ersoy R, Uzum A, et al. Prognostic value of glomerular C4d staining in patients with IgA nephritis. *Inter J Clin Exp Pathol*. (2014) 7:3299–304.
142. Rath A, Tewari R, Mendonca S, Badwal S, Nijhawan VS. Oxford classification of IgA nephropathy and C4d deposition; correlation and its implication. *J Nephropharmacol*. (2016) 5:75–9.
143. Rauterberg EW, Lieberknecht HM, Wingen AM, Ritz E. Complement membrane attack (MAC) in idiopathic IgA-glomerulonephritis. *Kidney Int*. (1987) 31:820–9. doi: 10.1038/ki.1987.72
144. Onda K, Ohsawa I, Ohi H, Tamano M, Mano S, Wakabayashi M, et al. Excretion of complement proteins and its activation marker C5b-9 in IgA nephropathy in relation to renal function. *BMC Nephrol*. (2011) 12:64. doi: 10.1186/1471-2369-12-64
145. Paunas TIF, Finne K, Leh S, Marti HP, Mollnes TE, Berven F, et al. Glomerular abundance of complement proteins characterized by proteomic analysis of laser-captured microdissected glomeruli associates with progressive disease in IgA nephropathy. *Clin Proteomics*. (2017) 14:30. doi: 10.1186/s12014-017-9165-x
146. Yu HH, Chu KH, Yang YH, Lee JH, Wang LC, Lin YT, et al. Genetics and immunopathogenesis of IgA nephropathy. *Clin Rev Allergy Immunol*. (2011) 41:198–213. doi: 10.1007/s12016-010-8232-0
147. He L, Peng Y, Liu H, Yin W, Chen X, Peng X, et al. Th1/Th2 polarization in tonsillar lymphocyte form patients with IgA nephropathy. *Ren Fail*. (2014) 36:407–12. doi: 10.3109/0886022X.2013.862809
148. Chintalacharuvu SR, Yamashita M, Bagheri N, Blanchard TG, Nedrud JG, Lamm ME, et al. T cell cytokine polarity as a determinant of immunoglobulin a (IgA) glycosylation and the severity of experimental IgA nephropathy. *Clin Exp Immunol*. (2008) 153:456–62. doi: 10.1111/j.1365-2249.2008.03703.x
149. Sun Q, Zhang J, Zhou N, Liu X, Shen Y. DNA methylation in cosmc promoter region and aberrantly glycosylated IgA1

associated with pediatric IgA nephropathy. *PLoS ONE*. (2015) 10:e0112305. doi: 10.1371/journal.pone.0112305
150. Schena FP, Cerullo G, Torres DD, Scolari F, Foramitti M, Amoroso A, et al. Role of interferon-gamma gene polymorphisms in susceptibility to IgA nephropathy: a family-based association study. *Eur J Hum Genet EJHG*. (2006) 14:488–96. doi: 10.1038/sj.ejhg.5201591
151. Yang L, Zhang X, Peng W, Wei M, Qin W. MicroRNA-155-induced T lymphocyte subgroup drifting in IgA nephropathy. *Int Urol Nephrol*. (2017) 49:353–61. doi: 10.1007/s11255-016-1444-3
152. Zhang Z, Wang H, Zhang L, Crew R, Zhang N, Liu X, et al. Serum levels of soluble ST2 and IL-10 are associated with disease severity in patients with IgA nephropathy. *J Immunol Res*. (2016) 2016:6540937. doi: 10.1155/2016/6540937
153. Lee TW, Kim MJ. Production of interleukin-2 (IL-2) and expression of IL-2 receptor in patients with IgA nephropathy. *Korean J Intern Med*. (1992) 7:31–8. doi: 10.3904/kjim.1992.7.1.31
154. Mitra S, Leonard WJ. Biology of IL-2 and its therapeutic modulation: mechanisms and strategies. *J Leukoc Biol*. (2018) 103:643–55. doi: 10.1002/JLB.2RI0717-278R
155. Paust HJ, Turner JE, Riedel JH, Disteldorf E, Peters A, Schmidt T, et al. Chemokines play a critical role in the cross-regulation of Th1 and Th17 immune responses in murine crescentic glomerulonephritis. *Kidney Int*. (2012) 82:72–83. doi: 10.1038/ki.2012.101
156. Sallustio F, Serino G, Cox SN, Dalla Gassa A, Curci C, De Palma G, et al. Aberrantly methylated DNA regions lead to low activation of CD4+ T-cells in IgA nephropathy. *Clin Sci*. (2016) 130:733–46. doi: 10.1042/CS20150711
157. Jogdand GM, Mohanty S, Devadas S. Regulators of Tfh cell differentiation. *Front Immunol*. (2016) 7:520. doi: 10.3389/fimmu.2016.00520
158. Zhang L, Wang Y, Shi X, Zou H, Jiang Y. A higher frequency of $CD4^+CXCR5^+$ T follicular helper cells in patients with newly diagnosed IgA nephropathy. *Immunol Lett*. (2014) 158:101–8. doi: 10.1016/j.imlet.2013.12.004
159. Sun Y, Liu Z, Liu Y, Li X. Increased frequencies of memory and activated B cells and follicular helper T cells are positively associated with high levels of activationinduced cytidine deaminase in patients with immunoglobulin A nephropathy. *Mol Med Rep*. (2015) 12:5531–7. doi: 10.3892/mmr.2015.4071
160. Huang ZQ, Raska M, Stewart TJ, Reily C, King RG, Crossman DK, et al. Somatic mutations modulate autoantibodies against galactose-deficient IgA1 in IgA nephropathy. *J Am Soc Nephrol*. (2016) 27:3278–84. doi: 10.1681/ASN.2014101044
161. Mazzoni A, Maggi L, Liotta F, Cosmi L, Annunziato F. Biological and clinical significance of T helper 17 cell plasticity. *Immunology*. (2019) 158:287–95. doi: 10.1111/imm.13124
162. Eisenstein EM, Williams CB. The T (reg)/Th17 cell balance: a new paradigm for autoimmunity. *Pediatr Res*. (2009) 65(5 Pt 2):26R—31R. doi: 10.1203/PDR.0b013e31819e76c7
163. Shan J, Feng L, Sun G, Chen P, Zhou Y, Xia M, et al. Interplay between mTOR and STAT5 signaling modulates the balance between regulatory and effective T cells. *Immunobiology*. (2015) 220:510–7. doi: 10.1016/j.imbio.2014.10.020
164. Lin FJ, Jiang GR, Shan JP, Zhu C, Zou J, Wu XR. Imbalance of regulatory T cells to Th17 cells in IgA nephropathy. *Scand J Clin Lab Invest*. (2012) 72:221–9. doi: 10.3109/00365513.2011.652158
165. Lin JR, Wen J, Zhang H, Wang L, Gou FF, Yang M, et al. Interleukin-17 promotes the production of underglycosylated IgA1 in DAKIKI cells. *Ren Fail*. (2018) 40:60–7. doi: 10.1080/0886022X.2017.1419972
166. Lu G, Zhang X, Shen L, Qiao Q, Li Y, Sun J, et al. CCL20 secreted from IgA1-stimulated human mesangial cells recruits inflammatory Th17 cells in IgA nephropathy. *PLoS ONE*. (2017) 12:e0178352. doi: 10.1371/journal.pone.0178352
167. Yang S, Chen B, Shi J, Chen F, Zhang J, Sun Z. Analysis of regulatory T cell subsets in the peripheral blood of immunoglobulin A nephropathy (IgAN) patients. *Genet Mol Res*. (2015) 14:14088–92. doi: 10.4238/2015.October.29.28
168. Huang H, Peng Y, Liu H, Yang X, Liu F. Decreased CD4+CD25+ cells and increased dimeric IgA-producing cells in tonsils in IgA nephropathy. *J Nephrol*. (2010) 23:202–9.
169. Huang H, Peng Y, Long XD, Liu Z, Wen X, Jia M, et al. Tonsillar CD4+CD25+ regulatory T cells from IgA nephropathy patients have decreased immunosuppressive activity in experimental IgA nephropathy rats. *Am J Nephrol*. (2013) 37:472–80. doi: 10.1159/000350533
170. He L, Peng X, Wang J, Tang C, Zhou X, Liu H, et al. Synthetic double-stranded RNA Poly(I:C) aggravates IgA nephropathy by triggering IgA class switching recombination through the TLR3-BAFF axis. *Am J Nephrol*. (2015) 42:185–97. doi: 10.1159/000440819
171. Xin G, Shi W, Xu LX, Su Y, Yan LJ, Li KS. Serum BAFF is elevated in patients with IgA nephropathy and associated with clinical and histopathological features. *J Nephrol*. (2013) 26:683–90. doi: 10.5301/jn.5000218
172. Zheng N, Fan J, Wang B, Wang D, Feng P, Yang Q, et al. Expression profile of BAFF in peripheral blood from patients of IgA nephropathy: correlation with clinical features and *Streptococcus pyogenes* infection. *Mol Med Rep*. (2017) 15:1925–35. doi: 10.3892/mmr.2017.6190
173. Muto M, Manfroi B, Suzuki H, Joh K, Nagai M, Wakai S, et al. Toll-Like receptor 9 stimulation induces aberrant expression of a proliferation-inducing ligand by tonsillar Germinal center B cells in IgA nephropathy. *J Am Soc Nephrol*. (2017) 28:1227–38. doi: 10.1681/ASN.2016050496
174. Zhai YL, Zhu L, Shi SF, Liu LJ, Lv JC, Zhang H. Increased APRIL expression induces IgA1 aberrant glycosylation in IgA nephropathy. *Medicine*. (2016) 95:e3099. doi: 10.1097/MD.0000000000003099
175. Takahara M, Nagato T, Nozaki Y, Kumai T, Katada A, Hayashi T, et al. A proliferation-inducing ligand (APRIL) induced hyper-production of IgA from tonsillar mononuclear cells in patients with IgA nephropathy. *Cell Immunol*. (2019) 341:103925. doi: 10.1016/j.cellimm.2019.103925
176. Martin-Penagos L, Benito-Hernandez A, San Segundo D, Sango C, Azueta A, Gomez-Roman J, et al. A proliferation-inducing ligand increase precedes IgA nephropathy recurrence in kidney transplant recipients. *Clin Transplant*. (2019) 33:e13502. doi: 10.1111/ctr.13502
177. Ye M, Peng Y, Liu C, Yan W, Peng X, He L, et al. Vibration induces BAFF overexpression and aberrant O-Glycosylation of IgA1 in cultured human tonsillar mononuclear cells in IgA nephropathy. *BioMed Res Inter*. (2016) 2016:9125960. doi: 10.1155/2016/9125960
178. Shao J, Peng Y, He L, Liu H, Chen X, Peng X. Capsaicin induces high expression of BAFF and aberrantly glycosylated IgA1 of tonsillar mononuclear cells in IgA nephropathy patients. *Hum Immunol*. (2014) 75:1034–9. doi: 10.1016/j.humimm.2014.08.205
179. Li W, Peng X, Liu Y, Liu H, Liu F, He L, et al. TLR9 and BAFF: their expression in patients with IgA nephropathy. *Mol Med Rep*. (2014) 10:1469–74. doi: 10.3892/mmr.2014.2359
180. McCarthy DD, Kujawa J, Wilson C, Papandile A, Poreci U, Porfilio EA, et al. Mice overexpressing BAFF develop a commensal flora-dependent, IgA-associated nephropathy. *J Clin Invest*. (2011) 121:3991–4002. doi: 10.1172/JCI45563
181. Suzuki Y, Suzuki H, Nakata J, Sato D, Kajiyama T, Watanabe T, et al. Pathological role of tonsillar B cells in IgA nephropathy. *Clin Dev Immunol*. (2011) 2011:639074. doi: 10.1155/2011/639074
182. Wu G, Peng YM, Liu H, Hou QD, Liu FY, Chen NL, et al. Expression of CD19(+)CD5(+)B cells and IgA1-positive cells in tonsillar tissues of IgA nephropathy patients. *Ren Fail*. (2011) 33:159–63. doi: 10.3109/0886022X.2011.552150
183. Yuling H, Ruijing X, Xiang J, Yanping J, Lang C, Li L, et al. $CD19^+CD5^+$ B cells in primary IgA nephropathy. *J Am Soc Nephrol*. (2008) 19:2130–9. doi: 10.1681/ASN.2007121303

Conflict of Interest: The authors declare that the research was conducted in the absence of any commercial or financial relationships that could be construed as a potential conflict of interest.

frontiers in Medicine

ORIGINAL RESEARCH
published: 27 March 2020
doi: 10.3389/fmed.2020.00080

Inhibition of Inflammatory Cytokine Expression Prevents High-Fat Diet-Induced Kidney Injury: Role of Lingonberry Supplementation

*Susara Madduma Hewage[1,2], Suvira Prashar[1,3], Samir C. Debnath[4], Karmin O[1,2,5] and Yaw L. Siow[1,2,3]**

[1] Canadian Centre for Agri-Food Research in Health and Medicine, St. Boniface Hospital Albrechtsen Research Centre, Winnipeg, MB, Canada, [2] Department of Physiology & Pathophysiology, University of Manitoba, Winnipeg, MB, Canada, [3] Agriculture and Agri-Food Canada, St. Boniface Hospital Albrechtsen Research Centre, Winnipeg, MB, Canada, [4] Agriculture and Agri-Food Canada, St. John's Research and Development Centre, St. John's, NL, Canada, [5] Department of Animal Science, University of Manitoba, Winnipeg, MB, Canada

OPEN ACCESS

Edited by:
Cheng Yang,
Fudan University, China

Reviewed by:
Bin Yang,
University of Leicester, United Kingdom
Hee-Seong Jang,
University of Nebraska Medical Center, United States

***Correspondence:**
Yaw L. Siow
chris.siow@canada.ca;
csiow@sbrc.ca

Specialty section:
This article was submitted to Nephrology, a section of the journal Frontiers in Medicine

Received: 12 December 2019
Accepted: 25 February 2020
Published: 27 March 2020

Citation:
Madduma Hewage S, Prashar S, Debnath SC, O K and Siow YL (2020) Inhibition of Inflammatory Cytokine Expression Prevents High-Fat Diet-Induced Kidney Injury: Role of Lingonberry Supplementation. Front. Med. 7:80. doi: 10.3389/fmed.2020.00080

Chronic low-grade inflammation is a major stimulus for progression of chronic kidney disease (CKD) in individuals consuming high-fat diet. Currently, there are limited treatment options for CKD other than controlling the progression rate and its associated complications. Lingonberry (*Vaccinium vitis-idaea* L.) is rich in anthocyanins with demonstrated anti-inflammatory effect. In the current study, we investigated the potential renal protective effect of lingonberry and its anthocyanin (cyanidin-3-glucoside) in high-fat diet fed obese mice and in human proximal tubular cells. Prolonged consumption of high-fat diets is strongly associated with obesity, abnormal lipid and glucose metabolism. Mice (C57BL/6J) fed a high-fat diet (62% kcal fat) for 12 weeks developed renal injury as indicated by an elevation of blood urea nitrogen (BUN) level as well as an increase in renal kidney injury molecule-1 (KIM-1), neutrophil gelatinase-associated lipocalin (NGAL) and renin expression. Those mice displayed an activation of nuclear factor kappa-light-chain-enhancer of activated B cells (NF-κB) and increased expression of inflammatory cytokines–monocyte chemoattractant-1 (MCP-1), tumor necrosis factor alpha (TNF-α), interleukin-6 (IL-6) in the kidneys. Mice fed a high-fat diet also had a significant elevation of inflammatory cytokine levels in the plasma. Dietary supplementation of lingonberry for 12 weeks not only attenuated high-fat diet-induced renal inflammatory response but also reduced kidney injury. Such a treatment improved plasma lipid and glucose profiles, reduced plasma inflammatory cytokine levels but did not affect body weight gain induced by high-fat diet feeding. Lingonberry extract or its active component cyanidin-3-glucoside effectively inhibited palmitic acid-induced NF-κB activation and inflammatory cytokine expression in proximal tubular cells. These results suggest that lingonberry supplementation can reduce inflammatory response and prevent chronic kidney injury. Such a renal protective effect by lingonberry and its active component may be mediated, in part, through NF-κB signaling pathway.

Keywords: chronic kidney disease, high-fat diet, lingonberry, cytokines, inflammation, NF-κB

INTRODUCTION

Chronic kidney disease (CKD) is a common kidney disease with a progressive decline of renal function (1). Obesity and metabolic syndrome are independent risk factors for the development of CKD (2). Obesity is prevalent in many countries around the world. Large cohort studies have shown that the incidence of CKD increases by 20–88% in obese individuals (3–5). There is increasing evidence that patients who survived acute kidney injury have increased risks in developing CKD (6). CKD has emerged as a serious economic threat to health care systems globally due to its increasing prevalence, complications (such as anemia, cardiovascular disease, bone, and mineral disorders), immense expenses associated with renal replacement therapy, high morbidity and mortality (1).

The pathophysiology of CKD is complex and incompletely understood. Several mechanisms by which obesity causes CKD have been proposed, which include renal lipid accumulation, inflammation and mitochondrial dysfunction (5, 7, 8). Chronic inflammatory response has been implicated as one of the important mediators contributing to kidney injury in patients with obesity (9). A study conducted in patients with chronic renal insufficiency revealed that kidney injury was positively correlated to the levels of proinflammatory cytokines, namely, tumor necrosis factor alpha (TNF-α) and interleukin-6 (IL-6) in the plasma (10). It was reported that casein-induced inflammatory stress promoted renal lipid accumulation and glomerular lesion formation in high-fat diet fed obese mice that displayed renal and systemic changes compatible to human obesity-related CKD (8). Chronic consumption of high-fat diets (HFD) is a major contributor to the development of obesity and metabolic abnormalities. In our previous studies, we observed an increased body weight gain and metabolic abnormalities (hyperlipidemia, hyperglycemia) in mice fed a HFD for 5–12 weeks (11–16). Recent studies demonstrated renal injury in diet-induced obese mice, a murine model of CKD (7, 17).

Currently, there is no specific treatment for CKD other than lowering the progression rate by controlling the CKD risk factors and its associated complications (edema, anemia, cardiovascular diseases, and bone and mineral disorders) (18). The most common medications prescribed for CKD patients include diuretics, erythropoietins, antihypertensive agents, statins and calcium and vitamin D supplements (18). Certain dietary restrictions are recommended to control the intake of protein, sugar, salt, and fiber content (18). In our previous study, we reported that supplementation of diet with lingonberry juice could protect rats against ischemia-reperfusion-induced acute kidney injury (19). Lingonberry (*Vaccinium vitis-idaea* L.) is an evergreen dwarf shrub native to North America and Eurasia throughout the Northern Hemisphere (20). The bright reddish color berries produced by these plants are edible and is opulent with anthocyanins compared to other commonly consumed berries (21). Anthocyanins are a group of water soluble flavonoids known for their antioxidant, anti-inflammatory, and anticancer properties (22). Lingonberry contains three types of anthocyanins, identified as cyanidin-3-galactoside, cyanidin-3-glucoside (C-3-Glu) and cyanidin-3-arabinoside (23). Among these, C-3-Glu is known to improve the redox status, energy, and glucose metabolism in rat kidneys (24). Furthermore, recent studies have revealed that lingonberry exhibits antidiabetic and renal protective properties (19, 25). However, its role in CKD has not been identified. In the current study, we investigated the potential renal protective effect of lingonberry and its anthocyanin (C-3-Glu) in HFD-induced obese mice and in human proximal tubular cells.

MATERIALS AND METHODS

Animal Model

Five weeks old C57BL/6J male mice were purchased from the University of Manitoba Central Animal Care Services (Winnipeg, MB, Canada). Animals were housed two per cage in a temperature- and humidity-controlled room with a 12 h dark−12 h light cycle, and freely accessible for water and feed. Mice were divided into three groups ($n = 10$): (1) Control (D12450J) diet consisted of 11% kcal fat, 18% kcal protein, and 71% kcal carbohydrate, (2) HFD (D12492) consisted of 62% kcal fat, 18% kcal protein, and 20% kcal carbohydrate, and (3) HFD supplemented with 5% Manitoba lingonberry (*Vaccinium vitis-idaea* ssp. *minus* (Lodd.) Hult.) (w/w) (D17022206). The animals were fed *ad libitum* for 12 weeks with the diets listed (Research Diets, Brunswick, NJ, USA). Fasting blood was collected at week 12 from the jugular vein after a 6 h fasting period to measure the following plasma analytes: triglyceride, total cholesterol, and urea/BUN, using the Cobas C111 Analyzer (Roche, Risch-Rotkreuz, Switzerland). Fasting blood glucose was measured at week 12 using AlphaTRAK 2 Blood Glucose Test Strips (Zoetis, Kirkland, QC, Canada). At the end of week 12, animals were sacrificed and their kidneys and blood were collected. All procedures were performed in accordance with the Guide to the Care and Use of Experimental Animals published by the Canadian Council on Animal Care and approved by the University of Manitoba Protocol Management and Review Committee.

Cell Culture

Human proximal tubule epithelial cells (HK-2) were purchased from American Type Culture Collection (CRL-2190, Manassas, VA, USA) and maintained in keratinocyte serum-free media supplemented with 5 ng/ml human recombinant epidermal growth factor and 50 ng/ml bovine pituitary extract (Life Technologies, Carlsbad, CA, USA) at 37°C in 95% oxygen−5% carbon dioxide atmosphere. The cells were sub-cultured at or below 90% confluency once every 2–3 days and passages between 5 and 20 were used for all the experiments. Depending on the assay, cells were seeded in 6-well plates or 100 mm dishes at a density of 2.0×10^5 cells per well or 2×10^6 cells per dish. Cells seeded in 6-well plate were pre-treated for 4 h either with cyanidin-3-glucoside (C-3-Glu) (2, 10, and 20 μM; Cerilliant Corp., Round Rock, TX, USA) or various dilutions of lingonberry extract (1:1,000, 1:500, and 1:200). The lingonberry (LB) extract was prepared as previously described (23). After the pre-treatment, the cells were incubated for 4 h with palmitic acid (Sigma-Aldrich. St. Louis, MO, USA; dissolved in 10% fatty

acid-free bovine serum albumin by gently shaking overnight at 37°C) prior to being added to the culture medium (16). In one set of experiments, cells were pre-incubated for 1 h with 100 μM ammonium pyrrolidinedithiocarbamate (PDTC; Sigma Aldrich), a selective inhibitor of NF-κB, prior to treatment with palmitic acid.

Cell Viability Assay

The influence of palmitic acid, C-3-Glu and LB extract on HK-2 cell viability was examined using the 3-(4,5-dimethylthiazol-2-yl)-2,5-diphenyltetrazolium bromide (MTT) assay. Cells were seeded in a 96-well plate at a density of 20,000 cells/well. After 24 h incubation, cells were treated with different concentrations of palmitic acid, C-3-Glu or LB extract for another 24 h. The yellow tetrazolium MTT (Sigma-Aldrich) was added to each well to yield a final concentration of 100 μM. The supernatant was aspirated 4 h later and the MTT formazan crystals were dissolved in dimethyl sulfoxide (DMSO; Thermo Fisher Scientific, Waltham, MA, USA). The absorbance at 540 nm was read using a SpectraMax M5 microplate reader (Molecular Devices, Sunnyvale, CA, USA).

Measurement of mRNA Expression

Relative mRNA expression of kidney injury molecule-1 (KIM-1), IL-6, monocyte chemoattractant protein-1 (MCP-1), neutrophil gelatinase-associated lipocalin (NGAL), renin and TNF-α, were measured using a StepOne Plus Real-Time qPCR (RT-qPCR) system (Applied Biosystems, Foster City, CA, USA). Briefly, total RNA was extracted from the HK-2 cells and the mouse kidney tissues with TRIzol (Thermo Fisher Scientific) and QIAzol (Qiagen, Hilden, Germany) reagents, respectively. HK-2 cells grown in 6-well plates were washed twice with ice cold PBS and the cell lysate was collected by adding 1 ml of TRIzol per well. Kidney tissues preserved in RNA*later* (Thermo Fisher Scientific) were homogenized with a handheld homogenizer (VWR 200, VWR, Radnor, PA, USA) in 1 ml of QIAzol reagent on ice. Total RNA was extracted according to the TRIzol reagent procedure for isolation of RNA as described by Chomczynski and Mackey (26). Extracted RNA was quantified using a NanoDrop One^{C} (Thermo Fisher Scientific) spectrophotometer. cDNA was synthesized by mixing 1X first-strand buffer, 10 mM dithiothreitol (DTT), 0.5 mM deoxynucleotide triphosphates (dNTPs), 10 ng/μl Oligo dT primers, 1 U/μl RNaseOUT recombinant ribonuclease inhibitor, 1 U/μl moloney murine leukemia virus (M-MLV) reverse transcriptase (Thermo Fisher Scientific), with 1 μg of total RNA in a total volume of 20 μl. Then the mixture was incubated for 60 min at 37°C and 2 min at 95°C. The RT-qPCR mixture contained 100 ng of cDNA, 1X iTaq Universal SYBR Green Super Mix (Bio-Rad, Hercules, CA, USA), 300 nM per primer and RNase-free water, in a total reaction mixture of 20 μl. The qPCR protocol was initiated as follows: the reaction mixture was subjected to initial denaturation at 95°C for 3 min followed by 45 cycles of denaturation step 95°C, 10 s and annealing. Annealing temperatures for TNF-α, IL-6, MCP-1, NGAL and renin were set at 58°C for 30 s while for KIM-1, it was set at 60°C for 15 s. For each primer a melt curve analysis was performed. All the samples were tested in triplicate and data were analyzed using the comparative C_T method (27) with gene expression level normalized to that of the housekeeping gene β-actin. The results were expressed as a percentage of the control group, which was set to 100%. Primer sequences used for the RT-qPCR were shown in the **Table 1**.

TABLE 1 | Primer sequences used for RT-qPCR.

Primer	Sequence 5′-3′	Accession number	Product length
Human			
IL-6	F: ACTCACCTCTTCAGAACGAATTG R: CCATCTTTGGAAGGTTCAGGTTG	XM_005249745.5	149 bp
MCP-1	F: CCCAAAGAAGCTGTGATCTTCA R: GTGTCTGGGGAAAGCTAGGG	NM_002982.4	186 bp
TNF-α	F: GAGGCCAAGCCCTGGTATG R: CGGGCCGATTGATCTCAGC	NM_000594.4	91 bp
β-Actin	F: AGATCAAGATCATTGCTCCTCCT R: GATCCACATCTGCTGGAAGG	NM_001101.5	95 bp
Mouse			
IL-6	F: GACTGATGCTGGTGACAACC R: GCCATTGCACAACTCTTTTC	NM_001314054.1	170 bp
MCP-1	F: AGGTCCCTGTCATGCTTCTG R: GCTGCTGGTGATCCTCTTGT	NM_011333.3	167 bp
TNF-α	F: GTCCCCAAAGGGATGAGAAG R: GCTCCTCCACTTGGTGGTTT	NM_001278601.1	93 bp
NGAL	F: ACGGACTACAACCAGTTCGC R: AATGCATTGGTCGGTGGGG	NM_008491.1	192 bp
KIM-1	F: TCCACACATGTACCAACATCAA R: GTCACAGTGCCATTCCAGTC	XM_011248784.2	98 bp
β-Actin	F: GATCAAGATCATTGCTCCTCCT R: AGGGTGTAAAACGCAGCTCA	XM_030254057.1	183 bp

Electrophoretic Mobility Shift Assay (EMSA)

LightShift Chemiluminescent EMSA Kit (Thermo Fisher Scientific) was used to measure the DNA binding affinity of NF-κB. In brief, nuclear proteins were extracted from the mouse kidney tissues and HK-2 cells as previously described (28). Nuclear proteins (2 μg) were incubated in a reaction mixture containing DNA-binding buffer, poly (dI-dC), and biotin-end-labeled oligonucleotides containing a consensus sequence specific for the NF-κB-binding site (5′-AGTTGAGGGGACTTTCCAGGC-3′) (Promega, Madison, WI, USA), according to manufacturer's instructions. The NF-κB oligonucleotide was labeled with biotin at the 3′ end using the Pierce Biotin 3′ End DNA labeling kit (Thermo Fisher Scientific). Following incubation, reaction mixtures were loaded in a 6% non-denaturing polyacrylamide gel to facilitate separation of DNA-protein complexes and transferred to a nylon membrane (Thermo Fisher Scientific) for detection using the Chemiluminescent Nucleic Acid Detection Module kit (Thermo Fisher Scientific).

Immunoblotting

An aliquot of the nuclear proteins (10 μg) prepared for EMSA was subjected to Western immunoblotting analysis

(28, 29). Briefly, the nuclear proteins were separated by electrophoresis in a 12% SDS-polyacrylamide gel and transferred onto nitrocellulose membrane (Bio-Rad) using a Trans-Blot Turbo Transfer System (Bio-Rad). The membranes were probed with anti-histone H3 antibody (SC-10809; Santa Cruz Biotechnology Inc., Dallas, TX, USA).

Proinflammatory Marker Analysis

Plasma TNF-α, IL-6, and MCP-1 protein levels were measured using a U-PLEX Biomarker Group 1 kit (MesoScale Discovery, Rockville, MD, USA). Briefly, an aliquot of plasma (25 μl) was loaded into a plate containing pre-coated biotinylated antibodies for specific inflammatory marker. The assay was performed according to the manufacturer's instructions and quantitative chemiluminescence data was obtained using the QuickPlex SQ 120 (MesoScale Discovery) followed by analysis using the Discovery Workbench 4.0 Software (MesoScale Discovery).

Histological Analysis and Immunohistochemistry

A portion of the kidney was immersion-fixed overnight in 10% neutral buffered formalin (10% formalin, 25 mM NaH_2PO_4, 45 mM Na_2HPO_4) and then embedded in paraffin (29). Paraffin-embedded sections were cut at a thickness of 5 μm and stained with hematoxylin and eosin (H&E) to evaluate the morphological changes. Paraffin embedded sections were used for immunostaining. In brief, tissue sections were boiled in EDTA antigen repairing buffer. The sections were naturally cooled and incubated with 3% hydrogen

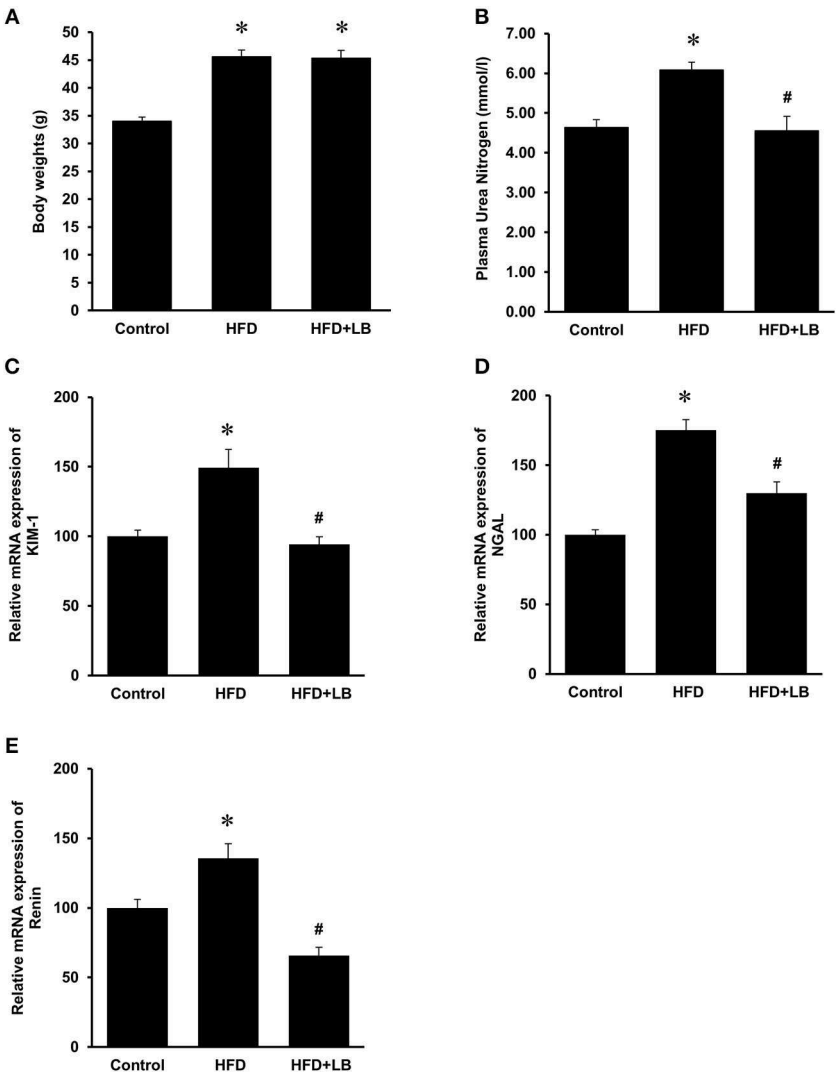

FIGURE 1 | Body weights and kidney injury parameters. Mice were fed a control diet, high-fat diet (HFD) or HFD supplemented with lingonberry (HFD+LB) for 12 weeks and **(A)** final body weights were measured. Kidney injury was examined by measuring **(B)** blood urea nitrogen (BUN), renal mRNA expression of **(C)** kidney injury molecule-1 (KIM-1), **(D)** neutrophil gelatinase-associated lipocalin (NGAL) and **(E)** renin. The results are expressed as the means ± SE ($n = 6$). $^{*}p < 0.05$ when compared with the value obtained from the control group. $^{\#}p < 0.05$ when compared with the value obtained from the HFD group.

peroxide solution at room temperature for 15 min to block the endogenous peroxidase activity. Slides were incubated overnight at 4°C with anti-F4/80 antibody (1:100 dilution, MCA497, Bio-Rad) or anti-MPO antibody (1:100 dilution, ab9535, Abcam, Cambridge, United Kingdom) in a humidified chamber. The sections were then incubated for 1 h with biotinylated goat anti-rat IgG or goat anti-rabbit IgG (1:200, Dako, Glostrup, Denmark), respectively, followed by incubation with streptavidin-horse radish peroxidase (HRP) conjugate (Zymed Laboratories, Inc., San Francisco, CA, USA). Finally, the slides were counterstained with Mayer's hematoxylin. For the negative controls, normal rabbit IgG and rat IgG were used as primary antibodies. All images were captured using an Olympus BX43 Upright Light Microscope (Olympus Corp., Tokyo, Japan) equipped with a Q-color 3 digital camera and analyzed using Image-Pro plus 7.0 (Media Cybernetics, Rockville, MD, USA).

Statistical Analysis

Data are presented as means ± standard error. Results were analyzed using one-way ANOVA followed by Newman–Keuls multiple comparison test. $P < 0.05$ were considered statistically significant. All statistical analyses were performed ProStat Version 6 software (Poly Software International, Pearl River, NY, USA).

RESULTS

Effect of HFD and Lingonberry Supplementation on Body Weight, Kidney Function and Metabolic Parameters

The initial average body weights of the mice ranged from 22.5–23.0 g. Feeding mice a HFD for 12 weeks caused a significant elevation in body weight as compared to mice fed a control diet (**Figure 1A**). Supplementation of lingonberry for 12 weeks did not change the body weight gain induced by the HFD feeding (**Figure 1A**). Kidney function was assessed by measuring BUN levels in the plasma, gene expression of KIM-1, NGAL and renin in the kidneys. HFD feeding resulted in a significant elevation of BUN levels in the plasma (**Figure 1B**) and a significant increase in the expression of KIM-1, NGAL, and renin mRNA in the kidneys (**Figures 1C–E**), indicating kidney function was impaired. Lingonberry supplementation reduced plasma BUN levels as well as renal KIM-1, NGAL and renin gene expression (**Figure 1**). Mice fed a HFD had a higher level of fasting blood glucose than the control group (**Figure 2A**). Lingonberry supplementation significantly reduced the fasting blood glucose level in mice fed a HFD (**Figure 2A**). There was also a significant increase in plasma levels of triglycerides (**Figure 2B**) and total cholesterol (**Figure 2C**) in mice fed a HFD. Lingonberry supplementation reduced plasma triglyceride and cholesterol levels to that similar to the control group (**Figures 2B,C**).

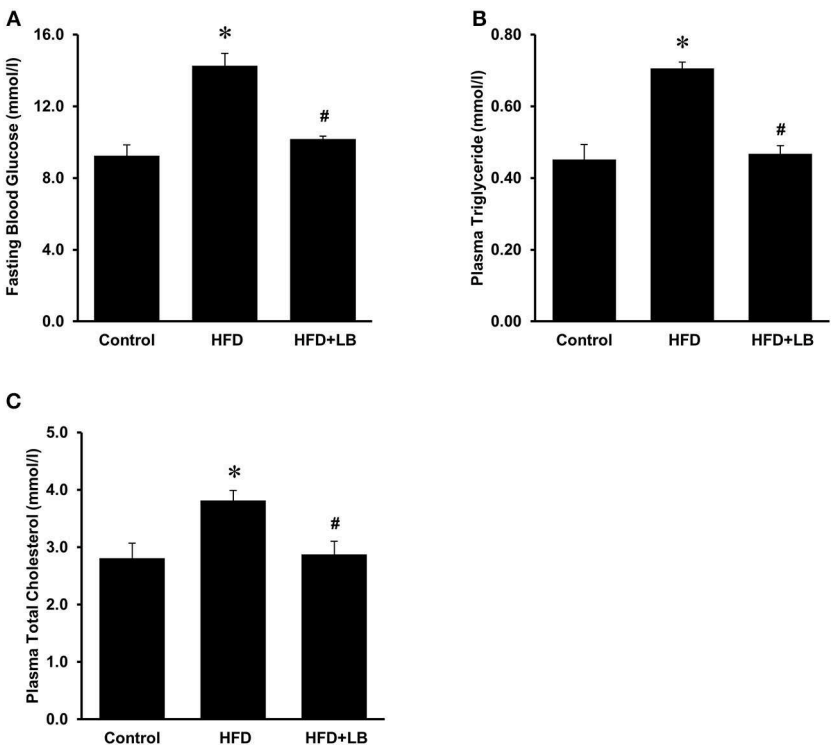

FIGURE 2 | Blood glucose and lipid profile in mice. Mice were fed a control diet, high-fat diet (HFD) or HFD supplemented with lingonberry (HFD+LB) for 12 weeks. **(A)** Blood glucose was measured after fasting for 6 h. Plasma **(B)** triglyceride and **(C)** total cholesterol were also measured. The results are expressed as the means ± SE ($n = 6$). *$p < 0.05$ when compared with the value obtained from the control group. $^{\#}p < 0.05$ when compared with the value obtained from the HFD group.

Effect of HFD and Lingonberry Supplementation on Inflammatory Cytokine Expression in the Kidneys and Plasma

Several proinflammatory cytokines were measured in the kidney tissue. Mice fed a HFD had a significant elevation of renal TNF-α, IL-6, and MCP-1 mRNA expression as compared to the control group (**Figures 3A–C**). Lingonberry supplementation attenuated the expression of these inflammatory cytokines in the kidneys (**Figure 3**). The transcription factor, NF-κB, is known to regulate inflammatory cytokine expression. Kidney nuclear proteins were prepared and an EMSA was carried out to determine the DNA binding activity of NF-κB. Mice fed a HFD had a significantly higher NF-κB/DNA binding activity than the control group (**Figure 3D**). Lingonberry supplementation effectively reduced NF-κB/DNA binding activity in the kidneys. The morphology of the kidney tissue was examined by using H&E staining. Mice fed a HFD had an increased renal deposition of inflammatory foci (characterized by dense aggregates of cells) as compared to the control group and the lingonberry supplemented group (**Figure 4**). To further identify the types of inflammatory cells in the kidney, immunohistochemical staining was performed (**Figure 5** and **Supplementary Figure 1**). The majority of inflammatory cells in the kidneys of HFD-fed mice were macrophages (**Figure 5A**) while neutrophils (**Figure 5B**) were also present but to a lesser extent. These results suggested that mice fed a HFD had an increased inflammatory response in the kidney while lingonberry supplementation could alleviate HFD-induced inflammatory cytokine expression. HFD fed mice also exhibited a significant elevation of plasma TNF-α, and MCP-1 protein levels as compared to the mice fed a control diet (**Figures 6A,C**). There was no significant difference in plasma IL-6 levels among mice fed the different diets (**Figure 6B**). Lingonberry supplementation effectively reduced plasma TNF-α, and MCP-1 protein levels (**Figures 6A,C**).

Induction of Inflammatory Cytokine Expression by Palmitic Acid in Kidney Proximal Tubular Cells

The HFD is rich in fatty acids and palmitic acid is one of the most abundant saturated fatty acids in the HFD. Palmitic acid treatment of human kidney proximal tubular cells

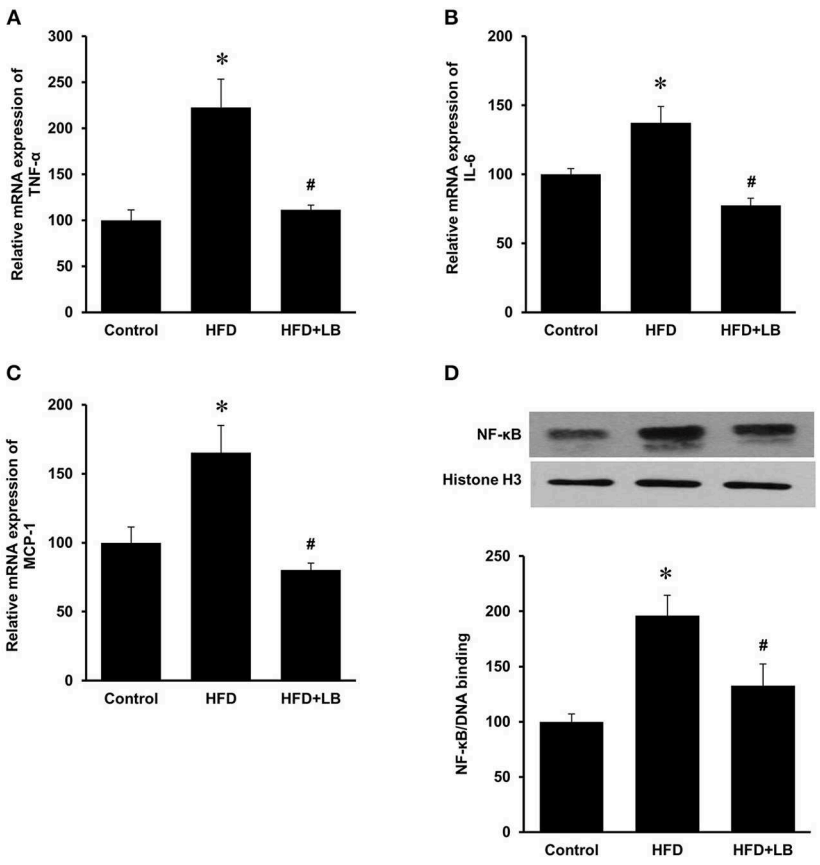

FIGURE 3 | Cytokine expression and NF-κB activation in mouse kidneys. Mice were fed a control diet, high-fat diet (HFD) or HFD supplemented with lingonberry (HFD+LB) for 12 weeks. The mRNA expression of **(A)** TNF-α, **(B)** IL-6, and **(C)** MCP-1 in kidneys were measured by using qPCR analysis. **(D)** The NF-κB/DNA binding activity was determined by EMSA. Histone in the nuclear content detected by Western immunoblotting analysis served as a loading control. The results are expressed as the means ± SE ($n = 6$). $^{*}p < 0.05$ when compared with the value obtained from the control group. $^{\#}p < 0.05$ when compared with the value obtained from the HFD group.

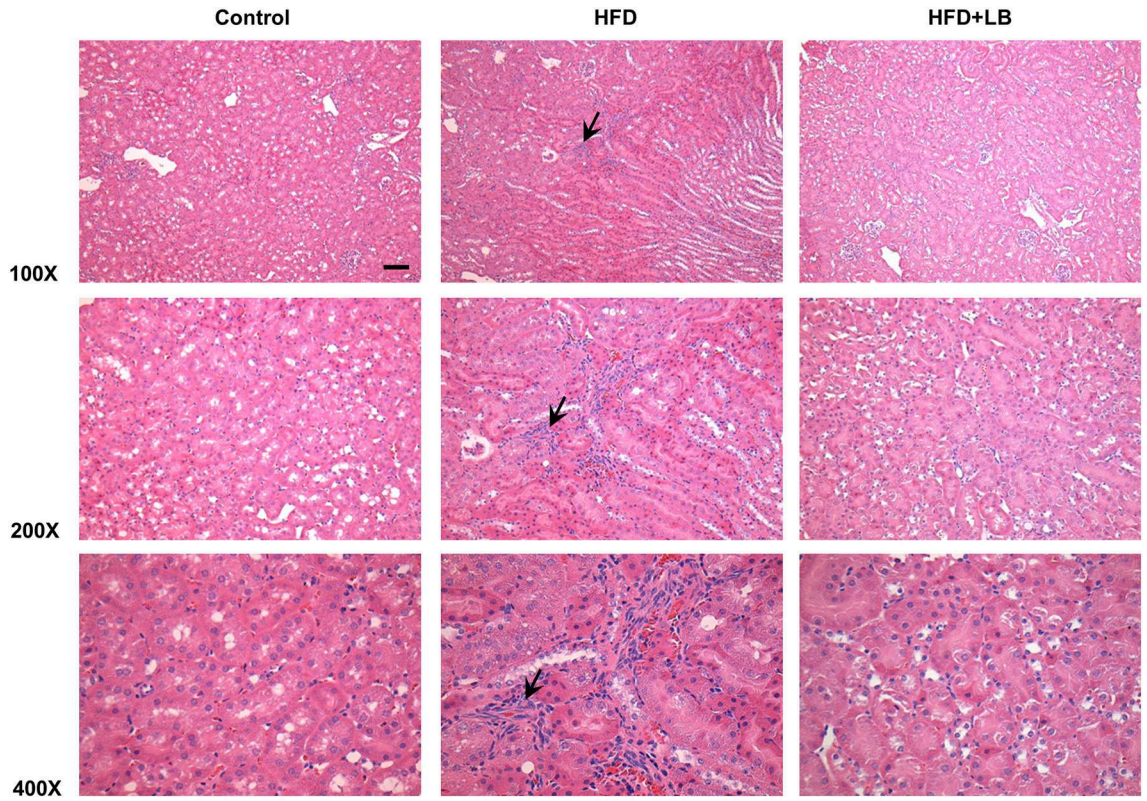

FIGURE 4 | Histological staining of mouse kidneys. Mice were fed a control diet, high-fat diet (HFD) or HFD supplemented with lingonberry (HFD+LB) for 12 weeks. Kidney histology was examined by hematoxylin and eosin (H&E) staining. Arrows point to inflammatory foci (Scale bar = 100 μm).

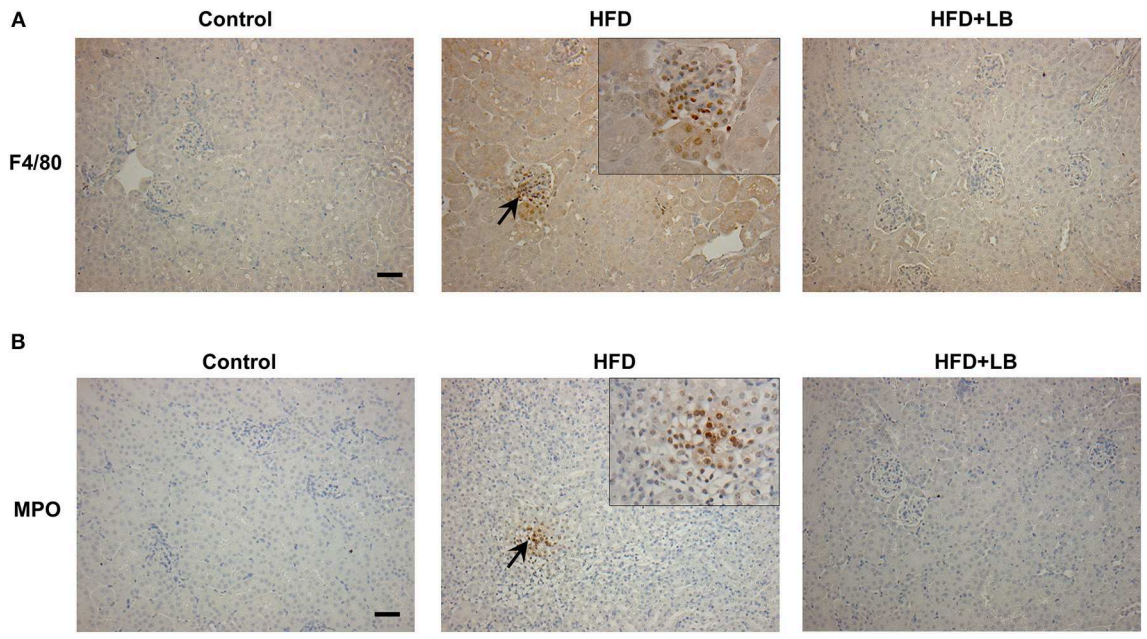

FIGURE 5 | Immunohistochemical staining of mouse kidneys. Mice were fed a control diet, high-fat diet (HFD) or HFD supplemented with lingonberry (HFD+LB) for 12 weeks. Paraffin embedded kidney sections were stained with **(A)** anti-F4/80 antibody to detect macrophages or **(B)** anti-MPO antibody to detect neutrophils in the inflamed areas. Arrows point to the infiltrated macrophages and neutrophils; the images were captured at 200X. Inset: Areas containing F4/80 or MPO positive cells were enlarged 2X (Scale bar = 100 μm).

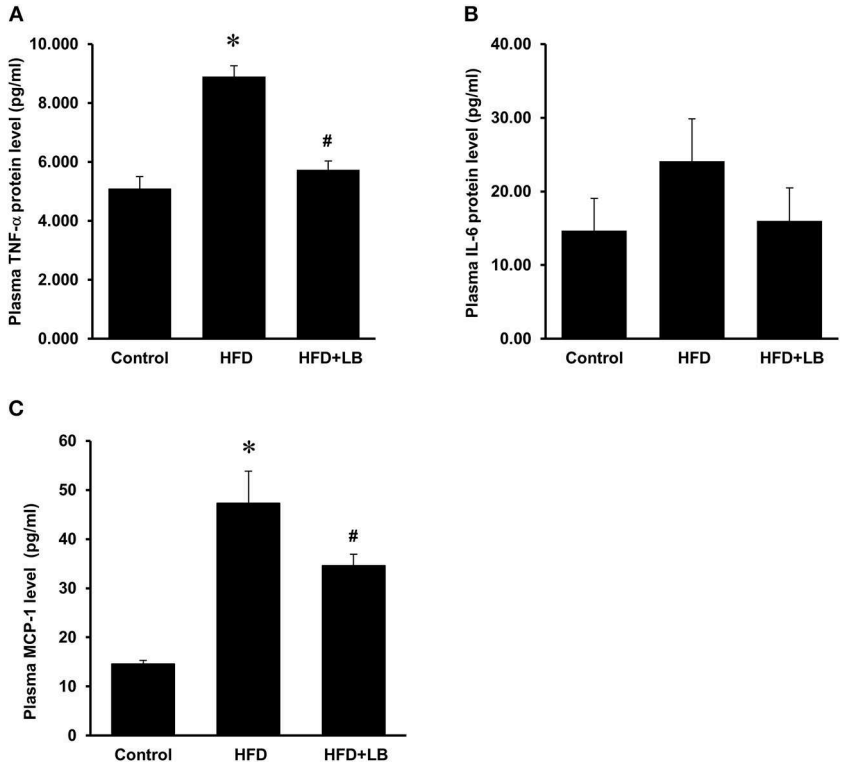

FIGURE 6 | Effect of lingonberry supplementation on inflammatory cytokines in plasma of HFD-fed mice. Mice were fed a control diet, high-fat diet (HFD) or HFD supplemented with lingonberry (HFD+LB) for 12 weeks. Plasma protein levels of **(A)** TNF-α, **(B)** IL-6, and **(C)** MCP-1 were analyzed by using a multiplex assay kit. The results were expressed as the means ± SE ($n = 4$). $^{*}p < 0.05$ when compared with the value obtained from the control group. $^{\#}p < 0.05$ when compared with the value obtained from the HFD group.

stimulated TNF-α, IL-6, and MCP-1 mRNA expression in a dose-dependent manner (**Figures 7A–C**). Incubation of cells with palmitic acid also activated NF-κB (**Figure 8A**). To further investigate the mechanism of HFD-induced inflammatory cytokine expression, cells were incubated with an NF-κB inhibitor pyrrolidine dithiocarbamate (PDTC) (**Figure 8A**). Inhibition of NF-κB activation by PDTC abolished palmitic acid-induced inflammatory cytokine expression in tubular cells (**Figures 8B–D**).

Effects of Lingonberry and Cyanidine-3-Glucoside on Palmitic Acid-Induced Inflammatory Cytokine Expression in Kidney Proximal Tubular Cells

Next, we examined the effect of lingonberry extract or C-3-Glu on palmitic acid-induced inflammatory cytokine expression in tubular cells. C-3-Glu is one of the major lingonberry anthocyanins that have been shown to have biological activities. Incubation of cells with lingonberry extract or C-3-Glu was shown to attenuate palmitic acid-induced NF-κB activation (**Figure 8A**). Upon further investigation, incubation of cells with lingonberry extract significantly reduced palmitic acid-induced TNF-α, IL-6, and MCP-1 mRNA expression (**Figures 9A–C**, respectively). Additionally, incubation of tubular cells with C-3-Glu also effectively attenuated palmitic acid-induced inflammatory cytokine expression in a dose-dependent manner (**Figures 10A–C**). The palmitic acid, lingonberry extract or C-3-Glu at the doses used in the present study did not reduce cell viability.

DISCUSSION

Inflammatory response is one of the important mechanisms for the development of CKD (30, 31). Results obtained from the present study demonstrated that mice fed a HFD for 12 weeks developed kidney injury with increased inflammatory cytokine expression that resembled the characteristics of CKD. Lingonberry supplementation significantly reduced HFD-induced kidney injury and inflammatory response without affecting body weight gain. Our results, for the first time, showed that lingonberry extract and its anthocyanin, cyanidin-3-glucoside, could attenuate fatty acid-induced inflammatory cytokine expression in kidney tubular cells. Such an inhibitory effect was mediated through the attenuation of NF-κB activation.

Obesity and its associated metabolic abnormalities are risk factors for the development of CKD, independent of hypertension and diabetes (2). In the current study, mice fed

a HFD for 12 weeks had more body weight gain as compared to the mice fed a control diet. The HFD-fed mice displayed hyperlipidemia and hyperglycemia, which resembled metabolic abnormalities seen in obese patients. HFD feeding exerted an adverse effect on kidneys as the plasma BUN levels and the expression of kidney injury biomarkers (NGAL, KIM-1, and renin) were significantly elevated. Kidney damage and inflammation can cause release of NGAL from neutrophils and kidney tubular epithelial cells (32). Overexpression of KIM-1 has also been shown to positively correlate with kidney injury (33), while inflammation and fibrosis can trigger the expression of KIM-1 at the luminal side of the proximal tubules (34). Increased tubular KIM-1 expression is an indication of ongoing tubular cell damage and dedifferentiation (35). The progression of nephron damage has also been correlated to the overexpression of renin, the initiator of renin-angiotensin axis (36). Development of renal fibrosis is a common outcome in the later stages of CKD (37). Transforming growth factor-β (TGF-β) has been identified as a key mediator of renal fibrosis (38, 39). In the current study, no significant change in TGF-β mRNA expression was observed in mice fed various diets for 12 week (see **Supplementary Table 1** and **Supplementary Figure 2**). It is plausible that the development of renal fibrosis may become apparent in mice after a longer period of HFD feeding (40). Supplementation of lingonberry effectively prevented HFD-induced kidney injury as indicated by a decreased expression of the kidney injury biomarkers (NGAL, KIM-1, and renin) and BUN. Such a renal protective effect by lingonberry did not appear to be associated with body weight changes.

Increased expression of inflammatory cytokines contributes to the development and progression of kidney disease. In the current study, there was a significant elevation of inflammatory cytokine expression in the kidneys (TNF-α, IL-6, MCP-1) of HFD-fed mice. Histological staining and immunohistochemistry of the kidneys revealed that the predominant inflammatory cells in the HFD-fed mice were macrophages and to a lesser extent neutrophils. There was a significant elevation of inflammatory cytokine expression in proximal tubular cells after incubation with palmitic acid, the most abundant saturated fatty acid in the HFD. MCP-1 is a potent chemokine that facilitates the migration of leukocytes such as monocytes into tissues including kidneys (41–43). Upon infiltration into tissues, monocytes differentiate into macrophages that are capable of producing inflammatory cytokines such as TNF-α and IL-6 as well as releasing reactive oxygen species to aggravate tissue injury. Elevation of TNF-α and IL-6 expression are linked to increased oxidative stress, endothelial dysfunction and renal fibrosis (44). In a human study with 37 health controls and 42 CKD patients, it was reported that MCP-1 levels were significantly higher in CKD patients, especially those with glomerular disease (45). The Chronic Renal Insufficiency Cohort (CRIC) Study showed that elevated circulating levels of TNF-α was associated with progression of CKD (46). In another study (47), patients with chronic nephropathies showed an early increase in IL-6 but the levels showed no further increase with severity of CKD. In the current study, there was a significant elevation of inflammatory cytokines (TNF-α and MCP-1) in the plasma of mice fed a HFD. Lingonberry supplementation reduced these inflammatory cytokine levels in the circulation. Several lines of evidence from the current study suggested that NF-κB activation might play an important role in HFD-induced renal inflammatory response. The DNA binding activity of NF-κB was markedly increased in the kidneys isolated from HFD-fed mice as well as in palmitic acid treated tubular cells. Inhibition of NF-κB activation by its inhibitor PDTC abolished palmitic acid-induced inflammatory cytokine expression. Chronic inflammation, as exhibited by a prolonged and increased expression of inflammatory cytokines can damage kidney structure and diminish kidney function. In accordance

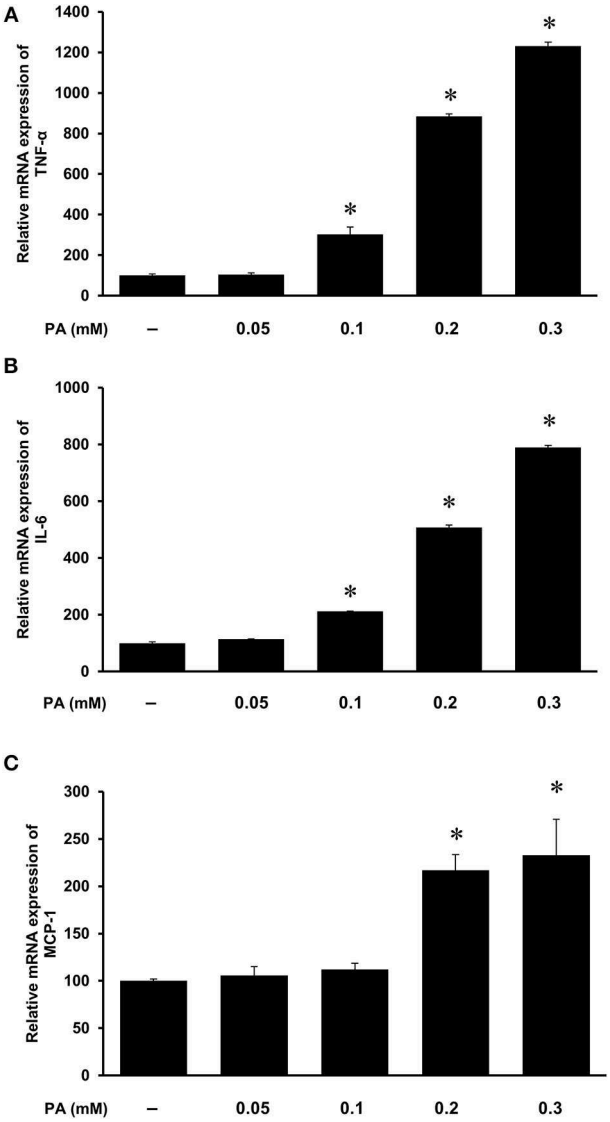

FIGURE 7 | Effect of palmitic acid on cytokine expression in human proximal tubular cells. Proximal tubular cells were incubated in the absence (control) or presence of palmitic acid (PA, 0.05, 0.1, 0.2, 0.3 mM) for 4 h. The mRNA expression of **(A)** TNF-α, **(B)** IL-6, and **(C)** MCP-1 were measured by using qPCR analysis. The results are expressed as the means ± SE ($n = 6$). *$p <$ 0.05 when compared with the value obtained from control cells.

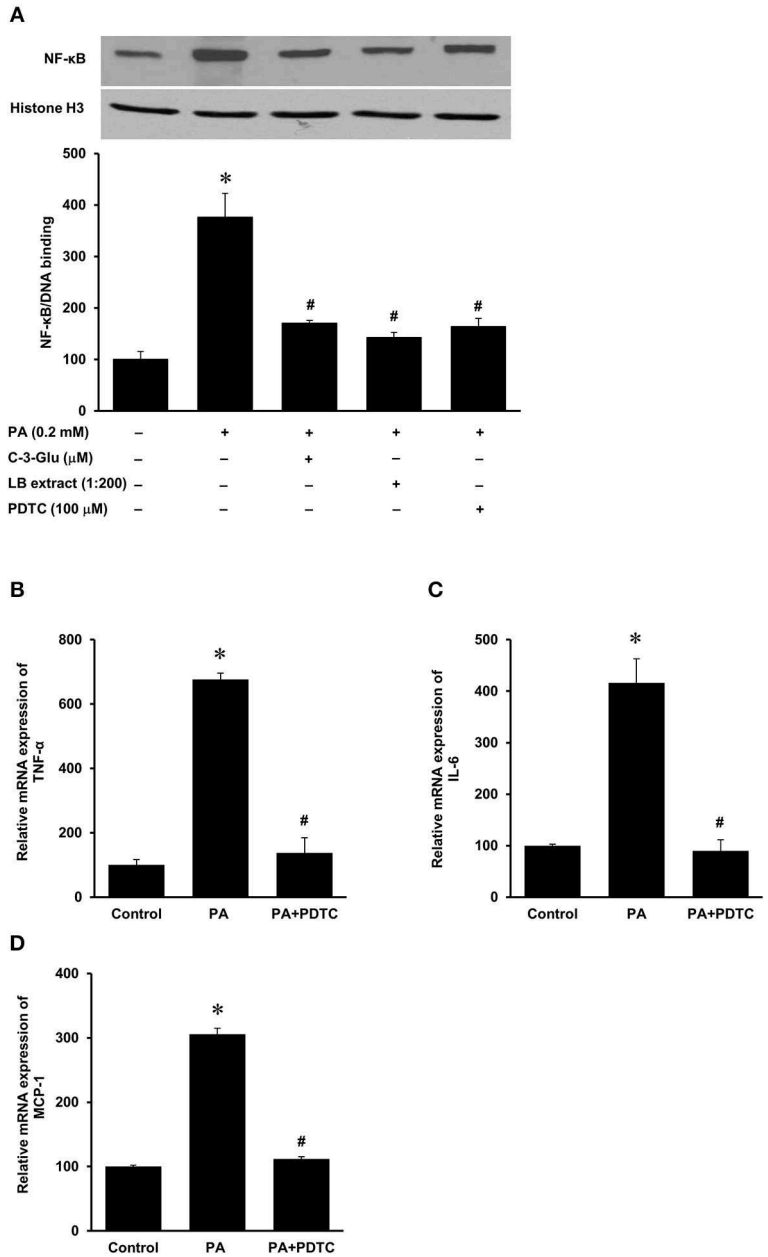

FIGURE 8 | Effect of palmitic acid on NF-κB activation in human proximal tubular cells. Proximal tubular cells were preincubated with either an NF-κB inhibitor (PDTC, 100 μM) for 1 h, C-3-Glu (20 μM) for 4 h, or lingonberry (LB) extract (1:200 dilution) for 4 h, followed by incubation with palmitic acid (0.2 mM) for another 30 min. **(A)** The NF-κB/DNA binding activity was determined by EMSA. Histone in the nuclear content detected by Western immunoblotting analysis served as a loading control. In another set of experiments, cells were incubated in the absence (control) or presence of PDTC (100 μM) for 1 h, prior to incubation with palmitic acid (0.2 mM) for 4 h. The mRNA expression of **(B)** TNF-α, **(C)** IL-6, and **(D)** MCP-1 was measured by using qPCR. The results are expressed as the means ± SE ($n = 6$). $^{*}p < 0.05$ when compared with the value obtained from control cells. $^{\#}p < 0.05$ when compared with the value obtained from palmitic cell treated cells.

with its protective effect on kidney function, lingonberry supplementation effectively attenuated NF-κB activation and inflammatory cytokine expression in the kidneys and plasma of mice fed a HFD. It should be noted that there was a differential effect of lingonberry extract on the expression of IL-6. This could be due to the multiple transcriptional regulation of IL-6 gene expression. Leonard et al. (48) reported that p38 and ERK MAPK pathways are important for the regulation of the production of IL-6 from the proximal tubular and glomerular mesangial regions of the nephron. Additionally, there may be potential involvement of the Jagged1-Notch signaling pathway (49). These signaling pathways may independently regulate the expression of IL-6. Aside from NF-κB, the involvement of other signaling pathways will be the focus of a separate future study.

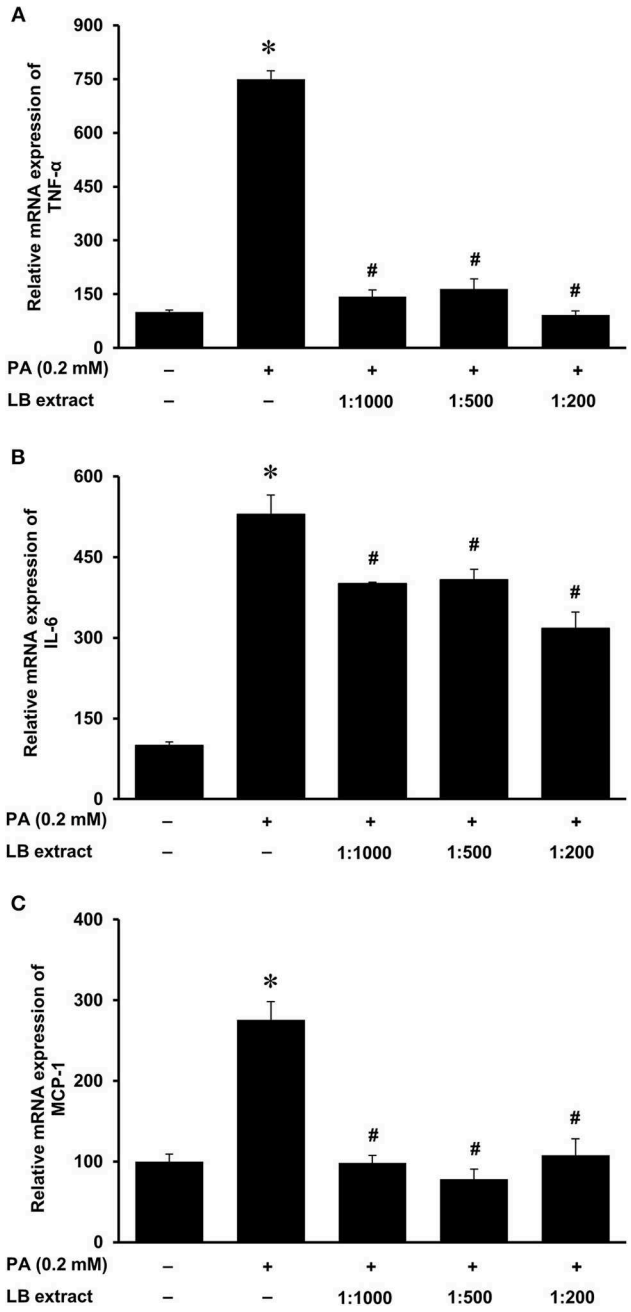

FIGURE 9 | Effect of lingonberry extract and palmitic acid on cytokine expression in human proximal tubular cells. Proximal tubular cells were incubated in the absence (control) or presence of lingonberry (LB) extracts (1:1,000, 1:500, or 1:200 dilution) for 4 h followed by incubation with palmitic acid (PA, 0.2 mM) for another 4 h. The mRNA expression of **(A)** TNF-α, **(B)** IL-6, and **(C)** MCP-1 were measured by using qPCR. The results are expressed as the means ± SE ($n = 6$). $^{*}p < 0.05$ when compared with the value obtained from control cells. $^{\#}p < 0.05$ when compared with the value obtained palmitic acid treated cells.

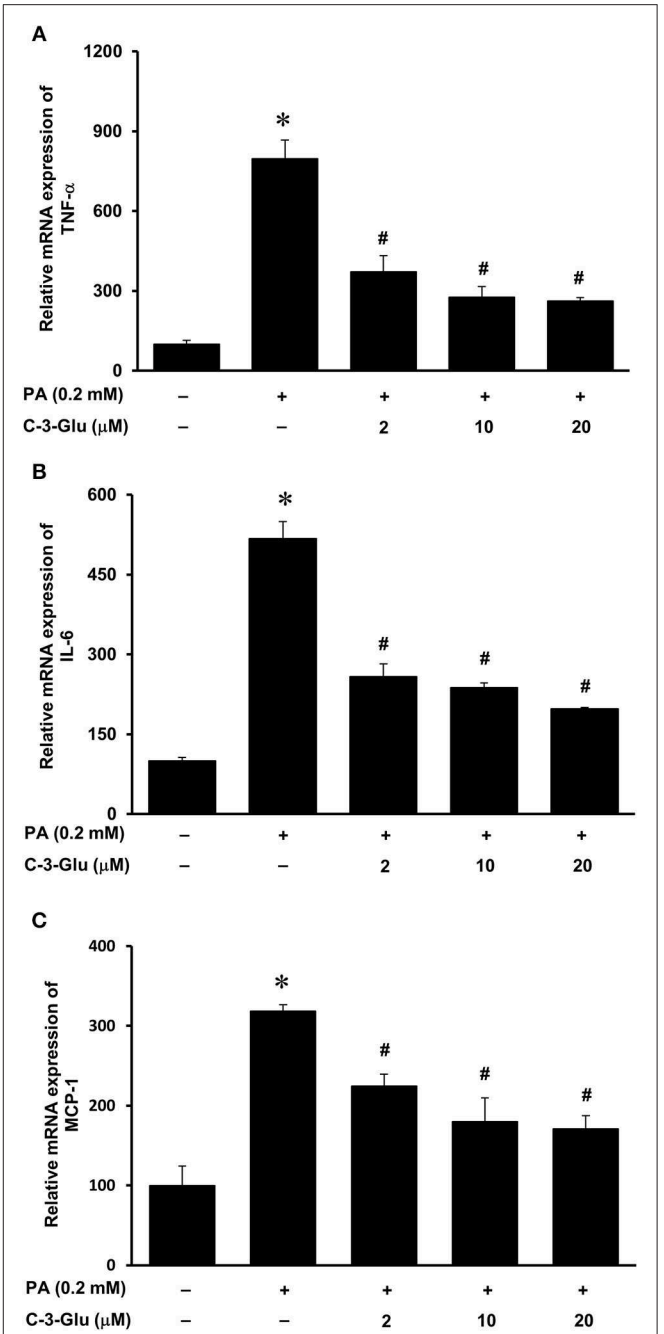

FIGURE 10 | Effect of cyanidin-3-glucoside and palmitic acid on cytokine expression in human proximal tubular cells. Proximal tubular cells were incubated in the absence (control) or presence of cyanidin-3-glucoside (C-3-Glu: 2, 10 or 20 μM) for 4 h followed by incubation with palmitic acid (PA) (0.2 mM) for another 4 h. The mRNA expression of **(A)** TNF-α, **(B)** IL-6, and **(C)** MCP-1 were measured by using qPCR. The results are expressed as the means ± SE ($n = 6$). $^{*}p < 0.05$ when compared with the value obtained from the control cells. $^{\#}p < 0.05$ when compared with the value obtained from palmitic acid treated cells.

Furthermore, incubation of tubular cells with lingonberry extract or its active ingredient C-3-Glu effectively attenuated palmitic acid-induced inflammatory cytokine expression in tubular cells. C-3-Glu is one of the most extensively studied anthocyanins shown to possess various potential beneficial effects against oxidative stress and inflammation (50), insulin resistance (51),

and dyslipidemia (52). Although C-3-Glu could be one of the potential bioactive compounds account for renal protective effect of lingonberry, future studies are warranted to evaluate the impact of other bioactive compounds in lingonberry. Taken together, our results suggested that attenuation of HFD-induced chronic inflammatory cytokine expression might be one of the mechanisms responsible for renal protective effect by lingonberry.

In conclusion, chronic consumption of HFD increases renal inflammatory cytokine expression and causes kidney injury. The current study, for the first time, demonstrates that dietary supplementation with lingonberry reduces HFD-induced inflammatory response and prevents kidney injury. Such a renal protective effect by lingonberry is, in part, mediated through the NF-κB signaling pathway. As current treatment option for patients with CKD is limited, lingonberry supplementation may serve as an alternative approach for the management of CKD.

DATA AVAILABILITY STATEMENT

All datasets generated for this study are included in the article/**Supplementary Material**.

ETHICS STATEMENT

The animal study was reviewed and approved by University of Manitoba Protocol Management and Review Committee.

AUTHOR CONTRIBUTIONS

YS and KO conceived and designed research. SM and SP performed experiments. SM, SP, KO, and YS analyzed data. YS, KO, SM, and SP interpreted results of experiments. SM prepared figures. YS, KO, and SM drafted manuscript. YS, KO, SM, SP, and SD edited, revised, and approved final version of manuscript.

FUNDING

SM was supported in part by a Mark and Pat Smerchanski Studentship Grant and by the estate of Margurite Jermaine Gerome (deceased). Project funding was provided by Agriculture and Agri-Food Canada Project ID J-001297 and J-002283.

ACKNOWLEDGMENTS

The authors wish to acknowledge the technical assistance of V. Sid and Y. Shang for animal handling procedures and C. Wijerathne for immunohistostaining.

SUPPLEMENTARY MATERIAL

The Supplementary Material for this article can be found online at: https://www.frontiersin.org/articles/10.3389/fmed.2020.00080/full#supplementary-material

REFERENCES

1. Zoccali C, Vanholder R, Massy ZA, Ortiz A, Sarafidis P, Dekker FW, et al. The systemic nature of CKD. *Nat Rev Nephrol*. (2017) 13:344–58. doi: 10.1038/nrneph.2017.52
2. Prasad GV. Metabolic syndrome and chronic kidney disease: current status and future directions. *World J Nephrol*. (2014) 3:210–9. doi: 10.5527/wjn.v3.i4.210
3. Garofalo C, Borrelli S, Minutolo R, Chiodini P, De Nicola L, Conte G. A systematic review and meta-analysis suggests obesity predicts onset of chronic kidney disease in the general population. *Kidney Int*. (2017) 91:1224–35. doi: 10.1016/j.kint.2016.12.013
4. Kovesdy CP, Furth SL, Zoccali C, World Kidney Day Steering C. Obesity and kidney disease: hidden consequences of the epidemic. *Can J Kidney Health Dis*. (2017) 4:1–10. doi: 10.1093/ckj/sfw139
5. Nehus E. Obesity and chronic kidney disease. *Curr Opin Pediatr*. (2018) 30:241–6. doi: 10.1097/MOP.0000000000000586
6. Sato Y, Yanagita M. Immune cells and inflammation in AKI to CKD progression. *Am J Physiol Renal Physiol*. (2018) 315:F1501–12. doi: 10.1152/ajprenal.00195.2018
7. Andres-Hernando A, Lanaspa MA, Kuwabara M, Orlicky DJ, Cicerchi C, Bales E, et al. Obesity causes renal mitochondrial dysfunction and energy imbalance and accelerates chronic kidney disease in mice. *Am J Physiol Renal Physiol*. (2019) 317:F941–8. doi: 10.1152/ajprenal.00203.2019
8. Yang P, Xiao Y, Luo X, Zhao Y, Zhao L, Wang Y, et al. Inflammatory stress promotes the development of obesity-related chronic kidney disease via CD36 in mice. *J Lipid Res*. (2017) 58:1417–27. doi: 10.1194/jlr.M076216
9. Navarro-Diaz M, Serra A, Lopez D, Granada M, Bayes B, Romero R. Obesity, inflammation, and kidney disease. *Kidney Int Suppl*. (2008) 74:S15–8. doi: 10.1038/ki.2008.518
10. Gupta J, Mitra N, Kanetsky PA, Devaney J, Wing MR, Reilly M, et al. Association between albuminuria, kidney function, and inflammatory biomarker profile in CKD in CRIC. *Clin J Am Soc Nephrol*. (2012) 7:1938–46. doi: 10.2215/CJN.03500412
11. Sarna LK, Wu N, Wang P, Hwang SY, Siow YL, O K. Folic acid supplementation attenuates high fat diet induced hepatic oxidative stress via regulation of NADPH oxidase. *Can J Physiol Pharmacol*. (2012) 90:155–65. doi: 10.1139/y11-124
12. Shang Y, Khafipour E, Derakhshani H, Sarna LK, Woo CW, Siow YL, et al. Short term high fat diet induces obesity-enhancing changes in mouse gut microbiota that are partially reversed by cessation of the high fat diet. *Lipids*. (2017) 52:499–511. doi: 10.1007/s11745-017-4253-2
13. Sid V, Shang Y, Siow YL, Hewage SM, House JD, O K. Folic acid supplementation attenuates chronic hepatic inflammation in high-fat diet fed mice. *Lipids*. (2018) 53:709–16. doi: 10.1002/lipd.12084
14. Sid V, Siow YL, Shang Y, Woo CW, O K. High-fat diet consumption reduces hepatic folate transporter expression via nuclear respiratory factor-1. *J Mol Med (Berl)*. (2018) 96:1203–13. doi: 10.1007/s00109-018-1688-8
15. Sid V, Wu N, Sarna LK, Siow YL, House JD, O K. Folic acid supplementation during high-fat diet feeding restores AMPK activation via an AMP-LKB1-dependent mechanism. *Am J Physiol Regul Integr Comp Physiol*. (2015) 309:R1215–25. doi: 10.1152/ajpregu.00260.2015
16. Wu N, Sarna LK, Hwang SY, Zhu Q, Wang P, Siow YL, et al. Activation of 3-hydroxy-3-methylglutaryl coenzyme A (HMG-CoA) reductase during high fat diet feeding. *Biochim Biophys Acta*. (2013) 1832:1560–8. doi: 10.1016/j.bbadis.2013.04.024
17. Wicks SE, Nguyen TT, Breaux C, Kruger C, Stadler K. Diet-induced obesity and kidney disease - In search of a susceptible mouse model. *Biochimie*. (2016) 124:65–73. doi: 10.1016/j.biochi.2015.08.001
18. Turner JM, Bauer C, Abramowitz MK, Melamed ML, Hostetter TH. Treatment of chronic kidney disease. *Kidney Int*. (2012) 81:351–62. doi: 10.1038/ki.2011.380
19. Isaak CK, Wang P, Prashar S, O K, Brown DC, Debnath SC, et al. Supplementing diet with Manitoba lingonberry juice reduces kidney

ischemia-reperfusion injury. *J Sci Food Agric*. (2017) 97:3065–76. doi: 10.1002/jsfa.8200
20. Debnath SC. Genetic diversity and erosion in berri. In: Ahuja MR, Jain SM, editors. *Genetic Diversity and Erosion in Plants*. Cham: Springer (2016). p. 75–129.
21. Zheng W, Wang SY. Oxygen radical absorbing capacity of phenolics in blueberries, cranberries, chokeberries, and lingonberries. *J Agric Food Chem*. (2003) 51:502–9. doi: 10.1021/jf020728u
22. Yao LH, Jiang YM, Shi J, Tomas-Barberan FA, Datta N, Singanusong R, et al. Flavonoids in food and their health benefits. *Plant Foods Hum Nutr*. (2004) 59:113–22. doi: 10.1007/s11130-004-0049-7
23. Isaak CK, Petkau JC, O K, Debnath SC, Siow YL. Manitoba Lingonberry (*Vaccinium vitis-idaea*) bioactivities in ischemia-reperfusion injury. *J Agric Food Chem*. (2015) 63:5660–9. doi: 10.1021/acs.jafc.5b00797
24. Vanzo A, Scholz M, Gasperotti M, Tramer F, Passamonti S, Vrhovsek U, et al. Metabonomic investigation of rat tissues following intravenous administration of cyanidin 3-glucoside at a physiologically relevant dose. *Metabolomics*. (2013) 9:88–100. doi: 10.1007/s11306-012-0430-8
25. Eid HM, Ouchfoun M, Brault A, Vallerand D, Musallam L, Arnason JT, et al. Lingonberry (*Vaccinium vitis-idaea* L.) exhibits antidiabetic activities in a mouse model of diet-induced obesity. *Evid Based Complement Alternat Med*. (2014) 2014:645812–23. doi: 10.1155/2014/645812
26. Chomczynski P, Mackey K. Short technical reports. Modification of the TRI reagent procedure for isolation of RNA from polysaccharide-and proteoglycan-rich sources. *Biotechniques*. (1995) 19:942–5.
27. Livak KJ, Schmittgen TD. Analysis of relative gene expression data using real-time quantitative PCR and the 2(-Delta Delta C(T)) Method. *Methods*. (2001) 25:402–8. doi: 10.1006/meth.2001.1262
28. Woo CW, Siow YL, O K. Homocysteine induces monocyte chemoattractant protein-1 expression in hepatocytes mediated via activator protein-1 activation. *J Biol Chem*. (2008) 283:1282–92. doi: 10.1074/jbc.M707886200
29. Woo CW, Siow YL, Pierce GN, Choy PC, Minuk GY, Mymin D, et al. Hyperhomocysteinemia induces hepatic cholesterol biosynthesis and lipid accumulation via activation of transcription factors. *Am J Physiol Endocrinol Metab*. (2005) 288:E1002–10. doi: 10.1152/ajpendo.00518.2004
30. Ramkumar N, Cheung AK, Pappas LM, Roberts WL, Beddhu S. Association of obesity with inflammation in chronic kidney disease: a cross-sectional study. *J Ren Nutr*. (2004) 14:201–7. doi: 10.1053/j.jrn.2004.07.009
31. Silverstein DM. Inflammation in chronic kidney disease: role in the progression of renal and cardiovascular disease. *Pediatr Nephrol*. (2009) 24:1445–52. doi: 10.1007/s00467-008-1046-0
32. Cai L, Rubin J, Han W, Venge P, Xu S. The origin of multiple molecular forms in urine of HNL/NGAL. *Clin J Am Soc Nephrol*. (2010) 5:2229–35. doi: 10.2215/CJN.00980110
33. van Timmeren MM, van den Heuvel MC, Bailly V, Bakker SJ, van Goor H, Stegeman CA. Tubular kidney injury molecule-1 (KIM-1) in human renal disease. *J Pathol*. (2007) 212:209–17. doi: 10.1002/path.2175
34. Ichimura T, Hung CC, Yang SA, Stevens JL, Bonventre JV. Kidney injury molecule-1: a tissue and urinary biomarker for nephrotoxicant-induced renal injury. *Am J Physiol Renal Physiol*. (2004) 286:F552–63. doi: 10.1152/ajprenal.00285.2002
35. Ichimura T, Bonventre JV, Bailly V, Wei H, Hession CA, Cate RL, et al. Kidney injury molecule-1 (KIM-1), a putative epithelial cell adhesion molecule containing a novel immunoglobulin domain, is up-regulated in renal cells after injury. *J Biol Chem*. (1998) 273:4135–42. doi: 10.1074/jbc.273.7.4135
36. Cao W, Jin L, Zhou Z, Yang M, Wu C, Wu L, et al. Overexpression of intrarenal renin-angiotensin system in human acute tubular necrosis. *Kidney Blood Press Res*. (2016) 41:746–56. doi: 10.1159/000450564
37. Eddy AA. Overview of the cellular and molecular basis of kidney fibrosis. *Kidney Int Suppl*. (2014) 4:2–8. doi: 10.1038/kisup.2014.2
38. Loeffler I, Wolf G. Transforming growth factor-beta and the progression of renal disease. *Nephrol Dial Transplant*. (2014) 29 (Suppl. 1):i37–45. doi: 10.1093/ndt/gft267
39. Biernacka A, Dobaczewski M, Frangogiannis NG. TGF-beta signaling in fibrosis. *Growth Factors*. (2011) 29:196–202. doi: 10.3109/08977194.2011.595714
40. Decleves AE, Zolkipli Z, Satriano J, Wang L, Nakayama T, Rogac M, et al. Regulation of lipid accumulation by AMP-activated kinase in high fat diet-induced kidney injury. *Kidney Int*. (2013) 85:611–23. doi: 10.1038/ki.2013.462
41. Hwang SY, Woo CW, Au-Yeung KK, Siow YL, Zhu TY, O K. Homocysteine stimulates monocyte chemoattractant protein-1 expression in the kidney via nuclear factor-kappaB activation. *Am J Physiol Renal Physiol*. (2008) 294:F236–44. doi: 10.1152/ajprenal.00331.2007
42. Sung FL, Zhu TY, Au-Yeung KK, Siow YL, O K. Enhanced MCP-1 expression during ischemia/reperfusion injury is mediated by oxidative stress and NF-kappaB. *Kidney Int*. (2002) 62:1160–70. doi: 10.1111/j.1523-1755.2002.kid577.x
43. Wang G, Woo CW, Sung FL, Siow YL, O K. Increased monocyte adhesion to aortic endothelium in rats with hyperhomocysteinemia: role of chemokine and adhesion molecules. *Arterioscler Thromb Vasc Biol*. (2002) 22:1777–83. doi: 10.1161/01.ATV.0000035404.18281.37
44. Stenvinkel P, Ketteler M, Johnson RJ, Lindholm B, Pecoits-Filho R, Riella M, et al. IL-10, IL-6, and TNF-alpha: central factors in the altered cytokine network of uremia–the good, the bad, and the ugly. *Kidney Int*. (2005) 67:1216–33. doi: 10.1111/j.1523-1755.2005.00200.x
45. Vianna HR, Soares CM, Silveira KD, Elmiro GS, Mendes PM, de Sousa Tavares M, et al. Cytokines in chronic kidney disease: potential link of MCP-1 and dyslipidemia in glomerular diseases. *Pediatr Nephrol*. (2013) 28:463–9. doi: 10.1007/s00467-012-2363-x
46. Richard L, Amdur RL, Feldman HI, Gupta J, Yang W, Kanetsky P, et al. Inflammation and Progression of CKD: The CRIC Study. *Clin J Am Soc Nephrol*. (2016) 11:1546–56. doi: 10.2215/CJN.13121215
47. Spoto B, Leonardis D, Parlongo RM, Pizzini P, Pisano A, Cutrupi S, et al. Plasma cytokines, glomerular filtration rate and adipose tissue cytokines gene expression in chronic kidney disease (CKD) patients. *Nutr Metab Cardiovasc Dis*. (2012) 22:981–8. doi: 10.1016/j.numecd.2011.01.005
48. Leonard M, Ryan MP, Watson AJ, Schramek H, Healy E. Role of MAP kinase pathways in mediating IL-6 production in human primary mesangial and proximal tubular cells. *Kidney Int*. (1999) 56:1366–77. doi: 10.1046/j.1523-1755.1999.00664.x
49. Qin Y, Sun B, Zhang F, Wang Y, Shen B, Liu Y, et al. Sox7 is involved in antibody-dependent endothelial cell activation and renal allograft injury via the Jagged1-Notch1 pathway. *Exp Cell Res*. (2019) 375:20–7. doi: 10.1016/j.yexcr.2019.01.008
50. Sivasinprasasn S, Pantan R, Thummayot S, Tocharus J, Suksamrarn A, Tocharus C. Cyanidin-3-glucoside attenuates angiotensin II-induced oxidative stress and inflammation in vascular endothelial cells. *Chem Biol Interact*. (2016) 260:67–74. doi: 10.1016/j.cbi.2016.10.022
51. Guo H, Xia M, Zou T, Ling W, Zhong R, Zhang W. Cyanidin 3-glucoside attenuates obesity-associated insulin resistance and hepatic steatosis in high-fat diet-fed and db/db mice via the transcription factor FoxO1. *J Nutr Biochem*. (2012) 23:349–60. doi: 10.1016/j.jnutbio.2010.12.013
52. Guo H, Liu G, Zhong R, Wang Y, Wang D, Xia M. Cyanidin-3-O-β-glucoside regulates fatty acid metabolism via an AMP-activated protein kinase-dependent signaling pathway in human HepG2 cells. *Lipids Health Dis*. (2012) 11:10. doi: 10.1186/1476-511X-11-10

Conflict of Interest: The authors declare that the research was conducted in the absence of any commercial or financial relationships that could be construed as a potential conflict of interest.

frontiers in Medicine

CASE REPORT
published: 28 April 2020
doi: 10.3389/fmed.2020.00148

A 14-Year Follow-Up of a Combined Liver-Pancreas-Kidney Transplantation: Case Report and Literature Review

Geng Zhang[1], Weijun Qin[1], Jianlin Yuan[1], Changsheng Ming[2], Shuqiang Yue[3], Zhengcai Liu[3], Lei Yu[1], Ming Yu[4], Xiaokang Gao[5], Yu Zhou[6], Longxin Wang[7], Xiaojian Yang[1], Kefeng Dou[3] and He Wang[1]**

[1] Department of Urology, Xijing Hospital, Fourth Military Medical University, Xi'an, China, [2] Institute of Organ Transplantation, Tongji Hospital, Tongji Medical College, Huazhong University of Science and Technology, Wuhan, China, [3] Department of Hepatobiliary, Xijing Hospital, Fourth Military Medical University, Xi'an, China, [4] Department of Ultrasound Diagnostics, Xijing Hospital, Fourth Military Medical University, Xi'an, China, [5] Department of Urology, General Hospital of Xinjiang Military Region, Urumqi, China, [6] Department of Urology, Central Theater Command General Hospital of The Chinese People's Liberation Army, Wuhan, China, [7] Urology Department, Maanshan People's Hospital, Maanshan, China

OPEN ACCESS

Edited by:
Cheng Yang,
Fudan University, China

Reviewed by:
Brian Duncan Tait,
Australian Red Cross Blood Service, Australia
Edward Seth Kraus,
Johns Hopkins University, United States

***Correspondence:**
Kefeng Dou
doukef@fmmu.edu.cn
He Wang
xjmwhw@126.com

Specialty section:
This article was submitted to Nephrology, a section of the journal Frontiers in Medicine

Received: 04 November 2019
Accepted: 06 April 2020
Published: 28 April 2020

Citation:
Zhang G, Qin W, Yuan J, Ming C, Yue S, Liu Z, Yu L, Yu M, Gao X, Zhou Y, Wang L, Yang X, Dou K and Wang H (2020) A 14-Year Follow-Up of a Combined Liver-Pancreas-Kidney Transplantation: Case Report and Literature Review. Front. Med. 7:148. doi: 10.3389/fmed.2020.00148

Objective: To investigate the long-term effect of triple organ transplantation (liver, kidney, and pancreas) in a patient with end-stage liver disease, post chronic hepatitis B, cirrhosis, chronic renal failure, and insulin-dependent diabetes mellitus caused by chronic pancreatitis and to explore the optimal surgical procedure.

Case: A 43-year-old man with progressive emaciation and hypourocrinia for 2 months. Results indicated exocrine pancreatic insufficiency and insulin-dependent diabetes related to chronic pancreatitis (CP) after developing end-stage hepatic and renal failure. Simultaneous piggyback orthotopic liver and heterotopic pancreas-duodenum and renal transplantation was performed in 2005. Pancreatic exocrine secretions were drained enterically to the jejunum, and the donor kidney was placed in the left iliac fossa. Patient was prescribed with prednisone, tacrolimus, mycophenolate mofetil, Rabbit Anti-human Thymocyte Immunoglobulin, and simulect for immunosuppression.

Results: Satisfactory hepatic and pancreatic functional recovery was achieved within 7 days post-surgery. The kidney was not functional, and continuous renal replacement therapy was used. However, the donor kidney was removed at day 16 post-surgery due to acute rejection reaction. A new renal transplantation at the same position was performed, and satisfactory kidney function from the new graft was achieved 3 days later. In 14 years of follow-up, patient has not had any rejection reactions or other complications such as pancreatitis, thrombosis, and localized infections. The patient is insulin independent with normal liver and renal functions. FK506+Pred was used for immunosuppression, and the tac tough level maintained 3.0–4.5 ng/ml. Lamivudine was prescribed for long-term use to inhibit HBV virus duplication.

Conclusion: Simultaneous piggyback orthotopic liver and heterotopic pancreas-duodenum and renal transplantation is a good therapeutic option for patients with exocrine pancreatic insufficiency and insulin-dependent diabetes combined with hepatic and renal failure.

Keywords: liver, pancreas, renal, simultaneous transplantation, diabetes mellitus

BACKGROUND

On January 17, 2005, we performed a pancreatic jejunal drainage and *in situ* piggyback type combined liver-pancreas-kidney transplantation in a patient with post-hepatitis B cirrhosis, hepatic insufficiency insulin, chronic renal insufficiency, accompanied dependent diabetes mellitus caused by chronic pancreatitis in our hospital. The patient has been followed up for more than 14 years and is the longest survivors of similar operations in the world. The follow-up information is reported as follows.

A 43-year-old man was detected positive for hepatitis B surface antigen in 1994, but was not followed-up regularly. From October 2004, progressive weight loss and decreased urine output was noted and the patient was admitted to the hospital on November 20, 2004. By January 2005, patient's body weight reduced by 15 kg, and preoperative body mass was 60.5 kg. Physical examination identified discomfort in the right upper abdomen and abdominal distension. Laboratory examination was as follows. Blood routine: white blood cells (WBC) 7.2×10^9/L, red blood cells (RBC) 3.4×10^{12}/L, Hb 6 g/L, PLT 70×10^{12}/L. Urine routine: protein + + +, occult blood ++. Liver function: alanine aminotransferase (ALT) 117 U/L, aspartate aminotransferase (AST) 113 U/L, total protein (TP) 50 g/L, albumin (ALB) 26.9 g/L, alkaline phosphatase (ALP) 99 U/L, γ-glutamyltranspeptidase (GGT) 109 U/L, total bilirubin (TBIL) 102 μmol/L. Renal function: blood urea nitrogen (BUN) 23.6 mmol/L, creatinine (CRE) 664 μmol / L. Hepatitis B series tips: hepatitis B surface antigen (HBsAg), hepatitis B e antibody (HBeAb), hepatitis B core antibody (anti-HBC) positive, HBV-DNA 1.5×10^7/ml. Ascites was yellow turbid with RBC $2{,}200 \times 10^6$/ml, WBC 50×10^6/ml, GLU 9.5 mmol/L, TP 9 g/L, ALB 6.0 g/L. Fasting and postprandial blood sugar were 10.8 and 18.4 mmol/L, respectively. Ultrasonography showed cirrhosis, a large amount of ascites, splenomegaly, large pancreatic head, and expansion of the main pancreatic duct. CT examination showed cirrhosis, ascites, portal hypertension, cholecystitis, atrophy of the pancreatic body and tail, significant expansion of the pancreatic duct, full pancreatic head, and atrophy of both kidneys. Magnetic resonance imaging showed cirrhosis with moderate ascites, obvious pancreatic duct dilatation, bilateral kidney atrophy, and cholecystitis. Renal dynamic imaging showed severe damage to both kidneys. The non-functional left and right renal glomerular filtration rate (GFR) were ∼3.73 ml/min/1.73 m^2 and 5.46 ml/min/1.73 m^2, respectively. The patient was diagnosed with post-hepatitis B cirrhosis, hepatic insufficiency with chronic renal insufficiency and chronic pancreatitis leading to insulin-dependent diabetes mellitus (IDDM). A simultaneous liver-pancreas-kidney transplantation surgery was planned.

The recipient blood type was type B, Rh+. The donor blood types were O-type and B-type. The panel reactive antibody (PRA) was negative for the recipient. The human leukocyte antigen (HLA) sites of the donors and recipient are shown in **Table 1**. Both pre-transplant lymphotoxicity tests were negative.

In the initial operation, the organs were obtained from donor 1 and trimmed using routine methods (1), and transplanted in the order of liver, kidney, and pancreas. Under general anesthesia, an incision under the bilateral costal margin was made, and a piggyback orthotopic liver transplantation was performed. Further, a conventional kidney transplantation was performed in the left axilla, and the pancreas was implanted into the right axilla. Carrel cuff of the abdominal aorta with superior mesenteric artery and celiac trunk were anastomosed end-to-side with external iliac artery, and portal vein of the transplant pancreas was anastomosed end-to-side with external iliac vein. The donor pancreaticoduodenal segment was anastomosed laterally with the upper jejunum. After anastomosis, the venous and arterial blood supply was opened, the drainage tube was placed, and the incision was sutured (**Figure 1**).

Following the operation, the liver and kidney function, blood and urine bilirubin, blood sugar, blood and urine routine, blood coagulation, D-dimer, serum C-peptide, blood and urine amylase, tacrolimus (FK506) blood concentration and immune index were monitored. Two doses of basiliximab were used to induction therapy. Three days after operation, acute rejection was considered and rabbit anti-human thymocyte immunoglobulin (ATG) was added, 100 mg/d for 7 days. The immunosuppressive regimen was FK506+ mycophenolate mofetil (MMF) + prednisone acetate (Pred).

One week after operation, ALT 57U/L, AST 43 U/L, ALB 36.9 g/L, TBIL 22 μmol/L, BU 26.5 mmol/L, CRE 683 μmol/L were re-examined. Insulin was completely discontinued. Continuous renal replacement therapy maintained a stable internal environment and blood and urine amylase were normal. Ultrasonography showed that the blood flow of the transplanted hepatic artery, portal vein, inferior vena cava, common bile duct, and pancreatic artery and vein was normal.

On the 16th day after operation, B-mode ultrasonography revealed that the blood flow perfusion of the transplanted kidney decreased significantly, the resistance index of the segmental artery blood flow increased to 1, 24 h urine volume was <300 ml, and PRA was negative. The patient was diagnosed with acute rejection of transplanted kidney. The original transplanted kidney was excised under general anesthesia and a second kidney transplantation (obtained from donor 2) was performed at the

TABLE 1 | Basic characteristics of the recipient and donors.

Recipient/donor	Gender	Age	Source of donors	Organ types	HLA sites					
Recipient	Male	43	—	—	A2	A33	B52	B54	DR9	DR13
Donor 1	Male	40	DCD	Liver; pancreas; right kidney	A2	A24	B15	B46	DR9	DR53
Donor 2	Male	52	DCD	Right kidney	A9	A28	B17	B50	DR4	DR11

DCD, donation after citizen's death; HLA, human leukocyte antigen.

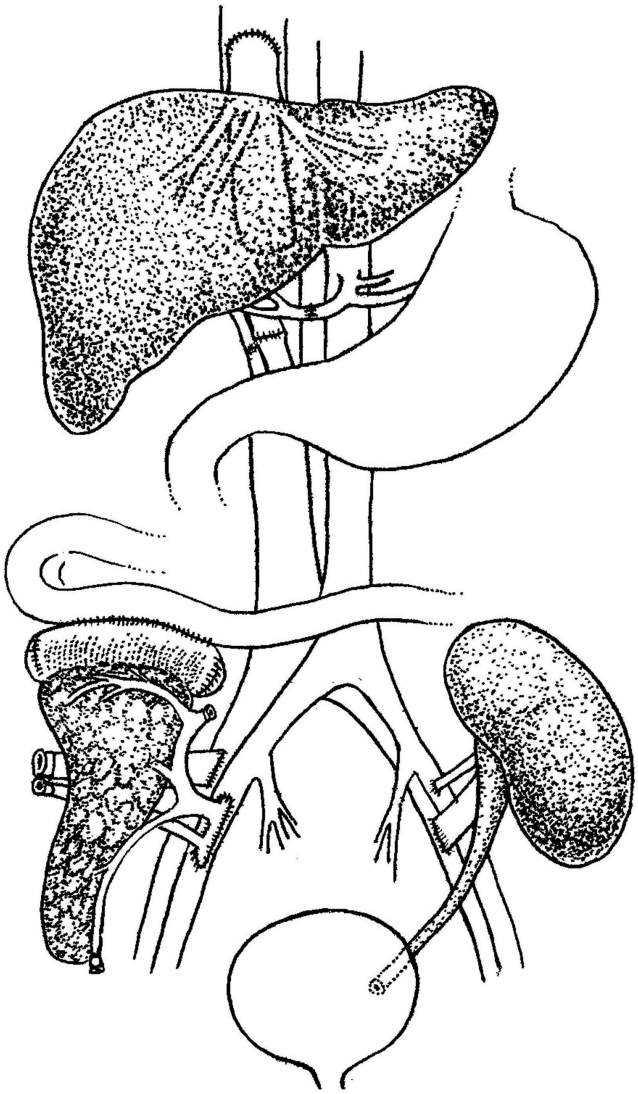

FIGURE 1 | Schematic diagram of the combined liver-pancreas-kidney transplantation. Transplantation was performed in the order of liver, kidney, and pancreas with piggyback orthotopic liver transplantation, conventional renal transplantation, and jejunal drainage of pancreas transplantation, respectively.

original transplanted site 16 days later after diagnosis of rejection of the first kidney. The pathological diagnosis of the original transplanted kidney was acute rejection. The first 24 h urine volume was 7,000 ml after the second operation. On the third day, renal function was reviewed: BUN 6.5 mmol/L, CRE155 μmol/L. One week after the second operation, the patient peripheral blood WBC was 2.1 × 10^9/L, RBC 1.4 × 10^{12}/L, Hb 5.2 g/L, PLT 6 × 10^{12}/L, PT 52 s, APTT 120 s, fibrinogen 1.2 g. Surgical wounds continued to ooze blood. Considering the occurrence of bone marrow suppression, MMF was discontinued and immunosuppressive therapy was maintained by FK506 + Pred regimen. The patient was hospitalized for 33 days and discharged after the function of the transplanted liver, kidney, and pancreas was stable.

One month after the operation, the patient returned to a normal diet and resumed social work 3 months later. The patient was regularly monitored for blood routine, liver function, kidney function, eGFR, electrolytes, blood sugar, blood lipids, hepatitis B virus DNA quantification and FK506 blood trough concentration. CT and ultrasound were routinely performed and medication was accordingly adjusted. No clinically visible rejection occurred after the second operation. Hepatitis B check was negative except for positive HBsAb. No other drugs were used except oral immunosuppressive agents, anti-hepatitis B immunoglobulin and lamivudine treatment. By June 2013, physical examination showed that the patient's body weight was 73 kg. Blood routine: WBC 7.6 × 10^9/L, RBC 4.4 × 10^{12}/L, Hb 11.8 g/L, PLT 110 × 10^{12}/L. Urine protein and occult blood were negative. Liver function: ALT 20 U/L, AST 19 U/L, TP 62 g/L, ALB 42 g/L, ALP 39 U/L, GGT 38 U/L, TBIL 19 μmol/L. Renal function: BUN 6.5 mmol/L, CRE 130 μmol/L, and blood uric acid 399 μmol/L. Fasting blood glucose was 4.3 mmol/L, postprandial blood glucose was 10.3 mmol/L, and HBV-DNA was <1,000/ml. The amount of FK506 was 1.5 mg twice daily, and the trough concentration was 3.0–4.5 ng/ml. The CT and ultrasound showed that the transplanted liver was *in situ*, the left lobe anterior and posterior diameter was 5.4 cm, and the upper and lower diameter was 3.4 cm, the right lobe anterior and posterior diameter was 11.5 cm, and the upper and lower diameter was 11.5 cm. The morphology was regular, the echo was moderately dense, and the distribution was uniform. The right hepatic artery blood flow velocity Vmax = 55.1 cm/s, RI = 0.71, CDFI showed the color blood flow was well filled. The inner diameter of the portal vein was 0.9 cm, and the blood flow velocity Vmean = 17 cm/s. CDFI showed that the color blood flow was well filled. The inner diameter of the hepatic vein was normal. The transplanted pancreas was located in the right iliac fossa, with a size of 2.7 cm at the head, 1.4 cm at the body, and 2.2 cm at the tail. The echo is moderately dense and evenly distributed. A color blood flow signal can be seen inside. The transplanted kidney was located in the left axilla, the size was 11.8 × 5.3 × 5.3 cm, the boundary was clear, the echo

in the parenchyma was dull, the renal pelvis and renal pelvis were separated, and the inner part was a liquid dark area. The maximum anteroposterior diameter was 0.7 cm. The blood flow velocity in the transplanted renal cortex was measured as Vmax = 89.2 cm/s, RI = 0.63. CDFI showed that the color flow was well filled.

DISCUSSION

Characteristics of Combined Liver-Pancreas-Kidney Transplantation

Treating end-stage liver disease and IDDM and renal failure with combined liver-pancreas-kidney transplantation is rare because patients with such conditions are rare. There is no inevitable internal relationship among end-stage liver disease, diabetes, and chronic renal failure. Surgical treatment of patients with liver, kidney, and pancreas failure is often difficult because of the patients' poor physical conditions. However, the combined liver-kidney transplantation and pancreas-kidney transplantation are relatively common, and intra- and postoperative management are becoming more advanced. Performing the combined liver-pancreas transplantation is rare, with fewer cases of combined liver-pancreas-kidney transplantation. In addition, the surgical process is complex, and the hemodynamic changes are unstable (2). There are many contradictions regarding the adjustments of medication during and after operation, which increases the difficulty of a successful combined liver-pancreas-kidney transplantation.

Organ transplantation is the best treatment choice for various types of solid organ failure when medical treatment is not effective. Therefore, kidney, liver, and heart transplantations, as well as various types of combined transplantation and organ cluster transplantation, have been performed in various parts of the world. However, because of the poor physical condition of patients, complicated surgical technique, and difficulty in intraoperative and postoperative treatments, the implementation of multiple solid organ combined transplantation is greatly limited.

Surgical indications for combined liver-kidney transplantation are as follows: systemic metabolic diseases such as primary hyperuricemia caused by liver and kidney failure; hereditary diseases such as congenital polycystic liver and polycystic kidney disease, leading to liver and kidney failure; liver and kidney failure caused by different etiologies such as chronic renal failure owing to chronic glomerulonephritis combined with advanced chronic cirrhosis or malignant liver tumors; hepatorenal syndrome; and Wolcott-Rallison syndrome (3). Hepatocirrhosis after viral hepatitis is the main indication of liver transplantation; however, hepatitis B virus reinfection must be prevented early after operation. In our patient, high-dose anti-hepatitis B immunoglobulin was administered to prevent hepatitis B virus infection during and after surgery, and long-term oral lamivudine inhibited the replication of hepatitis B virus. The serum HbsAb titer and hepatitis B virus DNA level were regularly examined, and the dosage of anti-hepatitis B immunoglobulin was adjusted according to the findings (4). Preventing the recurrence of hepatitis B and avoiding the occurrence of hepatitis B-related nephropathy can effectively ensure the long-term survival of patients (5). In 2017, Jiang et al. (6). performed combined liver-pancreas-kidney transplantation for a patient with hepatitis B cirrhosis and IDDM using block transplantation and achieved good results. Combined pancreas-kidney transplantation can treat diabetes mellitus and diabetic renal failure. Compared with single kidney transplantation, combined pancreas-kidney transplantation can improve the quality of life, prevent or slow down the progression of diabetic complications, and prolong the survival time of recipients and transplanted kidneys (5). A study reported that 1,000 patients who underwent combined pancreas-kidney transplantation had 1-, 10-, and 20-year survival rates of 97, 80, and 58%, respectively, which were significantly better than those of type I diabetes patients with uremia who underwent single living kidney transplantation (403 cases) and single cadaveric kidney transplantation (697 cases) during the same period. The 10-year survival rate of diabetic nephropathy patients receiving hemodialysis was only 9.6–11.2% (7). According to the data of the United Network for Organ Sharing in 2016, the 5- and 10-year pancreas graft function rates after combined pancreas-kidney transplantation were 64 and 38%, respectively (8). Our patient had post-hepatitis B cirrhosis, hepatic insufficiency insulin, and chronic renal insufficiency accompanied with IDDM caused by chronic pancreatitis. After combined liver-kidney-pancreas transplantation, exogenous insulin was discontinued, liver and kidney functions and blood sugar levels returned to normal, the wound recovered well without a serious infection, and satisfactory results were achieved. Therefore, we believe that patients who require organ transplantation and have diabetes, whether kidney or liver transplantation, as long as insulin therapy is needed, should consider combined transplantation with pancreas transplantation. In this combined transplantation, the organs required for transplantation are mostly obtained from the same donor that have the same genetic background and the same antigenicity. Compared with organs from different donors, the number of donor specific antibodies produced will be reduced. The symptoms of diabetes can be simultaneously corrected with uremia and liver failure. Therefore, the long-term effect of combined liver-pancreas-kidney transplantation for patients with diabetes and liver and renal failures should be better than that of combined liver-kidney transplantation.

In multiple organ transplants, the risk of graft-vs.-host disease (GVHD) increases when the organs come from the same donor. GVHD is a kind of pathological damage caused by the antigen sensitization, proliferation and differentiation of the host's major histocompatibility complex (MHC) recognized by the donor's T lymphocytes contained in the graft, and then attacking the host's digestive tract, skin and other organs. GVHD mainly occurs in patients with small bowel transplantation and hematopoietic stem cell transplantation (9). GVHD is a serious complication after liver transplantation. Its incidence is about 2%, but the mortality rate is high (10). GVHD that

occurs after solid organ transplantation mainly refers to: T lymphocytes present in the donor liver are activated after entering the recipient, and then cloned and expanded to attack the host tissues and organs. It is a serious complication after solid organ transplantation, with a mortality rate of more than 85% (11). The most commonly used diagnostic criteria for GVHD after solid organ transplantation are the three-point diagnostic criteria: patients with characteristic clinical symptoms and signs such as rash, fever, and diarrhea; the pathological examination and microbial culture of the involved and organs; evidence of donor lymphocytes found in peripheral blood or affected organs, such as the detection of donor lymphocyte DNA or HLA (12). Acute rejection occurred in this patient after the first transplant, and there was no evidence of GVHD.

Long-Term Survival Analysis

A number of phenomena indicate that transplanted livers have immuno-protective effects. For example, although patients with liver transplantation do not undergo PRA and HLA examination, the incidence of acute rejection remains low, and acute-type rejection is less common in patients who undergo organ transplantation in combination with liver transplantation. From an immunological point of view, although the mechanism of liver immune preference is still not completely understood, there are some hypotheses that may explain it. One explanation is that a large number of passenger white blood cells in the transplanted liver form micro-chimerism with recipient cells and stably circulate and regenerate in the recipient, so that the recipient's immune system receives the donor antigen as if it were a self-antigen (13). Starzl et al. (14) confirmed the existence of peripheral micro-chimerism in liver transplant recipients, suggesting that chimerism plays an important role in inducing immune tolerance and may increase long-term graft survival. Shimonkevitz et al. (15) revealed that the removal of the chimeric state disrupts the state of tolerance and leads to rejection. The hypothesis that the liver can alleviate the rejection of other combined transplantation organs also suggests that the liver can reduce the incidence of antibody-mediated rejection by adsorbing lymphocyte-toxic antibodies *in vivo*. In addition, hepatocytes can express soluble class I antigens after transplantation, which is an immune response effect of the liver (16). Moreover, some studies have reported that the alleviation of rejection by the liver in other combined grafts may be because of larger liver volume and more antigens, resulting in low immune responsiveness; thus, subsequently, the regenerative ability of the liver may mask the slow rejection (17). This can also be explained by the fact that the multiorgan combined transplantation causes the recipient's immune system to bear an excessive immune load, resulting in a state in which the host's immune response to foreign antigens is ineffective. Other studies suggest that this immune protective effect may be related to the immune adsorption of donor-specific antibodies, which may be mediated by hepatocytes and FoxP3+ T cells and the cascade reaction after the activation of indoleamine-2,3-dioxygenase (18, 19). In our case, the first transplanted kidney was excised because of acute rejection, which proved that transplanted livers cannot exert sufficient immunoprotective effects on other grafts in all cases. The second successful kidney transplantation may be the result of the co-adsorbing of the transplanted liver and excised kidney.

Selection of Immunological Factors and Immunosuppressive Programs

There were four mismatches in the first transplantion and six mismatches in the second transplantion. At that time, continuous renal replacement therapy (CRRT) was urgently needed by the patient, and the coagulation index of the patient would be seriously reduced after each dialysis, the bleeding tendency would be aggravated, and the maintenance of dialysis would be life-threatening. Therefore, although the matching results were not satisfactory, we still chose the second transplantation. In terms of epitope classification, A2, A9, A24, and A28 belong to the cross-reactive group (CREG) of A02C, B17, B15, B52, B50, and B46 belong to the CREG of B21C, DR4, DR9, and DR53 belong to the same CREG, so the increased donor antigen in the second transplantation does not significantly increase the potential risk of mismatch, which also can explain the good recovery of the patient.

Judging the degree of matching between donors and recipients and the producing of donor specific antibodies (DSA) by analyzing epitopes is a novel and effective method. HLA eplet matching can reflect the degree of incompatibility. Since this is a case in 2005, the HLA matching results at that time were detected by serological methods, and the results obtained were also serological results. However, the analysis of HLA eplet mismatches requires analysis with HLA high resolution results detected by sequence based typing (SBT). The existing serological HLA typing results cannot be converted to epitopes or eplets.

MMF was discontinued because of poor coagulation and serious bleeding in the early stage after the operation; moreover, continuous blood routine examination showed strong bone marrow suppression. Because of multiorgan transplantation, the antigenicity of the donor was relatively strong, and it was relatively easy to establish a balance with the recipient's immune system. Therefore, although the immunosuppressive regimen of FK506+Pred had been used for a long time, no clinical rejection occurred during the 14-year follow-up.

DECLARATION

The case obeys Declaration of Istanbul. No executed prisoner donor was used. The donors had signed informed consents before donation. The documentation of the organ donation consent has been lost due to several relocations and personnel adjustments.

DATA AVAILABILITY STATEMENT

All datasets generated for this study are included in the article/supplementary material.

ETHICS STATEMENT

Written informed consent was obtained from the individual(s) for the publication of any potentially identifiable images or data included in this article.

AUTHOR CONTRIBUTIONS

GZ, KD, and CM performed the operation. SY, ZL, and LY assisted in obtaining donors. MY was in charge of imaging diagnosis. XG, YZ, LW, and XY followed up patient and obtained data. JY, HW, and WQ concepted and supervised the study. All authors were involved in writing the paper and had final approval of the submitted and published versions.

FUNDING

This work was supported by Xijing Hospital clinical booster program - free exploration project (grant number XJZT18ML04).

ACKNOWLEDGMENTS

The author would like to thank the Department of laboratory and the Department of imaging diagnosis of Xijing Hospital for their support of patients' follow-up. At the same time, they would like to thank the nursing team of Urology and Hepatobiliary for their postoperative rehabilitation care.

REFERENCES

1. Nakache R, Merhav H. Rapid en bloc liver-pancreas-kidney procurement: more pancreas with better vascular supply. *Transplant Proc.* (2000) 32:755–6. doi: 10.1016/S0041-1345(00)00969-6
2. Matuszkiewicz-Rowinska J, Wieliczko M, Malyszko J. Renal replacement therapy before, during, and after orthotopic liver transplantation. *Ann Transplant.* (2013) 18:248–55. doi: 10.12659/AOT.883929
3. Tzakis AG, Nunnelley MJ, Tekin A, Buccini LD, Garcia J, Uchida K, et al. Liver, pancreas and kidney transplantation for the treatment of Wolcott-Rallison syndrome. *Am J Transplant.* (2015) 15:565–7. doi: 10.1111/ajt.13005
4. Dindoost P, Jazayeri SM, Alavian SM. Hepatitis B immune globulin in liver transplantation prophylaxis: an update. *Hepat Mon.* (2012) 12:168–76. doi: 10.5812/hepatmon.5124
5. Schenker P, Vonend O, Kruger B, Klein T, Michalski S, Wunsch A, et al. Long-term results of pancreas transplantation in patients older than 50 years. *Transpl Int.* (2011) 24:136–42. doi: 10.1111/j.1432-2277.2010.01172.x
6. Li J, Guo QJ, Cai JZ, Pan C, Shen ZY, Jiang WT. Simultaneous liver, pancreas-duodenum and kidney transplantation in a patient with hepatitis B cirrhosis, uremia and insulin dependent diabetes mellitus. *World J Gastroenterol.* (2017) 23:8104–8. doi: 10.3748/wjg.v23.i45.8104
7. Sollinger HW, Odorico JS, Becker YT, D'Alessandro AM, Pirsch JD. One thousand simultaneous pancreas-kidney transplants at a single center with 22-year follow-up. *Ann Surg.* (2009) 250:618–30. doi: 10.1097/SLA.0b013e3181b76d2b
8. Gruessner AC, Gruessner RW. Long-term outcome after pancreas transplantation: a registry analysis. *Curr Opin Organ Transplant.* (2016) 21:377–85. doi: 10.1097/MOT.0000000000000331
9. Taylor AL, Gibbs P, Bradley JA. Acute graft versus host disease following liver transplantation: the enemy within. *Am J Transplant.* (2004) 4:466–74. doi: 10.1111/j.1600-6143.2004.00406.x
10. Wu Z, Shi W. Rash as the first manifestation of acute graft-versus-host disease after orthotopic liver transplantation. *Eur J Dermatol.* (2011) 21:997–8. doi: 10.1684/ejd.2011.1506
11. Jacobs MT, Olson M, Ferreira BP, Jin R, Hachem R, Byers D, et al. The use of ruxolitinib for acute graft-versus-host disease developing after solid organ transplantation. *Am J Transplant.* (2019) 20:589–92. doi: 10.1111/ajt.15579
12. Triulzi DJ, Nalesnik MA. Microchimerism, GVHD, and tolerance in solid organ transplantation. *Transfusion.* (2001) 41:419–26. doi: 10.1046/j.1537-2995.2001.41030419.x
13. Dar W, Agarwal A, Watkins C, Gebel HM, Bray RA, Kokko KE, et al. Donor-directed MHC class I antibody is preferentially cleared from sensitized recipients of combined liver/kidney transplants. *Am J Transplant.* (2011) 11:841–7. doi: 10.1111/j.1600-6143.2011.03467.x
14. Starzl TE, Demetris AJ, Trucco M, Ramos H, Zeevi A, Rudert WA, et al. Systemic chimerism in human female recipients of male livers. *Lancet.* (1992) 340:876–7. doi: 10.1016/0140-6736(92)93286-V
15. Shimonkevitz RP, Bevan MJ. Split tolerance induced by the intrathymic adoptive transfer of thymocyte stem cells. *J Exp Med.* (1988) 168:143–56. doi: 10.1084/jem.168.1.143
16. Alqurashi S, Alsayyari AA, Abdullah K, Alwan A, Hajeer AH. Combined liver and kidney transplantation in a highly sensitized and positively cross-matched patient. *Saudi J Kidney Dis Transpl.* (2011) 22:757—60.
17. Creput C, Durrbach A, Menier C, Guettier C, Samuel D, Dausset J, et al. Human leukocyte antigen-G (HLA-G) expression in biliary epithelial cells is associated with allograft acceptance in liver-kidney transplantation. *J Hepatol.* (2003) 39:587–94. doi: 10.1016/S0168-8278(03)00354-4
18. Ingelsten M, Gustafsson K, Oltean M, Karlsson-Parra A, Olausson M, Haraldsson B, et al. Is indoleamine 2,3-dioxygenase important for graft acceptance in highly sensitized patients after combined auxiliary liver-kidney transplantation? *Transplantation.* (2009) 88:911–9. doi: 10.1097/TP.0b013e3181b72e49
19. Baan CC, Weimar W. How does auxiliary liver transplantation regulate alloreactivity in sensitized kidney transplant patients? *Transplantation.* (2011) 91:823–4. doi: 10.1097/TP.0b013e3182100f9a

Conflict of Interest: The authors declare that the research was conducted in the absence of any commercial or financial relationships that could be construed as a potential conflict of interest.

frontiers in Cell and Developmental Biology

ORIGINAL RESEARCH
published: 28 April 2020
doi: 10.3389/fcell.2020.00290

MicroRNA-381-3p Functions as a Dual Suppressor of Apoptosis and Necroptosis and Promotes Proliferation of Renal Cancer Cells

Cong Zhao[1,2,3†], Yifei Zhou[1,2,3†], Qiao Ran[1,2,3], Ying Yao[1,2,3], Haoran Zhang[1,2,3], Jie Ju[1,2,3], Tao Yang[1,2,3], Wei Zhang[1,2,3], Xiaoliang Yu[1,2,3] and Sudan He[1,2,3*]*

[1] State Key Laboratory of Radiation Medicine and Protection, Cyrus Tang Hematology Center and Collaborative Innovation Center of Hematology, Soochow University, Suzhou, China, [2] Center of Systems Medicine, Institute of Basic Medical Sciences, Chinese Academy of Medical Sciences and Peking Union Medical College, Beijing, China, [3] Suzhou Institute of Systems Medicine, Suzhou, China

OPEN ACCESS

Edited by:
Cheng Yang,
Fudan University, China

Reviewed by:
Zhigao Wang,
The University of Texas Southwestern Medical Center, United States
Liming Sun,
Chinese Academy of Sciences, China

***Correspondence:**
Xiaoliang Yu
yxlzark@sina.com
Sudan He
hesudan2018@163.com

[†] These authors have contributed equally to this work

Specialty section:
This article was submitted to Molecular Medicine, a section of the journal Frontiers in Cell and Developmental Biology

Received: 03 February 2020
Accepted: 03 April 2020
Published: 28 April 2020

Citation:
Zhao C, Zhou Y, Ran Q, Yao Y, Zhang H, Ju J, Yang T, Zhang W, Yu X and He S (2020) MicroRNA-381-3p Functions as a Dual Suppressor of Apoptosis and Necroptosis and Promotes Proliferation of Renal Cancer Cells. Front. Cell Dev. Biol. 8:290. doi: 10.3389/fcell.2020.00290

Renal cell carcinoma (RCC) is the most common type of kidney cancer. It has a poor prognosis, with approximately 20–30% of patients developing recurrent and/or metastatic diseases that is relatively high resistant to conventional therapy. Resisting cell death is a hallmark of cancer cells. Apoptosis is a form of programmed cell death mediated by the activation of caspases. Necroptosis is a form of regulated necrosis that relies on the activation of receptor-interacting protein kinase 1 (RIPK1), RIPK3 and mixed lineage kinase domain-like protein (MLKL), the substrate of RIPK3. Cancer cells often display apoptosis resistance via upregulation of anti-apoptotic genes and defective necroptosis due to the epigenetic silence of *Ripk3*. MicroRNAs (miRNAs) are non-coding small RNAs that are involved in numerous biological processes including cell proliferation, differentiation and death. In this study, we screened a set of ∼120 miRNAs for apoptosis-regulating miRNAs and identified miR-381-3p as a suppressor of TNF-induced apoptosis in various cancer cells. Ectopic expression of miR-381-3p inhibits the activation of caspase-8 and caspase-3. The expression level of miR-381-3p inversely correlates with the sensitivity of cancer cells to TNF-induced apoptosis. Moreover, we found that overexpression of miR-381-3p blocks TNF-induced necroptosis by inhibiting the activation of RIPK3 and MLKL. Of note, Kaplan-Meier Plotter analysis demonstrates that papillary RCC patients with high miR-381-3p expression have a lower overall survival than those with low expression level of miR-381-3p. Importantly, miR-381-3p overexpression promotes colony formation in human renal cancer cells. Thus, miR-381-3p acts as an oncogenic miRNA that counteracts both apoptotic and necroptotic signaling pathways. Our findings highlight miR-381-3p as a biomarker for predicting sensitivity to apoptosis and necroptosis, and as a possible therapeutic target for RCC.

Keywords: renal cell carcinoma, miR-381-3p, apoptosis, necroptosis, microRNA

INTRODUCTION

In multicellular organisms, cell death is crucial for the individual development and homeostasis maintenance. Apoptosis is a well-defined form of programmed cell death that is characterized with morphological changes including cell shrinkage, chromatin condensation, DNA fragmentation and the formation of membrane-surrounded apoptotic bodies (Kerr et al., 1972). Apoptosis is executed by a series of cysteine proteases called caspases (Thornberry and Lazebnik, 1998). In mammalian cells, apoptosis can be initiated by the activation of the intrinsic mitochondrial pathway or by the extrinsic death receptor pathway. Activation of mitochondria pathway results in the release of mitochondrial cytochrome c to the cytosol and subsequent assembly of the apoptosome, a protein complex comprised of cytochrome c, procaspase-9 and apoptotic protease activating factor-1 (Apaf-1) (Li et al., 1997). This event leads to the activation of caspase-9. Smac/Diablo acts as a pro-apoptotic protein that is released from mitochondria to the cytosol and interacts with inhibitors of apoptosis proteins (IAPs) to relieve IAPs-mediated inhibition of caspases. The extrinsic pathway is initiated by the binding of death ligands of the TNF receptor superfamily, including TNF-α, FasL, and TRAIL, to their respective death receptors: TNFR, Fas and TRAILR (Ashkenazi and Dixit, 1998; Peter and Krammer, 2003). Ligation of TNF to TNFR1 results in formation of a membrane protein complex (called Complex I) consisting of TNFR1, receptor-interacting protein kinases 1 (RIPK1), cIAP1/2, and TRAF2 (Micheau and Tschopp, 2003). RIPK1 is ubiquitinated in Complex I to mediate NF-κB activation (Ea et al., 2006; Li et al., 2006; Wu et al., 2006). Smac mimetic is a small molecule that can mimic the function of Smac protein (Li et al., 2004). In the presence of Smac mimetic, cIAP1/2 are degraded and this process promotes the deubiquitination of RIPK1 by CYLD (Wright et al., 2007; Hitomi et al., 2008). RIPK1 then forms a cytosolic protein complex (Complex II) with FADD and procaspase-8, leading to the activation of caspase-8 (Micheau and Tschopp, 2003; Wang et al., 2008). Activated caspase-9 or caspase-8 can cleave and activate the executor caspases such as caspase-3 and caspase-7, eventually leading to apoptosis.

Necroptosis is a form of regulated necrosis that displays morphological features including cell swelling and membrane rupture. Necroptosis can be induced by activation of the TNFR family of receptors (TNFR1, Fas, TRAILR) (Laster et al., 1988; Holler et al., 2000), TLR3 and TLR4 (He et al., 2011; Kaiser et al., 2013), interferon receptors (IFNRs) (Robinson et al., 2012) and pathogen infection (Nailwal and Chan, 2019). When capase-8 activity is impaired or inhibited by the caspase inhibitor zVAD, TNF-induced apoptosis switches to TNF-induced necroptosis (Laster et al., 1988; Vercammen et al., 1998). RIPK1 interacts with RIPK3 through their RIP homotypic interaction motif (RHIM) domains, leading to the activation of RIPK3 (Cho et al., 2009; He et al., 2009; Zhang et al., 2009). The activated RIPK3 phosphorylates the substrate protein MLKL (Sun et al., 2012; Zhao et al., 2012), followed by its oligomerization and translocation to the plasma membrane, eventually leading to necroptosis (He and Wang, 2018).

Renal cell carcinoma (RCC) accounts for ∼90% of kidney cancers and is one of the most lethal urological cancer. Around 20–30% patients with localized RCC have a recurrence and/or develop metastatic disease that is relatively high resistant to conventional chemotherapy and radiotherapy (Pantuck et al., 2001). Resisting cell death is considered as a hallmark of cancer cells. Cancer cells often display increased expression of anti-apoptotic genes, including IAPs and anti-apoptotic Bcl-2 family, which is associated with increased resistance of cancer cells to apoptotic stimuli (Pfeffer and Singh, 2018). Many cancer cells exert a defect in necroptosis due to epigenetic silence of *Ripk3* gene. MicroRNAs (miRNAs) are a type of small endogenous single-stranded non-coding RNAs that negatively regulate the expression of target genes by binding to their 3′-UTR region. Increasing evidence suggests that miRNAs are involved in the regulation of various biological processes, including cell proliferation, differentiation, and cell death (Negrini et al., 2009). Studies have shown that some microRNAs are involved in regulating apoptotic pathway in cancer cells (Su et al., 2015; Shirjang et al., 2020). For example, miR-187, miR-181c and miR-34a target TNF-α, leading to suppression of TNF-induced apoptosis (Rossato et al., 2012; Zhang et al., 2012; Guennewig et al., 2014). MiR-708 and miR-22 are downregulated in RCC samples. The overexpression of miR-708 induces apoptosis and suppresses clonogenicity in renal cancer cells (Saini et al., 2011). MiR-22 overexpression increases acetylated p53 and apoptosis by reducing the expression of SIRT1 (Zhang et al., 2016). Additionally, miR-155 inhibits necroptosis in human cardiomyocyte progenitor cells through targeting RIPK1 (Liu et al., 2011). Therefore, identification of miRNAs regulating apoptosis and necroptosis could offer new insights into exploring biomarkers or therapeutic targets for cancer.

In the present study, we discovered miR-381-3p as a dual suppressor of TNF-induced apoptosis and necroptosis in multiple cancer cells. MiR-381-3p interferes with TNF-induced apoptosis by inhibiting the activation of caspase-8 and caspase-3. In addition, miR-381-3p negatively regulates TNF-induced necroptosis through inhibiting the activation of RIPK3 and MLKL. Notably, Kaplan-Meier Plotter analysis has shown that RCC patients with high miR-381-3p expression correlates with a lower overall survival. Remarkably, miR-381-3p overexpression promotes cell proliferation and colony formation of human renal cancer cells.

MATERIALS AND METHODS

Cell Culture

HT-29, OSRC-2, 786, Panc-1, MKN45, and HEK-293T cells were from ATCC. RKO, SW480 and SW620 were kindly provided by Dr. Jianming Li (Soochow University). These cells were cultured in DMEM medium (Invitrogen) supplemented with 10% fetal bovine serum (Invitrogen) and 100 units/mL Penicillin-Streptomycin-Glutamine (Hyclone) in a humidified incubator at 37°C and 5% CO_2. HT-29 stably expressing Flag-RIPK3 was cultured in complete medium containing 2 μg/ml G418 (Calbiochem) as previously described (He et al., 2009).

Cell Viability Assay

Cells were seeded in 96-well plates and then treated as indicated. The cell viability was analyzed by using the Cell Titer-Glo Luminescent Cell Viability Assay kit (Promega, United States) according to the manufacturer's instructions.

Reagents and Antibodies

TNF-α recombinant protein was generated as previously described (Wang et al., 2008). The Smac mimetic compound was kindly provided by Dr. Xiaodong Wang (National Institute of Biological Sciences, Beijing). z-VAD was bought from Bachem (Babendorf, Switzerland). The following antibodies were used: hRIPK1 (BD Biosciences, 610458), p-hRIPK1 (CST, 65746), p-hRIPK3 (Abcam, 209384), p-hMLKL (Abcam, 187091), caspase-8 (CST, 9746), caspase-3 (CST, 9665), cleaved-caspase-3 (CST, 9664), PARP (CST, 9542), FADD (Abcam, 52935), TNFR1 (CST, 3736), TRADD (CST, 3684), TRAF2 (CST, 4712), p-IκB-α (CST, 9246), CYLD (CST, 4495), β-actin (Sigma, A2066). The antibodies recognizing human RIPK3 and MLKL were generated against full-length human recombination proteins.

MicroRNA Screening

Around 120 microRNAs were synthesized by GenePharma Co., Ltd. (Shanghai, China). MicroRNAs were diluted in Opti-MEM medium (Invitrogen, United States) and then transferred into 96-well plates. Lipo2000 was diluted in Opti-MEM medium and incubated for 5 min, then were added to those 96-well plates. After incubation for 20 min, Panc-1 cells were added into the plates at density of 3×10^3 cells per well. Forty-eight hours (h) after transfection, cells were treated with PBS or TNF-α/Smac mimetic for 24 h, followed by cell viability analysis. The negative control oligo (miR-NC) and a RIPK1 siRNA oligo were used as negative control and positive control, respectively.

SiRNA Transfection

The siRNA oligos were transfected into cells using Lipofectamine 2000 (Invitrogen, United States) according to the manufacturer's instructions. The siRNA oligos were purchased from GenePharma Co., Ltd. (Shanghai, China). The following siRNA oligos were used:

Oligo	Sequence (5′→3′)
miR-NC	AACGUACGCGGAAUACUUCGA
miR-381-3p	UAUACAAGGGCAAGCUCUCUGU
si-hCYLD	AAGGGTAGAACCTTTGCTAAA
si-hRIPK1	CCACTAGTCTGACGGATAA
si-hRIPK3	GCUACGAUGUGGCGGUCAA
si-hMLKL	CAAACTTCCTGGTAACTCA

Western Blot Analysis

Cell pellet was collected by centrifugation at 13000 × *g* for 1 min and resuspended in lysis buffer [20 mM Tris–HCl, pH 7.4, 150 mM NaCl, 10% glycerol, 1% Triton X-100, 1 mM Na_3VO_4, 25 mM β-glycerol phosphate, 0.1 mM PMSF, a complete protease inhibitor set (Roche)]. Cell lysate was incubated on ice for 20 min, and then centrifuged at 13000 × *g* for 20 min at 4°C. The supernatants were collected and subjected to further western blot analysis.

Real-Time Quantitative PCR Analysis

Total RNA was extracted from cells using Trizol Reagent (Invitrogen, United States) according to the manufacturer's instructions. RNA was reversely transcribed into cDNA using HiScript II Q RT SuperMix (Vazyme, China). The gene expression was determined by quantitative real time PCR using SYBR Green Master Mix (Biotool, United States) performed in a Roche LightCycler 480 II system. The following primers were used:

Gene	Sequence (5′→3′)
miR-381-3p	F: AAAGCGAGGTTGCCCTTTGT
	R: TACTCACAGAGAGCTTGCCC
U6	F: CTCGCTTCGGCAGCACA
	R: AACGCTTCACGAATTTGCGT
TNFR1	F: TGCCAGGAGAAACAGAACAC
	R: TCCTCAGTGCCCTTAACATTC
TRADD	F: GCTGTTTGAGTTGCATCCTAGC
	R: CCGCACTTCAGATTTCGCA
TRAF2	F: TCCCTGGAGTTGCTACAGC
	R: AGGCGGAGCACAGGTACTT
RIPK1	F: TGGGCGTCATCATAGAGGAAG
	R: CGCCTTTTCCATGTAAGTAGCA
GAPDH	F: GGAGCGAGATCCCTCCAAAAT
	R: GGCTGTTGTCATACTTCTCATGG

mRNA and miRNA expression levels were normalized against GAPDH and endogenous U6 small nuclear RNA (U6 snRNA), respectively.

Flow Cytometry Analysis

The Annexin V-FITC/PI apoptosis detection kit (BD Biosciences, United States) was used according to the manufacturer's instructions. Panc-1 cells were transfected with miR-NC, miR-381-3p or a RIPK1 siRNA oligo. After 60 h, cells were treated with TNF-α/Smac mimetic. Twenty-four hours later, cells were harvested, then washed with cold PBS and resuspended in staining buffer containing Annexin V- FITC. Then cells were incubated in the dark at room temperature for 20 min, followed by PI staining. Flow cytometry analysis was acquired on a Gallios Flow Cytometer (Beckman Coulter, United States) and data was then analyzed with software Kaluza Analysis.

Dual-Luciferase Reporter Assay

3′-UTR of human CYLD (hCYLD) was cloned into the pmirGLO vector (Promega, United States). The recombinant reporter plasmids were validated by DNA sequencing. CYLD-3′UTR

reporter plasmid was co-transfected with miR-NC or miR-381-3p into HEK-293T cells. Then cells were harvested in reporter lysis buffer. The luciferase activity was measured 48 h after transfection by Dual-Luciferase Reporter Assay System (Promega, United States). Luciferase activity was normalized to Renilla luciferase activity.

Colony Formation Assay

OSRC-2 and Panc-1 cells were transfected with miR-NC, miR-381-3p or siRIPK1 in 12-well plates. Forty-eight hours later, cells (8×10^2/well) were reseeded in 6-well plates, and culture media were replaced every 3 days. After around 7 days, cell colonies reached desirable size. Cells were fixed with 10% formalin and stained with Gimasa [Nanjing Jiancheng Chemical Industrial Co., Ltd. (Nanjing, China)] for counting. The total area of OSRC-2 cell colony formation was calculated using Image J software.

Overall Survival Analysis

The dataset of a total 290 patients with papillary RCC were obtained from the online database Kaplan-Meier Plotter[1]. The overall survival (OS) was analyzed with Kaplan-Meier Plotter and GraphPad Prism.

[1]http://kmplot.com/analysis/

Statistical Analysis

Data of cell survival rate are represented as the mean ± standard deviation of triplicates. Significance was evaluated using *t*-tests of GraphPad Prism software. *P*-values were determined by paired-samples *t*-tests. $^*P < 0.05$, $^{**}P < 0.01$, $^{***}P < 0.001$.

RESULTS

Identification of MiR-381-3p as a Suppressor of TNF-Induced Apoptosis

Apoptosis is a highly regulated process of cell death executed by caspases. To identify miRNAs involved in the cellular response to apoptosis, we screened a set of ∼ 120 miRNAs to identify candidate miRNAs regulating TNF-induced apoptosis, which is known to be induced by the treatment of TNF-α plus Smac mimetic (Wang et al., 2008). This screening was carried out in human pancreatic cancer Panc-1 cells, which are known to be sensitive to TNF-α/Smac mimetic. Panc-1 cells were transfected with these miRNAs for 48 h, and then were treated with TNF-a plus Smac mimetic. After 24 h, cell viability was determined by measuring the ATP levels. MiR-381-3p came out as one of the most effective hits that significantly suppressed TNF-induced apoptosis (**Figure 1A**). A siRNA oligo targeting RIPK1 was used as the positive control (**Figure 1A**). Further, we confirmed

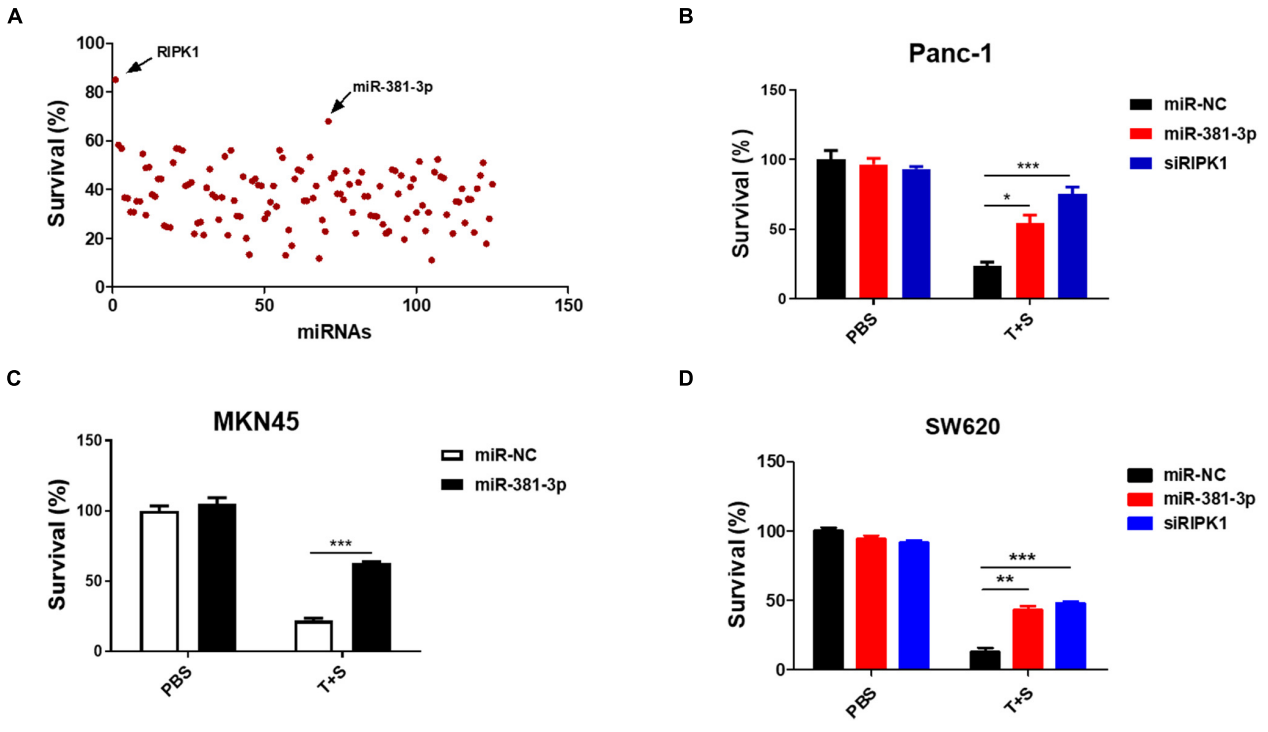

FIGURE 1 | MiR-381-3p inhibited TNF-induced apoptosis in human cancer cells. **(A)** Panc-1 cells cultured in 96-well plates were transfected with miRNAs from a small library of ∼120 miRNAs for 48 h, and subsequently treated with the control PBS or TNF-α (40 ng/ml) plus Smac mimetic (100 nM) (T + S) for 24 h. Cell viability was determined by measuring ATP levels. T: TNF-α; S: Smac mimetic. **(B–D)** Panc-1, MKN45 and SW620 cells were transfected with miR-381-3p for 60 h prior to the treatment with TNF-α plus Smac mimetic for 24 h, and then cell viability was determined. Identical concentrations of TNF-α and Smac mimetic were used in later experiments unless otherwise stated. $^*P < 0.05$, $^{**}P < 0.01$, $^{***}P < 0.001$.

that miR-381-3p efficiently inhibited TNF-induced apoptosis in multiple human cancer cell lines including pancreatic cancer Panc-1 cells, gastric carcinoma MKN45 cells, and colon cancer SW620 cells (**Figures 1B–D**).

MiR-381-3p Negatively Regulates Apoptosis by Suppressing Caspase-3 Activation

Since miR-381-3p has the ability to inhibit TNF-induced apoptosis, we sought to evaluate the effect of miR-381-3p on the Annexin V-positive cells and caspase activation. Annexin V staining is widely used for the detection of apoptotic cells with the exposure of phosphatidylserine at the outer surface of cell membrane. We transfected miR-381-3p into Panc-1 cells, and treated cells with PBS (as control) or TNF-α/Smac mimetic. The cells were stained with Annexin V and PI, followed by flow cytometry analysis. As shown in **Figure 2A**, transfection of miR-381-3p reduced the percentage of both Annexin V and PI positive cells in response to the treatment of TNF-α/Smac mimetic. As TNF-induced apoptosis is mediated via the activation of a series of caspases including caspase-8, an initiator caspase, and caspase-3, an executioner caspase, we next examined the effect of miR-381-3p on the activation of caspase-8 and caspase-3 by measuring their proteolytic cleavage. As shown in **Figures 2B,C**, miR-381-3p transfection reduced the cleavage of caspase-8 and the cleavage of caspase-3. Poly (ADP-ribose) polymerase (PARP) is a well-known substrate that is cleaved by activated caspases-3 during apoptosis. We found that miR-381-3p transfection inhibited the cleavage of PARP in both Panc-1 and MKN45 cells treated with TNF-α/Smac mimetic (**Figures 2D,E**). MiR-381-3p overexpression did not affect the expression levels of caspase-8, FADD and caspase-3 under normal culture conditions (**Figure 2B**), suggesting that miR-381-3p negatively regulates caspase-8 and caspase-3 activation, but not their expression

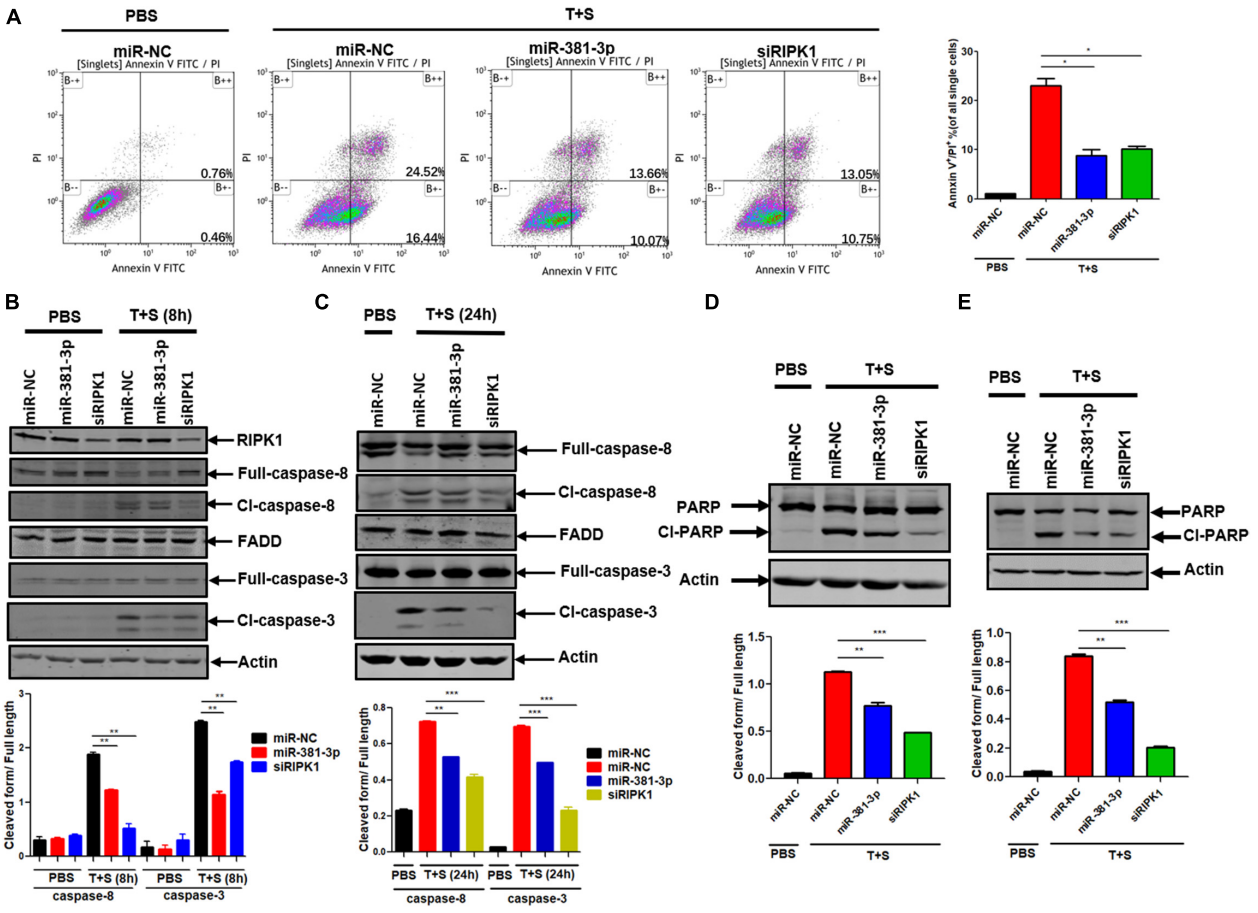

FIGURE 2 | MiR-381-3p negatively regulates apoptosis by suppressing caspase-3 activation. **(A)** Panc-1 cells were transfected with miR-NC, miR-381-3p or siRIPK1 for 60 h, respectively, and then were stained with Annexin V/PI for flow cytometric analysis of apoptosis. **(B,C)** Panc-1 cells were transfected with indicated miRNAs for 60 h and then treated with control PBS or TNF-α plus Smac mimetic for the indicated time. Cell lysates were collected, and aliquots of 40 μg were subjected to western blot analysis of caspase-8, FADD and caspase-3. The ratio of the cleaved form to full-length caspase-8 or caspase-3 was determined by software Image J (lower panel). **(D,E)** Panc-1 and MKN45 cells transfected with miR-381-3p were treated with TNF-α plus Smac mimetic, and analyzed by western blot for PARP cleavage. The ratio of the cleaved form to full-length PARP was also determined by software Image J (lower panel). Cl-caspase-8: cleaved caspase-8. Full caspase-8: full length caspase-8. $^{*}P < 0.05$, $^{**}P < 0.01$, $^{***}P < 0.001$.

levels. Collectively, these results demonstrate that miR-381-3p is capable of inhibiting apoptosis by interfering with caspase-8 and caspase-3 activation.

High Expression of MiR-381-3p Is Correlated With Resistance of Cancer Cells to Apoptosis and Poor Prognosis of RCC Patients

Apoptosis resistance is a hallmark of cancer cells. Having shown that miR-381-3p intervenes with the apoptosis pathway, we sought to examine the prognostic value of miR-381-3p expression in human patients with cancer using the online database Kaplan-Meier Plotter (see text footnote 1). Kaplan–Meier overall survival analysis showed that papillary RCC patients with high miR-381-3p expression level had a significantly shorter overall survival time than those patients with low miR-381-3p expression level (**Figure 3A**). Considering that miR-381-3p overexpression in both Panc-1 and MKN45 cells enhanced cell resistance to TNF-induced apoptosis, we hypothesized that there is a correlation between the miR-381-3p level and the sensitivity of cancer cells to TNF-induced apoptosis. We measured the expression levels of miR-381-3p mRNA in various human cancer cell lines including human renal cancer cell lines (OSRC-2 and 786), human colon cancer cell lines (HT-29, RKO and SW480 and SW620) in addition to Panc-1 and MKN45. Based on the relative expression level of miR-381-3p, we divided these cell lines into two groups: miR-381-3p high expression cell lines (HT-29, OSRC-2, 786, RKO) and miR-381-3p low expression cell lines (Panc-1, MKN45, SW480, and SW620) (**Figure 3B**). Notably, the miR-381-3p^{high} cells (HT-29, OSRC-2, 786, and RKO), displayed relatively lower sensitivity to TNF-induced apoptosis, compared with the miR-381-3p^{low} cells (Panc-1, MKN45, SW480, and SW620) (**Figure 3C**). Further correlation analysis showed a positive correlation between miR-381-3p expression level and resistance of cells to TNF-induced apoptosis (**Figure 3D**). Taken together, these results suggest that cellular miR-381-3p expression level in human cancer cell is negatively correlated with cell sensitivity to TNF-induced apoptosis.

MiR-381-3p Inhibits TNF-Induced Necroptosis

In addition to apoptosis, TNF is a classical trigger of necroptosis, which is highly regulated by RIPK1, RIPK3, and MLKL. To evaluate the effect of miR-381-3p on TNF-induced necroptosis,

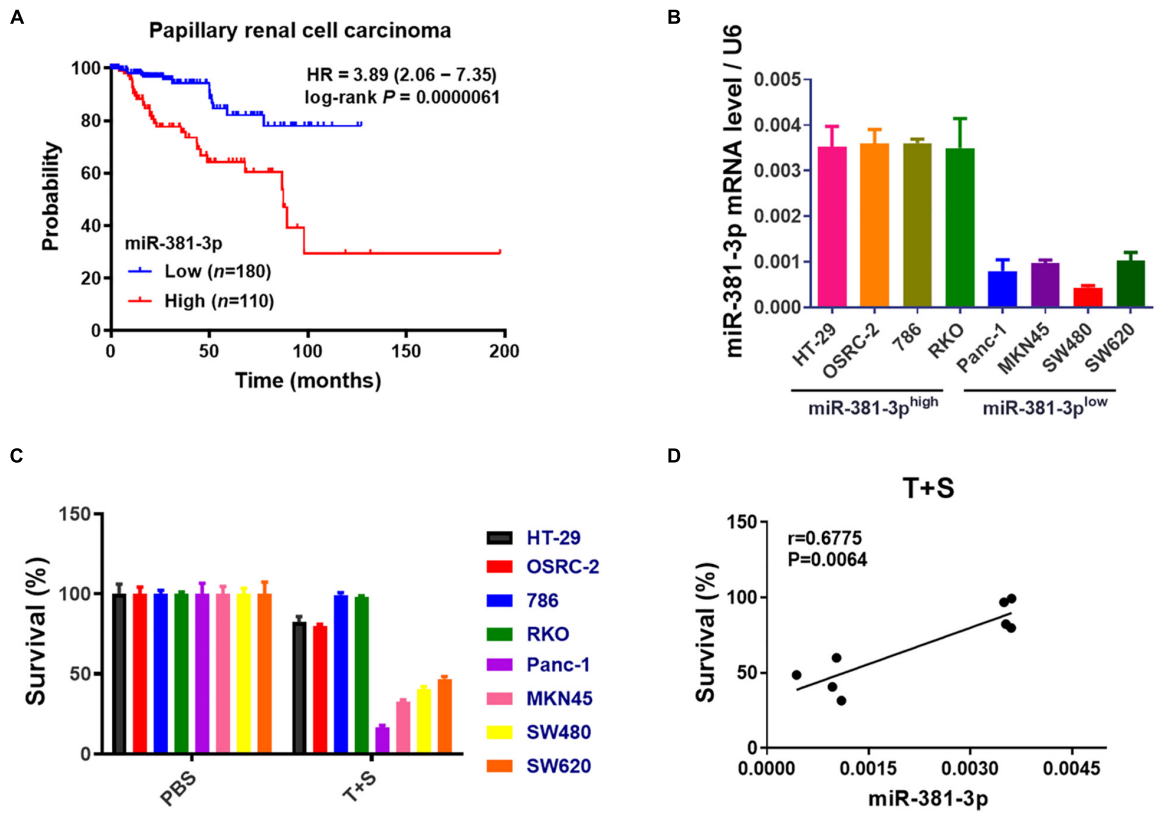

FIGURE 3 | High expression of miR-381-3p is correlated with resistance of cancer cells to apoptosis and poor prognosis of RCC patients. **(A)** The overall survival of papillary RCC patients was compared between individuals with high or low level of miR-381-3p. **(B)** Detection of miR-381-3p mRNA expression level in different human cancer cells by qRT-PCR analysis. U6 was used as an internal control. **(C)** Human cancer cells were treated with the control PBS or TNF-α/Smac mimetic for 24 h. Cell viability was determined by measuring ATP levels. **(D)** Correlation analysis revealed a positive correlation between relative miR-381-3p mRNA expression levels in human cancer cells and survival rate of cells treated with TNF-α/Smac mimetic.

both MKN45 and HT-29 cells were transfected with miR-NC or miR-381-3p, followed by treatment with necroptotic stimuli (TNF-α, Smac mimetic and z-VAD), which is known to induce TNF-mediated necroptosis (He et al., 2009). As shown in **Figures 4A,B**, overexpression of miR-381-3p in MKN45 and HT-29 cells resulted in reduced cell death, suggesting that miR-381-3p suppressed TNF-induced necroptosis. As OSRC-2 cells do not express RIPK3, we further evaluated the impact of miR-381-3p on necroptosis in OSRC-2 cells with ectopic expression of human RIPK3. Ectopic expression of RIPK3 in OSRC-2 cells resulted in death of around 30% cells upon necroptotic stimuli, while this effect was attenuated by miR-381-3p overexpression (**Figure 4C**). During TNF-induced necroptosis, activation of RIPK1 and RIPK3 leads to the phosphorylation of RIPK1 and RIPK3. The activated RIPK3 phosphorylates the substrate MLKL. We therefore examined the effect of miR-381-3p on the activation of RIPK1, RIPK3, and MLKL. MiR-381-3p transfection decreased the phosphorylation levels of both RIPK3 and MLKL in HT-29 cells treated with TNF-α/Smac mimetic/z-VAD, while overexpression of miR-381-3p had no effect on RIPK1 phosphorylation (**Figures 4D,E**). We further confirmed the inhibitory effect of miR-381-3p overexpression on RIPK3 phosphorylation in HT-29 cells which stably expressed RIPK3 with a 3X FLAG tag at the N-terminus (**Figure 4F**). These results demonstrate that miR-381-3p negatively regulates activation of RIPK3 and MLKL acting downstream of RIPK1 activation. To clarify whether miR-381-3p directly targets these key molecules in TNF-induced necroptosis, we evaluated the effect of miR-381-3p on the protein levels of RIPK1, RIPK3, and MLKL. It came out that the expression levels of these three proteins were not affected by miR-381-3p overexpression (**Figures 4G,H**), suggesting that miR-381-3p does not downregulate the levels of RIPK1, RIPK3, and MLKL. Taken together, miR-381-3p exerts an inhibitory effect on RIPK3 activation and necroptosis.

MiR-381-3p Does Not Directly Downregulate the Known Common Molecules Involved in TNF-Induced NF-κB Signaling and Cell Death

TNF is a pleiotropic cytokine that can activate NF-κB activation in addition to apoptosis and necroptosis. To assess the effect of miR-381-3p on TNF-induced NF-κB activation, we examined the effect of miR-381-3p on the level of IκB-α phosphorylation, which is a key step in NF-κB activation. As shown in **Figure 5A**, overexpression of miR-381-3p had no effect on the IκB-α phosphorylation, suggesting that miR-381-3p did not influence IκB-α phosphorylation in response to TNF-α receptor activation. Moreover, miR-381-3p exerted no impacts on the mRNA

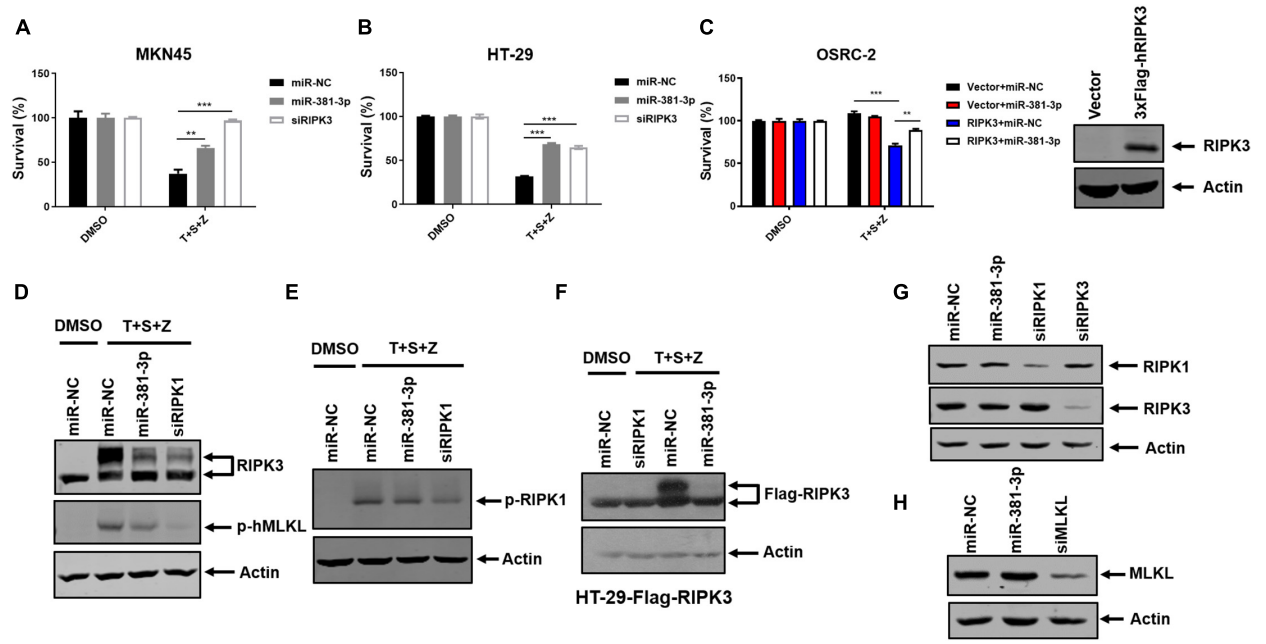

FIGURE 4 | MiR-381-3p inhibits TNF-induced necroptosis. **(A,B)** MKN45 and HT-29 cells were transfected with miR-381-3p for 60 h, and then were treated with the control DMSO or TNFα/Smac mimetic/z-VAD (20 μM) (T + S + Z) for indicated time. Cell viability was determined by measuring ATP levels. Z: z-VAD.**(C)** OSRC-2 cells were transfected with empty vector or human RIPK3 plasmid together with miR-NC or miR-381-3p. After 48 h, cells were treated with TNFα/Smac mimetic/z-VAD for 24 h. Cell viability was determined by measuring ATP levels. OSRC-2 cells were transfected with empty vector or human RIPK3 plasmid for 48 h, then the cell lysates were subjected to western blot analysis of RIPK3. **(D,E)** MiR-NC, miR-381-3p or siRIPK1 was transfected into HT-29 cells for 60 h, then treated with TNFα/Smac mimetic/z-VAD. Cell lysates were collected and subjected to western blot analysis of phos-RIPK3, phos-MLKL and phos-RIPK1. **(F)** HT-29 cells stably expressing Flag-RIPK3 (HT-29-Flag-RIPK3) were transfected with miR-NC, miR-381-3p or siRIPK1 for 60 h, followed by treatment as indicated. Cell lysates were collected and subjected to western blot analysis of Flag-RIPK3 level. **(G,H)** HT-29 cells were transfected with indicated miRNAs for 60 h. The cell lysates were subjected to western blot analysis of RIPK1, RIPK3, and MLKL levels. $^{**}P < 0.01$, $^{***}P < 0.001$.

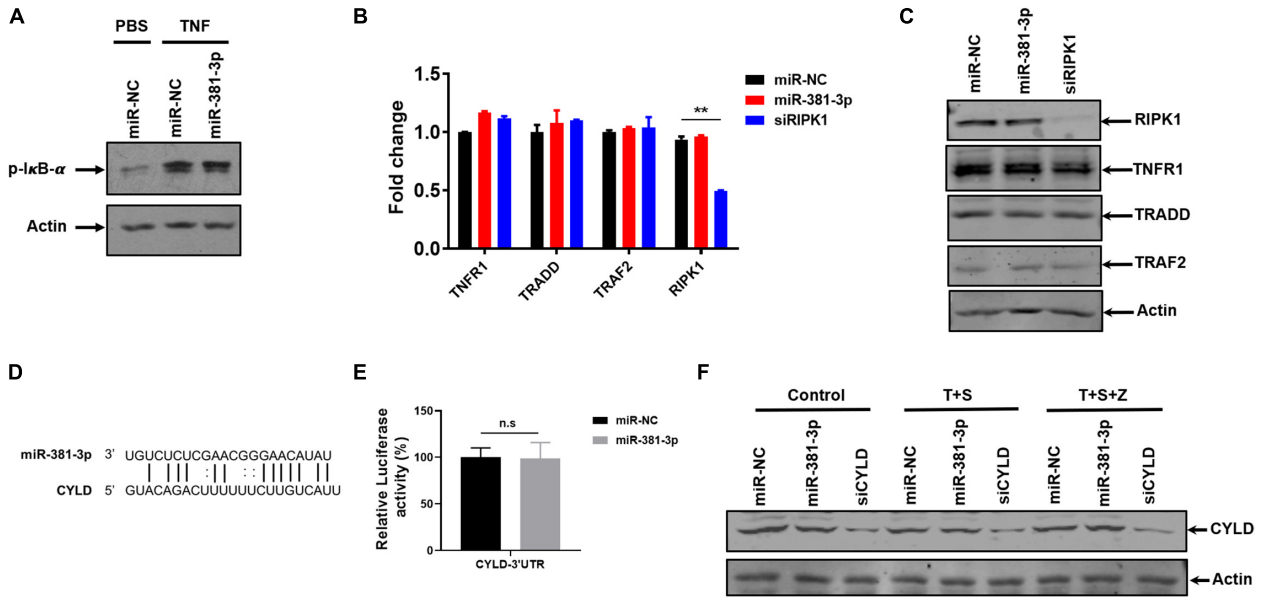

FIGURE 5 | MiR-381-3p does not directly downregulate the known common molecules involved in TNF-induced NF-κB signaling and cell death. **(A)** HT-29 cells were transfected with miR-NC or miR-381-3p for 60 h and then treated with the control PBS or TNF-α for 10 min, phos-IκB-α protein level was detected by western blot. **(B)** HT-29 cells were transfected with miR-NC or miR-381-3p for 60 h, and mRNA levels of *Tnfr1*, *Tradd*, *Traf2*, and *Ripk1* were determined via qRT-PCR. **(C)** HT-29 cells were transfected with miR-NC or miR-381-3p for 60 h. Cell lysates were collected and subjected to western blot analysis of TNFR1, TRADD, TRAF2, and RIPK1. **(D)** MiR-381-3p and its putative binding sequence in the 3′-UTR of CYLD. **(E)** MiR-NC or miR-381-3p was co-transfected with pmir-GlO-CYLD-3′UTR into HEK-293T cells, and luciferase activity was measured. **(F)** HT-29 cells were transfected with miR-381-3p for 60 h, and then were treated with the control PBS, TNF-α/Smac mimetic or TNFα/Smac mimetic/z-VAD for 6 h. Cell lysates were collected and subjected to western blot analysis of CYLD protein level. $^{**}P < 0.01$.

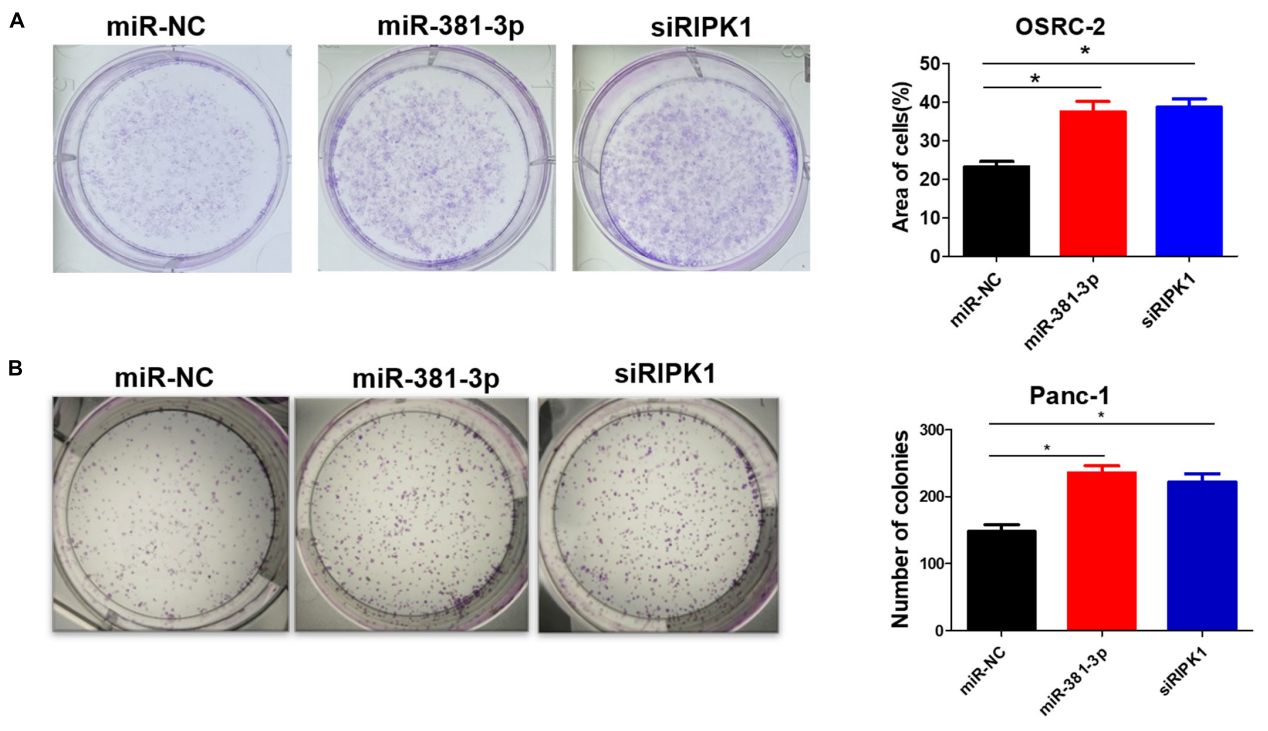

FIGURE 6 | MiR-381-3p promotes human renal cancer cell growth and colony formation. **(A)** Human renal cancer OSRC-2 cells were transfected with miR-NC, miR-381-3p or RIPK1 siRNA oligo, followed by colony formation assay. **(B)** Panc-1 cells were transfected with miR-NC, miR-381-3p or RIPK1 siRNA oligo and then colony formation assay was performed. $^{*}P < 0.05$.

expression levels of molecules involved in the TNFR complex including TNFR1, TRADD, TRAF2, and RIPK1 (**Figure 5B**). Given that miRNAs may regulate gene expression through suppressing mRNA translation, we further examined whether the protein levels of these genes in the TNFR complex were affected by miR-381-3p overexpression. The result showed that miR-381-3p had no effect on the protein levels of TNFR1, TRADD, TRAF2, and RIPK1 (**Figure 5C**). To further investigate possible target of miR-381-3p in the regulation of apoptosis and necroptosis, we searched the miRNA database (microRNA), and found a putative miR-381-3p-binding site located within the 3′-UTR of CYLD (Cylindromatosis) (**Figure 5D**). CYLD is a de-ubiquitin enzyme which removes ubiquitin chains on RIPK1 to facilitate both TNF-induced apoptosis and necroptosis (Wright et al., 2007). To evaluate whether CYLD is a direct target of miR-381-3p, we generated luciferase report gene of 3′-UTR of CYLD containing the predicted miR-381-3p-binding site. We found that transfection of miR-381-3p did not affect the luciferase signal of 3′-UTR of CYLD (**Figure 5E**). Moreover, overexpression of miR-381-3p had no obvious impact on CYLD protein level when cells were either cultured under normal condition or treated with apoptotic or necroptotic stimuli (**Figure 5F**). Collectively, these results suggest that miR-381-3p does not directly downregulate the known common molecules involved in TNF-induced NF-κB signaling, apoptosis and necroptosis.

MiR-381-3p Promotes Human Renal Cancer Cell Growth and Colony Formation

High expression of miR-381-3p not only enhanced resistance of renal cancer cells to apoptosis and necroptosis (**Figures 1**, **4**), but also was highly correlated with poor prognosis of RCC patients (**Figure 3A**). Therefore, we speculated that miR-381-3p might contribute to cell proliferation and clonogenicity in renal cancer cells. We further explore the effect of miR-381-3p on colony formation of human renal carcinoma cells. As shown in **Figure 6A**, miR-381-3p overexpression significantly increased OSRC-2 cell colony formation. Consistently, miR-381-3p overexpression promoted the colony formation in Panc-1 cells (**Figure 6B**). These results suggest that miR-381-3p promotes survival and proliferation of cancer cells including renal cancer cells.

DISCUSSION

Cancer cells escape from immunosurveillance by developing strategies to avoid apoptotic and necrotic cell death. The ability of cancer cells to evade cell death usually limits the efficacy of anticancer therapies. Emerging evidence has suggested that miRNAs play important roles as oncogenes or tumor suppressors in various cancers including RCC. In this study, we identify miR-381-3p as a dual suppressor of apoptosis and necroptosis with an oncogenic role in renal cell cancer.

MiR-381-3p has been demonstrated as either oncogenic or tumor suppressive miRNA in various tumor types depending on the target mRNAs. For instance, miR-381-3p overexpression promotes cancer cell proliferation in glioblastoma cells and osteosarcoma cells by targeting the brain relative specific expression gene LRRC4 (Tang et al., 2011; Li et al., 2016). On the contrary, miR-381-3p functions as a tumor suppressor gene in rectal cancer and prostate cancer through suppression of UBE2C (Zhang et al., 2018; Hu et al., 2019). Through a cell-based screening for miRNAs regulating apoptosis, we found that miR-381-3p negatively regulates TNF-induced apoptosis in multiple human cancer cell lines. MiR-381-3p overexpression inhibits the activation of caspase-8 and caspase-3 (**Figures 2B,C**). In addition, miR-381-3p blocks TNF-induced necroptosis through suppressing activation of RIPK3 and MLKL, whereas it has no impact on RIPK1 phosphorylation (**Figures 4C–E**). Taken together, our study reveals that miR-381-3p plays a crucial role in counteracting both apoptosis and necroptosis in cancer cells.

Considering that miR-381-3p is a dual suppressor of apoptosis and necroptosis, we speculated that it may target common molecules involved in apoptotic and necroptotic cell death. In fact, miR-381-3p overexpression does not affect the expression levels of RIPK1 and CYLD (**Figures 4F**, **5E**). Of note, miR-381-3p specifically inhibits TNF-induced apoptosis and necroptosis, while it has no effect on TNF-induced NF-κB activation (**Figure 5A**), suggesting that molecules involved in the TNFR complex are not the functional targets of miR-381-3p. Consistently, miR-381-3p does not downregulate the mRNA and protein levels of molecules in the TNFR complex including TNFR1, TRADD, TRAF2, and RIPK1 (**Figures 5B,C**). Future studies will be required to explore the direct targets of miR-381-3p in regulating TNF-induced apoptosis and necroptosis.

Our study demonstrates that miR-381-3p expression varies among different types of human cancer cell lines, which negatively correlates with tumor cell sensitivity to TNF-induced apoptosis (**Figures 3B–D**). MiR-381-3p expression is relatively high in human renal carcinoma cells. Remarkably, papillary RCC patients with high expression level of miR-381-3p is associated with a poor prognosis (**Figure 3A**). Indeed, miR-381-3p overexpression promotes clonogenicity of human renal cancer cells (**Figure 6A**). Thus, miR-381-3p could be a biomarker for predicting sensitivity to apoptosis and necroptosis, and may be a potential target for renal cancer therapy.

DATA AVAILABILITY STATEMENT

All datasets generated for this study are included in the article/supplementary material.

AUTHOR CONTRIBUTIONS

SH and XY designed this study and revised the manuscript. CZ and YZ performed the molecular biology studies and colony formation, analyzed the data, and drafted the manuscript. QR, YY, HZ, and JJ performed cell culture and qRT-PCR. TY and WZ performed flow cytometry analysis and plasmid construction.

FUNDING

This work was supported by the National Natural Science Foundation of China (31671436, 31830051, 31900526, 31771533, and 31600133), a Project Funded by the Priority Academic Program Development of Jiangsu Higher Education Institutions, China Postdoctoral Science Foundation funded project (2019M650563), Natural Science Foundation of Jiangsu Province Grant (BK20160314), Fok Ying Tung Education Foundation for Young Teachers (151020), and CAMS Initiative for Innovative Medicine (CAMS-I2M, 2016-I2M-1-005, and 2019-I2M-1-003).

REFERENCES

Ashkenazi, A., and Dixit, V. M. (1998). Death receptors: signaling and modulation. *Science* 281, 1305–1308. doi: 10.1126/science.281.5381.1305

Cho, Y. S., Challa, S., Moquin, D., Genga, R., Ray, T. D., Guildford, M., et al. (2009). Phosphorylation-driven assembly of the RIP1-RIP3 complex regulates programmed necrosis and virus-induced inflammation. *Cell* 137, 1112–1123. doi: 10.1016/j.cell.2009.05.037

Ea, C. K., Deng, L., Xia, Z. P., Pineda, G., and Chen, Z. J. (2006). Activation of IKK by TNFalpha requires site-specific ubiquitination of RIP1 and polyubiquitin binding by NEMO. *Mol. Cell* 22, 245–257. doi: 10.1016/j.molcel.2006.03.026

Guennewig, B., Roos, M., Dogar, A. M., Gebert, L. F., Zagalak, J. A., Vongrad, V., et al. (2014). Synthetic pre-microRNAs reveal dual-strand activity of miR-34a on TNF-alpha. *RNA* 20, 61–75. doi: 10.1261/rna.038968.113

He, S., Liang, Y., Shao, F., and Wang, X. (2011). Toll-like receptors activate programmed necrosis in macrophages through a receptor-interacting kinase-3-mediated pathway. *Proc. Natl. Acad. Sci. U.S.A.* 108, 20054–20059. doi: 10.1073/pnas.1116302108

He, S., Wang, L., Miao, L., Wang, T., Du, F., Zhao, L., et al. (2009). Receptor interacting protein kinase-3 determines cellular necrotic response to TNF-alpha. *Cell* 137, 1100–1111. doi: 10.1016/j.cell.2009.05.021

He, S., and Wang, X. (2018). RIP kinases as modulators of inflammation and immunity. *Nat. Immunol.* 19, 912–922. doi: 10.1038/s41590-018-0188-x

Hitomi, J., Christofferson, D. E., Ng, A., Yao, J., Degterev, A., Xavier, R. J., et al. (2008). Identification of a molecular signaling network that regulates a cellular necrotic cell death pathway. *Cell* 135, 1311–1323. doi: 10.1016/j.cell.2008.10.044

Holler, N., Zaru, R., Micheau, O., Thome, M., Attinger, A., Valitutti, S., et al. (2000). Fas triggers an alternative, caspase-8-independent cell death pathway using the kinase RIP as effector molecule. *Nat. Immunol.* 1, 489–495. doi: 10.1038/82732

Hu, J., Wu, X., Yang, C., Rashid, K., Ma, C., Hu, M., et al. (2019). Anticancer effect of icaritin on prostate cancer via regulating miR-381-3p and its target gene UBE2C. *Cancer Med.* 8, 7833–7845. doi: 10.1002/cam4.2630

Kaiser, W. J., Sridharan, H., Huang, C., Mandal, P., Upton, J. W., Gough, P. J., et al. (2013). Toll-like receptor 3-mediated necrosis via TRIF, RIP3, and MLKL. *J. Biol. Chem.* 288, 31268–31279. doi: 10.1074/jbc.M113.462341

Kerr, J. F., Wyllie, A. H., and Currie, A. R. (1972). Apoptosis: a basic biological phenomenon with wide-ranging implications in tissue kinetics. *Br. J. Cancer* 26, 239–257. doi: 10.1038/bjc.1972.33

Laster, S. M., Wood, J. G., and Gooding, L. R. (1988). Tumor necrosis factor can induce both apoptic and necrotic forms of cell lysis. *J. Immunol.* 141, 2629–2634.

Li, H., Kobayashi, M., Blonska, M., You, Y., and Lin, X. (2006). Ubiquitination of RIP is required for tumor necrosis factor alpha-induced NF-kappaB activation. *J. Biol. Chem.* 281, 13636–13643. doi: 10.1074/jbc.M600620200

Li, L., Thomas, R. M., Suzuki, H., De Brabander, J. K., Wang, X., and Harran, P. G. (2004). A small molecule Smac mimic potentiates TRAIL- and TNFalpha-mediated cell death. *Science* 305, 1471–1474. doi: 10.1126/science.1098231

Li, P., Nijhawan, D., Budihardjo, I., Srinivasula, S. M., Ahmad, M., Alnemri, E. S., et al. (1997). Cytochrome c and dATP-dependent formation of Apaf-1/caspase-9 complex initiates an apoptotic protease cascade. *Cell* 91, 479–489. doi: 10.1016/s0092-8674(00)80434-1

Li, Y., Zhao, C., Yu, Z., Chen, J., She, X., Li, P., et al. (2016). Low expression of miR-381 is a favorite prognosis factor and enhances the chemosensitivity of osteosarcoma. *Oncotarget* 7, 68585–68596. doi: 10.18632/oncotarget.11861

Liu, J., van Mil, A., Vrijsen, K., Zhao, J., Gao, L., Metz, C. H., et al. (2011). MicroRNA-155 prevents necrotic cell death in human cardiomyocyte progenitor cells via targeting RIP1. *J. Cell. Mol. Med.* 15, 1474–1482. doi: 10.1111/j.1582-4934.2010.01104.x

Micheau, O., and Tschopp, J. (2003). Induction of TNF receptor I-mediated apoptosis via two sequential signaling complexes. *Cell* 114, 181–190. doi: 10.1016/s0092-8674(03)00521-x

Nailwal, H., and Chan, F. K. (2019). Necroptosis in anti-viral inflammation. *Cell Death Differ.* 26, 4–13. doi: 10.1038/s41418-018-0172-x

Negrini, M., Nicoloso, M. S., and Calin, G. A. (2009). MicroRNAs and cancer–new paradigms in molecular oncology. *Curr. Opin. Cell Biol.* 21, 470–479. doi: 10.1016/j.ceb.2009.03.002

Pantuck, A. J., Zisman, A., and Belldegrun, A. S. (2001). The changing natural history of renal cell carcinoma. *J. Urol.* 166, 1611–1623. doi: 10.1097/00005392-200111000-00003

Peter, M. E., and Krammer, P. H. (2003). The CD95(APO-1/Fas) DISC and beyond. *Cell Death Differ.* 10, 26–35. doi: 10.1038/sj.cdd.4401186

Pfeffer, C. M., and Singh, A. T. K. (2018). Apoptosis: a target for anticancer therapy. *Int. J. Mol. Sci.* 19:448. doi: 10.3390/ijms19020448

Robinson, N., McComb, S., Mulligan, R., Dudani, R., Krishnan, L., and Subash, S. (2012). Type I interferon induces necroptosis in macrophages during infection with *Salmonella enterica* serovar Typhimurium. *Nat. Immunol.* 13, 954–962. doi: 10.1038/ni.2397

Rossato, M., Curtale, G., Tamassia, N., Castellucci, M., Mori, L., Gasperini, S., et al. (2012). IL-10-induced microRNA-187 negatively regulates TNF-alpha, IL-6, and IL-12p40 production in TLR4-stimulated monocytes. *Proc. Natl. Acad. Sci. U.S.A.* 109, E3101–E3110. doi: 10.1073/pnas.1209100109

Saini, S., Yamamura, S., Majid, S., Shahryari, V., Hirata, H., Tanaka, Y., et al. (2011). MicroRNA-708 induces apoptosis and suppresses tumorigenicity in renal cancer cells. *Cancer Res.* 71, 6208–6219. doi: 10.1158/0008-5472.CAN-11-0073

Shirjang, S., Mansoori, B., Asghari, S., Duijf, P. H., Mohammadi, A., Gjerstorff, M., et al. (2020). Corrigendum to "MicroRNAs in cancer cell death pathways: apoptosis and necroptosis" [Free Radic. Biol. Med. 139 (2019) 1-15]. *Free Radic. Biol. Med.* 146:402. doi: 10.1016/j.freeradbiomed.2019.06.014

Su, Z., Yang, Z., Xu, Y., Chen, Y., and Yu, Q. (2015). MicroRNAs in apoptosis, autophagy and necroptosis. *Oncotarget* 6, 8474–8490. doi: 10.18632/oncotarget.3523

Sun, L., Wang, H., Wang, Z., He, S., Chen, S., Liao, D., et al. (2012). Mixed lineage kinase domain-like protein mediates necrosis signaling downstream of RIP3 kinase. *Cell* 148, 213–227. doi: 10.1016/j.cell.2011.11.031

Tang, H., Liu, X., Wang, Z., She, X., Zeng, X., Deng, M., et al. (2011). Interaction of hsa-miR-381 and glioma suppressor LRRC4 is involved in glioma growth. *Brain Res.* 1390, 21–32. doi: 10.1016/j.brainres.2011.03.034

Thornberry, N. A., and Lazebnik, Y. (1998). Caspases: enemies within. *Science.* 281, 1312–1316. doi: 10.1126/science.281.5381.1312

Vercammen, D., Beyaert, R., Denecker, G., Goossens, V., Van Loo, G., Declercq, W., et al. (1998). Inhibition of caspases increases the sensitivity of L929 cells to necrosis mediated by tumor necrosis factor. *J. Exp. Med.* 187, 1477–1485. doi: 10.1084/jem.187.9.1477

Wang, L., Du, F., and Wang, X. (2008). TNF-alpha induces two distinct caspase-8 activation pathways. *Cell* 133, 693–703. doi: 10.1016/j.cell.2008.03.036

Wright, A., Reiley, W. W., Chang, M., Jin, W., Lee, A. J., Zhang, M., et al. (2007). Regulation of early wave of germ cell apoptosis and spermatogenesis by deubiquitinating enzyme CYLD. *Dev. Cell* 13, 705–716. doi: 10.1016/j.devcel.2007.09.007

Wu, C. J., Conze, D. B., Li, T., Srinivasula, S. M., and Ashwell, J. D. (2006). Sensing of Lys 63-linked polyubiquitination by NEMO is a key event in

NF-kappaB activation [corrected]. *Nat. Cell Biol.* 8, 398–406. doi: 10.1038/ncb1384

Zhang, D. W., Shao, J., Lin, J., Zhang, N., Lu, B. J., Lin, S. C., et al. (2009). RIP3, an energy metabolism regulator that switches TNF-induced cell death from apoptosis to necrosis. *Science* 325, 332–336. doi: 10.1126/science.1172308

Zhang, L., Dong, L. Y., Li, Y. J., Hong, Z., and Wei, W. S. (2012). The microRNA miR-181c controls microglia-mediated neuronal apoptosis by suppressing tumor necrosis factor. *J. Neuroinflammation* 9:211. doi: 10.1186/1742-2094-9-211

Zhang, S., Zhang, D., Yi, C., Wang, Y., Wang, H., and Wang, J. (2016). MicroRNA-22 functions as a tumor suppressor by targeting SIRT1 in renal cell carcinoma. *Oncol. Rep.* 35, 559–567. doi: 10.3892/or.2015.4333

Zhang, Y., Tian, S., Li, X., Ji, Y., Wang, Z., and Liu, C. (2018). UBE2C promotes rectal carcinoma via miR-381. *Cancer Biol. Ther.* 19, 230–238. doi: 10.1080/15384047.2017.1416939

Zhao, J., Jitkaew, S., Cai, Z., Choksi, S., Li, Q., Luo, J., et al. (2012). Mixed lineage kinase domain-like is a key receptor interacting protein 3 downstream component of TNF-induced necrosis. *Proc. Natl. Acad. Sci. USA* 109, 5322–5327. doi: 10.1073/pnas.1200012109

Conflict of Interest: The authors declare that the research was conducted in the absence of any commercial or financial relationships that could be construed as a potential conflict of interest.

frontiers in Medicine

ORIGINAL RESEARCH
published: 06 May 2020
doi: 10.3389/fmed.2020.00178

Transcriptome Profiling Reveals Indoxyl Sulfate Should Be Culpable of Impaired T Cell Function in Chronic Kidney Disease

Fangfang Xiang[1,2,3], *Xuesen Cao*[1], *Bo Shen*[1], *Xiaohong Chen*[1], *Man Guo*[1], *Xiaoqiang Ding*[1,2,3,4] *and Jianzhou Zou*[1,2,3,4]*

[1] *Department of Nephrology, Zhongshan Hospital, Fudan University, Shanghai, China,* [2] *Shanghai Key Laboratory of Kidney and Blood Purification, Shanghai, China,* [3] *Shanghai Institute of Kidney and Dialysis, Shanghai, China,* [4] *Shanghai Medical Center for Kidney, Shanghai, China*

Introduction: Chronic inflammation and immune system dysfunction have been evaluated as major factors in the pathogenesis of chronic kidney disease (CKD), contributing to the high mortality rates observed in these populations. Uremic toxins seem to be the potential "missing link." Indoxyl sulfate (IS) is one of the protein-bound renal toxins. It participates in multiple pathologies of CKD complications, yet its effect on immune cell has not been studied. This study aimed to explore the genome-wide expression profile in human peripheral blood T cells under stimulation by IS.

Methods: In this study, we employed RNA-sequencing transcriptome profiling to identify differentially expressed genes (DEGs) responding to IS stimulation in human peripheral T cells *in vitro*. Flow cytometry and western blot were used to verify the discovery in RNA-sequencing analysis.

Results: Our results yielded a total of 5129 DEGs that were at least twofold up-regulated or down-regulated significantly by IS stimulation and half of them were concentration-specific. Analysis of T cell functional markers revealed a quite different transcription profile under various IS concentration. Transcription factors analysis showed the similar pattern. Aryl hydrocarbon receptor (AhR) target genes CYP1A1, CYP1B1, NQO1, and AhRR were up-regulated by IS stimulation. Pro-inflammatory genes TNF-α and IFN-γ were up-regulated as verified by flow cytometry analysis. DNA damage was induced by IS stimulation as confirmed by elevated protein level of p-ATM, p-ATR, p-BRCA1, and p-p53 in T cells.

Conclusion: The toxicity of IS to T cells could be an important source of chronic inflammation in CKD patients. As an endogenous ligand of AhR, IS may influence multiple biological functions of T cells including inflammatory response and cell cycle regulation. Further researches are required to promulgate the underling mechanism and explore effective method of reserving T cell function in CKD.

Keywords: T cell, indoxyl sulfate, aryl hydrocarbon receptor, chronic kidney disease, RNA-sequencing

OPEN ACCESS

Edited by:
Songjie Cai,
Brigham and Women's Hospital, United States

Reviewed by:
Milena Barcza Stockler-Pinto, Universidade Federal Fluminense, Brazil
Hee-Seong Jang, University of Nebraska Medical Center, United States

***Correspondence:**
Jianzhou Zou
zou.jianzhou@zs-hospital.sh.cn

Specialty section:
This article was submitted to Nephrology, a section of the journal Frontiers in Medicine

Received: *09 January 2020*
Accepted: *16 April 2020*
Published: *06 May 2020*

Citation:
Xiang F, Cao X, Shen B, Chen X, Guo M, Ding X and Zou J (2020) Transcriptome Profiling Reveals Indoxyl Sulfate Should Be Culpable of Impaired T Cell Function in Chronic Kidney Disease. Front. Med. 7:178. doi: 10.3389/fmed.2020.00178

INTRODUCTION

Chronic inflammation and immune system dysfunction have been evaluated as major factors in the pathogenesis of chronic kidney disease (CKD), contributing to the high mortality rates observed in these populations. As a main component of cellular immunity, T cells play a leading role in defense of pathogens, immune homeostasis and immune surveillance. The impact of uremia on the immune system has been previously studied in end-stage renal disease (ESRD) patients. Betjes et al. (1, 2) described a decline of T cell numbers especially naive T cells with an increased susceptibility to activation-induced apoptosis, expansion of terminally differentiated T cells with highly secretion of proinflammatory cytokines and lack of adequate antigen-specific T cell differentiation which may be the probable cause of high risk of infection in these patients. Uremic toxins have been suggested as a potential "missing link" between CKD and cardiovascular disease (CVD) since higher CVD risk in these patients cannot be sufficiently explained by classic factors. However, there are few studies on the mechanism of T cell dysfunction caused by uremic toxins.

Indoxyl sulfate (IS) is a renal toxin that accumulates in blood of uremic patients with 97.4% bound to serum albumin (3). The serum level of IS in healthy humans is almost undetectable, whereas in uremic patients, it escalates to 236 μg/ml (4). IS plays an important role in the progression of renal disease, CVD, bone metabolism disorders and other complications by promoting oxidative stress and inflammatory response (5). IS also affects T cell differentiation. It has been reported that IS aggravates experimental autoimmune encephalomyelitis by stimulating Th17 differentiation (6) and lessens allergic asthma by regulating Th2 differentiation (7). As one of the endogenous ligands of aryl hydrocarbon receptor (AhR), IS probably make effect through AhR. Emerging evidence suggests that AhR is a key sensor allowing immune cells to adapt to environmental conditions and changes in AhR activity have been associated with autoimmune disorders and cancer (8). However, it remains largely unknown if whether IS or AhR are responsible for the T cell disfunction in uremic patients.

In the past decade, next-generation sequencing technology has emerged as an effective tool to investigate the gene expression profiling of a species under specific conditions. The advantages of speed, precision and high-efficiency performance of RNA sequencing (RNA-seq) encouraged us to explore the genome-wide expression profile in human peripheral blood T cells under stimulation by IS.

METHODS

Cell Isolation and Activation

Buffy coats from healthy donors were obtained from Zhongshan Hospital, Fudan University. This study has been approved by the Medical Ethics committee of Zhongshan Hospital, Fudan University. Peripheral blood mononuclear cells were separated by density-gradient centrifugation using Ficoll-Paque Plus (GE healthcare Bio-Science, Uppsala, Sweden) and were further processed for separation of T cells using CD3 MicroBeads (MiltenyiBiotec, Auburn, USA). T cells were cultured in RPMI medium (Eurobio, Les Ulis, France) supplemented with 20 IU/mL penicillin, 20 μg/mL streptomycin, and 10% decomplemented FBS (Life Technologies), and stimulated with Dynabeads® T-Expander beads coated with anti-CD3 and anti-CD28 Abs (Life Technologies) at a 1:1 cell/bead ratio in the absence of IL-2 (30 U/ml). Then IS stimulation experiments were conducted by treating T cells with different IS concentration for 96 h.

RNA Sequencing

Total RNA was extracted from each sample using TRIzol reagent (Invitrogen, Carlsbad, CA, USA) following the manufacturer's protocol. The RNA concentration and purity were checked by OD A260/A280 (>1.8) and A260/A230 (>1.6). The quality and quantity of RNA obtained from each sample was checked using the NanoPhotometer® spectrophotometer (IMPLEN, CA, USA). RNA concentration was measured using Qubit® RNA Assay Kit in Qubit®2.0 Flurometer (Life Technologies, CA, USA). RNA integrity was assessed using the RNA Nano 6000 Assay Kit of the Bioanalyzer 2100 system (Agilent Technologies, CA, USA). A total amount of 3 μg RNA per sample was used as input material for the RNA sample preparations. Sequencing libraries were generated using NEBNext® Ultra TM RNA Library Prep Kit for Illumina® (NEB, USA) following manufacturer's recommendations and index codes were added to attribute sequences to each sample. The clustering of the index-coded samples was performed on a cBot Cluster Generation System using TruSeq PE Cluster Kit v3-cBot-HS (Illumia) according to the manufacturer's instructions. After cluster generation, the library preparations were sequenced on an Illumina Hiseq platform and 125 bp/150 bp paired-end reads were generated.

RNA-Seq Data Processing

Clean reads were obtained by removing reads containing adapter, reads containing ploy-N and low-quality reads from raw data. Reference genome and gene model annotation files were downloaded from genome website directly. Index of the reference genome was built using Hisat2 v2.0.5 and paired-end clean reads were aligned to the reference genome using Hisat2v2.0.5. The read counts of each transcript were normalized to the length of the individual transcript and to the total mapped read counts in each sample and were expressed as FPKM. Differential expression analysis of two groups was performed using the DESeq2 R package (1.16.1). *P*-values were adjusted using the Benjamini and Hochberg's approach for controlling the false discovery rate. In the analysis, a criterion of $|\log_2(\text{fold-change})| > 0$ and an adjusted $P < 0.05$ were assigned as differentially expressed. Hierarchical clustering was utilized to present the selected significant down-regulated and up-regulated genes. The cluster Profiler R package was used to perform the gene ontology (GO) enrichment analysis (http://www.geneontology.org). Kyoto Encyclopedia of Genes and Genomes (KEGG, https://www.genome.jp/kegg) and Reactome (https://reactome.org) pathway analysis were performed to understand the function and interactions among differentially expressed genes.

Flow Cytometry Analysis

After culture, purified T cells were washed twice in PBS with 1% FBS and subsequently stained for 30 min at 4°C with the following fluorescein-conjugated monoclonal antibodies: human anti-CD3-PE (Biolegend, San Diego, CA), anti-CD4-APC (Biolegend, San Diego, CA), anti-CD8-PerCP/CY5.5(Biolegend and San Diego, CA). Stained cells were resuspended for 30 min at 4°C in Cytofix/Cytoperm fixation/permeabilization solution (Thermo Fisher Scientific, Waltham, MA, USA), according to the manufacturer's instructions. Once permeabilized, cells were washed twice and stained for intracellular cytokines with the following mAbs: human anti-IFNγ-FITC (Biolegend, San Diego, CA), anti–TNF-α-650^{TM} (Biolegend, San Diego, CA). A total of 200,000 events were acquired by the BD LSRFortessa^{TM} flow cytometer (BD Bioscience, San Jose, CA, USA). FlowJo v10.1 software (Tree Star, Ashland, OR, USA) was used for date analysis.

Western Blot Analysis

The cells were washed twice with cold PBS and then lysed in RIPA buffer supplemented with complete EDTA-free Protease Inhibitor Cocktail (Roche Applied Science, Mannheim, Germany) and PhosStop Phosphatase Inhibitor Cocktail (Roche Applied Science) on ice for 30 min. The cell lysates were sonicated five times for 10 s each and centrifuged at 11,000 g for 30 min at 4°C. The supernatants were subsequently collected. Protein concentrations were measured using a BCA protein assay kit (Pierce, Inc., Rockford, IL).

Protein samples of 50 μg were separated by sodium dodecyl sulfate polyacrylamide gel electrophoresis and transferred to a PVDF membrane (Millipore, Inc.). Immunoblotting was conducted using rabbit anti-phospho-ATR (Ser 428) antibody, rabbit anti-phospho-BRCA1 (Ser 1524) antibody, rabbit anti-phospho-ATM (Ser1981) antibody, mouse anti-phospho-p53 (Ser15) antibody, rabbit anti-AhR antibody, anti-rabbit IgG antibody, anti-mouse IgG antibody. All antibodies were purchased from Cell Signaling Technology, Inc. (1:1,000). The ECL-enhanced chemiluminescence system (Amersham) was used for detection. Images were quantified by Image J1.34 Software. The intensity of band was normalized to the GAPDH.

Statistical Analysis

Data were reported as mean ± SD. Statistical analysis was performed using the GraphPad Prism5 software. The one-way ANOVA was used for multiple group comparisons. The paired Student's *t*- test was used for a single comparison between two groups, and the non-parametric *t*-test was also chosen if the sample size was too small and not fit Gaussian distribution.

RESULTS

Purity of T Cells and RNA-Seq Profiling Analysis

The purity of T cells was >97%, as confirmed by flow cytometry (**Figure 1A**). In this study, after filtered adapter and low-quality reads, about 44.25–62.64 million clean reads were obtained for all samples (**Table S1**). Hierarchical clustering based on Pearson correlation coefficients showed high correlation (0.969–1.00) among samples in each group and IS stimulation groups were distinctly separated from control group (**Figure 1B**).

There were 5129 DEGs that were at least twofold up-regulated or down-regulated significantly by IS stimulation and half of them were concentration-specific. Compared with the control group, there were 2535 DEGs in the group treated by 200 μM IS, of which 1101 DEGs were up-regulated and 1434 DEGs were down-regulated. Group treated by 500 μM IS had 2382 DEGs, of which 1131 DEGs were up-regulated and 1251 DEGs were down-regulated. Group treated by 1,000 μM IS had 4090 DEGs, of which 2178 DEGs were up-regulated and 1912 DEGs were down-regulated (**Figure 1C**). 1332 were common DEGs in all groups treated by various concentrations of IS compared with the control groups (**Figure 1D**). Of all common 1332 DEGs, 29 DEGs were up-regulated and 15 DEGs were down-regulated in a concentration dependent manner. **21** DEGs were up-regulated or down-regulated at 200μM but reversely regulated when IS concentration was higher. These DEGs were listed in **Figure 2**.

Functional Categories and Enriched Pathways by RNA-Seq Analysis

We firstly focused on the T cell functional markers including cluster of differentiation, cytokine and cytokine receptor. Two hundred and seventy two genes were screened (**Table S2**) and 87 differently expressed genes were found under filtering conditions (corrected $P < 0.0001$ and FPKM>1), which were listed in **Table 1**. These genes were involved in T cell activation, adhesion and signal transduction. 19 genes including LTA, LTB, CXCL8, and CCR7 were up-regulated at IS concentration of 200 μM. Twenty genes including TNF-α, IFN-γ and CD40L were up-regulated when IS concentration were higher. 41 genes including IL2, CD28, PD1, and CTLA4 were down-regulated at IS concentration of 200 μM; some of them returned to normal or even up-regulated when IS concentration were higher. The effects of IS stimulation on AhR activation were shown in **Figure 2E**. mRNA levels of AhR target genes, CYP1A1, CYP1B1, NQO1, and AhRR were increased by IS stimulation, indicating a transcriptionally active form of AhR.

Next, we focused on transcription factor (TF) responsive to IS stimulation. TF analysis of differentially expressed genes were extracted directly from the AnimalTFDB database. 114 TFs differentially expressed when compared to the control group under filtering conditions (corrected $P < 0.0001$). The three mostly altered TF families were zf-C2H2, bHLH, and TF-bZIP separately (**Figure 3**). Most TFs were differentially expressed at IS concentration of 200 μM, of which 24 TFs were up-regulated and 64 TFs were down-regulated. With a similar pattern of T cell functional markers, many of these TFs were diversely regulated when IS concentration was higher. Eighteen more TFs were differentially expressed when IS concertation raised to 500 μM and 9 TFs were only differentially expressed at IS concentration of 1,000 μM. Myc, BHLHE40, SOX4, CREM, and HIC1 were

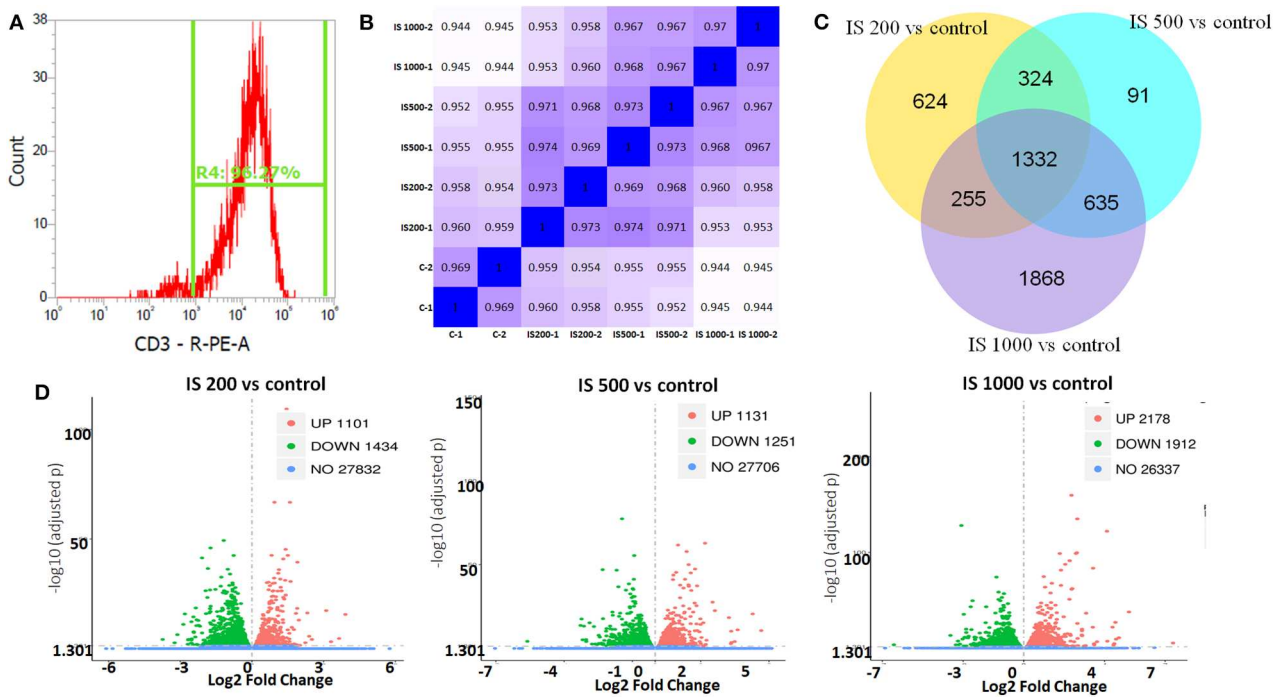

FIGURE 1 | T cell purity and global patterns of RNA-seq profiling. **(A)** The purity of T cells confirmed by flow cytometry; **(B)** Hierarchical clustering based on Pearson correlation coefficients among samples in IS groups; **(C)** Volcano plot showed the numbers of up and down regulated DEGs in each IS groups compared to the control group; **(D)** Veen figure showed the common and different DEGs in each IS groups.

up-regulated in a concentration dependent manner. Several major regulators of T cell differentiation were also affected by IS stimulation. STAT1, STAT4, NF κ B1 (P50/P105), GATA3, Foxp3, Smad3, and IRF2 were significantly up-regulated. STAT3, STAT5B, STAT6, T-bet, MAF, Runx2, Runx1, BCL6, and NFATC1 were significantly down-regulated at IS concentration of 200 μM. Except for STAT5B and STAT6, these TFs were relatively up-regulated at 500 μM or 1,000 μM. STAT2 was significantly down-regulated when IS concentration was higher than 500 μM (**Figure 4**).

GO term enrichment analysis of the 2040 DEGs in IS 500 μM group revealed 182 significantly enriched GO terms under filtering conditions (corrected $P < 0.001$). The top 10 GO terms of the three aspects [Biological Process (BP), Molecular Function (MF) and Cellular Component (CC)] were shown in **Figure 5A**. The enriched GO terms on BP and MF were mainly related to immune function (e.g., "T cell activation," "antigen receptor-mediated signaling pathway," "leukocyte cell-cell adhesion," "leukocyte differentiation"), gene expression (e.g., "regulation of transcription from RNA polymerase II promoter in response to stress"). The top GO terms on CC were proteasome complex and focal adhesion. Reactome pathway analysis revealed lots of enriched terms concerning cell cycle especially DNA damage in the top 20 (e.g., "Autodegradation of the E3 ubiquitin ligase COP1," "p53-Independent DNA Damage Response"). The top 20 Reactome pathway terms were shown in **Figure 5B**.

Effects of IS on Inflammation and DNA Damage in Human Peripheral T Cells

To validate RNA-seq results, flow cytometry was performed on two most common pro-inflammatory factors TNF-α and IFN-γ. After 4 days of stimulation, secretion of TNF–α and IFN-γ were significantly elevated in T cells (**Figure 6**).

To verify the pathway enrichment results that IS induced DNA damage in T cells, proteins related to DNA damage response (DDR) were tested by western blot. Protein level of p-ATM, p-ATR, p-p53, and p-BRCA1 were significantly higher in IS intervention group and so was AhR (**Figure 7**).

DISCUSSION

The RNA-seq provided a rapid and cost-effective way to obtain all transcribed mRNA expression profiles within a specific period. Here we studied the transcriptome of human peripheral T cells to understand gene expression profiles under IS stimuli. Interestingly, we found quite different transcription profile under various concentration of IS stimulation indicating IS may have different effects on T cell function at distinct stages of CKD. As reported earlier, serum level of IS averages 35.5 mg/ml and escalate to maximum value of 236 mg/ml in dialysis patients

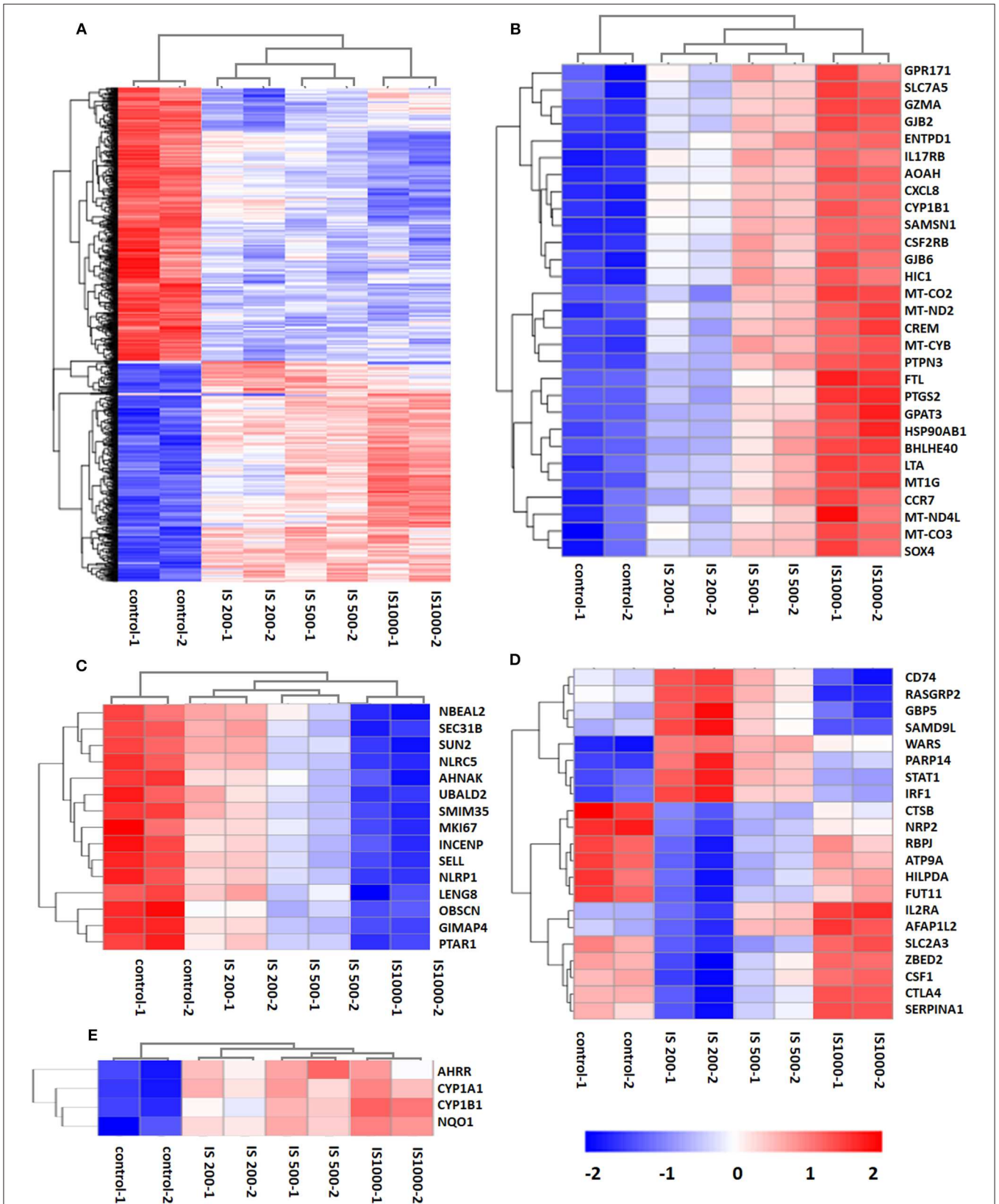

FIGURE 2 | Hierarchical cluster analysis of patterns of DEGs. **(A)** 1,332 common DEGs in all IS groups compared with the control groups; **(B)** 29 DEGs up-regulated by IS simulation in a concentration dependent manner; **(C)** 15 DEGs down-regulated by IS stimulation in a concentration dependent manner; **(D)** 20 DEGs up-regulated or down-regulated at 200 μM but reversely regulated when IS concentration was higher; **(E)** AhR target genes CYP1A1, CYP1B1, NQO1, and AhRR were up-regulated by IS stimulation.

TABLE 1 | Differentially expressed genes of T cell functional markers on IS stimulation.

	Gene name
Up-regulated at 200 μM	LTA, LTB, CXCL8, IL17RB, IL7R, IL9R, CSF2RB, TNFSF8, SIRPG, CCR7, CCR8, CD38, ENTPD1, CD48, ITGA4, CD74, CD96, SLC7A5, TNFSF10
Down-regulated at 200 μM	CD28, CTLA4, PDCD1, IL2, IL2RB, IL4R, DPP4, LAG3, IL1RN, IL4I1, IL21, SEMA7A, ITGAX, TNFRSF1B, TNFRSF4, ADAM8, SELPLG, DDR1, ITGB2, CD200, IL10RA, CD22, IGF1R, CD24, CD276, TNFRSF8, CD3E, CD4, CD47, ITGA3, ITGA5, CD5, CD6, SELL, CD7, CD82, THY1, ADGRE5, CD99, TNFRSF13C, SLAMF1
Up-regulated at 500 μM	IL2RA, TNF, CD40LG, IL23R, IL13, IL18R1, HMMR, CD2, TFRC, CD84, LTA, LTB, CXCL8, IL17RB, IL7R, IL9R, CSF2RB, TNFSF8, SIRPG, CCR7, CCR8, CD38, ENTPD1, CD48, ITGA4, CD74, CD96, SLC7A5, TNFSF10
Down-regulated at 500 μM	IL31RA, CD37, CD28, CTLA4, PDCD1, IL2, IL4R, DPP4, LAG3, IL1RN, IL4I1, IL21, ITGAX, TNFRSF4, ADAM8, SELPLG, DDR1, ITGB2, CD200, IL10RA, CD22, IGF1R, CD24, CD276, CD3E, CD4, CD47, ITGA3, ITGA5, CD5, CD6, SELL, CD7, CD82, THY1, ADGRE5, CD99, TNFRSF13C
Up-regulated at 1,000 μM	IFNG, FASLG, IL26, TNFRSF9, PTPRJ, CXCR6, CD226, CD69, CD9, LTA, LTB, CXCL8, IL17RB, IL9R, CSF2RB, TNFSF8, SIRPG, CCR7, CCR8, CD38, ENTPD1, CD48, ITGA4, CD96, SLC7A5, TNFSF10, IL2RA, TNF, CD40LG, IL23R, IL13, IL18R1, HMMR, CD2, TFRC, CD84, CTLA4, IL2RB, SEMA7A
Down-regulated at 1,000 μM	IL11RA, MUC1, CD8B2, IL3RA, FGFR1, CD74, IL31RA, CD37, CD28, IL2, IL4R, DPP4, LAG3, IL1RN, IL4I1, IL21, ITGAX, TNFRSF4, ADAM8, SELPLG, ITGB2, CD200, IL10RA, CD22, IGF1R, CD24, CD3E, CD4, CD47, ITGA3, ITGA5, SELL, CD7, THY1, ADGRE5, CD99, TNFRSF13C, TNFRSF1B

(4, 9). In the current study, the intervention concentration of IS covered the medium and high serum IS level in uremic patients.

By screening transcription of T cell functional markers including cluster of differentiation, cytokine and cytokine receptor, we found lots of pro-inflammatory genes were up-regulated such as TNF-α, IFN-γ, CD40L, and CXCL8. Flow cytometry further proved that IS elevated the secretion of TNF -α and IFN-γ in T cells. In addition, IS down regulated CD28 expression, which could be vital since $CD4^+CD28^-$ T cell has been well-proved to be closely related to chronic inflammation and clinical CVD events in CKD patients (10). CD7 and CD26, the two factors reported been down-regulated in chronic inflammatory diseases (11, 12), were also down-regulated by IS intervention. Many molecules known as immune checkpoint inhibitor, which activating in evolving immune activation cascade and contributing inhibitory signals to dampen an overexuberant response, were down-regulated, including PD1, CTLA4, LAG3, and CD200 (13–15). Down-regulation of these genes could aggravate inflammation. These results highly suggested that the toxicity of IS to T cells could be an important source of chronic inflammation in CKD or uremic patients. Many factors would contribute to chronic inflammatory status in CKD, including increased production of proinflammatory cytokines, oxidative stress, acidosis, altered metabolism of adipose tissue and even some treatment *per se* such as hemodialysis (16). Immune cells activated by uremic milieu produce more proinflammatory cytokines and aggravate the inflammation condition as a vicious circle. The most well-documented studies were that patients with ESRD typically had an expansion of proinflammatory $CD4^+CD28^-$ T cell and $CD14^+CD16^{++}$ monocyte populations, which were considered to be novel, non-traditional cardiovascular risk factors (2). Besides cytokines, retention of uremic toxins should be the key mechanism that underlie the generation of oxidative stress and inflammation. As matter of fact, the crosstalk between gut microbiota and CKD has become a new focus for studying the mechanism of inflammation in these patients. IS and p-cresyl sulfate, generated by protein fermentation in intestine, are potential candidates since they were not only associated with CKD progression but also related to poor prognosis in ESRD patients (17, 18). Our study shed a light into the mechanism of immune disturbance in CKD patients.

As an endogenous ligand of AhR, IS is functioning through AhR along with many other uremic toxins, such as indole-3-acetic acid and indoxyl-β-D glucuronide (19, 20). AhR is a ligand-activated transcription factor and is involved in the regulation of multiple cellular pathways such as inflammatory responses, cell cycle regulation and hormone signaling (21). Physiological functions of AhR may require tightly controlled and transient signaling, and sustained AhR signaling may underlie pathological responses (22). Accumulation of IS in CKD patients could cause prolonged AhR activation; it further leading to a pathological change. Recently, a clinical study confirmed that CKD patients displayed a strong AhR-activating potential, which is not only strongly correlated with serum IS level but also correlated with CVD risk (23). In the current study, the expression of AhR protein and known AhR-regulated genes such as CYP1A1, CYP1B1, NQO1, and AhRR were up-regulated, indicating a transcriptionally active form of AhR, which was consistent with the previous study (7). When analyzing transcription factors, we found some critical TFs such as STAT1, STAT3, IRF4 were differentially expressed at IS concentration of 200 μM, but were diversely regulated when IS concentration was higher. In addition, the plasma IS concentration of CKD patients is far beyond the scope of this experimental design, and it remains a question how TFs react at lower IS concentration. It seems that the effect of IS on T cells are quite different depending on various IS concentration. At present, we cannot fully understand the mechanism of TFs rebound. We speculate this may be related to the characteristics of AhR function, since lots of previous studies have shown that activated AhR could function oppositely by different kinds of ligand or even one ligand in different concentrations (24, 25). It is worth noting that in GO and Reactome analysis, we found a lot of enriched items were concerning cell cycle especially DNA damage. Western blot also

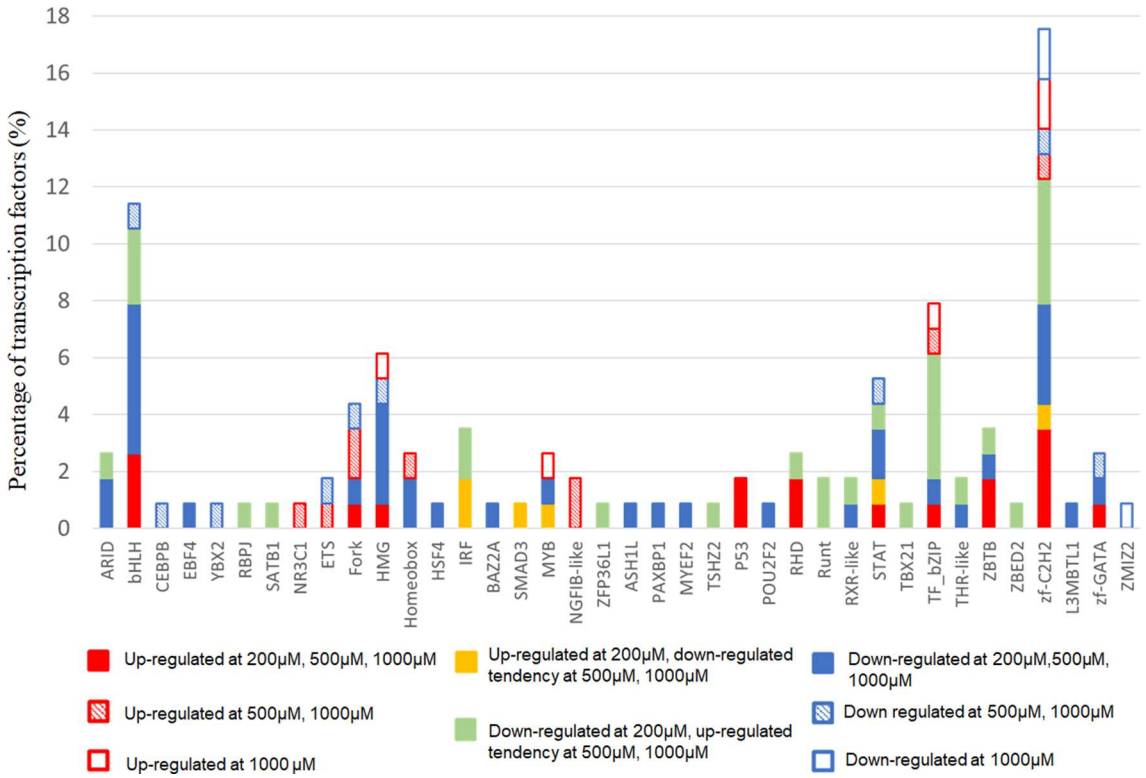

FIGURE 3 | The distribution of TF families. The x-axis represents different TF families (gene names were presented directly if there was only one TF in this TF family), the y-axis represents the percentage of corresponding TF family in total differentially expressed TFs.

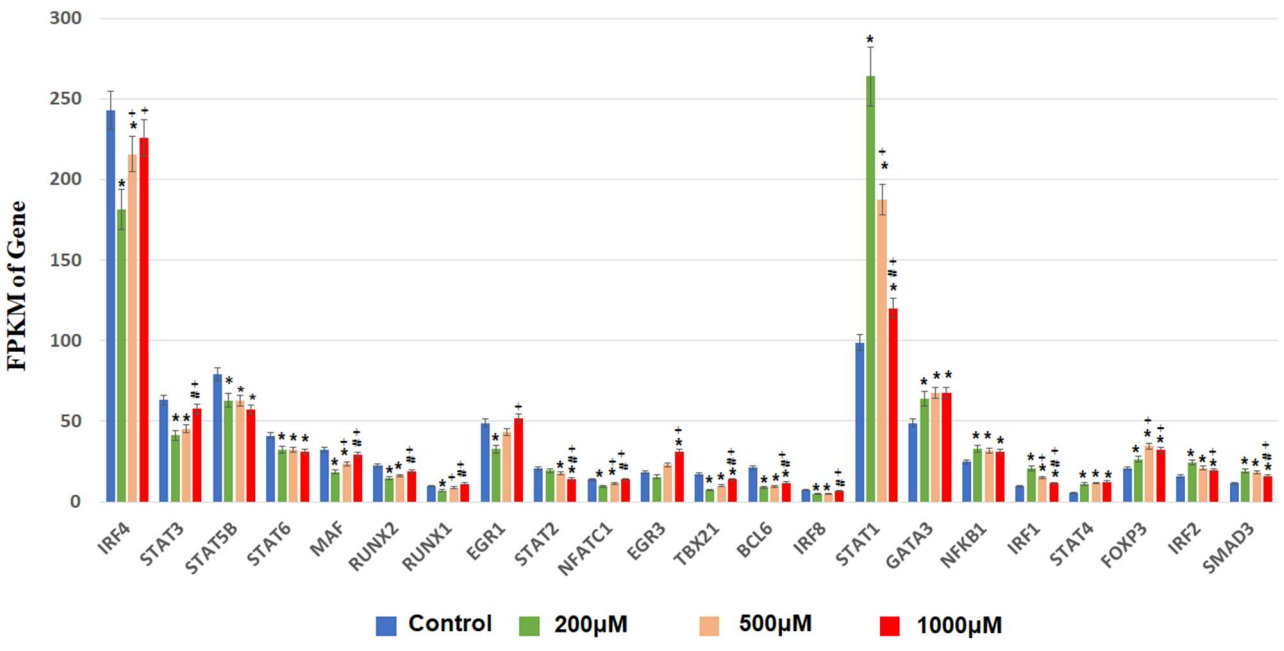

FIGURE 4 | FPKM of TFs involved in T cell differentiation in each IS group. The x-axis represents FPKM, the y-axis represents gene name and IS concentration. *corrected $P < 0.05$ compared with control group; $^{+}$corrected $P < 0.05$ compared with IS 200 μM group; $^{\#}$corrected $P < 0.05$ compared with IS 1,000 μM group.

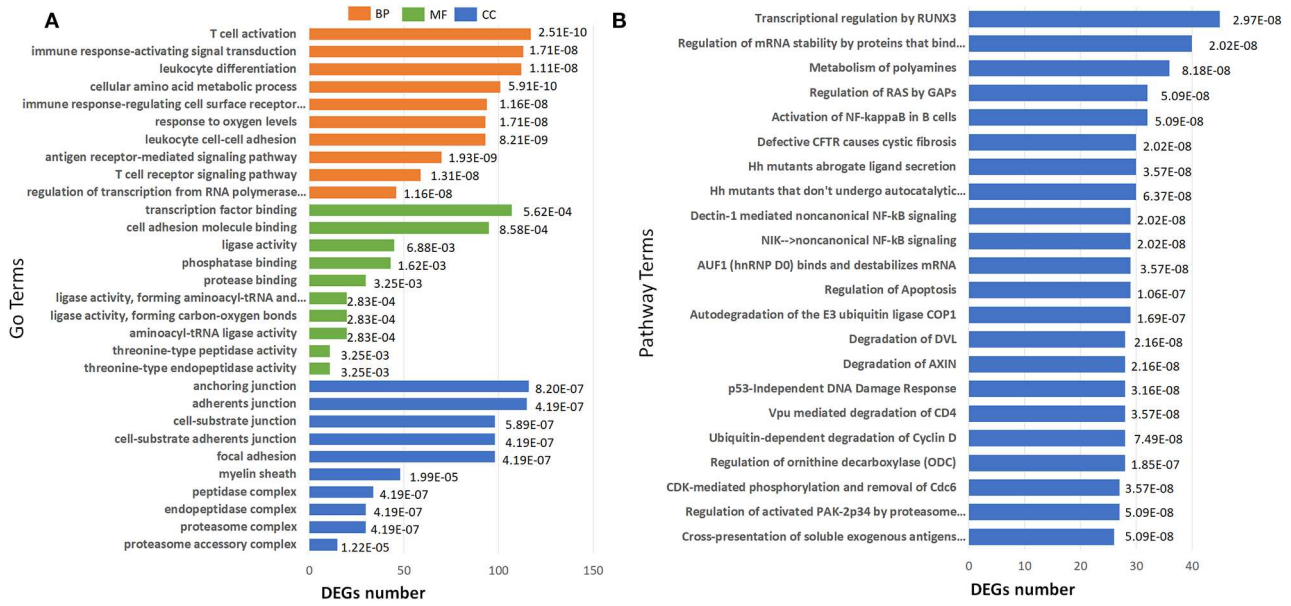

FIGURE 5 | Barplots of significantly enriched terms. **(A)** GO enrichment and **(B)** Reactome enrichment terms under corrected $P < 0.001$. The x-axis represents differentially expressed genes number, the y-axis represents GO or Reactome pathway terms; the numbers in the plot are the corrected *P*-values.

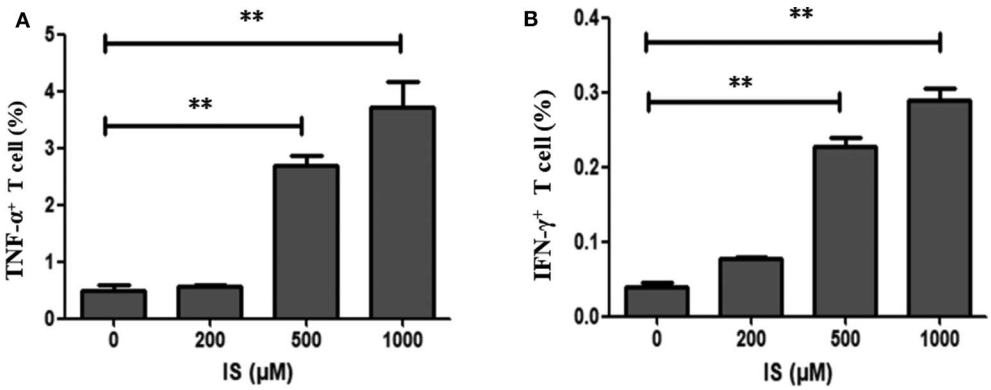

FIGURE 6 | Secretion of TNF–α and IFN-γ in T cells by IS intervention. **(A)** Secretion of TNF–α was significantly elevated in T cells in IS 500 μM group and IS 1,000 μM group; **(B)** Secretion of IFN-γ was significantly elevated in T cell in IS 500μM group and IS 1,000 μM group. $^{**}P < 0.001$ compared with the control group.

confirmed that the expression of DDR proteins including p-ATM, p-ATR, p-p53, and p-BRCA1 were up-regulated under IS stimulation. Therefore, we suggest that IS may cause DNA damage, which could further lead to T cell senescence. Notably, T cell senescence has been considered a major contributor of inflammation and crucial mechanism of complications in CKD (11, 26, 27), thus it should be paid enough attention that IS may lead to DNA damage. We can't get answer here whether IS directly leads to DNA damage through AhR, or indirectly through inflammation or oxidative stress. But the first case is reasonable since it has been well-proved that activation of AhR could directly cause DNA damage in other settings (28, 29).

Our study had several limitations. First, this study was based on IS effect on T cells from healthy donors. Since inflammatory response in T cells of CKD patients could be different compared to the response in healthy T cells treated with IS, further research focused on patients' T cells should be conducted to providing better understanding of effect of IS on T cell function in CKD. Secondly, this research only presented an image of influence by IS to T cells, studies with the aim of understanding molecular mechanism are needed.

In conclusion, our study shows that the toxicity of IS to T cells could be an important source of chronic inflammation in CKD patients. As an endogenous ligand of AhR, IS may participate in multiple cellular pathways such as inflammatory response and cell cycle regulation, which are closely related to impaired T cell function in CKD patients. We hope that this study will encourage other laboratories around the world to get

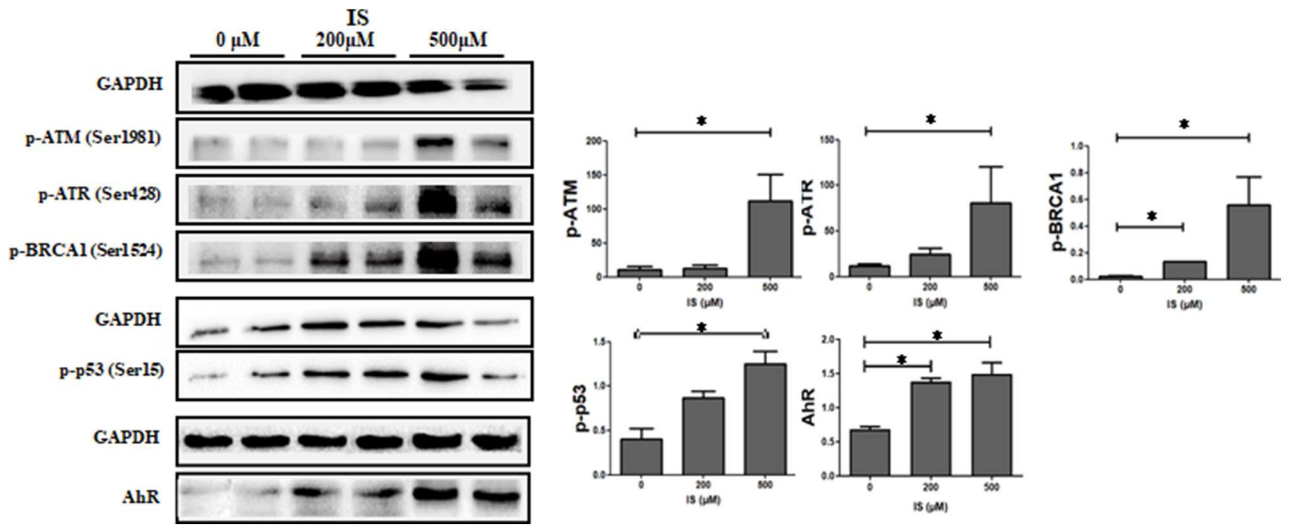

FIGURE 7 | Expression of DDR protein in T cells by IS intervention. Protein level of p-ATM, p-ATR, p-p53 and p-BRCA1 were significantly higher in IS 500 μM group compared with the control group. Protein level of p-BRCA1 were also increased in IS 200 μM group. AhR were also up-regulated in IS 200 μM and IS 500 μM group. *$P < 0.05$ compared with the control group.

more in-depth knowledge of the molecular mechanism of uremia associated immune dysfunction and make efforts to improve the clinical prognosis of CKD patients.

DATA AVAILABILITY STATEMENT

The datasets generated for this study can be found in the SRA, PRJNA599948.

ETHICS STATEMENT

The studies involving human participants were reviewed and approved by Ethical Committee, Zhongshan Hospital, Fudan University. The patients/participants provided their written informed consent to participate in this study.

AUTHOR CONTRIBUTIONS

FX conducted the experiment and drafted the paper. JZ and XCa designed the experiments. MG and XCh provided technical support. XD and BS revised the manuscript. All authors read and approved the final manuscript.

FUNDING

This work was supported by the Shanghai Clinical Medical Center for Kidney Disease Project support by Shanghai Municipal Health Commission (No. 2017ZZ01015) and Shanghai Municipal Hospital Frontier Technology Project supported by Shanghai Shen Kang Hospital Development Center (No. SHDC12018127).

SUPPLEMENTARY MATERIAL

The Supplementary Material for this article can be found online at: https://www.frontiersin.org/articles/10.3389/fmed.2020.00178/full#supplementary-material

Table S1 | Clean reads for all samples.

Table S2 | T cell markers screened for DEGs.

REFERENCES

1. Betjes MGH, Langerak AW, van der Spek A, de Wit EA, Litjens NHR. Premature aging of circulating T cells in patients with end-stage renal disease. *Kidney Int*. (2011) 80:208–17. doi: 10.1038/ki.2011.110
2. Betjes MGH. Immune cell dysfunction and inflammation in end-stage renal disease. *Nat Rev Nephrol*. (2013) 9:255–65. doi: 10.1038/nrneph.2013.44
3. Niwa T, Takeda N, Tatematsu A, and Maeda K (1988). Accumulation of indoxyl sulfate, an inhibitor of drug-binding, in uremic serum as demonstrated by internal-surface reversed-phase liquid chromatography. *Clinical Chemistry*. 34, 2264–2267. doi: 10.1093/clinchem/34.11.2264
4. Vanholder R, Schepers E, Pletinck A, Nagler EV, Glorieux G. The uremic toxicity of indoxyl sulfate and p-cresyl sulfate: a systematic review. *JASN*. (2014) 25:1897–907. doi: 10.1681/ASN.2013101062
5. Tan X, Cao X, Zou J, Shen B, Zhang X, Liu Z, et al. Indoxyl sulfate, a valuable biomarker in chronic kidney disease and dialysis. *Hemodial Int*. (2017) 21:161–7. doi: 10.1111/hdi.12483
6. Hwang Y, Hwang S, Yun M, Kim J, Oh G, Park J. Indoxyl 3-sulfate stimulates Th17 differentiation enhancing phosphorylation of c-Src and STAT3 to worsen experimental autoimmune encephalomyelitis. *Toxicol Lett*. (2013) 220:109–17. doi: 10.1016/j.toxlet.2013.04.016
7. Hwang Y, Yun M, Jeong K, Park J. Uremic toxin indoxyl 3-sulfate regulates the differentiation of Th2 but not of Th1 cells to lessen

allergic asthma. *Toxicol Lett*. (2014) 225:130–8. doi: 10.1016/j.toxlet.2013.11.027
8. Shinde R, McGaha TL. The aryl hydrocarbon receptor: connecting immunity to the microenvironment. *Trends Immunol*. (2018) 39:1005–20. doi: 10.1016/j.it.2018.10.010
9. Cao X, Chen J, Zou J, Zhong Y, Teng J, Ji J, et al. Association of indoxyl sulfate with heart failure among patients on hemodialysis. *CJASN*. (2015) 10:111–9. doi: 10.2215/CJN.04730514
10. Betjes MGH, Meijers RWJ, de Wit LEA, Litjens NHR. A killer on the road: circulating CD4(+)CD28null T cells as cardiovascular risk factor in ESRD patients. *J Nephrol*. (2012) 25:183. doi: 10.5301/jn.5000057
11. Klemann C, Wagner L, Stephan M, von Horsten S. Cut to the chase: a review of CD26/dipeptidyl peptidase-4's. (DPP4) entanglement in the immune system. *Clin Exp Immunol*. (2016) 185:1–21. doi: 10.1111/cei.12781
12. Haftcheshmeh SM, Tajbakhsh A, Kazemi M, Esmaeili SA, Mardani F, Fazeli M, et al. The clinical importance of CD4(+) CD7(-) in human diseases. *J Cell Physiol*. (2019) 234:1179–89. doi: 10.1002/jcp.27099
13. Walker LSK, Sansom DM. The emerging role of CTLA4 as a cell-extrinsic regulator of T cell responses. *Nat Rev Immunol*. (2011) 11:852–63. doi: 10.1038/nri3108
14. Andrews LP, Marciscano AE, Drake CG, Vignali DA. LAG3. (CD223) as a cancer immunotherapy target. *Immunol Rev*. (2017) 276:80–96. doi: 10.1111/imr.12519
15. Gorczynski RM, Zhu F. Checkpoint blockade in solid tumors and B-cell malignancies, with special consideration of the role of CD200. *Cancer Manag Res*. (2017) 9:601–9. doi: 10.2147/CMAR.S147326
16. Mihai S, Codrici E, Popescu ID, Enciu A, Albulescu L, Necula LG, et al. Inflammation-related mechanisms in chronic kidney disease prediction, progression, and outcome. *J Immunol Res*. (2018) 2018:2180316–73. doi: 10.1155/2018/2180373
17. Meijers BKI, Evenepoel P. The gut-kidney axis: indoxyl sulfate, p-cresyl sulfate and CKD progression. *Nephrol Dialysis Transpl*. (2011) 26:759–61. doi: 10.1093/ndt/gfq818
18. Al KS, Shatat IF. Gut microbiome and kidney disease: a bidirectional relationship. *Pediatr Nephrol*. (2017) 32:921–31. doi: 10.1007/s00467-016-3392-7
19. Heath-Pagliuso S, Rogers WJ, Tullis K, Seidel SD, Cenijn PH, Brouwer A, et al. Activation of the Ah receptor by tryptophan and tryptophan metabolites. *Biochemistry*. (1998) 37:11508–15. doi: 10.1021/bi980087p
20. Schroeder JC, DiNatale BC, Murray IA, Flaveny CA, Liu Q, Laurenzana EM, et al. The uremic toxin 3-indoxyl sulfate is a potent endogenous agonist for the human aryl hydrocarbon receptor. *Biochemistry*. (2010) 49:393–400. doi: 10.1021/bi901786x
21. Stockinger B, Meglio PD, Gialitakis M, Duarte JH. The aryl hydrocarbon receptor: multitasking in the immune system. *Annu Rev Immunol*. (2014) 32:403–32. doi: 10.1146/annurev-immunol-032713-120245
22. Mitchell KA, Elferink CJ. Timing is everything: consequences of transient and sustained AhR activity. *Biochem Pharmacol*. (2009) 77:947–56. doi: 10.1016/j.bcp.2008.10.028
23. Dou L, Poitevin S, Sallée M, Addi T, Gondouin B, McKay N, et al. Aryl hydrocarbon receptor is activated in patients and mice with chronic kidney disease. *Kidney Int*. (2018) 93:986–99. doi: 10.1016/j.kint.2017.11.010
24. Quintana FJ, Basso AS, Iglesias AH, Korn T, Farez MF, Bettelli E, et al. Control of T(reg) and T(H)17 cell differentiation by the aryl hydrocarbon receptor. *Nature*. (2008) 453:65–71. doi: 10.1038/nature06880
25. Ehrlich AK, Pennington JM, Bisson WH, Kolluri SK, Kerkvliet NI. TCDD, FICZ, and other high affinity AhR ligands dose-dependently determine the fate of CD4+ T cell differentiation. *Toxicol Sci*. (2018) 161:310–20. doi: 10.1093/toxsci/kfx215
26. Jimenez R, Carracedo J, Santamara R, Soriano S, Madueo JJ, Ramyrez CR, et al. Replicative senescence in patients with chronic kidney failure. *Kidney Int*. (2005) 68:S11–5. doi: 10.1111/j.1523-1755.2005.09903.x
27. Crépin T, Legendre M, Carron C, Vachey C, Courivaud C, Rebibou J, et al. Uraemia-induced immune senescence and clinical outcomes in chronic kidney disease patients. *Nephrol Dialysis Transpl*. (2018) 35:624–32. doi: 10.1093/ndt/gfy276
28. Das DN, Panda PK, Sinha N, Mukhopadhyay S, Naik PP, Bhutia SK. DNA damage by 2,3,7,8-tetrachlorodibenzo-p-dioxin-induced p53-mediated apoptosis through activation of cytochrome P450/aryl hydrocarbon receptor. *Environ Toxicol Pharmacol*. (2017) 55:175–85. doi: 10.1016/j.etap.2017.08.012
29. Liu Y, Zhang H, Zhang H, Niu Y, Fu Y, Nie J, et al. Mediation effect of AhR expression between polycyclic aromatic hydrocarbons exposure and oxidative DNA damage among Chinese occupational workers. *Environ Pollut*. (2018) 243:972–7. doi: 10.1016/j.envpol.2018.09.014

Conflict of Interest: The authors declare that the research was conducted in the absence of any commercial or financial relationships that could be construed as a potential conflict of interest.

frontiers in Medicine

ORIGINAL RESEARCH
published: 08 May 2020
doi: 10.3389/fmed.2020.00153

Serum N-terminal Pro-B-type Natriuretic Peptide Predicts Mortality in Cardiac Surgery Patients Receiving Renal Replacement Therapy

Ying Su[1†], Jun-yi Hou[1†], Yi-jie Zhang[1†], Guo-guang Ma[1], Guang-wei Hao[1], Jing-chao Luo[1], Zhe Luo[1,2] and Guo-wei Tu[1*]*

[1] Department of Critical Care Medicine, Zhongshan Hospital, Fudan University, Shanghai, China, [2] Department of Critical Care Medicine, Xiamen Branch, Zhongshan Hospital, Fudan University, Xiamen, China

OPEN ACCESS

Edited by:
Songjie Cai,
Brigham and Women's Hospital,
United States

Reviewed by:
Maria-Eleni Roumelioti,
University of New Mexico,
United States
Hu Linkun,
Soochow University, China
Karmin O.,
University of Manitoba, Canada

***Correspondence:**
Zhe Luo
luo.zhe@zs-hospital.sh.cn
Guo-wei Tu
tu.guowei@zs-hospital.sh.cn

[†]These authors have contributed equally to this work

Specialty section:
This article was submitted to Nephrology, a section of the journal Frontiers in Medicine

Received: *22 January 2020*
Accepted: *07 April 2020*
Published: *08 May 2020*

Citation:
Su Y, Hou J, Zhang Y, Ma G, Hao G, Luo J, Luo Z and Tu G (2020) Serum N-terminal Pro-B-type Natriuretic Peptide Predicts Mortality in Cardiac Surgery Patients Receiving Renal Replacement Therapy. Front. Med. 7:153. doi: 10.3389/fmed.2020.00153

Background: N-terminal pro-B-type natriuretic peptide (NT-proBNP) is a useful cardiac biomarker that is associated with acute kidney injury (AKI) and mortality after cardiac surgery. However, its prognostic value in cardiac surgical patients receiving renal replacement therapy (RRT) remains unclear.

Objectives: Our study aimed to assess the prognostic value of NT-proBNP in patients with established AKI receiving RRT after cardiac surgery.

Methods: A total of 163 cardiac surgical patients with AKI requiring RRT were enrolled in this study. Baseline characteristics, hemodynamic variables at RRT initiation, and NT-proBNP level before surgery, at RRT initiation, and on the first day after RRT were collected. The primary outcome was 28-day mortality after RRT initiation.

Results: Serum NT-proBNP levels in non-survivors was markedly higher than survivors before surgery (median: 4,096 [IQR, 962.0–9583.8] vs. 1,339 [IQR, 446–5,173] pg/mL; $P < 0.01$), at RRT initiation (median: 10,366 [IQR, 5,668–20,646] vs. 3,779 [IQR, 1,799–11,256] pg/mL; $P < 0.001$), and on the first day after RRT (median: 9,055.0 [IQR, 4,392–24,348] vs. 5,255 [IQR, 2,134–9,175] pg/mL; $P < 0.001$). The area under the receiver operating characteristic curve of NT-proBNP before surgery, at RRT initiation, and on the first day after RRT for predicting 28-day mortality was 0.64 (95% CI, 0.55–0.73), 0.71 (95% CI, 0.63–0.79), and 0.68 (95% CI, 0.60–0.76), respectively. Consistently, Cox regression revealed that NT-proBNP levels before surgery (HR: 1.27, 95% CI, 1.06–1.52), at RRT initiation (HR: 1.11, 95% CI, 1.06–1.17), and on the first day after RRT (HR: 1.17, 95% CI, 1.11–1.23) were independently associated with 28-day mortality.

Conclusions: Serum NT-proBNP was an independent predictor of 28-day mortality in cardiac surgical patients with AKI requiring RRT. The prognostic role of NT-proBNP needs to be confirmed in the future.

Keywords: acute kidney injury, renal replacement therapy, biomarker, N-terminal pro-B-type natriuretic peptide, mortality

INTRODUCTION

Acute kidney injury (AKI) is a frequent but serious complication for patients undergoing cardiac surgery, with an increased risk of hospital mortality and prolonged length of hospital stay (1). Patients who develop severe AKI requiring renal replacement therapy (RRT) represent nearly 2–6% of patients after cardiac surgery, and RRT dependency results in high mortality (2–6). However, few biomarkers and effective scoring systems have been validated as prognostic factors in this high risk population (7, 8).

Serum N-terminal pro-B-type natriuretic peptide (NT-proBNP), as an inactive polypeptide of the pre-prohormone brain natriuretic peptide (BNP), is synthesized and released by cardiomyocytes in response to pressure and volume overload (9–11). Increasing evidence has shown that the NT-proBNP level is associated with AKI after cardiac surgery (12–15), medical (non-surgical) patients in cardiac intensive care units (16), or unselected critically ill patients (17). Several studies have also validated NT-proBNP as a predictor of mortality in cardiac surgery patients (12, 14, 18, 19). However, little is known about the prognostic value of NT-proBNP in cardiac surgery patients with established AKI. Therefore, the purpose of this study was to investigate the prognostic value of NT-proBNP in cardiac surgery patients with established AKI requiring RRT.

MATERIALS AND METHODS

Study Population

From January 2018 to October 2019, consecutive AKI patients after cardiac surgery who required RRT in the cardiac surgical intensive care unit (ICU) of Zhongshan Hospital, Fudan University, Shanghai, China, were prospectively enrolled.

AKI was diagnosed according to the Kidney Disease Improving Global Outcomes (KDIGO) classification (20). Patients were excluded if they met the following criteria: age < 18 years, ICU length of stay < 48 h, pre-admission chronic RRT or previous history of end-stage renal disease [defined by an estimated glomerular filtration rate (eGFR) < 15 mL/min/1.73 m^2], and receiving RRT before cardiac surgery.

RRT Indications and Management

Indications for RRT included metabolic acidosis (pH < 7.2), hyperkalemia > 6.0 mmol/L, evidence of fluid overload refractory to diuretics, urine output < 0.5 mL/kg/h for more than 6 h under optimized conditions (preload optimization, titration of vasopressors, and use of diuretics), and severe azotemia (serum creatinine level > 4 mg/dL and/or >3-fold increase in serum creatinine level compared with baseline). RRT was initiated within 6 h of meeting the above criteria. The method of RRT (continuous or intermittent technique, duration, and interval between sessions) depended on the clinical state of individual patients, usually the continuous technique in unsteady hemodynamic phase and then succeeded by intermittent techniques after stabilization. The modality of RRT included continuous venovenous hemofiltration (CVVH), continuous venovenous hemodiafiltration (CVVHDF), intermittent hemodialysis (IHD), and intermittent sustained low efficiency dialysis (SLED), which were used based on the discretion of clinicians to achieve optimal hemodynamic status and metabolic control. Blood flow was usually kept between 180 to 220 mL per minute. The prescribed effluent flow was kept above 25 mL per kilogram per hour. The replacement or dialysate solution used was bicarbonate. Femoral or internal jugular double-lumen dialysis catheter was used for vascular access.

Data Collection

Baseline demographics, co-morbidities, and pre-operative laboratory data including NT-proBNP, serum creatinine (sCr), and blood urea nitrogen (BUN) were recorded. Information regarding the surgical procedure was obtained. The eGFR was calculated based on the Modification of Diet in Renal Disease (MDRD) equation. Day 0 was defined as the day of RRT initiation, and day 1 was defined as the first day after RRT initiation. RRT indications, hemodynamic variables, and clinical characteristics at RRT initiation which included central venous pressure (CVP), mean artery pressure (MAP), vasoactive agent dosages, and Acute Physiology and Chronic Health Evaluation II (APACHE-II) scores were collected.

Serum samples for laboratory assessments were obtained for each patient on day 0 (within 6 h before RRT initiation) and day 1 (within 18 h after RRT initiation). The NT-proBNP levels were measured using the Elecsys Electro-chemo luminescent assay (Cobase 411 analyzer, Roche Diagnostics, Mannheim, Germany) in the clinical chemistry laboratory of the Zhongshan Hospital. The measurement range was 5 to 35,000 pg/mL and the total coefficient of variation was 3.9–4.4% according to multicenter measurements of the automated Roche NT-proBNP assay (21).

Outcome

The primary outcome of this study was 28-day mortality from the day of RRT initiation. Patients who survived to day 28 were censored at day 28. Secondary outcomes were duration of invasive mechanical ventilation, length of stay in the ICU and hospital, ICU mortality, hospital mortality, and RRT dependency at day 28 in survivors.

Statistical Analysis

The normality of distribution of continuous variables was evaluated using the Kolmogorov-Smirnov test. Continuous variables are shown as the mean ± standard deviation (SD) or median interquartile range [IQR], as appropriate. Categorical variables were presented as numbers and percentages. For skewed data, ln transformation of NT-proBNP, troponin T, and APACHE II score was performed (presented as ln-NT-proBNP, ln-troponin T, and ln-APACHE II score, respectively). Baseline characteristics were compared using the Student's *t*-test or Mann-Whitney *U*-test for continuous variables and the chi-square test or Fisher's exact test for categorical variables. We used receiver operating characteristic (ROC) curves to examine the performance of variables to predict 28-day mortality. The area under the curve (AUC) was derived from ROC curves. Survival curves were plotted and compared across different NT-proBNP levels. Cox proportional hazards regressions were performed to evaluate prognostic values of NT-proBNP. Variables with a *P*

< 0.1 in univariate analyses were introduced into multivariable models (stepwise variable-selection method). Analyses were performed using the SPSS software package, version 13.0 (SPSS, Inc., Chicago, IL, USA). Two-sided $p < 0.05$ was defined as statistically significant.

RESULTS

From January 2018 to October 2019, a total of 8,429 patients undergoing cardiac surgery were screened for inclusion. Of these, 2,903 patients had AKI after cardiac surgery and 186 patients required RRT. Of those, 23 patients were excluded, including 12 patients receiving RRT before surgery, eight patients who died within 48 h after surgery, and three patients with missing data. Finally, 163 patients that received RRT were included for analysis (**Figure 1**).

Patient characteristics

The baseline characteristics grouped by 28-day mortality are presented in **Table 1**. There were no significant differences in age, sex, hypertension, and diabetes mellitus. Non-survivors had higher pre-operative troponin *T* (median: 0.03 [IQR, 0.02–0.14] vs. 0.02 [IQR, 0.01–0.05] ng/mL; $P = 0.03$), NT-proBNP (median: 4,096 [IQR, 962.0–9,583.8] vs. 1,339 [IQR, 446–5,173] pg/mL; $P < 0.01$), sCr levels (mean: 173.4, SD ± 92.1 vs. 141.3 SD ± 78.1 μmol/L; $P = 0.03$) and lower BMI (mean: 22.7, SD ± 4.0 vs. 24.1, SD ± 4.4 kg/m^2; $P = 0.04$) compared with survivors. The type of surgery was comparable between the two groups. The cardiopulmonary bypass (CPB) time and aortic clamp time were higher in non-survivors compared to survivors (all $P < 0.05$).

The clinical characteristics at RRT initiation are shown in **Table 2**. The indications for RRT included severe azotemia (25.8%), oliguria (97.5%), metabolic acidosis (6.1%), and electrolyte disorders (3.1%). There were no differences in indications of RRT, urine output before RRT initiation, and hemodynamic variables including MAP, CVP, and the dosage of vasoactive drugs between two groups. The APACHE II score (mean: 18, SD ± 8 vs. 15, SD ± 6; $P < 0.01$), NT-proBNP (median: 10,366 [IQR, 5,668–20,646] vs. 3,779 [IQR, 1,799–11,256] pg/mL; $P < 0.001$) and serum lactate level (mean: 5.88, SD ± 5.19 vs. 3.76, SD ± 3.63 mmol/L; $P < 0.01$) at RRT initiation were higher in non-survivors, while the eGFR (mean: 20.9, SD ± 10.3 vs. 25.2, SD ± 15.7 mL/min/1.73 m^2; $P = 0.04$) and serum bicarbonate level (mean: 23.2, SD ± 4.1 vs. 25.7, SD ± 4.2 mmol/L; $P < 0.001$) were lower. On day 1 after RRT initiation, NT-proBNP (median: 9,055.0 [IQR, 4,392–24,348] vs. 5,255 [IQR, 2,134–9,175] pg/mL; $P < 0.001$) and serum lactate level (mean: 4.74, SD ± 4.68 vs. 1.90, SD ± 1.30 mmol/L; $P < 0.001$) were still higher in non-survivors, while serum bicarbonate level (mean: 23.0, SD ± 4.2 vs. 25.6, SD ± 3.7 mmol/L; $P < 0.001$) was lower.

Outcome

The 28-day mortality of our cohort was 39.3% (64/163; **Table 3**). Concerning the clinical course, 43.6% patients (71/163) received tracheostomy during the ICU stay. The mean duration of invasive

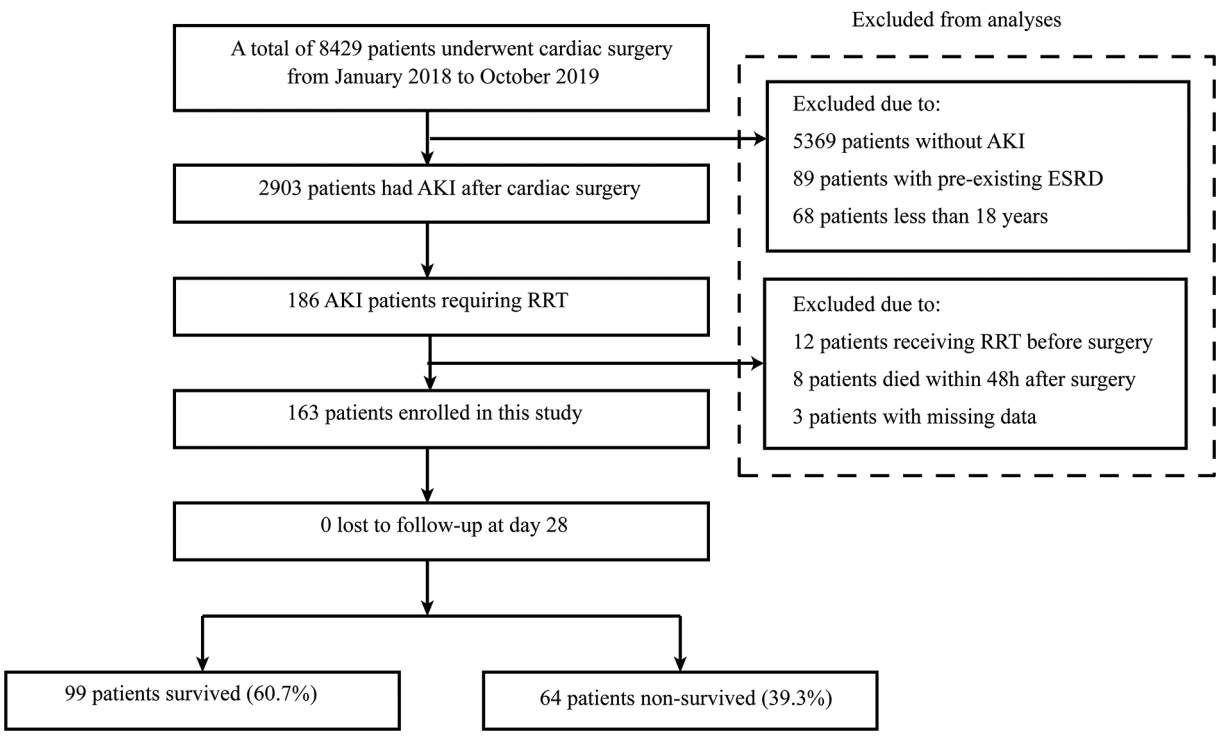

FIGURE 1 | Flow chart of this study. AKI, acute kidney injury; RRT, renal replacement therapy; ESRD, end-stage renal disease.

TABLE 1 | Clinical characteristics of patients grouped by 28-day mortality.

	All patients ($n = 163$)	Survivors ($n = 99$)	Non-survivors ($n = 64$)	*P*-value
Age (years)	56.5 ± 14.7	56.7 ± 14.4	56.3 ± 15.3	0.89
Sex (male), *n* (%)	110 (67.5)	68 (68.7)	42 (65.6)	0.73
BMI (kg/m^2)	23.5 ± 4.3	24.1 ± 4.4	22.7 ± 4.0	0.04
Comorbidities				
Hypertension, *n* (%)	103 (63.2)	60 (60.6)	43 (67.2)	0.41
Diabetes mellitus, *n* (%)	25 (15.3)	16 (16.2)	9 (14.1)	0.83
CAD, *n* (%)	27 (16.6)	12 (12.1)	15 (23.4)	0.08
Prior cardiac surgery, *n* (%)	37 (22.7)	25 (25.3)	12 (18.8)	0.44
Pre-operative laboratory data				
BUN_{pre-op} (mmol/L)	12.9 ± 10.4	11.7 ± 7.4	14.7 ± 13.6	0.15
$cTnT_{pre-op}$ (ng/mL)	0.03 [0.01,0.06]	0.02 [0.01,0.05]	0.03 [0.02,0.14]	0.03
NT-$proBNP_{pre-op}$ (pg/mL)	1924 [523,7277]	1339 [446,5173]	4096 [962.0,9583.8]	<0.01
sCr_{pre-op} (μmol/L)	154.41 ± 85.32	141.3 ± 78.1	173.4 ± 92.1	0.03
$Procalcitonin_{pre-op}$ (ng/mL)	0.23 [0.05,0.68]	0.07 [0.05,0.44]	0.25 [0.10,1.00]	0.10
$eGFR_{pre-op}$ (MDRD) (mL/min/1.73 m^2)	54.00 ± 32.13	58.1 ± 33.0	48.0 ± 30.1	0.06
Type of surgery, *n* (%)				
CABG only	14 (8.6)	8 (8.1)	16 (25.0)	0.78
Valve only	58 (35.6)	37 (37.4)	21 (32.8)	0.62
CABG and valve	9 (5.5)	4 (4.0)	5 (7.8)	0.32
Aortic surgery	41 (25.2)	27 (27.3)	14 (21.9)	0.47
Valve and large vessels	20 (12.3)	13 (13.1)	7 (10.9)	0.81
Other cardiac surgery	21 (12.9)	10 (1.1)	11 (17.2)	0.23
Intraoperative parameters				
CPB time (min)	193 [152,238]	182 [148,227]	206 [161,252]	0.03
Aortic clamp time (min)	75 [60,93]	73 [58,90]	82 [65,94]	0.04

Continuous variables are shown as the mean (±SD) or median [interquartile range, IQR], as appropriate. Categorical variables are shown as a number (%). BMI, body mass index; BUN, blood urea nitrogen; CAD, coronary artery disease; CABG, coronary artery bypass grafting; CPB, cardiopulmonary bypass; sCr, serum creatinine; eGFR, estimated glomerular filtration rate using the abbreviated Modification of Diet in Renal Disease (MDRD) equation; cTnT, troponin T; NT-proBNP, N-terminal pro-B-type natriuretic peptide; pre-op, pre-operative.

mechanical ventilation was 11, SD ± 11 days. The rate of dependence on RRT among survivors at 28 days was 12.1% (12/99). The length of ICU and hospital stay were longer in non-survivors compared with survivors (mean: 21.0, SD ± 16.0 vs.14, SD ± 10 days and 39, SD ± 26 vs. 21, SD ± 13 days, all $P < 0.01$; **Table 3**).

Value of Variables to Predict 28-Day Mortality

ROC curves were constructed to evaluate the performance of variables to predict 28-day mortality (**Figure 2**). The AUC, optimal cutoff value, sensitivity, and specificity of each variable are shown in **Table 4**. The APACHE II score (AUC 0.60, SD ± 0.05), NT-$proBNP_{pre-op}$ (AUC 0.64, SD ± 0.05), NT-$proBNP_{day0}$ (AUC 0.71, SD ± 0.04), and NT-$proBNP_{day1}$ (AUC 0.68, SD ± 0.04) had a modest power for prediction of 28-day mortality (all $P < 0.05$). There were no statistically significant differences in the AUC among above indicators (all $P > 0.05$). A NT-$proBNP_{pre-op}$ cutoff value of ≥3,632.5 pg/mL had a sensitivity of 53.1% and a specificity of 71.4%. A NT-$proBNP_{day0}$ threshold of ≥5,539 pg/mL had a sensitivity of 78.1% and a specificity of 62.2%. A NT-$proBNP_{day1}$ threshold of ≥7,841 pg/mL had a sensitivity of 64.1% and a specificity of 71.4%.

Variables for Prediction of 28-day Mortality

According to the ROC curves, the cut-off value of NT-$proBNP_{pre-op}$, NT-$proBNP_{day0,}$ and NT-$proBNP_{day1}$ levels were set at 3,632.5, 5,539, and 7,841 pg/mL, respectively (**Table 4**). Patients with higher NT-$proBNP_{pre-op}$ levels (≥3,632.5 pg/mL), NT-$proBNP_{day0}$ (≥5,539 pg/mL), and NT-$proBNP_{day1}$ (≥7,841 pg/mL) levels were at a higher risk of mortality (all $P < 0.001$, log-rank test). Survival curves for 28-day mortality are shown in **Figure 3**.

The predictive variables of 28-day mortality were evaluated using Cox proportional hazards regression. In univariable analysis, ln-APACHE II score, ln-NT -$proBNP_{pre-op}$, ln-NT -$proBNP_{day0}$, ln-NT -$proBNP_{day1}$, lactate $_{day0}$, lactate $_{day1}$, HCO_3^- day0, and HCO_3^- day1 were significantly associated with 28-day mortality (**Table 5**). To account for the possible influence of NT-proBNP levels on 28-day mortality, multivariable models were constructed (**Table 6**). In multivariable analysis, ln NT -$proBNP_{pre-op}$, ln NT-$proBNP_{day0,}$ and ln NT-$proBNP_{day1}$ were independently associated with 28-day mortality (all $P < 0.05$).

TABLE 2 | Patient characteristics at RRT initiation grouped by 28-day mortality.

	All patients (n = 163)	Survivors (n = 99)	Non-survivors (n = 64)	P-value
LOS before RRT initiation (day)	1 [1, 3]	1 [1, 2]	1.5 [1, 7.8]	0.02
Indication for RRT				
Severe azotemia, *n* (%)	42 (25.8)	21 (21.2)	21 (32.8)	0.10
Oliguria, *n* (%)	159 (97.5)	96 (97.0)	63 (98.4)	1.00
Metabolic acidosis, *n* (%)	10 (6.1)	4 (4.0)	6 (9.4)	0.19
Electrolyte disorders, *n* (%)	5 (3.1)	2 (2.0)	3 (4.7)	0.38
Urine output before RRT initiation (mL/kg/h)	0.45 ± 0.24	0.45 ± 0.25	0.45 ± 0.23	0.96
Patients on IABP, *n* (%)	8 (4.9)	4 (4.0)	4 (6.3)	0.71
Patients on ECMO, *n* (%)	26 (15.9)	9 (9.1)	17 (26.6)	<0.01
Heart rate (bpm)	106.8 ± 18.5	105.6 ± 19.1	108.6 ± 17.4	0.30
Mean arterial pressure (mmHg)	75.0 ± 15.1	75.2 ± 14.9	74.8 ± 15.6	0.87
CVP (mmHg)	17 ± 4	17 ± 4	17 ± 3	0.66
Norepinephrine dose (μg/kg/min)	0.19 [0.11, 0.20]	0.19 [0.10, 0.28]	0.20 [0.12, 0.26]	0.89
Epinephrine dose (μg/kg/min)	0.15 [0.09, 0.27]	0.15 [0.06, 0.27]	0.18 [0.10, 0.27]	0.11
APACHE II score	16 ± 7	15 ± 6	18 ± 8	<0.01
RRT dose (mL/kg/h)	38.34 ± 11.14	37.50 ± 11.21	39.63 ± 11.00	0.23
Laboratory data at RRT initiation				
BUN_{day0} (mmol/L)	20.6 ± 13.2	19.0 ± 10.4	23.5 ± 16.7	0.08
$cTnT_{day0}$ (ng/mL)	1.20 [0.36, 2.54]	1.21 [0.54, 2.40]	0.94 [0.21, 4.38]	0.47
$NT\text{-}proBNP_{day0}$ (pg/mL)	5,876 [2,221, 12,816]	3,779 [1,799, 11,256]	10,366 [5,668, 20,646]	<0.001
sCr_{day0} (μmol/L)	286.51 ± 12.02	276.5 ± 124.4	302.0 ± 112.2	0.19
$Procalcitonin_{day0}$ (ng/mL)	4.16 [1.53, 13.56]	4.15 [1.49, 11.79]	4.20 [1.94, 17.28]	0.50
$eGFR_{day0}$ (MDRD) (mL/min/1.73 m^2)	23.47 ± 13.97	25.2 ± 15.7	20.9 ± 10.3	0.04
$Bicarbonate_{day0}$ (mmol/L)	24.7 ± 4.4	25.7 ± 4.2	23.2 ± 4.1	<0.001
$Lactate_{day0}$ (mmol/L)	4.60 ± 4.42	3.76 ± 3.63	5.88 ± 5.19	<0.01
Laboratory data on the first day after RRT initiation				
BUN_{day1} (mmol/L)	15.95 ± 7.21	15.5 ± 6.3	16.6 ± 8.45	0.41
$cTnT_{day1}$ (ng/mL)	1.20 [0.60, 3.18]	1.14 [0.58, 2.86]	1.27 [0.61, 3.31]	0.51
$NT\text{-}proBNP_{day1}$ (pg/mL)	6,494 [2,684, 12,817]	5,255 [2,134, 9,175]	9055.0 [4,392, 24,348]	<0.001
sCr_{day1} (μmol/L)	250.27 ± 95.16	247.0 ± 88.0	255.3 ± 105.8	0.60
$Procalcitonin_{day1}$ (ng/mL)	6.25[2.20, 17.76]	5.75[1.97, 17.04]	7.32[3.45, 19.67]	0.35
$eGFR_{day1}$ (MDRD) (mL/min/1.73 m^2)	26.8 ± 16.2	27.3 ± 18.0	26.1 ± 13.1	0.65
$Bicarbonate_{day1}$ (mmol/L)	24.6 ± 4.1	25.6 ± 3.7	23.0 ± 4.2	<0.001
$Lactate_{day1}$ (mmol/L)	3.09 ± 3.47	1.90 ± 1.30	4.74 ± 4.68	<0.001

Results are presented as the mean (± SD) or median [IQR], as appropriate. LOS, length of stay; NT-proBNP, N-terminal pro-B-type natriuretic peptide; cTnT, troponin T; BUN, blood urea nitrogen; sCr, serum creatinine; eGFR, estimated glomerular filtration rate using the abbreviated Modification of Diet in Renal Disease (MDRD) equation; RRT, renal replacement therapy; CVP, central venous pressure; ECMO, extracorporeal membrane oxygenation; IABP, intra-aortic balloon pump. Day 0 was defined as the day at RRT initiation, while day 1 was defined as the first day after RRT initiation.

TABLE 3 | Clinical outcome grouped by 28-day mortality.

	All patients (n = 163)	Survivors (n = 99)	Non-survivors (n = 64)	P-value
Patients on tracheostomy, *n* (%)	71 (43.6)	40 (40.4)	31 (48.4)	0.34
Duration of IMV (day)	11 ± 11	11 ± 12	11 ± 7	0.78
Dependence on RRT among survivors at day 28, *n* (%)	/	12 (12.1%)	/	/
ICU mortality, *n* (%)	73 (44.8)	9 (9.1)	64 (100)	<0.001
Hospital mortality, *n* (%)	73 (44.8)	9 (9.1)	64 (100)	<0.001
Length of ICU stay (day)	18 ± 14	21 ± 16	14 ± 10	0.001
Length of hospital stay (day)	32 ± 23	39 ± 26	21 ± 13	<0.001

Results are presented as the mean (±SD). RRT, renal replacement therapy; IMV, invasive mechanical ventilation.

DISCUSSION

To our knowledge, this is the first study investigating the prognostic value of NT-proBNP in cardiac surgery patients with established AKI requiring RRT. Serum NT-proBNP levels in non-survivors was markedly higher than survivors before surgery, at RRT initiation and on the first day after RRT initiation. Consistently, ROC curves revealed that NT-pro-BNP levels (pre-op, day 0 or day 1) had a modest power for predicting 28-day mortality. Cox proportional hazards regression analyses revealed that NT-proBNP levels before surgery, at RRT initiation, and on the first day after RRT initiation were independently associated with 28-day mortality.

Recent studies have reported several biomarkers to predict mortality at RRT initiation in critically ill patients. Serum neutrophil gelatinase associated lipocalin (NGAL) at initiation of RRT was identified as a prognostic biomarker in unselected critically ill patients (22). Plasma c-terminal FGF-23 (cFGF-23) at inception of RRT was correlated with higher 90-day overall mortality and predicted worse kidney recovery in survivors in critically ill patients with AKI (23). NT-proBNP and procalcitonin (PCT) have also been identified as prognostic markers in septic AKI patients requiring RRT (24). However, there are no definitive biomarkers for outcome prediction in AKI patients requiring RRT after cardiac surgery.

Natriuretic peptides (NPs), specifically NT-proBNP and B-type natriuretic peptide (BNP), are released by cardiomyocytes in response to stress and pressure overload. NT-proBNP is an inactive N-terminal fragment produced from the cleavage

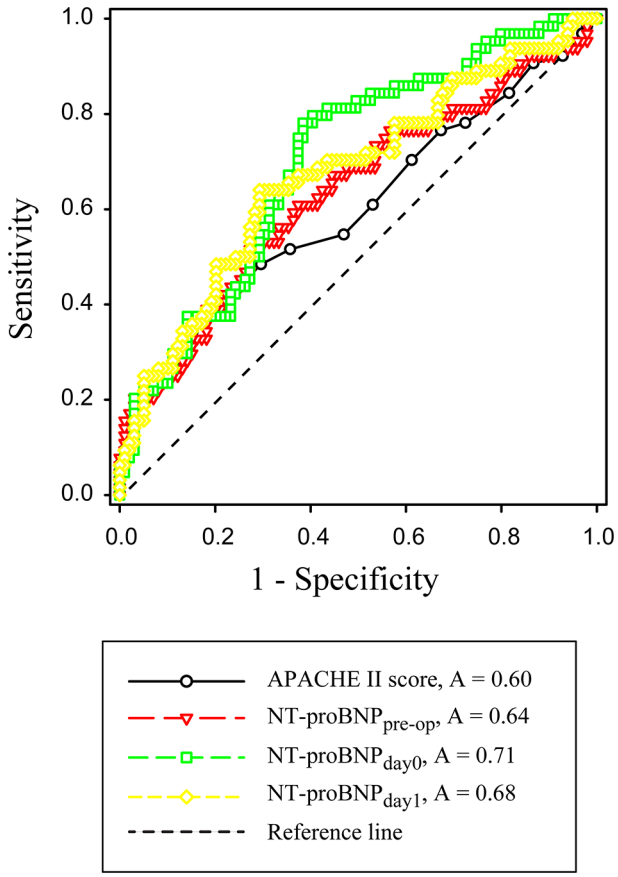

FIGURE 2 | Receiver operating characteristic curves for APACHE II score, $NT\text{-}proBNP_{pre-op}$, $NT\text{-}proBNP_{day0}$ and $NT\text{-}proBNP_{day1}$. APACHE-II, Acute Physiology and Chronic Health Evaluation II; $NT\text{-}proBNP_{pre-op}$, preoperative NT-proBNP level; $NT\text{-}proBNP_{day0}$, NT-proBNP level at RRT initiation; $NT\text{-}proBNP_{day1}$, NT-proBNP level on the first day after RRT initiation.

TABLE 5 | Predictors of 28-day mortality by univariate Cox regression analysis.

Variables	Standard β	Hazard ratio	95% CI	*P*-value
BMI	−0.07	0.93	0.87–0.99	0.03
CAD	0.66	1.93	1.08–3.44	0.03
Ln-APACHE II score	0.75	2.11	1.17–3.82	0.01
$eGFR_{pre-op}$	−40.007	0.99	0.99–1.00	0.13
$eGFR_{day0}$	−0.016	0.98	0.96–1.01	0.13
$eGFR_{day1}$	−0.003	0.99	0.98–1.01	0.71
$Ln\text{-}NT\text{-}proBNP_{pre-op}$	0.23	1.26	1.07–1.48	<0.01
$Ln\text{-}cTnT_{pre-op}$	0.14	1.15	0.99–1.35	0.08
$Ln\text{-}NT\text{-}proBNP_{day0}$	0.54	1.71	1.34–2.18	<0.001
$Bicarbonate_{day0}$	−0.11	0.89	0.84–0.95	<0.001
$Lactate_{day0}$	0.08	1.08	1.03–1.14	0.001
$Ln\text{-}NT\text{-}proBNP_{day1}$	0.47	1.60	1.25–2.05	<0.001
$Bicarbonate_{day1}$	−0.18	0.83	0.78–0.89	<0.001
$Lactate_{day1}$	0.17	1.18	1.12–1.25	<0.001

CI, Confidence; BMI, body mass index; CAD, coronary artery disease; APACHE-II, Acute Physiology and Chronic Health Evaluation II; eGFR, estimated glomerular filtration rate using the abbreviated Modification of Diet in Renal Disease (MDRD) equation; NT-proBNP, N-terminal pro-B-type natriuretic peptide; cTnT, troponin T; pre-op, pre-operative. Ln-variable is the logarithm of the variable. Day 0 was defined as the day at RRT initiation, while day 1 was defined as the first day after RRT initiation.

TABLE 4 | Performance of variables in predicting 28-day mortality.

	AU ROC	95% CI	P	Cut-off	Sensitivity (%)	Specificity (%)
APACHE II score	0.60 ± 0.05	0.51–0.69	0.032	≥19.5	37.5	81.6
$NT\text{-}proBNP_{pre-op}$	0.64 ± 0.05	0.55–0.73	0.003	≥3632.5	53.1	71.4
$NT\text{-}proBNP_{day0}$	0.71 ± 0.04	0.63–0.79	0.000	≥5,539	78.1	62.2
$NT\text{-}proBNP_{day1}$	0.68 ± 0.04	0.60–0.76	0.000	≥7,841	64.1	71.4

Results are presented as the mean (±SD). AUROC, area under the receiver operating characteristic curve; CI, confidence interval; Acute Physiology and Chronic Health Evaluation II, APACHE-II; pre-op, preoperative; cTnT, troponin T; NT-proBNP, N-terminal pro-B-type natriuretic peptide. Day 0 was defined as the day at RRT initiation, while day 1 was defined as the first day after RRT initiation.

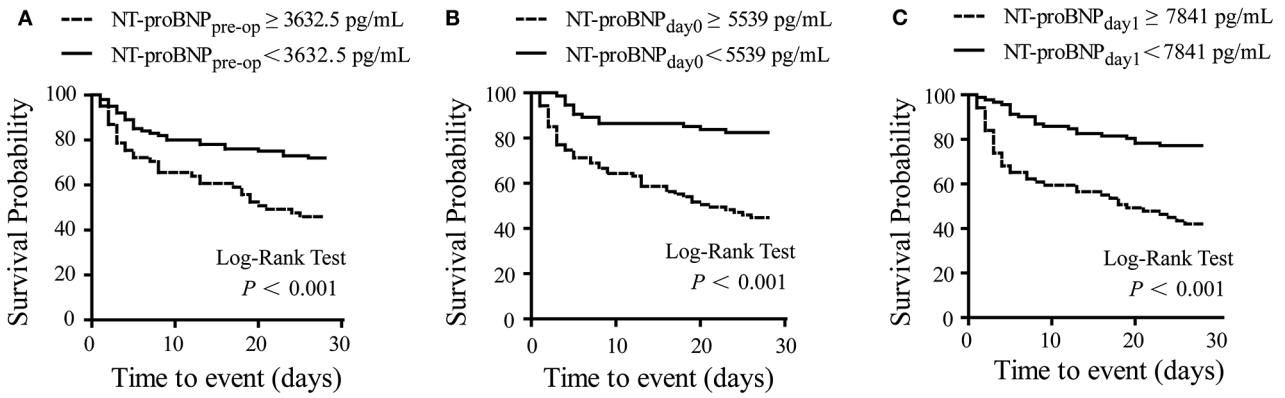

FIGURE 3 | Kaplan-Meier curve for survival. Survival probability in patients with low and high NT-proBNP levels. A significant difference was observed with higher risk of survival events in patients with NT-proBNP$_{pre-op}$ ≥ 3,632.5 pg/mL **(A)**, NT-proBNP$_{day0}$ ≥ 5,539 pg/mL **(B)**, and NT-proBNP$_{day1}$ ≥7,841 pg/mL **(C)**. Log-rank *P*-value shown on graphs. NT-proBNP$_{pre-op}$, preoperative NT-proBNP level; NT-proBNP$_{day0}$, NT-proBNP level at RRT initiation; NT-proBNP$_{day1}$, NT-proBNP level on the first day after RRT initiation.

TABLE 6 | Independent predictors of 28-day mortality by multivariate Cox regression analysis.

	Hazard ratio (95 % CI)	*P*-value
Model 1		
CAD	1.91 (1.03–3.52)	0.04
Ln-APACHE II score	2.01 (1.09–3.71)	0.03
Ln-NT-proBNP$_{pre-op}$	1.27 (1.06–1.52)	0.01
Model 2		
CAD	2.08 (1.14–3.80)	0.02
Ln-NT-proBNP $_{day0}$	1.90 (1.47–2.47)	<0.001
Lactate$_{day0}$	1.11 (1.06–1.17)	<0.001
Model 3		
Ln-NT-proBNP$_{day1}$	1.52 (1.18–1.97)	0.001
Lactate$_{day1}$	1.17 (1.11–1.23)	<0.001

Model 1 adjusted for BMI, CAD, ln-APACHE II score, ln-NT-proBNP$_{pre-op}$, GFR$_{pre-op}$ and ln-cTnT$_{pre-op}$.

Model 2 adjusted for BMI, CAD, ln-APACHE II score, ln-NT-proBNP$_{day0}$, eGFR$_{day0}$, lactate$_{day0}$, bicarbonate$_{day0}$.

Model 2 adjusted for BMI, CAD, ln-APACHE II score, ln-NT-proBNP$_{day1}$, eGFR$_{day1}$, lactate$_{day1}$, bicarbonate$_{day1}$.

CI, Confidence; BMI, body mass index; CAD, coronary artery disease; APACHE-II, Acute Physiology and Chronic Health Evaluation II; eGFR, estimated glomerular filtration rate using the abbreviated Modification of Diet in Renal Disease (MDRD) equation; NT-proBNP, N-terminal pro-B-type natriuretic peptide; cTnT, troponin T; pre-op, pre-operative. Ln-variable is the logarithm of the variable. Day 0 was defined as the day at RRT initiation, while day 1 was defined as the first day after RRT initiation.

of proBNP (9–11). Elevated NT-proBNP levels are usually associated with cardiac dysfunction or heart failure after cardiac surgery and portend a poor outcome (14, 25–27). Decreases in NT-proBNP during follow-up were associated with reduced morbidity and mortality in patients with heart failure (28–30). In addition, recent evidence showed that NT-proBNP also represents a useful prognostic biomarker in septic patients (31–33), non-cardiac surgery patients (34), patients without heart failure (35), and an unselected cohort of critically ill patients (36, 37).

In the present study, NT-pro-BNP levels (pre-op, day 0 or day 1) had a modest power for prediction of 28-day mortality. Although the AUC of NT-proBNP$_{day0}$ was larger than NT-proBNP$_{pre-op}$ or NT-proBNP$_{day1}$, the differences were not statistically significant. Multivariable COX regression analysis also confirmed that serum NT-proBNP levels (pre-op, day 0 or day 1) were independent predictors of 28-day mortality. Several mechanisms may explain the relationship between NT-proBNP and mortality in cardiac surgery patients requiring RRT. First, elevated NT-proBNP are most likely released from stressed myocardium, suggesting that patients with higher NT-proBNP levels may have more severe cardiac dysfunction (27). In this study, the patients receiving RRT tended to be hemodynamically unstable with vasoactive drugs maintenance and high CVP level at RRT initiation, which indicated a reduced cardiac function. Second, all patients in this study had impaired renal function and low GFR at the initiation of RRT. Elevated NT-proBNP levels in this cohort may be partially due to decreased clearance by the kidneys or decreased renal responsiveness to BNP (9). It has been demonstrated that NT-proBNP is associated significantly with progression to end-stage renal disease in patients with chronic kidney disease (38, 39). Even in critically ill patients without underlying cardiac disease, NT-proBNP was independently associated with the maximum stage of AKI and need for RRT (17), which was correlated with high mortality. Third, inflammatory status might also account for increased levels of BNPs, apart from cardiac and renal dysfunction (40). In this study, non-survivors had longer CPB time and aortic clamp time than survivors, which led to a more severe systemic inflammatory reaction and consequently increased the risk of mortality (41, 42).

Several limitations in this study should be addressed. First, the conclusion may be restricted by the small sample size. Second, as the frequency of NT-proBNP measurement is low, the change in NT-proBNP during the clinical course was not analyzed in this study. Finally, as the cohort included patients with severe AKI requiring RRT, we should be cautious to interpret the

prognostic capacity in cardiac surgical patients with mild or moderate AKI.

CONCLUSION

Serum NT-proBNP was an independent predictor of 28-day mortality in cardiac surgical patients with AKI requiring RRT. Large studies are needed to validate the prognostic role of NT-proBNP.

DATA AVAILABILITY STATEMENT

All datasets generated for this study are included in the article/supplementary material.

ETHICS STATEMENT

This prospective study was approved by the Ethics Committee of Zhongshan Hospital, Fudan University (No. B2016-147R) and conducted in accordance with the Declaration of Helsinki. Written informed consent was obtained from legal representatives of participants.

AUTHOR CONTRIBUTIONS

YS, GT, and ZL contributed to study design. YS, JH, YZ, GM, GH, and JL contributed to participants enrollment. JH and YZ contributed to study management and data collection. YS and GT contributed to manuscript writing. GT and ZL contributed to data analyses and manuscript revision. All authors have read and approved the final manuscript.

FUNDING

This article was supported by grants from the Research Funds of Zhongshan Hospital (2019ZSYXQN34, 2019ZSQN13, 2018ZSQN53, and XYYX201922) and the Research Fund of Shanghai Municipal Health Commission (2019ZB0105).

REFERENCES

1. Dasta JF, Kane-Gill SL, Durtschi AJ, Pathak DS, Kellum JA. Costs and outcomes of acute kidney injury (AKI) following cardiac surgery. *Nephrol Dial Transplant.* (2008) 23:1970–4. doi: 10.1093/ndt/gfm908
2. Thiele RH, Isbell JM, Rosner MH. AKI associated with cardiac surgery. *Clin J Am Soc Nephrol.* (2015) 10:500–14. doi: 10.2215/CJN.07830814
3. Tu GW, Xu JR, Liu L, Zhu DM, Yang XM, Wang CS, et al. Preemptive renal replacement therapy in post-cardiotomy cardiogenic shock patients: a historically controlled cohort study. *Ann Transl Med.* (2019) 7:534. doi: 10.21037/atm.2019.09.140
4. Yang XM, Tu GW, Gao J, Wang CS, Zhu DM, Shen B, et al. A comparison of preemptive versus standard renal replacement therapy for acute kidney injury after cardiac surgery. *J Surg Res.* (2016) 204:205–12. doi: 10.1016/j.jss.2016.04.073
5. Bastin AJ, Ostermann M, Slack AJ, Diller GP, Finney SJ, Evans TW. Acute kidney injury after cardiac surgery according to risk/injury/failure/loss/end-stage, acute kidney injury network, and kidney disease: improving global outcomes classifications. *J Crit Care.* (2013) 28:389–96. doi: 10.1016/j.jcrc.2012.12.008
6. Hobson CE, Yavas S, Segal MS, Schold JD, Tribble CG, Layon AJ, et al. Acute kidney injury is associated with increased long-term mortality after cardiothoracic surgery. *Circulation.* (2009) 119:2444–53. doi: 10.1161/CIRCULATIONAHA.108.800011
7. Maccariello E, Soares M, Valente C, Nogueira L, Valenca RV, Machado JE, et al. RIFLE classification in patients with acute kidney injury in need of renal replacement therapy. *Intensive Care Med.* (2007) 33:597–605. doi: 10.1007/s00134-007-0535-0
8. Chertow GM, Soroko SH, Paganini EP, Cho KC, Himmelfarb J, Ikizler TA, et al. Mortality after acute renal failure: models for prognostic stratification and risk adjustment. *Kidney Int.* (2006) 70:1120–6. doi: 10.1038/sj.ki.5001579
9. Daniels LB, Maisel AS. Natriuretic peptides. *J Am Coll Cardiol.* (2007) 50:2357–68. doi: 10.1016/j.jacc.2007.09.021
10. Lugnier C, Meyer A, Charloux A, Andres E, Geny B, Talha S. The endocrine function of the heart: physiology and involvements of natriuretic peptides and cyclic nucleotide phosphodiesterases in heart failure. *J Clin Med.* (2019) 8:1746. doi: 10.3390/jcm8101746
11. Nishikimi T, Nakagawa Y. Does impaired processing of pro-B-type (or brain) natriuretic peptide cause decreased plasma BNP levels in obese heart failure patients? *Ann Transl Med.* (2019) 7:S221. doi: 10.21037/atm.2019.08.56
12. Belley-Cote EP, Parikh CR, Shortt CR, Coca SG, Garg AX, Eikelboom JW, et al. Association of cardiac biomarkers with acute kidney injury after cardiac surgery: a multicenter cohort study. *J Thorac Cardiovasc Surg.* (2016) 152:245–51. doi: 10.1016/j.jtcvs.2016.02.029
13. Patel UD, Garg AX, Krumholz HM, Shlipak MG, Coca SG, Sint K, et al. Preoperative serum brain natriuretic peptide and risk of acute kidney injury after cardiac surgery. *Circulation.* (2012) 125:1347–55. doi: 10.1161/CIRCULATIONAHA.111.029686
14. Lurati BG, Bolliger D, Seeberger E, Kasper J, Grapow M, Koller MT, et al. Troponin T and B-type natriuretic peptide after on-pump cardiac surgery: prognostic impact on 12-month mortality and major cardiac events after adjustment for postoperative complications. *Circulation.* (2014) 130:948–57. doi: 10.1161/CIRCULATIONAHA.113.007253
15. Zelt J, Mielniczuk LM, Liu PP, Dupuis JY, Chih S, Akbari A, et al. Utility of novel cardiorenal biomarkers in the prediction and early detection of congestive kidney injury following cardiac surgery. *J Clin Med.* (2018) 7:540. doi: 10.3390/jcm7120540
16. Naruse H, Ishii J, Takahashi H, Kitagawa F, Nishimura H, Kawai H, et al. Predicting acute kidney injury using urinary liver-type fatty-acid binding protein and serum N-terminal pro-B-type natriuretic peptide levels in patients treated at medical cardiac intensive care units. *Crit Care.* (2018) 22:197. doi: 10.1186/s13054-018-2120-z
17. Haines R, Crichton S, Wilson J, Treacher D, Ostermann M. Cardiac biomarkers are associated with maximum stage of acute kidney injury in critically ill patients: a prospective analysis. *Crit Care.* (2017) 21:88. doi: 10.1186/s13054-017-1674-5
18. Litton E, Ho KM. The use of pre-operative brain natriuretic peptides as a predictor of adverse outcomes after cardiac surgery: a systematic review and meta-analysis. *Eur J Cardiothorac Surg.* (2012) 41:525–34. doi: 10.1093/ejcts/ezr007
19. Holm J, Vidlund M, Vanky F, Friberg O, Hakanson E, Walther S, et al. EuroSCORE II and N-terminal pro-B-type natriuretic peptide for risk evaluation: an observational longitudinal study in patients undergoing coronary artery bypass graft surgery. *Br J Anaesth.* (2014) 113:75–82. doi: 10.1093/bja/aeu088
20. Kellum JA, Lameire N. Diagnosis, evaluation, and management of acute kidney injury: a KDIGO summary (Part 1). *Crit Care.* (2013) 17:204. doi: 10.1186/cc11454
21. Yeo KT, Wu AH, Apple FS, Kroll MH, Christenson RH, Lewandrowski KB, et al. Multicenter evaluation of the Roche NT-proBNP assay and comparison to the Biosite Triage BNP assay. *Clin Chim Acta.* (2003) 338:107–15. doi: 10.1016/j.cccn.2003.08.016
22. Kumpers P, Hafer C, Lukasz A, Lichtinghagen R, Brand K, Fliser D, et al. Serum neutrophil gelatinase-associated lipocalin at inception of renal

replacement therapy predicts survival in critically ill patients with acute kidney injury. *Crit Care.* (2010) 14:R9. doi: 10.1186/cc8861
23. Wu VC, Shiao CC, Chi NH, Wang CH, Chueh SJ, Liou HH, et al. Outcome prediction of acute kidney injury biomarkers at initiation of dialysis in critical units. *J Clin Med.* (2018) 7:202. doi: 10.3390/jcm7080202
24. Sheng X, Yang J, Yu G, Fei Y, Bao H, Yin J, et al. Procalcitonin and N-terminal pro-B-type natriuretic peptide for prognosis in septic acute kidney injury Patients receiving renal replacement therapy. *Blood Purif.* (2019) 48:262–71. doi: 10.1159/000501388
25. Seoudy H, Kuhn C, Frank J, Eden M, Rangrez AY, Lutter G, et al. Prognostic implications of N-terminal pro-B-type natriuretic peptide in patients with normal left ventricular ejection fraction undergoing transcatheter aortic valve implantation. *Int J Cardiol.* (2019) 301:195–9. doi: 10.1016/j.ijcard.2019.11.101
26. Ramkumar N, Jacobs JP, Berman RB, Parker DM, MacKenzie TA, Likosky DS, et al. Cardiac biomarkers predict long-term survival after cardiac surgery. *Ann Thorac Surg.* (2019) 108:1776–82. doi: 10.1016/j.athoracsur.2019.04.123
27. Palazuelos J, Rubio AM, Clares MP. Prognostic implications of baseline NT-proBNP before cardiac surgery. *J Thorac Cardiovasc Surg.* (2016) 152:252–3. doi: 10.1016/j.jtcvs.2016.03.011
28. Savarese G, Musella F, D'Amore C, Vassallo E, Losco T, Gambardella F, et al. Changes of natriuretic peptides predict hospital admissions in patients with chronic heart failure: a meta-analysis. *JACC Heart Fail.* (2014) 2:148–58. doi: 10.1016/j.jchf.2013.11.007
29. Felker GM, Ahmad T. Natriuretic peptides and primary prevention: the new world? *J Am Coll Cardiol.* (2013) 62:1373–5. doi: 10.1016/j.jacc.2013.06.009
30. Zile MR, Claggett BL, Prescott MF, McMurray JJ, Packer M, Rouleau JL, et al. Prognostic implications of changes in N-terminal pro-B-type natriuretic peptide in patients with heart failure. *J Am Coll Cardiol.* (2016) 68:2425–36. doi: 10.1016/j.jacc.2016.09.931
31. Wang F, Wu Y, Tang L, Zhu W, Chen F, Xu T, et al. Brain natriuretic peptide for prediction of mortality in patients with sepsis: a systematic review and meta-analysis. *Crit Care.* (2012) 16:R74. doi: 10.1186/cc11331
32. Varpula M, Pulkki K, Karlsson S, Ruokonen E, Pettila V. Predictive value of N-terminal pro-brain natriuretic peptide in severe sepsis and septic shock. *Crit Care Med.* (2007) 35:1277–83. doi: 10.1097/01.CCM.0000261893.72811.0F
33. Brueckmann M, Huhle G, Lang S, Haase KK, Bertsch T, Weiss C, et al. Prognostic value of plasma N-terminal pro-brain natriuretic peptide in patients with severe sepsis. *Circulation.* (2005) 112:527–34. doi: 10.1161/CIRCULATIONAHA.104.472050
34. Duceppe E, Patel A, Chan M, Berwanger O, Ackland G, Kavsak PA, et al. Preoperative N-terminal pro-B-type natriuretic peptide and cardiovascular events after noncardiac surgery: a cohort study. *Ann Intern Med.* (2019). doi: 10.7326/M19-2501. [Epub ahead of print].
35. Fukushima N. Is B-type natriuretic peptide (BNP) similarly associated with mortality in patients with and without heart failure? *Ann Transl Med.* (2018) 6:S9. doi: 10.21037/atm.2018.08.46
36. Wang F, Pan W, Pan S, Wang S, Ge Q, Ge J. Usefulness of N-terminal pro-brain natriuretic peptide and C-reactive protein to predict ICU mortality in unselected medical ICU patients: a prospective, observational study. *Crit Care.* (2011) 15:R42. doi: 10.1186/cc10004
37. Meyer B, Huelsmann M, Wexberg P, Delle KG, Berger R, Moertl D, et al. N-terminal pro-B-type natriuretic peptide is an independent predictor of outcome in an unselected cohort of critically ill patients. *Crit Care Med.* (2007) 35:2268–73. doi: 10.1097/01.CCM.0000284509.23439.5B
38. Sundqvist S, Larson T, Cauliez B, Bauer F, Dumont A, Le Roy F, et al. Clinical value of natriuretic peptides in predicting time to dialysis in Stage 4 and 5 chronic kidney disease patients. *PLoS ONE.* (2016) 11:e159914. doi: 10.1371/journal.pone.0159914
39. Desai AS, Toto R, Jarolim P, Uno H, Eckardt KU, Kewalramani R, et al. Association between cardiac biomarkers and the development of ESRD in patients with type 2 diabetes mellitus, anemia, and CKD. *Am J Kidney Dis.* (2011) 58:717–28. doi: 10.1053/j.ajkd.2011.05.020
40. Rudiger A, Fischler M, Harpes P, Gasser S, Hornemann T, von Eckardstein A, et al. In critically ill patients, B-type natriuretic peptide (BNP) and N-terminal pro-BNP levels correlate with C-reactive protein values and leukocyte counts. *Int J Cardiol.* (2008) 126:28–31. doi: 10.1016/j.ijcard.2007.03.108
41. Madhavan S, Chan SP, Tan WC, Eng J, Li B, Luo HD, et al. Cardiopulmonary bypass time: every minute counts. *J Cardiovasc Surg.* (2018) 59:274–81. doi: 10.23736/S0021-9509.17.09864-0
42. Dvirnik N, Belley-Cote EP, Hanif H, Devereaux PJ, Lamy A, Dieleman JM, et al. Steroids in cardiac surgery: a systematic review and meta-analysis. *Br J Anaesth.* (2018) 120:657–67. doi: 10.1016/j.bja.2017.10.025

Conflict of Interest: The authors declare that the research was conducted in the absence of any commercial or financial relationships that could be construed as a potential conflict of interest.

frontiers in Medicine

ORIGINAL RESEARCH
published: 02 June 2020
doi: 10.3389/fmed.2020.00201

Kidney Ischemia-Reperfusion Elicits Acute Liver Injury and Inflammatory Response

Yue Shang[1,2], *Susara Madduma Hewage*[1,3], *Charith U. B. Wijerathne*[1,2], *Yaw L. Siow*[1,3,4], *Cara K. Isaak*[1,3] *and Karmin O*[1,2,3]*

[1] St. Boniface Hospital Research Centre, Winnipeg, MB, Canada, [2] Department of Animal Science, University of Manitoba, Winnipeg, MB, Canada, [3] Department of Physiology and Pathophysiology, University of Manitoba, Winnipeg, MB, Canada, [4] Agriculture and Agri Food Canada, St. Boniface Hospital Research Centre, Winnipeg, MB, Canada

Ischemia-reperfusion (IR) is a common risk factor that causes acute kidney injury (AKI). AKI is associated with dysfunction of other organs also known as distant organ injury. The liver function is often compromised in patients with AKI and in animal models. However, the underlying mechanisms are not fully understood. Inflammatory response plays an important role in IR-induced tissue injury. Although increased proinflammatory cytokines have been detected in the kidney and the distant organs after renal IR, their original sources remain uncertain. In the present study, we investigated the acute effect of renal IR on hepatic inflammatory cytokine expression and the mechanism involved. Sprague-Dawley rats that were subjected to renal IR (ischemia for 45 min followed by reperfusion for 1 h or 6 h) had increased plasma levels of creatinine, urea, and transaminases, indicating kidney and liver injuries. There was a significant increase in the expression of proinflammatory cytokine mRNA (MCP-1, TNF-α, IL-6) in the kidney and liver in rats with renal IR. This was accompanied by a significant increase in proinflammatory cytokine protein levels in the plasma, kidney, and liver. Activation of a nuclear transcription factor kappa B (NF-κB) was detected in the liver after renal IR. The inflammatory foci and an increased myeloperoxidase (MPO) activity were detected in the liver after renal IR, indicating hepatic inflammatory response and leukocyte infiltration. These results suggest that renal IR can directly activate NF-κB and induce acute production of proinflammatory cytokines in the liver. Renal IR-induced hepatic inflammatory response may contribute to impaired liver function and systemic inflammation.

Keywords: kidney, liver, ischemia-reperfusion, inflammation, acute kidney injury

OPEN ACCESS

Edited by:
Cheng Yang,
Fudan University, China

Reviewed by:
Bin Yang,
University of Leicester, United Kingdom
Shengdi Wu,
Fudan University, China
Lixin Wei,
Second Military Medical University, China

***Correspondence:**
Karmin O
karmino@sbrc.ca

Specialty section:
This article was submitted to Nephrology, a section of the journal Frontiers in Medicine

Received: *02 January 2020*
Accepted: *24 April 2020*
Published: *02 June 2020*

Citation:
Shang Y, Madduma Hewage S, Wijerathne CUB, Siow YL, Isaak CK and O K (2020) Kidney Ischemia-Reperfusion Elicits Acute Liver Injury and Inflammatory Response. Front. Med. 7:201. doi: 10.3389/fmed.2020.00201

INTRODUCTION

Acute kidney injury (AKI) is characterized by a rapid decline in kidney function over a short period of time and is associated with a high mortality. AKI often leads to multiple organ dysfunctions known as distant organ injury (1–5). Kidney ischemia-reperfusion (IR) is one of the most common causes for AKI (6–8). It occurs in clinical situations such as kidney transplantation, cardiac surgery, sepsis, and in critically ill patients. Despite the advancement in renal replacement therapy, the mortality in patients with AKI that is complicated by multiple-organ dysfunction remains high

worldwide (estimated to be 50%). In experimental animals, renal IR is shown to cause distant organ injury in the heart, lung, brain, intestine, and liver (1, 9–15). Clinical studies have shown that AKI patients with multiple organ dysfunctions have worse prognosis than those who have AKI alone (16, 17). Although the remote effects of AKI have been noted for a long time, the precise mechanisms responsible for pathological changes in the distant organs are not well-understood.

Liver function is often impaired in patients with AKI and in animal models with renal IR or nephrectomy (1, 9, 15, 18). It appears that AKI patients with a complication of liver dysfunction have poorer clinical outcomes (16, 17, 19, 20). Oxidative stress, systemic inflammatory response and increased leukocyte trafficking have been implicated in AKI associated distant organ injury. In experimental animals, AKI-induced liver injury manifests with increased oxidative stress, hepatocyte necrosis, elevated cytokines, and leukocyte infiltration (3, 15, 16, 21). Liver plays a central role in metabolism, redox balance, immune regulation, and detoxification. Our recent study has shown that renal IR causes liver injury with reduced hepatic production of glutathione, a major endogenous antioxidant. We have identified that renal IR directly inhibits hepatic glutathione production through downregulation of Nrf-2 mediated glutathione biosynthesis pathway, leading to oxidative stress in rats (15). Renal IR-induced redox imbalance in the liver may contribute to local and systemic oxidative stress (15, 21).

Inflammatory response plays a critical role in IR-induced tissue injury (22). Upon renal IR, proinflammatory cytokines generated in the kidney are considered as major contributors to local and systemic inflammation (13, 23–26). Nuclear factor-kappa B (NF-κB) is one of the key transcription factors that regulates the expression of proinflammatory cytokines and immune response (26, 27). Our previous study showed that IR stimulated chemokine MCP-1 expression through the activation of NF-κB in the kidney (26, 28). Although increased levels of cytokine proteins in the liver were detected in mice 5 h after renal IR (16), in rats 6 h and 24 h after renal IR (21) and in pigs 48 h after renal IR (29), the origin(s) of increased cytokines in the liver after renal IR were not well-identified. It was suggested that the remote effect of renal IR might be initiated by impaired renal clearance or increased influx of cytokines derived from the kidney or from increased mononuclear phagocyte production (24). However, it is unclear whether renal IR can acutely elicit distant organ inflammatory response through directly triggering NF-κB activation and cytokine expression in the liver. Further research is required to identify the molecular mechanisms underlying renal IR-induced distant organ inflammatory response. In the present study, we investigated the early impact of renal IR on liver function and inflammatory response as well as the potential mechanism involved.

MATERIALS AND METHODS

Animal Model

Renal IR was induced in rats as described in our previous studies (15, 28, 30, 31). In brief, Sprague–Dawley rats (250–300 g, male, Central Animal Care Services, University of Manitoba, Winnipeg, MB, Canada) were anesthetized through inhalation of 3% isoflurane/oxygen gas prior to surgery. Renal ischemia was induced by clamping the left kidney pedicle for 45 min. At the end of ischemia, the clamp was removed to allow reperfusion in the left kidney with right nephrectomy. Rats were sacrificed at 1 or 6 h after reperfusion. As a control (sham-operated), rats were subjected to the same surgical procedure without inducing renal ischemia and were sacrificed at the corresponding time points. Blood was collected and centrifuged at 3,000 *g* for 20 min for plasma preparation. All procedures were performed in accordance with the Guide to the Care and Use of Experimental

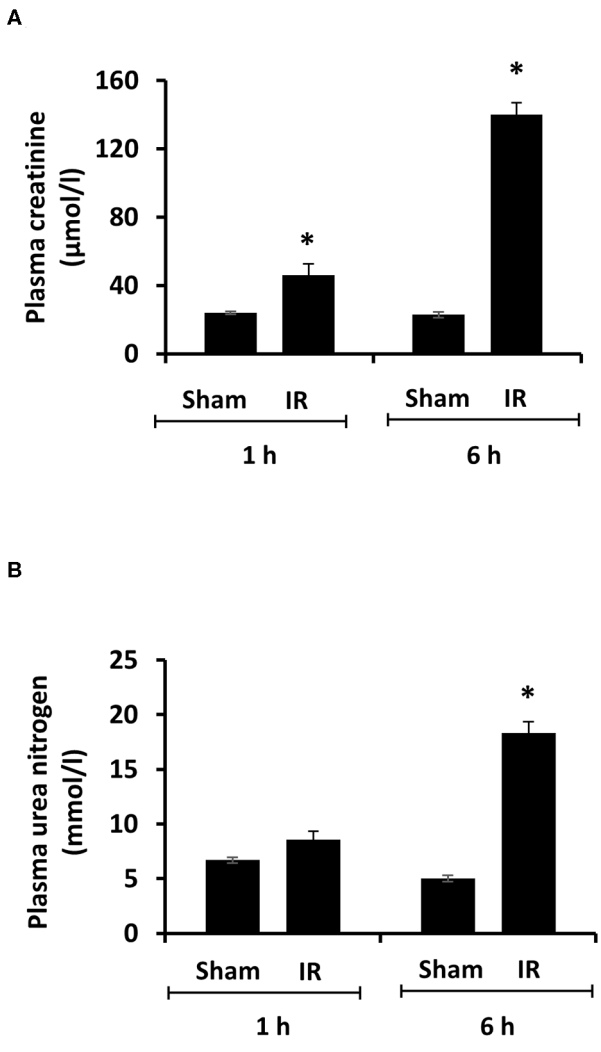

FIGURE 1 | Effect of kidney ischemia-reperfusion on kidney function. The left kidney of rats was subjected to 45 min ischemia followed by 1 hour (1 h) or 6 hours (6 h) of reperfusion (IR). As a control, rats were subjected to a sham-operation without inducing ischemia (Sham). Plasma creatinine **(A)** and urea nitrogen **(B)** were measured. Results are expressed as mean ± SE ($n = 5$ for each group). *$p < 0.05$ when compared with the value obtained from the sham-operated group.

Animals published by the Canadian Council on Animal Care and approved by the University of Manitoba Protocol Management and Review Committee.

Biochemical Analysis

Plasma creatinine, urea, alanine aminotransferase (ALT), and aspartate aminotransferase (AST) were measured by using the Cobas C111 Analyzer (Roche, Risch-Rotkreuz, Switzerland). Cytokines in the plasma, kidney, and liver were measured by using the electrochemiluminescent sandwich ELISA array from Meso Scale Discovery (Rockville, MD, USA). Liver myeloperoxidase (MPO) activity was measured by using a fluorometric assay with a commercial MPO Activity Assay Kit (ab111749, Abcam Inc., Toronto, ON, Canada).

Real-Time Polymerase Chain Reaction (PCR) Analysis

Total RNAs were isolated from the kidney and liver with Trizol reagent (Invitrogen, Carlsbad, CA, USA). The mRNA of MCP-1, TNF-α, and IL-6 was determined by a real-time polymerase chain reaction (PCR) analysis using the iQ5 real-time PCR detection system (Bio-Rad, Mississauga, ON, Canada) and normalized with β-actin (23, 31, 32). The primers (Thermo Fisher Scientific, Waltham, MA, USA) used for rat mRNA measurement were: MCP-1 (119 bp), 5′- CAGAAACCAGCCAACTCTCA-3′ (forward) and 5′- AGACAGCACGTGGATGCTAC-3′ (reverse) (GeneBank accession number NM_031530), TNF-α (215 bp), 5′- CCCAGACCCTCACACTCAGAT-3′ (forward) and 5′- TTG TCCCTTGAAGAGAACCTG-3′ (reverse) (GenBank, accession number NM_012675), IL-6 (161 bp), 5′- CCGGAGAGGAG ACTTCACAG-3′ (forward) and 5′-ACAGTGCATCATCGCT GTTC-3′ (reverse) (GenBank accession number NM_012589) and β-actin (198 bp), 5′- ACAACCTTCTTGCAGCTCCTC-3′ (forward) and 5′- GACCCATACCCACCA TCACA-3′ (reverse) (GenBank accession number NM_031144).

Electrophoretic Mobility Shift Assay (EMSA)

The binding activity of NF-κB with DNA was measured by electrophoretic mobility shift assay (EMSA) (Thermo Fisher Scientific, Waltham, MA, USA). In brief, nuclear proteins were prepared from the liver after renal IR or sham-operation as described in our previous studies (31). Nuclear proteins (2 μg) were incubated with biotin-labeled oligonucleotides containing a consensus sequence specific for the NF-κB/DNA binding site (5′-AGTTGAGGGGACTTTCCCAGGC-3′) (Promega, Madison,

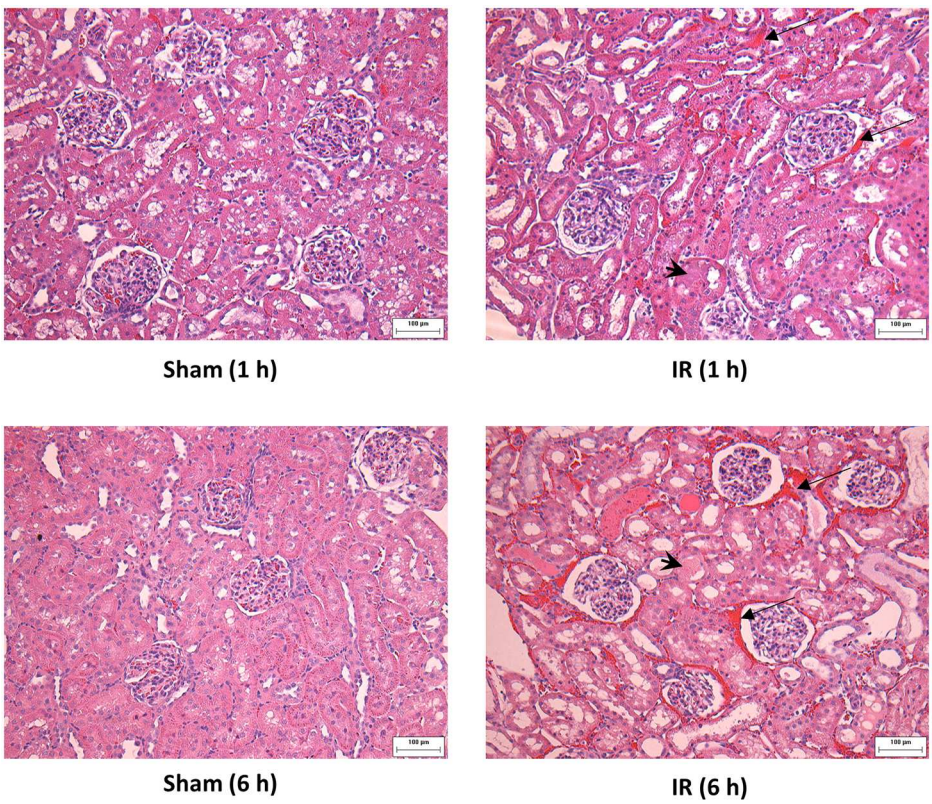

FIGURE 2 | Effect of kidney ischemia-reperfusion on histological change in the kidney. The left kidney of rats was subjected to 45 min ischemia followed by 1 hour (1 h) or 6 hours (6 h) of reperfusion (IR). As a control, rats were subjected to a sham-operation without inducing ischemia (Sham). The histological structure of kidney was examined by hematoxylin and eosin (H&E) staining and analyzed at ×200 magnification. Kidneys of the IR group showed tubular necrosis (arrowheads), interstitial congestion of red blood cells (arrow), and glomerulus enlargement compared with the Sham group (scale bar = 100 μm).

WI, USA). To confirm an equal loading of proteins for each sample, nuclear histone H3 protein was measured by Western immunoblotting analysis. Liver nuclear proteins (10 μg) were separated by electrophoresis in a 12% SDS-polyacrylamide gel. Proteins in the gel were transferred to a nitrocellulose membrane that was first probed with anti-histone H3 polyclonal antibodies (1:1,000, SC-10809, Dallas, TX, USA) followed by HRP-conjugated anti-rabbit IgG secondary antibodies (1:1,000, #7074, New England Biolabs, Ipswich, MA, USA). The protein bands were visualized by using Luminata Crescendo chemiluminescent HRP detection reagent (Millipore, Burlington, MA, USA) and quantified with the Quantity One 1-D Analysis Software (Bio-Rad).

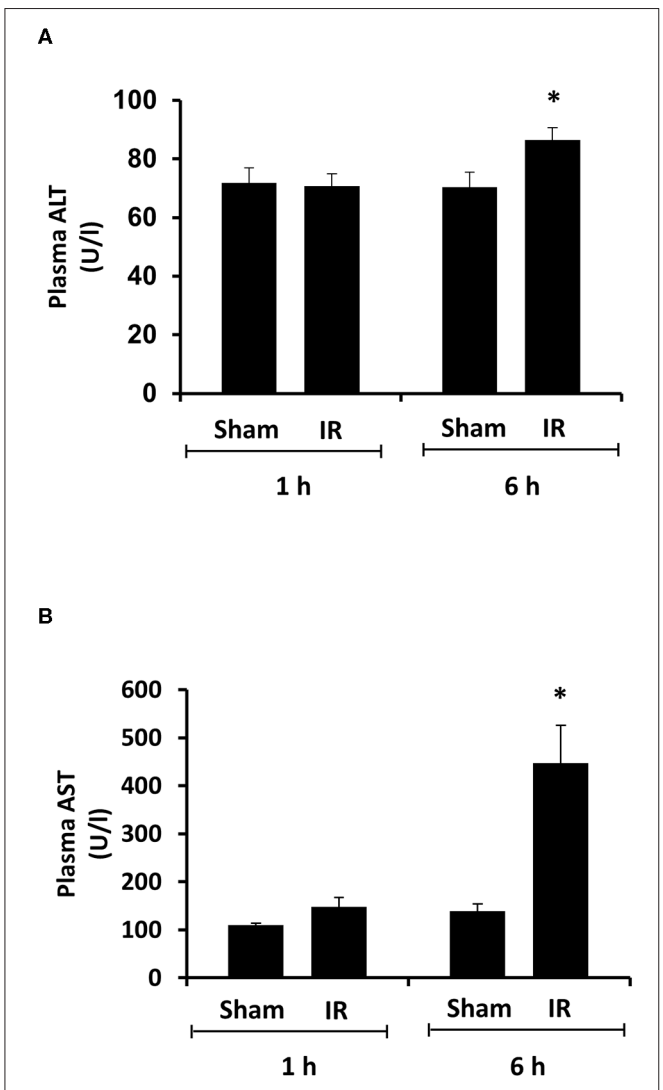

FIGURE 3 | Effect of kidney ischemia-reperfusion on liver function. The left kidney of rats was subjected to 45 min ischemia followed by 1 hour (1 h) or 6 hours (6 h) of reperfusion (IR). As a control, rats were subjected to a sham-operation without inducing ischemia (Sham). Plasma alanine transaminase (ALT) **(A)** and aspartate aminotransferase (AST) **(B)** were measured. Results are expressed as mean ± SE ($n = 5$ for each group). *$p <$ 0.05 when compared with the value obtained from the sham-operated group.

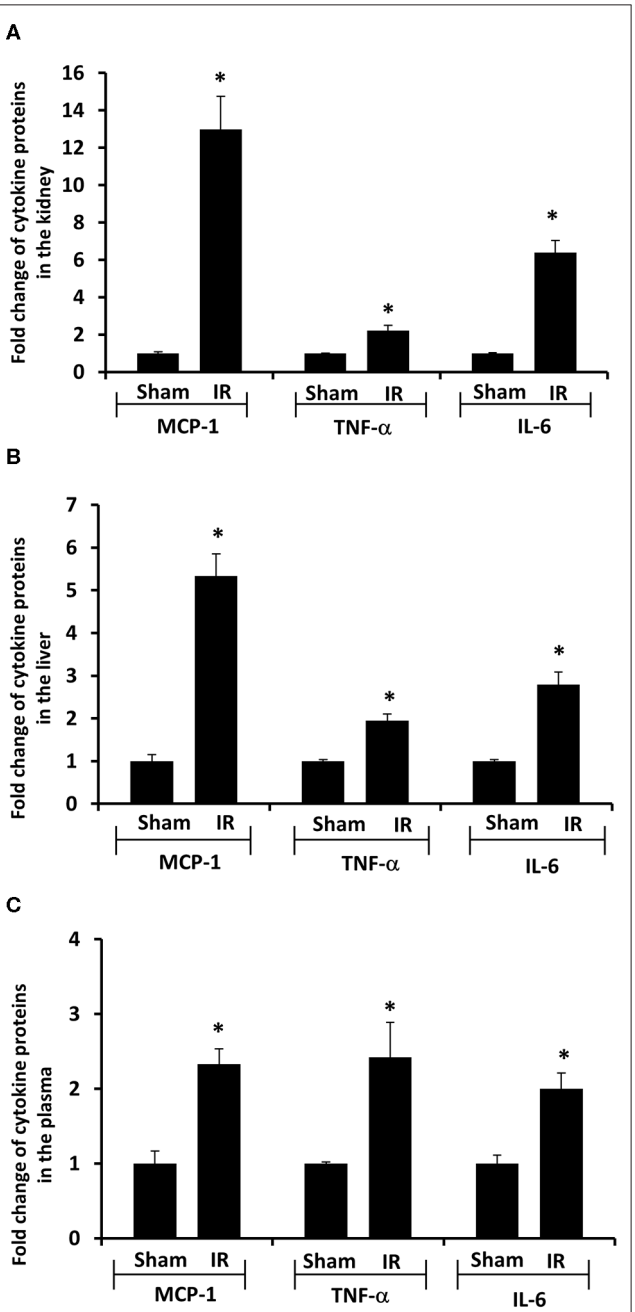

FIGURE 4 | Effect of kidney ischemia-reperfusion on cytokine protein levels in the kidney, liver, and plasma. The left kidney of rats was subjected to 45 min ischemia followed by 6 hours (6 h) of reperfusion (IR). As a control, rats were subjected to a sham-operation without inducing ischemia (Sham). The protein expressions of MCP-1, TNF-α, and IL-6 were measured in the kidney **(A)**, liver **(B)**, and plasma **(C)** by using ELISA. For reference, the cytokine levels in the sham group were MCP-1 (kidney 3.9 ng/g tissue, liver 100 pg/g tissue, plasma 13.63 ng/ml), TNF-α (kidney 200 ng/g tissue, liver 41 pg/g tissue, plasma 1.2 pg/ml), IL-6 (kidney 3.2 ng/g tissue, liver 1,880 pg/g tissue, plasma 1.8 pg/ml). Results are expressed as fold change to the Sham ($n = 5$ for each group). *$p <$ 0.05 when compared with the value obtained from the sham-operated group.

Histological Examination

For histological examination, a portion of the kidney or liver was immersion fixed in 10% neutral-buffered formalin followed by embedding in paraffin. The paraffin-embedded cross sections (5 μm) were prepared and stained with hematoxylin and eosin (H&E) to examine histological changes in the kidney and the liver as described in our previous studies (28). The images were captured by using Olympus BX43 Upright Light Microscope with

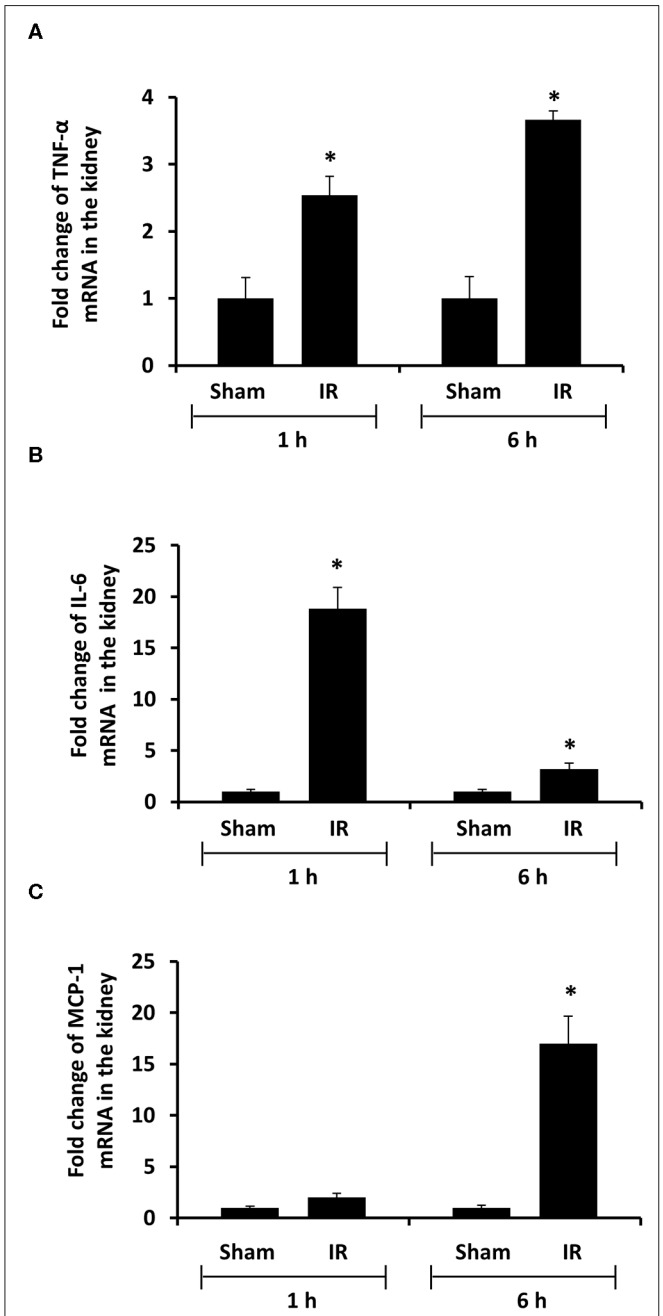

FIGURE 5 | Effect of kidney ischemia-reperfusion on cytokine mRNA expression in the kidney. The left kidney of rats was subjected to 45 min ischemia followed by 1 hour (1 h) or 6 hours (6 h) of reperfusion (IR). As a control, rats were subjected to a sham-operation without inducing ischemia (Sham). The mRNA expressions of TNF-α **(A)**, IL-6 **(B)**, and MCP-1 **(C)** were determined in the kidney by a real-time PCR analysis. Results are expressed as fold change to the Sham ($n = 5$ for each group). *$p < 0.05$ when compared with the value obtained from the sham-operated group.

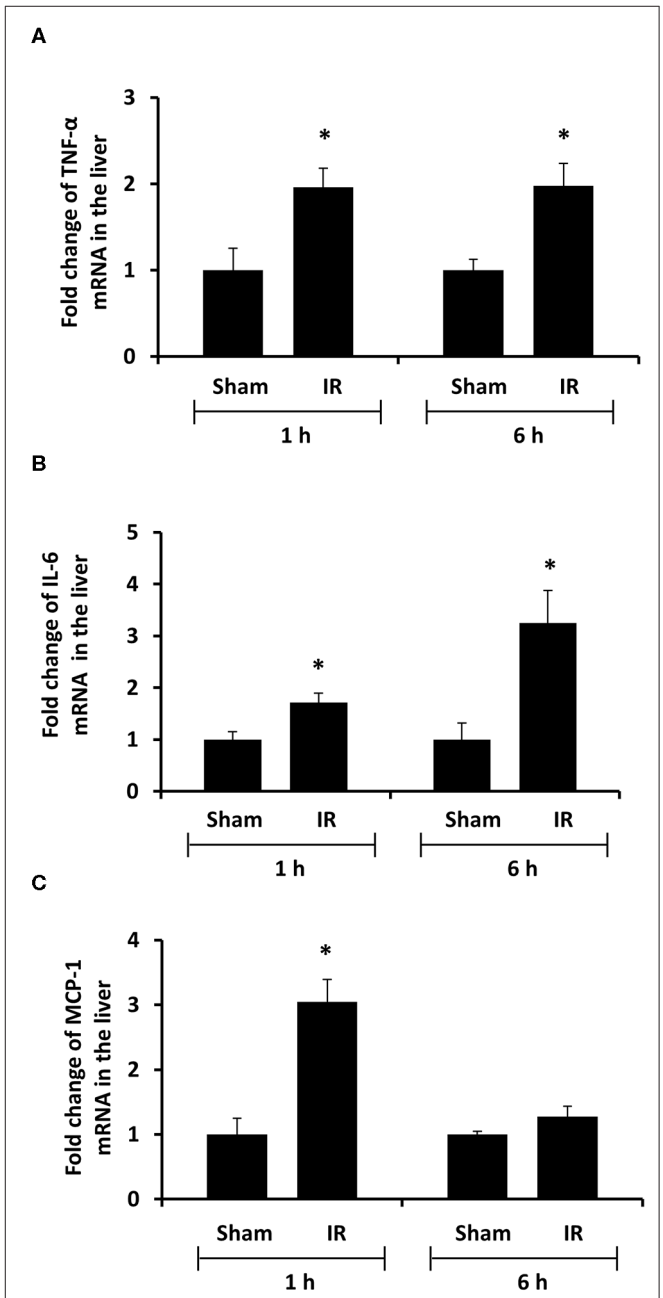

FIGURE 6 | Effect of kidney ischemia-reperfusion on cytokine mRNA expression in the liver. The left kidney of rats was subjected to 45 min ischemia followed by 1 hour (1 h) or 6 hours (6 h) of reperfusion (IR). As a control, rats were subjected to a sham-operation without inducing ischemia (Sham). The mRNA expression of TNF-α **(A)**, IL-6 **(B)**, and MCP-1 **(C)** was determined in the liver by a real-time PCR analysis. Results are expressed as fold change to the Sham ($n = 5$ for each group). *$p < 0.05$ when compared with the value obtained from the sham-operated group.

an Olympus QColor3 digital camera (Olympus Corporation, Tokyo, Japan) and analyzed using Image-Pro plus 7.0 (Media Cybernetics, Bethesda, MD, USA).

Statistical Analysis

Results were analyzed using a two-tailed Student's *t*-test. *P*-value < 0.05 were considered statistically significant.

RESULTS

Renal Ischemia-Reperfusion Impaired Kidney and Liver Function

Renal ischemia for 45 min followed by reperfusion for 1 or 6 h caused a significant elevation of plasma creatinine and urea levels (**Figure 1**), indicating that IR impaired kidney function. IR also caused histological changes in the kidney. The H&E staining showed tubular necrosis, glomerulus enlargement and interstitial congestion of red blood cells in the kidneys of rats subjected to renal IR (**Figure 2**). There was a significant increase in plasma ALT and AST levels in rats at 6 h after renal IR as compared to sham-operated rats (**Figure 3**), indicating liver injury. These results suggested that renal IR not only caused kidney injury but also impaired liver function.

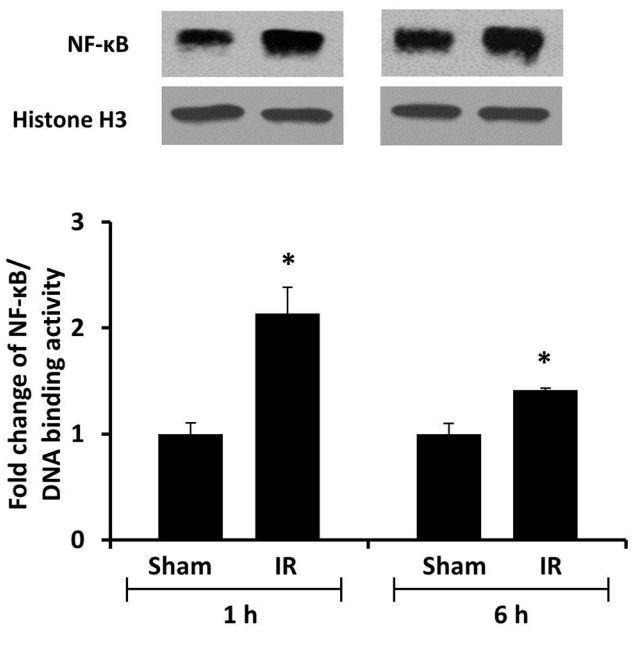

FIGURE 7 | The DNA binding activity of NF-κB in the liver. The left kidney of rats was subjected to 45 min ischemia followed by 1 hour (1 h) or 6 hours (6 h) of reperfusion (IR). As a control, rats were subjected to a sham-operation without inducing ischemia (Sham). Liver nuclear proteins were prepared. The DNA binding activity of NF-κB in the liver was determined by EMSA. Histone H3 was determined by Western immunoblotting analysis and used as an internal control. Results are expressed as fold change to the Sham ($n = 5$ for each group). *$p < 0.05$ when compared with the value obtained from the sham-operated group.

Elevation of Proinflammatory Cytokine Levels in the Kidney, Liver, and Plasma

Next, we measured proinflammatory cytokines in the plasma, kidney, and liver. Renal IR resulted in a significant increase in TNF-α, IL-6, and MCP-1 protein levels in the kidney, liver and plasma (**Figure 4**). These results suggested that renal IR not only increased local inflammatory response but also elevated proinflammatory cytokine levels in a distant organ (liver) and in the circulation.

Renal Ischemia-Reperfusion Increased the Expression of Proinflammatory Cytokine Expression in The Kidney and Liver

To investigate the source of increased proinflammatory cytokines in the local and distant organs, we measured proinflammatory cytokine gene expression in the kidney and liver. There was a significant increase in TNF-α, IL-6, and MCP-1 mRNA in both kidney and liver tissues in rats that were subjected to renal IR (**Figures 5**, **6**). A significant elevation of TNF-α and IL-6 mRNA was detected in the kidney (**Figures 5A,B**) and liver (**Figures 6A,B**) at 1 h or 6 h after renal IR. However, an elevation of MCP-1 mRNA expression was detected in the kidney at 6 h after renal IR (**Figure 5C**). Interestingly, an elevation of MCP-1 mRNA expression was detected in the liver at 1 h after IR (**Figure 6C**). Taken together, these results suggested that renal IR not only caused local inflammatory response but also stimulated the expression of proinflammatory cytokines in the distant organ(s), which might contribute, in part, to an elevation of these cytokines in the circulation.

Renal Ischemia-Reperfusion Activated Transcriptional Factor NF-κB in the Liver

We previously observed that renal IR caused an activation of NF-κB, a main transcription factor for cytokine expression, in the kidney (26). To investigate whether renal IR also activated NF-κB in a distant organ, liver nuclear proteins were prepared and the activation of NF-κB was examined by EMSA. There was a significant increase in the NF-κB/DNA binding activity in the liver of rats at 1 h or 6 h after renal IR (**Figure 7**). The liver morphology was examined by H&E staining. There was deposition of inflammatory foci (characterized by dense aggregates of cells) in the liver of rats after renal IR (**Figure 8**). The MPO activity was measured to determine the presence of neutrophils in the liver. The hepatic MPO activity was significantly increased as early as 1 h after renal IR and remained elevated at 6 h after renal IR (**Figure 9**).

DISCUSSION

In the present study, rats that were subjected to renal IR developed kidney and liver injuries as manifested by increased plasma creatinine, urea, and transaminases (ALT, AST) levels along with histological changes. Increased proinflammatory cytokine mRNA expression was detected in the kidney and liver shortly after the onset of renal IR. In correspondence, the levels of inflammatory cytokine proteins (MCP-1, TNF-α, IL-6) were

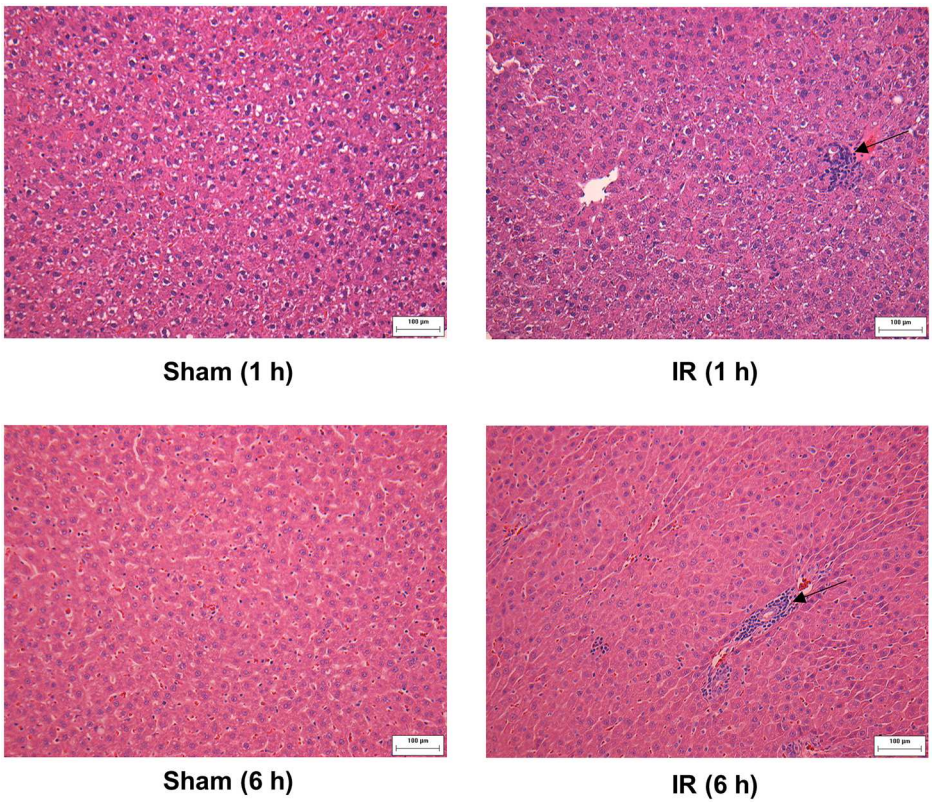

FIGURE 8 | Effect of kidney ischemia-reperfusion on pathohistological change of the liver. The left kidney of rats was subjected to 45 min ischemia followed by 1 hour (1 h) or 6 hours (6 h) of reperfusion (IR). As a control, rats were subjected to a sham-operation without inducing ischemia (Sham). The histological structure of liver was examined by hematoxylin and eosin (H&E) staining (magnification ×200). Arrows point to inflammatory foci (scale bar = 100 μm).

significantly elevated in the kidney, liver and plasma. These results suggest that renal IR can quickly stimulate inflammatory cytokine production locally as well as in distant organs such as in the liver, which augments systemic inflammation and may, in turn, exacerbate kidney injury.

Previous studies conducted by our laboratory and others showed an elevation of proinflammatory cytokine expression in the kidney upon IR (16, 23, 24, 26). Increased proinflammatory cytokine expression is considered as one of the important mechanisms for IR-induced tissue injuries. Increased levels of cytokine proteins were detected in the circulation and distant organs in mice and rats with IR or nephrectomy-induced AKI (16, 33). However, the origin(s) of elevated proinflammatory cytokines have not been well-defined. It has been suggested that an increased production and a decreased clearance by the kidneys upon IR may lead to elevated cytokine levels in the circulation and the distant organs (14).

The present study revealed a significant increase in proinflammatory cytokine levels in the kidney, liver, and plasma at 6 h after renal IR. Although it was plausible that proinflammatory cytokines produced in originally injured organ, namely, kidney could lead to systemic and distant organ inflammation, several lines of evidence indicated that renal IR could also stimulate the production of cytokines in a distant organ. First, activation of NF-κB was detected in the liver of rats at the early time points 1 h and 6 h after renal IR. NF-κB is a transcription factor that plays an important role in the inflammatory response by up-regulating cytokine expression. Multiple pathways have been proposed in the activation of NF-κB. We previously reported that renal IR led to a significant elevation of plasma homocysteine (Hcy) levels (15, 23, 30, 34). Hcy at an elevated level, which is also known as hyperhomocysteinemia, can elicit inflammatory response through activation of transcription factors including NF-κB (35–37). It was plausible that Hcy at elevated levels might serve as one of mediators that contributed to NF-κB activation in the distance organs such as liver during renal IR. Acute activation of NF-κB in response to renal IR could lead to a rapid increase in inflammatory cytokine expression in the liver. Secondly, an elevation of TNF-α, IL-6, and MCP-1 mRNA expression was detected in the liver as early as 1 h after the onset of renal IR, suggesting that an acute up-regulation of proinflammatory cytokine production occurred in a distant organ (liver). This, in turn, might contribute to increased cytokine levels in the circulation. MCP-1 is a potent chemotactic protein that stimulates monocyte/neutrophil infiltration into tissues. We previously reported that there was a significant increase in MCP-1 expression in the kidney at 2 h after renal IR (26). The

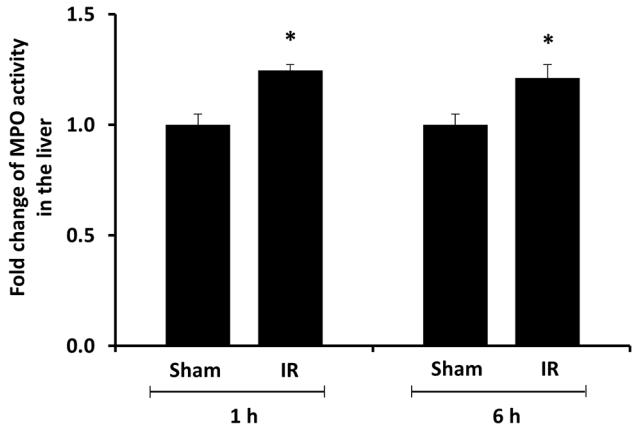

FIGURE 9 | Effect of kidney ischemia-reperfusion on myeloperoxidase activity in the liver. The left kidney of rats was subjected to 45 min ischemia followed by 1 hour (1 h) and 6 hours (6 h) of reperfusion (IR). As a control, rats were subjected to a sham-operation without inducing ischemia (Sham). The myeloperoxidase (MPO) activity were determined in the liver. Results are expressed as fold change to the Sham. Results are expressed as mean ± SE ($n = 4$–5 for each group). *$p < 0.05$ when compared with the value obtained from the sham-operated group.

expression of MCP-1 in the kidney remained elevated 24 h after renal IR (23, 26). Up-regulation of MCP-1 expression by IR might be tissue-specific and time-dependent. In the present study, a significant elevation of MCP-1 mRNA expression was detected in the liver but not in the kidney at 1 h after renal IR. However, a stimulation of MCP-1 expression in the liver was rather transient when compared to its expression in the kidney upon renal IR. Renal IR also stimulated the expression of other proinflammatory cytokines. An elevation of TNF-α and IL-6 mRNA expression was detected in the kidney and liver at 1 or 6 h after renal IR. Furthermore, inflammatory foci were detected in the liver of rats that were subjected to renal IR. This was accompanied by an increased MPO enzymatic activity in the liver tissue. The MPO is a peroxidative enzyme that is abundantly expressed in neutrophil granulocytes. An elevation of hepatic MPO activity indicated neutrophil accumulation in the liver after renal IR. However, the involvement of other inflammatory cells in distant organ injury remains to be investigated. Taken together, these results suggested that increase proinflammatory cytokine production in the kidney and the distant organ(s) could lead to an elevation of cytokine levels in the circulation, which, in turn, might contribute to systemic inflammation during AKI. Future studies are warranted to investigate whether early intervention can alleviate renal IR-induced local and distant organ inflammatory response.

In conclusion, renal IR not only causes kidney injury but also results in liver dysfunction. Inflammation is a hallmark of IR-induced kidney and distant organ injury, which can augment the already high morbidity and mortality in patients with AKI. Although increased proinflammatory cytokine production in the kidney is regarded as one of the important mechanisms leading to systemic and distant organ injury, our results clearly demonstrate that renal IR can directly induce acute production of proinflammatory cytokines in the liver. This, in turn, may contribute to systemic inflammatory response and exacerbate kidney injury. Activation of NF-κB may be involved in renal IR-induced inflammatory cytokine production in the liver. Better understanding of the local and distant organ responses to AKI will help identify new therapeutic targets and ultimately improve the clinical outcomes.

DATA AVAILABILITY STATEMENT

All datasets generated for this study are included in the article/supplementary material.

ETHICS STATEMENT

The animal study was reviewed and approved by University of Manitoba Protocol Management and Review Committee.

AUTHOR CONTRIBUTIONS

KO and YLS conceived and designed research and drafted the manuscript. YS, CW, SM, and CI performed the experiments and analyzed the data. YS, CW, and SM prepared the figures. CW, SM, YS, CI, YLS, and KO edited and revised the manuscript.

FUNDING

This study was supported, in part, by the Natural Sciences and Engineering Research Council of Canada, the St. Boniface Hospital Foundation, and the Molson's Foundation.

ACKNOWLEDGMENTS

The authors wish to acknowledge the technical assistance of V. Sid for tissue collection procedure.

REFERENCES

1. Grams ME, Rabb H. The distant organ effects of acute kidney injury. *Kidney Int*. (2012) 81:942–8. doi: 10.1038/ki.2011.241
2. Yap SC, Lee HT. Acute kidney injury and extrarenal organ dysfunction: new concepts and experimental evidence. *Anesthesiology*. (2012) 116:1139–48. doi: 10.1097/ALN.0b013e31824f951b
3. Doi K, Rabb H. Impact of acute kidney injury on distant organ function: recent findings and potential therapeutic targets. *Kidney Int*. (2016) 89:555–64. doi: 10.1016/j.kint.2015.11.019
4. Miyazawa S, Watanabe H, Miyaji C, Hotta O, Abo T. Leukocyte accumulation and changes in extra-renal organs during renal ischemia reperfusion in mice. *J Lab Clin Med*. (2002) 139:269–78. doi: 10.1067/mlc.2002.122832
5. Husain-Syed F, Rosner MH, Ronco C. Distant organ dysfunction in acute kidney injury. *Acta Physiol*. (2020) 228:e13357. doi: 10.1111/apha.13357

6. Thadhani R, Pascual M, Bonventre JV. Acute renal failure. *N Engl J Med*. (1996) 334:1448–60. doi: 10.1056/NEJM199605303342207
7. Mehta RL, Pascual MT, Soroko S, Savage BR, Himmelfarb J, Ikizler TA, et al. Spectrum of acute renal failure in the intensive care unit: the PICARD experience. *Kidney Int*. (2004) 66:1613–21. doi: 10.1111/j.1523-1755.2004.00927.x
8. Lameire N, van Biesen W, Vanholder R. Acute renal failure. *Lancet*. (2005) 365:417–30. doi: 10.1016/S0140-6736(05)70238-5
9. Hassoun HT, Grigoryev DN, Lie ML, Liu M, Cheadle C, Tuder RM, et al. Ischemic acute kidney injury induces a distant organ functional and genomic response distinguishable from bilateral nephrectomy. *Am J Physiol Renal Physiol*. (2007) 293:F30–40. doi: 10.1152/ajprenal.00023.2007
10. Kelly KJ. Distant effects of experimental renal ischemia/reperfusion injury. *J Am Soc Nephrol*. (2003) 14:1549–58. doi: 10.1097/01.ASN.0000064946.94590.46
11. Liu M, Liang Y, Chigurupati S, Lathia JD, Pletnikov M, Sun Z, et al. Acute kidney injury leads to inflammation and functional changes in the brain. *J Am Soc Nephrol*. (2008) 19:1360–70. doi: 10.1681/ASN.2007080901
12. Druml W. Systemic consequences of acute kidney injury. *Curr Opin Crit Care*. (2014) 20:613–9. doi: 10.1097/MCC.0000000000000150
13. Ologunde R, Zhao H, Lu K, Ma D. Organ cross talk and remote organ damage following acute kidney injury. *Int Urol Nephrol*. (2014) 46:2337–45. doi: 10.1007/s11255-014-0766-2
14. Lane K, Dixon JJ, MacPhee IA, Philips BJ. Renohepatic crosstalk: does acute kidney injury cause liver dysfunction? *Nephrol Dial Transplant*. (2013) 28:1634–47. doi: 10.1093/ndt/gft091
15. Shang Y, Siow YL, Isaak CK, Karmin O. Downregulation of glutathione biosynthesis contributes to oxidative stress and liver dysfunction in acute kidney injury. *Oxid Med Cell Longev*. (2016) 2016:9707292. doi: 10.1155/2016/9707292
16. Park SW, Chen SW, Kim M, Brown KM, Kolls JK, D'Agati VD, et al. Cytokines induce small intestine and liver injury after renal ischemia or nephrectomy. *Lab Invest*. (2011) 91:63–84. doi: 10.1038/labinvest.2010.151
17. Bagshaw SM, Laupland KB, Doig CJ, Mortis G, Fick GH, Mucenski M, et al. Prognosis for long-term survival and renal recovery in critically ill patients with severe acute renal failure: a population-based study. *Crit Care*. (2005) 9:R700–9. doi: 10.1186/cc3879
18. Chertow GM, Christiansen CL, Cleary PD, Munro C, Lazarus JM. Prognostic stratification in critically ill patients with acute renal failure requiring dialysis. *Arch Intern Med*. (1995) 155:1505–11. doi: 10.1001/archinte.155.14.1505
19. Liano F, Pascual J. Epidemiology of acute renal failure: a prospective, multicenter, community-based study. Madrid acute renal failure study group. *Kidney Int*. (1996) 50:811–8. doi: 10.1038/ki.1996.380
20. Mehta RL. Refining predictive models in critically ill patients with acute renal failure. *J Am Soc Nephrol*. (2002) 13:1350–7. doi: 10.1097/01.ASN.0000014692.19351.52
21. Golab F, Kadkhodaee M, Zahmatkesh M, Hedayati M, Arab H, Schuster R, et al. Ischemic and non-ischemic acute kidney injury cause hepatic damage. *Kidney Int*. (2009) 75:783–92. doi: 10.1038/ki.2008.683
22. Thurman JM. Triggers of inflammation after renal ischemia/reperfusion. *Clin immunol*. (2007) 123:7–13. doi: 10.1016/j.clim.2006.09.008
23. Wang P, Isaak CK, Siow YL, Karmin O. Downregulation of cystathionine β-synthase and cystathionine γ-lyase expression stimulates inflammation in kidney ischemia-reperfusion injury. *Physiol Rep*. (2014) 2:e12251. doi: 10.14814/phy2.12251
24. Lee DW, Faubel S, Edelstein CL. Cytokines in acute kidney injury (AKI). *Clin Nephrol*. (2011) 76:165–73. doi: 10.5414/CN106921
25. Akcay A, Nguyen Q, Edelstein CL. Mediators of inflammation in acute kidney injury. *Mediators Inflamm*. (2009) 2009:137072. doi: 10.1155/2009/137072
26. Sung FL, Zhu TY, Au-Yeung KK, Siow YL, Karmin O. Enhanced MCP-1 expression during ischemia/reperfusion injury is mediated by oxidative stress and NF-kappaB. *Kidney Int*. (2002) 62:1160–70. doi: 10.1111/j.1523-1755.2002.kid577.x
27. Lawrence T. The nuclear factor NF-kappaB pathway in inflammation. *Cold Spring Harb Perspect Biol*. (2009) 1:a001651. doi: 10.1101/cshperspect.a001651
28. Wang P, Zhu Q, Wu N, Siow YL, Aukema H, Karmin O. Tyrosol attenuates ischemia-reperfusion-induced kidney injury via inhibition of inducible nitric oxide synthase. *J Agric Food Chem*. (2013) 61:3669–75. doi: 10.1021/jf400227u
29. Gardner DS, De Brot S, Dunford LJ, Grau-Roma L, Welham SJ, Fallman R, et al. Remote effects of acute kidney injury in a porcine model. *Am J Physiol Renal Physiol*. (2016) 310:F259–71. doi: 10.1152/ajprenal.00389.2015
30. Prathapasinghe GA, Siow YL, Karmin O. Detrimental role of homocysteine in renal ischemia-reperfusion injury. *Am J Physiol Renal Physiol*. (2007) 292:F1354–63. doi: 10.1152/ajprenal.00301.2006
31. Wu N, Siow YL, Karmin O. Ischemia/reperfusion reduces transcription factor Sp1-mediated cystathionine β-synthase expression in the kidney. *J Biol Chem*. (2010) 285:18225–33. doi: 10.1074/jbc.M110.132142
32. Hwang SY, Sarna LK, Siow YL, Karmin O. High-fat diet stimulates hepatic cystathionine β-synthase and cystathionine gamma-lyase expression. *Can J Physiol Pharmacol*. (2013) 91:913–9. doi: 10.1139/cjpp-2013-0106
33. Andres-Hernando A, Dursun B, Altmann C, Ahuja N, He Z, Bhargava R, et al. Cytokine production increases and cytokine clearance decreases in mice with bilateral nephrectomy. *Nephrol Dial Transplant*. (2012) 27:4339–47. doi: 10.1093/ndt/gfs256
34. Prathapasinghe GA, Siow YL, Xu Z, Karmin O. Inhibition of cystathionine-beta-synthase activity during renal ischemia-reperfusion: role of pH and nitric oxide. *Am J Physiol Renal Physiol*. (2008) 295:F912–22. doi: 10.1152/ajprenal.00040.2008
35. Wang G, Siow YL, Karmin O. Homocysteine stimulates nuclear factor kappaB activity and monocyte chemoattractant protein-1 expression in vascular smooth-muscle cells: a possible role for protein kinase C. *Biochem J*. (2000) 352(Pt 3):817–26. doi: 10.1042/bj3520817
36. Au-Yeung KK, Woo CW, Sung FL, Yip JC, Siow YL, Karmin O. Hyperhomocysteinemia activates nuclear factor-kappaB in endothelial cells via oxidative stress. *Circ Res*. (2004) 94:28–36. doi: 10.1161/01.RES.0000108264.67601.2C
37. Cheung GT, Siow YL, Karmin O. Homocysteine stimulates monocyte chemoattractant protein-1 expression in mesangial cells via NF-kappaB activation. *Can J Physiol Pharmacol*. (2008) 86:88–96. doi: 10.1139/Y08-002

Conflict of Interest: The authors declare that the research was conducted in the absence of any commercial or financial relationships that could be construed as a potential conflict of interest.

frontiers in Cell and Developmental Biology

ORIGINAL RESEARCH
published: 05 June 2020
doi: 10.3389/fcell.2020.00398

Cathepsin S and Protease-Activated Receptor-2 Drive Alloimmunity and Immune Regulation in Kidney Allograft Rejection

Yutian Lei[1†], Benjamin Ehle[2†], Santhosh V. Kumar[1], Susanne Müller[3], Solange Moll[4], Andrew F. Malone[5], Benjamin D. Humphreys[5,6], Joachim Andrassy[2*] and Hans-Joachim Anders[1*]*

[1] Division of Nephrology, Department of Medicine IV, University Hospital, LMU Munich, Munich, Germany, [2] Division for General, Visceral, Transplant, Vascular and Thoracic Surgery, University Hospital, LMU Munich, Munich, Germany, [3] Department of Pathology, University of Munich, Munich, Germany, [4] Institute of Clinical Pathology, University Hospital Geneva, Geneva, Switzerland, [5] Division of Nephrology, Department of Medicine, Washington University in Saint Louis School of Medicine, St. Louis, MO, United States, [6] Department of Developmental Biology, Washington University in Saint Louis School of Medicine, St. Louis, MO, United States

OPEN ACCESS

Edited by:
Songjie Cai,
Brigham and Women's Hospital and Harvard Medical School, United States

Reviewed by:
Robert L. Fairchild,
Cleveland Clinic, United States
Toshiaki Tanaka,
Sapporo Medical University, Japan

***Correspondence:**
Yutian Lei
leiyutian1234@gmail.com
Joachim Andrassy
joachim.andrassy@med.uni-muenchen.de
Hans-Joachim Anders
Hans-Joachim.Anders@med.uni-muenchen.de

[†] These authors have contributed equally to this work

Specialty section:
This article was submitted to Molecular Medicine, a section of the journal Frontiers in Cell and Developmental Biology

Received: 03 February 2020
Accepted: 29 April 2020
Published: 05 June 2020

Citation:
Lei Y, Ehle B, Kumar SV, Müller S, Moll S, Malone AF, Humphreys BD, Andrassy J and Anders H-J (2020) Cathepsin S and Protease-Activated Receptor-2 Drive Alloimmunity and Immune Regulation in Kidney Allograft Rejection. Front. Cell Dev. Biol. 8:398. doi: 10.3389/fcell.2020.00398

Alloantigen presentation is an essential process in acute allorejection. In this context, we speculated on a pathogenic role of cathepsin S (Cat-S), a cysteine protease known to promote antigenic peptide loading into MHC class II and to activate protease-activated receptor (PAR)-2 on intrarenal microvascular endothelial and tubular epithelial cells. Single-cell RNA sequencing and immunostaining of human kidney allografts confirmed Cat-S expression in intrarenal mononuclear phagocytes. *In vitro*, Cat-S inhibition suppressed CD4 + T cell lymphocyte activation in a mixed lymphocyte assay. *In vivo*, we employed a mouse model of kidney transplantation that showed preemptive Cat-S inhibition significantly protected allografts from tubulitis and intimal arteritis. To determine the contribution of PAR-2 activation, first, Balb/c donor kidneys were transplanted into Balb/c recipient mice without signs of rejection at day 10. In contrast, kidneys from C57BL/6J donor mice revealed severe intimal arteritis, tubulitis, interstitial inflammation, and glomerulitis. Kidneys from *Par2*-deficient C57BL/6J mice revealed partial protection from tubulitis and lower intrarenal expression levels for *Fasl*, *Tnfa*, *Ccl5*, and *Ccr5*. Together, we conclude that Cat-S and PAR-2 contribute to immune dysregulation and kidney allograft rejection, possibly involving Cat-S-mediated activation of PAR-2 on recipient parenchymal cells in the allograft.

Keywords: kidney transplantation, cathepsin S, allorejection, proteinase-activated receptor-2, animal model of transplantation

INTRODUCTION

Among the different forms of renal replacement, therapy kidney transplantation, when available, is the preferred option for most patients with end-stage kidney disease (Wolfe et al., 1999; Robinson et al., 2016). Alloimmunity remains an important factor limiting graft survival, and life-long treatment with relatively non-specific immunosuppressants has remained the standard of care

to date for the vast majority of patients (Durrbach et al., 2010). More selective interference with alloimmunity may broaden the range of options for those patients facing drug toxicity.

Presentation of alloantigen's is a central path mechanism of alloimmunity and involves MHC class II molecules on professional antigen-presenting cells (Borges et al., 2016; Robson et al., 2018). Within antigen-presenting cells, the maturation of MHC class II molecules is tightly regulated, whereby the invariant chain covers the peptide-binding domain up to when peptide loading occurs and the molecule is shuttled to the cell surface (Roche and Frusta, 2015; Robson et al., 2018). Cathepsin (Cat-) S is one of several proteases that chop the invariant chain in a stepwise process (Shi et al., 1999; Roche and Frusta, 2015); hence, Cat-S deficiency or pharmaceutical Cat-S inhibition prevents MHC class II–mediated (auto)antigen presentation (Rise et al., 1996, 1998; Dresden et al., 1999; Saugus et al., 2002; Stickle et al., 2012). Indeed, Cat-S inhibition effectively suppresses the immune dysregulation in numerous experimental autoimmune diseases (Saugus et al., 2002; Baugh et al., 2011; Rupanagudi et al., 2015; Tato et al., 2017).

Beyond its role inside cells, monocytes/macrophages, neutrophils, and endothelial cells secrete Cat-S in the extracellular space where it processes several matrix proteins (Lutgens et al., 2007; Reiser et al., 2010). For example, its elastase activity contributes to vascular wall degeneration in atherosclerosis and aortic aneurysm formation (Shi et al., 2003; Sukhova et al., 2003; Rodgers et al., 2006; Aikawa et al., 2009; Samokhin et al., 2010; Qin et al., 2012; Figueiredo et al., 2015). Indeed, increased serum levels of Cat-S are associated with several cardiovascular risk factors including chronic kidney disease (Jobs et al., 2011, 2013; Lv et al., 2012). As a new finding, we and others recently described that Cat-S activates protease-activated receptor (PAR)-2 on vascular endothelial cells in a thrombin-like manner (Elmariah et al., 2014; Zhao et al., 2014; Kumar et al., 2016). Cat-S-driven PAR-2 activation induced endothelial dysfunction, a central path mechanism in microvascular complications of diabetic mellitus or systemic autoimmunity (Kumar et al., 2016; Tato et al., 2017).

As both mechanisms, MHC class II–mediated antigen presentation and microvascular injury also contribute to immune dysregulation and allograft dysfunction in solid organ transplantation, we hypothesized that interfering with either Cat-S or PAR-2 would attenuate organ injury in a robust model of allograft rejection. To address this concept, we decided for a rigorous mouse model of acute kidney allograft rejection without further immunosuppressive therapy.

MATERIALS AND METHODS

Single-Cell RNA Sequencing of Human Kidney Biopsies

Tissue Processing

The renal biopsy was minced into small pieces with a razor blade and incubated at 37°C in freshly prepared dissociation buffer containing 0.25% trypsin and 40 U/ml DNase I, filtered resuspended in buffer (9% OptiPrep). Nuclei from normal human nephrectomy tissue were isolated with Nuclei EZ Lysis buffer with protease inhibitor and RNase inhibitor. Samples were cut into <2-mm pieces, homogenized, and incubated on ice for 5 min with an additional 2 ml of lysis buffer. The homogenate was filtered, centrifuged, resuspended in suspension Buffer (1 × PBS, 0.07% BSA, 0.1% RNase inhibitor), and counted.

InDrops Single-Cell RNA-Seq

InDrops was performed as described (Klein et al., 2015). In brief, cells were diluted into 60,000 cells/ml in 9% OptiPrep buffer. Single-cell encapsulation was carried out using an inDrops instrument and microfluidic chip manufactured by 1CellBio. In total, 4000 cells were collected. Library preparation was performed according to the protocol provided by the manufacturer. Libraries were sequenced by HiSeq 2500 with a sequencing depth of 50K mapped reads/cell.

10× Single-Nucleus RNA-Seq

RNAs from 6000 single nuclei loaded into one lane of the 10 × Genomics 3-prime V2 platform were encapsulated, barcoded, and reversed transcribed. The library was sequenced in HiSeq 2500 with a sequencing depth of 12.5K mapped reads/cell.

Data Preprocessing

We used the inDrops computational pipeline, dropEst (Klein et al., 2015), to process the single-cell InDrops data. We used STAR to map the high-quality reads to the human genome (GRCh38). We next ran the dropEst program to estimate the accurate molecular counts, which generated a UMI count matrix for each gene in each cell. We used the zUMIs computational pipeline to process the single nuclei data according to protocol (Parekh et al., 2018). In brief, fastq files were filtered for low-quality barcodes and unique molecular identifier (UMIs). Next, cDNA reads were mapped to the reference genome using STAR. Count matrices were generated for exon + intron overlapping reads. These count matrices were used for downstream analysis.

Unsupervised Clustering and Cell Type Identification

UMI count matrices were loaded into the R package Seurat. For normalization, the DGE matrix was scaled by total UMI counts, multiplied by 10,000, and transformed to log space. Only genes found to be expressed in >10 cells were retained. Cells with a relatively high percentage of UMIs mapped to mitochondrial genes (≥0.3) were discarded. Moreover, cells with fewer than 300 or more than 4,000 detected genes were omitted, resulting in 4,487 cells. We also regressed out the variants arising from library size and percentage of mitochondrial genes using the function RegressOut in R package Seurat. The highly variable genes were identified using the function MeanVarPlot with the parameters x.low.cutoff = 0.0125, x.high.cutoff = 6, and y.cutoff = 1, resulting in an output of 2,404 highly variable genes. The expression level of highly variable genes in the cells was scaled and centered along each gene and was conducted to principal component analysis. Based on PCElbowPlot and PCHeatmap Seurat function analysis, we first selected 20 PCs for two-dimensional t-distributed stochastic neighbor embedding (tSNE), implemented by the Seurat software with the default parameters. Based on the

tSNE map, sixteen clusters were identified using the function FindCluster in Seurat with the resolution parameter set to 0.6. We applied the same unsupervised clustering analysis on the single nucleus dataset. After filtering low-quality nuclei, 4,609 nuclei with >400 genes expressed were imported into Seurat for clustering analysis. In total, we identified 13 cell types in the single nucleus dataset, which included macrophages and endothelial cells. Integrated analysis of rejecting and normal human kidney was performed using the Seurat function IntegrateData.

Immunohistochemistry in Human Renal Biopsies

Human renal tissue, fixed in formaldehyde and embedded in paraffin, was selected from the files of the Service of Pathology, University Hospital Geneva: control normal renal tissue was obtained from two patients with nephrectomy performed for neoplasia, involving the possibility of tumor-related immune exhaustion. Five biopsy specimens were obtained from renal transplant patients with acute T cell–mediated rejection. For all biopsy specimens, standard analyses were performed. Each patient gave informed consent before enrollment. The institutional ethical committee board approved the clinical protocol (CEREH number 03-081). The research was performed according to the Helsinki's declaration principles. For immunostaining, serial paraffin sections were stained with the primary antibodies anti-cathepsin S (monoclonal mouse anti-human Cat-S, LSBio, Seattle, WA, United States) and anti-CD68 (DakoCytomation, Glostrup, Denmark) or double stained with anti-cathepsin S and anti-CD68. Counterstaining was performed using Mayer hematoxylin. Negative controls included the absence of the primary antibody (not shown).

Bone Marrow–Derived Dendritic Cell Isolation and Differentiation

For bone marrow–derived dendritic cell (BMDC) preparation, cells were isolated and cultured according to a standard method with minor modifications (Han et al., 1999). Briefly, bone marrow cells were cultured in RPMI 1640 media supplemented with 1% penicillin and streptomycin, 10% of fetal calf serum (S0115, EMD Millipore, United States), 20 ng/ml of mouse recombinant IL-4 and GM-CSF (ImmunoTools, Friesoythe, Germany). At day 8, non-adherent cells were transferred to a fresh plate, primed by 500 μg/ml lipopolysaccharide (LPS, Sigma) for another 24 h, and used for MLR. In BMDC stimulation assays, non-adherent cells were transferred to 12-well plate at 2×10^6/ml at day 8, stimulated with indicated stimuli for 24 h, and analyzed by flow cytometry.

Mixed Lymphocyte Reaction

For *in vitro* assessment of allogenic T-cell activation, mixed lymphocyte reaction (MLR) was set up by incubating T cell–enriched splenocytes together with bone marrow–derived dendritic cells (BMDCs). C57BL/6 (H-2b) and Balb/c (H-2d) mice were used at the age of 7–15 weeks. For T cell preparation, pan T-cells were enriched from splenocytes by a magnetic bead–based negative selection method (Mouse Pan T-cell Isolation Kit II, Miltenyi Biotec, Germany) according to the manufacturer's instruction (purity >90%, data not shown). Purified T cells were labeled with 5 μM carboxyfluorescein succinimidyl ester (CFSE) dye (CellTrace^{TM} CFSE Cell Proliferation Kit, Invitrogen) for 5 min according to the manufacturer's instruction. For proliferation assay, 1.5×10^5 CFSE-labeled T cells and 1×10^5 of primed BMDCs were cocultured in round bottom 96-well plate (Nunc, Germany) for 4 days. Mixed cells were afterward analyzed by flow cytometry to evaluate the proliferation.

Flow Cytometry Analysis

Single-cell suspensions from BMDC stimulation assay or MLR were washed in cold DPBS (PAN Biotech, Germany) twice and suspended in cold FACS buffer (DPBS with 1% BSA and 0.05% sodium azide). Single-cell suspensions were first treated with anti-mouse CD16/32 antibody (BioLegend, United States). Cells from BMDC stimulation assay were stained for anti-mouse CD11c-PE (clone HL3, BioLegend, United States) and anti-mouse MHCII-FITC (clone M5/114.15.2, BioLegend, United States). Cells from MLR were stained for anti-mouse CD8-PE (clone 53-6,7, BioLegend, United States) and then stained for anti-mouse CD4-APC antibody (RM4-4 clone, BioLegend, United States). Samples were analyzed on a flow cytometry analyzer (BD FACSCalibur). For analysis of proliferation, after gating in live/CD4 + CD8- or live/CD4-CD8 +, CFSE histograms were deconvoluted to differentiate each daughter generation from parent cells by software (FlowJo, version 7.6.5) (**Supplementary Figure S1A**). Division index was calculated by the ratio of the total number of divisions over the number of cells at start of culture.

Lactate Dehydrogenase Cytotoxicity Assay

Lactate dehydrogenase (LDH) cytotoxicity assay was set up by mixing 1.5×10^5 of CFSE-stained T cells and 1×10^5 of LPS-primed BMDCs in RPMI 1640 media supplemented with 1% penicillin and streptomycin and 10% of fetal calf serum. Cells were incubated for 4 days. At day 4, cell death was evaluated using LDH cell cytotoxicity assay kit (Roche, Mannheim, Germany) according to the manufacturer's protocol.

Animal Study Design

C57BL/6J (H2b) and Balb/c (H2d) mice were obtained from Charles River (Sulzfeld, Germany) and used at the age of 8–12 weeks. *Par2*-/- mice in the C57BL/6J background were purchased from Jackson Laboratory (Bar Harbor, ME, United States). Offspring were genotyped by polymerase chain reaction (PCR) of genomic DNA derived from tail clippings. Animals were assigned by stratified randomization to different groups co-housed in groups of five in filter top cages with unlimited access to food and water. Cages, nestlets, food, and water were sterilized by autoclaving before use. Humane endpoints were monitored throughout the study. All experiments were conducted according to the European equivalent of the NIH's Guide for the Care and Use of Laboratory Animals and had been approved by the local government authorities.

Kidney transplantations were performed as previously described (Skoskiewicz et al., 1973). Following a midline abdominal incision, the left kidney, aorta, and inferior vena cava of the donor were fully exposed and mobilized. The kidney was procured en bloc including the renal vein; the renal artery, along with a small aortic cuff; and the ureter. The vessels of the graft were anastomosed end-to-side to the recipient's abdominal aorta and inferior vena cava using 10-0 nylon sutures (AROSurgical, Newport Beach, CA, United States). For urinary tract reconstruction, the ureter was directly anastomosed into the bladder using a pull-through (Han et al., 1999). The times of cold and warm ischemia of the graft were maintained at 40 and 30 min, respectively. The native kidneys of the recipient remained untouched as this was a non-life-sustaining approach.

Primary Endpoint: Harvested allografts were split in half and either paraffin embedded or snap frozen and kept at −80°C. Light microscopy was performed on HE- and PAS-stained whole cross sections of kidney allografts. An experienced blinded nephropathologist (S. M.) evaluated and scored for tubulitis, intimal arteritis, interstitial inflammation, and glomerulitis as well as periarteritis using a 4-point-score (0–3) and assigned a score according to the Banff criteria (Haas et al., 2014).

Secondary Endpoints: Real-time reverse transcription-polymerase chain reaction (RT-PCR). Gene expression was assessed by real-time quantitative RT-PCR as described (Lech et al., 2010). In brief, total RNA was isolated using an RNA extraction kit (Life Technologies, Darmstadt, Germany) according to the manufacturer's instructions. After isolation of RNA, cDNA was generated using reverse transcriptase (Superscript II; Invitrogen, Carlsbad, CA, United States). A SYBR Green Dye detection system was used for quantitative real-time PCR on Light Cycler 480 (Roche, Mannheim, Germany) using SYBR Green (SABiosciences) as marker and 18s rRNA as a housekeeping gene. Gene-specific primers blasted with ensemble-BLAST and NCBI primer-BLAST (Metabion, Martinsried, Germany) were used. The following are forward and reverse gene-specific primers, respectively (300 nM; Metabion, Martinsried, Germany): 18s, GCAATTATTCCCCATGAACG and AGG GCCTCACTAAACCATCC; *Ifng*, TGAGCTCATTGAATGCTT GG and ACAGCAAGGCGAAAAAGGAT; *Fasl*, TTAAATGGG CCACACTCCTC and ACTCCGTGAGTTCACCAACC; *Ctss*, GAGTCCCATAGCCAACCACAAG and AAGCGGTGTCTATG ACGACCC; and *Ccl5*, GTGCCCACGTCAAGGAGTAT and CCACTTCTTCTCTGGGTTGG; *Ccr5*, GTCTACTTTCTCTT CTGGACTCC and CCAAGAGTCTCTGTTGCCTGCA; *Foxp3*, CTGGACACCCATTCCAGACT and TTCATGCATCAGCTC TCCAC; *Il2ra*, GCGTTGCTTAGGAAACTCCTGG and GCATA GACTGTGTTGGCTTCTGC, *Cd8b1*, GAATGTGAAGCCAGA GGACAGTG and GGGCAGTTGTAGGAAGGACATC; *Cd4*, GTTCAGGACAGCGACTTCTGGA and GAAGGAGAACTCC GCTGACTCT. Non-template controls consisting of all used reagents were negative for target and housekeeping genes. To reduce the risk of false-positive crossing point, the high-confidence algorithm was used. The melting curve profiles were analyzed for every sample to detect eventual unspecific products or primer dimers.

Histology was a secondary endpoint. Kidneys were fixed in 4% formalin, embedded in paraffin. Immunostaining was performed as described using anti-mouse MHC-II (1:100, clone M5/114.15.2, eBioscience, United States) (Kumar et al., 2016).

Statistical Analysis

Normal data distribution was tested using the Shapiro–Wilk test. Comparisons between two groups were performed with Student's *t*-test or Mann–Whitney *U* test. Comparison of multiple groups was performed with ANOVA or Kruskal–Wallis test; a multiple comparison test was performed with Dunnett or Dunn's correction, respectively. A value of $p < 0.05$ was considered to indicate statistical significance. Data are presented as mean ± SD.

RESULTS

Cathepsin S–Positive Cells Accumulate in Rejecting Human Kidney Allografts

We compared single-cell Cat-S expression (CTSS) in human kidney allograft with mixed rejection and normal human kidney (Wu et al., 2018). Integrated analysis of rejecting and normal human kidney identified 16-cell clusters including all major tubular and immune cell types and endothelial cells (**Figure 1A**). Compared to normal kidney, high expression of CTSS is seen in macrophages and intercalated cells (**Figures 1B** upper, **1C** left). To confirm these data, we performed immunostaining in biopsies from transplanted patients diagnosed with kidney allograft rejection, as well as biopsies from healthy controls. As shown in **Figure 2A**, Cat-S-positive cells were sparse in the interstitium of healthy kidneys and were most likely expressed by CD68 + cells. In contrast, we found numerous CD68/Cat-S double-positive cells accumulating in rejected allografts (**Figure 2B**). Together, Cat-S was strongly expressed inside human kidney allografts.

Cathepsin S Inhibition Suppresses Alloimmune Lymphocyte Proliferation *in vitro*

As Cat-S is a non-redundant component in MHC class II–driven antigen presentation, it should also drive MHC class II–related alloantigen presentation and alloimmunity. We tested this concept by performing mixed lymphocyte assays (**Figure 3A**) and measured CD4 + T lymphocyte division as a readout for alloantigen-specific lymphocyte activation. As shown in **Figure 3B**, Cat-S inhibition did not significantly affect BMDC MHC class II expression. In MLR, however, Cat-S inhibitor–treated groups had less proportion of divided CD4 + T cells (**Figure 3C**). Quantification of the division index also showed that the Cat-S inhibitor suppressed CD4 + T cell and CD8 + T cell division in a dose-dependent manner (**Figures 3D,E**). This effect was independent of cytotoxicity of the Cat-S inhibitor as LDH release was identical in all groups (**Figure 3F**). Thus, we conclude that Cat-S inhibition blocks alloimmune CD4 + and CD8 + T lymphocyte proliferation *in vitro*.

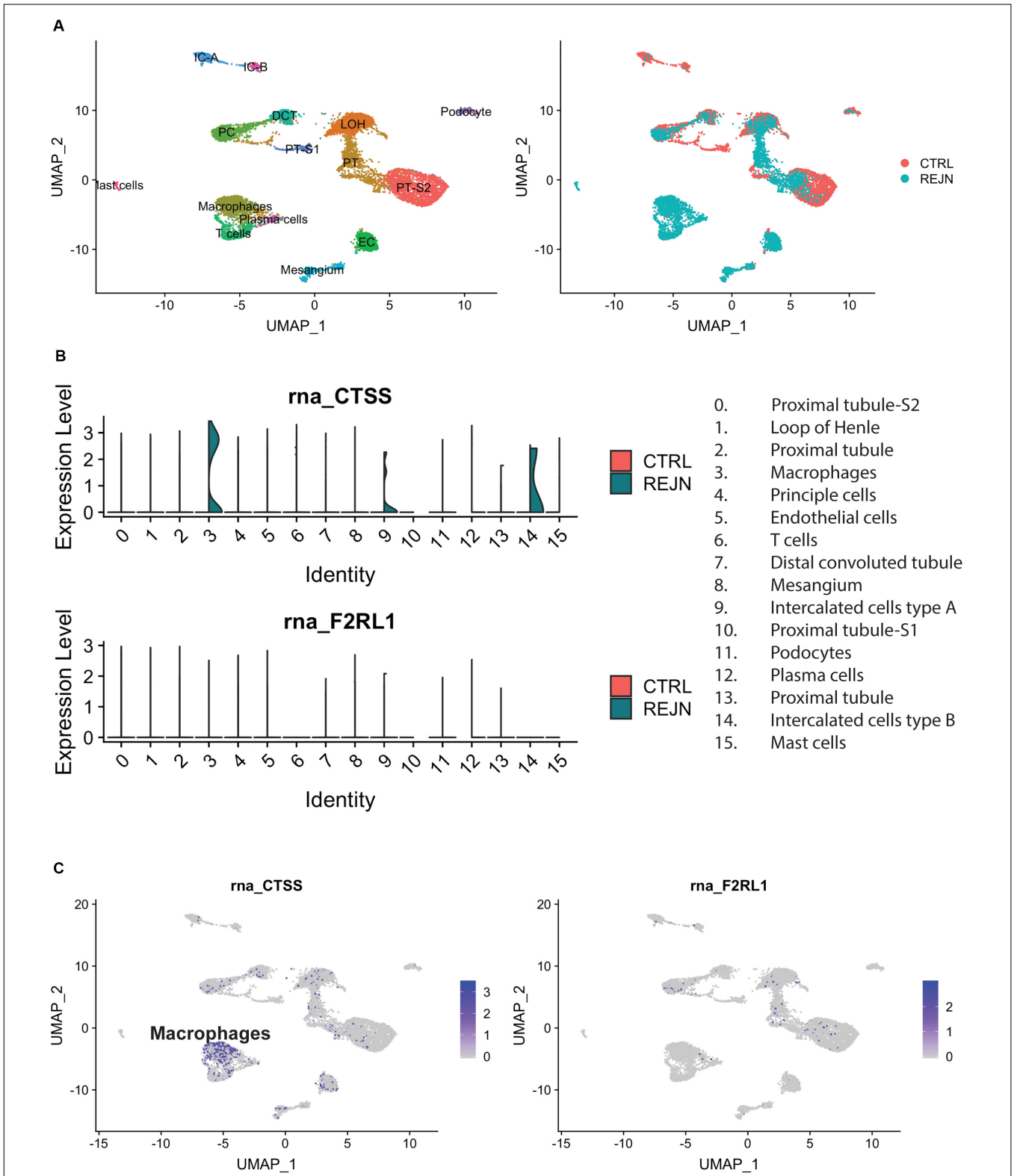

FIGURE 1 | Cat-S and PAR-2 gene expression in healthy and rejected human kidney biopsies by single-cell RNA-seq. **(A)** UMAP plots of combined correlation analysis of a mixed rejection kidney transplant biopsy and a healthy human kidney tissue sample. Left: cell clusters labeled by cell type. Right: clusters labeled according to rejection (blue) or healthy (red) kidney. **(B)** Violin plots of Cat-S (*CTSS*) and PAR-2 (*F2RL1*) gene expression per cell type, in rejection (green) and healthy (red). Upper: *CTSS* expression. Lower: *F2RL1* expression. **(C)** Feature UMAP plots of Cat-S (left) and PAR2 (right) expression. Purple color demotes high gene expression.

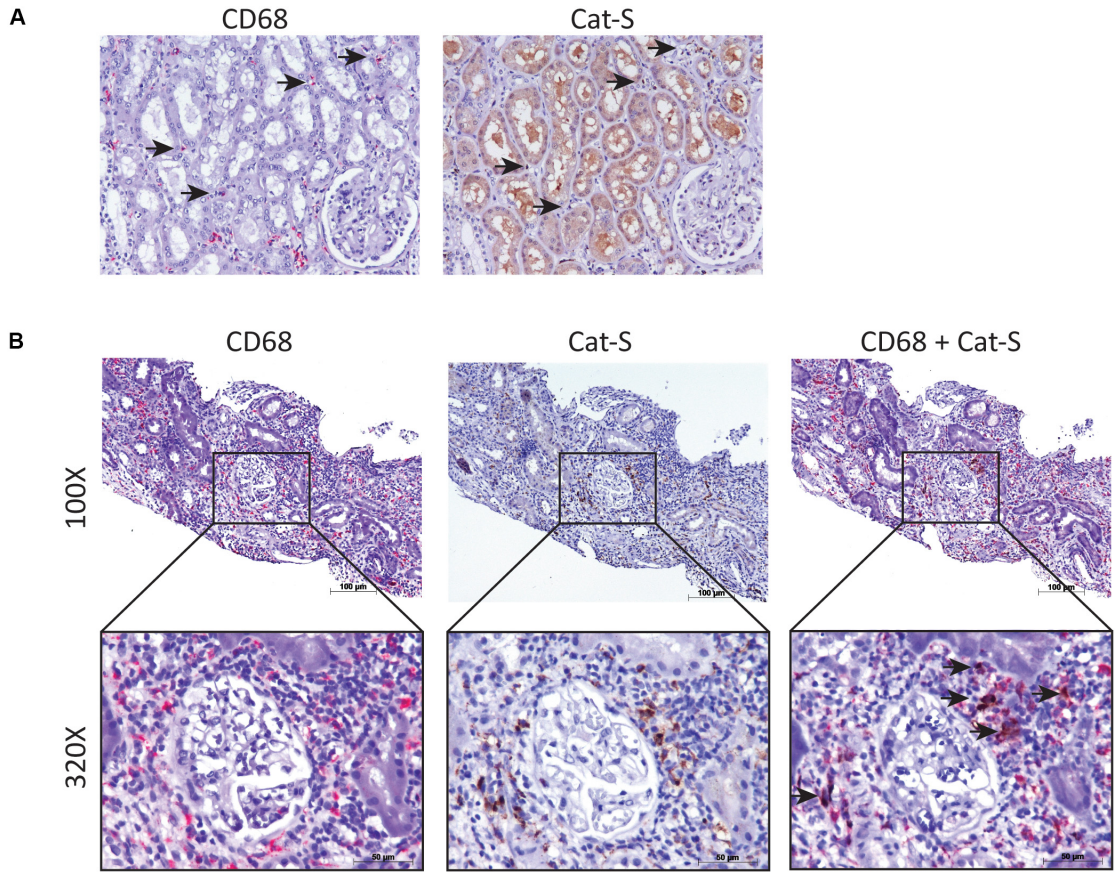

FIGURE 2 | Cat-S expression in kidney biopsies from renal transplant patients with acute T cell–mediated rejection by immunostaining. **(A)** Cat-S and CD68 staining in health human kidney tissue. Consecutive kidney slides were stained for CD68 (left, in red) and Cat-S (right, in brown). CD68-positive cells and Cat-S-positive cells were marked by black arrows. Magnification 200×. **(B)** Cat-S and CD68 staining in rejecting human kidney allografts. CD68 single staining (left), Cat-S single staining (middle), and Cat-S/CD68 double staining (right) was performed on tissues from patients undergoing kidney rejection. Cat-S/CD68 double-positive cells were marked by black arrow.

Preemptive Cathepsin S Inhibition Attenuates Acute Kidney Allograft Rejection

Based on these findings, we tested whether Cat-S inhibition can attenuate kidney allograft rejection *in vivo*. We set up an experimental model based on C57BL/6J (H2b)–recipient mice (**Figure 4A**). We investigated the Cat-S expression in transplanted kidneys. Compared to syngeneic controls, allograft showed numerous Cat-S-positive cells accumulating in the interstitium, especially around vessels (**Figure 4B**). Likewise, Cat-S gene expression was also significantly induced in allograft (**Figure 4C**). Transplanting a kidney from a donor of the same strain showed minimal differences in the histological picture compared to the native kidneys 10 days after the surgery, implying that the transplant procedure *per se* was reliably performed and did not cause tissue damage by ischemia–reperfusion injury (**Figure 4D**). In contrast, kidneys from Balb/c (H2d) donor mice showed signs of severe rejection with tubulitis, glomerulitis, intimal arteritis, and interstitial inflammation (**Figure 4D**). Treating recipient mice with the Cat-S inhibitor RO5461111 completely abrogated tubulitis, intimal arteritis, but not glomerulitis and interstitial inflammation (**Figure 4D**). As a further sign of intrarenal inflammation, quantitative RT-PCR of total kidney RNA revealed increased levels of proinflammatory mediators such as *Ccl5*, *Ccr5*, *Fasl*, and *Ifng* (**Figure 4E**). Cat-S inhibition reduced intrarenal expression levels of above genes. Cat-S inhibition also reduced *Cd4* and *Cd8b1* gene expression (**Figure 4F**). However, it did not affect Foxp3 or Il2ra gene expression (**Supplementary Figure S1B**). The Cat-S inhibitor also did not affect MHC class II expression in graft (**Figure 4G** and **Supplementary Figure S1D**). Cat-S inhibition reduced intrarenal expression levels of the above genes (**Figure 4E**). Taken together, Cat-S inhibition substantially attenuates kidney allograft rejection.

Lack of *Par2* in the Kidney Allograft Attenuates Acute Rejection in Recipient Balb/c Mice

PAR-2 is a G protein receptor and acts as the receptor for many extracellular enzymes, such as Cat-S, trypsin, and tryptase.

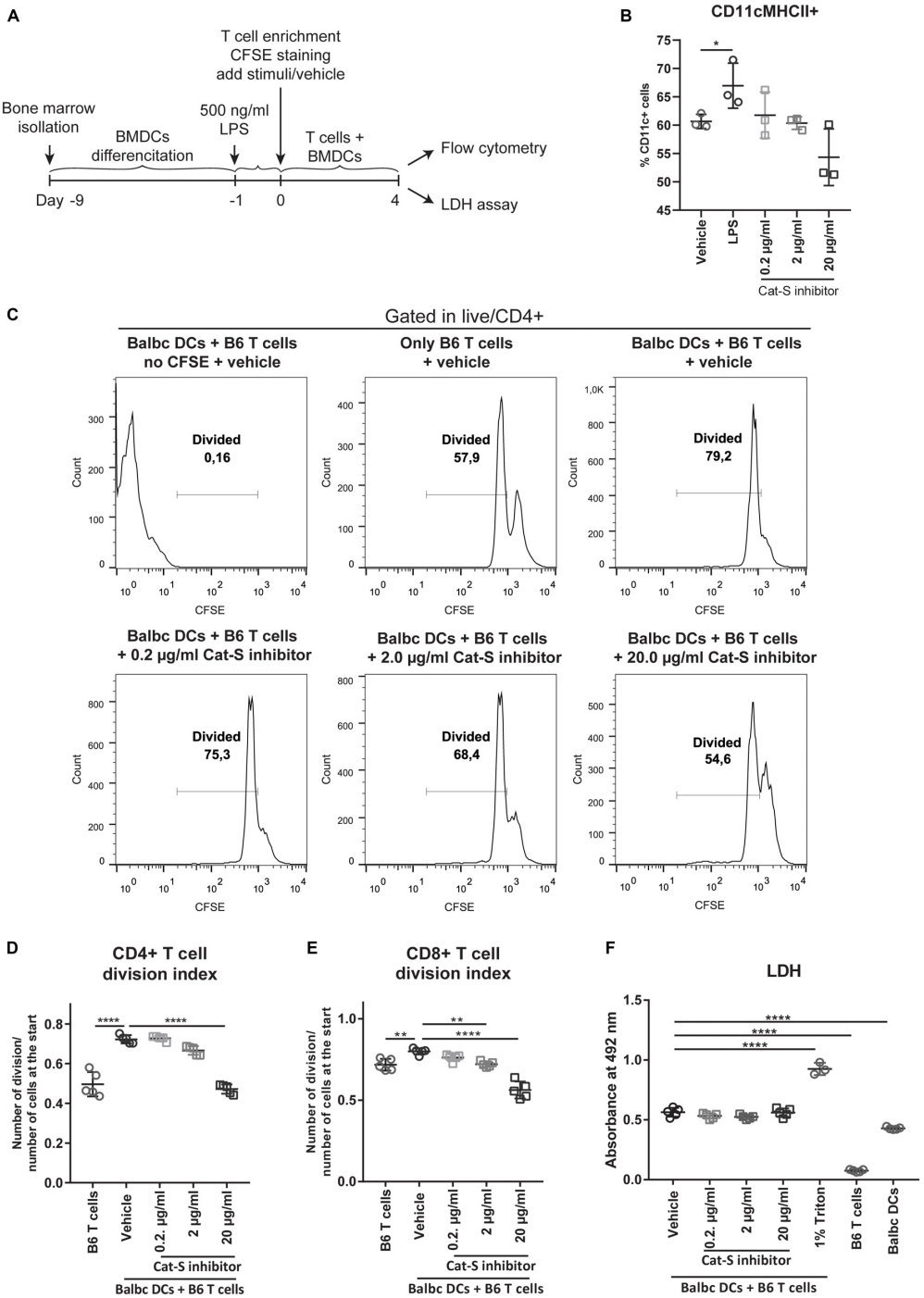

FIGURE 3 | Effect of Cat-S inhibitor on MLR and cytotoxicity. **(A)** Experiment design of mixed lymphocyte reaction for proliferation and LDH assay. LPS-primed BMDCs (Balb/c) and CFSE-stained T cells (C57BL/6J) were used as stimulator and responder, respectively. Mixed cells were cocultured for 4 days and analyzed by flow cytometry or LDH assay. **(B)** BMDC stimulation assays. BMDCs were stimulated with 500 ng/ml LPS, Cat-S inhibitor, or vehicle for 24 h and analyzed for MHC-II expression among CD11c + cells. **(C)** CD4 + T cell proliferation monitored using CFSE labeling. Mixed cells were in the presence of 0.2, 2, 20 µg/ml, or vehicle, and proliferation was analyzed by flow cytometry at 4 days of culture. As controls, mixed cells with no CFSE were treated as the same way as vehicle but without CFSE staining; single T cells were treated with vehicle but without adding BMDCs. After gating in CD4 + cells, divided cells were gated in the histograms of the CFSE channel. A representative experiment from two separate experiments is shown. For each experiment, one mouse was used for BMDC differentiation and two mice were used for T cell isolation. Two or three replications was made from each T cell host for MLR. **(D)** Division index of CD4 + T cells. Based on the deconvoluted histograms of the CFSE channel, the division index was calculated by the ratio of the total number of divisions over the number of cells at start of culture. **(E)** The division index of CD8 + T cells. **(F)** LDH assay for Cat-s inhibitor–treated cells. Supernatant of mixed cell culture was analyzed at day 4 by LDH. $^{*}p < 0.05$, $^{**}p < 0.01$, $^{****}p < 0.0001$.

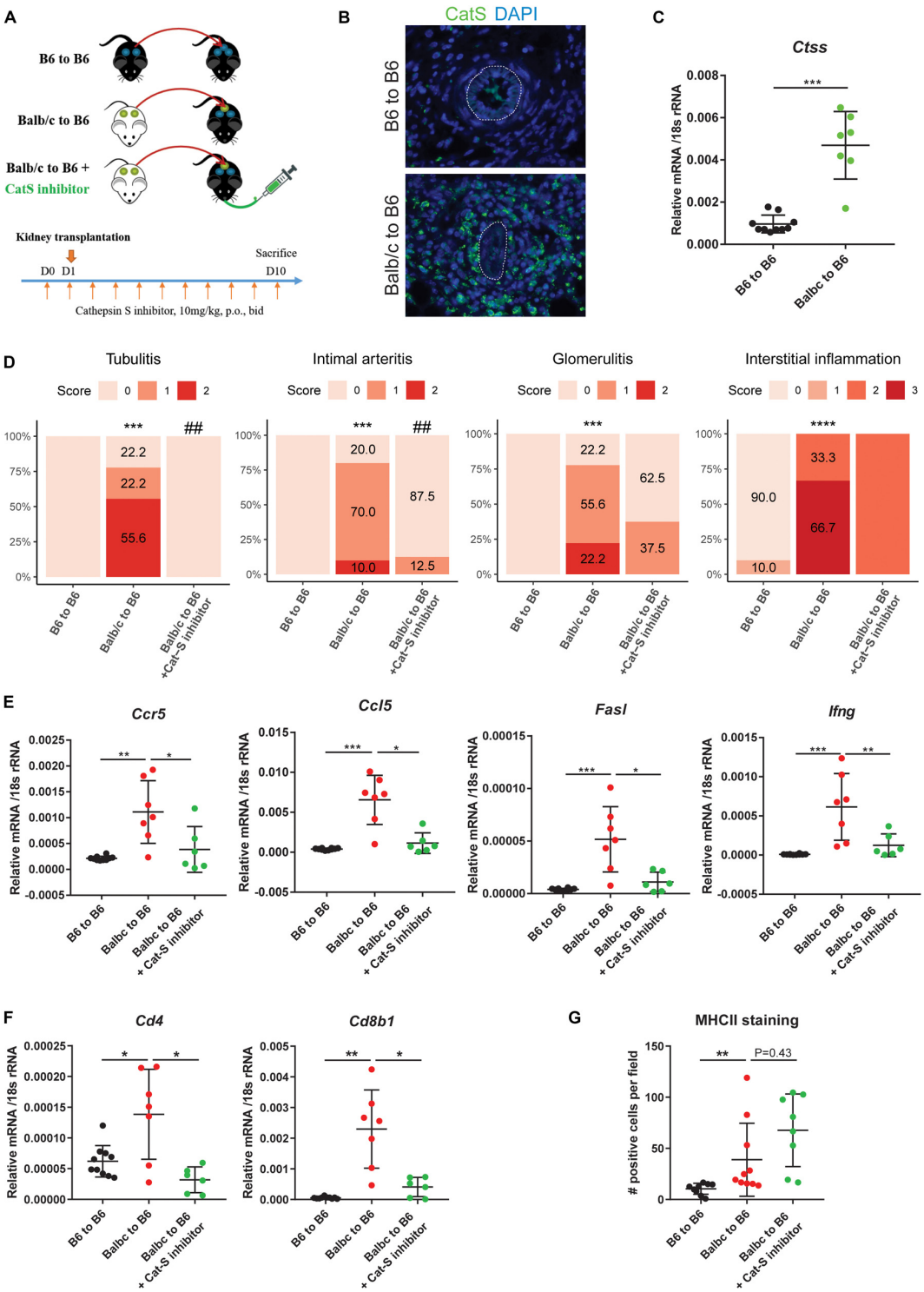

FIGURE 4 | Cathepsin S inhibition attenuated renal allograft rejection *in vivo*. **(A)** Experimental design. Wild-type C57BL/6 kidneys (syngeneic) or wild-type Balb/c kidneys (allogeneic) were transplanted into wild-type C57BL/6 mice. Allogenic recipients were orally administrated with either vehicle or Cat-S inhibitor 10 mg/kg twice daily for a total of 11 days. At day 10 after transplantation, mice were analyzed. **(B)** Cat-S staining in mouse kidney grafts from syngeneic (B6 to B6) and allogeneic group (Balb/c to B6). White dash lines represent for vessels. Magnification 200×. **(C)** *Ctss* mRNA expression in mouse kidney grafts. **(D)** Histological score for mouse kidney grafts. Tubulitis, intimal arteritis, glomerulitis, and interstitial inflammation were quantified by Banff scoring method. $^{***}p < 0.001$ Balb/c to B6 vs. B6 to B6; $^{****}p < 0.0001$ Balb/c to B6 vs. B6 to B6; $^{\#\#}p < 0.01$ Balb/c to B6 vs. Balb/c to B6 + Cat-S inhibitor. $N = 10$ for B6 to B6, $n = 9$–10 for Balb/c to B6, $n = 8$–10 for Balb/c to B6 + Cat-S inhibitor. **(E)** Proinflammation gene expression in mouse kidney grafts by RT-qPCR. **(F)** Cd4 and Cd8b1 gene expression in mouse kidney grafts. **(G)** Quantification of interstitial MHC-II positive cells in mouse kidney graft. $^{*}p < 0.05$; $^{**}p < 0.01$; $^{***}p < 0.001$. B6 represents for C56BL/6J.

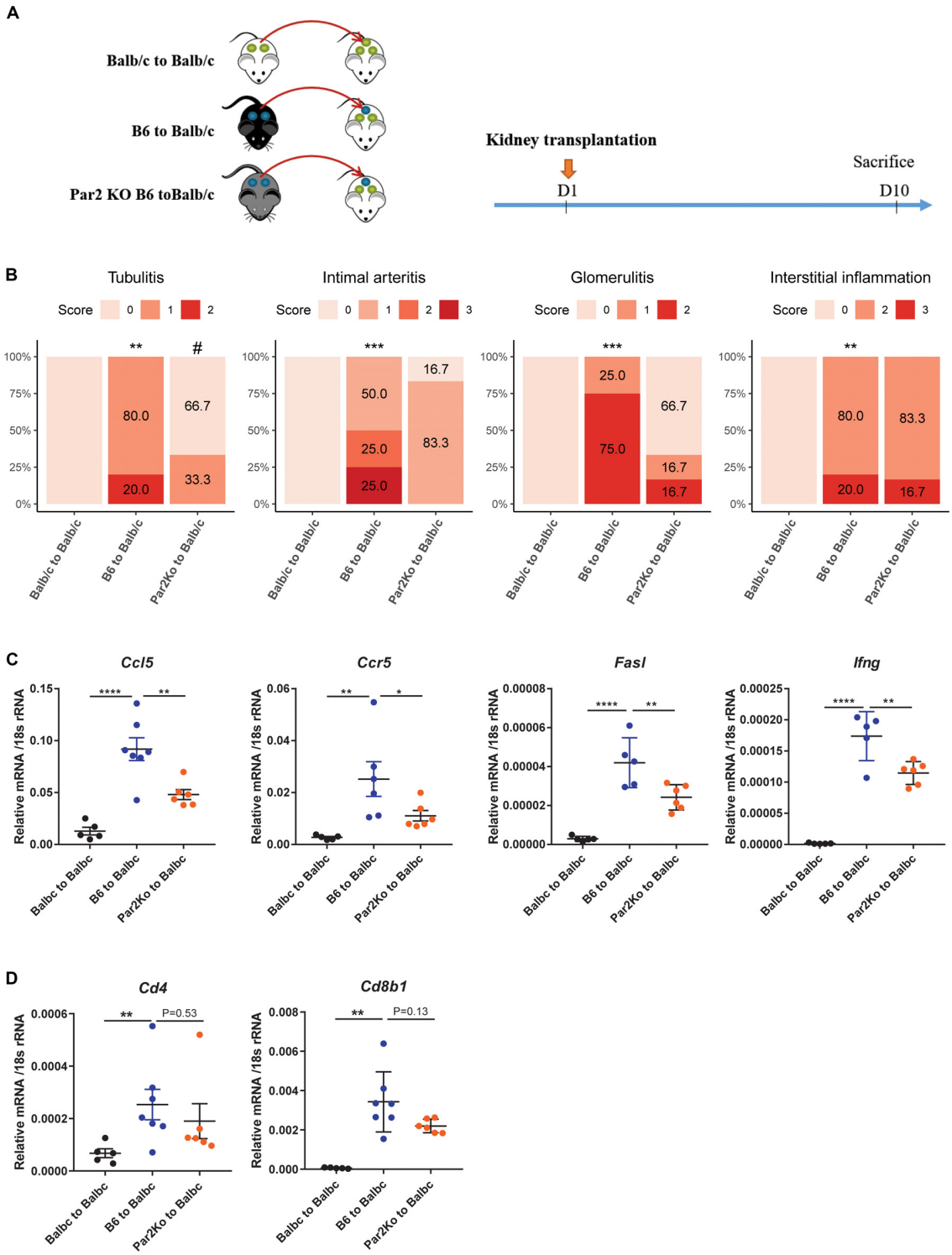

FIGURE 5 | *Par2* deficiency in grafts attenuated renal allograft rejection *in vivo*. **(A)** Experimental design. Wild-type Balb/c kidneys (syngeneic) or wild-type C57BL/6 (allogeneic) were transplanted to wild-type Balb/c mice. *Par2*-deficient kidneys from C67BL/6 background (allogeneic) were transplanted into wild-type Balb/c mice. At day 10 after transplantation, mice were sacrificed for analysis. **(B)** Histological score for mouse kidney grafts. Tubulitis, intimal arteritis, glomerulitis, and interstitial inflammation were quantified by the Banff scoring method. $^{**}p < 0.01$ B6 to Balb/c vs. Balb/c to Balb/c, $^{***}p < 0.001$ B6 to Balb/c vs. Balb/c to Balb/c, $^{\#}p < 0.05$ B6 to Balb/c vs. Par2KO to Balb/c. $N = 4$ for Balb/c to Balb/c, $n = 4$–6 for B6 to Balb/c, $n = 6$ for Par2KO to Balb/c. **(C)** Proinflammation gene expression in mouse kidney grafts by RT-qPCR. **(D)** *Cd4* and *Cd8b1* gene expression in mouse kidney grafts. $^{*}p < 0.05$, $^{**}p < 0.01$, $^{***}p < 0.001$, $^{****}p < 0.0001$. B6 represents for C56BL/6J. Par2KO represent for *Par2* deficiency.

The Cat-S/PAR-2 axis was previously reported to play a role in itch, pain, and diabetic microvasculopathy (Kumar et al., 2016; Zhao et al., 2014; Mihara et al., 2016). Interestingly, using single-cell sequencing data of human kidney allograft rejection, we found F2RL1, the human gene encoding for PAR-2 to be expressed at low levels by several renal parenchymal cell types including endothelial cells and tubular epithelial cells (**Figures 1B** lower, **1C** right). We therefore asked whether PAR-2 also plays a role in this setting. We designed the animal experiment as shown in **Figure 5A**. Compared to kidneys from wild-type B6 donors, kidneys from *Par2*-deficient donor mice showed significantly less tubulitis, non-significant trends toward less glomerulitis, and less intimal arteritis, and no effect on interstitial inflammation (**Figure 5B**). However, *Par2*-deficient allografts also showed reduced expression of the inflammatory genes *Ccl5*, *Ccr5*, *Fasl*, and *Ifng* (**Figure 5C**). In contrast to mice treated with Cat-S inhibitor, Par2-deficient allografts did not show reduced mRNA expression of Cd4 and Cd8b1 (**Figure 5D**) and of *Foxp3* and Il-2ra (**Supplementary Figure S1C**). Together, donor *Par2* deficiency attenuates acute allograft rejection.

DISCUSSION

We had hypothesized that interfering with either Cat-S or PAR-2 would attenuate kidney injury in a robust model of renal allograft rejection. We tested this concept using a pharmacological inhibitor of Cat-S and genetic *Par2* deficiency in different versions of the same kidney transplant model in mice based on the two strains C57Bl/6J (H2b) and Balb/c (H2d). By avoiding additional immunosuppressive therapy, we tested the role of these targets in severe acute rejection. The results confirm the hypothesis and identify Cat-S/PAR-2 as potential molecular targets in the context of solid organ transplantation.

Alloantigen recognition is a central path mechanism of alloimmunity. Both donor- and recipient-derived antigen-presenting cells activate recipient alloreactive T cells to proliferate and circulate, a process leading to alloantigen recognition inside the graft and local alloimmunity, i.e., rejection. These processes involve both MHC class I and II molecules of which peptide loading into MHC class II but not class I molecules is controlled by Cat-S (Rise et al., 1996). In support of this concept, Cat-S inhibition suppressed lymphocyte proliferation in a mixed lymphocyte assay, an accepted *in vitro* model of alloantigen recognition (Ansari and Strom, 2010). Our *in vivo* data further demonstrate that preemptive Cat-S inhibition was sufficient to suppress some aspects of acute renal allograft rejection, namely, tubulitis and arteritis, while, e.g., interstitial inflammation was hardly affected. This may relate to the contribution of MHC class I–mediated alloantigen recognition, and this suggests that monotherapy with a Cat-S inhibitor may be insufficient to control allograft rejection. In this regard, alloimmunity significantly differs from autoimmunity, which can be well controlled by Cat-S inhibitor monotherapy (Rupanagudi et al., 2015; Tato et al., 2017).

However, we and others have previously shown that Cat-S inhibition also prevents Cat-S-mediated activation of PAR-2 on vascular endothelial cells and thereby attenuates endothelial dysfunction–related organ injury (Kumar et al., 2016). In the setting of kidney transplantation, this would imply a potential dual renoprotective effect of Cat-S inhibition, one on alloantigen recognition and one of microvascular injury in the allograft. Indeed, our data show a considerable renoprotective effect of genetic *Par2* deficiency in the allograft. This genetic approach overcomes some of the concerns related to small molecule inhibitors such as exposure, dosing, dosing intervals, and specificity. Nevertheless, we found similar renoprotective effects as compared to the Cat-S inhibitor, indicating that the renoprotective effects of the Cat-S inhibitor largely relate to its activity at PAR-2. However, *Par2* deficiency also abrogates the activity of other serum proteases such as thrombin, which can have similar biological effects (Mihara et al., 2016). Although specific targeting of PAR-2 with drugs would be feasible, in the setting of solid organ transplantation targeting the dual activity of Cat-S appears more promising, potentially in combination with an immunosuppressive drug that also controls MHC class I–mediated alloimmunity.

Obviously, our study presents with some limitations. First, we could not ultimately prove that the *Par2*-dependent effects relate to Cat-S activity. Also, other proteases such as thrombin induce PAR-2 signaling on endothelium and tubular epithelial cells (Vesey et al., 2013; Mihara et al., 2016). Second, because of the robust nature of the acute rejection, it was difficult to quantify immune cell infiltrates and endothelial integrity properly and the life-non-sustaining transplantation technique did not allow testing for renal function. Finally, it would have been desirable to validate the experiments with Cats-deficient mice but such mice fulfilling the microbial requirements of our animal facility could not be obtained.

Together, Cat-S and PAR-2 are potential molecular targets in acute renal allograft rejection. Further studies will evaluate its potential in models that mimic more closely the clinical scenario of acute (and chronic) human allograft rejection.

DATA AVAILABILITY STATEMENT

The datasets generated for this study can be found in the GSE109564 and GSE114156.

ETHICS STATEMENT

The studies involving human participants were reviewed and approved by Committee board University of Geneva (CEREH number 03-081). The patients/participants provided their written informed consent to participate in this study. The animal study was reviewed and approved by Regierung von Oberbayern, Germany.

AUTHOR CONTRIBUTIONS

JA, SK, and H-JA designed the study. BE, SK, and YL performed the mouse study. SuM performed the Banff scoring of mouse kidney. YL and SK performed the *in vitro* study and the mouse sample analysis except Banff scoring. SoM performed the immunostaining of human biopsies. AM and BH performed the single-cell sequencing. YL and H-JA prepared the manuscript. All authors revised and approved the final version of the manuscript.

FUNDING

YL was supported by China Scholarship Council Scholarship. Parts of this project were prepared as a doctoral thesis at the Faculty of Medicine, University of Munich, by BE. This study was supported by the Deutsche Forschungsgemeinschaft (AN372/24-1 to H-JA).

ACKNOWLEDGMENTS

We thank Dan Draganovic, Jana Mandelbaum, Yvonne Minor, Lidia Anguiano Gómez, and Thomas Cagarelli for their expert technical assistance.

SUPPLEMENTARY MATERIAL

The Supplementary Material for this article can be found online at: https://www.frontiersin.org/articles/10.3389/fcell.2020.00398/full#supplementary-material

FIGURE S1 | (A) Gating strategy for proliferation analysis of mixed lymphocyte reaction. **(B)** Foxp3 and Il2ra gene expression in mouse kidney grafts from mice treated with Cat-S inhibitor or vehicle. **(C)** Foxp3 and Il2ra gene expression in mouse kidney grafts from wild type or Par2 deficient mice. **(D)** Representative images of MHC-II staining in mouse kidney grafts treated with Cat-S inhibitor or vehicle. Magnification, 200×.

REFERENCES

Aikawa, E., Aikawa, M., Libby, P., Figueiredo, J. L., Rusanescu, G., Iwamoto, Y., et al. (2009). Arterial and aortic valve calcification abolished by elastolytic cathepsin S deficiency in chronic renal disease. *Circulation* 119, 1785–1794. doi: 10.1161/CIRCULATIONAHA.108.827972

Ansari, M. J., and Strom, T. B. (2010). "Chapter 42 - novel diagnostics in transplantation," in *Chronic Kidney Disease, Dialysis, and Transplantation*, 3rd Edn, eds J. Himmelfarb and M. H. Sayegh (Philadelphia: W.B. Saunders), 609–619. doi: 10.1016/b978-1-4377-0987-2.00042-x

Baugh, M., Black, D., Westwood, P., Kinghorn, E., McGregor, K., Bruin, J., et al. (2011). Therapeutic dosing of an orally active, selective cathepsin S inhibitor suppresses disease in models of autoimmunity. *J. Autoimmun.* 36, 201–209. doi: 10.1016/j.jaut.2011.01.003

Borges, T. J., Murakami, N., and Riella, L. V. (2016). Current status of alloimmunity. *Curr. Opin. Nephrol. Hypertens.* 25, 556–562. doi: 10.1097/mnh.0000000000000267

Dresden, C., Bryant, R. A., Lennon-Dumenil, A. M., Villadangos, J. A., Bryant, P. W., Shi, G. P., et al. (1999). Cathepsin S controls the trafficking and maturation of MHC class II molecules in dendritic cells. *J. Cell Biol.* 147, 775–790. doi: 10.1083/jcb.147.4.775

Durrbach, A., Francois, H., Beaudreuil, S., Jacquet, A., and Charpentier, B. (2010). Advances in immunosuppression for renal transplantation. *Nat. Rev. Nephrol.* 6, 160–167. doi: 10.1038/nrneph.2009.233

Elmariah, S. B., Reddy, V. B., and Lerner, E. A. (2014). Cathepsin S signals via PAR2 and generates a novel tethered ligand receptor agonist. *PloS One* 9:e99702. doi: 10.1371/journal.pone.0099702

Figueiredo, J. L., Aikawa, M., Zheng, C., Aaron, J., Lax, L., Libby, P., et al. (2015). Selective cathepsin S inhibition attenuates atherosclerosis in apolipoprotein E-deficient mice with chronic renal disease. *Am. J. Pathol.* 185, 1156–1166. doi: 10.1016/j.ajpath.2014.11.026

Haas, M., Sis, B., Racusen, L. C., Solez, K., Glotz, D., Colvin, R. B., et al. (2014). Banff 2013 meeting report: inclusion of c4d-negative antibody-mediated rejection and antibody-associated arterial lesions. *Am. J. Transplant.* 14, 272–283. doi: 10.1136/bmjopen-2017-020904

Han, W. R., Murray-Segal, L. J., and Mottram, P. L. (1999). Modified technique for kidney transplantation in mice. *Microsurgery* 19, 272–274. doi: 10.1002/(sici)1098-2752(1999)19:6<272::aid-micr3>3.0.co;2-l

Jobs, E., Ingelsson, E., Riserus, U., Nerpin, E., Jobs, M., Sundstrom, J., et al. (2011). Association between serum cathepsin S and mortality in older adults. *JAMA* 306, 1113–1121. doi: 10.1001/jama.2011.1246

Jobs, E., Riserus, U., Ingelsson, E., Sundstrom, J., Jobs, M., Nerpin, E., et al. (2013). Serum cathepsin S is associated with decreased insulin sensitivity and the development of type 2 diabetes in a community-based cohort of elderly men. *Diabetes Care* 36, 163–165. doi: 10.2337/dc12-0494

Klein, A. M., Mazutis, L., Akartuna, I., Tallapragada, N., Veres, A., Li, V., et al. (2015). Droplet barcoding for single-cell transcriptomics applied to embryonic stem cells. *Cell* 161, 1187–1201. doi: 10.1016/j.cell.2015.04.044

Kumar, S. V., Darisipudi, M. N., Steiger, S., Devarapu, S. K., Tato, M., Kukarni, O. P., et al. (2016). Cleavage of protease-activated receptor-2 on endothelial cells promotes microvascular diabetes complications. *J. Am. Soc. Nephrol.* 27, 1635–1649. doi: 10.1681/ASN.2015020208

Lech, M., vila-Ferrufino, A. A., Skuginna, V., Susanti, H. E., and Anders, H. J. (2010). Quantitative expression of RIG-like helicase, NOD-like receptor and inflammasome-related mRNAs in humans and mice. *Int. Immunol.* 22, 717–728. doi: 10.1093/intimm/dxq058

Lutgens, S. P., Cleutjens, K. B., Daemen, M. J., and Heeneman, S. (2007). Cathepsin cysteine proteases in cardiovascular disease. *FASEB J.* 21, 3029–3041. doi: 10.1096/fj.06-7924com

Lv, B. J., Lindholt, J. S., Cheng, X., Wang, J., and Shi, G. P. (2012). Plasma cathepsin S and cystatin C levels and risk of abdominal aortic aneurysm: a randomized population-based study. *PloS One* 7:e41813. doi: 10.1371/journal.pone.0041813

Mihara, K., Ramachandran, R., Saifeddine, M., Hansen, K. K., Renaux, B., Polley, D., et al. (2016). Thrombin-mediated direct activation of proteinase-activated receptor-2: another target for thrombin signaling. *Mol. Pharmacol.* 89, 606–614. doi: 10.1124/mol.115.102723

Parekh, S., Ziegenhain, C., Vieth, B., Enard, W., and Hellmann, I. (2018). zUMIs - A fast and flexible pipeline to process RNA sequencing data with UMIs. *GigaScience* 7:giy059. doi: 10.1093/gigascience/giy059

Qin, Y., Cao, X., Guo, J., Zhang, Y., Pan, L., Zhang, H., et al. (2012). Deficiency of cathepsin S attenuates angiotensin II-induced abdominal aortic aneurysm formation in apolipoprotein E-deficient mice. *Cardiovasc. Res.* 96, 401–410. doi: 10.1093/cvr/cvs263

Reiser, J., Adair, B., and Reinheckel, T. (2010). Specialized roles for cysteine cathepsins in health and disease. *J. Clin. Investig.* 120, 3421–3431. doi: 10.1172/jci42918

Rise, R. J., Mitchell, R. N., Villadangos, J. A., Shi, G. P., Palmer, J. T., Karp, E. R., et al. (1998). Cathepsin S activity regulates antigen presentation and immunity. *J. Clin. Investig.* 101, 2351–2363. doi: 10.1172/jci1158

Rise, R. J., Wolf, P. R., Bromme, D., Natkin, L. R., Villadangos, J. A., Ploegh, H. L., et al. (1996). Essential role for cathepsin S in MHC class II-associated invariant chain processing and peptide loading. *Immunity* 4, 357–366. doi: 10.1016/s1074-7613(00)80249-6

Robinson, B. M., Akizawa, T., Jager, K. J., Kerr, P. G., Saran, R., and Pisoni, R. L. (2016). Factors affecting outcomes in patients reaching end-stage kidney disease worldwide: differences in access to renal replacement therapy, modality use,

and haemodialysis practices. *Lancet* 388, 294–306. doi: 10.1016/S0140-6736(16)30448-2

Robson, K. J., Ooi, J. D., Holdsworth, S. R., Rossjohn, J., and Kitching, A. R. (2018). HLA and kidney disease: from associations to mechanisms. *Nat. Rev. Nephrol.* 14, 636–655. doi: 10.1038/s41581-018-0057-8

Roche, P. A., and Frusta, K. (2015). The ins and outs of MHC class II-mediated antigen processing and presentation. *Nat. Rev. Immunol.* 15, 203–216. doi: 10.1038/nri3818

Rodgers, K. J., Watkins, D. J., Miller, A. L., Chan, P. Y., Karanam, S., Brissette, W. H., et al. (2006). Destabilizing role of cathepsin S in murine atherosclerotic plaques. *Arterioscler. Thromb. Vasc. Biol.* 26, 851–856. doi: 10.1161/01.atv.0000203526.75772.4b

Rupanagudi, K. V., Kulkarni, O. P., Lichtnekert, J., Darisipudi, M. N., Mulay, S. R., Schott, B., et al. (2015). Cathepsin S inhibition suppresses systemic lupus erythematosus and lupus nephritis because cathepsin S is essential for MHC class II-mediated CD4 T cell and B cell priming. *Ann. Rheum. Dis.* 74, 452–463. doi: 10.1136/annrheumdis-2013-203717

Saugus, K., Ishimaru, N., Yanagi, K., Arakaki, R., Ogawa, K., Saito, I., et al. (2002). Cathepsin S inhibitor prevents autoantigen presentation and autoimmunity. *J. Clin.Investig.* 110, 361–369. doi: 10.1172/jci0214682

Samokhin, A. O., Lythgo, P. A., Gauthier, J. Y., Percival, M. D., and Bromme, D. (2010). Pharmacological inhibition of cathepsin S decreases atherosclerotic lesions in Apoe-/- mice. *J. Cardiovasc. Pharmacol.* 56, 98–105. doi: 10.1097/FJC.0b013e3181e23e10

Shi, G. P., Sukhova, G. K., Kuzuya, M., Ye, Q., Du, J., Zhang, Y., et al. (2003). Deficiency of the cysteine protease cathepsin S impairs microvessel growth. *Circ. Res.* 92, 493–500. doi: 10.1161/01.res.0000060485.20318.96

Shi, G. P., Villadangos, J. A., Dranoff, G., Small, C., Gu, L., Haley, K. J., et al. (1999). Cathepsin S required for normal MHC class II peptide loading and germinal center development. *Immunity* 10, 197–206. doi: 10.1016/s1074-7613(00)80020-5

Skoskiewicz, M., Chase, C., Winn, H. J., and Russell, P. S. (1973). Kidney transplants between mice of graded immunogenetic diversity. *Transplant. Proc.* 5, 721–725.

Stickle, C., Quecke, P., Ruckrich, T., Burster, T., Reich, M., Weber, E., et al. (2012). Cathepsin S dominates autoantigen processing in human thymic dendritic cells. *J. Autoimmun.* 38, 332–343. doi: 10.1016/j.jaut.2012.02.003

Sukhova, G. K., Zhang, Y., Pan, J. H., Wada, Y., Yamamoto, T., Naito, M., et al. (2003). Deficiency of cathepsin S reduces atherosclerosis in LDL receptor-deficient mice. *J. Clin. Investig.* 111, 897–906. doi: 10.1172/jci200314915

Tato, M., Kumar, S. V., Liu, Y., Mulay, S. R., Moll, S., Popper, B., et al. (2017). Cathepsin S inhibition combines control of systemic and peripheral pathomechanisms of autoimmune tissue injury. *Sci. Rep.* 7:2775. doi: 10.1038/s41598-017-01894-y

Vesey, D. A., Suen, J. Y., Seow, V., Lohman, R. J., Liu, L., Gobe, G. C., et al. (2013). PAR2-induced inflammatory responses in human kidney tubular epithelial cells. *Am. J. Physiol. Renal Physiol.* 304, F737–F750. doi: 10.1152/ajprenal.00540.2012

Wolfe, R. A., Ashby, V. B., Milford, E. L., Ojo, A. O., Ettenger, R. E., Agodoa, L. Y., et al. (1999). Comparison of mortality in all patients on dialysis, patients on dialysis awaiting transplantation, and recipients of a first cadaveric transplant. *N. Engl. J. Med.* 341, 1725–1730. doi: 10.1056/nejm199912023412303

Wu, H., Malone, A. F., Donnelly, E. L., Kirita, Y., Uchimura, K., Ramakrishnan, S. M., et al. (2018). Single-cell transcriptomics of a human kidney allograft biopsy specimen defines a diverse inflammatory response. *J. Am. Soc. Nephrol.* 29, 2069–2080. doi: 10.1681/ASN.2018020125

Zhao, P., Lieu, T., Barlow, N., Metcalf, M., Veldhuis, N. A., Jensen, D. D., et al. (2014). Cathepsin S causes inflammatory pain via biased agonism of PAR2 and TRPV4. *J. Biol. Chem.* 289, 27215–27234. doi: 10.1074/jbc.M114.599712

Conflict of Interest: The authors declare that the research was conducted in the absence of any commercial or financial relationships that could be construed as a potential conflict of interest.

frontiers in Medicine

ORIGINAL RESEARCH
published: 10 July 2020
doi: 10.3389/fmed.2020.00305

Histone Methylation Inhibitor DZNep Ameliorated the Renal Ischemia-Reperfusion Injury *via* Inhibiting TIM-1 Mediated T Cell Activation

Jiawei Li[1,2†], *Yue Qiu*[2,3†], *Long Li*[4†], *Jiyan Wang*[1,2], *Yin Celeste Cheuk*[1,2], *Ruirui Sang*[2], *Yichen Jia*[1,2], *Jina Wang*[1,2], *Yi Zhang*[2,5*] *and Ruiming Rong*[1,2*]

[1] Department of Urology, Zhongshan Hospital, Fudan University, Shanghai, China, [2] Shanghai Key Laboratory of Organ Transplantation, Shanghai, China, [3] Department of Critical Care Medicine, Zhongshan Hospital, Fudan University, Shanghai, China, [4] Department of Urology, Shanghai Ninth People's Hospital, Shanghai Jiaotong University School of Medicine, Shanghai, China, [5] Biomedical Research Center, Institute for Clinical Sciences, Zhongshan Hospital, Fudan University, Shanghai, China

OPEN ACCESS

Edited by:
Songjie Cai,
Brigham and Women's Hospital,
United States

Reviewed by:
Gurvinder Kaur,
All India Institute of Medical Sciences, India
Hee-Seong Jang,
University of Nebraska Medical Center, United States

***Correspondence:**
Yi Zhang
yzhang_med@fudan.edu.cn
Ruiming Rong
rong.ruiming@zs-hospital.sh.cn

[†]These authors have contributed equally to this work

Specialty section:
This article was submitted to Nephrology, a section of the journal Frontiers in Medicine

Received: 26 January 2020
Accepted: 27 May 2020
Published: 10 July 2020

Citation:
Li J, Qiu Y, Li L, Wang J, Cheuk YC, Sang R, Jia Y, Wang J, Zhang Y and Rong R (2020) Histone Methylation Inhibitor DZNep Ameliorated the Renal Ischemia-Reperfusion Injury via Inhibiting TIM-1 Mediated T Cell Activation. Front. Med. 7:305. doi: 10.3389/fmed.2020.00305

Renal ischemia-reperfusion injury (IRI) after renal transplantation often leads to the loss of kidney graft function. However, there is still a lack of efficient regimens to prevent or alleviate renal IRI. Our study focused on the renoprotective effect of 3-Deazaneplanocin A (DZNep), which is a histone methylation inhibitor. We found that DZNep significantly alleviated renal IRI by suppressing nuclear factor kappa-B (NF-κB), thus inhibiting the expression of inflammatory factors in renal tubular epithelial cells *in vivo* or *in vitro*. After treatment with DZNep, T cell activation was impaired in the spleen and kidney, which correlated with the downregulated expression of T-cell immunoglobulin mucin (TIM)-1 on T cells and TIM-4 in macrophages. In addition, pretreatment with DZNep was not sufficient to protect the kidney, while administration of DZNep from before to after surgery significantly ameliorated IRI. Our findings suggest that DZNep can be a novel strategy for preventing renal IRI following kidney transplantation.

Keywords: renal IRI, DZNep, TIM-1, T cells, NF-κB

INTRODUCTION

Ischemia-reperfusion injury (IRI) is the leading cause of renal function impairment after renal transplantation. It can induce a series of pathological phenomena, including renal inflammation and fibrosis, and eventually lead to the loss of kidney graft function or acute or chronic rejection, which affects the patient's quality of life (1–3).

The adaptive immune system plays an essential role in renal IRI (4–8). T cells mediate IRI or rejection, impair the recovery of kidney grafts, and even induce renal interstitial fibrosis. Therefore, inhibiting the activation of T cells has the potential to promote the functional recovery of kidney grafts.

T-cell immunoglobulin mucin (TIM) molecules, or kidney injury molecules (KIM) when expressed in the kidney, are costimulatory molecules critical in regulating adaptive immunity. There are eight TIM genes in mice (TIM-1 to 8) and three in humans (TIM-1,3,4) encoded by

the TIM family (9). Recent evidence (10) has indicated the high expression of TIM-1 on the surface of activated $CD4^+$ T cells after liver IRI. When using a TIM-1 monoclonal antibody (RMT1-10) to block TIM-1 function, T cell activation was reduced significantly. In $RAG^{-/-}$ mice (T cell deficient), RMT1-10 had no effect on liver IRI. A similar result was also found in mice with renal IRI (11). Such reports reveal that TIM-1 is highly correlated with T cell activation. Thus, TIM-1 could be a potential target for intervention in T cell-mediated injury.

Recently, research has focused on epigenetic modifications. Epigenetic modifications are critical for protecting the function of grafts (12). Histone methylation, a common epigenetic modification, takes part in cell proliferation and differentiation. It has been reported that the histone methyltransferase Ezh2 mediates the functional alteration of T cells (13) and drives them to differentiate into various subtypes and impair their activation and proliferation (14). Acting as an inhibitor of Ezh2, 3-Deazaneplanocin A (DZNep) has been used to treat leukemia (15, 16), tumors (17), and other malignant diseases. Recent research has broadened its potential therapeutic effects in ischemic brain injury by promoting microglial activation (18) and tubulointerstitial fibrosis by inhibiting the expression of fibrogenic genes. It has become an ideal medication for epigenetic therapy owing to its reversible effects on gene expression. A previous study found that DZNep had an inhibitory effect on graft-versus-host disease (GVHD) in a kidney or bone marrow transplantation model, and it can only induce apoptosis of activated T cells but has no effect on naïve T cells (19).

In this study, we demonstrated that DZNep treatment can alleviate renal IRI in mice by inhibiting T cell activation through direct and indirect pathways. The indirect pathway may involve the impairment of interactions between T cells and macrophages by the TIM-1–TIM-4 axis. DZNep may have a better protective effect when used postoperatively. Our findings suggest that DZNep can be a novel strategy for preventing renal IRI following kidney transplantation.

METHODS

Mice and Model of Renal IRI

Male C57BL/6 mice (20–25 g) were obtained from Shanghai SLAC Laboratory Animal Co., Ltd. Renal IRI was performed as follows: briefly, the bilateral renal pedicles were occluded for 45 min using non-traumatic clamps, and mice were sacrificed 36 h after reperfusion. For survival rate analysis, mice were observed for 7 d, and euthanized. Before surgery, mice were randomly divided into six groups ($n = 6$) according to the different treatments: (1) sham group (without renal pedicle occlusion); (2) DZNep group (DZNep treated without renal pedicle occlusion); (3) IRI group (with renal pedicles occlusion); (4) IRI+DZNep pretreatment group (mice were pretreated with DZNep for 2 days before surgery); (5) IRI+DZNep post-treatment group (mice were pretreated with DZNep immediately after reperfusion and 1 d after surgery); (6) IRI+DZNep group (mice were treated with DZNep for 2 days before surgery, right after reperfusion, and 1 d after surgery). DZNep (100μL 1 mg/kg) was subcutaneously injected at the bilateral inguinal area every time. DZNep was purchased from the National Cancer Institute (NCI), dissolved in sterile phosphate-buffered saline, and stored at −20°C. The experimental protocols were approved by the Animal Ethical Committee of Zhongshan Hospital, Fudan University.

Assessment of Renal Damage

Serum creatinine (SCr) and blood urea nitrogen (BUN) levels were measured with an autoanalyzer (HITACHI 7600 P automatic biochemical analyzer [Japan]). Renal specimens were fixed with a 10% buffered formalin solution and hematoxylin and eosin (H&E) stained to determine histological injury. Ten random sections per slide (200×) were evaluated. Renal damage was graded as 0–4 based on the percentage of damaged tubules of each sample as previously described (20). Injury included cell vacuolization, cell necrosis, and interstitial infiltration.

Immunohistochemistry

Fixed kidney sections were dewaxed, rehydrated, and incubated with either myeloperoxidase (MPO) to assess neutrophil infiltration (1:200, Thermo Fisher) or CD4 monoclonal antibody for T cells (1:500, Abcam).

Cell Culture

The renal tubular epithelial cell line (TCMK-1 cells) was obtained from the ATCC® CRL-3216™ American Type Culture Collection (Manassas, VA).

Cells were cultured in Dulbecco's modified Eagle medium F12 (Gibco, NY, USA) supplemented with 10% fetal bovine serum (Gibco, NY), 100 IU/mL penicillin, and 100 μg/mL streptomycin. Mouse splenic cells were ground and filtered from mouse spleens, and naïve $CD4^+$ T cells were separated by microbeads (Miltenyi Biotec, NY) and later cultured in RPMI 1640 medium (Gibco, NY). Cells were maintained in a humidified atmosphere containing 5% CO_2 and 95% O_2 at 37°C. Splenic cells were further stimulated with ConA and seeded in 96-well plates (1×10^5 cells/well) in the absence or presence of DZNep for 3 days. The proportion of $CD4^+CD69^+$ T cells was evaluated by flow cytometry.

Hypoxia/Reoxygenation (H/R) Model and Treatment

For H/R stimulation, TCMK-1 cells were cultured in glucose/serum-free medium under hypoxic conditions (94% N_2, 1% O_2, and 5% CO_2) for 24 h, followed by 2 h in normal media and normoxic conditions (5% CO_2 and 95% O_2). Cells in the control group were incubated under normoxic conditions. Cells in the DZNep group were pretreated with DZNep (40 μM) for 24 h followed by H/R stimulation.

Cell Isolation and Flow Cytometric Analysis

To obtain a splenic single cell suspension, the mouse spleen was ground and filtered. The kidneys were cut into small pieces and digested in Hank's Balanced Salt Solution (Gibco) supplemented with 10% type IV collagenase (Gibco) and 0.002% DNase I (Gibco) at 37°C for 30 min. Dissociated cells were filtered and centrifuged at 1,000 rpm. Splenic and renal kidney cells

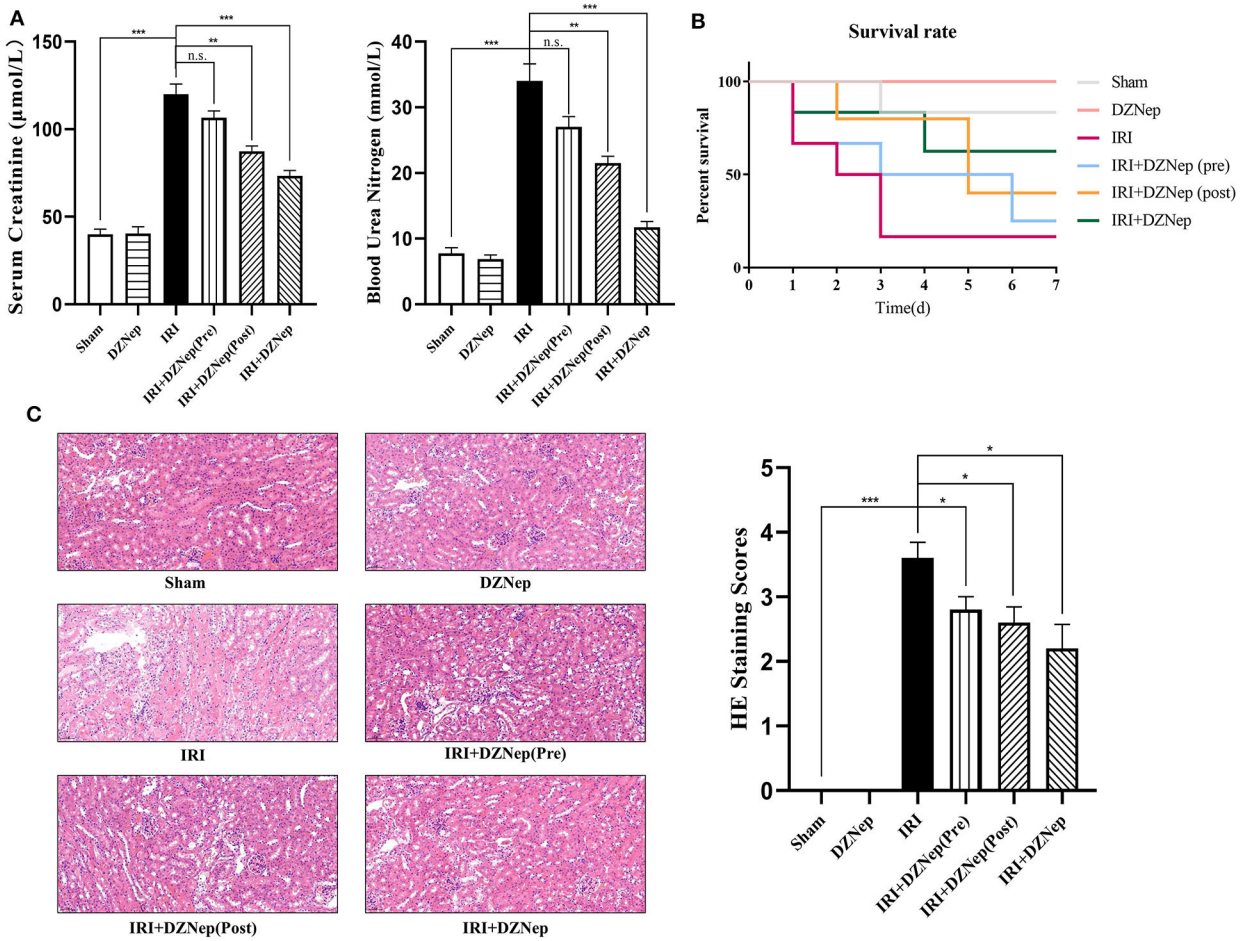

FIGURE 1 | DZNep alleviated renal dysfunction after IRI. **(A)** Serum of mice in each group were tested for serum creatine (SCr) and blood urea nitrogen (BUN) level ($n = 6$). **(B)** 72-h survival rate in each group ($n = 6$). **(C)** Tubular injury level in different group indicated by H&E staining. Tubular injury scoring was made and shown at the right ($n = 6$). $^{n.s.}P \geq 0.05$, $^{*}P < 0.05$, $^{**}P < 0.01$, $^{***}P < 0.001$.

were suspended in PBS+10% FBS (Gibco) and incubated with CD4-PE (eBioscience, CA), CD69-APC, TIM1-FITC antibody (BioLegend, CA), TIM4- PerCP-eFluor 710, and F4/80-FITC (Thermo Fisher Scientific) at 4°C for 30 min. After washing, flow cytometric analyses were performed using a FACScan and Canto cytometer (BD Biosciences).

Realtime PCR

Total RNA was extracted from kidney tissue using TRIzol (Invitrogen Life Technologies) and transcribed into cDNA using HiScript II Q RT SuperMix for qPCR (Vazyme). Realtime PCR was performed using the iQ5 Real-time PCR instrument (Bio-Rad) with a SYBR green PCR mix (Yeasen). Gene expression levels were normalized to the GAPDH gene. The primer sequences are listed as follows (mice, 5′ '-3''): interleukin (IL)-6, F: CTGCAAGAGACTTCCATCCAG, R: AGTGGTAT AGACAGGTCTGTTGG; IL-10, F: CTTACTGACTGGCATG AGGATCA, R: GCAGCTCTAGGAGCATGTGG; IFN-γ, F: GCCACGGCACAGTCATTGA, R: TGCTGATGGCCTGATT GTCTT; TNF-α, F: CAGGCGGTGCCTATGTCTC; R: CGAT CACCCCGAAGTTCAGTAG; KIM-1, F: ACATATCGTGGA ATCACAACGAC; R: ACTGCTCTTCTGATAGGTGACA; and neutrophil gelatinase-associated lipocalin (NGAL), F: TGGCCCTGAGTGTCATGTG, R: CTCTTGTAGCTCATAGA TGGTGC.

ELISA

Whole blood of mice was centrifuged for 4,000 rpm for 5 min to obtain serum. KIM-1 expression in serum was detected using a TIM-1 (HAVCR1) Mouse ELISA Kit (Thermo Fisher).

Western Blot Analysis

Total protein was extracted using lysis buffer and a 1% protease inhibitor cocktail. After centrifuging for 15 min at 12,000 g, the supernatant was transferred to a new tube and stored at −80°C. A Bradford protein assay kit was used to determine the concentration of total protein. Total protein was separated on SDS-poly-acrylamide gels, transferred to polyvinylidene difluoride membranes, blocked with 5%

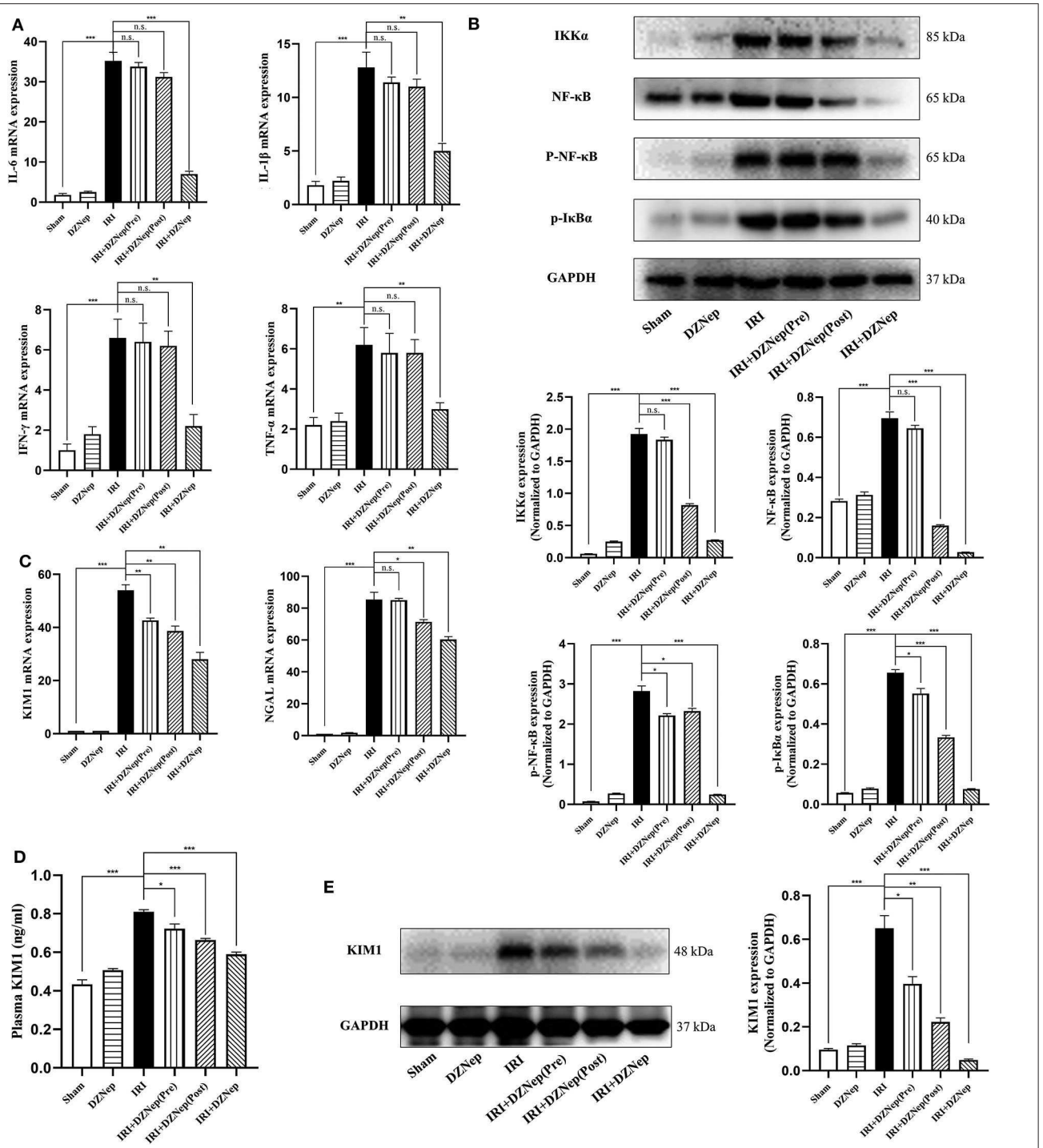

FIGURE 2 | DZNep decreased the expression of inflammatory agents and injury relative molecules in renal IRI. **(A)** The relative mRNA expression level of IL-6, IL-10, IFN-γ, and TNF-α in mice kidney ($n = 6$). **(B)** Western blot analysis of protein expression in NF-κB signaling pathway ($n = 6$). The expression level was normalized to GAPDH. **(C)** Relative mRNA expression of KIM-1 and NGAL in mice kidneys ($n = 6$). **(D)** KIM-1 expression level in plasma ($n = 6$). **(E)** Western blot analysis of protein expression of KIM-1 in mice kidneys. The expression level was normalized to GAPDH. $^{n.s.}P \geq 0.05$, $^{*}P < 0.05$, $^{**}P < 0.01$, $^{***}P < 0.001$.

non-fat dried milk, and incubated overnight with KIM-1 (eBioscience), anti-IKKα, anti-NF-κB, anti-p-NF-κB, p-IκB (Cell Signaling Technology, Beverly, MA, USA, 1:1000), and GAPDH (Abcam, Cambridge, UK,1:1000). The membranes were washed with TBST and probed with HRP goat anti-rabbit IgG (H+L) cross-adsorbed secondary antibody (Thermo

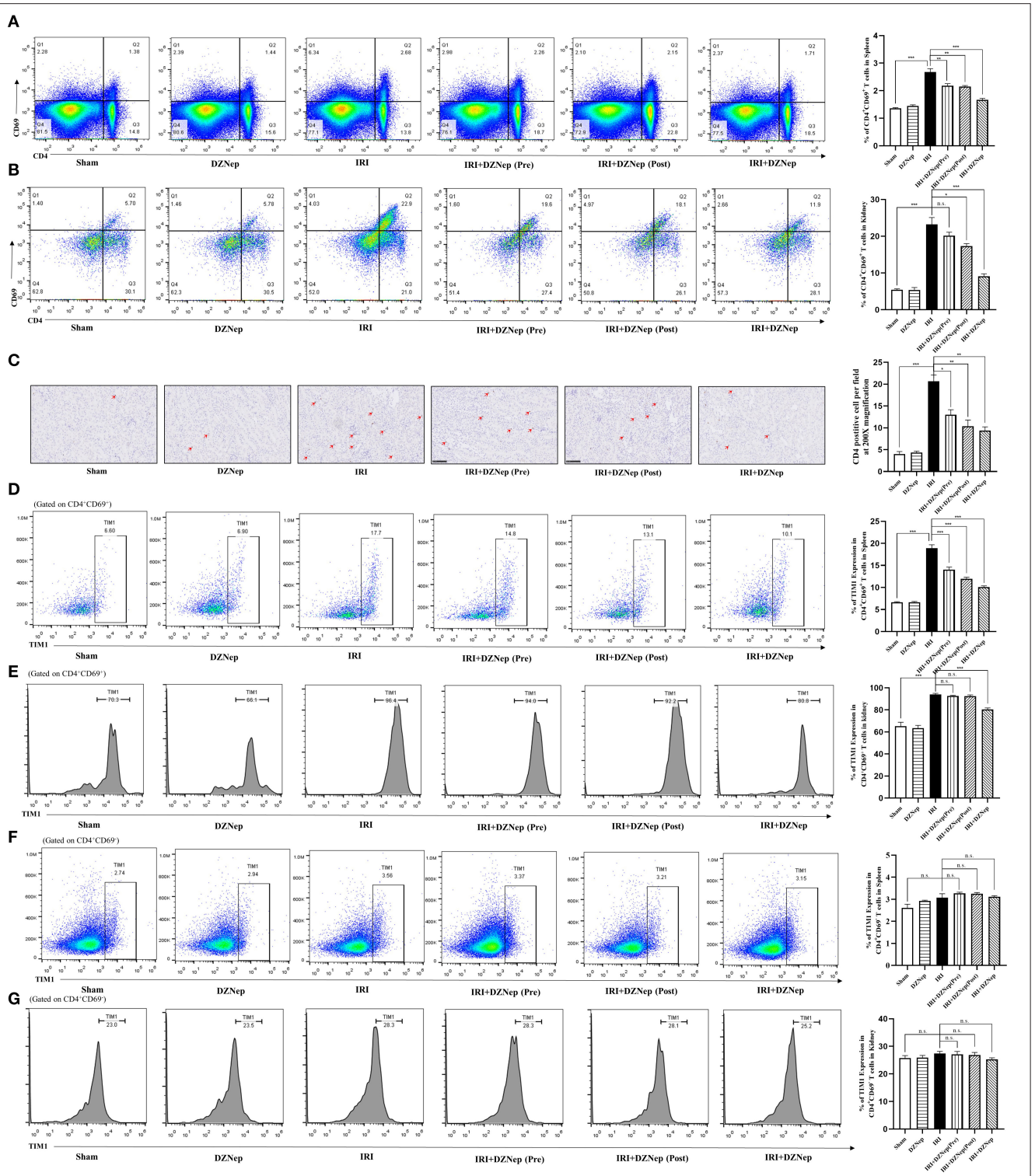

FIGURE 3 | DZNep downregulated TIM-1 expression in activated $CD4^+$T cells after IRI. **(A)** $CD4^+CD69^+$T cells in spleen were gated using flowcytometry. **(B)** The proportion of $CD4^+CD69^+$T cells in mice kidney. **(C)** Immunochemistry stained $CD4^+$T cells in kidney. Histogram showed the average cell count of $CD4^+$T cells per field ($n = 18$, 200X). **(D)** TIM-1 level in $CD4^+CD69^+$ T cells of mice spleen. **(E)** TIM-1 level in $CD4^+CD69^+$ T cells of mice kidney. **(F)** TIM-1 level in $CD4^+CD69^-$ T cells of mice spleen. **(G)** TIM-1 level in $CD4^+CD69^-$ T cells of mice kidney. $^{n.s.}P \geq 0.05$, $^*P < 0.05$, $^{**}P < 0.01$, $^{***}P < 0.001$.

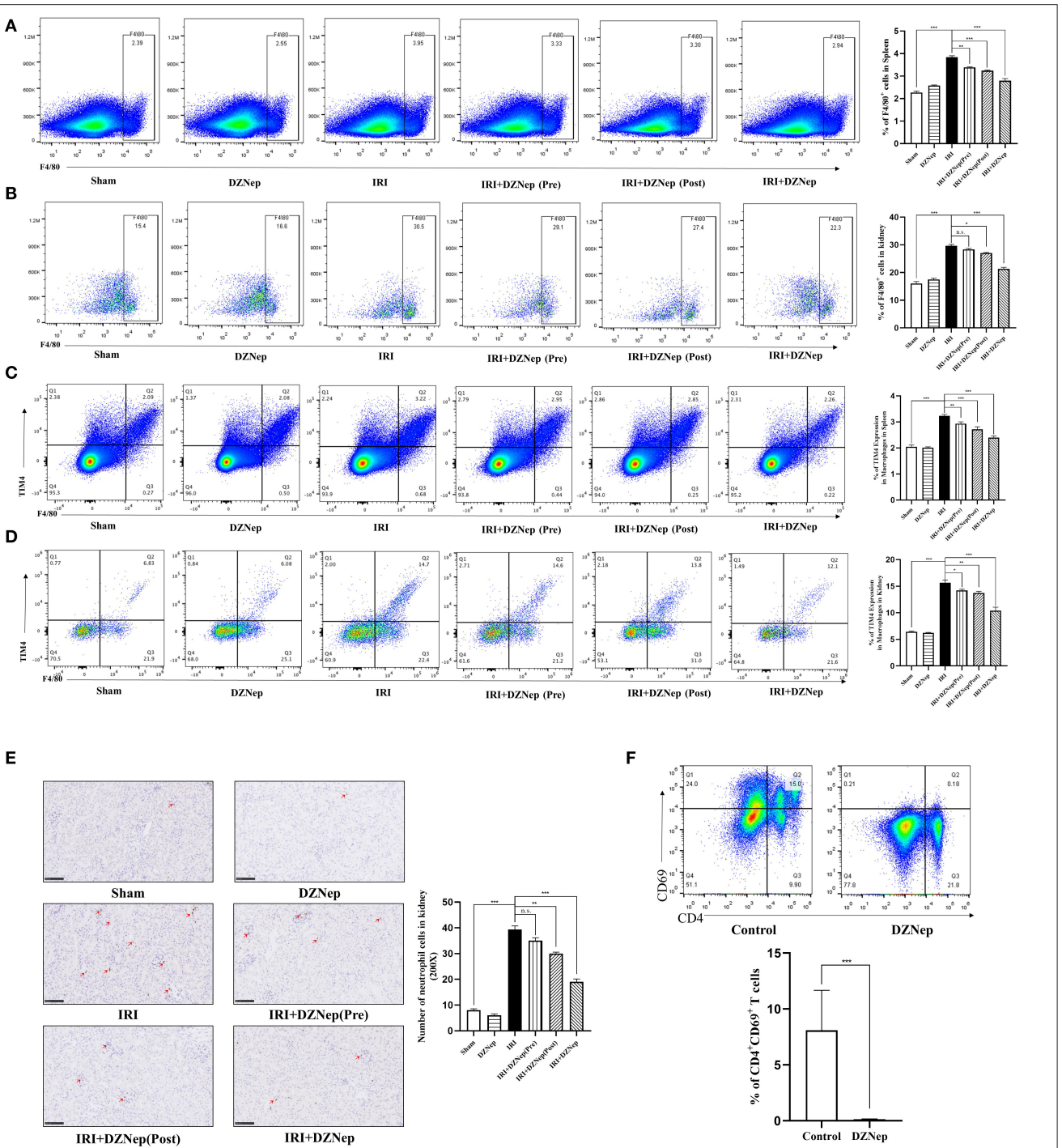

FIGURE 4 | DZNep could impair activation of T cells by direct and indirect pathway. **(A)** The proportion of macrophages in mice spleen. **(B)** The proportion of macrophages in mice kidney. **(C)** TIM-4 level in macrophages of mice spleen. **(D)** TIM-4 level in macrophages of mice kidney. **(E)** MPO staining of neutrophils in mice kidney sections and neutrophil count in each group ($n = 18$, 200X). **(F)** Flow-cytometry evaluated the proportion of $CD4^+CD69^+$ T cells in spleen cells after 3 days culture with absence or presence of DZNep. $^{n.s.}P \geq 0.05$, $^{*}P < 0.05$, $^{**}P < 0.01$, $^{***}P < 0.001$.

Fisher Scientific, 1:10000). Proteins were visualized and captured using a chemiluminescence image analysis system (Tanon, 5200 Multi).

Statistical Analysis

GraphPad Prism 10 was used for data analysis. Data are presented as the mean ± standard error of the mean (SEM). A two-tailed

independent Student's *t*-test was conducted after a demonstration of the homogeneity of variance with an *F*-test. The survival endpoints were analyzed using the Kaplan-Meier method. A $P < 0.05$ was defined as statistically significant.

RESULT

DZNep Alleviated Renal Dysfunction After Ischemia-Reperfusion Injury

We first evaluated the renal protective effect of DZNep in renal IRI and optimal administration time. DZNep was applied preoperatively, postoperatively, or from before to after surgery (details are shown in the Methods section). The SCr and BUN concentrations were measured 36 h post-reperfusion, which were significantly increased in the IRI group and reduced with DZNep treatment. Additionally, the reduction in SCr and BUN concentrations was especially significant in the IR+DZNep group (**Figure 1A**). The survival rate, regardless of the time of DZNep administration, improved after 7 days (**Figure 1B**). H&E staining also demonstrated that DZNep could alleviate kidney injury after IRI. The 4-point scoring system was also used to evaluate tissue injury and found that injury scores were lower in DZNep treated group than in the IR group (**Figure 1C**). These results indicated that DZNep could alleviate renal IRI, especially through continued use from before to after surgery. In addition, DZNep had long-term effects on improving the survival rate.

DZNep Decreased Proinflammatory Responses and Inhibited Inflammatory Reactions in IRI

The mRNA expression of proinflammatory cytokines IL-6, IL-1β, IFN-γ, and TNF-α increased after IRI and was reduced by DZNep treatment (**Figure 2A**). After IRI, the expression of the NF-κB signaling pathway was found to be activated. According to our results, IKKα, NF-κB, p-NF-κB, and p-IκBα differed significantly between the IR and sham groups, and decreased after DZNep treatment (**Figure 2B**). The realtime PCR, ELISA, and western blot analyses revealed a downregulation of KIM-1 in the kidney and plasma after treatment with DZNep, regardless of when treatment was initiated (**Figures 2C–E**). Another indicator for renal injury, neutrophil gelatinase-associated lipocalin (NGAL), was only downregulated in the post- and continued-treated DZNep groups (**Figure 2C**). These results confirmed an anti-inflammatory and mitigatory effect of DZNep in renal IRI. However, pretreatment with DZNep was insufficient to suppress inflammation. The continued-treated DZNep group presented the most significant protective effect.

DZNep Reduced the Activation of $CD4^+$ T Cells and Inhibited TIM-1 Expression

It has been reported that DZNep can induce apoptosis of activated T cells in a bone marrow transplantation model. Thus, we investigated the effect and relative mechanism of DZNep on $CD4^+$ T cells in renal IRI. Flow cytometry showed that $CD4^+CD69^+$ T cells (activated T helper cells) were downregulated in the spleen and kidney after treatment with DZNep (**Figures 3A,B**), indicating a significant impairment in the activation of $CD4^+$ T cells induced by DZNep. Immunohistochemistry also confirmed a significant decline in $CD4^+$ cells in DZNep-treated IRI kidneys (**Figure 3C**).

Since TIM-1 is involved in the activation of $CD4^+$ T cells, we evaluated the expression level of TIM-1 in $CD4^+CD69^+$ and $CD4^+CD69^-$ T cells (activated and inactivated T cells, respectively). As expected, TIM-1 was elevated in $CD4^+CD69^+$ T cells after IRI in both the spleen and kidney (**Figures 3D,E**), but remained unchanged in $CD4^+CD69^-$ T cells (**Figures 3F,G**). In addition, DZNep significantly downregulated TIM-1 expression in $CD4^+CD69^+$ T cells (**Figures 3D,E**) but had no effect on $CD4^+CD69^-$ T cells (**Figures 3F,G**). Thus, we could infer that TIM-1 plays a role in the activation of CD4+ T cells in IRI, and DZNep impaired the activation of $CD4^+$ T cells by inhibiting the expression of TIM-1 on the surface. Interestingly, despite the trend, pretreatment of DZNep did not impair T cell activation and downregulate TIM-1 expression significantly in the kidney (**Figures 3B,E**), which was in accordance with SCr, BUN, and other injury related indicators.

DZNep May Impair the Activation of T Cells *via* Direct and Indirect Pathways

Since DZNep can widely affect other major inflammatory cells, such as macrophages and neutrophils, we conducted further experiments to determine whether DZNep impairs the activation of T cells via direct or indirect pathways. Macrophages accumulated in the IRI spleen and kidney, and this accumulation was mitigated after treatment with DZNep (**Figures 4A,B**). Notably, TIM-4, the ligand of TIM-1, was also significantly downregulated in macrophages (**Figures 4C,D**) after treatment with DZNep, indicating that DZNep may impair T cell activation by affecting the interaction of macrophages and T cells by modulating the TIM-1-TIM-4 axis. In addition, Neutrophils showed a similar trend in the kidney (**Figure 4E**). To determine whether DZNep has a direct effect on T cells, we cultured activated mouse splenic T cells (activated by conA) with or without DZNep. T cell activation was still impaired without interaction with other cells after treatment with DZNep (**Figure 4F**). Thus, DZNep has a direct effect on T cell activation.

DZNep Downregulated the NF-κB Signaling Pathway in TCMK-1 Cells

TCMK-1 cells were used to confirm the anti-inflammatory effect of DZNep *in vitro*. TCMK-1 cells were exposed to H/R. KIM-1 and NGAL expression as well as components of the NF-κB signaling pathway were all downregulated in DZNep-treated TCMK-1 cells (**Figures 5A,B**). Therefore, DZNep can protect the renal tubular cells from exacerbated inflammation directly in renal IRI.

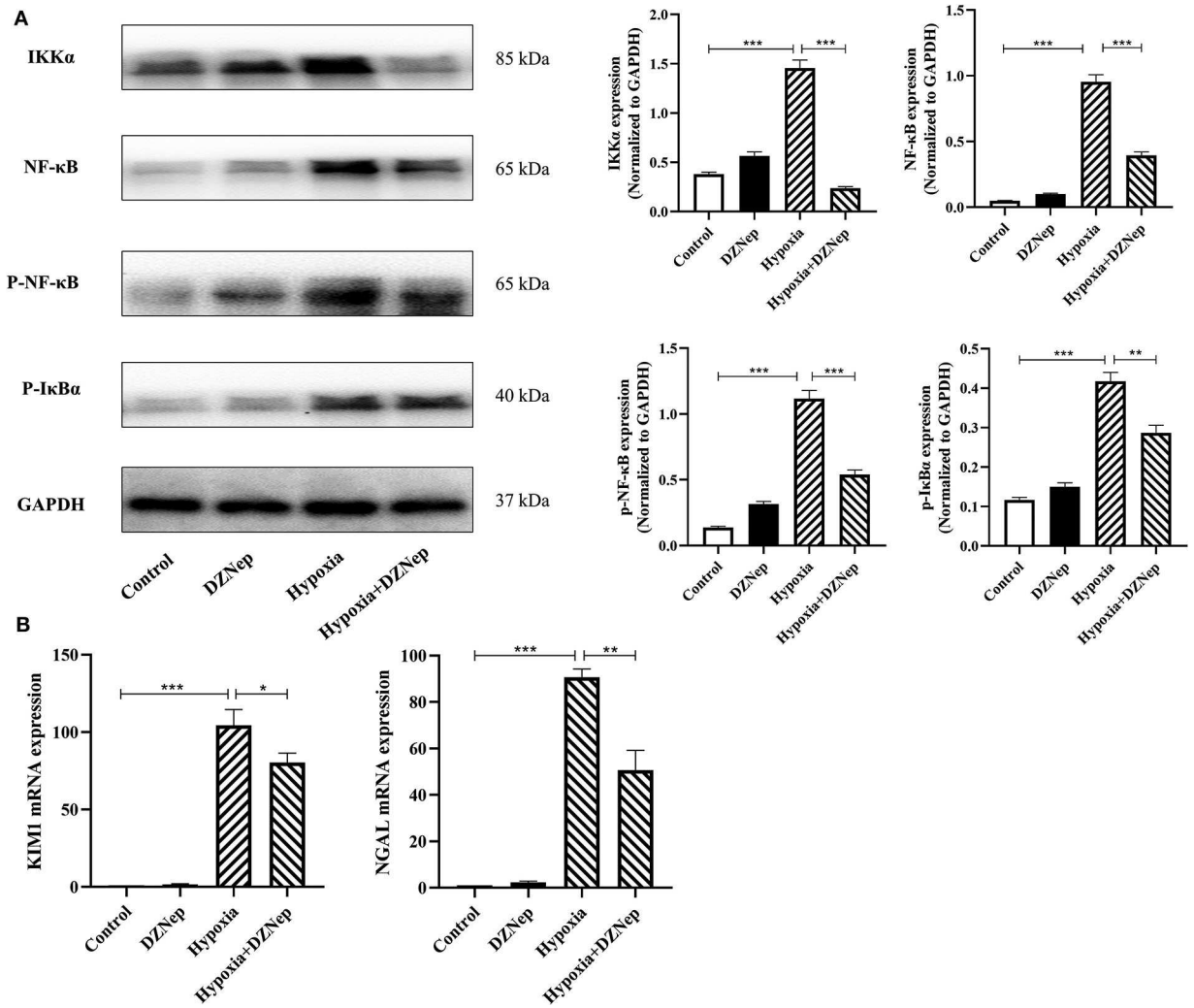

FIGURE 5 | DZNep downregulated expression of KIM-1 and NF-κB signaling pathway in TCMK-1 cells. **(A)** Realtime PCR revealed KIM-1 and NGAL relative mRNA expression. **(B)** Western blot analysis of NF-κB signaling pathway protein expression in TCMK-1 cells. The expression level was normalized to GAPDH. $^{*}P < 0.05$, $^{**}P < 0.01$, $^{***}P < 0.001$.

DISCUSSION

In this study, we investigated the therapeutic effects and optimal administration time of DZNep in renal IRI for the first time. DZNep treatment from before to after surgery showed adequate renal protective effects, while treating with DZNep only before surgery was insufficient to alleviate injury. After treatment with DZNep, the renal injury and inflammatory reaction were ameliorated and T cell activation was directly and significantly impaired by DZNep, with a downregulation of TIM-1 transcription in activated T cells and decreased TIM-4 expression in macrophages.

IRI is the common cause of acute renal failure in both allograft and native kidneys. Researchers have found that T cells play a key role in renal IRI (8). Depletion of T cells improved the outcomes of IRI and was believed to be a promising therapeutic target in preventing allograft rejection. However, complete depletion of T cells is unrealistic for clinical practice and experiments using knockout mice may not reflect the intervention effects in wild-type mice or humans. With advances in the understanding of chromatin remodeling and epigenetic changes during T cell development and function, epigenetic therapy targeting T cells is rapidly developing. Histone methylation is more stable than other histone modification forms, which could provide a long-term maintenance of chromatin states that cannot be silenced by DNA methylation (17, 21, 22). Therefore, medication targeting histone methylation in T cells may be more reliable for long-term intervention among post-transplant patients. EZH2 was associated with cytokine gene expression in T cells (13, 23). As an inhibitor of histone EZH2, DZNep was reported

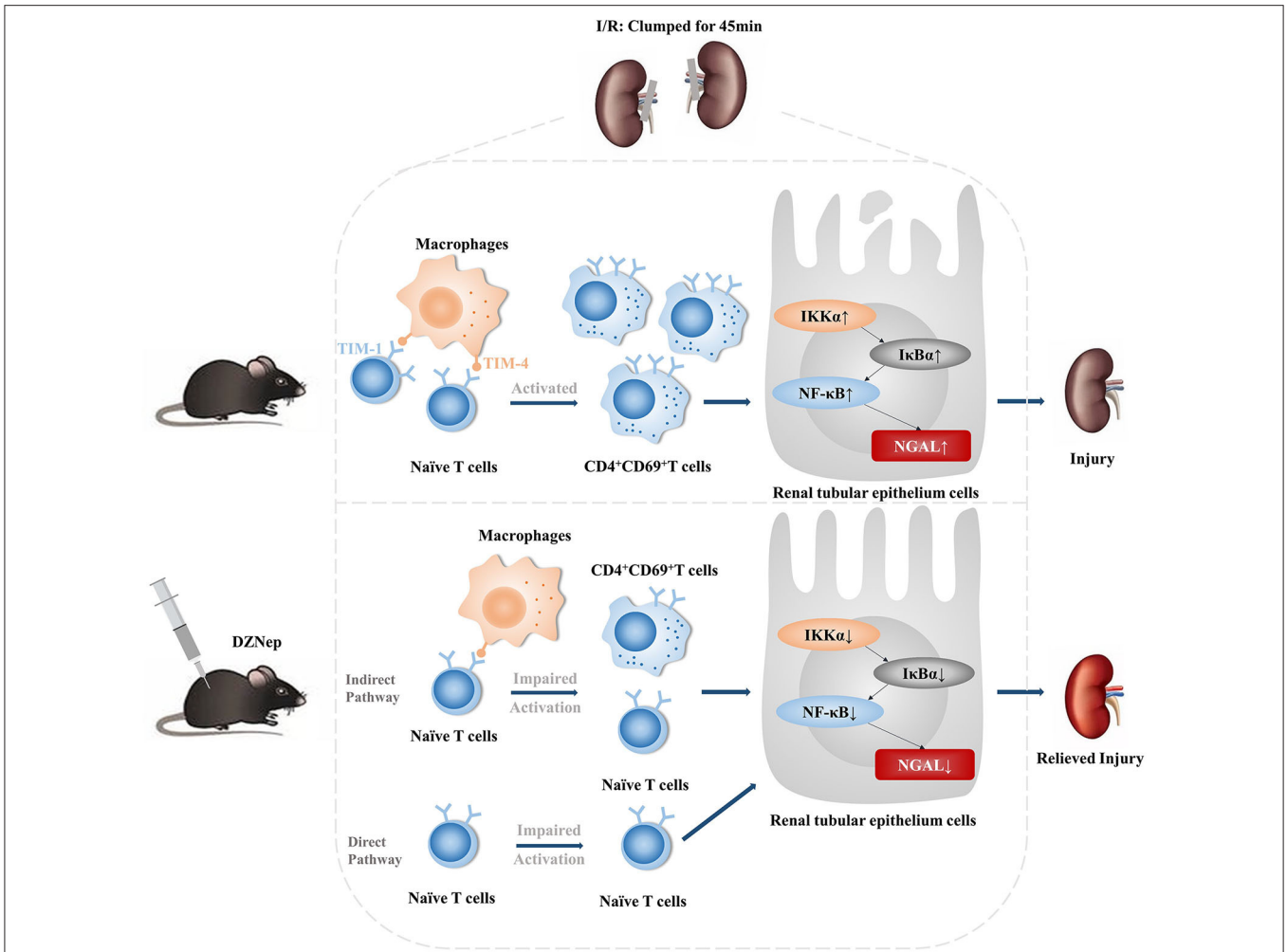

FIGURE 6 | The pictorial summary of DZNep on renal IRI. DZNep treatment in I/R mice could significantly downregulated TIM-1 expression on naïve T cells and impaired their activation. DZNep could alleviate mice renal IRI by inhibiting T cell activation in direct and indirect pathway. The indirect pathway might be involved in the impaired interaction between T cells and macrophages by TIM-1: TIM-4 axis. And DZNep could have a better protective effect when used postoperatively.

to have protective effects in ischemic brain injury (18) and tubulointerstitial fibrosis (24). In our study, DZNep ameliorated the renal IRI and injury of the renal tubular cells *in vivo* and *in vitro* and such protective effects persisted and improved the survival rate in our 3-days follow-up. In addition, the activation of T cells was still impaired when cultured solely with DZNep, indicating a direct action of DZNep on T cell activation, which has not been previously reported. Therefore, DZNep may become a promising therapeutic for modulating the function of T cells in renal IRI.

The TIM-1-TIM-4 axis was suggested as a novel intervention target for IRI. Direct inhibition or induced depression of TIM-1 and TIM-4 protected against liver and cerebral IRI (25–29). Blocking the TIM-1-TIM-4 pathway by anti-TIM monoclonal antibody also diminished inflammation and improve apoptosis and survival in renal IRI (11). The TIM-1-TIM-4 axis is involved in the activation and proliferation of all T cells, including Tregs (29–32), and impacts the infiltration and activation of macrophages and neutrophils as well (10). Eventually, we found that TIM-1 was elevated in activated T cells after renal IRI, and DZNep treatment significantly downregulated TIM-1 expression. In addition, since TIM-4 is highly restricted to antigen-presenting cells, we also evaluated the expression level of TIM-4 in macrophages and found that TIM-4 expression in macrophages was in parallel with TIM-1. Macrophages were also recruited less to the kidney after treatment with DZNep. Thus, TIM-1 and TIM-4 may be involved in the interaction of macrophages and T cells, and may be an indirect mechanism for DZNep-mediated impairment of T cell activation.

Another aspect of our study was to determine the optimal administration time of DZNep. To our surprise, pretreatment with DZNep showed an unsatisfactory protective effect against renal injury, while post-treatment with DZNep significantly inhibited the injury. Based on this phenomenon, we suspect that the renal protective effect of DZNep mainly involves

blocking the deterioration process after the occurrence of injury, rather than prompting cells to undergo adaptive changes in advance. Combining the fact that TIM-1 expression was only downregulated in activated T cells while it remained unchanged in naïve T cells, we inferred that DZNep had no effect on T cells in the resting state and can block the activation process of T cells by inhibiting TIM-1 expression. However, the underlying mechanism requires further exploration.

In conclusion, our study demonstrated that DZNep ameliorated acute renal injury and inflammatory responses in a renal IRI murine model by modulating $CD4^+$ T cell activation. DZNep also inhibited the recruitment of neutrophils by $CD4^+$ T cells. The modulation effect of DZNep on T cells may involve histone methylation and subsequent downregulation of TIM-1 (**Figure 6**).

DATA AVAILABILITY STATEMENT

All datasets generated for this study are included in the article/supplementary material.

ETHICS STATEMENT

The animal study was reviewed and approved by Animal Ethical Committee of Zhongshan Hospital, Fudan University.

AUTHOR CONTRIBUTIONS

JL, LL, YZ, and RR: conceived the project, designed the project, extracted and analyzed data, and approved the final manuscript. YQ: drafted the manuscript. JiyW, YC, YJ, JinW, and RS: conducted the experiments. All authors contributed to the article and approved the submitted version.

FUNDING

This work was supported by the National Key R&D Program of China (2018YFA0107501 to RR), National Natural Science Foundation of China (81400688 to YZ, 81770747 and 81970646 to RR).

REFERENCES

1. Cravedi P, Heeger PS. Corrigendum. Complement as a multifaceted modulator of kidney transplant injury. *J Clin Invest.* (2015) 125:1365. doi: 10.1172/JCI81182
2. Ponticelli C. Ischaemia-reperfusion injury: a major protagonist in kidney transplantation. *Nephrol Dial Transplant.* (2014) 29:1134–40. doi: 10.1093/ndt/gft488
3. Schroppel B, Legendre C. Delayed kidney graft function: from mechanism to translation. *Kidney Int.* (2014) 86:251–8. doi: 10.1038/ki.2014.18
4. Rabb H, Daniels F, O'Donnell M, Haq M, Saba SR, Keane W, et al. Pathophysiological role of T lymphocytes in renal ischemia-reperfusion injury in mice. *Am J Physiol Renal Physiol.* (2000) 279:F525–31. doi: 10.1152/ajprenal.2000.279.3.F525
5. Ysebaert DK, De Greef KE, De Beuf A, Van Rompay AR, Vercauteren S, Persy VP, et al. T cells as mediators in renal ischemia/reperfusion injury. *Kidney Int.* (2004) 66:491–6. doi: 10.1111/j.1523-1755.2004.761_4.x
6. Pinheiro HS, Camara NO, Noronha IL, Maugeri IL, Franco MF, Medina JO, et al. Contribution of CD4+ T cells to the early mechanisms of ischemia-reperfusion injury in a mouse model of acute renal failure. *Braz J Med Biol Res.* (2007) 40:557–68. doi: 10.1590/S0100-879X2007000400015
7. Xue C, Liu Y, Li C, Li Y, Yang T, Xie L, et al. Powerful protection against renal ischemia reperfusion injury by T cell-specific NF-κB inhibition. *Transplantation.* (2014) 97:391–6. doi: 10.1097/01.TP.0000438622.89310.95
8. Yokota N, Daniels F, Crosson J, Rabb H. Protective effect of T cell depletion in murine renal ischemia-reperfusion injury. *Transplantation.* (2002) 74:759–63. doi: 10.1097/00007890-200209270-00005
9. Lee J, Phong B, Egloff AM, Kane LP. TIM polymorphisms–genetics and function. *Genes Immun.* (2011) 12:595–604. doi: 10.1038/gene.2011.75
10. Zhang Y, Ji H, Shen X, Cai J, Gao F, Koenig KM, et al. Targeting TIM-1 on CD4 T cells depresses macrophage activation and overcomes ischemia-reperfusion injury in mouse orthotopic liver transplantation. *Am J Transplant.* (2013) 13:56–66. doi: 10.1111/j.1600-6143.2012.04316.x
11. Rong S, Park JK, Kirsch T, Yagita H, Akiba H, Boenisch O, et al. The TIM-1:TIM-4 pathway enhances renal ischemia-reperfusion injury. *J Am Soc Nephrol.* (2011) 22:484–95. doi: 10.1681/ASN.2010030321
12. Mas VR, Le TH, Maluf DG. Epigenetics in kidney transplantation: current evidence, predictions, and future research directions. *Transplantation.* (2016) 100:23–38. doi: 10.1097/TP.0000000000000878
13. Koyanagi M, Baguet A, Martens J, Margueron R, Jenuwein T, Bix M. EZH2 and histone 3 trimethyl lysine 27 associated with Il4 and Il13 gene silencing in Th1 cells. *J Biol Chem.* (2005) 280:31470–7. doi: 10.1074/jbc.M504766200
14. Tumes DJ, Onodera A, Suzuki A, Shinoda K, Endo Y, Iwamura C, et al. The polycomb protein Ezh2 regulates differentiation and plasticity of $CD4^+$ T helper type 1 and type 2 cells. *Immunity.* (2013) 39:819–32. doi: 10.1016/j.immuni.2013.09.012
15. Zhou J, Bi C, Cheong LL, Mahara S, Liu SC, Tay KG, et al. The histone methyltransferase inhibitor, DZNep, up-regulates TXNIP, increases ROS production, and targets leukemia cells in AML. *Blood.* (2011) 118:2830–39. doi: 10.1182/blood-2010-07-294827
16. Jiang X, Lim CZ, Li Z, Lee PL, Yatim SM, Guan P, et al. Functional characterization of D9, a novel deazaneplanocin A (DZNep) analog, in targeting acute myeloid leukemia (AML). *PLoS ONE.* (2015) 10:e0122983. doi: 10.1371/journal.pone.0122983
17. Miranda TB, Cortez CC, Yoo CB, Liang G, Abe M, Kelly TK, et al. DZNep is a global histone methylation inhibitor that reactivates developmental genes not silenced by DNA methylation. *Mol Cancer Ther.* (2009) 8:1579–88. doi: 10.1158/1535-7163.MCT-09-0013
18. Chen J, Zhang M, Zhang X, Fan L, Liu P, Yu L, et al. EZH2 inhibitor DZNep modulates microglial activation and protects against ischaemic brain injury after experimental stroke. *Eur J Pharmacol.* (2019) 857:172452. doi: 10.1016/j.ejphar.2019.172452
19. He S, Wang J, Kato K, Xie F, Varambally S, Mineishi S, et al. Inhibition of histone methylation arrests ongoing graft-versus-host disease in mice by selectively inducing apoptosis of alloreactive effector T cells. *Blood.* (2012) 119:1274–82. doi: 10.1182/blood-2011-06-364422
20. Hesketh EE, Czopek A, Clay M, Borthwick G, Ferenbach D, Kluth D, et al. Renal ischaemia reperfusion injury: a mouse model of injury and regeneration. *J Vis Exp.* (2014) 51816. doi: 10.3791/51816
21. Berger SL. The complex language of chromatin regulation during transcription. *Nature.* (2007) 447:407–12. doi: 10.1038/nature05915
22. Jenuwein T, Allis CD. Translating the histone code. *Science.* (2001) 293:1074–80. doi: 10.1126/science.1063127
23. Lee CG, Sahoo A, Im SH. Epigenetic regulation of cytokine gene expression in T lymphocytes. *Yonsei Med J.* (2009). 50:322–30. doi: 10.3349/ymj.2009.50.3.322
24. Mimura I, Hirakawa Y, Kanki Y, Nakaki R, Suzuki Y, Tanaka T, et al. Genome-wide analysis revealed that DZNep reduces tubulointerstitial

fibrosis via down-regulation of pro-fibrotic genes. *Sci Rep.* (2018) 8:3779. doi: 10.1038/s41598-018-22180-5
25. Zheng L, Huang Y, Wang X, Wang X, Chen W, Cheng W, et al. Inhibition of TIM-4 protects against cerebral ischaemia-reperfusion injury. *J Cell Mol Med.* (2019) 24:1276–85. doi: 10.1111/jcmm.14754
26. Zhang Y, Liu Y, Chen H, Zheng X, Xie S, Chen W, et al. TIM-1 attenuates the protection of ischemic preconditioning for ischemia reperfusion injury in liver transplantation. *Am J Transl Res.* (2017) 9:3665–75.
27. Zhang Y, Shen Q, Liu Y, Chen H, Zheng X, Xie S, et al. Hepatic ischemic preconditioning alleviates ischemia-reperfusion injury by decreasing TIM4 expression. *Int J Biol Sci.* (2018) 14:1186–95. doi: 10.7150/ijbs.24898
28. Zheng Y, Wang L, Chen M, Liu L, Pei A, Zhang R, et al. Inhibition of T cell immunoglobulin and mucin-1 (TIM-1) protects against cerebral ischemia-reperfusion injury. *Cell Commun Signal.* (2019) 17:103. doi: 10.1186/s12964-019-0417-4
29. Ji H, Liu Y, Zhang Y, Shen XD, Gao F, Busuttil RW, et al. T-cell immunoglobulin and mucin domain 4 (TIM-4) signaling in innate immune-mediated liver ischemia-reperfusion injury. *Hepatology.* (2014) 60:2052–64. doi: 10.1002/hep.27334
30. Mariat C, Sanchez-Fueyo A, Alexopoulos SP, Kenny J, Strom TB, Zheng XX. Regulation of T cell dependent immune responses by TIM family members. *Philos Trans R Soc Lond B Biol Sci.* (2005) 360:1681–5. doi: 10.1098/rstb.2005.1706
31. Meyers JH, Chakravarti S, Schlesinger D, Illes Z, Waldner H, Umetsu SE, et al. TIM-4 is the ligand for TIM-1, and the TIM-1-TIM-4 interaction regulates T cell proliferation. *Nat Immunol.* (2005) 6:455–64. doi: 10.1038/ni1185
32. Tan X, Jie Y, Zhang Y, Qin Y, Xu Q, Pan Z. Tim-1 blockade with RMT1-10 increases T regulatory cells and prolongs the survival of high-risk corneal allografts in mice. *Exp Eye Res.* (2014) 122:86–93. doi: 10.1016/j.exer.2014.02.019

Conflict of Interest: The authors declare that the research was conducted in the absence of any commercial or financial relationships that could be construed as a potential conflict of interest.

frontiers in Medicine

CASE REPORT
published: 23 September 2020
doi: 10.3389/fmed.2020.00500

The Double-Edged Sword of Immunosuppressive Therapy in Kidney Transplantation: A Rare Case Report of Pulmonary Mucormycosis Post-Transplant and Literature Review

Hengcheng Zhang[1,2†], Ke Wang[1†], Hao Chen[1†], Li Sun[1], Zijie Wang[1], Shuang Fei[1], Ruoyun Tan[1] and Min Gu[1*]*

[1] Department of Urology, The First Affiliated Hospital of Nanjing Medical University, Nanjing, China, [2] Transplantation Research Center, Brigham & Women's Hospital and Harvard Medical School, Boston, MA, United States

OPEN ACCESS

Edited by:
Cheng Yang,
Fudan University, China

Reviewed by:
Brian Duncan Tait,
Australian Red Cross Blood Service, Australia
Gaurav Gupta,
Virginia Commonwealth University, United States

***Correspondence:**
Min Gu
Lancetgu@aliyun.com
Ruoyun Tan
tanruoyun112@vip.sina.com

[†] These authors have contributed equally to this work

Specialty section:
This article was submitted to Nephrology, a section of the journal Frontiers in Medicine

Received: 04 January 2020
Accepted: 21 July 2020
Published: 23 September 2020

Citation:
Zhang H, Wang K, Chen H, Sun L, Wang Z, Fei S, Tan R and Gu M (2020) The Double-Edged Sword of Immunosuppressive Therapy in Kidney Transplantation: A Rare Case Report of Pulmonary Mucormycosis Post-Transplant and Literature Review. Front. Med. 7:500. doi: 10.3389/fmed.2020.00500

Immunosuppressive therapy is improving the graft survival of kidney transplant recipients and increasing the potential risk of infection. Pulmonary mucormycosis is a rare post-operative infection complication characterized with rapid deterioration and high mortality. In this case, a 33-year-old patient underwent a kidney transplantation with regular immunosuppressive therapy. Soon, 38 days post-transplant, pulmonary patchy shadows can be seen in the radiological examination and rounded into a large cavity formation with splenic rupture 25 days later. The diagnosis of mucormycosis was confirmed by lung biopsy and spleen histopathology. This case is a reminder that early diagnosis is imperative, meanwhile, rational antifungal therapy, timely elimination of immunosuppressants, and alternatively, abandoning the graft should be prudently assessed in the treatment of mucormycosis.

Keywords: case report, pulmonary, infection, mucor, immunosuppressant, mucormycosis, kidney transplantation

INTRODUCTION

With the use of immunosuppressants, the incidence of rejection after kidney transplantation has dropped considerably in the past few decades (1), which has brought benefits to end-stage renal disease patients and contributes to prolonged graft survival (2, 3). However, as a double-edged sword, the immunosuppressive agents also dramatically reduce the immunity of patients to viruses, bacteria, and other pathogens, thus increasing the risk of peri-operative infection (4, 5). It has been demonstrated that the pulmonary fungal infection is one of the major types of growing infections after renal transplantation, associated with insidious episodes, rapid progression, and severe disease (6, 7). Among these mycoses, aspergillosis is the most common fungal pathogen accounting for more than half of cases (8). However, pulmonary mucosal infections in kidney graft recipients, characterized by rapid progression, high mortality, poor prognosis, and diagnostic difficulties, are rare, occur much less frequently than aspergillosis, and are seldom reported in detail (9, 10).

In the case report, we described a kidney transplantation patient who suffered grievous pulmonary mucormycosis with further deterioration, followed by concurrent splenic infectious

foci (**Figure 1**). We reviewed the relevant references, discussed the course of this case and put forward some reflections on the treatment of peri-operative pulmonary mucor infection in kidney transplantation recipients.

CASE PRESENTATION

A 33-year-old man with end-stage renal disease who underwent 1 year of hemodialysis was admitted to our center for renal replacement therapy. After comprehensive related examinations and the exclusion of contraindications, he received a kidney transplantation from a donor after cardiac death with negative pathogen culture results of blood and kidney lavage fluid. The surgery went smoothly with the cold-ischemia estimated at 12 h along with a warm-ischemia at 10 min. Prevention of infection with linezolid, caspofungin was performed after the operation routinely. We treated this patient with 20 mg basiliximab pre-transplant and then 20 mg basiliximab on the fourth day after transplantation for immunosuppression induction. Considering the long duration of delayed graft function (DGF), we also used the antithymocyte globulin to prevent acute rejection afterward (in total 175 mg, equal to 3.5 mg/kg). The consecutive immunosuppressive therapy included tacrolimus, mycophenolate mofetil, and methylprednisolone.

Hemodialysis was carried out intermittently due to post-operative continuous DGF. Eight days after surgery, a routine B-ultrasound showed a small amount of effusion on the upper lateral side of the graft. Ten days later, the patient reported peri-renal pain. An abdominal computed tomography (CT) examination revealed mixed density mass shadow in the upper and medial inferior right side of the kidney graft, hematoma was considered (**Figure 2**). The hematoma enlarged to 64 × 54 mm in the superior side and 95 × 37mm in the medial side in the next 2 days and had no significant changes shortly thereafter. Considering there was no indication for emergency operation, correct coagulation function, anti-infection, immunosuppression, and other conservative treatments were continued.

On 38 days post-transplantation, the chest CT revealed multiple small nodules and patchy shadows in the left and right lower lobes of the lung. In addition, the patient was positive for serum fungal galactomannan (GM) detection (1.176 μg/L, the normal reference value is <0.5 μg/L) and had an elevator procalcitonin at 0.442 ng/ml (<0.05 ng/ml is normal value) with normal body temperature and no other obvious clinical symptoms. The patient was regarded as having a pulmonary infection and treated with caspofungin (50 mg, qd), voriconazole (200 mg, q12 h), sulperazon (1.5 g, q12 h), and ganciclovir (250 mg, qod) by intravenous drip. A bronchoalveolar lavage was performed subsequently, which showed pulmonary mucosa was slightly congested without obvious secretion. Oral anti-immune rejection medications were reduced to tacrolimus 0.5 mg/12 h, mycophenolate mofetil 0.25 g/12 h, and methylprednisolone 24 mg/d.

After seven days of treatment, radiological examination revealed new lesions and the cavity formation in the upper left lung. Based on the examination, multidisciplinary consultation advised that fungal lung infections were possible (aspergillus or mucor), which needs early and definitive diagnosis by biopsy. However, after being informed of the possible complications of lung biopsy, the patient and family refused to biopsy and requested conservative treatment in consideration of the current coagulation profile. The voriconazole was changed to amphotericin B liposome, and cotrimoxazole was treated to prevent bacterial infections. After continuous treatment for several days, the patient began to develop hemoptysis and dark red secretions in the sputum. A chest CT showed consolidation of the left upper lobe with ground-glass opacity and multiple nodules in both lungs. Following informed consent, a CT-guided percutaneous lung biopsy was immediately performed to identify the pathogen under regional anesthesia. The results indicated that fungal hyphae and spores could be seen in the biopsies with a high suspicion of mucormycosis (**Figure 3A**). All oral immunosuppressants were stopped except methylprednisolone, which was gradually reduced to 4 mg/d. Following multidisciplinary consultation and discussion with the patient and relatives, he agreed to abandon the graft immediately and underwent embolization of the transplanted renal artery instead of a transplant nephrectomy to avoid the potential risk of intolerance of surgery. The antibody combination was adjusted as following: amphotericin B liposome (50 mg, qd), posaconazole (400 mg, q12 h), and meropenem (1 g, q8 h). Ten days later, a chest CT showed the cavity in the upper left lung as larger than that in the previous examination. On 78 days after transplantation, the patient suffered acute abdominalgia accompanied by vomiting, high fever, shock, and confusion, meanwhile, the blood pressure dropped to 64/45 mmHg. An emergency exploratory laparotomy was performed and showed a hemorrhage of the spleen, which was then cut off. The pathological results of spleen tissue submitted revealed multiple necroses under capsule with visible mycelium and spores of mold (**Figure 3B**). Despite initial remarkable improvements, the patient developed a round-like mixed slightly low-density shadow in his right cerebellum showed in a brain CT scan on 85 days post-transplant. The patient and his family abandoned any treatment and soon left the hospital. His death was confirmed a few days after follow-up.

DISCUSSION

In recent years, the incidence of pulmonary fungal infections in the clinic has increased rapidly, especially in kidney transplantation recipients (11). The risk factors of pulmonary mycosis post-transplant include further surgery, administration of immunosuppressants, and the short-time use of or without anti-inflammatory drugs (12, 13). To date, fungal infection was still the leading cause of early death in solid organ transplantation recipients (14, 15). Mucor is a rare conditioned pathogen that can severely endanger hypo-immune recipients using various immunosuppressants. Here, we report the complete episode, diagnosis, and treatment process of

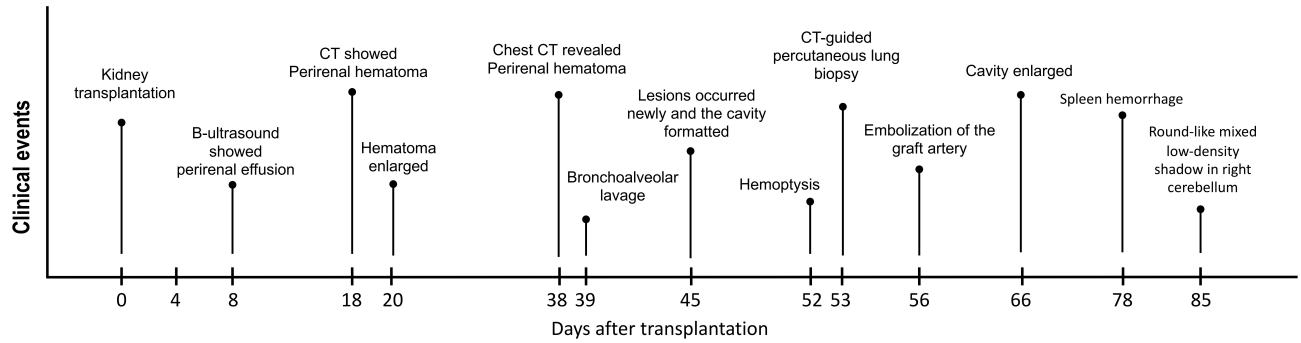

FIGURE 1 | The clinical course of the patient. The pivotal clinical events after surgery of this kidney transplant recipient are showed in this figure.

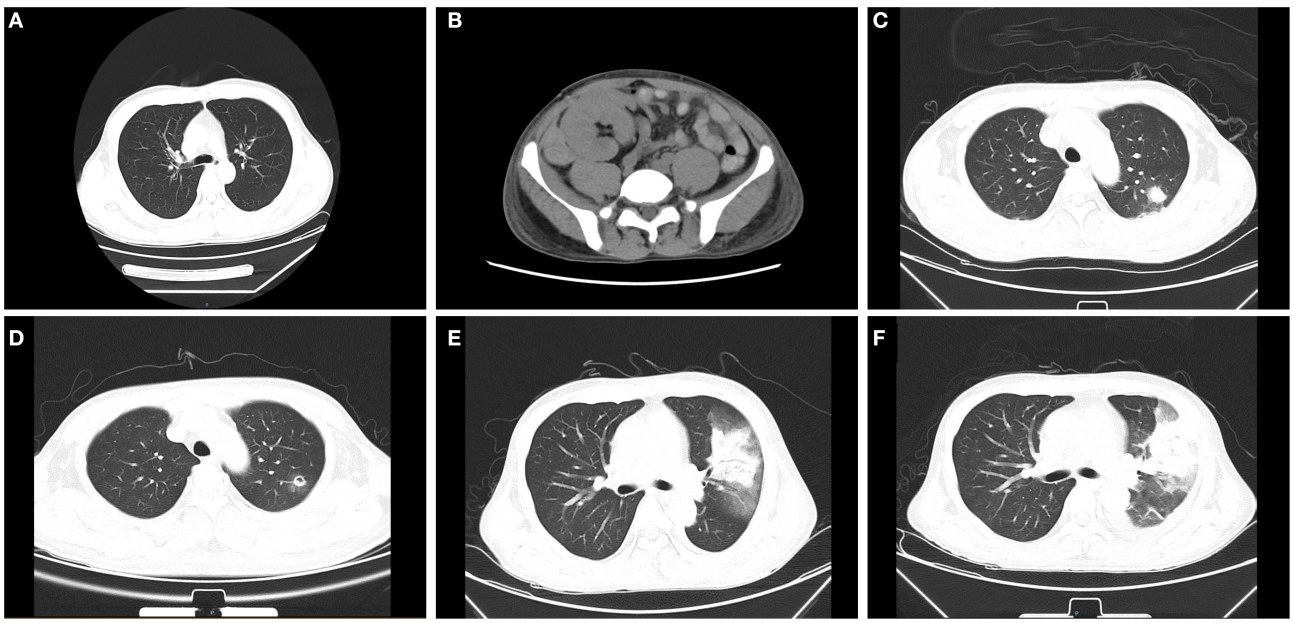

FIGURE 2 | Abdominal and chest computed tomography (CT) scans before and after mucor infection. **(A)** The pre-transplant chest CT is presented without obvious abnormality. **(B)** On 18 days post-transplant, abdominal CT examination revealed a mixed density mass shadow in the medial inferior right side of kidney graft, hematoma considered. **(C)** The chest CT revealed patchy shadows in the left lung on 38 days after transplantation. **(D)** After 7 days of initial treatment, the cavity formed in the left lung can be seen in radiological examination. **(E)** A chest CT showed consolidation of the left upper lobe with a ground-glass density shadow, multiple nodules in both lungs on 52 days. **(F)** A chest CT showed the cavity in the upper left lung had become larger than that in the previous examination 2 weeks earlier.

pulmonary mucormycosis in the patient who underwent a kidney transplantation.

In this patient, DGF and clinical potential graft rejection may be reasons for hematomas appearing early after surgery and compression of the transplanted kidney by a peri-renal hematoma may also exacerbate graft ischemia, delay functional recovery, and limit the patient's absolute bed rest, additionally leading to increased water load and the risk of pulmonary infection (16). It is therefore necessary to discuss the treatment of peri-renal hematoma associated with post-operative transplantation. Peri-renal hematoma is an early complication after renal transplantation, associated with coagulation dysfunction caused by chronic uremia, vascular anastomosis, blocked drainage, and early activity in post-operative patients (12, 17), which may compress blood vessels and renal parenchyma as well as cause oliguria, promote DGF, and even lead to graft loss (18–20). Timely treatment of post-operative peri-renal hematoma is essential. However, there exists a controversy regarding treatment, conservative treatment such as anti-rejection and hemodialysis or surgical intervention like percutaneous drainage, surgical decortication, or laparoscopic intervention are all applicable without definite indications (21, 22). In short, we all agree that expanding hematoma, affecting the blood flow and function of graft, should be explored and evacuated opportunely (23).

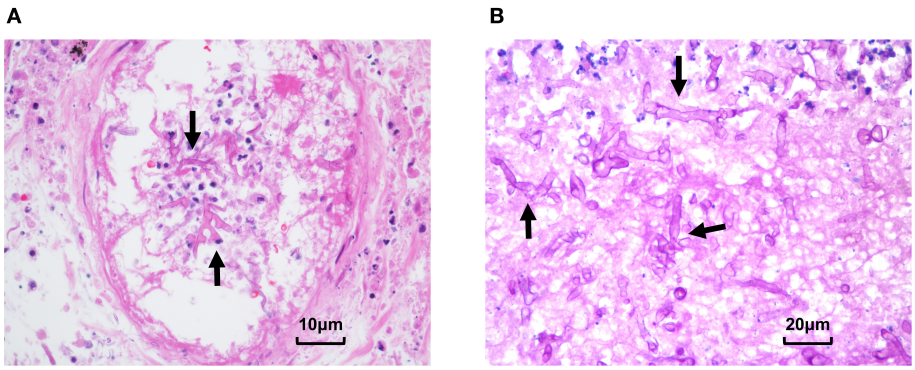

FIGURE 3 | Pathological presentation of pulmonary and splenic mucormycosis. **(A)** Percutaneous lung biopsy showed alveolar epithelial hyperplasia, interstitial hyperemia, inflammatory cell infiltration, and fungal hyphae and spores can be seen in necrotic tissues. **(B)** Pathological results of spleen tissue showed multifocal necrosis was formed under the spleen capsule with mycelia and spores (Arrow: mycelia).

Mucormycosis develops rapidly, has a poor prognosis, and is rarely reported in kidney recipients (24). Considering that mucoromycetes are pathogens that are present in the environment and cause opportunistic infections in immunocompromised individuals, we first identified the foci of infection in the lungs and confirmed the presence of mucor in lung tissue biopsies, the source of this mucormycosis was likely to be the pulmonary infection. In this case, it takes just 15 days from patchy shadows seen in radiological examination to large cavity formation and splenic rupture with fungal infections 25 days later. Early and reliable diagnosis along with the identification of pathogens is necessary for treatment (25). This patient with idiopathic peri-transplantation hematoma, hard on palpation, and abnormal coagulation, a kidney biopsy may result in aggravation of peri-transplantation hematoma or even a rupture of the transplanted kidney. We used lung biopsy and spleen histopathology to confirm the diagnosis of mucormycosis, which usually manifested as negative in the serological examination and non-specific clinical presentations (26). Many researchers are committed to finding new methods for making the diagnosis of mucormycosis earlier leading to improve survival. A previous study reported that mucorales specific T cells detected by an enzyme-linked immunospot can be a surrogated diagnostic marker (27). Molecular assays such as conventional polymerase chain reaction, DNA sequence, and melt curve analysis provide an alternative auxiliary method for the diagnosis (28–30). More attention and effort should be paid to the early diagnosis of mucor infection. It is currently agreed that only amphotericin B and its liposomes, and posaconazole are effective medicines for treating mucor (31). The liposomal amphotericin B is recommended as a first-line therapy because of less renal toxicity (32, 33). A retrospective cohort study of antifungals among inpatients of invasive aspergillosis or mucormycosis highlighted the importance of invasive fungal infection monitoring during hospitalization and the use of appropriate prophylaxis and treatment (34). Other cases have also pointed out that pre-emptive treatment is critical for the rarely seen mucormycosis in organ transplantation recipients (35, 36). There is a contradiction between the treatment of mucormycosis and the use of immunosuppressants against graft rejection. Firstly, immunosuppression promotes the invasion of pathogens. On the other hand, drug-drug interactions, the dose of tacrolimus should be reduced by 60–75% when receiving posaconazole typically (37), which should be evaluated carefully (31). At the early stage of infection, the effective dose of immunosuppressants can be maintained. With the development of the disease, cell proliferation inhibitors should be stopped in time. Then, all inhibitors other than glucocorticoids should be stopped immediately with the rapidly developing and refractory infections. Considering the more than 60% mortality rate in pulmonary mucormycosis after kidney transplantation (38–40), abandoning the graft is a way to reduce loss and advance survival.

In conclusion, we reported the case of pulmonary mucormycosis in kidney transplantation recipients. Prevention and early diagnosis are essential due to the uncontrollable progression of mucor infection. The authors reviewed three key treatments including rational antifungal therapy, timely elimination of immunosuppressants, and abandoning the graft if necessary.

ETHICS STATEMENT

Written informed consent was obtained from the individual(s) for the publication of any potentially identifiable images or data included in this article.

AUTHOR CONTRIBUTIONS

HZ and KW reviewed the case and wrote the article. HC collected the clinical data and revised the report. LS and ZW were involved in collecting clinical data and providing related literature. SF participated in the post-operative management of this case. RT and MG led the treatment of the patient and revised the

manuscript. All authors contributed to the article and approved the submitted version.

FUNDING

This research was supported by the National Natural Science Foundation of China (grant numbers 81900684, 81870512, 81770751, 81570676, 81470981, and 81100532), Project of Jiangsu Province for Important Medical Talent (grant number ZDRCA2016025), the 333 High Level Talents Project in Jiangsu Province (grant numbers BRA2017532, BRA2016514, and BRA2015469), the Standardized Diagnosis and Treatment Research Program of Key Diseases in Jiangsu Province (grant number BE2016791), the Open Project Program of Health Department of Jiangsu Province (grant number JSY-2-2016-099), and the Jiangsu Province Natural Science Foundation Program (grant number BK20191063).

ACKNOWLEDGMENTS

Thanks to all medical workers dedicated to organ transplantation and all the donors and patients.

REFERENCES

1. Zhang H, Shi G, Hu Q, Zhang H, Zheng M, Jiang K, et al. Transcriptional dissection of differentially expressed long non-coding RNAs and messenger RNAs reveals the potential molecular mechanism after kidney transplantation. *Ann Transl Med.* (2019) 7:458. doi: 10.21037/atm.2019.08.60
2. Lim MA, Kohli J, Bloom RD. Immunosuppression for kidney transplantation: where are we now and where are we going? *Transplant Rev.* (2017) 31:10–7. doi: 10.1016/j.trre.2016.10.006
3. Zhang J, Zhang H, Wang Z, Yang H, Chen H, Cheng H, et al. BTLA suppress acute rejection via regulating TCR downstream signals and cytokines production in kidney transplantation and prolonged allografts survival. *Sci Rep.* (2019) 9:12154. doi: 10.1038/s41598-019-48520-7
4. Cai S, Chandraker A. Cell therapy in solid organ transplantation. *Curr Gene Ther.* (2019) 19:71–80. doi: 10.2174/1566523219666190603103840
5. Fishman JA. Infection in organ transplantation. *Am J Transplant*. (2017) 17:856–79. doi: 10.1111/ajt.14208
6. Kinnunen S, Karhapaa P, Juutilainen A, Finne P, Helantera I. Secular trends in infection-related mortality after kidney transplantation. *Clin J Am Soc Nephrol.* (2018) 13:755–62. doi: 10.2215/CJN.11511017
7. Limper AH, Knox KS, Sarosi GA, Ampel NM, Bennett JE, Catanzaro A, et al. American thoracic society fungal working: an official american thoracic society statement: treatment of fungal infections in adult pulmonary and critical care patients. *Am J Respir Crit Care Med.* (2011) 183:96–128. doi: 10.1164/rccm.2008-740ST
8. Enoch DA, Yang H, Aliyu SH, Micallef C. The changing epidemiology of invasive fungal infections. *Methods Mol Biol.* (2017) 1508:17–65. doi: 10.1007/978-1-4939-6515-1_2
9. Neofytos D, Fishman JA, Horn D, Anaissie E, Chang CH, Olyaei A, et al. Epidemiology and outcome of invasive fungal infections in solid organ transplant recipients. *Transpl Infect Dis.* (2010) 12:220–9. doi: 10.1111/j.1399-3062.2010.00492.x
10. Zhang Q, Liu H, Qiu S, Wang W, Yang L, Chen H, et al. A rare case of pulmonary coinfection by lichtheimia ramosa and aspergillus fumigatus in a patient with delayed graft function after renal transplantation. *Transplant Proc.* (2019) 51:551–5. doi: 10.1016/j.transproceed.2018.12.006
11. Stelzmueller I, Lass-Floerl C, Geltner C, Graziadei I, Schneeberger S, Antretter H, et al. Zygomycosis and other rare filamentous fungal infections in solid organ transplant recipients. *Transpl Int.* (2008) 21:534–46. doi: 10.1111/j.1432-2277.2008.00657.x
12. Haberal M, Boyvat F, Akdur A, Kirnap M, Ozcelik U, Yarbug Karakayali F. Surgical complications after kidney transplantation. *Exp Clin Transplant.* (2016) 14:587–95. doi: 10.6002/ect.2016.0290
13. Petrikkos G, Skiada A, Lortholary O, Roilides E, Walsh TJ, Kontoyiannis PD. Epidemiology and clinical manifestations of mucormycosis. *Clin Infect Dis.* (2012) 54(Suppl. 1):S23–34. doi: 10.1093/cid/cir866
14. Baddley JW, Andes DR, Marr KA, Kontoyiannis DP, Alexander BD, Kauffman CA, et al. Pappas: factors associated with mortality in transplant patients with invasive aspergillosis. *Clin Infect Dis.* (2010) 50:1559–67. doi: 10.1086/652768
15. Farmakiotis D, Kontoyiannis PD. Emerging issues with diagnosis and management of fungal infections in solid organ transplant recipients. *Am J Transplant.* (2015) 15:1141–7. doi: 10.1111/ajt.13186
16. Chen G, Zhang Z, Gu J, Qiu J, Wang C, Kung R, et al. Incidence and risk factors for pulmonary mycosis in kidney transplantation. *Transplant Proc.* (2010) 42:4094–8. doi: 10.1016/j.transproceed.2010.10.010
17. Hedges SJ, Dehoney SB, Hooper JS, Amanzadeh J, Busti JA. Evidence-based treatment recommendations for uremic bleeding. *Nat Clin Pract Nephrol.* (2007) 3:138–53. doi: 10.1038/ncpneph0421
18. Salgado OJ, Vidal AM, Semprun P, Garcia R. Conservative management of an extensive renal graft subcapsular hematoma arising during living donor nephrectomy. Role of Doppler sonographic post-transplant follow-up. *J Clin Ultrasound.* (2010) 38:164–7. doi: 10.1002/jcu.20644
19. Ay N, Beyazit U, Alp V, Duymus R, Sevuk U, Anil M, et al. Rupture of a subcapsular hematoma after kidney transplant: case report. *Exp Clin Transplant.* (2017) 15:358–60. doi: 10.6002/ect.2014.0270
20. Chung J, Caumartin Y, Warren J, Luke PP. Acute page kidney following renal allograft biopsy: a complication requiring early recognition and treatment. *Am J Transplant.* (2008) 8:1323–8. doi: 10.1111/j.1600-6143.2008.02215.x
21. Davies MC, Perry JM. Urological management of 'page kidney'. *BJU Int.* (2006) 98:943–4. doi: 10.1111/j.1464-410X.2006.06432.x
22. Ciftci S, Stuart Wolf J. Laparoscopic treatment of page kidney: a report of two cases and review of the literature. *Turk J Urol.* (2013) 39:126–30. doi: 10.5152/tud.2013.024
23. Di Carlo HN, Darras FS. Urologic considerations and complications in kidney transplant recipients. *Adv Chronic Kidney Dis.* (2015) 22:306–11. doi: 10.1053/j.ackd.2015.04.003
24. Patel MH, Patel RD, Vanikar AV, Kanodia KV, Suthar KS, Nigam LK, et al. Invasive fungal infections in renal transplant patients: a single center study. *Ren Fail.* (2017) 39:294–8. doi: 10.1080/0886022X.2016.1268537
25. Lin E, Moua T, Limper HA. Pulmonary mucormycosis: clinical features and outcomes. *Infection.* (2017) 45:443–8. doi: 10.1007/s15010-017-0991-6
26. He R, Hu C, Tang Y, Yang H, Cao L, Niu R. Report of 12 cases with tracheobronchial mucormycosis and a review. *Clin Respir J.* (2018) 12:1651–60. doi: 10.1111/crj.12724
27. Potenza L, Vallerini D, Barozzi P, Riva G, Forghieri F, Zanetti E, et al. Mucorales-specific T cells emerge in the course of invasive mucormycosis and may be used as a surrogate diagnostic marker in high-risk patients. *Blood.* (2011) 118:5416–9. doi: 10.1182/blood-2011-07-366526
28. Springer J, Lackner M, Ensinger C, Risslegger B, Morton CO, Nachbaur D, et al. Clinical evaluation of a mucorales-specific real-time PCR assay in tissue and serum samples. *J Med Microbiol.* (2016) 65:1414–21. doi: 10.1099/jmm.0.000375
29. Kasai M, Harrington SM, Francesconi A, Petraitis V, Petraitiene R, Beveridge MG, et al. Detection of a molecular biomarker for zygomycetes by quantitative PCR assays of plasma, bronchoalveolar lavage, and lung tissue in a rabbit model of experimental pulmonary zygomycosis. *J Clin Microbiol.* (2008) 46:3690–702. doi: 10.1128/JCM.00917-08
30. Skiada A, Lass-Floerl C, Klimko N, Ibrahim A, Roilides E, Petrikkos G. Challenges in the diagnosis and treatment of mucormycosis. *Med Mycol.* (2018) 56:93–101. doi: 10.1093/mmy/myx101
31. Gavalda J, Meije Y, Fortun J, Roilides E, Saliba F, Lortholary O, et al. Invasive fungal infections in solid organ transplant recipients. *Clin Microbiol Infect.* (2014) 20(Suppl. 7):27–48. doi: 10.1111/1469-0691.12660

32. Tissot F, Agrawal S, Pagano L, Petrikkos G, Groll AH, Skiada A, et al. ECIL-6 guidelines for the treatment of invasive candidiasis, aspergillosis and mucormycosis in leukemia and hematopoietic stem cell transplant patients. *Haematologica.* (2017) 102:433–44. doi: 10.3324/haematol.2016.152900
33. Cornely OA, Arikan-Akdagli S, Dannaoui E, Groll AH, Lagrou K, Chakrabarti A, et al. ESCMID and ECMM joint clinical guidelines for the diagnosis and management of mucormycosis. *Clin Microbiol Infect*. (2014) 20(Suppl. 3)5–26. doi: 10.1111/1469-0691.12371
34. Stull K, Esterberg E, Ajmera M, Candrilli S, Kitt TM, Spalding JR, et al. Use of antifungals and outcomes among inpatients at risk of invasive aspergillosis or mucormycosis in the USA: a retrospective cohort study. *Infect Dis Ther.* (2019) 8:641–55. doi: 10.1007/s40121-019-00267-4
35. Peng H, Xiao J, Wan H, Shi J, Li J. Severe gastric mycormycosis infection followed by cytomegalovirus pneumonia in a renal transplant recipient: a case report and concise review of the literature. *Transplant Proc.* (2019) 51:556–60. doi: 10.1016/j.transproceed.2018.12.023
36. Thomas S, Pawar B, Fernandes D, Nayar S, George P, Cherian S. An unusual case of pulmonary mucormycosis. *Transplant Proc.* (2018) 50:3943–5. doi: 10.1016/j.transproceed.2018.06.001
37. Sansone-Parsons A, Krishna G, Martinho M, Kantesaria B, Gelone S, Mant GT. Effect of oral posaconazole on the pharmacokinetics of cyclosporine and tacrolimus. *Pharmacotherapy.* (2007) 27:825–34. doi: 10.1592/phco.27.6.825
38. Bodro M, Sabe N, Gomila A, Ayats J, Baliellas C, Roca J, et al. Risk factors, clinical characteristics, and outcomes of invasive fungal infections in solid organ transplant recipients. *Transplant Proc.* (2012) 44:2682–5. doi: 10.1016/j.transproceed.2012.09.059
39. Einollahi B, Rostami Z. Mucormycosis after kidney transplantation. *Saudi J Kidney Dis Transpl.* (2013) 24:576–7. doi: 10.4103/1319-2442.111070
40. Kuy S, He C, Cronin DC. Renal mucormycosis: a rare and potentially lethal complication of kidney transplantation. *Case Rep Transplant*. (2013) 2013:915423. doi: 10.1155/2013/915423

Conflict of Interest: The authors declare that the research was conducted in the absence of any commercial or financial relationships that could be construed as a potential conflict of interest.

frontiers in Medicine

ORIGINAL RESEARCH
published: 25 November 2020
doi: 10.3389/fmed.2020.531999

Plasma Soluble CD146 as a Potential Diagnostic Marker of Acute Rejection in Kidney Transplantation

Jun Liao[1†], Qian Fu[1†], Wenfang Chen[2†], Jun Li[1], Wenhui Zhang[2], Huanxi Zhang[1], Yifang Gao[1,3], Shicong Yang[2], Bowen Xu[1], Huiting Huang[1], Jiali Wang[4], Xirui Li[1], Longshan Liu[1] and Changxi Wang[1,3]**

[1] Organ Transplant Center, The First Affiliated Hospital of Sun Yat-sen University, Guangzhou, China, [2] Department of Pathology, The First Affiliated Hospital of Sun Yat-sen University, Guangzhou, China, [3] Guangdong Provincial Key Laboratory on Organ Donation and Transplant Immunology, Guangzhou, China, [4] Department of Nephrology, The First Affiliated Hospital of Sun Yat-sen University, Guangzhou, China

OPEN ACCESS

Edited by:
Cheng Yang,
Fudan University, China

Reviewed by:
Yang Lyu,
Washington University in St. Louis, United States
Helong Dai,
Central South University, China

***Correspondence:**
Longshan Liu
liulshan@mail.sysu.edu.cn
Changxi Wang
wangchx@mail.sysu.edu.cn

[†]These authors have contributed equally to this work

Specialty section:
This article was submitted to Nephrology, a section of the journal Frontiers in Medicine

Received: 02 February 2020
Accepted: 21 September 2020
Published: 25 November 2020

Citation:
Liao J, Fu Q, Chen W, Li J, Zhang W, Zhang H, Gao Y, Yang S, Xu B, Huang H, Wang J, Li X, Liu L and Wang C (2020) Plasma Soluble CD146 as a Potential Diagnostic Marker of Acute Rejection in Kidney Transplantation. Front. Med. 7:531999. doi: 10.3389/fmed.2020.531999

Previous studies have implicated the role of CD146 and its soluble form (sCD146) in the pathogenesis of inflammatory diseases. However, the association between CD146 and acute rejection in kidney transplant patients remains unexplored. In this study, fifty-six patients with biopsy-proved rejection or non-rejection and 11 stable allograft function patients were retrospectively analyzed. Soluble CD146 in plasma was detected in peripheral blood by enzyme linked immunosorbent assay (ELISA), and local CD146 expression in graft biopsy was detected by immunohistochemistry. We found that plasma soluble CD146 in acute rejection recipients was significantly higher than in stable patients without rejection, and the biopsy CD146 staining in the rejection group was higher than that of the non-rejection group. Multivariate analysis demonstrated soluble CD146 as an independent risk factor of acute rejection. The area under the receiver operating characteristic curve (AUC) of sCD146 for AR diagnosis was 0.895, and the optimal cut-off value was 75.64 ng/ml, with a sensitivity of 87.8% and a specificity of 80.8%, which was better than eGFR alone ($P = 0.02496$). Immunohistochemistry showed CD146 expression in glomeruli was positively correlated with the Banff-g score, and its expression in tubules also had a positive relationship with the Banff-t score. Therefore, soluble CD146 may be a potential biomarker of acute rejection. Increased CD146 expression in the endothelial or tubular epithelial cells may imply that endothelial/epithelial dysfunction is involved in the pathogenesis of immune injury.

Keywords: kidney transplantation, acute rejection, biomarker, melanoma cell adhesion molecule, endothelial dysfunction

INTRODUCTION

Kidney transplantation is a preferred treatment for patients with end stage renal disease (ESRD), improving quality of life and survival more so than dialysis (1). While current immunosuppressants have improved the short-term outcomes of kidney transplantation, long-term allograft loss remains a significant conundrum. Acute rejection (AR) as a result of alloimmune injury due to individual genetic differences and inadequate immunosuppression occurs in 10–20% of kidney transplant recipients and could cause allograft dysfunction. Repeated rejection episodes undoubtedly

aggravate long-term renal allograft survival (2, 3). Early detection and intervention of ongoing allogeneic immune response may hinder development of rejection, alleviate immunological lesions, sustain renal function, and improve long-term graft survival. The early monitoring strategy prevents the need for later costly treatment of rejection and subsequent allograft dysfunction and provides more cost-effective benefits. In current clinical practice, acute rejection is suspected when renal function parameters such as serum creatinine and urine protein are abnormal or unstable. Renal allograft biopsy is then implemented as a gold-standard procedure to determine the diagnosis of rejection. The change of renal function parameters often lags behind the ongoing immune response and pathological lesions. Renal biopsy, as an invasive technique, may lead to surgical complications, such as bleeding, hematuria, perirenal hematoma, arteriovenous fistulas, and even graft loss (4–6), limiting its clinical usage as a consecutive monitoring tool. The needs of non-invasive or less invasive biomarkers which are necessary to discriminate rejection early from other disorders causing graft dysfunction are unmet in the field of kidney transplantation.

CD146, known as melanoma cell adhesion molecule (MCAM), is an integral membrane glycoprotein, which belongs to the immunoglobulin superfamily. Different from other widely expressed cell adhesion molecules, its expression is mainly limited to endothelial cells and pericytes (7). Besides, there are about 1–2% of lymphocytes that are detected as CD146-positive. CD146 on lymphocytes enhances production of proinflammatory cytokines and prompts inflammation (8, 9). The soluble form of CD146 (sCD146) derives from the shedding of membrane CD146 (10), and has been detected in the supernatant of endothelial cell culture medium and in the peripheral blood of patients and healthy population. Membrane CD146 and soluble CD146 can both function in cell-cell conjunction and vessel integrity, and are associated with cell signaling, migration, proliferation, differentiation, and angiogenesis (11, 12), as well as the pathogenesis of multiple illnesses including autoimmune diseases (13–15), tumors (16–19), acute heart failure (20–22), and ischemic disorders (23, 24).

A previous study found a significant increase of sCD146 in patients with chronic renal failure (CRF) compared to the heathy control, and this increase was correlated with elevated endothelial expression of CD146 in renal biopsies. It was indicated CD146 reflected the degree of endothelial dysfunction which is one of the critical changes in CRF (25). In a cohort of kidney transplantation, Malyszko and his colleagues found circulating sCD146 was higher in recipients with coronary artery disease (CAD), and this phenomenon was more apparent in patients with lower renal allograft function (26). Studies have shown the activation and injury of endothelial cells is an essential event in the initial of either T cell-mediated rejection (TCMR) or antibody-mediated rejection (ABMR). To date, clinical implication of CD146 in monitoring acute rejection after kidney transplantation has not been well-explored. We hypothesize circulating sCD146 or CD146 expression in renal allografts increases in kidney transplant patients with acute rejection. In this study, plasma sCD146 and CD146 expression in allograft biopsies of renal transplant recipients were examined to evaluate the capability of sCD146 as a less invasive biomarker of acute rejection.

Abbreviations: ABMR, antibody-mediated rejection; ANOVA, analysis of variance; AR, acute rejection; AUC, area under the curve; BBB, blood brain barrier; CAD, coronary artery disease; CAN, chronic allograft nephropathy; CNINT, calcineurin inhibitors nephrotoxin; CNS, central nervous system; CRF, chronic renal failure; EDTA, ethylenediaminetetra-acetic acid; ELISA, enzyme linked immunosorbent assay; ESRD, end stage renal disease; eGFR, estimated glomerular filtration rate; IBD, inflammatory bowel disease; IF/TA, interstitial fibrosis and tubular atrophy; IQR, interquartile range; MCAM, melanoma cell adhesion molecule; NPV, negative predictive value; PBS, phosphate buffered saline; PPV, positive predictive value; ROC, receiver operating characteristic curve; TCMR, T cell mediated rejection.

PATIENTS AND METHODS

Study Subjects

Kidney transplantation recipients who received indicated allograft biopsies from May 2016 to May 2019 in Organ Transplant Center, The First Affiliated Hospital of Sun Yat-sen University were included in this study. A total of 143 patients who underwent a renal allograft biopsy and had blood samples were included in the study. Patients with the following conditions were excluded: (1) systematic autoimmune diseases including systemic lupus erythematosus (SLE), antineutrophil cytoplasmic antibody (ANCA) glomerulonephritis, inflammatory bowel diseases (IBD), Crohn's disease and multiple sclerosis, etc; (2) diabetes mellitus; (3) active infection; (4) tumors; (5) no peripheral blood samples available before the day of biopsy. We also excluded the mixed rejection in order to more clearly figure out whether there is a difference between two types of rejection. In practice, 56 patients who met the criteria were included in the cohort analysis. Furthermore, we also enrolled 11 renal transplant patients from a surveillance program after kidney transplantation, who visited the outpatient clinic of our center at the same period, as a control group reflecting postoperative normal state. These controls had a stable allograft function, and no history of kidney diseases, diabetes, cardiovascular events, or autoimmune disorders. Hypertension, if present, was treated with a maximum of one class of antihypertensive drugs.

This study was approved by the institutional ethics committee and was conducted according to the standards of the Declaration of Helsinki. Informed consent was obtained from all subjects.

Clinical and laboratory data was collected including blood count, blood urea nitrogen, serum creatinine, serum electrolytes (potassium, sodium, and calcium), urine analysis, immunosuppression (calcineurin inhibitor trough level), and donor specific antibody (DSA). Estimated glomerular filtration rate (eGFR) was calculated according to MDRD formula (27).

Diagnosis of Acute Rejection

All biopsies were reviewed by two independent pathologists according to the Banff classification (28, 29). Acute rejection includes antibody-mediated rejection (ABMR) and T cell-mediated rejection (TCMR). Briefly, the diagnostic criteria of acute ABMR are (1) histologic evidence of acute tissue

injury, including one or more of the following: microvascular inflammation, intimal or transmural arteritis, acute thrombotic microangiopathy, and acute tubular injury; (2) evidence of antibody interaction with vascular endothelium, including at least one of the following: linear C4d staining in peritubular capillaries, at least moderate microvascular inflammation, and increased expression of gene transcriptions in the biopsy tissue indicative of endothelial injury; (3) serologic evidence of donor-specific antibodies. Acute TCMR is defined as significant interstitial inflammation and foci of moderate or severe tubulitis and/or different levels of intimal arteritis.

Examination of Plasma sCD146 With Enzyme Linked Immunosorbent Assay (ELISA)

Peripheral blood samples were collected in plastic tubes containing ethylenediaminetetraacetic acid (EDTA) and were centrifuged at 3,000 rpm for 15 min. The supernatants were stored at −80°C until they were analyzed. Repeated thawing and freezing of the blood samples were forbidden. At the day of testing, the samples were simultaneously thawed and analyzed in triplicate. The concentration of sCD146 was determined by ELISA (RayBio® Human MCAM ELISA Kit, RayBiotech, USA) according to the manufacturer's instructions.

Detection of CD146 Expression in Allograft Biopsies With Immunohistochemistry (IHC) Staining

CD146 immunohistochemistry staining was only performed in patients with biopsy, excluding the stable controls. Sections from formalin-fixed and paraffin-embedded tissues were dewaxed in xylene and ethanol. After antigen retrieval and endogenous peroxidase blocking, the sections were incubated with primary anti-CD146 antibody (rabbit monoclonal antibody; Abcam, Cambridge, UK), then were washed with phosphate buffered saline (PBS) before application of the anti-rabbit secondary antibody. Following 3 washes with PBS, the sections were developed with 3,3′-diaminobenzidine (DAB), and then counterstained with hematoxylin and eosin (H&E).

CD146 staining was calculated with a semi-quantitative score, as previously described (30, 31). The method, scoring the extent of CD146 staining in renal glomeruli and tubules, was as follows: Under a 200-fold microscopic field of view, 5 microscopic visions were randomly selected. In each vision, we estimated each glomerulus as follows: score 0, absence of specific staining; score 1, <25% area has specific staining for CD146; score 2, 25–50%; score 3, 50–75%; and score 4, >75%, and calculated the arithmetic average of the glomerular scores of one vision. The staining of tubular compartment was also scored on a scale of 0–4, using the same method. Then the mean value of the glomerular and tubular scores in 5 random visions were regarded as the semi-quantitative score of the glomerular and tubular CD146 staining in one patient. Representative PSAM staining of ABMR, TCMR and IF/TA are shown in **Supplement Figure 1**.

Statistical Analysis

Continuous variables were described as mean and standard deviation, or median (interquartile range), as appropriate after testing for normality using the Shapiro-Wilk test. Categorical variables were described as number (percentage). Differences between the two groups were assessed with *t*-test, Wilcoxon rank sum test, or Fisher's exact test. One-way analysis of variance (ANOVA) with Tukey's multiple comparisons test or Kruskal-Wallis test with Dunn's multiple comparisons test were used when more than two groups were compared. The correlation of sCD146 and eGFR was assessed by Pearson test. Receiver operating characteristic curve (ROC) analysis of plasma sCD146 level and eGFR, and calculation of the corresponding area under the curve (AUC) was performed. The difference between two AUCs was compared using the Delong test. The optimal cut-off point was defined by the Yoden index. Logistic regression analysis was used to assess the risk factors for acute rejection. A value of $P < 0.05$ was considered to indicate statistical significance. Internal validation was performed using 2000-bootstrap resamples and the optimism-corrected AUC was also calculated. The seed for randomization was 20200101. All statistical analyses were performed using GraphPad Prism (v.7.04) and R software (v.2.10.1).

RESULTS

From May 2016 to May 2019, 56 patients, who met the inclusion and exclusion criteria and had matched blood samples, and 11 outpatients with stable allograft function were included in this study. The active rejection subgroup contained ACMR ($n = 21$) and TBMR ($n = 20$). The non-rejection cohort contained interstitial fibrosis and tubular atrophy (IF/TA, $n = 7$), calcineurin inhibitors (CNIs) nephrotoxicity ($n = 4$), and normal tissue ($n = 4$). The indication of biopsy included elevated serum creatinine ($n = 37$), proteinuria ($n = 10$), or both ($n = 9$). Patient characteristics are summarized in **Table 1**. Rejection patients had a mean age of 38.2 ± 10.7 years; 82.9% of rejection patients were male. At baseline, they were 245 [IQR, 149-1506] days after transplantation, had a mean eGFR of 43.9 ± 18.5 mL/min/1.73 m^2, a median urinary protein excretion of 0.27 [IQR, 0.16–0.72] g/24 h. Non-rejection patients had a mean age of 32.1 ± 8.1 years; 73.3% patients were male. They were 430 [IQR, 163.5-2811] days after transplantation, had a mean eGFR of 56.6 ± 25.4 mL/min/1.73 m^2, a median urinary protein excretion of 0.29 [IQR, 0.21–0.49] g/24 h stable controls had a mean age of 40.6 ± 10.3 years; 54.5% patients were male. They were 196 [IQR, 171–587] days after transplantation, had a mean eGFR of 74±22.6 mL/min/1.73 m^2, a median urinary protein excretion of 0.17 [IQR, 0.1-0.21] g/24 h. All patients were primary transplant recipients, and received calcineurin inhibitors, mycophenolate, and prednisone as maintenance immunosuppressive therapy.

Soluble CD146 Level Was Higher in Renal Transplantation Patients With Rejection

sCD146 level in the rejection group (89.8 ± 12.8 ng/ml) was significantly higher than that in the non-rejection group (73.8 ±

7.9 ng/ml, $P < 0.0001$) and control subjects (62.8 ± 8.3 ng/ml, $P < 0.0001$). The non-rejection group was slightly higher than the stable group ($P = 0.0557$) (**Figure 1A**). We then compared the differences of sCD146 levels between the six subgroups, i.e., TCMR, ABMR, IF/TA, CNI nephropathy, the normal tissue, and stable subjects. The sCD146 level in ABMR patients (90.0 ± 14.1 ng/ml) was higher than that in CNI nephropathy (69.5 ± 3.3 ng/ml, $P = 0.0193$), normal tissue on biopsy (70.3 ± 5.5 ng/ml, $P = 0.0272$) and stable subjects (62.8 ± 8.3 ng/ml, $P < 0.0001$), but TCMR (89.5±11.8 ng/ml, $P > 0.9999$) and IF/TA (78.2 ± 9.0 ng/ml, $P = 0.1798$). The sCD146 level of TCMR patients was higher than that of CNI ($P = 0.0252$), normal tissue ($P = 0.0351$), and control group ($P < 0.001$), but IF/TA ($P = 0.2255$) (**Figure 1B**).

TABLE 1 | Characteristics of kidney transplantation patients.

Clinical Characteristics	Patients with biopsy		Stable patients
	Rejection	Non-rejection	
Number of patients	41	15	11
Age at enrollment, y	38.2 ± 10.7	32.1 ± 8.1	40.6 ± 10.3
Men, *n* (%)	34 (82.9)	11 (73.3)	6 (54.5)
Post-transplant time d (IQR)[a]	245 (149, 1506)	430 (163.5, 2811)	196 (171, 587)
Donor type, *n* (%)			
Deceased donor	25 (61)	10 (66.7)	6 (54.5)
Living donor	16 (39)	5 (33.3)	5 (45.5)
Donor age, y	43.6 ± 15.4	42.3 ± 15.4	38.1 ± 17.7
Donor gender, Men, *n* (%)	26 (63.4)	9 (60)	5 (45.5)
Cold ischemia time, min	7.5 ± 4.2	10 ± 5.2	6.9 ± 3.5
HLA mismatch	2.2 ± 0.8	1.9 ± 0.9	1.6 ± 0.8
DSA MFI_{max} (IQR)	5635 (4618, 7590.5)[c]	–	–
eGFR[b] $[ml*min^{-1}*(1.73m^2)^{-1}]$	43.9 ± 18.5* ####	56.6 ± 25.4*	74.0 ± 22.6
Serum creatinine μmol/L	180.5 ± 71.5* ####	132.2 ± 46.1	87.0 ± 14.9
Proteinuria g/24 h (IQR)	0.27* (0.16, 0.72)	0.29* (0.21, 0.49)	0.17 (0.1, 0.21)

*Compared with the group of stable patients, *P < 0.05.*
Compared with the group of non-rejection, ####P < 0.0001.
[a]*IQR, interquartile range.*
[b]*eGFR, estimated glomerular filtration rate.*
[c]*the data is derived from ABMR subgroup.*

Plasma sCD146 Significantly Contributed to Discrimination of Acute Rejection

As shown in **Figure 2**, sCD146 levels were negatively correlated with allograft function (Pearson $r = -0.38$, $P = 0.0015$). The diagnostic value of sCD146 for acute rejection may be affected by renal function. Thus, the logistic regression analysis was performed (**Table 2**). In the univariate model, sCD146 level, eGFR, and serum creatinine level were correlated with the occurrence of acute rejection. We included the parameters of which $P < 0.10$ into the multivariate logistic analysis. It was found that sCD146 level was the only independent risk factor of acute rejection.

ROC curve analysis of sCD146 level and eGFR for the diagnosis of acute rejection was performed. The AUC of sCD146 was 0.895 (95% CI: 0.821–0.968; ($P < 0.001$), and the AUC of eGFR was 0.735 (95%CI: 0.605–0.865; $P = 0.001$). The optimal cut-off value of sCD146 was 75.64 ng/ml, the sensitivity was 87.8%, the specificity was 80.8%, and the corresponding positive predictive value (PPV) and negative predictive value (NPV) were 87.8 and 80.8%, respectively. Examination using the DeLong

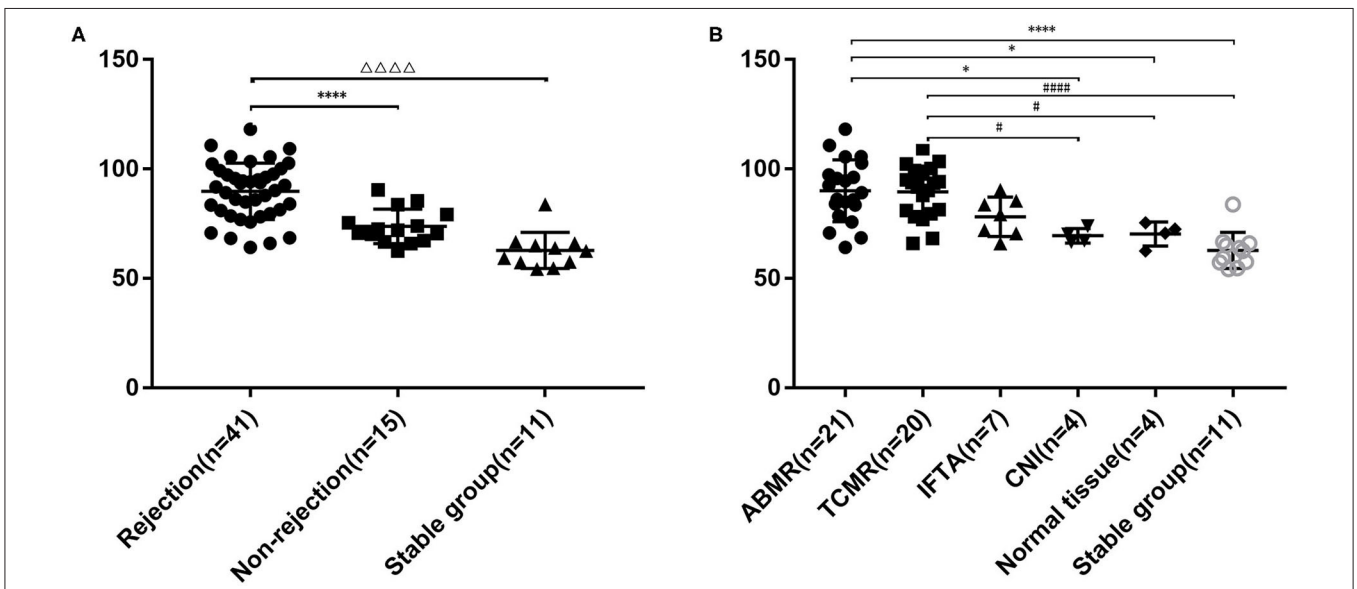

FIGURE 1 | Plasma sCD146 level in kidney transplant patients with or without rejection and stable patients. **(A)** Comparison of sCD146 levels between patients with and without rejection and stable patients. The statistical differences among groups were assessed by one-way ANOVA. Statistical significance: $^{\Delta\Delta\Delta\Delta}P < 0.0001$, $^{****}P < 0.0001$. **(B)** Comparison of sCD146 levels between patients with ABMR, TCMR, IF/TA, CNI, normal allograft tissue, and stable kidney function. The statistical differences among groups were assessed by one-way ANOVA. Statistical significance: $^{*}P < 0.05$, $^{****}P < 0.0001$, $^{\#}P < 0.05$, and $^{\#\#\#\#}P < 0.0001$.

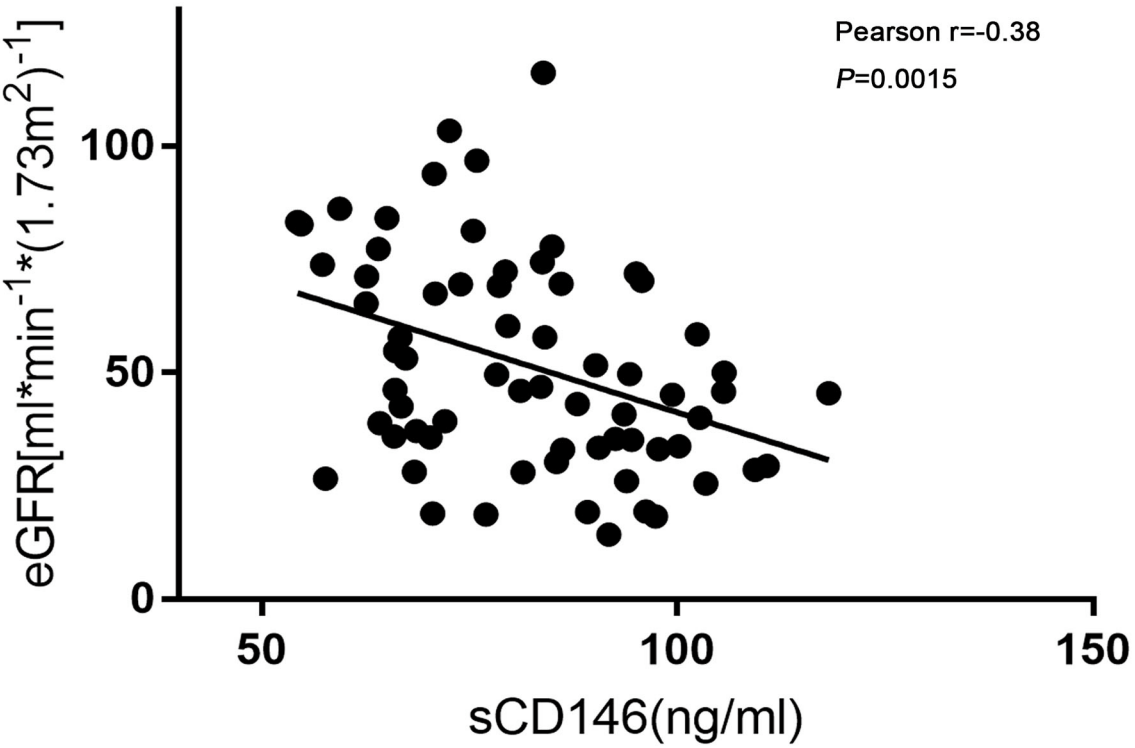

FIGURE 2 | Correlation of sCD146 and eGFR. Soluble CD146 was negatively correlated with eGFR. Pearson $r = -0.38$, $P = 0.0015$.

TABLE 2 | Univariate and multivariate logistic regression analysis for parameters of diagnostics of acute rejection.

	univariate		multivariate	
	OR (95%CI)	*P*	OR (95%CI)	*P*
sCD146	1.159 (1.083, 1.241)	<0.001	1.156 (1.069, 1.251)	<0.001
eGFR	0.959 (0.935, 0.984)	0.001	0.996 (0.997, 1.038)	0.853
Creatinine	1.023 (1.010, 1.036)	0.001	1.016 (0.997, 1.036)	0.108

test found a significant difference between the AUC of sCD146 and the AUC of eGFR ($P = 0.02496$) (**Figure 3**). Furthermore, we established a combination model of sCD146 and eGFR to evaluate its diagnostic value for acute rejection, looking forward to enhancing sCD146's effectiveness. The combination model had an AUC of 0.912 (95%CI: 0.845–0.979) ($P < 0.001$), sensitivity of 82.9%, and specificity of 88.5%. The model also showed good diagnostic performance in internal validation (optimism-corrected AUC: 0.9042). The difference of the AUC between the combined model and eGFR alone ($P = 0.003$) was significant, but the combined model was not superior to sCD146 alone ($P = 0.3697$). The model also showed good diagnostic performance in internal validation (optimism-corrected AUC is 0.9042). The results suggest sCD146 significantly contributed to the diagnosis of acute rejection.

ROC curve analysis of sCD146 level and eGFR for the diagnosis of ABMR was performed, too. The AUCs of sCD146 (AUC = 0.725) and the combination model (AUC = 0.717) are better than eGFR (AUC = 0.566), respectively ($P < 0.05$). But the AUCs of sCD146 and the combination model are not significantly different ($P > 0.05$) (**Supplement Figure 2**).

Local Expression of CD146 Increased in Renal Allograft Biopsies With Acute Rejection

CD146 expression in renal allograft biopsy sections was examined with IHC staining. Representative slide images of allograft biopsies are shown in **Figure 4**. The semi-quantitative scoring analysis of CD146 staining shows that the rejection group had more and stronger positive areas of CD146 expression in allograft glomeruli and tubules than the non-rejection group (**Figures 5A,C**). Considering the differences in the pathogenesis and pathological manifestations of ABMR and TCMR, we separated the two types of rejection and compared the expression of glomeruli and tubules, respectively (**Figures 5B,D**). The allograft biopsied from ABMR biopsies had more positive areas of CD146 expression in the glomerular compartment, while the range of tubular CD146 expression was relatively modest. We did not observe much positive expression in peritubular capillaries, so it was difficult to judge the condition of peritubular capillaries CD146 expression. In contrast, in patients with TCMR

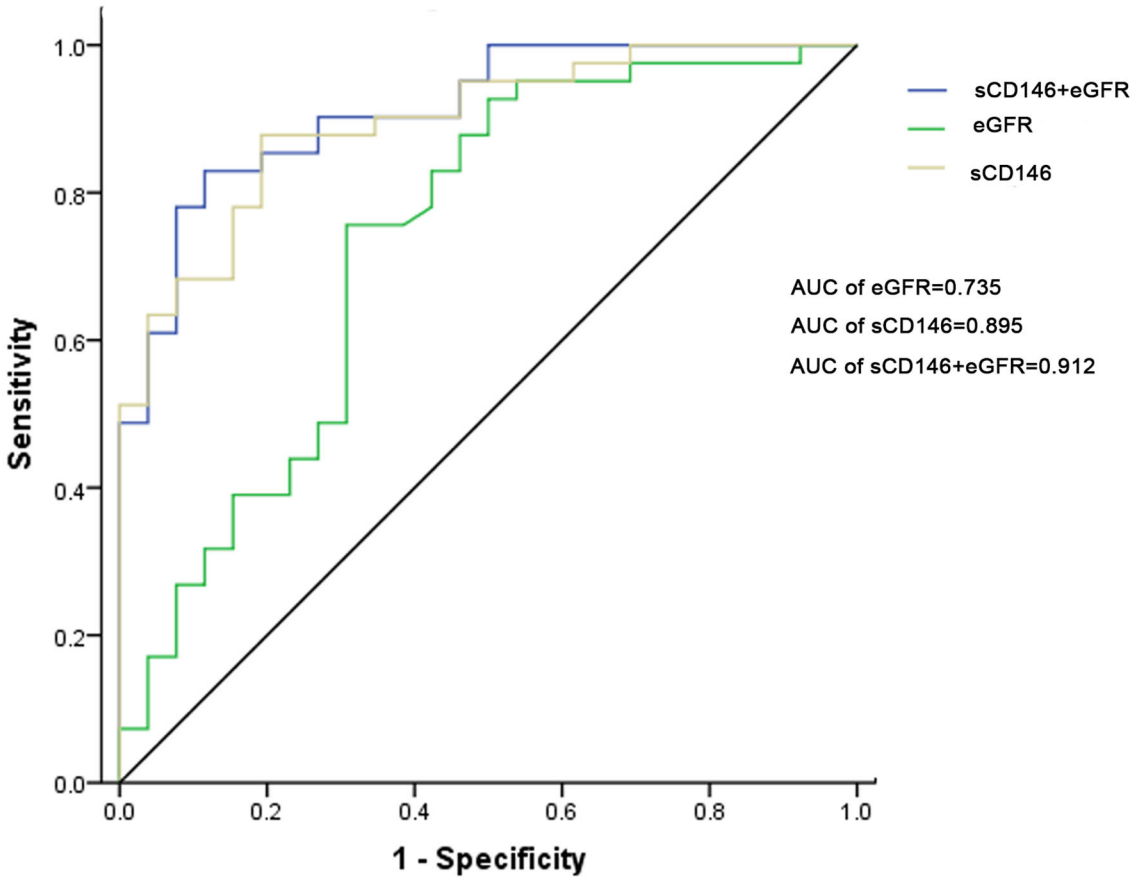

FIGURE 3 | ROC curves for sCD146, eGFR, and the combination model to diagnose acute rejection. The AUC of sCD146 was higher than that of eGFR ($P = 0.02496$). The AUC of the combination model was not higher than that of sCD146 ($P = 0.3697$), but higher than that of eGFR ($P = 0.003$).

the staining expression of the tubular compartment was higher than that of the glomerular compartment. These data suggest that an increased, distribution-different expression of CD146 in glomeruli and tubules may be associated with these two kinds of rejections that were, respectively, characterized by glomerulitis and tubulitis.

Allograft Expression of CD146 Was Associated With Banff Score

The correlation of CD146 expression in renal biopsy specimens with Banff score was further analyzed. The median values of glomerular and tubular CD146 staining scores were defined as the corresponding cut-offs. The high glomerular CD146 expression was defined as glomerular semi-quantitative score $\geq$1.7, and the high tubular CD146 expression was defined as tubular semi-quantitative score $\geq$1.5. Our results showed that high glomerular CD146 expression was positively correlated with increased Banff g score ($P < 0.0001$), and high tubular CD146 expression was positively correlated with increased Banff t score ($P < 0.0001$) (**Figure 6**). These results suggest that CD146 expression in renal biopsy specimens may be useful for evaluating the severity of inflammatory infiltration in acute rejection.

DISCUSSION

The results of this study suggest that plasma sCD146 level may be useful for monitoring acute rejection in renal transplant recipients, and sCD146 might function as a pro-inflammatory marker which facilitates the development of rejection.

Prior studies have shown that CD146 and its soluble form are associated with endothelial dysfunction or injury and play a crucial role in inflammatory diseases. Bardin et al. reported that CD146 expression was increased in endothelial cells from intestinal biopsy specimens from patients with active IBD, Crohn's disease or ulcerative colitis, especially in actively inflamed areas. The results reflected the important role of CD146 in endothelial dysfunction, vascular permeability, and vessel proliferation (14). Studies of multiple sclerosis, which is an inflammatory disease of the central nervous system, showed the expression of CD146 in the blood-brain-barrier promoted the transmigration of leukocytes, effectively triggering

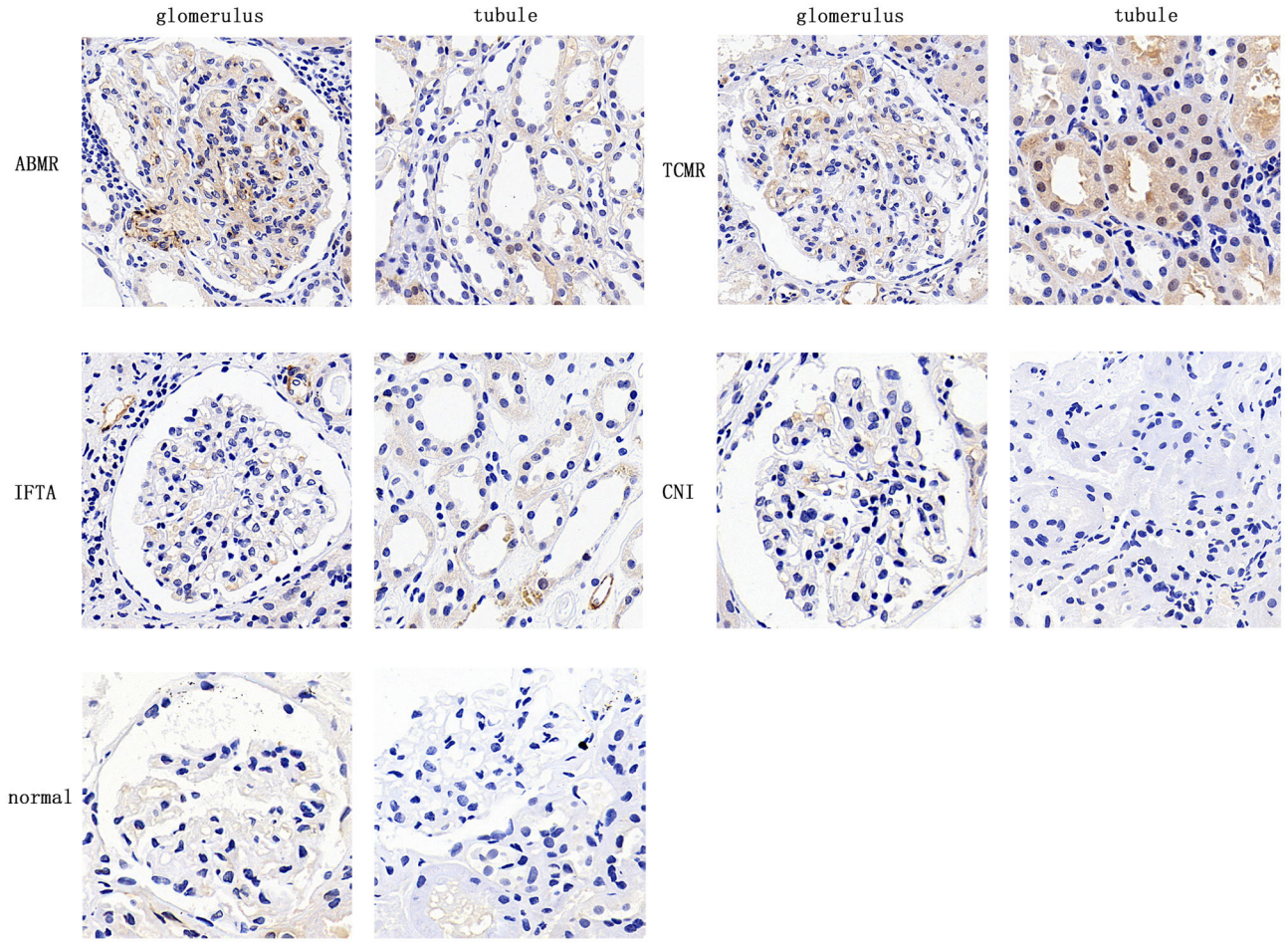

FIGURE 4 | Expression of CD146 in allograft biopsy specimens of kidney transplant patients. Representative image of CD146 staining in 5 groups (×400).

focal inflammation (13, 15, 32). Higher sCD146 levels in the cerebrospinal fluid of patients with multiple sclerosis are also correlated with the disease severity. In the current study, we found that the level of sCD146 was higher in recipients with acute rejection, implying the allografts were in an active inflammatory phase, in accordance with the previous research results about inflammation related diseases. Endothelial dysfunction has a significant impact on the pathogenesis of acute rejection (33), so we claimed that sCD146, as a marker of endothelial dysfunction, may be useful for estimating the severity of inflammation and the seriousness of acute rejection.

When designing the study, we excluded the mixed rejection patients because of the consideration of the different mechanisms of ABMR and TCMR, which might differ the concentrations of sCD146. The main feature of ABMR is that the antigens of vascular endothelial cells are recognized by various antibodies, causing a series of subsequent rejection effects, however, TCMR involves the infiltration of mononuclear lymphocytes into renal tubules and interstitial. Unexpectedly, the plasma levels in both rejection subgroups were elevated. Three possibilities may explain the phenomenon: (1) TCMR is also involved in intimal arteritis, which can cause an increase in soluble CD146; (2) renal tubular epithelial cells are induced to express CD146 (30), which resulted in increased plasma concentration after shedding; (3) the experimental or statistical error caused by the too-small sample size.

We found that a sCD146 plasma level of 75.64 ng/ml had a specificity of 87.8% and a sensitivity of 80.8% for predicting acute rejection, with an AUC of 0.895. We further established a combination model suing sCD146 and eGFR, which had an AUC of 0.912, a sensitivity of 82.5%, and a specificity of 88.9% for discriminating acute rejection. According to our model, the detection of sCD146 alone had a high sensitivity and specificity, which meant that patients who used sCD146 level to detect whether acute rejection occurs might have relatively satisfactory diagnostic accuracy. When combined with eGFR to form a joint model, the AUC of the novel model seems to improve up to 0.912, but statistical analysis does not support this modest improvement. In patients with abnormal or unstable renal function after transplantation, sCD146 may have the potential to

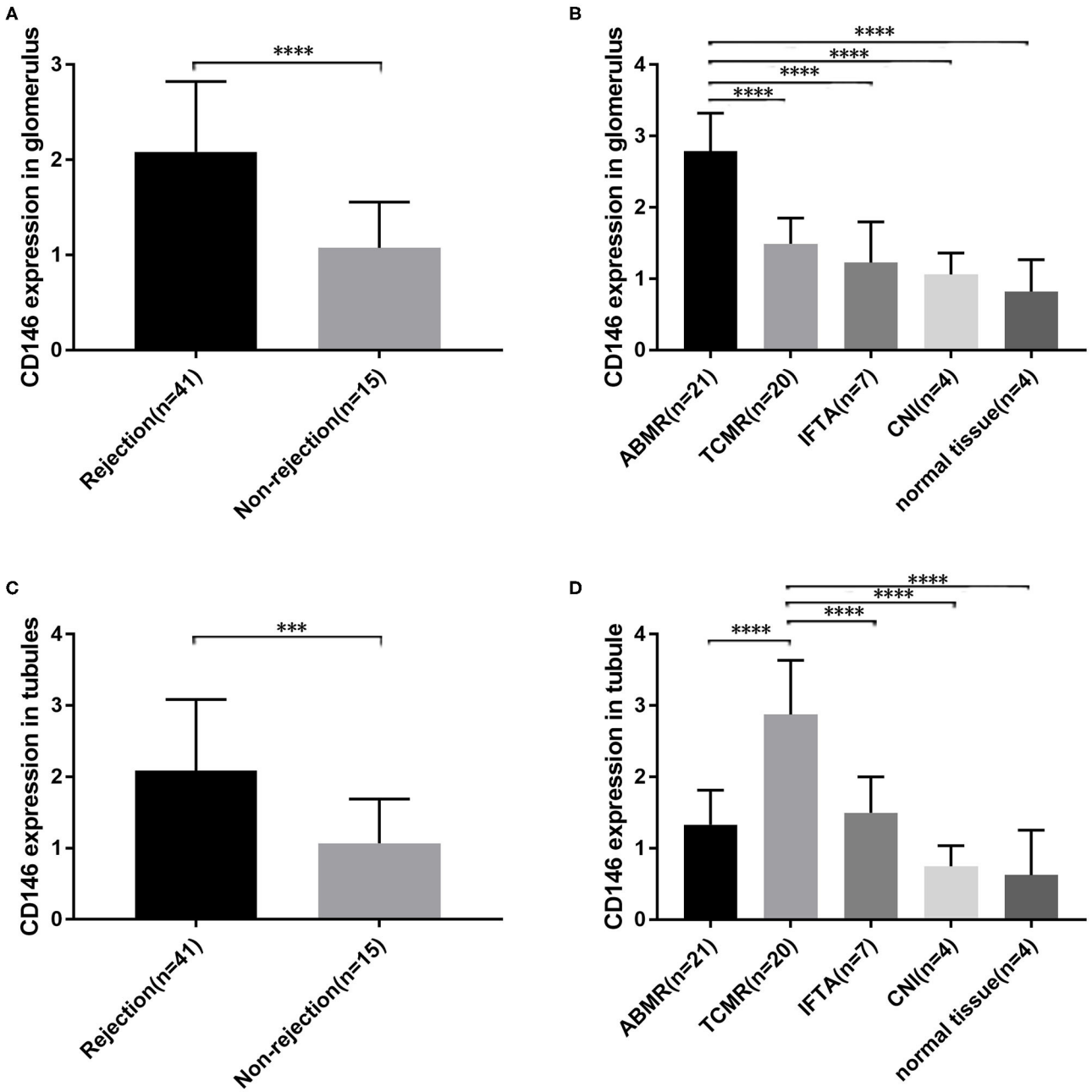

FIGURE 5 | Semi-quantitative scoring of CD146 expression in different parts. **(A,C)** Semi-quantitative scoring of CD146 staining of glomerular and tubular compartments between the rejection groups and non-rejection group. **(B,D)** Semi-quantitative scoring of CD146 staining of glomerular and tubular compartments between the five subgroups. The statistical differences among groups were assessed by Student's *t*-test and one-way ANOVA. Statistical significance: $^{***}P < 0.001$, $^{****}P < 0.0001$.

be a sensitive indicator for the occurrence of allograft rejection. Although allograft biopsy is still the gold standard, the detection of sCD146 level could complement the diagnostic efficiency of common clinical indicators and increase the accuracy of diagnosis of acute rejection.

We also found the staining degree of CD146 was greater in biopsy specimens of acute rejection. It is reasonable to deduce that the increased plasma sCD146 level might come from the allografts undergoing rejection by Logistic regression analysis. CD146 could make endothelial cells to remodel their cytoskeleton, facilitating certain kinds of leukocytes and small activated molecules to pass through the barriers and then infiltrate local inflammatory tissues (34). Interestingly, the distribution pattern of CD146 staining was not the same in

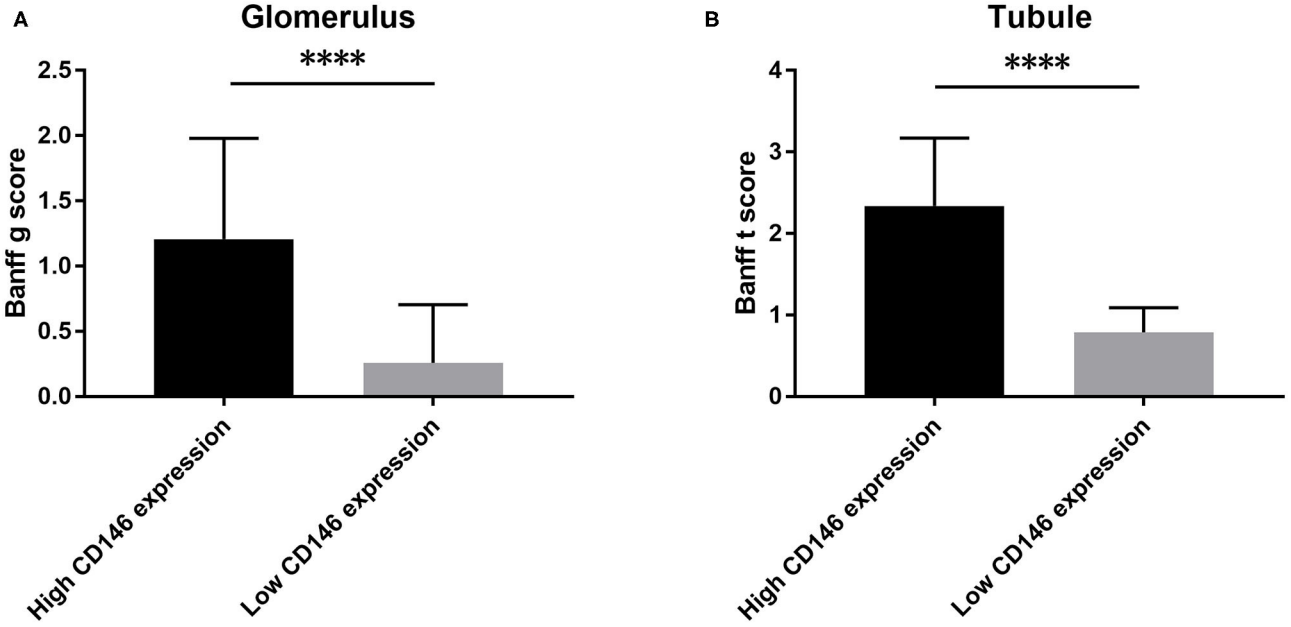

FIGURE 6 | Association of CD146 expression and Banff score. **(A)** The correlation of CD146 expression in glomerulus and Banff g score. **(B)** The correlation of CD146 expression in tubule and Banff t score. Statistical significance: ****$P < 0.0001$.

ABMR and TCMR. In ABMR, CD146 staining was greater in the glomerular compartment, while in TCMR staining was concentrated in the tubules. In addition, glomerular CD146 staining was positively correlated with biopsy Banff g score, and tubular staining was correlated with Banff t score. These data may support the hypothesis that high expression of CD146 is associated with the severity of local inflammation.

As previously described, CD146 expression is limited to certain cells and tissues. Moreover, the normal distribution of CD146 expression will change under certain condition of diseases. Some cell types that do not initially express CD146, such as renal tubular epithelial cells, will highly express it (25). Changes of the expression pattern of CD146 in cells may imply transformation of the function and structure of these cells. In this study, the expression of CD146 was different between the TCMR and ABMR groups. There was up-regulation of CD146 in the tubular region of patients with TCMR and the glomerular region of patients with ABMR, which is consistent with the respective pathological changes—tubulitis and glomerulitis.

To our best knowledge, this is the first study to explore the relation of sCD146/CD146 and acute renal rejection. Besides the new findings of this study, there are some limitations. Firstly, this was a single center retrospective study with a relatively small sample size. Secondly, the value of sCD146 for diagnosis of acute rejection needs further external evaluation. Thirdly, the potential mechanism explaining how CD146 contributes to the acute rejection requires further investigation.

In summary, our findings suggest that sCD146 may be useful for diagnosing acute rejection episodes in renal transplant recipients. The increased expression of CD146 may reflect endothelial or tubular epithelial dysfunction in the pathogenesis of immune injury.

DATA AVAILABILITY STATEMENT

All datasets generated for this study are included in the article/**Supplementary-Material**.

ETHICS STATEMENT

The studies involving human participants were reviewed and approved by the ethics committee of the first affiliated hospital of Sun Yat-sen University. The patients/participants provided their written informed consent to participate in this study.

AUTHOR CONTRIBUTIONS

JLia and QF conception and design, collection and assembly of data, data analysis and interpretation, manuscript writing, final approval of manuscript. WC, WZ, and SY pathological examination and analysis, final approval of manuscript. JLi, BX, and HH collection and assembly of data, data analysis and interpretation, final approval of manuscript. YG, JW, and XL laboratory experiments. HZ statistical analysis. LL and CW conception and design, financial support, data interpretation, manuscript writing, final approval of manuscript.

ACKNOWLEDGMENTS

This project was supported by the National Natural Science Foundation of China (81870511, 81670680, 81700655), Science and Technology Planning Project of Guangdong Province, China (2014B020212006, 2015B020226002, 2017A020215012), Guangdong Natural Science Foundation (2018A030313016), Key Scientific and Technological Program

of Guangzhou City (201803040011), Guangdong Provincial Key Laboratory on Organ Donation and Transplant Immunology (2013A061401007, 2017B030314018), and Guangdong Provincial International Cooperation Base of Science and Technology (Organ Transplantation, 2015B050501002).

SUPPLEMENTARY MATERIAL

The Supplementary Material for this article can be found online at: https://www.frontiersin.org/articles/10.3389/fmed.2020.531999/full#supplementary-material

REFERENCES

1. Oniscu GC, Brown H, Forsythe JL. Impact of cadaveric renal transplantation on survival in patients listed for transplantation. *J Am Soc Nephrol.* (2005) 16:1859–65. doi: 10.1681/ASN.2004121092
2. Chapman JR, O'Connell PJ, Nankivell BJ. Chronic renal allograft dysfunction. *J Am Soc Nephrol.* (2005) 16:3015–26. doi: 10.1681/ASN.2005050463
3. Nankivell BJ, Kuypers DR. Diagnosis and prevention of chronic kidney allograft loss. *Lancet*. (2011) 378:1428–37. doi: 10.1016/S0140-6736(11)60699-5
4. Huraib S, Goldberg H, Katz A, Cardella CJ, deVeber GA, Cook CT, et al. Percutaneous needle biopsy of the transplanted kidney: technique and complications. *Am J Kidney Dis.* (1989) 14:13–7. doi: 10.1016/S0272-6386(89)80087-3
5. Wilczek HE. Percutaneous needle biopsy of the renal allograft. A clinical safety evaluation of 1129 biopsies. *Transplantation*. (1990) 50:790–7. doi: 10.1097/00007890-199011000-00010
6. Tapia-Canelas C, Zometa R, O López-Oliva M, Jiménez C, Rivas B, Escuin F, et al. [Complications associated with renal graft biopsy in transplant patients]. *Nefrologia*. (2014) 34:115–9. doi: 10.3265/Nefrologia.pre2013.Nov.12232
7. Lehmann JM, Holzmann B, Breitbart EW, Schmiegelow P, Riethmüller G, Johnson JP. Discrimination between benign and malignant cells of melanocytic lineage by two novel antigens, a glycoprotein with a molecular weight of 113,000 and a protein with a molecular weight of 76,000. *Cancer Res.* (1987) 47:841–5.
8. van den Bosch TPP, Hilbrands LB, Kraaijeveld R, Litjens NHR, Rezaee F, Nieboer D, et al. Pre-transplant numbers of CD16(+) monocytes as a novel biomarker to predict acute rejection after kidney transplantation: a pilot study. *Am J Transplant.* (2017) 17:2659–67. doi: 10.1111/ajt.14280
9. Dagur PK, Tatlici G, Gourley M, Samsel L, Raghavachari N, Liu P, et al. CD146+ T lymphocytes are increased in both the peripheral circulation and in the synovial effusions of patients with various musculoskeletal diseases and display pro-inflammatory gene profiles. *Cytometry B Clin Cytom.* (2010) 78:88–95. doi: 10.1002/cyto.b.20502
10. Bardin N, Blot-Chabaud M, Despoix N, Kebir A, Harhouri K, Arsanto JP, et al. CD146 and its soluble form regulate monocyte transendothelial migration. *Arterioscler Thromb Vasc Biol*. (2009) 29:746–53. doi: 10.1161/ATVBAHA.108.183251
11. Dagur PK, McCoy JP. Endothelial-binding pro-inflammatory T cells identified by MCAM (CD146) expression: characterization and role in human autoimmune diseases. *Autoimmun Rev*. (2015) 14:415–22. doi: 10.1016/j.autrev.2015.01.003
12. Wang Z, Yan X. CD146, a multi-functional molecule beyond adhesion. *Cancer Lett*. (2013) 330:150–62. doi: 10.1016/j.canlet.2012.11.049
13. Ito T, Tamura N, Okuda S, Tada K, Matsushita M, Yamaji K, et al. Elevated serum levels of soluble CD146 in patients with systemic sclerosis. *Clin Rheumatol.* (2017) 36:119–24. doi: 10.1007/s10067-016-3434-3
14. Bardin N, Reumaux D, Geboes K, Colombel JF, Blot-Chabaud M, Sampol J, et al. Increased expression of CD146, a new marker of the endothelial junction in active inflammatory bowel disease. *Inflamm Bowel Dis.* (2006) 12:16–21. doi: 10.1097/01.MIB.0000194181.46930.88
15. Duan H, Luo Y, Hao H, Feng L, Zhang Y, Lu D, et al. Soluble CD146 in cerebrospinal fluid of active multiple sclerosis. *Neuroscience*. (2013) 235:16–26. doi: 10.1016/j.neuroscience.2013.01.020
16. Ilie M, Long E, Hofman V, Selva E, Bonnetaud C, Boyer J, et al. Clinical value of circulating endothelial cells and of soluble CD146 levels in patients undergoing surgery for non-small cell lung cancer. *Br J Cancer.* (2014). 110:1236–43. doi: 10.1038/bjc.2014.11
17. Stalin J, Nollet M, Garigue P, Fernandez S, Vivancos L, Essaadi A, et al. Targeting soluble CD146 with a neutralizing antibody inhibits vascularization, growth and survival of CD146-positive tumors. *Oncogene*. (2016) 35:5489–500. doi: 10.1038/onc.2016.83
18. Dufies M, Nollet M, Ambrosetti D, Traboulsi W, Viotti J, Borchiellini D, et al. Soluble CD146 is a predictive marker of pejorative evolution and of sunitinib efficacy in clear cell renal cell carcinoma. *Theranostics*. (2018) 8:2447–58. doi: 10.7150/thno.23002
19. Xing S, Luo Y, Liu Z, Bu P, Duan H, Liu D, et al. Targeting endothelial CD146 attenuates colitis and prevents colitis-associated carcinogenesis. *Am J Pathol.* (2014) 184:1604–16. doi: 10.1016/j.ajpath.2014.01.031
20. Kubena P, Arrigo M, Parenica J, Gayat E, Sadoune M, Ganovska E, et al. Plasma levels of soluble CD146 reflect the severity of pulmonary congestion better than brain natriuretic peptide in acute coronary syndrome. *Ann Lab Med.* (2016) 36:300–5. doi: 10.3343/alm.2016.36.4.300
21. Van Aelst LNL, Arrigo M, Placido R, Akiyama E, Girerd N, Zannad F, et al. Acutely decompensated heart failure with preserved and reduced ejection fraction present with comparable haemodynamic congestion. *Eur J Heart Fail.* (2018) 20:738–47. doi: 10.1002/ejhf.1050
22. Gayat E, Caillard A, Laribi S, Mueller C, Sadoune M, Seronde MF, et al. Soluble CD146, a new endothelial biomarker of acutely decompensated heart failure. *Int J Cardiol.* (2015) 199:241–7. doi: 10.1016/j.ijcard.2015.07.039
23. Harhouri K, Kebir A, Guillet B, Foucault-Bertaud A, Voytenko S, Piercecchi-Marti MD, et al. Soluble CD146 displays angiogenic properties and promotes neovascularization in experimental hind-limb ischemia. *Blood*. (2010) 115:3843–51. doi: 10.1182/blood-2009-06-229591
24. Stalin J, Harhouri K, Hubert L, Garrigue P, Nollet M, Essaadi A, et al. Soluble CD146 boosts therapeutic effect of endothelial progenitors through proteolytic processing of short CD146 isoform. *Cardiovasc Res.* (2016) 111:240–51. doi: 10.1093/cvr/cvw096
25. Bardin N, Moal V, Anfosso F, Daniel L, Brunet P, Sampol J, et al. Soluble CD146, a novel endothelial marker, is increased in physiopathological settings linked to endothelial junctional alteration. *Thromb Haemost.* (2003). 90:915–20. doi: 10.1160/TH02-11-0285
26. Małyszko J, Małyszko JS, Brzosko S, Wołczynski S, Myśliwiec M. Markers of endothelial cell activation/injury: CD146 and thrombomodulin are related to adiponectin in kidney allograft recipients. *Am J Nephrol*. (2005). 25:203–10. doi: 10.1159/000085827
27. Kuan Y, Hossain M, Surman J, El Nahas AM, Haylor J. GFR prediction using the MDRD and Cockcroft and Gault equations in patients with end-stage renal disease. *Nephrol Dial Transplant.* (2005) 20:2394–401. doi: 10.1093/ndt/gfi076
28. Haas M, Sis B, Racusen LC, Solez K, Glotz D, Colvin RB, et al. Banff 2013 meeting report: inclusion of c4d-negative antibody-mediated rejection and antibody-associated arterial lesions. *Am J Transplant.* (2014) 14:272–83. doi: 10.1111/ajt.12590
29. Loupy A, Haas M, Solez K, Racusen L, Glotz D, Seron D, et al. (2015). The Banff 2015 kidney meeting report: current challenges in rejection classification and prospects for adopting molecular pathology. *Am J Transplant*. (2017) 17:28–41. doi: 10.1111/ajt.14107
30. Fan Y, Fei Y, Zheng L, Wang J, Xiao W, Wen J, et al. Expression of endothelial cell injury marker Cd146 correlates with disease severity and predicts the renal outcomes in patients with diabetic nephropathy. *Cell Physiol Biochem.* (2018) 48:63–74. doi: 10.1159/000491663

31. Fan Y, Xiao W, Li Z, Li X, Chuang PY, Jim B, et al. RTN1 mediates progression of kidney disease by inducing ER stress. *Nat Commun.* (2015) 6:7841. doi: 10.1038/ncomms8841
32. Breuer J, Korpos E, Hannocks MJ, Schneider-Hohendorf T, Song J, Zondler L, et al. Blockade of MCAM/CD146 impedes CNS infiltration of T cells over the choroid plexus. *J Neuroinflamm.* (2018) 15:236. doi: 10.1186/s12974-018-1276-4
33. Cardinal H, Dieude M, Hebert MJ. Endothelial dysfunction in kidney transplantation. *Front Immunol.* (2018) 9:1130. doi: 10.3389/fimmu.2018.01130
34. Cerutti C, Ridley AJ. Endothelial cell-cell adhesion and signaling. *Exp Cell Res.* (2017) 358:31–8. doi: 10.1016/j.yexcr.2017.06.003

Conflict of Interest: The authors declare that the research was conducted in the absence of any commercial or financial relationships that could be construed as a potential conflict of interest.

Advantages of publishing in Frontiers

OPEN ACCESS
Articles are free to read for greatest visibility and readership

FAST PUBLICATION
Around 90 days from submission to decision

HIGH QUALITY PEER-REVIEW
Rigorous, collaborative, and constructive peer-review

TRANSPARENT PEER-REVIEW
Editors and reviewers acknowledged by name on published articles

Frontiers
Avenue du Tribunal-Fédéral 34
1005 Lausanne | Switzerland

Visit us: www.frontiersin.org
Contact us: frontiersin.org/about/contact

REPRODUCIBILITY OF RESEARCH
Support open data and methods to enhance research reproducibility

DIGITAL PUBLISHING
Articles designed for optimal readership across devices

FOLLOW US
@frontiersin

IMPACT METRICS
Advanced article metrics track visibility across digital media

EXTENSIVE PROMOTION
Marketing and promotion of impactful research

LOOP RESEARCH NETWORK
Our network increases your article's readership